UNIVERSITÀ DEGLI STUDI DI MILANO

DOTTORATO DI RICERCA IN SCIENZE DELLA TERRA

Ciclo XXXIII

DIPARTIMENTO DI SCIENZE DELLA TERRA

TESI DI DOTTORATO DI RICERCA

Calcareous nannofossil biostratigraphy and paleoecology of the late Turonian to Early Campanian interval and of Oceanic Anoxic Event 3.

GEO/01 04/A2

DOTTORANDO

FRANCESCO MINIATI

TUTOR
Prof.ssa ELISABETTA ERBA

COORDINATORE DEL DOTTORATO
Prof. FERNANDO CAMARA ARTIGAS

Abstract i

Chapter 1 1

Introduction 1

Chapter 2 5

Calcareous nannofossil biozonations of the Upper Cretaceous. 5

2.1. The biozation of Sissingh (1977). 7

2.1.1 The revised biozation of Perch-Nielsen (1985). 11

2.2 The biozation of Roth (1978). 13

2.4 The biozation of Burnett (1998). 21

Chapter 3 33

The Oceanic Anoxic Event 3. 33

3.1 The Oceanic Anoxic Events 3 35

3.2 Calcareous nannofossil across the Coniacian-Santonian OAE3. 40

Chapter 4 47

Materials and methods. 47

4.1 Studied sections. 47

4.1.1 DSDP Site 364. 47

4.1.2 ODP Site 959. 50

4.1.3 ODP Site 1261 52

4.1.4 Bottaccione section. 54

4.1.5 Seaford Head. 55

4.1.6 Tanzania TDP39 58

4.1.7 ODP Site 763 61

4.2 Sample preparation techniques. 63

4.3 Semiquantitative biostratigraphy. 64

4.4. Quantitative abundances. 65

4.5. Paleocological indicies of Temperature and Fertility 66

4.6. Statistical analyses. 67

Chapter 5 68

Results. 68

5.1 DSDP Site 364 68

5.1.1 Biostratigraphy 68

5.1.2 Nannofossil paleoecology and paleoceanography 70

5.1.3 The Coniacian-Santonian OAE3 at DSDP Site 364 80

5.2 ODP Site 959 82

5.2.1 Biostratigraphy 82

5.2.2 Nannofossil paleoecology and paleoceanography 83

5.2.3 The Coniacian-Santonian OAE3 at ODP Site 959 94

5.3 ODP Site 1261 96

5.3.1 Biostratigraphy 96

5.3.2 Nannofossil paleoecology and paleoceanography 97
5.4 Seaford Head 105
5.4.1 Biostratigraphy 105
5.4.2 Nannofossil paleoecology and paleoceanography 107
5.4.3 The Coniacian-Santonian OAE3 at Seaford Head 118
5.5 Tanzania TD39 120
5.5.1 Biostratigraphy 120
5.5.2 Nannofossil paleoecology and paleoceanography 122
5.5.3 The Coniacian-Santonian OAE3 at TDP39 131
5.6 ODP Site 763 132
5.6.1 Biostratigraphy 132
5.6.2 Nannofossil paleoecology and paleoceanography. 134
5.6.3 The Coniacian-Santonian OAE3 at ODP Site 763 141
Chapter 6 144
Discussion 144
6.1 Changes of surface-water fertility during the Coniacian-Santonian OAE3 144
6.2 Abundance changes of genera *Micula* and *Marthasterites* across the Coniacian-Santonian OAE3 151
Chapter 7 161
Conclusions 161
References 167
Appendix 1 186
Systematic Paleontology 186
Appendix 2 235
Taxonomic list 235
Appendix 3 243
Plates 243
Appendix 4 248
Table of papers with biostratigraphic and paleocological nannofossil data for the Turonian-Campanian 248
Appendix 5 249
Range chart of DSDP Site 364 249
Appendix 6A 250
Correlation matrix of DSDP 364 250
Appendix 7 253
Range chart of ODP Site 959 253
Appendix 8A 254

Correlation matrix of ODP Site 959 ..... **254**
Appendix 9 ..... **257**
Range chart of ODP Site 1261 ..... **257**
Appendix 10A **258**
Correlation matrix of ODP Site 1261 ..... **258**
Appendix 11 ..... **260**
Range chart of Seaford Head **260**
Appendix 12A **261**
Correlation matrix of Seaford Head **261**
Appendix 13 ..... **265**
Range chart of TDP39 ..... **265**
Appendix 14A **266**
Correlation matrix of - TDP39 ..... **266**
Appendix 15 ..... **270**
Range chart of ODP Site 763 ..... **270**
Appendix 16A **271**
Correlation matrix of ODP Site 763 ..... **271**
Appendix 17 ..... **274**
Miniati et al., 2020 ..... **274**
Acknowledgements

Abstract

The Late Cretaceous was punctuated by several periods of global perturbations of the climate-ocean system that lead to widespread organic carbon-rich marine black shale deposition, termed Oceanic Anoxic Events (OAEs). The OAE3 represents the last episode of anoxia dated as Coniacian-Santonian. Compared to previous anoxic events, OAE3 has a regional extension, rather than a global significance, since it is confined to the equatorial-south Atlantic Ocean and adjacent basins (e.g. Caribbean Basin, Western Interior Basin). Another major difference of OAE3 relative to previous OAEs resides in the absence of a prominent $\delta^{13}C$ anomaly, but the occurrence of several minor positive and negative excursions in the Coniacian-Santonian interval. Moreover, the deposition of organic carbon-rich sediments (black shales) seems to be diachronous even in the central-south Atlantic Ocean.

This PhD project focused on calcareous nannofossil biostratigraphy and paleoceanography of the Late Turonian to Early Campanian time interval (Late Cretaceous), and specifically of the Coniacian-Santonian. Nannofossil assemblages were investigated semiquantitatively and quantitatively to obtain a detailed biostratigraphic framework for assessing the paleoenvironmental changes across OAE3.

The study was performed on Deep Sea Drilling Project (DSDP) and Ocean Drilling Program (ODP) sites and on-land sections, situated in the equatorial and south Atlantic Ocean, the Indian Ocean and the Anglo-Paris Basin. The results of my investigation were integrated with data from literature in order to achieve a solid framework of events for the Coniacian-Santonian time interval and provide a paleoceanographic characterization of OAE3.

A detailed revision of the taxonomy was accomplished for solving a few taxonomic incongruities and obtain a unified updated nomenclature. This was the basis for the coherent high-resolution biostratigraphy of the selected sites, in order to establish dating and correlations at supra-regional scale. The four standards biozonation schemes available for the Upper Cretaceous were applied to attain the maximum resolution and test their individual applicability in different oceanic basins and oceanographic settings.

The major objective of this PhD thesis was the reconstruction of presumed paleoceanographic changes across OAE3 as recorded by abundance and composition of calcareous nannofossil assemblages. Quantitative analyses of calcareous nannofossil assemblages allowed the characterization of paleotemperature and nutrient changes prior, during and after OAE3. Nannofossil-based paleotemperature obtained in this study and documented in the literature do not show significant changes in the studied successions, perhaps due to unresolved unambiguous temperature-related taxa in the Late Cretaceous and/or minor (subtle) temperature changes across OAE3. As far as paleofertility is

concerned, the nannofossil taxa indicative of higher nutrient content display very different patterns at the various sites, suggesting that OAE3 was not characterized by a global fertilization episode. Indeed, fertility remained globally low with the exception of upwelling areas characterized by meso-eutrophic conditions also in the intervals preceding and following OAE3.

The quantitative analyses conducted in this study pointed out relatively large fluctuations in abundance of genera *Micula* and *Marthasterites* in the Coniacian-Santonian interval. These abundance peaks could be correlated with analogous events described in the literature, even if with different values of abundance at the various sites/sections. Two *Marthasterites (M. furcatus)* abundance peaks and five *Micula* (*M. staurophora*) abundance peaks were distinguished across OAE3. The paleoecological affinity of *Micula*, and specifically *M. staurophora,* as well as that of genus *Marthasterites* remains unexplained, so the causes of their abundance peaks continue to be elusive. However, the distinctive fluctuations in nannofossil assemblages indicate profound paleoceanographic changes during the Coniacian-Santonian. The onset of OAE3 coincides with a major increase in abundance (and locally dominance) of *M. furcatus* suggesting the rapid establishment of new and peculiar paleoceanographic conditions at widespread to global scale. The most altered paleoceanographic conditions were reached in the core of OAE3 with the synchronous maximum abundance (climax) of *M. staurophora* at global scale.

In addition to their value for paleoenvironmental reconstructions, the identified *Micula* and *Marthasterites* abundance peaks turned out to be extremely useful for complementing/implementing the biostratigraphic characterization of the Turonian/Coniacian, Coniacian/Santonian and Santonian/Campanian boundaries and might be introduced as additional events in future nannofossil zonations for the Late Cretaceous.

Chapter 1

Introduction

The Late Cretaceous was characterized by important changes in oceanic chemistry, structure and circulation with the gradual opening of oceanic gateways and a long-term climatic cooling. These changes contributed to the progressive fading of intermittent periods of anoxia (Oceanic Anoxic Events, OAEs) leading to the deposition of the youngest OAE, during the Coniacian-Santonian time interval, named OAE3. Profound differences distinguish OAE3 from the previous episodes of global anoxia, since it was most probably restricted to the equatorial to mid-latitudinal Atlantic Ocean and adjacent basins (e.g., Caribbean Basin, Western Interior Basin), and to the South Atlantic (Wagreich et al. 2009, 2012). In addition, the temporal distribution of the organic-rich sediments seems to be not synchronous among the different basins. Another major difference resides in the absence of a distinctive $\delta^{13}C$ anomaly, being characterized by several minor positive and negative excursions in the Coniacian-Santonian interval (Jarvis et al., 2006). In the present study, I follow the definition of OAE3 given by Wagreich et al. (2009, 2012)

Calcareous nannoplankton have a wide geographical and latitudinal distribution and represent an extremely useful biostratigraphic tool as well as a proxy for paleoceanographic reconstructions. Calcareous nannoplankton proliferation and crisis reflect changes of surface water conditions (temperature, fertility, salinity, chemistry and CO_2), and affect the inorganic and organic carbon cycle in the oceans at short, medium and long term.

This PhD project is focused on calcareous nannofossil biostratigraphy and paleoceanography of the Late Turonian to Early Campanian time interval (Late Cretaceous), including the OAE3 of Coniacian-Santonian age. This study was performed on samples from various ODP/DSDP Sites and on-land sections, situated in: a) the equatorial and south Atlantic ODP Site 1261(Demerara Rise), ODP Site 959 (Ivory Coast–Ghana), and DSPD Site 364 (Angola Basin); b) the Anglo-Paris Basin (Seaford Head section); c) Indian Ocean: Tanzania TDP 39 and ODP Site 763. A detailed revision of the taxonomy is considered crucial for the coherent high-resolution biostratigraphy of the selected sites, in order to establish dating and correlations at supra-regional scale. The four standards biozonation schemes available for the Upper Cretaceous (Sissingh,1977; Roth. 1978; Bralower et al., 1995; Burnett, 1998) have been applied to attain the maximum resolution and test their individual applicability in different oceanic basins and oceanographic settings.

The major objective of this PhD thesis is the reconstruction of presumed paleoceanographic changes across OAE3 as recorded by abundance and composition of calcareous nannofossil assemblages. A literature survey conducted to evaluate the available information about calcareous nannofossil paleoecology of the Coniacian-Santonian time interval, revealed the reconstruction of nannofossil paleocology in different areas in terms of changes in paleotemperature and paleofertility. However, unlike other Mesozoic OAEs, studies conducted so far show that OAE3 lacks specific changes in calcareous nannofossil assemblages although increases in abundance of *Marthasterites furcatus* and *Micula staurophora* have been observed.
Quantitative analyses of abundance and diversity of calcareous nannofloras will be performed to delineate the surface ocean state and dynamics prior, during and after the most recent episode of Mesozoic anoxia. Since Wagreich et al. (2009, 2012) describe Coniacian-Santonian oxygen depletion at regional scale in the central-south Atlantic Ocean, the selected sites are located at Demerara Rise, and in the Ivory Coast–Ghana and Angola Basin. My investigation was extended to the Indian ocean and the Anglo-Paris Basin to quantify nannofloral changes in different oceanic basins. The comparison and integration of my results with literature data will allow to distinguish synchroneity/diachroneity of changes in nannofossil abundance and composition as well as the occurrence of reproducible responses to paleoenvironmental perturbations at local, regional or global scale.

Thesis outline:
In *Chapter 2* I present an overview of the available calcareous nannofossil biozonations for the Late Cretaceous time interval.
In *Chapter 3* I illustrate the OAE3 and present an overview of the calcareous nannofossil literature available for the late Turonian-early Campanian time interval.
In *Chapter 4* I describe all the studied successions, illustrating the sample preparation techniques and the criteria adopted for calcareous nannofossil investigations.
In *Chapter 5* the results are reported separately for each studied section/site.
In *Chapter 6* I discuss calcareous nannofossil changes observed across the OAE3 interval.
In *Chapter 7* the conclusions are compiled.

In the Appendices I present:

- a taxonomy description/revision of every species used as marker in Upper Cretaceous biozonations, specifically for the Turonian – Campanian time interval (Appendix 1).
- The taxonomic list of all taxa encountered in this study (Appendix 2).
- Calcareous nannofossil plates (Appendix 3).

- Tables with the list of the studied papers (Appendix 4).
- Calcareous nannofossil range charts, and matrix correlation for every investigated section (Appendices 5-16).
- The recently published paper on the Santonain/Campanian boundary (Miniati et al., 2020) (Appendix 17).

Chapter 2
Calcareous nannofossil biozonations of the Upper Cretaceous

The first attempt to establish a biostratigraphy based on calcareous nannofossils for the Cretaceous, was done by Stradner (1963): he studied different sections situated in West Europe, and recognized seven successive associations. A similar assemblage zonation from European sections and stratotypes was also described by Stover (1966), Reinhardt (1966) and Black (1971). Radomski (1967) described the first range zones for the Cretaceous, whereas Gartner (1968), Bukry (1969) and Cepek and Hay (1969) published tentative biozonations from Unites States sections using calcareous nannofossils. Manivit (1971, 1972) analyzed sections from France and proposed a zonation for the Aptian to Danian interval. She also tried to make a correlation between Europe and the United States using calcareous nannofossils together with ammonite and planktonic foraminiferal zones.

In the 1970s the oceanic exploration conducted by the Deep Sea Drilling Project (DSDP) provided new data from oceanic sites, leading to important implementation also of calcareous nannofossil biostratigraphy. New zonations were established as direct results of new data collected from the various oceans ad at different latitudes (Buky and Bramlette, 1970; Worsley, 1971; Perch-Nielsen, 1972; Roth and Thierstein, 1972; Bukry,1973a; Roth, 1973; Thierstein, 1974; Martini, 1976). The first global zonation for the Cretaceous was established by Thierstein (1976), based on a large dataset from both land and DSDP sections and comprising a tentative correlation with magnetostratigraphy. He also highlighted the paleoenvironmental restrictions of some calcareous nannofossil taxa that can be responsible of diachroneity of events recorded in different areas.

Verbeek (1976, 1977) published a zonation for the middle-Upper Cretaceous based on calcareous nannonofossil associations from Tunisia, southern Spain and stratotype sections in France. Sissingh (1977, 1978) completed the investigations of European stratotypes and proposed a new nannofossil zonation for the entire Cretaceous calibrated in stage-stratotypes, data from the El Kef section in western Tunisia, and drill samples from the North Sea, Oman and Turkey.

Roth (1978) compiled his biozonation mainly based on data from DSDP material and introduced oceanic stages. The Roth's zonation showed the correlation potential of nannofossil biostratigraphy from onshore to oceanic sequences, establishing a connection between the "European stratotypes".

In the 1980s, the most relevant works are those of Crux (1982) who studied sections from SE England providing a correlation between nannofossil bioevents and macrofossil zones of northern Europe. Perch-

Nielsen (1985) implemented Sissingh (1977) zonation with a number of additional events both from Boreal and Tethyan areas establishing one of the most used and solid framework for dating Upper Cretaceous successions.

The investigation conducted on calcareous nannofossils of the Cretaceous European stratotypes highlighted an incomplete stratigraphic record in most of these sections. For this reason, at the Symposium on Cretaceous Stage Boundaries held in Copenhagen in 1983 and the follow-up conference in Brussels in 1995 it was decided to focus calcareous nannofossil studies on proposed stage boundary sections (see summary of Burnett,1996) and apply integration with other fossil groups.

In the Gubbio area, Monechi and Thierstein (1985) correlated nannofossils and planktonic foraminifera with magnetostratigraphy in the Campanian-Maastrichtian interval. Bralower (1988) analyzed the Cenomanian/Turonian boundary interval in different regions of the Western Interior, Europe and Tunisia, establishing a high-resolution biostratigraphic scheme. Bralower et al. (1995) revised Roth's (1978) zonation introducing additional nannofossil events and integrating nannofossils with planktonic foraminifera, bentonite radiometric ages and polarity chrons.

During the 1990s, new calcareous nannofossil biozonations were produced and mainly focussed on higher latitudes areas: Burnett (1990) provided a Boreal zonation for the Campanian and Watkins et al. (1996) established a new Upper Cretaceous nannofossil biostratigraphy for the Southern Ocean based on data from DSDP/ODP sites.

Bergen and Sikora (1999) published an integrated Upper Cretaceous microfossil scheme for the southern Norwegian chalk mainly based on samples from wells and circum North Sea outcrops.

In 1998 Burnett published an Upper Cretaceous zonation based on old and new bioevents from both oceanic and epicontinental paleoenvironments. She distinguished between three paleobiogeographical areas (provinces), correlating the events with European and American macrofossil zones. In a successive paper (Lees, 2002) she implemented the "austral" biozonation with new data from DSDP and ODP sites in the Indian Ocean. Fritsen et al. (2000) revised Burnett (1998) zonation for the Upper Cretaceous of the North Sea, integrating the nannofossil events with planktonic foraminifera (King et al, 1989).

At present, several questions are still open concerning the age calibration of nannofossil events, their correlation with other fossil groups and provincialism of different nannofossil taxa.

In the following chapters I present the overview of the four most widely used Upper Cretaceous nannofossil zonations by Sissingh (1977) as revised by Perch-Nielsen (1985), Roth (1978), Bralower et al. (1995) and Burnett (1998).

2.1. The biozation of Sissingh (1977).

The calcareous nannofossil zonation presented by Sissingh (1977) for the Cretaceous includes the analyses of on-land sections and offshore explorations wells. The Upper Cretaceous zonation was mainly based on calcareous nannofossil assemblages of the Tunisian section of Dyr el Kef, stratotype sections and other important successions in France. In addition, data from sections in The Netherlands, New Jersey (U.S.) and from industrial well spot-samples from Oman, Turkey and the North Sea region were also considered (Figure 2.1.1). As far as the Lower Cretaceous is concerned, together with the Dyr el Kef section, the dataset included sections situated in northern France, west Germany and England (Speeton Clay Formation).

Sissingh (1977) recognized in the Cretaceous a total of 26 formal zones, some of them divided in informal subzone of secondary value. Each zone was termed following an alphanumerical notation (Cretaceous Coccoliths - CC#) according on the first (FO) or last (LO) occurrences of relatively

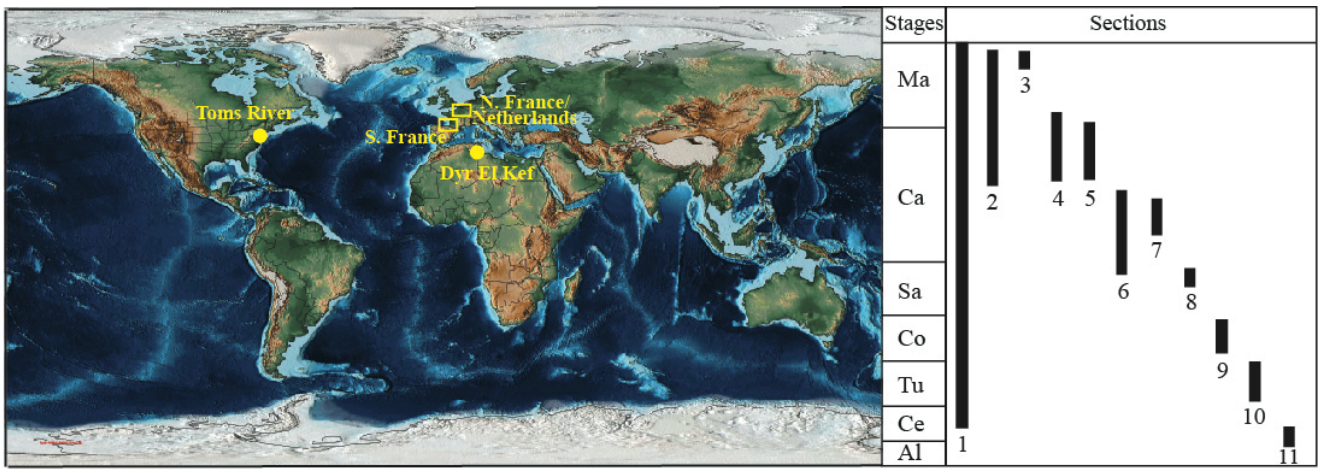

Figure 2.1 - Summary of sections and stratigraphic intervals studied by Sissingh (1977). 1: Dyr El Kef (191 samples); 2: Toms River (9 samples);3: ENCI Quarry (19 samples);4: Aubeterre (20 samples);5: Le Maine-Blanc, Barret, Breuillare, Gironde Estuary, Montmoreau, Brossac (16 samples);6: Grande Champagne (2 samples);7: Sens (8 samples); 8: Javresac, Saintes St. Laurant – Louzac (7 samples); 9: Cognac (5 samples); 10: Cher Valley (16 samples);11: St. Ulphace Théligny-Moulin de l'Aunay, Ballon (10 samples).

abundant taxa, easily identifiable with light microscope. A composite Cretaceous range chart of nannofossil species was compiled to define zonal or sub-zonal boundaries, also integrating data from Thierstein (1973) for the Lower Cretaceous. More attention was paid by Sissingh (1977) to the Upper Cretaceous with identification of several zones and subzone, compare to the Lower Cretaceous. A correlation between the nannofossil and foraminiferal zonation was established based on the analyses of the same samples previously used for planktonic foraminiferal studies in the Dyr el Kef section (Postuma (1971) (Figure 2.1.2).

Sissingh (1977) also highlighted the different paleoecological affinities of some biostatigraphic markers, that result more common, respectively, at lower latidudes (*Bukryaster hayi*, *Calculites aculeus*, *Lithraphidites quadratus*, *Micula murus*, *Tetralithus nitidus*, *Uniplanarius trifidus*) or higher latitudes (*Nephrolithus frequens*), and concluded that his biozonation is more reliable for lower latitudes.
The calcareous nannofossil zones and subzones for the Upper Cretaceous established by Sissingh (1977), summarized in Figure 2.1.2, are synthetized below reporting the occurrence in the studied sections, the age assignments and the correlation with planktonic foraminiferal biozonation (Postuma, 1971).

- **CC10-*Microrhabdulus decoratus* zone** (Sissingh,1977). Definition: from the FO of *Microrhabdulus decoratus* to the FO of *Tetralithus pyramidus* (= *Quadrum gartneri).* Ref. section: El Kef. Age assignment: Late Cenomanian; planktonic foraminiferal zone: *R. cushmani.*
- **CC11-*Tetralithus pyramidus* zone** (Cepek and Hay, 1969 emend. Sissingh,1977). Definition: from the FO of *Tetralithus pyramidus* (= *Quadrum gartneri)* to the FO *Lucianorhabdus maleformis.* Ref. sections: El Kef, Cher Valley, Kansas (Cepek and Hay, 1969). Age assignment: Early Turonian; planktonic foraminiferal zone: *R. cushmani-G. helvetica*.
- **CC12-*Lucianorhabdus maleformis* zone** (Sissingh,1977). Definition: from the FO of *Lucianorhabdus maleformis* to the FO of *Eiffellithus eximius.* Ref. sections: El Kef, Central Pacific (Roth, 1973), Indian Ocean (Thierstein, 1974). Age assignment: Late Turonian; planktonic foraminiferal zone: *G. helvetica.* Remarks: The base of this zone can be approximated also with the LO of *Lucianorhabdus compactus* (basal Turonian Stratotype) or the FO of *Eiffellithus eximius*.
- **CC13-*Marthasterites furcatus* zone** (Čepek and Hay, 1969 emend. Sissingh,1977). Definition: from the FO *Marthasterites furcatus* to the FO of *Micula staurophora*. Ref. sections: El Kef, Central Pacific (Roth, 1973), Indian Ocean (Thierstein, 1974). Age assignment: Early Coniacian; planktonic foraminiferal zone: *G. schneegansi.*
- **CC14-*Micula staurophora* zone** (Čepek and Hay, 1969 emend. Sissingh,1977). Definition: from the FO of *Micula staurophora* to the FO of *Reinhardtites anthophorus*. Ref. sections: El Kef, Indian Ocean (Thierstein, 1974). Age assignment: Late Coniacian; planktonic foraminiferal zone: *G. schneegansi*.
- **CC15-*Reinhardtites anthophorus* zone** (Sissingh,1977). Definition: from the FO of *Reinhardtites anthophorus* to the FO of *Lucianorhabdus cayeuxii*. Ref. section: El Kef. Age assignment: Early Santonian; planktonic foraminiferal zone: *G. concavata/G. carinata.*
- **CC16-*Lucianorhabdus cayeuxii* zone** (Sissingh,1977). Definition: from the FO of *Lucianorhabdus cayeuxii* to the FO of *Calculites obscurus.* Ref. sections: El Kef, Saintes, Javresac, St. Laurent-

Louzac, Gimeux, Alabama (Čepek and Hay, 1969). Age assignment: Late Santonian; planktonic foraminiferal zone: *G. concavata/G. carinata.*

- **CC17-*Calculites obscurus* zone** (Sissingh,1977). Definition: from the FO of *Calculites obscurus* to the FO of *Aspidolithus parcus*. Ref. sections: El Kef, The Netherlands, Oman, Alabama (Cepek and Hay, 1969). Age assignment: earliest Campanian; planktonic foraminiferal zone: *G. elevata* (basal).
- **CC18-*Aspidolithus parcus* zone** (Sissingh,1977). Definition: from the FO of *Aspidolithus parcus* (s.l.) to the LO of *Marthasterites furcatus.* Ref. sections: El Kef, Genté, Oman, Great Britain, Alabama (Čepek and Hay, 1969), Central Pacific (Roth, 1973). Age assignment: Early Campanian; planktonic foraminiferal zone: *G. elevata.* This zone can be subdivided in two subzones:

  CC18a subzone. Definition: from the FO of *Aspidolithus parcus* (s.l.) to the FO of *Bukryaster hayi.*

  CC18b subzone. Definition: from the FO of *Bukryaster hayi* to the LO of *Marthasterites furcatus.*
- **CC19-*Calculites ovalis* zone** (Sissingh,1977). Definition: from the LO of *Marthasterites furcatus* to the FO of *Ceratolithoides aculeus.* Ref. sections: El Kef, Oman, Alabama (Čepek and Hay, 1969), Central Pacific (Roth, 1973). Age assignment: Early Campanian; planktonic foraminiferal zone: *G. elevata.* This zone can be subdivided in two subzones:

  CC19a subzone. Definition: from the LO of *Marthasterites furcatus* to the LO of *Bukryaster hayi.*

  CC19b subzone. Definition: from the LO of *Bukryaster hayi* to the FO of *Ceratolithoides aculeus.*
- **CC20-*Ceratolithoides aculeus* zone** (Čepek and Hay, 1969 emend. Sissingh,1977). Definition: from the FO of *Ceratolithoides aculeus* to the FO of *Tetralithus nitidus* (= *Uniplanarius gothicus*). Ref. sections: Toms River, Aubeterre, Oman, Alabama (Čepek and Hay, 1969), Central Pacific (Roth, 1973). Age assignment: Early Campanian; planktonic foraminiferal zone: *G. elevata.*
- **CC21- *Tetralithus nitidus* zone** (Sissingh,1977). Definition: from the FO of *Tetralithus nitidus* (= *Uniplanarius gothicus)* and the FO of *Tetralithus trifidus* (= *Uniplanarius trifidus*). Ref. sections: El Kef, Aubeterre, Gironde, Estuary, Montmoreau, Brossac, Turkey, Oman, Central Pacific (Roth, 1973). Age assignment: Late Campanian; planktonic foraminiferal zone: *G. elevata.* This zone can be subdivided in three subzones:

  CC21a subzone. Definition: from the FO of *Uniplanarius gothicus* to the FO of *Ceratolithoides arcuatus.*

  CC21b subzone. Definition: from the FO of *Ceratolithoides arcuatus* to the LO of *Ceratolithoides arcuatus*.

  CC21c subzone. Definition: from the LO of *Ceratolithoides arcuatus* to the FO *Uniplanarius trifidus*
- **CC22- *Tetralithus trifidus* zone** (Bukry and Bramlette, 1970). Definition: from the FO of *Uniplanarius trifidus* to the LO of *Reinhardtites anthophorus.* Ref. sections: El Kef, Gironde/Estuary,

Aubeterre, Toms River, Turkey, Oman, Central Pacific (Roth, 1973). Age assignment: Late Campanian; planktonic foraminiferal zone: *G. elevata.* This zone can be subdivided in two subzones:

CC22a subzone. Definition: from the FO of *Uniplanarius trifidus* to the FO of *Reinhardtites levis*.

CC22b subzone. Definition: from the FO of *Reinhardtites levis* to the LO of *Reinhardtites anthophorus.*

- **CC23 *Tranolithus phacelosus* zone** (Sissingh,1977). Definition: from the LO of *Reinhardtites anthophorus* to the LO of *Tranolithus phacelosus* (= *Tranolithus orionatus*). Ref. sections: El Kef, Gironde/Estuary, Aubeterre, Toms River, Turkey, Oman, Central Pacific (Roth, 1973). Age assignment: Late Campanian; planktonic foraminiferal zone: *G. elevata.* This zone can be subdivided in two subzones:

  CC23a subzone. Definition: from the LO of *Reinhardtites anthophorus* to the LO of *Aspidolithus parcus*.

  CC23b subzone. Definition: from the LO of *Aspidolithus parcus* to the LO of *Tranolithus orionatus*
- **CC24 *Reinhardtites levis* zone** (Sissingh,1977). Definition: from the LO *Tranolithus phacelosus* (= *Tranolithus orionatus*) to the LO of *Reinhardtites levis*. Ref. sections: El Kef, Aubeterre, Denmark, Great Britain, Central Pacific (Roth, 1973); age assignment: Early Maastrichtian; planktonic foraminiferal zone: *G. gansseri*.
- **CC25 *Arkhangelskiella cymbiformis* zone** (Sissingh,1977). Definition: from the LO of *Reinhardtites levis* to the FO of *Nephrolithus frequens* or *Micula murus* (Perch-Nielsen, 1972). Ref. sections: Alabama (Cepek and Hay, 1969), North Atlantic (Perch-Nielsen, 1972), Central Pacific (Roth, 1973), W. Tunisia (Dry el Kef), The Netherlands (Maastricht), New jersey (Toms River), Denmark, Great Britain. Age assignment: Late Maastrichtian; planktonic foraminiferal zone: *G. mayaroensis.* This zone can be subdivided in three subzones:

  CC25a subzone. Definition: from the LO of *Reinhardtites levis* to the FO of *Arkhangelskiella cymbiformis.*

  CC25b subzone. Definition: from the FO of *Arkhangelskiella cymbiformis* to the FO of *Lithraphidites quadratus.*

  CC25c subzone. Definition: from the FO of *Lithraphidites quadratus* to the FO of *Nephrolithus frequens* or *Micula murus.*
- **CC26 *Nephrolithus frequens* zone** (Čepek and Hay, 1969). Definition: from the FO and LO of *Nephrolithus frequens*. Ref. sections: El Kef, Toms River, Maastricht. Age assignment: Late Maastrichtian, boreal and tropical preference respectively; planktonic foraminiferal zone: *G. mayaroensis.*

2.1.1 The revised biozonation of Perch-Nielsen (1985).

The calcareous nannofossil zonation of Sissingh (1977) was revised by Perch-Nielsen (1979, 1983, 1985) adding numerous zonal and subzonal markers. She used a dataset that included nannofossil events from different areas and latitudes with the aim of improving the applicability of Sissingh (1977) zonation, both at lower and higher latitudes, making it more cosmopolitan. The calcareous nannofossil zones and subzones for the Upper Cretaceous as modified by Perch-Nielsen (1985) are shown in Figure 2.1.2. The most important changes introduced by Perch-Nielsen (1985) are summarized below.

- **CC9-*Eiffellithus turriseiffelii* zone** (Thierstein emnd. Sissingh,1977). This zone is divided in two subzones according, respectively, to the LO of *Hayesites albiensis* (Manivit et al. 1977) together with the FO of *Crucicribrum anglicum* and the LO of *Watznaueria britannica*, *Braarudosphaera africana* and FO *Corollithion kennedyi*.
- **CC10-*Microrhabdulus decoratus* zone** (Sissingh,1977). This zone corresponds to the *Lithraphidites acutus* zone of Manivit et al. (1977) delimitated at top by the FO of *Quadrum gartneri*.
- **CC13-*Marthasterites furcatus* zone** (Čepek and Hay, 1969 emend. Sissingh,1977). The FO of *Lithastrinus septenarius* is noticed after the FO of *Marthasterites furcatus* and before the FO *of Micula staurophora*.
- **CC15-*Reinhardtites anthophorus* zone** (Sissingh,1977). The FO of *Lithastrinus grillii* together with the FO of *Micula concava* are suggested as additional marker for the base of this zone.
- **CC16-*Lucianorhabdus cayeuxii* zone** (Sissingh,1977). The LO of *Lithastrinus septenarius* can be used together with the FO *Lucianorhabdus cayeuxii* to indicate the base of this zone.
- **CC17- *Calculites obscurus* zone** (Sissingh,1977). Perch-Nielsen (1979) suggested the use of the LO *Eprolithus floralis* as substitute marker of *Calculites obscurus*.
- **CC18- *Aspidolithus parcus* zone** (Sissingh,1977). This zone is divided in two subzones according, to the FO of *Bukryaster hayii* and FO *Ceratolithoides verbeekii*, respectively.
- **CC21- *Tetralithus nitidus* zone** (Sissingh,1977). This zone was divided by Sissingh (1977) in three subzones using the range of *Ceratolithoides arcuatus*. However, according to Perch-Nielsen (1985) *Ceratolithoides arcuatus* is absent at higher latitudes (North Sea).
- **CC22- *Tetralithus trifidus* zone** (Bukry and Bramlette, 1970). This zone is divided by Perch-Nielsen (1985) in three subzones using in addition to the FO *Reinhardtites levis* of Sissingh (1977) the FO of *Lithastrinus grillii*.
- **CC23- *Tranolithus phacelosus* zone** (Sissingh,1977). Perch-Nielsen (1979) noticed that the LO

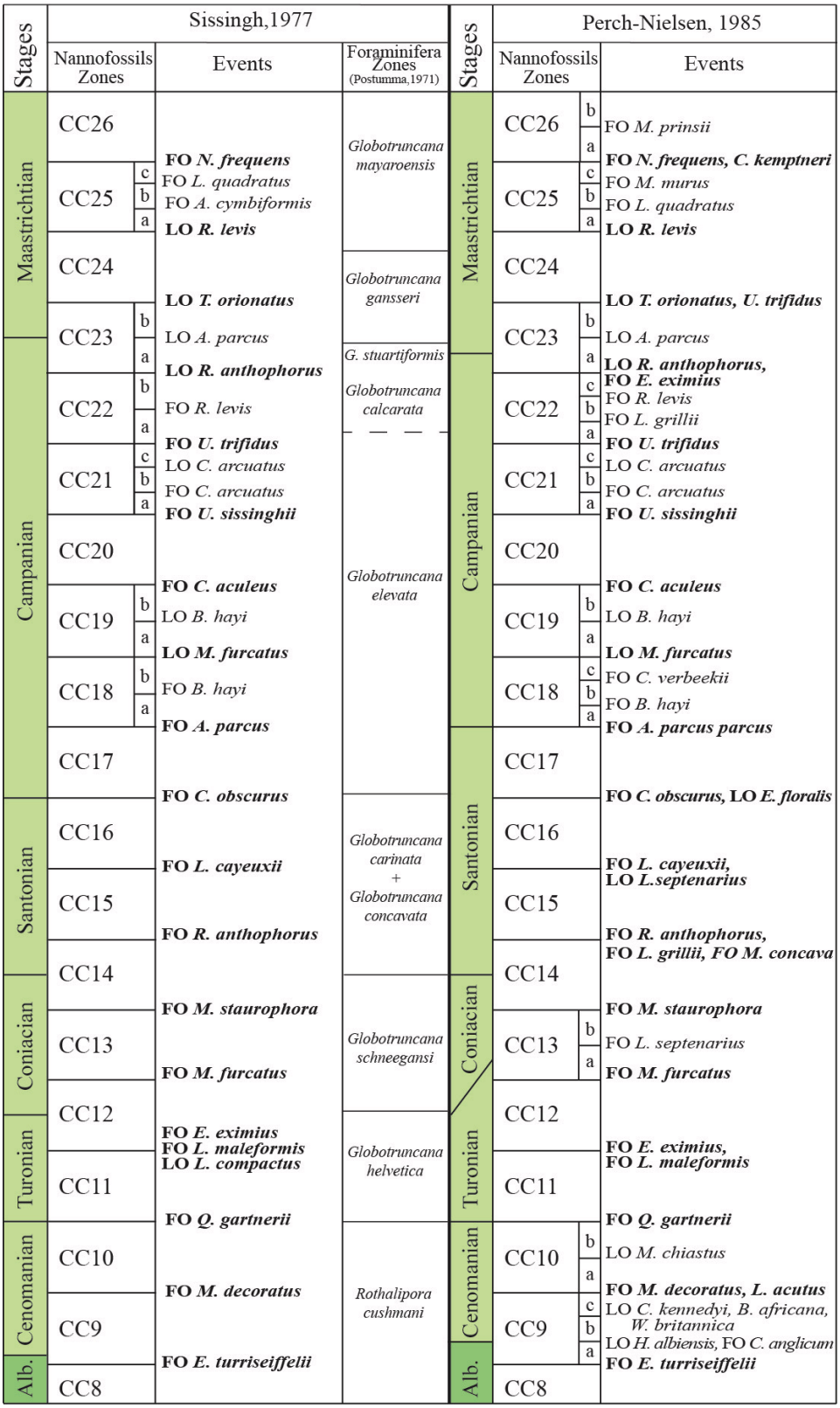

Figure 2.1.1 - Biozonations of Sissingh (1977) and Perch-Nielsen (1985). Zonal markers are indicated in bold. Nannofossil zones are arbitrarily given equal lengths/duration and, therefore, stages are not in scale. Foraminifera zonation is after Postuma (1971) as in the original zonation.

Eiffellithus eximius coincides with the LO of *Reinhardtites anthophorus*. This zone corresponds to the upper part of the *Uniplanarius trifidus* zone of some authors (Bukry and Bramlette, 1970, Martini,1976, Roth,1978, Doeven,1983).

- **CC25 *Arkhangelskiella cymbiformis* zone** (Sissingh,1977). Perch-Nielsen (1985) divided this zone in three subzones using the FO of *Lithraphidites quadratus* and the FO of *Micula murus,* respectively. Both species represent reliable biostratigraphic markers at lower latitudes.
- **CC26 *Nephrolithus frequens* zone** (Čepek and Hay, 1969). According to Perch-Nielsen (1985) *N. frequens* is a common taxon at higher latitudes ad represents a good marker for this time interval. At lower latitudes, the interval between the FO of *Lithraphidites qudratus* and the top Maastrichtian can be divided into three subzones using the FO of *M. murus* and FO of *Micula prinsii,* respectively.

2.2 The biozonation of Roth (1978).

The calcareous nannofossil zonation proposed by Roth (1978), for the Upper Cretaceous was based on a compilation of data from Roth (1973), Thierstein (1974, 1976), Bukry (1975) and Verbeek (1976). As show in Figure 2.2.1 the dataset used by Roth (1978) was mainly based on samples collected during DSDP Legs.

The Upper Cretaceous was subdivided by Roth (1978) into 13 zones named following an alphanumerical notation (Nannofossils Cretaceous - NC#) and are predominantly based on first occurrences of marker taxa (Figure 2.2.2). Stage calibration was obtained using correlation to stratotype sections that, however, resulted to introduce uncertainties (as show in Figure 2.2.2 by the grey rectangles). According to Roth (1978) such uncertainties were related to problems in the occurrence and preservation of calcareous plankton in most Cretaceous stratotype sections, and for this reason, he introduces Oceanic Stages extending the work of Bukry (1973a) to the Cretaceous.

Each stratotype section for Oceanic Stages was defined in a specific hole drilled by DSDP and the boundaries were defined by biostratigraphic events. A correlation of the Oceanic Stages with the aim of achieving a chronostratigraphic framework for oceanic stratigraphy. The Oceanic Stages of Late Cretaceous age are:

- **Tenerifian (Cenomanian-Early Turonian):** includes nannofossil zones NC11, NC12. From FO of *Lithraphidites acutum* to FO of *Tetralithus pyramidus* (*Quadrum gartneri*). Ref. sections: DSDP Site 137; DSDP Site 258.
- **Naturalistian (Middle-Late Turonian):** includes nannofossil zones NC13, NC14. From FO of *Tetralithus pyramidus* (*Quadrum gartneri*) to FO of *Marthasterites furcatus*. Ref. section: DSDP Site 258.

- **Howlandian (Coniacian-Santonian):** includes nannofossil zones NC15, NC16, NC17. From FO of *Marthasterites furcatus* to FO of *Aspidolithus parcus*. Ref. sections: DSDP Site 137; DSDP Site 258.
- **Bermudan (Campanian-Maastrichtian):** includes nannofossil zones NC18, NC19, NC20, NC21, NC22, NC23. It extends from the FO of *Aspidolithus parcus* to the extinction of Cretaceous nannofossils. Ref. sections: DSDP Site 10.

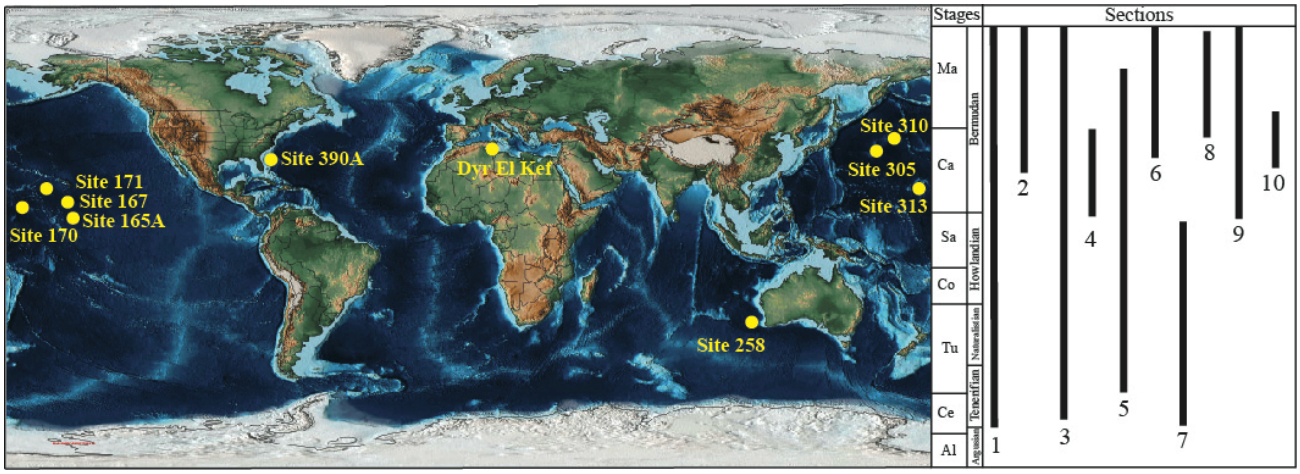

Figure 2.2.1 - Summary of the locations and stratigraphic intervals considered by Roth (1978). 1: Dyr El Kef (66 samples);2: DSDP Site 165 (17 samples);3: DSDP Site 167(48 samples);4: DSDP Site 170(17 samples); 5: DSDP Site 171(59 samples);6: DSDP Site 305 (no range charts);7: DSDP Site 258 (43 samples);8: DSDP Site 390 (12 samples);9: DSDP Site 310 no range charts;10: DSDP Site 313 no range charts.

The calcareous nannofossil zonation for the Upper Cretaceous presented by Roth (1978) is summarized in Figure 2.2.2. Each zone and subzone are discussed below reporting the oceanic stage and the corresponding chronostratigraphic age.

- **NC11- *Lithraphidites acutus* zone.** Definition: from the FO of *Lithraphidites acutus* to the LO of *Lithraphidites acutus*. Age assignment: Tenerifian (Cenomanian).
- **NC12- *Gartenrago obliquum* zone.** Definition: from the LO of *Lithraphidites acutus* to the FO of *Micula staurophora*/ *Tetralithus pyramidus*. Age assignment: Tenerifian (Early Turonian). Remarks: The lower part of this zone is characterized by the FO of *Gartnerago obliquum*.
- **NC13- *Micula staurophora* zone.** Definition: from the FO of *Micula staurophora* to the FO of *Kamptnerius magnificus*. Age assignment: Naturalistian (Turonian).
- **NC14- *Kamptnerius magnificus* zone.** Definition: from the FO *Kamptnerius magnificus* to the FO of *Marthasterites furcatus/Eiffellithus eximius*. Age assignment: Naturalistian (Late Turonian).
- **NC15- Martasterites furcatus zone.** Definition: from the FO Marthasterites furcatus/Eiffellithus

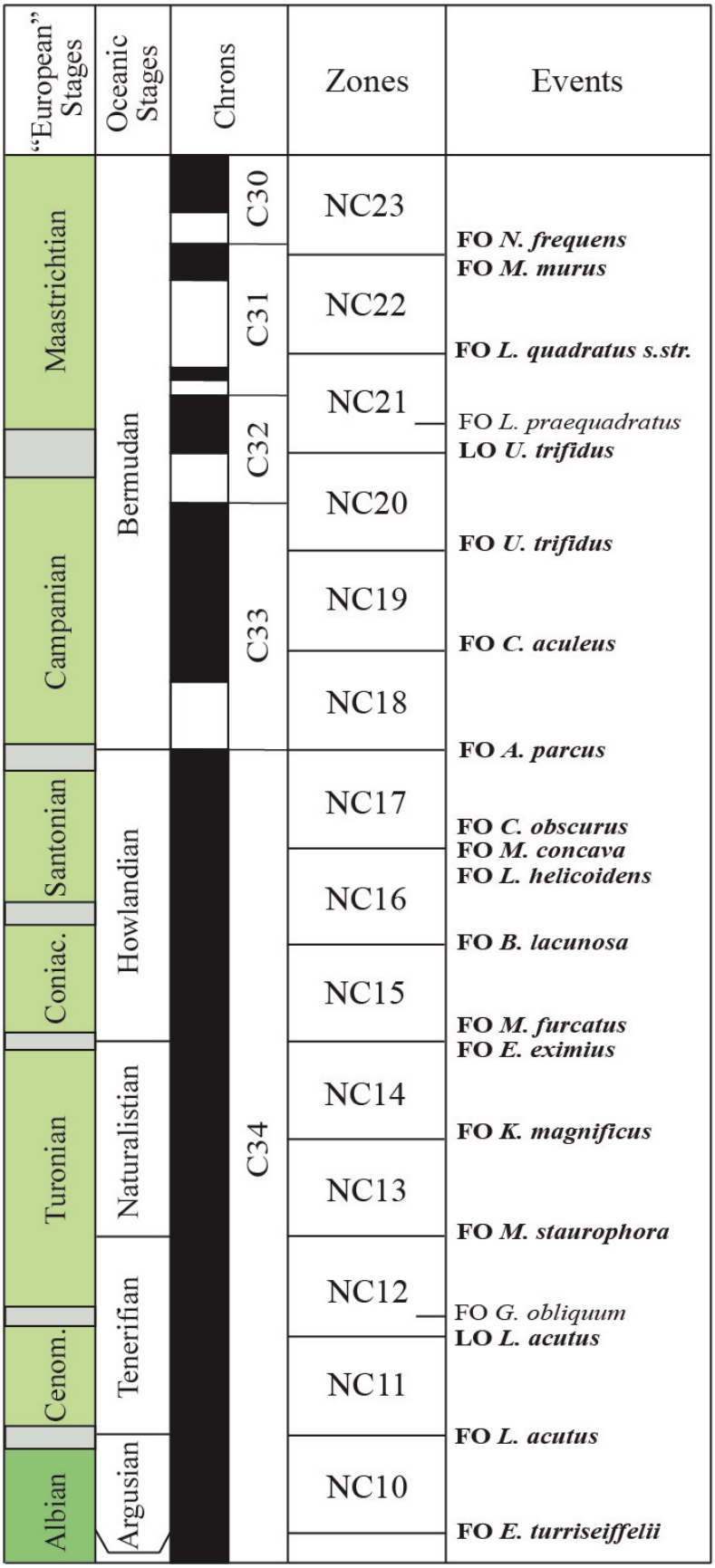

Figure 2.1.2 - Biozonation of Roth (1978). Zonal markers are indicated in bold. Nannofossil zones are arbitrarily given equal lengths/duration and, therefore, Stages are not in scale.

eximius to the FO of *Broinsonia lacunosa* (=*Aspidolithus parcus expansus)*. Age assignment: Howlandian (Turonian/Coniacian boundary interval).

- **NC16- *Broinsonia lacunosa* zone.** Definition: from the FO of *Broinsonia lacunosa* (= *Aspidolithus parcus expansus* to the FO of *Tetralithus obscurus/ Micula concava/ Lithraphidites helicoideus.* Age assignment: Howlandian (Coniacian)
- **NC17- *Tetralithus obscurus-Micula concava* zone.** Definition: from the FO *Tetralithus obscurus/ Micula concava/ Lithraphidites helicoidens* to the FO of *Aspidolithus parcus*. Age assignment: Howlandian (Santonian)
- **NC18- *Aspidolithus parcus* zone.** Definition: from the FO of *Aspidolithus parcus* to the FO of *Tetralithus aculeus*. Age assignment: Bermudan (Early Campanian).
- **NC19- *Tetralithus aculeus* zone.** Definition: from the FO of *Tetralithus aculeus* to the LO of *Uniplanarius trifidus*. Age assignment: Bermudan (Campanian).
- **NC20- *Tretralithus trifidus* zone.** Definition: from the FO *Tetralithus trifidus* (=*Uniplanarius trifidus*) to the LO of *Tetralithus trifidus*. Age assignment: Bermudan (late Campanian).
- **NC21- *Litraphidites praequadratus* zone.** Definition: from the LO *Tetralithus trifidus* to the FO of *Lithraphidites quadratus.* Age assignment: Bermudan (Campanian/Maastrichtian boundary interval). Remarks: The lower part of this zone is characterized by the FO of *Litraphidites praequadratus.*
- **NC21- *Litraphidites praequadratus* zone.** Definition: from the LO *Tetralithus trifidus* to the FO of *Lithraphidites quadratus.* Age assignment: Bermudan (Campanian/Maastrichtian boundary interval). Remarks: The lower part of this zone is characterized by the FO of *Litraphidites praequadratus.*
- **NC22- *Litraphidites quadratus* zone.** Definition: from the FO *Lithraphidites quadratus* to the FO of *Nephrolithus frequens/Micula murus.* Age assignment: Bermudan (Maastrichtian).
- **NC23- *Micula murus* - *Neprolithus frequens* zone.** Definition: from the FO *Nephrolithus frequens/Micula murus* to the top of Maastrichtian. Age assignment: (Late Maastrichtian).

2.3 The biozonation of Bralower et al. (1995).

Bralower et al. (1995) produced a calcareous nannofossil biostratigraphic scheme for the Cretaceous that originated from that of Roth (1978). The revision was based on a literature survey and a partial reinvestigation of various DSDP/ODP Sites and on-land sections.

The revision of Roth's zonation for the Upper Cretaceous includes data from Bralower (1988) and Bralower and Siessier (1992) (Figure 2.3.1). Additional nannofossil events were introduced with the aim of improving the biostratigraphic resolution. The new zones/ subzones were defined by Bralower et al. (1995) following the

alphanumerical notation of Roth (1978) coded with an asterisk (*) when one or both basal/top biohorizon was/were changed (NC#*).

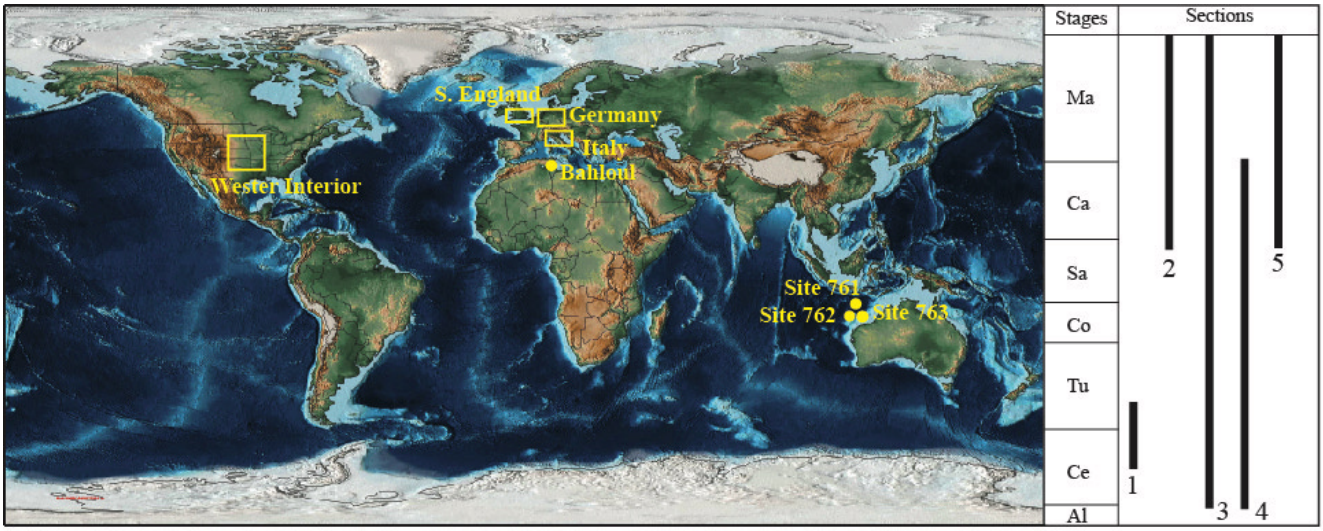

Figure 2.3.1 - Summary of the locations and stratigraphic intervals considered by Bralower et al. (1995). 1: Blue Point, Lohali Point, Rock Canyon, Riding Mountain, South Ferriby, Elsham, Shakespeare Cliff, Wunstorf, Hannover-Misburg, Sohlde, Danish Graben, Cismon, Bahloul; 2: ODP Site 761; 3:ODP Site 762 ;4: ODP Site 763; 5: Bottaccione (Monechi and Thierstein, 1985).

The calcareous nannofossil zonation was integrated with the planktonic foraminifera zonation of Sliter (1989, 1992) (Figure 2.3.2).

A correlation between the microfossil biostratigraphy and the geomagnetic polarity timescale was presented by Bralower et al. (1995) as reported in Figure 2.3.2. This correlation was based on the investigation of the Gubbio sequence (Alvarez et al. 1977; Monechi and Thierstein, 1985; Premoli Silva and Sliter, 1995), South Atlantic (Poor et al, 1983; Tauxe et al. 1983; Boersma, 1984; Manivit, 1984; Chave, 1984; Stradner and Steinmetz, 1984; Huber,1991) Southern Ocean (Huber, 1990; Pospichal and Wise, 1990), Pacific (Monechi et al, 1985) and the eastern Indian Ocean (Galbrun, 1992; Bralower and Sissier,1992).

Moreover, the calcareous nannofossil zonation was calibrated by Bralower et al. (1995) with radiometric ages of Obradovich (1993) who applied $^{40}Ar/^{39}Ar$ dating to bentonite layers interbedded in calcareous plankton and ammonite- dated sections of the Western Interior Basin. According to Bralower et al. (1995) the analyses of the nannofossil content of most succession used by Obradovich (1993) for the stage designation, and age determination allowed to solve a correlations problem between Western Interior stratigraphy, mainly based on macrofossil zones, and European stage boundaries.

The calcareous nannofossil zones and subzones for the Upper Cretaceous are summarized in Figure 2.3.2 and discussed below reporting the age assignments and the correlation with planktonic foraminiferal

biozones (Sliter, 1989,1992).

- **NC10 – *Eiffellithus turriseiffelii* zone (Roth, 1978).** Definition: from the FO of ***Eiffellithus*** *turriseiffelii* to the FO of ***Lithraphidites acutus***. Age assignment: Late Albian – Cenomanian; planktonic foraminiferal zone top *R. appenninica-R. brotzeni* Zone. This zone was subdivided in two subzones:

  NC10a subzone. Definition: from the FO of ***Eiffellithus*** *turriseiffelii* to the FO of *Corollithion kennedyi.* Age: basal Cenomanian.

  NC10b subzone. Definition: from the FO of *Corollithion kennedyi* to the FO of *Lithraphidites acutus.*
- **NC11- *Lithraphidites acutus* zone (Bralower et al. 1995).** Definition: from the FO of *Lithraphidites acutus* to the LO of *Axopodorhabdus albianus*. Age assignment: Cenomanian; top of *R. reicheli-R. cushmani* planktonic foraminiferal Zone. Remarks: This zone is characterized by the FO of *Ahmuellerella octoradiata* and the LO of *Corollithion kennedyi.*
- **NC12*- *Rhagodiscus asper* zone (Bralower et al. 1995).** Definition: from the LO of *Axopodorhabdus albianus* to the LO *Rhagodiscus asper*. Age assignment: Early Turonian; *W. archeocretacea* planktonic foraminiferal Zone. This zone was subdivided into two subzones:

  NC12a subzone. Definition: from the LO of *Axopodorhabdus albianus* to the LO of *Helenea chiastia*.

  NC12b subzone. Definition: from the LO of *Helenea chiastia* to the LO of *Rhagodiscus asper.*
- **NC13*- *Eprolithus floralis* zone (Bralower et al. 1995).** Definition: from the FO of *Lithraphidites acutus* to the LO of *Axopodorhabdus albianus*. Age assignment: Turonian; *H. helvetica* planktonic foraminiferal Zone.
- **NC14- *Kamptnerius magnificus* zone (Roth, 1978).** Definition: from the FO of *Kamptnerius magnificus* to the FO of *Marthasterites furcatus*. Age assignment: Late Turonian; *M. sigali* planktonic foraminiferal Zone.
- **NC15- *Marthasterites furcatus* zone (Roth, 1978).** Definition: from the FO *Marthasterites furcatus* to the FO of *Micula staurophora*. Age assignment: Coniacian; *M. sigali – D. concavata* planktonic foraminiferal Zones.
- **NC16*-*Micula decussata* zone (Bralower et al. 1995).** Definition: from the FO of *Micula staurophora* to the FO of *Lucianorhabdus cayeuxii*. Age assignment: latest Coniacian- Early Santonian; *D. concavata-D. asymetrica* planktonic foraminiferal Zones.
- **NC17*- *Lucianorhabdus cayeuxii* zone (Bralower et al. 1995).** Definition: from the FO *Lucianorhabdus cayeuxii* to the FO of *Aspidolithus parcus*. Age assignment: Late Santonian; *D. asymetrica* planktonic foraminiferal Zone.

- **NC18- *Aspidolithus parcus* zone (Roth, 1978).** Definition: from the FO *Aspidolithus parcus* to the FO of *Ceratolithoides aculeus*. Age assignment: Early Campanian; *G. elevata-G. verticosa* planktonic foraminiferal Zones. This zone was subdivided by Bralower et al. (1995) into two subzones:

  NC18a* subzone. Definition: from the FO *Aspidolithus parcus* to the LO of *Lithastrinus grillii.*

  NC18b* subzone. Definition: from the LO of *Lithastrinus grillii* to the FO of *Ceratolithoides aculeus*.

- **NC19 - *Tetralithus aculeus* zone (Roth, 1978).** Definition: from the FO of *Ceratolithoides aculeus* to the FO of *Uniplanarius trifidus*. Age assignment: Campanian; *G. verticosa* planktonic foraminiferal Zone. This zone was subdivided by Bralower et al. (1995) into two subzones:

  NC19a* subzone. Definition: from the FO of *Ceratolithoides aculeus* to the FO of *Uniplanarius gothicus.*

  NC19b* subzone. Definition: from the FO of *Uniplanarius gothicus* to the FO *Uniplanarius trifidus.*

- **NC20-*Tretralithus trifidus* zone (Roth, 1978).** Definition: from the FO *Uniplanarius trifidus* to the LO of *Uniplanarius trifidus*. Age assignment: latest Campanian- Early Maastrichtian; this calcareous nannofossil zone corresponds to four planktonic foraminiferal zones *G. calcarata*, *G. havanaensis*, *G. aegyptica, G. gansseri*.

- **NC21-*Litraphidites praequadratus* zone (Roth, 1978).** Definition: from the LO of *Uniplanarius trifidus* to the FO of *Lithraphidites quadratus*. Age assignment: Early Maastrichtian; *G. gansseri - A. mayoroensis* planktonic foraminiferal Zones.This Zone was subdivided by Bralower et al. (1995) into two subzones:

NC21a* subzone. Definition: from the LO of *Uniplanarius trifidus* to the LO of *Reinhardites levis*

  NC21b* subzone. Definition: from the LO of *Reinhardites levis* to the FO of *Lithraphidites quadratus*.

- **NC22-*Litraphidites quadratus* zone (Roth, 1978).** Definition: from the FO *Lithraphidites quadratus* to the FO of *M. murus.* Age assignment: Late Maastrichtian; *A. mayaroensis* planktonic foraminiferal Zone.

- **NC23-*Micula murus* zone (Roth, 1978).** Definition: from the FO of *Micula murus* to the top of Maastrichtian. Age assignment: Late Maastrichtian; *A. mayaroensis* planktonic foraminiferal Zone.

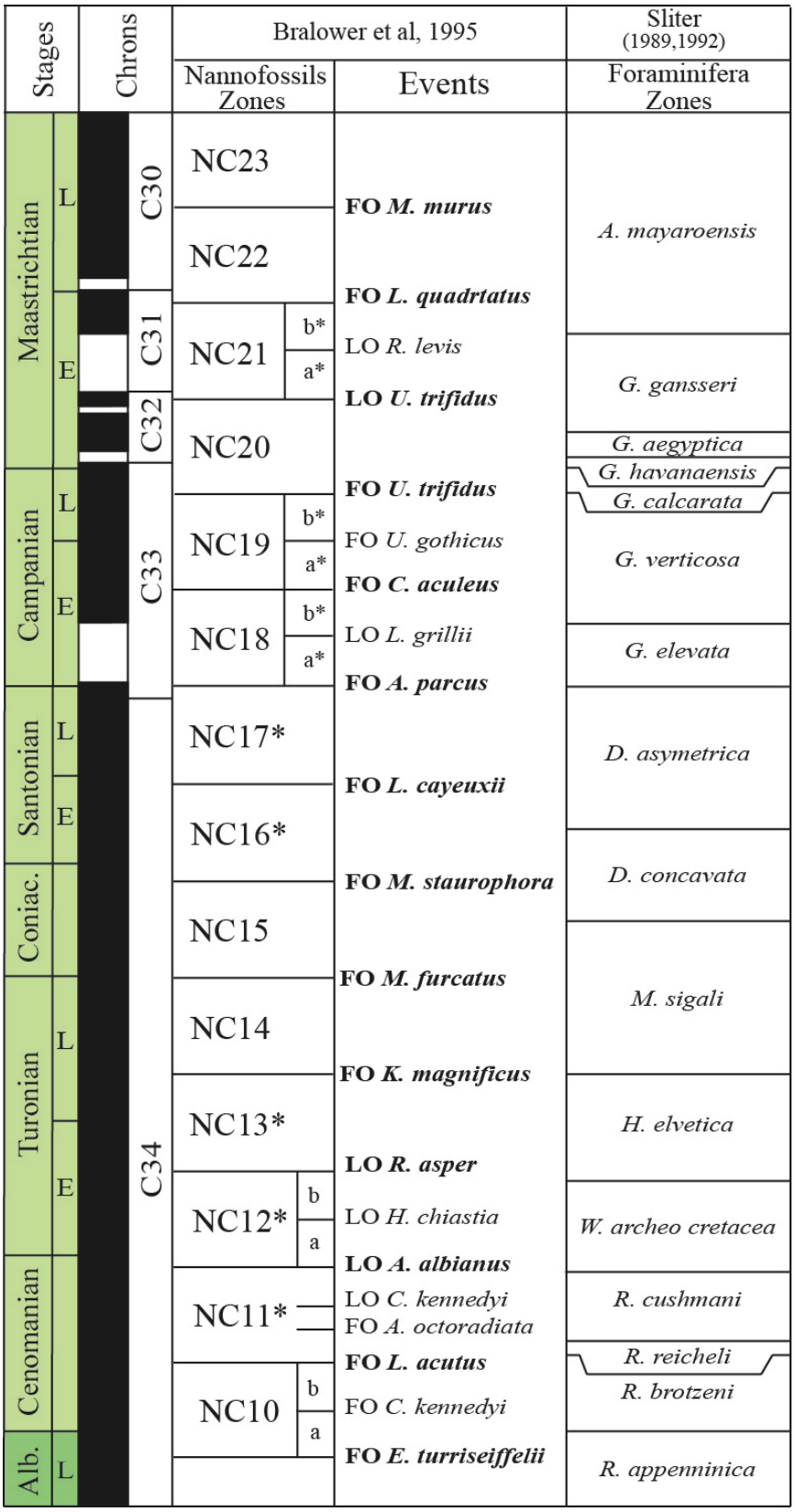

Figure 2.3.2 - Biozonation of Bralower et al. (1995). Zonal markers are indicated in bold. Nannofossil zones are arbitrarily given equal lengths/duration and, therefore, Stages are not in scale. Foraminifera zonations after Sliter (1989,1992).

2.4 The biozonation of Burnett (1998).

The calcareous nannofossil zonation presented by Burnett (1998) results from an integration of literature data with new events identified and calibrated at different paleolatitudes and biogeographic provinces from both oceanic and shelf paleoenvironment. The zonation includes data from different areas (Figure 2.4.1): Europe (Belgium, Bulgaria, Czech Republic, Denmark, England, France, Germany, The Netherlands, North Sea, Poland), Russia, South Africa, USA, Australia, Pakistan, Indian, Atlantic and Pacific oceans (Burnett, 1988; Burnett et al., 1992a, b; Kennedy et al., 1992; Gale et al., 1996; Burnett and Whitham, 1999; Lees, 2002 and unpublished data). The tethyan-intermediate (TP) zonation

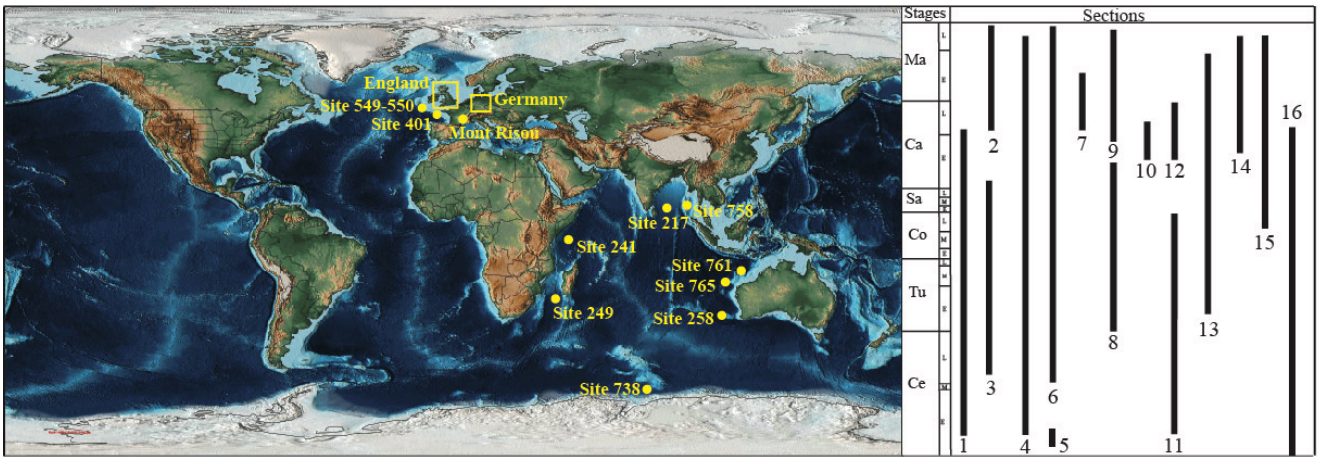

Figure 2.4.1 - Summary of the locations and stratigraphic intervals considered by Burnett, 1998. 1: Trunch Borehole (88 samples); 2: DSDP Site 401 (9 samples);3: Kent (59 samples);4: DSDP Site 549 (38 samples);5: Mont Risou (40 samples); 6: DSDP Site 550 (130 samples); 7: Lagerdorf and Kronsmoor (38 samples); 8: NE England (72 samples);9DSDP Site 217 (71 samples); 10: DSDP Site 258 (50 samples);11: DSDP Site 258 (50 samples);12: DSDP Site 249 (41 samples); 13:ODP Site 738C (39 samples);14: ODP Site 758 (61 samples);15: ODP Site 761 (34 samples):16 ODP Site 765 (21 samples).

originate in most part from the previous works of Sissingh (1977) and Perch-Nielsen (1985). The biozonation adopted an alphanumerical notation (Upper Cretaceous - UC#) and are based on first and last occurrences of selected species. Nannofossil events were calibrated with macrofossil events in Europe and United States, and with stage-boundary events (Burnett, 1996). Burnett (1998) produced three different zonations according to three different regions: Tethyan-intermediate (TP); Austral (AP); Boreal (BP). Whereas the biozones can be correlated globally the subzones can differ between provinces. Calcareous nannofossil zones and subzones for the Upper Cretaceous are summarized in Figure 2.4.2 and discussed below reporting the age assignment and the correlation with macrofossil bizonations (MFZ) (Burnett, 1998).

Calcareous nannofossil zones and subzones for the Upper Cretaceous are summarized in Figure 2.4.2 and discussed below reporting the age assignment and the correlation with macrofossil bizonations (MFZ) (Burnett, 1998).

- **UC0 zone (Burnett, 1998).** Definition: from the FO *Eiffellithus turriseiffelii* to the FO of *Corollithion kennedyi.* Age assignment: Late Albian to Early Cenomanian; macrofossil zone: inflatum to mantelli MFZ (macrofossil zone), carcitanense MFsZ (macrofossil subzone). Remarks: This zone is equivalent to the BC27 zone of Bown et al. (1998) and is subdivided into three subzones.

  UC0a subzone. Definition: from the FO *Eiffellithus turriseiffelii* to the LO of *Hayesites albiensis*.

  UC0b subzone. Definition: from the LO *Hayesites albiensis* to the FO of *Calculites anfranctus.*

  UC0c subzone. Definition: from the FO *Calculites anfranctus* to the FO of *Corollithion kennedyi*.
- **UC1 zone (Burnett, 1998).** Definition: from the FO *Corollithion kennedyi* to the FO of *Gartnerago segmentatum*. Age assignment: Early Cenomanian; macrofossil zone: mantelli MFZ, carcitanense MFsZ to basal dixoni MFZ. This zone was subdivided into four subzones:

  UC1a subzone. Definition: from the FO of *Corollithion kennedyi* to the LO of *Watznaueria britannica.*

  UC1b subzone. Definition: from the LO *Watznaueria britannica* to the LO of *Gartnerago chiasta.*

  UC1c subzone. Definition: from the LO *Gartnerago chiasta* to the FO of *Helicolithus anceps*.

  UC1d subzone. Definition: from the FO *Helicolithus anceps* to the FO of of *Gartnerago segmentatum.*
- **UC2 zone (Burnett, 1998).** Definition: from the FO of *Gartnerago segmentatum* to the FO of *Lithraphidites acutus*. Age assignment: Early to Middle Cenomanian; macrofossil zone: basal dixoni MFZ to basal rhotomagense MFZ. This zone was subdivided into three subzones:

  UC2a subzone. Definition: from the FO of *Gartnerago segmentatum* to the FO of *Zeugrhabdotus xenotus.*

  UC2b subzone. Definition: from the FO *Zeugrhabdotus xenotus* to the FO of *Cylindralithus sculptus.*

  UC2c subzone. Definition: from the FO *Cylindralithus sculptus* to the FO of *Lithraphidites acutus*.
- **UC3 zone (Burnett, 1998).** Definition: from the FO of *Lithraphidites acutus* to the FO of *Cylindralithus biarcus.* Age assignment: Middle to Late Cenomanian; macrofossil zone: basal rhotomagense MFZ to geslinianum MFZ. This zone was subdivided into five subzones:

  UC3a subzone. Definition: from the FO of *Lithraphidites acutus* to the LO of *Gartnerago theta.*

  UC3b subzone. Definition: from the LO *Gartnerago theta* to the LO of *Staurolithites gausorhethium.*

  UC3c subzone. Definition: from the LO *Staurolithites gausorhethium* to the LO of *Gartnerago nanum.*

  UC3d subzone. Definition: from the LO *Gartnerago nanum* to the LO of *Corollithion kennedyi.*

  UC3e subzone. Definition: from the LO of *Corollithion kennedyi* to the FO of *Cylindralithus biarcus.*

- **UC4 zone (Burnett, 1998).** Definition: from the FO *Cylindralithus biarcus* to the LO of *Lithraphidites acutus.* Age assignment: Late Cenomanian; macrofossil zone: geslinianum MFZ. This zone was subdivided into two subzones:

  UC4a subzone. Definition: from the FO of *Cylindralithus biarcus* to the LO of *Cretarhabdus striatus.*

  UC4b subzone. Definition: from the LO *Cretarhabdus striatus* to the LO of *Lithraphidites acutus.*

  UC5 zone (Burnett, 1998). Definition: from the LO *Lithraphidites acutus* to the LO of *Helenea chiastia*. Age assignment: Late Cenomanian to Early Turonian; macrofossil zone: geslinianum MFZ to devonense MFZ. This zone was subdivided into three subzones:

  UC5a subzone. Definition: from the FO of *Lithraphidites acutus* to the LO of *Axopodorhabdus albianus.*

  UC5b subzone. Definition: from the LO *Axopodorhabdus albianus* to the FO of *Quadrum intermedium* (5 elements). Remarks: The LO of *R. asper* and the FO of *Q. intermedium* with 6 and 7 elements in each cycle, occur in this subzone.

  UC5c subzone. Definition: from the FO of *Quadrum intermedium* (5 elements) to the LO of *Helenea chiastia*. Remarks: *Cylindralithus coronatus* and *Eprolithus octopetalus* have their FOs in this subzone.

- **UC6 zone (Burnett, 1998).** Definition: from the LO *Helenea chiastia* to the FO of *Quadrum gartneri*. Age assignment: Early Turonian; macrofossil zone: devonense and labiatus MFZs. This zone is equivalent to the subzone CC10b of Perch-Nielsen (1985) and was subdivided into two subzones:

  UC6a subzone. Definition: from the LO of *Helenea chiastia* to the FO of *Eprolithus moratus.*

  UC6b subzone. Definition: from the FO *Eprolithus moratus* to the FO of *Quadrum gartneri.*

- **UC7 zone (Burnett, 1998).** Definition: from the FO of *Quadrum gartneri* to the FO of *Eiffellithus eximius*. Age assignment: Early Turonian; macrofossil zone: labiatus MFZ. Remnarks: This zone is equivalent to zone CC11 of Perch-Nielsen (1979a).

- **UC8 zone (Burnett, 1998).** Definition: from the FO of *Eiffellithus eximius* to the FO of *Lithastrinus septenarius*. Age assignment: Early to Middle Turonian; macrofossil zone: Iabiatus MFZ to lata MFZ. This zone can be subdivided into two subzones:

  UC8a Subzone. Definition: from the FO of *Eiffellithus eximius* to the FO of *Lucianorhabdus quadrifidus*.

  UC8b Subzone. Definition: from the FO of *Lucianorhabdus quadrifidus* to the FO of *Lithastrinus septenarius*. In the Austral province, this zone can be subdivided using the more abundant species of *T. ecclesiastica* as follows:

  UC8a^{AP} Subzone. Definition: from the FO of *Eiffellithus eximius* to the FO of *Thiersteinia*

ecclesiastica.

UC8b^{AP} Subzone. Definition: from the FO of *Thiersteinia ecclesiastica* to the FO of *Lithastrinus septenarius*.

- **UC9 zone (Burnett, 1998).** Definition: from the FO of *Lithastrinus septenarius* to the FO of *Micula stauraphora*. Age assignment: Middle Turonian to Early or Middle Coniacian; macrofossil zone: lata MFZ to cortestudinarium MFZ. Remarks: This zone is equivalent to subzone CC13b of Perch-Nielsen (l985a) and can be subdivided into three subzones.

  UC9a subzone. Definition: from the FO of *Lithastrinus septenarius* to the FO of *Zeugrhabdotus biperforatus*

  UC9b subzone. *Definition:* from the FO of *Zeugrhabdotus biperforatus* to the FO of *Aspidolithus parcus expansus*.

  UC9c Subzone. Definition: from the FO of *Aspidolithus parcus expansus* to the FO of *Micula staurophora*.

  In the Austral province, the FO of *Zeugrhabdotus kerguelenensis* allows the identification of two AP subzones as follows:

  UC9a^{AP} subzone. Definition: from the FO of *Lithastrinus septenarius* to the FO of *Zeugrhabdotus kerguelenensis*.

  UC9b^{AP} subzone. Definition: from the FO of *Zeugrhabdotus kerguelenensi*s to the FO of *Micula staurophora*.

- **UC10 zone (Burnett, 1998).** Definition: from the FO of *Micula staurophora* to the FO of *Lithastrinus grillii*. Age assignment: Middle? to Late Coniacian; macrofossil zone: cortestudinarium MFZ to coranguinum MFZ. In the Austral province, this zone can be subdivided into two subzones as follows:

  UCl0a ^{AP} subzone. Definition: from the FO of *Micula staurophora* to the LO of *Zeugrhabdotus kerguelenensis*.

  UCl0b ^{AP} subzone. Definition: from the LO of *Zeugrhabdotus kerguelenensis* to the LO of *Quadrum gartneri*.

- **UC11 zone (Burnett, 1998).** Definition: from the FO of *Lithastrinus grillii* to the LO of *Lithastrinus septenarius*. Age assignment: Late Coniacian to Early? Santonian; macrofossil zone:
  coranguinum MFZ to coranguinum MFZ.

  UC11a subzone. Definition: from the FO of *Lithastrinus grillii* to the LO of *Quadrum gartneri*.

  UC11b subzone. Definition: from the LO of *Quadrum gartneri* to the FO of *Lucianorhabdus cayeuxii*.

UC11c subzone. Definition: from the FO of *Lucianorhabdus cayeuxii* to the LO of *Lithastrinus septenarius*.

- **UC12 zone (Burnett, 1998).** Definition: from the LO of *Lithastrinus septenarius* to the FO of *Arkhangelskiella cymbiformis*. Age assignment: Early Santonian to Early Campanian; macrofossil zone: uppermost coranguinum MFZ to granulataquadrata or pilula MFZ.
- **UCl3 zone (Burnett, 1998).** Definition: from the FO of *Arkhangelskiella cymbiformis* to the FO of *Aspidolithus parcus parcus*. Age assignment: Early Campanian; macrofossil zone: granulataquadrata or pilula MFZ to lingua/quadrata or pilula MFZ. In the Boreal province, this zone can be subdivided into two subzones as follows:

  UCl3a^{BP} subzone. Definition: from the FO of *Arkhangelskiella cymbiformis* to the consistent FO of *Orastrum campanensis*.

  UC13b^{BPs}ubzone. Definition: from the FO of consistent *Orastrum campanensis* to the FO of *Aspidolithus parcus parcus.*
- **UC14 zone (Burnett, 1998).** Definition: from the FO of *Aspidolithus parcus parcus* to the FO of *Misceomarginatus pleniporus*. Age assignment: Early to late Early Campanian; macrofossil zone: lingua/quadrata or piluIa MFZ to pilula/ senonensis or quadrata MFZ. This zone can be subdivided in subzones according to paleoceanographic province as follows:

  UC14a subzone. Definition: from the FO of *Aspidolithus parcus parcus* to the FO of *Aspidolithus parcus constrictus*.

  UC14b ^{BP} subzone. Definition. from the FO of *Aspidolithus parcus constrictus* to the FO of *Misceomarginatus pleniporus*. Remarks: the LO of *E. floralis* is observed in this subzone at intermediate and Austral locations.

  UC14b^{TP} subzone. Definition: from the FO of *Aspidolithus parcus constrictus* to the FO of *Bukryaster hayi*.

  UC14c^{TP} subzone. Definition: from the FO of *Bukryaster hayi* to the FO of *Ceratolithoides verbeekii*. Remarks: equivalent to subzone CC18b of Perch-Nielsen (1985).

  UC14d^{TP} subzone. Definition: from the FO of *Ceratolithoides verbeekii* to the FO of *Misceomarginatus pleniporus*.
- **UC15 zone (Burnett, 1998).** Definition: from the FO of *Misceomarginatus pleniporus* to the LO *of Eiffellithus eximius*. Age assignment: late Early to Late Campanian; macrofossil zone: pilula/senonensis or? quadrata MFZ to the grimmensis/ granulosus or mucronata MFZ. This zone can be subdivided into subzones according to paleoceanographic province as follows:

UC15a^{BP} subzone. Definition: from the FO of *Misceomarginatus pleniporus* to the LO of *Cylindralithus biarcus*.

UC15b^{BP} subzone. Definition: from the LO of *Cylindralithus biarcus* to the FO of *Heteromarginatus bugensis*.

UC15c^{BP} subzone. Definition: from the FO of *Heteromarginatus bugensis* to the FO of *Prediscosphaera stoveri*.

UC15d^{BP} subzone. Definition: from the FO of *Prediscosphaera stoveri* to the LO of *Orastrum campanensis*.

UC15e^{BP} subzone. Definition: from the LO of *Orastrum campanensis* to the LO of *Eiffellithus eximius*.

UC15a^{TP} subzone. Definition: from the FO of *Misceomarginatus pleniporus* to the FO of *Ceratolithoides aculeus*.

UC15b^{TP} subzone. Definition: from the FO of *Ceratolithoides aculeus* to the FO of *Uniplanarius sissinghii*. Remarks: this subzone is equivalent to the zone CC20 of Sissingh (1977).

UC15c^{TP} subzone. Definition: from the FO of *Uniplanarius sissinghii* to the FO of *Uniplanarius trifidus*. This subzone corresponds to the zone CC21 of Sissingh (1977).

UC15d^{TP} subzone. Definition: from the FO of *Uniplanarius trifidus* to the FO of *Eiffellithus parallelus*.

UCl5e^{TP} subzone. Definition: from the FO of *Eiffellithus parallelus* to the LO of *Eiffellithus eximius*.

UCl5a^{AP} subzone. Definition: from the FO of *Misceomarginatus pleniporus* to the LO of *Biscutum dissimilis*.

UCl5b^{AP} subzone. Definition: from the LO of *Biscutum dissimilis* to the LO of *Eiffellithus eximius*.

- **UCl6 zone (Burnett, 1998).** Definition: from the LO of *Eiffellithus eximius* to the LO of *Aspidolithus parcus constrictus*. Age assignment: Late Campanian; macrofossil zone: grimmensis/ granulosus or mucronata MFZ to lanceolata MFZ. This zone can be subdivided into four subzones only in the Boreal province as follows:

  UCl6a^{BP} subzone. Definition: from the LO of *Eiffellithus eximius* to the LO of *Heteromarginatus bugensis*.

  UCl6b^{BP} subzone. Definition: from the LO of *Heteromarginatus bugensis* to the LO of Tortolithus *caistorensis*.

  UCI6c^{BP} subzone. Definition: from the LO of *Tortolithus caistorensis* to the LO of *Monomarginatus quaternarius*.

UCI6d^{BP} subzone. Definition: from the LO of *Monomarginatus quaternarius* to the LO of *Aspidolithus parcus constrictus*.

- **UCl7 zone (Burnett, 1998).** Definition: from the LO of *Aspidolithus parcus constrictus* to the LO of *Tranolithus orionatus*. Age assignment: Late Campanian (Ianceolata MFZ) to late Early Maastrichtian; macrofossil zone: lanceolata MFZ to the sumensis MFZ or Brachiopod Zone 4. Remarks: This zone is equivalent to CC23b of Sissingh (1977).
- **UC18 zone (Burnett, 1998).** Definition: from the LO of *Tranolithus orionatus* to the LO of *Reinhardtites levis.* Age assignment: late Early Maastrichtian; macrofossil zone: sumensis MFZ or Brachiopod Zones 4 to 5). This zone is equivalent to zone CC24 of Sissingh (1977).

  UC18a^{AP} subzone. Definition: from the LO of *Tranolithus orionatus* to the LO of *Biscutum coronum*.

  UC18b ^{AP} subzone. Definition: from the LO of *Biscutum coronum* to the LO of *Reinhardtites levis*.
- **UC19 zone (Burnett, 1998).** Definition: from the LO of *Reinhardtites levis* to the FO of *Lithraphidites quadratus*. Age assignment: late Early to early Late Maastrichtian; macrofossil zone: sumensis MFZ or Brachiopod Zone 5 to the lower Upper Maategulatus/junior MFZ or Brachiopod Zone 8. This zone is equivalent to subzone CC25a of Perch-Nielsen (l985a).
- **UC20 zone (Burnett, 1998).** Definition: from the FO of *Lithraphidites quadratus* to the LO of unreworked, non-survivor Cretaceous taxa. Age assignment: Late Maastrichtian to the Cretaceous/Tertiary boundary; macrofossil zone: tegulatus/ junior MFZ or Brachiopod Zone 8. This zone can be subdivided into subzones according to paleoceanographic provinces as follows:

  UC20a^{BP} subzone. Definition: from the FO of *Lithraphidites quadratus* to the FO of *Nephrolithusfrequens*.

  UC20b^{BP} subzone. Definition: from the FO of *Nephrolithus frequens* to the FO of *Arkhangelskiella maastrichtiana*.

  UC20c^{BP} subzone. Definition: from the FO of *Arkhangelskiella maastrichtiana* to the FO of *Cribrosphaerella daniae*.

  UC20d^{BP} subzone. Definition: from the FO of *Cribrosphaerella daniae* to the LO of unreworked, non-survivor Cretaceous nannofossil taxa.

  UC20a^{TP} subzone. Definition: from the FO of *Lithraphidites quadratus* to the FO of *Micula murus*. This subzone is equivalent to subzone CC25b of Perch-Nielsen (1985a).

  UC20b^{TP} subzone. Definition: from the FO of *Micula murus* to the FO of *Ceratolithoides kamptneri*.

  UC20c ^{TP} subzone. Definition: from the FO of *Ceratolithoides kamptneri* to the FO of *Micula prinsii*.

  UC20d^{TP} subzone. Definition: rom the FO of *Micula prinsii* to the LO of unreworked, non-survivor

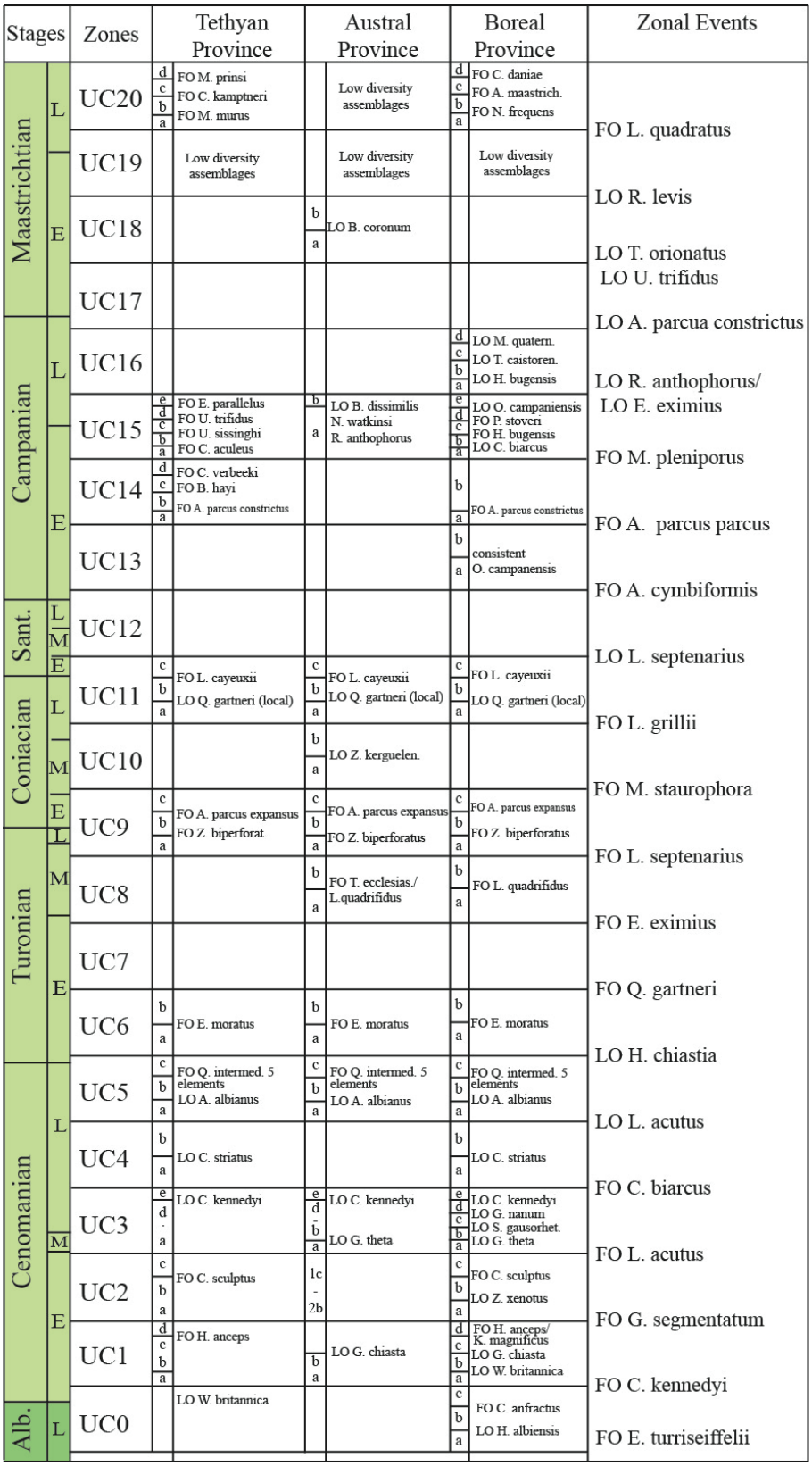

Figure 2.4.2 - Biozonation of Burnett (1998). Zonal markers are indicated in bold. Nannofossil zones are arbitrarily given equal lengths/duration and, therefore, stages are not in scale.

UC20d^{TP} subzone. Definition: rom the FO of *Micula prinsii* to the LO of unreworked, non-survivor Cretaceous nannofossil taxa.

2.5 Comparison between the four Upper Cretaceous nannofossil zonations.

The four examined biozonations for the Late Cretaceous (Sissingh, 1997; Roth, 1978; Bralower et al., 1995; Burnett, 1998) are compiled in Figure 2.5.1, and integrated with planktonic foraminiferal biozonations (modified after Coccioni and Premoli Silva, 2015 and Robaszynski and Caron, 1995), following the timescale and magnetic polarity of Gradstein et al. (2012).

The Burnett (1998) zonation shows the highest number of nannofossil events compared to the other schemes. She added numerous events observed in the North Sea area, reaching the highest biostratigraphic resolution for the Late Cretaceous. This is more evident in time intervals characterized by few nannofossil events. A total of five main events was recognized by Burnett (1998) in the Cenomanian compared to one event of Sissingh (1977) and two of Roth (1978) and Bralower et al. (1995). Similarly, in the Santonian and in the Early Maastrichtian, the number of events recognized is higher in Burnett (1998) biozonations compared to other ones. The biostratigraphic resolution achieved by Sissingh (1977) is similar to Burnett's (1998) one, but is higher in the Early-Middle Campanian and the Coniacian time intervals. Roth (1978) and Bralower et al. (1995) adopted less bioevents – but cosmopolitan and diagenesis-resistant - to define their zones and subzones compared to Sissingh (1977) and Burnett (1998). The resolution of the zonation of Roth (1978), revised by Bralower et al. (1995), remains lower except in the Cenomanian/Turonian boundary interval and in the Maastrichtian. In all the four zonations the Late Campanian still remains with a low resolution in terms of zones, although Burnett (1998) added numerous subzones in this interval. Integrating the four available zonations a total of 82 events can be used with nine bioevents present in all zonations (in red in Figure 2.5.1).events can be used with nine bioevents present in all zonations (in red in Figure 2.5.1).

These are:

- the FO of *E. turriseiffelii;*
- the FO of *L. acutus*;
- the FO of *A. parcus parcus*;
- the FO of *C. aculeus*;
- the FO of *U. trifidus*;
- the LO of *U. trifidus*;
- the FO of *L. quadratus*

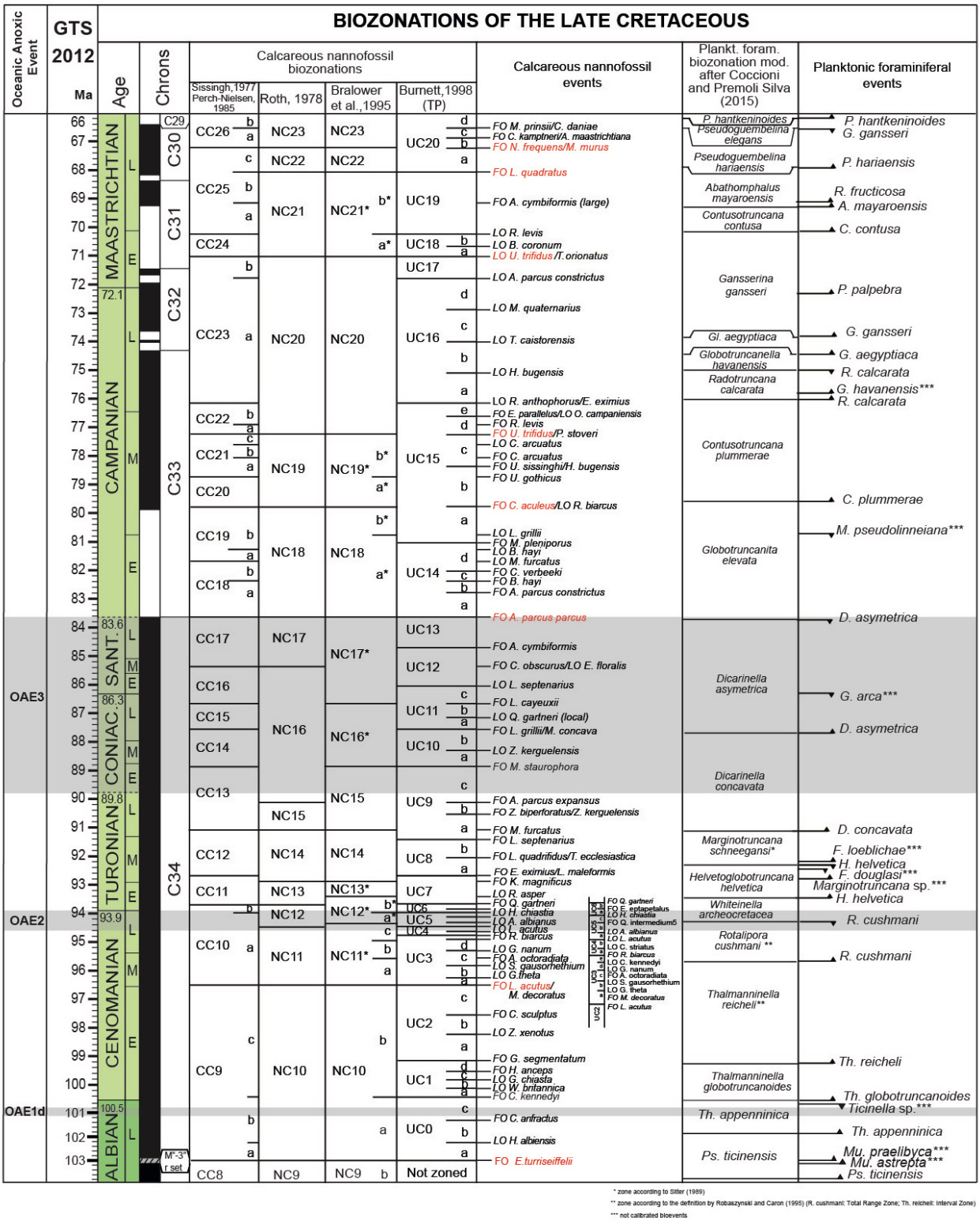

Figure 2.5.1 - Late Cretaceous integrated calcareous nannofossil, planktonic foraminiferal biozonations and magnetostratigraphy. Timescale and magnetostratigraphy are after Gradstein et al. (2012). Calcareous nannofossil biozonations by Sissingh (1977) as modified by Perch-Nielsen (1985), Roth (1978), Bralower et al., (1995) and Burnett (1998) are illustrated and nannofossil events adopted by all Authors are marked in red. Planktonic foraminiferal biozonation is modified after Coccioni and Premoli Silva (2015) and Robaszynski and Caron (1995). Late Cretaceous oceanic anoxic events (OAEs) are also plotted.

events can be used with nine bioevents present in all zonations (in red in Figure 2.5.1).These are:

- the FO of *E. turriseiffelii;*
- the FO of *L. acutus*;
- the FO of *A. parcus parcus*;
- the FO of *C. aculeus*;
- the FO of *U. trifidus*;
- the LO of *U. trifidus*;
- the FO of *L. quadratus*
- the FOs of *N. frequens* and *M. murus*.

Three zonations, Sissingh (1977), Bralower et al. (1995) and Burnett (1998) have in common five events. These are: the FO of *C. kennedy*; the LO of *H. chiasta*; the FO *M. furcatus*; the *M. staurophora*; the FO *L. cayeuxii*; the LO *R. levis*. The FO of *Q. gartenrii* is in common between the zonation of Sissingh (1977), Roth (1978) and Burnett (1998), whereas the FO of *M. furcatus* is and event used in the zonations of Sissingh (1977), Roth (1978) and Bralower et al. (1995).

Six events were adopted exclusively by Burnett (1998) as zonal marker (FO of *G. segmentatum*, FO of *R. biarcus*, FO of *L. septenarius*, LO of *L. septenarius*, FO of *A. cymbiformis*, FO of *M. pleniporus*), whereas two events (FO of *M. decoratus*, LO of *M. furcatus*) are used exclusively by Sissingh (1977), whereas only one (LO of *R. asper*) is included in the zonation of Bralower et al., (1995). The rest of zonal (markers) events can be correlated between at least two zonation.

Chapter 3
The Oceanic Anoxic Event 3.

The Mesozoic sedimentary successions are punctuated by several organic carbon-rich horizons that coincide with anomalies in the carbon isotope records (Jenkyns, 2010; Robinson et al., 2017). The early phase of the Deep Sea Drilling Project provided evidence of Cretaceous black shales from previously unsampled oceanic basins. As on-land, the recovered pelagic successions showed that organic carbon-rich lithologies are confined to specific geologically short intervals (0.5 to 2 million years) suggesting a global to regional oxygen-depletion of bottom waters.

The term "Oceanic Anoxic Event" (OAE) was coined by Schlanger and Jenkyns (1976) after the recovery of mid-Cretaceous black shales at sites drilled in the Pacific Ocean. Such lithologic units were recognized as equivalent and coeval of well-known lithostratigraphic markers previously described in the Tethys and Atlantic Oceans. The term OAE was originally defined to signify time intervals during which black shale deposition was prevalent at a global scale. The original definition was, therefore, based on lithologic criteria and applied to two time intervals, namely the Aptian-Albian (OAE1) and the Cenomanian–Turonian (OAE2). Later investigations on land and in the oceans pointed out the occurrence of the Coniacian–Santonian OAE3 (Arthur and Schlanger, 1979; Jenkyns, 1980) and of the Toarcian OAE (Jenkyns, 1985, 1988). Based on integrated and higher resolution stratigraphy of the sedimentary record of organic-rich black shales, Arthur et al. (1990) subdivided OAE1 into discrete events OAE1a, OAE1b, OAE1c and OAE1d, still using the sedimentary record of organic C-rich black shales.

Despite the original definition of OAEs (Schlanger and Jenkyns,1976) was based on lithostratigraphic criterion, the development of C and O stable isotopic chemostratigraphy led the $\delta^{13}C$ record to become one of the most important tool for identifying, correlating and characterizing OAEs (e.g., Erba, 2004; Weissert and Erba, 2004; Jenkyns, 2010; Robinson et al., 2017; Erba et al., 2019). In fact, all OAEs are associated with anomalies (positive and/or negative shifts) of $\delta^{13}C$ record measured on carbonates and organic matter, both in marine and terrestrial sections, interpreted as the result of perturbations of the global carbon cycle (Jenkyns, 2010). Actually, high-resolution stratigraphy of Cretaceous OAEs has revealed that black shale intervals are diachronous in many cases, with anoxic conditions rarely reached, whereas also fully oxic continental and shallow marine successions record the global carbon cycle anomalies (Robinson et al., 2017; Erba et al., 2019).

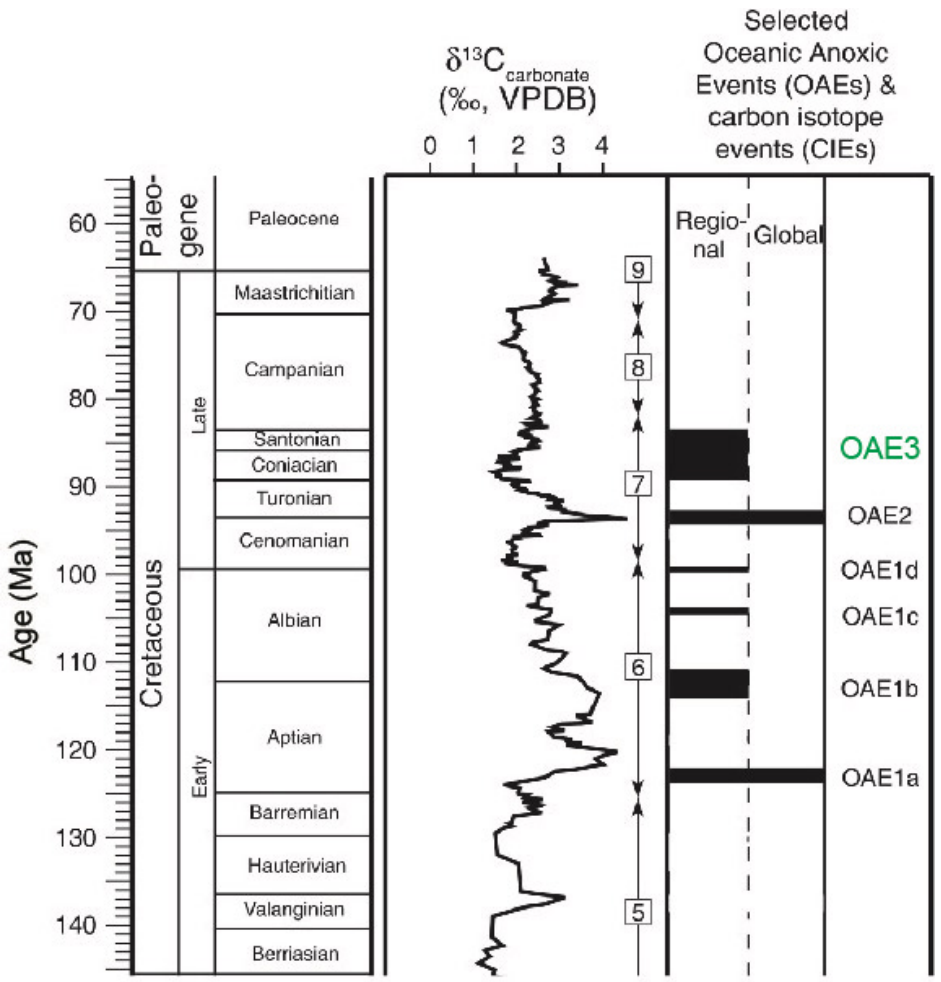

Figure 3.1 - Bulk carbonate carbon isotope ($\delta^{13}C_{carb}$) stratigraphy of the Cretaceous (modified after Robinson et al. 2017). The stratigraphic position of OAE1; OAE2 and OAE3 (green) are reported with black bands. Carbon-isotope data from: (5) Weissert et al. (1998); (6) Erbacher et al. (1996); (7) Jenkyns et al. (1994); (8) Jarvis et al. (2002); and (9) Abramovich et al. (2003).

The OAEs were generally associated with warm climate responsible for accelerated weathering and continental run-off, ocean stratification and local upwelling. All these processes concurred to an increase in the nutrient input to marine ecosystems (Jenkyns, 1999; Erba, 2004; Bottini et al., 2015). Furthermore, fertilization may have been increased by submarine volcanic activity and changes in ocean circulation (Larson and Erba, 1999; Erba, 2004; Parente et al., 2008; Erba et al., 2015). Thus, enhanced primary productivity together with expanded of the oxygen minimum zone (OMZ) led to the deposition and preservation of a large amount of organic matter (Robinson et al., 2017). A debate persists for disentangling the process most relevant in the accumulation of organic matter in pelagic settings. Specifically, available data suggest two contrasting models: a) enhanced preservation due to the oxygen depletion, b) increased primary productivity promoting higher fluxes of organic matter through the water column and consequent expansion of the OMZ reaching the seafloor (Arthur et al. 1990; Jenkyns, 2010).

Together with sedimentological and geochemical evidence, an important constrain to the paleoceanographic interpretations was also given by studies of the biogenic components of pelagic sediments. Due to the role of the biological pump (photosynthesis) and biomineralization, the increase in abundance and/or crises of phytoplankton affects the inorganic and organic carbon cycle and adsorption of CO_2 in the oceans (Erba, 2004). Among them, calcareous nannoplankton (coccolithophore algae) have a wide geographical and latitudinal distribution and represent a proxy for paleoceanographic reconstruction as their proliferation/crisis is affected by changes in ocean temperature, fertility, salinity, chemistry and CO_2. Therefore, fossil coccoliths and nannoliths can be used to trace ecological affinities and adaptation to paleoceanographic perturbations (Erba, 2004).

The individual OAEs differs in the magnitude of the $\delta^{13}C$ excursion, in the mechanism operating during the events, as well as the global or regional distribution of black shales. As for the Cretaceous is concerned, the Early Aptian OAE1a and latest Cenomanian OAE 2 have a global distribution and are associated with large $\delta^{13}C$ excursion, interpreted as a consequence of burial of organic matter during episodes of enhanced productivity. The decrease in the $^{87}Sr/^{86}Sr$ record reveals that both these OAEs occurred during periods of construction of submarine large igneous provinces (LIPs) and specifically the Ontong Java and Caribbean Plateaus, that presumably induced increased atmospheric CO_2 and a climate change to greenhouse conditions (Erba 1994, 2004; Larson and Erba, 1999; Jenkyns, 2003, 2010; Erba et al., 2015).

The OAE3 represents the last OAE of the Cretaceous and has been identified based on black shales of varying age and duration occurred during the Coniacian-Santonian time interval. Unlike OAE 1a and OAE 2, organic carbon-rich sediments are mainly restricted to the Equatorial Atlantic Ocean and adjacent basins, whereas most of the oceanic basins experienced fully oxic conditions during that period (Arthur and Fisher, 1977; Leckie et al., 2002; Wang et al., 2011).

3.1 The Oceanic Anoxic Event 3

The OAE3 was identified on the basis of black shale deposits of different age and duration occurred during the Coniacian-Santonian time interval. It was recognized for the first time by Arthur and Schlanger (1979). The features that differentiate the OAE3 from OAE1 and OAE2 comprise: a) the variable geographical and temporal distribution of organic-rich sediments; b) its long and not constrained duration; and 3) the absence of a main $\delta^{13}C$ isotopic excursion. Moreover, unlike other OAEs, OAE3 correlates with a cooling phase from the mid-Cretaceous super greenhouse to the Paleogene onset of icehouse conditions.

The Coniacian-Santonian also represents a time interval of widespread deposition of red oxic deep-water sediments, termed Cretaceous Oceanic Red Beds (CORBs; Hu et al., 2005). CORBs have been identified in all major Cretaceous oceans, from the Tethys to the Atlantic and the Pacific (Figure 3.2) (Hu et al., 2005; Wang and Hu, 2005). These CORBs include red limestones, marlstones, claystones, and cherts, and are interpreted as proving the widespread occurrence of oxygen-rich bottom waters.

A survey of the regional distribution of Coniacian-Santonian black shale attributed to OAE3 was given by Wagner et al. (2004) (Figure 3.1.1). Detailed studies on the sedimentological and geochemical record of OAE3 black shales was conducted in the equatorial Atlantic at ODP Site 959 (Ivory Coast–Ghana transform margin), and on the opposite side of the Atlantic, at the ODP Sites 1257–1261 (Demerara Rise). At these ODP sites the recovery of cyclic black shales was interpreted to represent precession and eccentricity orbital cycles (Hofmann et al., 2003; Beckmann et al., 2005; März et al., 2008, 2009).

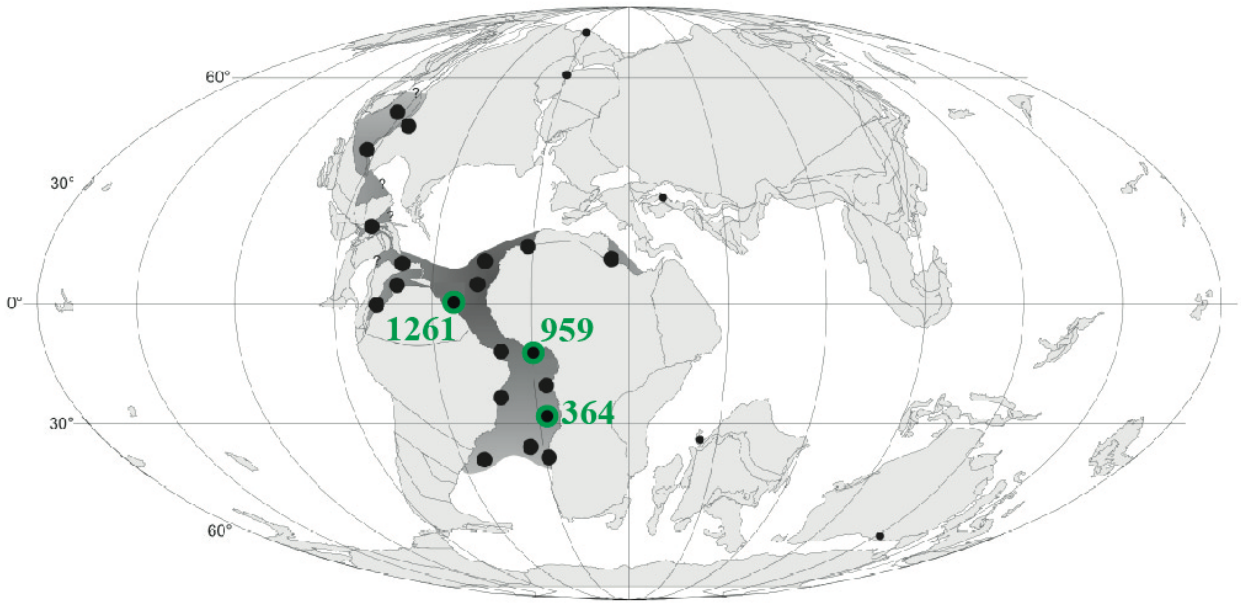

Figure 3.1.1 - Plate reconstruction around the Coniacian–Santonian boundary. The area of significant OAE3 black shale sedimentation is documented (large black circles) in the low latitude Atlantic and marginal basins and seaways (based on compilations of Wagner et al., 2004; Hofmann and Wagner, 2011; Wagreich, 2009), and other locations with reported local black shales (small black circles). In green are indicated ODP Site 1261 (Demerara Rise), ODP Site 959 (Deep Ivorian Basin) and DSDP Site 364 (Angola Basin) studied here. (Modified after Wagreich, 2012).

Here, the black shales constitute a more or less continuous succession from the OAE2 up to the Upper Santonian or Lower Campanian (Wagner et al., 2004; Friedrich and Erbacher, 2006; Wagreich, 2009).

Coeval organic carbon-rich sediments are also found in the continental slopes of North America (ODP site 603) and the southern South Atlantic (DSDP site 361; Dean et al., 1984). In South America OAE3 black shales are present from the shelf seas to deep-water basins as the Maracaibo Basin, western Venezuela (Luna and Querecual Formation) and Colombia (Lomagorda Formation) (Davis et al., 1999; Erlich et al., 1999; Erlich et al., 2000; Martinez, 2003; De Romero et al., 2003; Rey et al., 2004). Even here, the sedimentation is characterized by cyclic couplets of laminated black shales up to the Lower Campanian (e.g. De Romero et al., 2003; Rey et al., 2004).

The U.S. Western Interior is another area where the OAE3 was recognized. The Niobara Formation shows a discontinuous record of light-dark chalk, Middle-Late Coniacian to Santonian in age (Arthur et al., 1985; Dean and Arthur, 1998). Coniacian-Santonian black shales were also found in Brazil, northern Namibia, Angola, Gabon, northwest Africa and Morocco (Sachse et al., 2012), Libya, and Egypt (Wagner et al., 2004; Wagreich, 2009).

Black shales of the same age but with a more restricted distribution are found in Pakistan, Western Greenland, Sverdrup Basin in Arctic Canada, and southern Australia (Wagner et al., 2004) (Figure 3.1.2). However, in these locations, the presence of terrestrial organic matter (Gallagher et al., 2005) suggests local factors controlling organic-rich sedimentation rather than a global event (Hu et al., 2005). It is worth mentioning that no organic-rich strata of Coniacian-Santonian age are found in the Tethys, Pacific and Indian Oceans.

The stratigraphic distribution of OAE3 black shales shows differences in age in various basins and, as a consequence, oxygen depletion appears to be diachronous (Figure 3.1.2). The differences in age of black shale deposition can be explained by a strong regional control. For instance, the sedimentation of organic carbon-rich facies in the equatorial Atlantic are probably due to its configuration in terms of width and depth. The presence of a restricted circulation, semi-closed deep basins and high runoff from Africa and South America, together with enhanced productivity driven by high nutrient supply and upwelling due to the shifts in the position of the Intertropical Convergence Zone (ITCZ) resulted in anoxia over the equatorial Atlantic (Hofmann and Wagner, 2011). At Demerara Rise (ODP Leg 207) the final opening of the Equatorial Atlantic Seaway, in the late Santonian to early Campanian (Friedrich and Erbacher,2006), resulted in a deep-water exchange leading to the end of the black shales deposition. Otherwise, the organic-rich deposits of the Western Interior Seaway are interpreted as the consequence of sea level changes and water mass dynamics associated with the incursion of Tethyan water masses in a relatively shallow epicontinental sea (Tessin et al., 2019).

As already mentioned, OAE3 differs from previous OAEs for the very minor anomalies in the $\delta^{13}C$ record. According to the composite curve of Jarvis et al. (2006), only minor positive excursions of a maximum of 0.5‰ (White Fall event, Middle Coniacian; Horseshoe Bay event) are recorded during the

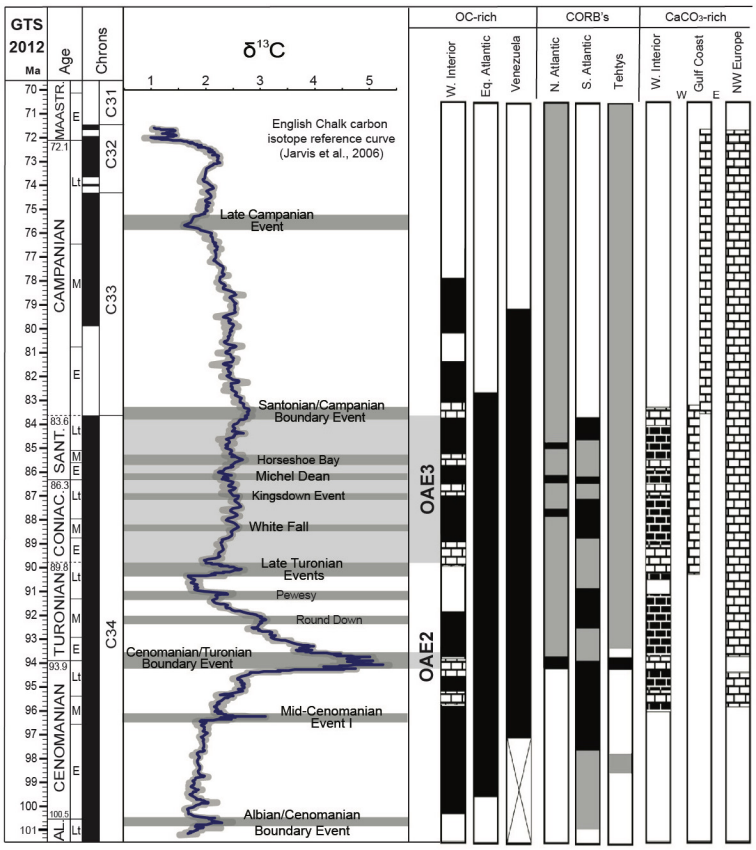

Figure 3.1.2 - Carbon isotopic reference curve from the Albian–Maastrichtian English Chalk (from Jarvis et al., 2006). Light gray bands highlight the stratigraphic position of OAE2 and OAE3 that are compared with the black shales records in the different areas (modified after Locklair et al., 2011). Dark grey bands identify C isotopic events (Jarvis et al., 2006).

Coniacian–Santonian time interval (Figure 3.1.2). Instead, during OAE1a and OAE2 the main carbon isotope excursions are in the order of a > 2 ‰ shift. OAE3 was considered by Wagreich (2012) as a long-lasting (5.8 Myr) event extending through the Coniacian-Santonian time interval (89.3–83.5 Ma; Ogg et al., 2004). The occurrence of only minor carbon isotopic excursions, and the local deposition of organic carbon-rich strata, point to a regional rather than global perturbation associated with OAE3 (Locklair et al. 2011). Based on the available data of spatial and temporal distribution of organic carbon-rich intervals and carbon isotope changes, Wagreich et al. (2009, 2012) suggested that OAE3 represents an Atlantic event distributed over a longer time span (about 5.8 Myr), associated to anoxic conditions at least from the Coniacian to the Santonian.

In the present study, I follow the definition of OAE3 given by Wagreich et al. (2009, 2012) and, consequently, the Coniacian-Santonian interval of each analyzed section has been considered as

equivalent of OAE3. According to the calcareous nannofossil biozonations adopted in this study (see discussion in Chapter 2), the OAE3 correlates with the following biozones (Figure 3.13):

* top of CC13 to CC17 Zones of Sissingh (1977),
* NC16 to NC17 of Roth (1978),
* top of NC15 to NC17* Zones of Bralower et al., (1995)
* UC9c to UC13 Zones of Burnett (1998).

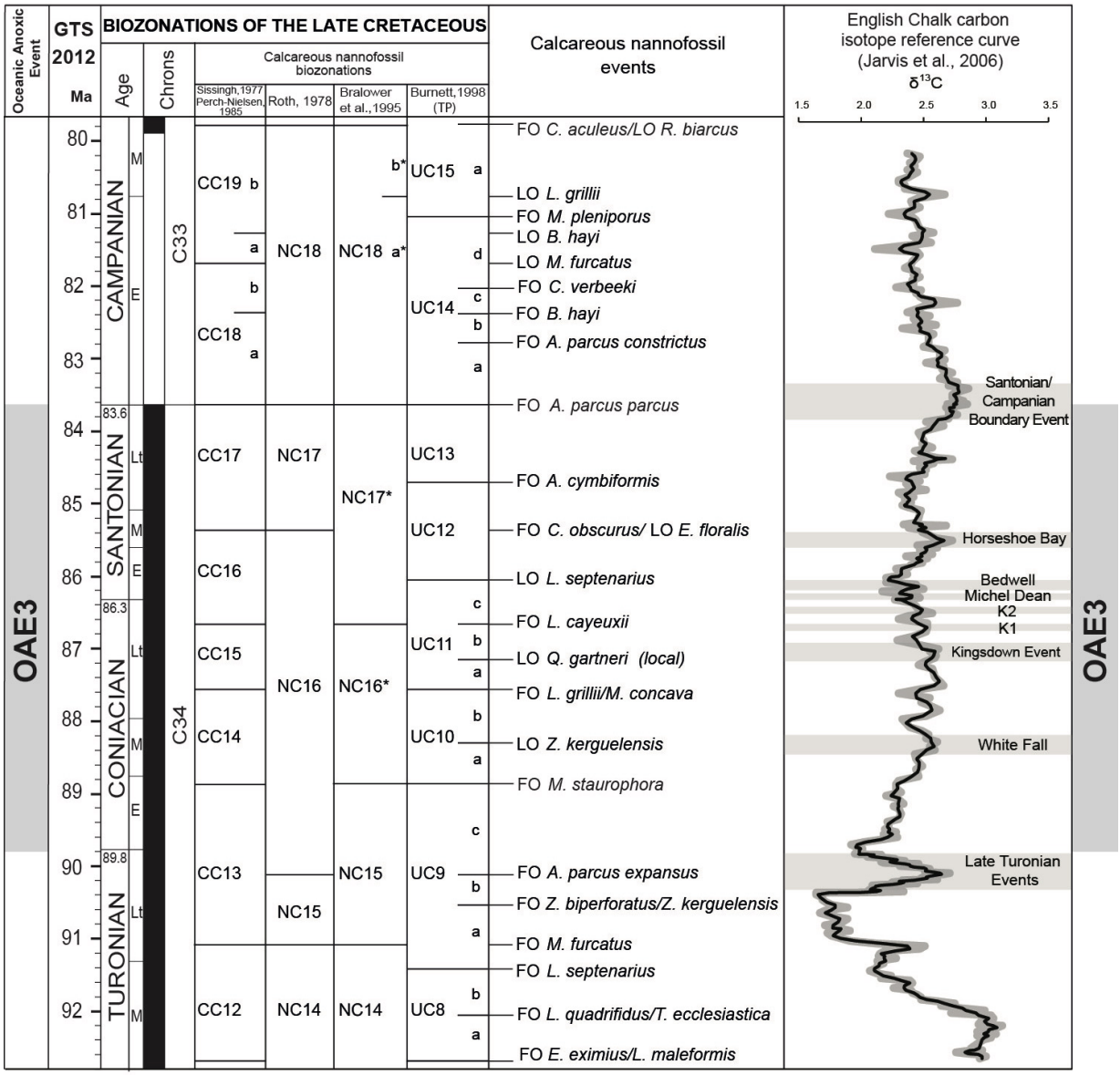

Figure 3.1.3 - Turonian – Campanian integrated calcareous nannofossil biozonations, polarity chrons and chronostratigraphy. Timescale after Gradstein et al. (2012). Calcareous nannofossil biozonations: Sissingh (1977) as modified by Perch-Nielsen (1985), Roth (1978), Bralower et al., (1995) and Burnett (1998). The OAE3 interval according to Wagreich et al. (2009; 2012) is highlight in grey.

The OAE3 starts at the Turonian/Coniacian boundary and terminates at the Santonian/Campanian boundary. The Turonian/Coniacian boundary lies between the FO of *M. furcatus* and FO of *M.*

staurophora, respectively, in the CC13 Zone of Sissingh (1977), NC16 Zone of Roth (1978) and NC15 zone of Bralower et al. (1995). Otherwise, in the Burnett's (1998) Zonation the Turonian/Coniacian boundary lie between the FO of *Aspidolithus parcus expansus* and the FO of *Micula staurophora* in the UC9c Subzone. As already mentioned, Jarvis et al. (2006) recognized only minor positive $\delta^{13}C$ excursions in the Coniacian-Santonian time interval in the English Chalk, these are: Kingsdown Event, K1, K2, Michel Dean, Bedwell and Horseshoe Bay (Figure 3.1.3).

3.2 Calcareous nannofossil across the Coniacian-Santonian OAE3

A literature survey was conducted to evaluate the available information about calcareous nannofossil biostratigraphy and paleoecology of the Coniacian-Santonian time interval. The analyzed papers deal with various localities and are focused on a time interval that spans from the Middle Turonian: CC12, NC14 and UC8 Zones to the Early Campanian: CC19b, NC18, NC18a* and UC15a Zones. A total of 58 papers were considered. The results of this survey are presented in Appendix 4 organized chronologically, from the most recent to the older paper. All the information are summarized in the table as follows:1) Author; 2) Realm; 3) Basin; 4) Section; 5) Time interval studied 6) Methodology; 7) Taxonomy; 8) Biostratigraphy; 9) Plates; 10) Range chart; 11) Paleoceanography;12) Paleoecology; 13) Morphometries;14) Principal component analyses; 15) Cluster Analyses; 16) New biozonation; 17) Lithostratigraphy; 18) Ammonite stratigraphy; 19) Foraminiferal biostratigraphy; 20) Inoceramid bivalves; 21) Crinoids; 22) Echinoids; 23) Palynology/Ostracods; 24) Chemostratigraphy (C-O isotopes); 25) Magneto stratigraphy; 26) Ciclostratigraphy; 27) Notes.

The stratigraphic distribution of sections with calcareous nannofossil biostratigraphy data for the Coniacian-Santonian time interval are summarized in Figure 3.2.1. These comprise various on-land sections and DSDP/ODP Sites located in the Tethys Ocean, Boreal Sea, Basque-Cantabrian area, Atlantic Ocean, Western Interior Basin, South America and Indian Ocean.

The Tethys Ocean was sampled in Alpine and Apennines successions (Wolfgring et al., 2018; Wagreich et al., 2010;Tremolada, 2002), the Carpathian area (Švábenická, 2012; Cetean et al., 2011; Melinte-Dobrinescu, 2010; Melinte-Dobrinescu and Bojar, 2010, Melinte and Lamolda , 2007) and the southern Tethys (Razmjooei et al., 2020a; Faris et al., 2019; Farouk et al., 2018; Razmjooei et al., 2018 and Razmjooei et al., 2014; Farouk et al., 2017;Wolfgring et al., 2017; Farouk et al., 2016; Razmjooei et al., 2014; Farouk and Faris, 2012; Bauer et al., 2001).

Only three successions span the Coniacian-Santonian interval entirely: the Bottaccione section in central Italy (Tremolada, 2002), the Fizesti Formation, Haţeg regions, in Romanian Carpathians (Melinte-Dobrinescu, 2010) and the Dokan section in Kurdistan (Faris et al., 2019).

The deposition in the Sinai region (Southern Tethys) during the Cenomanian-Santonian was characterized by hiatuses and condensed intervals, due to regional tectonics and sea level changes, in addition to global eustatic sea level changes (Farouk and Faris, 2012; Bauer et al., 2001).

In the Tethyan successions, an integrated calcareous nannofossil and planktonic foraminifera biostratigraphy is widely adopted by many researchers (Appendix 4).

In the Basque-Cantabrian area, the Olazagutia section represents the GSSP for the Coniacian-Santonian boundary (Lamolda et al., 2014, Howe et al., 2007).

The available data for the Boreal Sea show that the Seaford Head section in South-East England (Sussex) is the only succession that spans the Coniacian-Santonian time interval entirely (Hampton et al., 2007). Data from multiple wells and composite on land sections are available for the North Sea (Berken and Sikora, 1999 and Fritsen et al., 2000), Germany (Püttmann et al., 2018) and North-East England (Burnett and Whitham,1999). Moreover, Lees (2008), Sikora et al. (2004), Kędzierski (1998), Howe et al. (2007) and Dubicka et al. (2017) focused, respectively, on the Turonian/Coniacian, Coniacian/Santonian and Santonian/Campanian boundaries.

The calcareous nannofossil biostratigraphy of Boreal Sea successions is generally integrated with benthic foraminifera and macrofossils as inoceramid bivalves, crinoids and echinoids (Appendix 4).

In the Atlantic Ocean, the DSDP Site 549 and 551 drilled in the Goban Spur Basin (Linnert et al., 2011) extends from the middle Coniacian to the Maastrichtian. The Cenomanian-Turonian portion of Site 549 is characterized by the presence of some gaps in the sedimentary record due to the poor core recovery. Other sites lack of the middle-upper Santonian as ODP Site 959 (Watkins et al.,1998) and ODP Site 1261 (Erbacher et al., 2004). Sites drilled in the Pelotas Basin (southern Brazil) recovered stratigraphic successions characterized by a gap between the upper Coniacian and the lower/middle Santonian (Guerra et al., 2012). Moreover, in this area the lack of classic nannofossil marker species resulting in the establishment of a regional calcareous nannofossil zonal scheme with a low biostratigraphic resolution, that prevents supra-regional correlations.

As far as the Western Interior Basin is concerned, particular attention was focused on calcareous nannofossil assemblages across the Turonian/Coniacian boundary (Corbett et al., 2014; Walaszcyk et al., 2012; Sikora et al.,2004), Coniacian/Santonian boundary (Blair and Watkins,2009; Gale et al., 2008; Howe et al.,2007) and Santonian/Campanian boundary (Kita et al., 2017; Gale et al., 2007). Only Da Gama et al. (2014) covered the entire OAE3 interval documenting both calcareous nannofossil biostratigraphy and paleoecology.

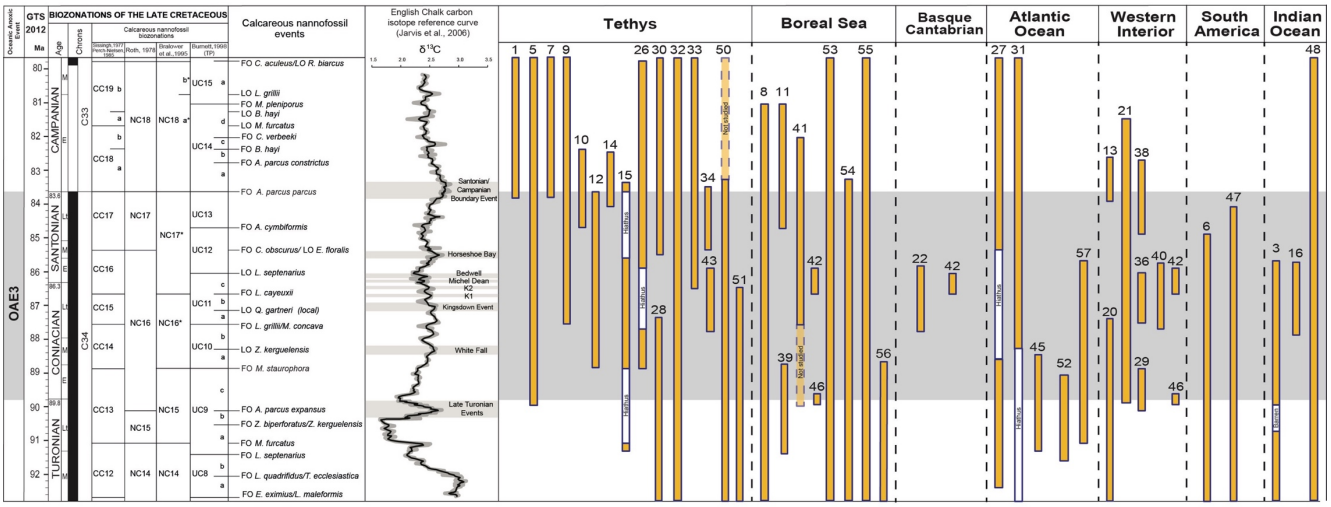

Figure 3.2.1 - Stratigraphic distribution of calcareous nannofossil biostratigraphy data according to available literature. The complete list of papers is in Appendix 4. (1) Razmjooei et al., 2020a; (5) Faris et al., 2019;(6) Pérez Panera et al., (2019); (7) Farouk et al., 2018;(8) Püttmann et al., 2018; (9) Razmjooei et al., 2018 and Razmjooei et al., 2014;(10) Wolfgring et al., 2018; (11) Dubicka et al. (2017); (12) Farouk et al., 2017;(13) Kita et al., (2017); (14) Wolfgring et al., 2017; (15) Farouk et al., 2016;(16) Jiménez Berrocoso et al., 2015; (20) Corbett et al., (2014); (21) Da Gama et al., 2014; (22) Lamolda et al., (2014); (26) Farouk and Faris (2012);(27) Guerra et al., (2012); (28) Švábenická (2012);(29) Walaszcyk et al., (2012); (30) Cetean et al., (2011); (31) Linnert et al., (2011);(32) Melinte-Dobrinescu (2010); (33) Melinte-Dobrinescu and Bojar (2010); (34) Wagreich et al., (2010); (36) Blair and Watkins (2009); (38) Gale et al., (2008); (39) Lees (2008); (40) Gale (2007); (41) Hampton et al., (2007); (42) Howe et al., (2007); (43) Melinte and Lamolda (2007); (45) Erbacher et al, 2004; (46) Sikora et al., (2004); (47) De Romero et al., 2003; (48) Lees (2002); (50) Tremolada (2002); (51) Bauer et al., (2001); (52) Gebhardt (2001); (53)Berken and Sikora (1999); (54) Burnett and Whitham (1999); (55) Fritsen et al.,1999; (56) Kedzierki (1998); (57) Watkins et al., (1998).

In South America, the Cenomanian-Campanian interval is represented by La Luna Formation. This was studied by Pérez Panera et al. (2019) and De Romero et al. (2003) in the Magdalena Valley Basin (Colombia) and the Maracaibo Basin (Venezuela), respectively. The presence of poorly preserved nannofossil assemblages characterized by dissolution and recrystallization with dominance of only most dissolution-resistant species led to the development of an informal calcareous nannofossil zonal scheme for this formation.

An exhaustive report of calcareous nannofossil biostratigraphy for the Indian Ocean was given by Lees (2002), also for the Coniacian-Santonian time interval (DSDP/ODP Sites 738C, 258, 761B,765C). A succession dated as Coniacian-Santonian in age was drilled at the TDP39 in Tanzania (Jiménez Berrocoso et al., 2015). More recently, Watkins and Guerra (2020) presented a calcareous nannofossil

biostratigraphy and paleoecology from the Turonian- middle Santonian interval recovered at IODP Site U1512 in the Australian-Antarctic Basin.

In the last few years the calcareous nannofossil paleoecology across the Coniacian-Santonian time interval has received more attention compared to the past. Figure 3.2.2 shows the available calcareous nannofossil paleocological information for different areas: for each section, the stratigraphic interval studied is indicated.

In the Tethys area, nannofossil paleocological reconstructions are available from middle east sections (Razmjooei et al., 2020b; Al Rawahi and Dunkley Jones, 2019) and the Carpathians (Švábenická and Bubík, 2014; Švábenická, 2012; Melinte and Lamolda, 2007). The available data for the Boreal Sea, include the North Sea (Berken and Sikora, 1999) and the Seaford Head section (Hampton et al., 2007). Quantitative data were produced by Melinte and Lamolda (2002) for the Olazagutia section in the Basque-Cantabrian area. In the Atlantic Ocean nannofossil palecological data are available for the Pelotas Basin in southern Brazil (Guerra et al., 2012) and DSDP Site 549 drilled in the Goban Spur Basin (Linnert et al., 2011). A few sections were characterized in the Western Interior Basin (De Gama et al., 2014; Blair and Watkins, 2009).

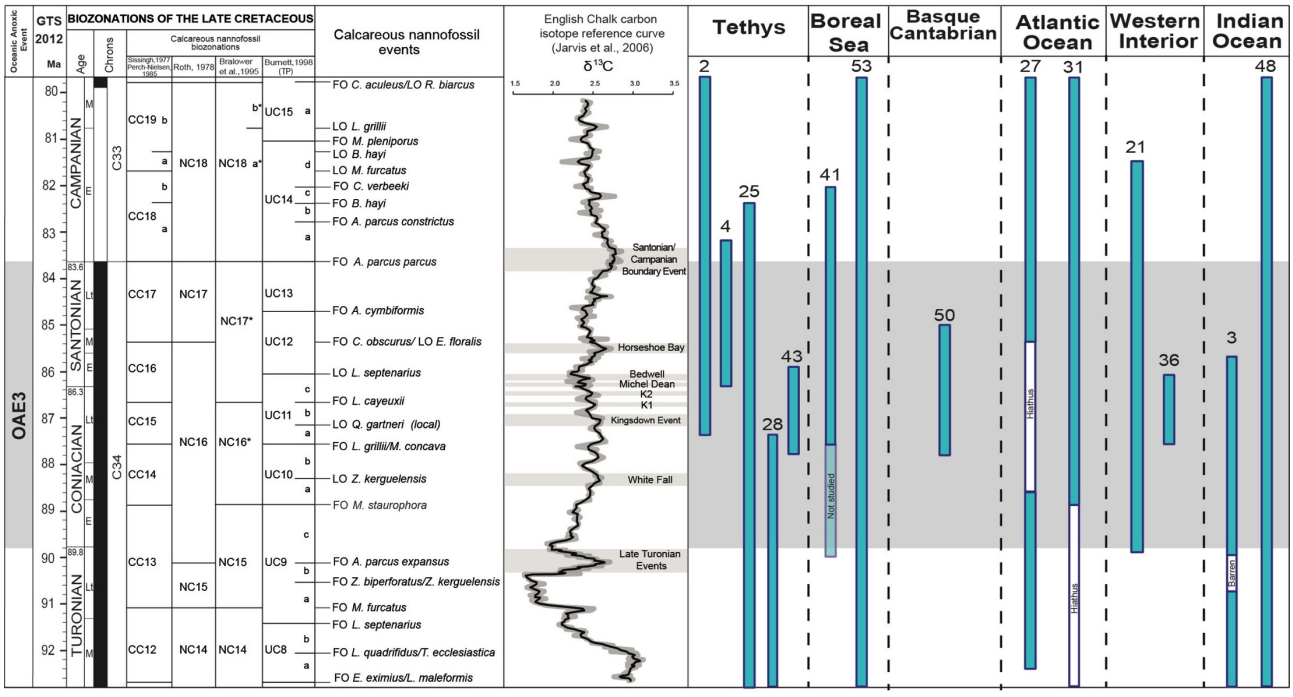

Figure 3.2.2 - Stratigraphic distribution of calcareous nannofossil quantitative data. The complete list of papers is in Appendix 4. (2) Razmjooei et al., (2020) b; (3) Watkins and Guerra (2020); (4) Al Rawahi and Dunkley Jones (2019); (21) Da Gama et al., 2014; (25) Švábenická and Bubík (2014); (27) Guerra et al., (2012); (28) Švábenická (2012); (31) Linnert et al., (2011); (36) Blair and Watkins (2009); (41) Hampton et al., (2007);(43) Melinte and Lamolda (2007); ; (48) Lees (2002) ;(50) Melinte and Lamolda (2002);(53)Berken and Sikora (1999).

In the Indian Ocean, Lees (2002) used changes of calcareous nannofossil assemblages to reconstruct the evolution of different paleoclimatic zones trough the Late Cretaceous. A more detailed paleoclimate evolution was proposed by Watkins and Guerra (2020) from the IODP Site U1512 in the Australian-Antarctic Basin.

Unlike other Mesozoic OAEs, the OAE3 lacks specific changes in calcareous nannofossil assemblages. In the Carpathians, the Turonian/Coniacian boundary transition is characterized by an increase in *Marthasterites furcatus* in the associations, defined by Švábenická (2012) and Švábenická and Bubík (2014) as "*Marthasterites furcatus* acme". This acme starts above the FO of *Aspidolithus parcus expansus* and the LO of *Helicolithus turonicus* in the UC9c zone, equivalent to the CC13, NC16 and NC15* Zones, just before the FO of *Cremnoceramus waltersdorfensis* that marks the Turonian/Coniacian boundary. The top of the "*Marthasterites furcatus* acme" was found below the FO of *Micula staurophora*, in the early Coniacian. In the Bohemian Basin, the relative amount of *M. furcatus* in the assemblage was observed to fluctuate between the 5-6% at the base of the acme up to 27 % (Figure 2.3.2), and to range from 5% to 13.5% in the Pavlovské vrchy klippes (Švábenická and Bubík, 2014). The "*Marthasterites furcatus* acme" was interpreted by Švábenická and Bubík (2014) and Švábenická (2012) as a consequence of a fluctuation of the sea-level to a more nearshore condition. According to Švábenická and Bubík (2014), the presence of common *M. furcatus* in the Bohemian Basin could reflect a widespread sea level fluctuation occurring during the Turonian-Coniacian transition that may correspond to the acme event in *Braarudosphaera* and *Nannoconus* observed by Wyton et al. (2007) in south-east England. A similar interpretation for the paleoecology of *M. furcatus* was also suggested by Watkins (pers. comun. 2019, INA Lyon Summer School) that considers this species more common in nearshore/epeiric seas than in deep ocean.

In the Western Interior, De Gama et al. (2014) observed an acme of *M. furcatus* in the UC9 Zone of the Niobrara Formation (Figure 2.3.2) and an acme of *M. furcatus* was also reported by Bergen and Sikora (1999) in the early Coniacian (KN30 Zone) of the North Sea.

Another increase in *M. furcatus* was also observed in early Campanian UC14a zone of the Pavlovské vrchy klippes (Švábenická and Bubík, 2014). In this area, this acme was found to correspond with an increase in *Lucianorhabdus* spp., *K. magnificus* and a decrease in *W. barnesiae* (Figure 2.3.2). Švábenická and Bubík (2014) associated this event to a decrease in surface water temperature and shallower conditions.

Melinte and Lamolda (2002) observed, in latest Coniacian of the Olazagutia section a high abundance of *Micula* spp. (*Micula staurophora* and *Micula concava*). This was found just below the FO of *Cladoceramus undulatoplicatus* (Coniacian/Santonian boundary), between the FO *L. cayeuxii* and the

LO of *L. septenarius* (Melinte and Lamolda, 2002), within the UC11c Zone, equivalent to the CC16, NC16 and NC17* Zones. A variation from 4% to 8% was observed for *M. staurophora* whereas *M. concava* displays relative abundances from 2% to 12% of the assemblages (Figure 2.3.2). At Olazagutia, the increase in *M. staurophora* slightly precedes that of *M. concava* associated with the increase of *Lucianorhabdus* spp. (*L. maleformis*, *L. quadrifidus* and *L. cayeuxii*) from 6% up to the 21% (Figure 2.3.2) in the earliest Santonian (Melinte and Lamolda, 2002; Lamolda et al., 2014). *Calculites* spp. (*C. ovalis*, *C. pernicensis* and *C. obscurus*) show low values across the Coniacian/Santonian boundary, with an increase in the early Santonian (Melinte and Lamolda, 2002). A sharp drop in *H. trabeculatus* was observed by Howe et al. (2007) in the UC11c Zone of the Olazagutia section, below the FO of *Cladoceramus undulatoplicatus*.

A similar pattern of *Micula* spp., *Lucinorhabdus* spp. and *Calculites* spp. was observed by Melinte and Lamolda (2007) in the UC11c/CC16 Zone of Romanian Carpathian. Here, *M. staurophora* is found to be common (5-20%) in the uppermost Coniacian, whereas *M. concava* is found to reach 15-18% below the FO of *Texanites* spp. and FO of *Dicarinella asymmetrica* (Figure 2.3.2). The beginning of the increase in abundance of *Lucianorhabdus* spp. (*L. maleformis*; *L. quadrifidus*; *L. cayeuxii* and *L. inflatus*) is slightly older than that of *M. concava,* reaching up to 26% of the assemblage. *Calculites* spp. *(C. obscurus, C. ovalis* and *C. pernicensis*) show an increase in relative abundance up to 13% in the early Santonian (Figure 2.3.2).

A sharp increase of *M. staurophora* (from 2 %–3% to > 15 %) was observed in the UC12-UC13 Zone of the Fiqua Formation (Oman) by Al Rawahi and Dunkley Jones (2019) (Figure 2.3.2). Here, the increase of *M. staurophora* (up to 15%), precedes an interval characterized by lower *W. barnesiae*, associated with an elevated abundance of fertility-related taxa *B. constans*, *Z. erectus, Discorhabdus ignotus* (e.g. Roth and Bowdler, 1981; Roth and Krumbach, 1986; Erba, 1992; Herrle, 2003; Herrle et al., 2003) and a peak of *C. signum* (from < 5% to > 40 %,). According to Al Rawahi and Dunkley Jones (2019) this increase in fertility-related taxa might indicate episodes of increased nutrient supply.

At Seaford Head (SE England) Hampton et al. (2007) highlighted an "influx" of *M. staurophora,* across the UC11iii – lower UC12 Zone (Figure 2.3.2) followed by an increase of *L. cayeuxii* and *L. maleformis* (Figure 2.3.2) in the middle Santonian (UC12 zone) up to the upper Santonian (UC13ii zone). The top of the UC13ii zone is marked by an "influx" of *C. obscurus* close to the LO of *Marsupites testudinarius.* Moreover, the highest occurrence of common *H. trabeculatus* was observed in the UC11iii/UC11c Zone close to the LO of *Cladoceramus undulatoplicatus* (Hampton et al., 2007; Howe et al., 2007).

A minor increase in abundance of *Micula* spp. (about 3%) was reported by Linnert et al. (2011) in the UC11c-UC12 Zone of Goban Spur (DSDP Site 549, Figure 2.3.2). Here, the relative abundance of *Micula* spp. increase started in the early Campanian (UC14b-d zone) and reaches its maximum (about

25%) in the late Campanian (UC15e zone). At DSDP Site 549, the highest abundance of *H. trabeculatus* (about 5%) was observed in the UC11c-UC12 Zone (Linnert et al., 2011).

In the Western Interior Basin, Blair and Watkins (2009) do not report the presence of abundant *Micula* spp. at the Coniacian/Santonian transition in the Ten Mile Creek and Locality 13 sections (Figure 2.3.2). Otherwise, an increase in *Micula* spp. was observed by De Gama et al. (2014) in the late Coniacian - early Santonian from wells drilled in the Niobrara Formation (Figure 2.3.2).

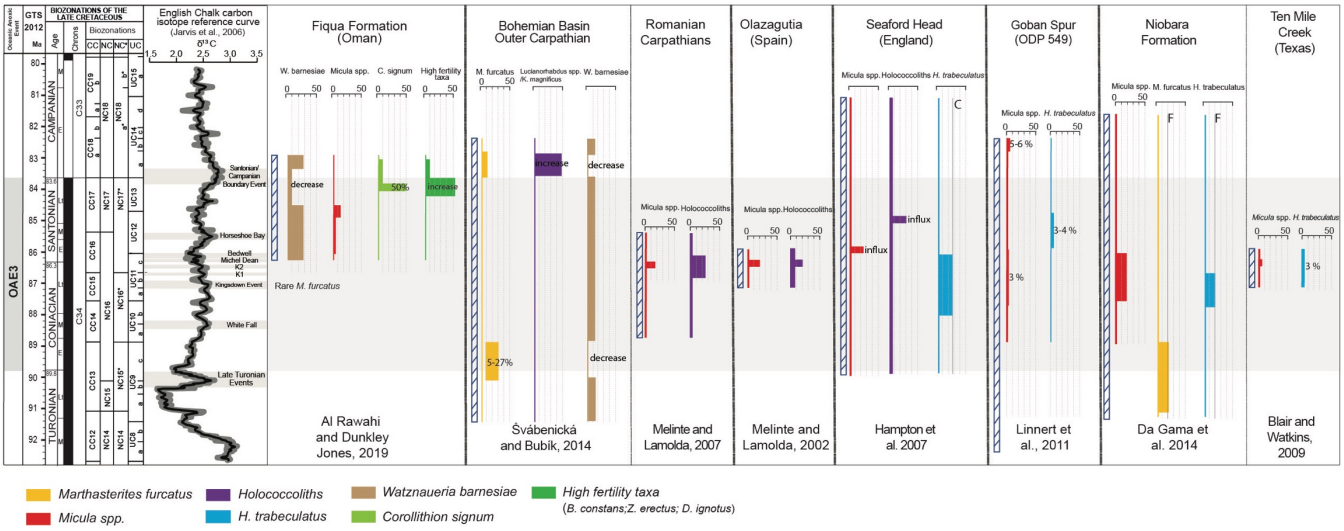

Figure 3.2.3 - Synthesis of the published calcareous nannofossil quantitative data across the OAE3.

In the Western Interior Basin, Blair and Watkins (2009) found the occurrence of abundant *H. trabeculatus* at the Coniacian/Santonian transition both at Ten Mile Creek and Locality 13, respectively with the 6.8 and 8.6% of the assemblages. However, De Gama et al. (2014) placed the top of *H. trabeculatus* acme in the UC10-UC11 zone of the Niobrara Formation.

Chapter 4
Materials and methods.

4.1 Studied sections.

Stratigraphic sections from land and oceanic sites were investigated though the Turonian-Campanian interval (Figure 4.1). As far as oceanic settings are concerned, DSDP/ODP Sites from the equatorial and south Atlantic were selected: ODP Site 959 (Ivory Coast–Ghana), ODP Site 1261(Demerara Rise) and DSPD Site 364 (Angola Basin). Successions were also investigated from the Tethys Ocean (Bottaccione section, Umbria-Marche Basin), the Anglo-Paris Basin (Seaford Head) and Indian Ocean (Tanzania TDP 39 and ODP Site 763).

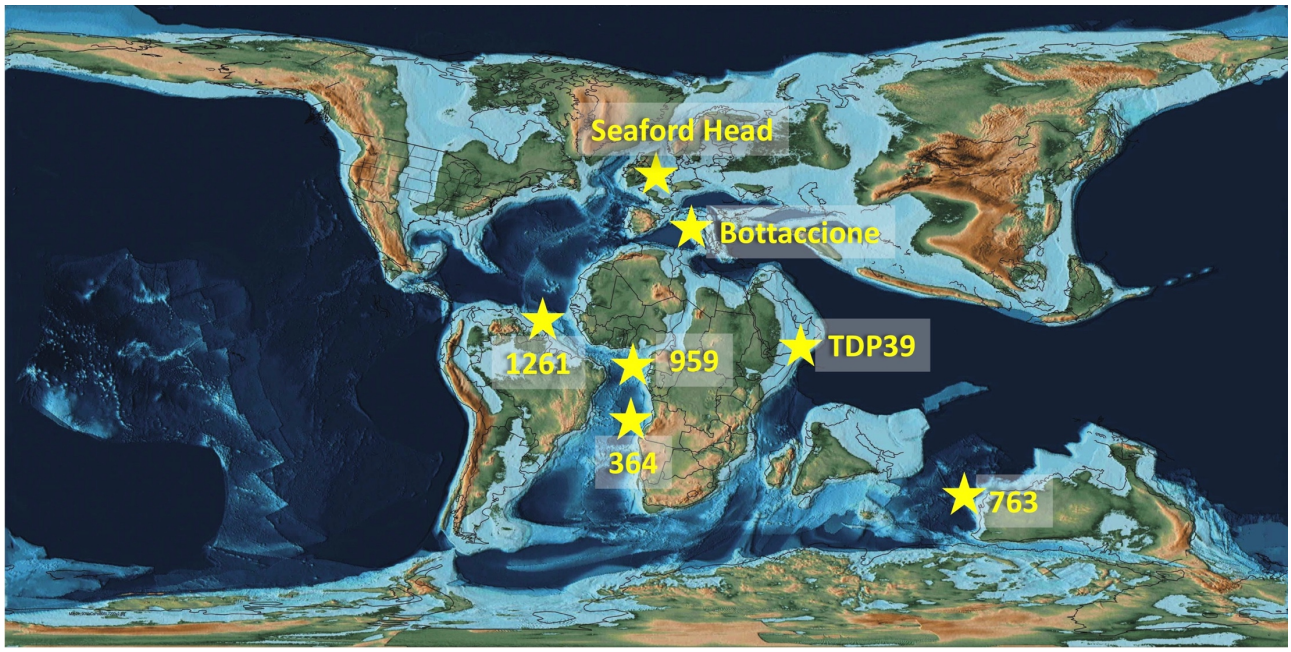

Figure 4.1 - Location of the studied sections in a paleogeographic reconstruction at 90 Ma (PALEOMAP PaleoAtlas; Scotese, 2016).

4.1.1 DSDP Site 364.

DSDP Site 364 is located along the eastern margin of the Angola Basin at about 100 miles offshore of Angola southwest Luanda (11°34.32'S;11°58.30'E) at a water depth of 2448 meters (Figure 4.1.1.1). Only one hole was drilled at this site with a total of 46 cores recovered and a total length of cored section of 427.5 meters (Bolli et al., 1978). The penetrated sequence extends in age from the Pleistocene to the late Albian, just above the evaporite and salt formations (Proto-Decima, 1978). DSDP Site 364 was spot

cored and cores were taken with an average spanning of 10 meters with a recovery of 69,1% (Bolli et al., 1978).

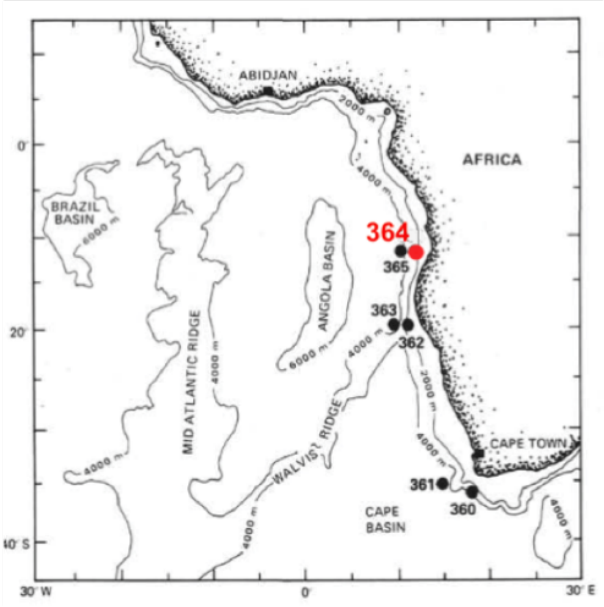

Figure 4.1.1.1 - Location of DSDP Leg 40 Site 364 (modified after Bolli et al., 1978).

Sampling: A total of 50 slides, were analyzed both for biostratigraphic and quantitative analyses, with a sampling resolution of 1 sample/2-3m. The considered interval covers the Campanian (core 40-364-15R) to Late Coniacian/Upper Turonian (core 40-364-23R). All the studied samples were prepared following the settling slide techniques.

Two lithologic units were distinguished in the studied stratigraphic interval (Units 4 and 5; Figure 4.1.1.2). Unit 4 (core 40-364-7 to core 40-364-19), consisting in a nannofossil chalk (up to 95% nannofossils), is divided in subunit 4a (cores 40-364-7 to 40-364-15) and subunit 4b (cores 40-364-16 to 40-364-19). The latter is characterized by abundant intercalations of terrigenous mudstones. Subunit 4a consists of yellow brown, light gray, brown and reddish yellow nannofossil chalk, whereas subunit 4b consists of brown, light brown, and pale brown nannofossil chalk. Unit 5 was described as marly chalk with black shales. It was divided in two subunits 5a (cores 40-364-20 to 40-364-22) and 5b (cores 40-364-23 to 40-364-25) on the base of abundance of black shales. Subunit 5a consists of greenish gray to brown nannofossil chalk and marly nannofossil chalk interbedded with thin sapropels, whereas subunit 5b consists of greenish gray and dark greenish gray marly chalk and calcareous mudstone interlayered with abundant black sapropelic shale.

Previous studies on calcareous nannofossil assemblages at DSDP Site 364 were published by Proto Decima et al. (1978) and reported in the "The Initial Reports of the Deep-Sea Drilling Project ". The biozonations used for the Late Cretaceous were those of Čepek and Hay (1969), Martini (1969, 1976),

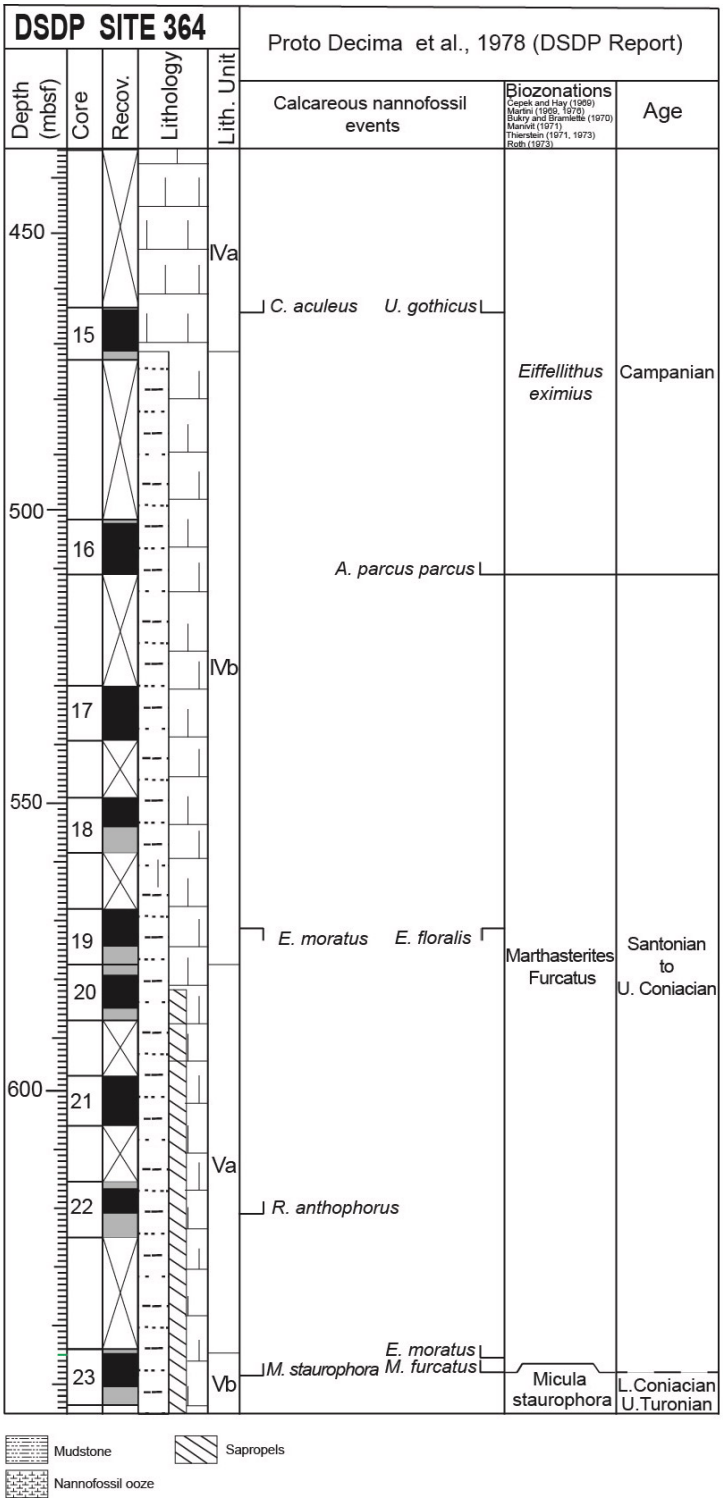

Figure 4.1.1.2. - Litho-biostratigraphic summary of Site DSDP 364. Lithostratigraphy and core recovery are from Bolli et al. (1978). Calcareous nannofossil biozonation is according to Proto Decima et al. (1978).

Bukry and Bramlette (1970), Manivit (1971), Perch-Nielsen (1972, 1977), and Roth (1973). At DSDP Site 364 an almost complete sequence of Late Cretaceous was recognized. Three zones were established in the interval between Cores 40-364-15R and 23R (Figure 4.1.1.2). The FO *A. parcus parcus* in Core

40-364-16R marks the base of the Campanian *Eiffellithus eximius* zone (Cores 40-364-15R and 16R), whereas the FO of *Marthasterites furcatus* was used to place the base of the Coniacian-Santonian *Marthasterites furcatus* zone (Cores 40-364-17R to 40-364-23R-3). Section 40-364-23R-4 was assigned to the Late Coniacian/Late Turonian *M. staurophora* zone due to the presence of *M. staurophora*.

4.1.2 ODP Site 959.

ODP Site 959 was drilled during Leg 159 on a small plateau close to the top of Côte d'Ivoire-Ghana Marginal Ridge on southern side of the Deep Ivorian Basin (3°37.656'N, 2°44.149'W), at about 2100 meters of water depth (Mascle et al., 1996; Figure 4.1.2.1). A total of 78 cores were drilled with a 741.10 meters of penetrated section (with 57.9% of recovery) extending in age from the early Oligocene to the late Albian (Mascle et al., 1996).

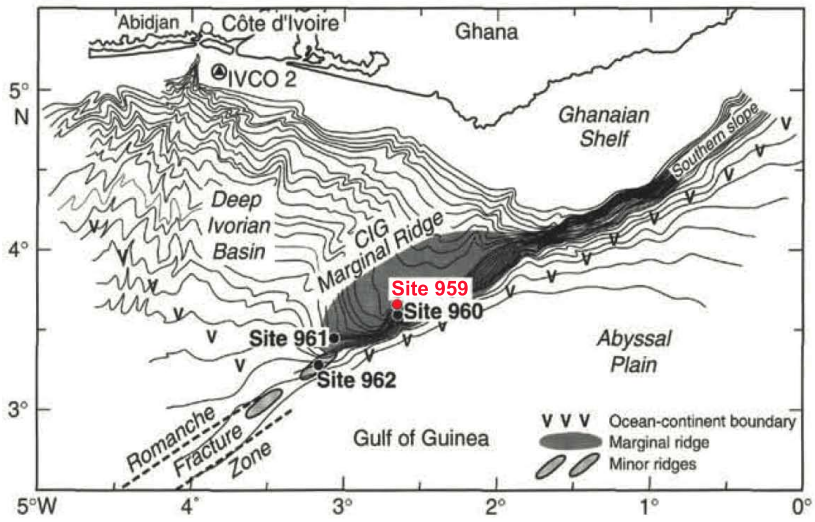

Figure 4.1.2.1 - Location of ODP Leg 150 Site 959 (modified after Mascle et al., 1996).

Sampling: The biostratigraphic analysis at Site ODP 959 was performed on a total of 29 slides sampled at about 1 m of resolution through the lower Turonian to lower Santonian (core 159-959-68R to core 159-959-65R; Figure 4.1.3.2). Among these, 20 samples were analyzed for quantitative abundances. All the studied samples were prepared following the settling slide techniques. Ten samples, were processed following the organic matter removal of Shamrock et al. (2015) because found to be particularly rich in organic matter. Two lithologic units (Mascle et al., 1996) were distinguished in the considered stratigraphic interval (Units 3 to 4) (Fig. 4.1.2.2). Unit 3 consists of black claystone and extends from core 159 959D-43R through core 159-959D-66R. The upper part of Unit 3 resulted to be entirely barren f calcareous microfossils, while the lowermost part (cores 59-959D-66R and lower 159-959D-65R) contains some carbonate-bearing lithologies that include calcareous microfossils.

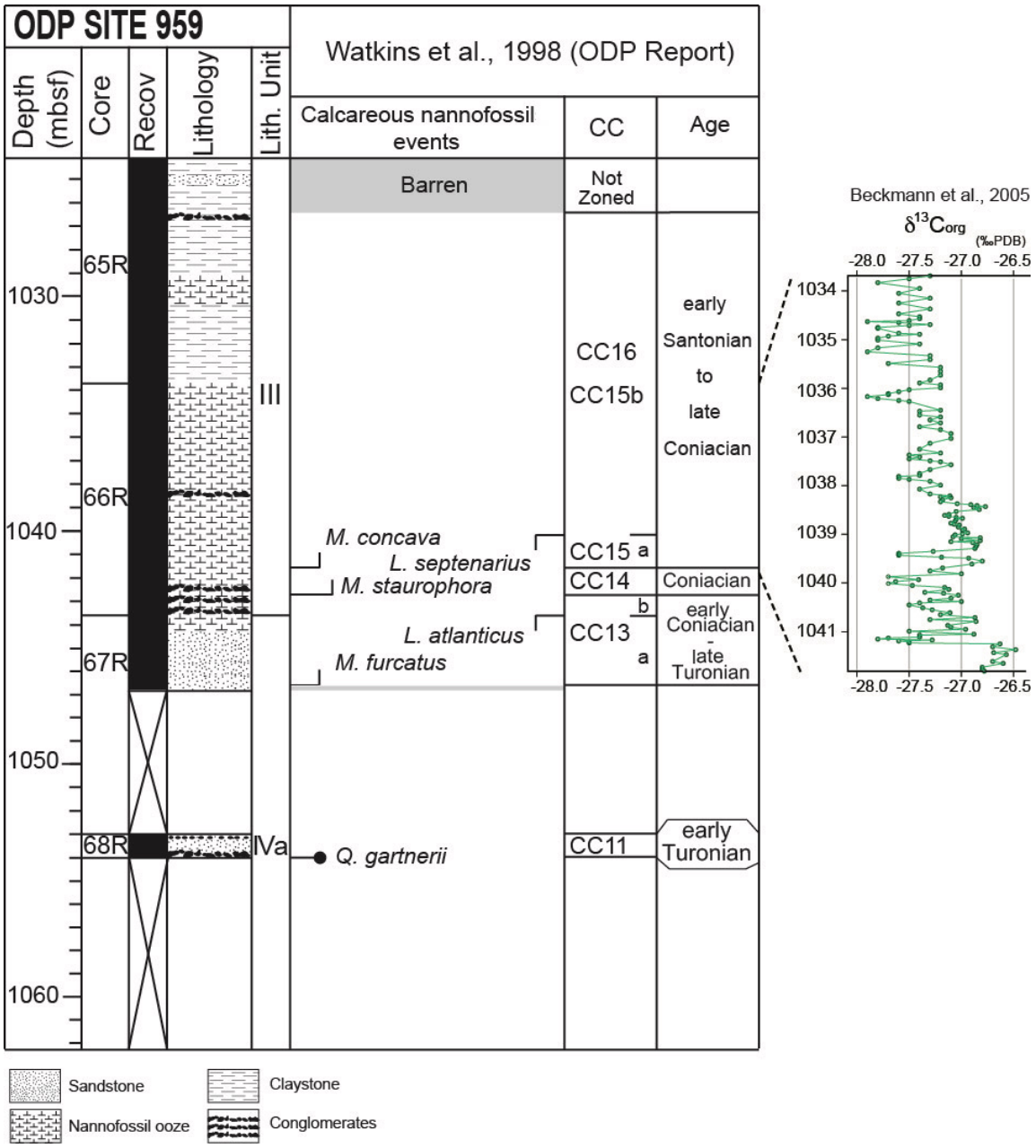

Figure 4.1.2.2 - Litho-biostratigraphic summary Site ODP 959. Lithostratigraphy and core recovery are from Mascle et al. (1998). Calcareous nannofossil biozonation is according to Watkins et al. (1998). $\delta^{13}C_{org}$ record from Beckmann et al. (2004).

According to Pletsch et al., (2001) the black shales in cores 59-959D-65R and 159-959D-66R follow a highly cyclic pattern, attributed to the fluctuation in continental supply and changes in the rate of organic carbon production at processional scale (Hofman et al., 2003; Beckmann et al., 2004). Unit 4 is characterized by the occurrence of sandy limestone, sandy dolomite, calcareous sandstone and limestone (cores 159-959D-67R through 159-959D-70R). Two subunits were recognized: 1) Subunit 4a consists of calcareous sandstones and organic-rich claystone including thin conglomeratic beds with phosphatic

pebbles and glauconitic clasts; 2) Subunits 4b is composed of bioclastic limestones with some sandy limestones.

Previous studies on calcareous nannofossils at ODP SITE 959 were performed by Watkins et al. (1998) as published in the "Proceedings of the Ocean Drilling Program, Scientific Results" (Mascle et al., 1998). The majority of Cretaceous sediments recovered at ODP Site 959 are non-calcareous and, therefore, impossible to date by calcareous nannofossils (e.g. from Core 159-959D-49R through section 159-959D-65R-2). The studied stratigraphic interval includes calcareous hemipelagic sediments that contain calcareous nannofossils. According to Watkins et al. (1998), this interval includes nannofossil zones CC16 (late Santonian) to CC11 of early Turonian age (Figure 4.1.3.2). However, a gap is present in the stratigraphic record due to poor recovery, and zone CC12 is absent.

Detailed studies on the sedimentological and geochemical record of the interval across Cores 59-959D-65R and 159-959D-66R was presented by Hofmann et al. (2003), Wagner et al. (2004) and Beckmann et al. (2004). In Figure 4.1.3.2 the $\delta^{13}C_{org}$ record of Beckmann et al. (2004) is showed.

4.1.3 ODP Site 1261.

ODP Site 1261 is situated at ~350 km north of Suriname, on the gently dipping northwest-facing slope of Demerara Rise (9°2.9168′N, 54°19.0384′W; Figure 4.1.3.1). A total of two holes were drilled at Site 1261: 51 cores in the Hole A and 15 in Hole B with a total of 478 meters-thick section and a 68% of recovery. The penetrated sequence extends in age from the Pleistocene to the Cenomanian (Erbacher et al., 2004).

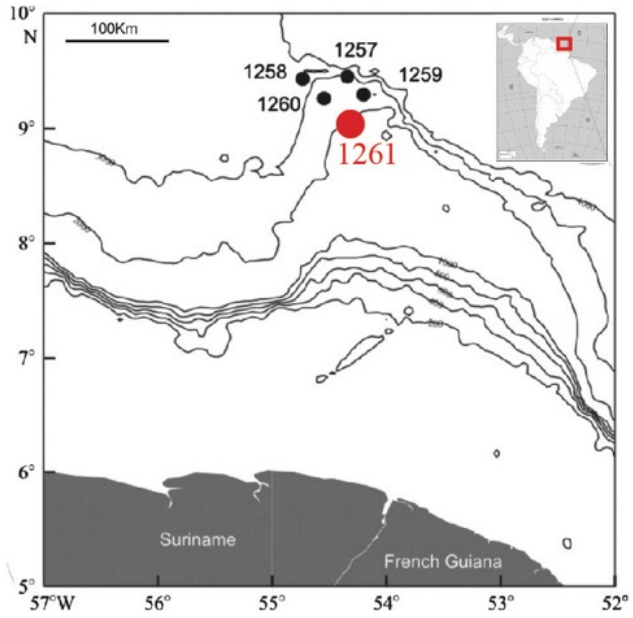

Figure 4.1.3.1 - Location of ODP Site 1261. Other sites drilled on the Demerara Rise during Leg 207 are also reported (modified after Hardas and Mutterlose, 2006).

Sampling: A total of 87 samples from Hole A were examined for calcareous nannofossil quantitative analyses, collected with a resolution of 1 sample every 20 cm. The considered interval spans from the Turonian to the late Coniacian (Russo, 2014). This includes core 207-1261A-41R to 43R. All the studied samples were prepared as settling slides.

One lithologic unit (Erbacher et al., 2004) was distinguished in the considered stratigraphic interval (Unit 4; Figure 4.1.3.2). Unit 4 consists of black, finely laminated claystone with organic matter to olive-gray laminated clayey limestone and clayey chalk with nannofossil, and extends from cores 207-1261A-41R through 50R. Unit 4 shows cyclic alternations of centimeter to decimeter scale of laminated claystone and laminated nannofossil chalk and limestone (Erbacher et al., 2004).

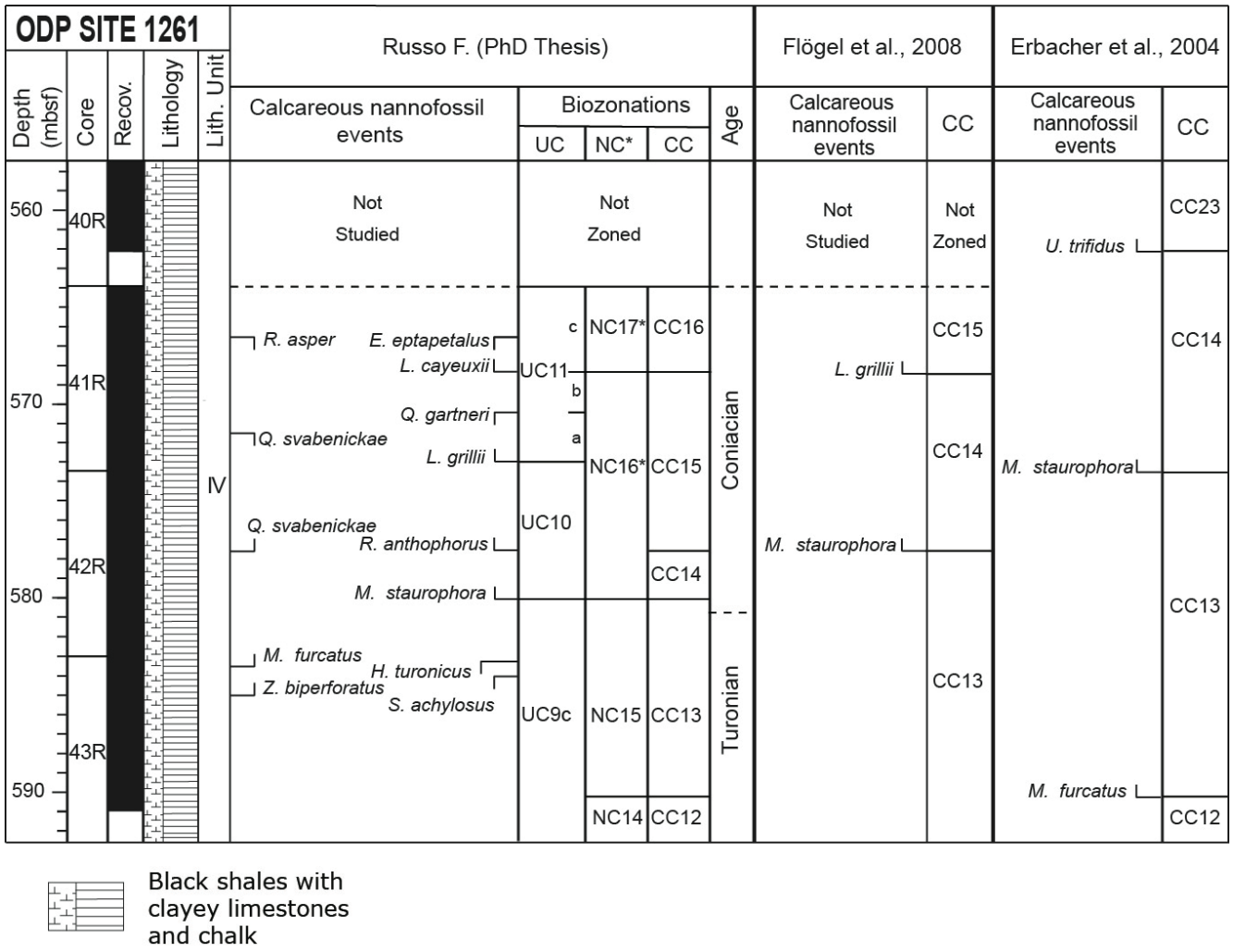

Figure 4.1.3.2 - Litho-biostratigraphic summary Site ODP 1261. Lithostratigraphy and core recovery are from (Erbacher et al., 2004). Calcareous nannofossil biozonation are according to Erbacher et al. (2004), Flögel et al. (2008) and Russo (2014).

Previous studies of calcareous nannofossils were included in the Proceedings of the Ocean Drilling Program (Erbacher et al., 2004). The nannofossil record highlighted the presence of a gap in the upper part. In fact, core 207-1261A-40R was assigned to the Late Campanian-Early Maastrichtian due to the identification of the CC23 Zone of Sissingh (1977). Whereas, the interval from cores 207-1261A-41R through 43R corresponds to nannofossil zones CC14/CC13 and CC12 of Sissingh (1977), and a Coniacian-Turonian age was derived (Figure 4.1.4.2). A biostratigraphic revision of the interval (cores 207-1261A-41R to 43R) was carried out by Flögel et al. (2008). The studied interval includes nannofossil zones CC15 to CC13 of Sissingh (1977), according to the FOs of *L. grillii, M. staurophora* and *M. furcatus,* respectively (Figure 2.1.3.2).
Russo (2014, PhD Thesis) recognized five bioevents within the interval from Cores 207-1261A-41R to 43R (Figure 2.1.3.2), allowing the identification of the CC16-CC12 zones of Sissingh (1977), NC17*-NC14* zones of Bralower et al. (1995) and UC9c to UC11c zones of Burnett (1998). These events are the FOs of *L. cayeuxii*, *L. grillii*, *R. anthophorus*, *M. staurophora* and *M. furcatus*.

4.1.4 Bottaccione section.

The following description is taken from the paper by Miniati et al. (2020) reported in Appendix 17. The Bottaccione section, located near the city of Gubbio in central Italy (coordinates: 43°21'56.05" N, 12°34'57.56" E; Fig. 4.1.4.1), consists of a continuous Jurassic to Paleocene pelagic sequence deposited in the Umbria-Marche Basin (central-western Tethys).

The portion of the Bottaccione section investigated here is entirely comprised in the Scaglia Rossa Formation and is exposed in the Bottaccione Gorge. The Scaglia Rossa Formation spans from the lower Turonian to the middle Eocene (e.g., Arthur and Fischer, 1977; Cresta et al., 1989) and consists of pink to red pelagic limestone that is a lithified nannofossil-planktonic foraminiferal ooze, sedimented at some 1500 m paleodepth (Arthur and Premoli Silva, 1982). Bedding thickness ranges from 10 to 30 cm with common stylolites in the thicker beds. The Cretaceous Scaglia Rossa is divided in two members, the lower R1 member (Turonian- lower Campanian) is characterized by chert nodules and layers and the upper R2 member (lower Campanian-Maastrichtian) is predominantly made of pink to red-brown limestone without chert (Alvarez and Montanari, 1988). The Bottaccione sequence represents a reference section used also in the Geologic Time Scale (GTS2012, Gradstein et al., 2012) for the Late Cretaceous.
<u>*Sampling*</u>: A total of 45 samples were analyzed from the Bottaccione section as simple smear slides that were studied for the biostratigraphic revision of the Santonian/Campanian boundary (Miniati et al., 2020; Appendix 17). The sampling resolution was of a sample every 0.50 cm, that was increased to 0.10

cm across the boundary (220 m and 221 m).

Figure 4.1.4.1 - A) Location of the Bottaccione section. B) Schematic picture of the outcrop. The dashed lines indicate the position of the stage boundaries along the succession, the Santonian/Campanian boundary is in red (modified after Coccioni and Premoli Silva, 2015). C) Photograph of the outcrop across the C34n/C33r magnetostratigraphic boundary at 221.525 ± 0.075 m (after Maron and Muttoni, accepted).

Calcareous nannofossil assemblages of the Cretaceous of the Bottaccione section were investigated in the 60s and 70s (Mohler, 1966; Monechi and Pirini, 1975; Monechi, 1977). Monechi and Thierstein (1985) established a first nannofossil biostratigraphy of the upper Campanian - lower Eocene interval of the Bottaccione section calibrated with planktonic foraminifera (Premoli Silva, 1977; Napoleone et al., 1983) and magnetostratigraphy (Alvarez et al., 1977). Gardin et al. (2001) revised and implemented the biostratigraphy of the Santonian - Maastrichtian interval and Tremolada (2002) focused on the upper Albian - lowermost Campanian interval, in both cases investigating the samples previously used for planktonic foraminiferal studies by Premoli Silva and Sliter (1995).

4.1.5 Seaford Head.

The Seaford Head section is exposed along the costal cliffs between Brighton and Eastbourne in the East Sussex (United Kingdom). The succession consists of Upper Turonian-Lower Campanian white nannofossil chalks that lie on an asymmetric anticline that dips at approximately 15° to the west (Figure 4.1.5.1). The Seaford Head section has been divided in various formations and members (Mortimore,1986; Figure 4.1.5.2).

At the base of the succession there is the Lewes Nodular Chalk composed of hard to very hard nodular chalk and hardgrounds with interbedded soft to medium hard chalk and marlstone.

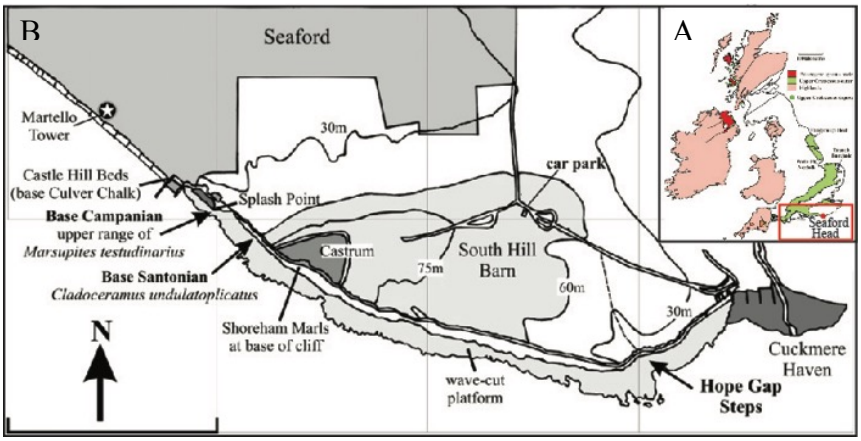

Figure 4.1.5.1 - A: Map showing the position of Seaford Head, Sussex, on the south coast of England. B: Map of Seaford Head indicating the position of the stage boundaries. (modified after Hampton et al., 2007).

The Shoreham Marl 2 marks the base of the overlying Seaford Chalk composed of white chalk, with semi-continuous nodular and tabular flint.

The Seaford Chalk is followed by the Newhaven Chalk Formation consisting of white chalk with numerous marl seams and flint bands. At the top of the succession there is the Culver Chalk Formation composed of white chalk, relatively marl-free with flint seams. A detailed lithostratigraphy highlights the presence of a large number of marker-beds, mostly corresponding to marly chalk beds, flint layers and fossil-rich beds (Mortimore, 1986, Mortimore et al., 2001). These marker beds are not restricted to Seaford Head but are widely used throughout the Anglo-Paris Basin (Mortimore and Pomerol,1987; Bristow et al., 1997).

Sampling: A total of 82 samples were analyzed for calcareous nannofossil biostratigraphy and quantitative analyses. These were collected from the base of the section (Lewes Nodular Chalk) up to 162 m (Culver Chalk). The applied sampling resolution was of 1 sample every 2 m. All samples were prepared following the method of Thibault and Gardin (2006).

Previous biostratigraphic studies of the Seaford head section include calcitic macrofossil (Mortimore, 1986; Thibault et al., 2016a), calcareous nannofossil and foraminifera (mostly benthic; Hampton et al., 2007). Inoceramid bivalves are relatively abundant and some of them are age-diagnostic, as the FO of C*ladoceramus undulatolplicatus* (Michel Dean Flint), index fossil for the Santonian. An integrated study of foraminifera and calcareous nannofossils was presented by Hampton et al. (2007). The calcareous nannofossil biostratigraphy followed the biozonation of Burnett (1998) as modified by Fritsen et al. (2000). The analyzed sequence includes the basal Seaford Chalk Formation (Belle Tout Beds) up to the

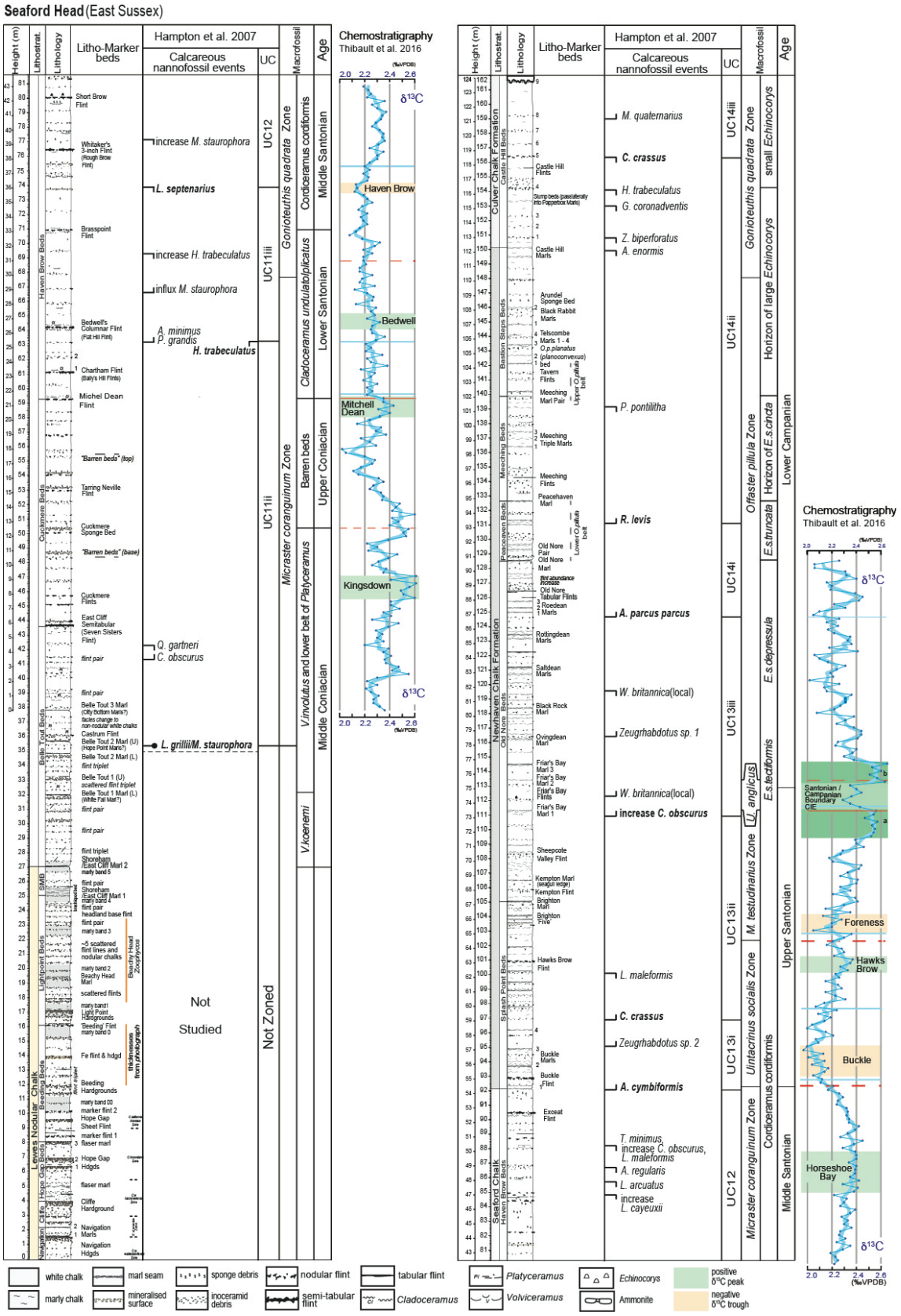

Figure 4.1.5.2 - Detailed log of the Seaford Head section. Lithostratigraphy is after Mortimore (1986) and Mortimore et al. (2001). Calcareous nannofossil biozonation is according to Hampton et al. (2007). Macrofossil biostratigraphy is after Mortimore (1986). Bulk carbonate carbon isotopes after Thibault et al. (2016a).

Culver Chalk. In this interval, the nannofossil zones UC11ii to UC14 were recognized of Middle Coniacian-Early Campanian age (Hampton et al., 2007; Figure 4.1.5.2). In particular, the following calcareous nannofossil events were used by Hampton et al. (2007): the presence of *L. grillii* and *M. staurophora* at the base of the studied interval, the LO of *H. trabeculatus*, the LO *L. septenarius*, FO *A. cymbiformis*, FO *C. crassus*, increase of *C. obscurus*, FO *A. parcus parcus*, FO *R. levis*, LO *C. crassus*. In addition to these events, Hampton et al. (2007) report the presence of several secondary events including changes in relative abundance of some taxa. An increase of *M. staurophora* was observed between the UC11iii and the UC12 zones, as well as an increase of *C. obscurus* between the UC13iii and the UC14i zones (Figure 4.1.5.2). The Seaford Head section represents one of the reference sections for stable isotope curves based on the English Chalk record. Analyses of bulk oxygen and carbon stable isotopes provided a high-resolution record with the definition of many positive and negative anomalies useful for global correlations (Jenkyns et al., 1994; Jarvis et al., 2006; Thibault et al., 2016a; Figure 4.1.5.2). Due to its biostratigraphic and chemostratigraphic record, the Seaford Head section was previously considered as a potential candidate for the GSSP for the Coniacian/Santonian and the Santonian/Campanian boundaries (Hancock and Gale,1996; Lamolda and Hancock,1996).

4.1.6 Tanzania TDP39.

The Tanzania Drilling Project (TDP) Site 39 was drilled in southeastern Tanzania between Kilwa and Lindi (Figure 4.1.6.1). Here, Upper Cretaceous marine successions deposited in the Mandawa and Ruvuma Basins are exposed (Salam and Abdula,1995). A total of 40 cores were recovered at TDP39 with a total length of cored section of 101 meter-thick (Jiménez Berrocoso et al., 2015).

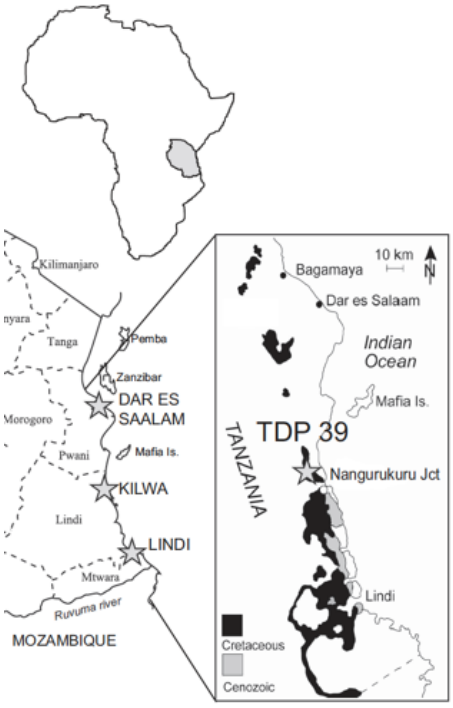

Figure 4.1.6.1 - Location of the Tanzania Drilling Project (TDP) 39 in south east costal Tanzania. (Petrizzo et al., 2017).

Sampling: A total of 53 samples were exanimated for both calcareous nannofossil biostratigraphy and quantitative analyses. Samples were collected through the whole TDP39 succession with a sampling resolution of 1 sample every 2 m and prepared as settling slides.

The penetrated sequence includes Coniacian–Santonian sediments of moderate to high completeness. The interval between Cores 40 to 30 belongs to the Lindi Formation, composed of dark gray, lithified, silty claystone with common thin laminations. A gradational contact in Cores 30 to 29 marks the transition between the Lindi Formation and the overlying Nangurukuru Formation.
The overlying interval (Cores 29 to 1) is mainly composed of light gray, mostly massive, calcareous, clayey siltstones of the Nangurukuru Formation. Cores 14to 21 and 24 to 28 show cm-thick, dark gray, possibly clay-rich, intervals with abundant bioturbation (Chondrites) alternating with cm-thick, lighter gray intervals with rare bioturbation. These alternating intervals was interpreted as possible result of changes in redox condition near the sediment–seawater interface associated with Ocean Anoxic Event 3 (Jiménez Berrocoso et al., 2015).
The TDP 39 succession was interpreted as deposited in an outer shelf to upper slope environment below the storm-wave base, due to the presence of common planktonic microfossils and rare ammonites and bivalves that would indicate a more open-ocean condition.
Cretaceous nannofossil biostratigraphy was presented by Jiménez Berrocoso et al. (2015). The stratigraphic succession of TDP39 Core spans from the UC10 Zone (middle-late Coniacian) to the UC12 Zone (early Santonian) of Burnett (1998) based on the presence of *M. staurophora* from the base of the section, FO of *L. grillii* at 53.05m and LO *L. septenarius* at 21.05m (Figure 4.1.6.2).

A detailed description of the TDP 39 planktonic foraminiferal assemblages together with a bulk stable isotope record was given by Petrizzo et al. (2017). The $\delta^{13}C$ values range from -2.43‰ to 1.70 ‰ with various positive and the negative oscillations of 1 to 2 ‰ (Figure 4.1.6.2). These changes were interpreted as mainly driven by local factors, such as sources of dissolved inorganic carbon of the water in which biogenic carbonate precipitated, and/or remineralization of organic matter and diagenetic changes in the sediment column (Petrizzo et al., 2017). For this reason, the identification of the Micheal Dean and Kingsdow positive shifts at 22m and 65m remain questionable (Figure 4.1.6.2).

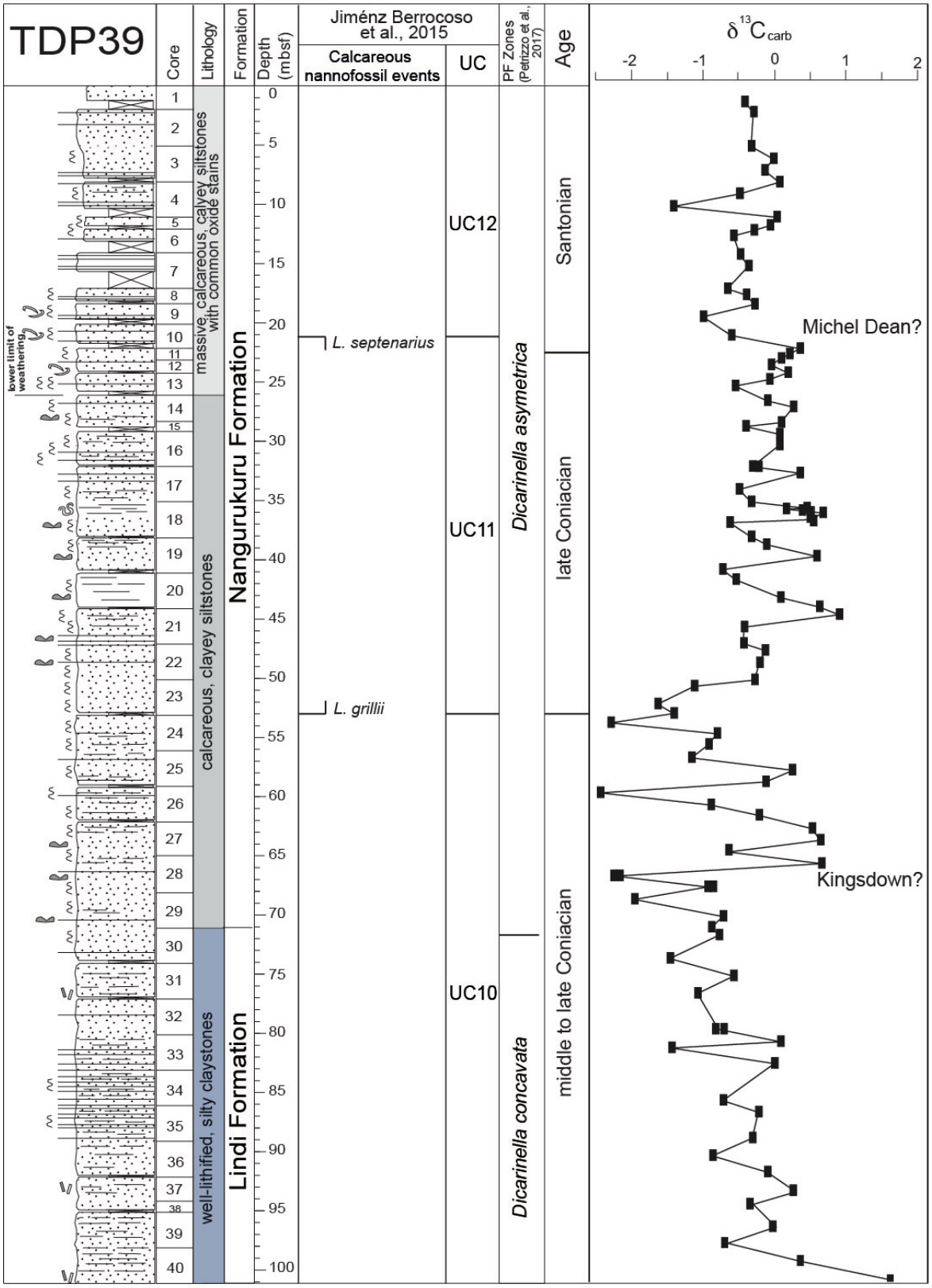

Figure 4.1.6.2 - Detailed log of the TDP39 section/core. Lithostratigraphy and chemostratigraphy after Petrizzo et al. (2017). Calcareous nannofossil biozonation is according to Jiménez-Berrocoso et al. (2015).

4.1.7 ODP Site 763.

ODP Site 763 was drilled on the western part of the central Exmouth Plateau off NW Australia in the eastern Indian Ocean (20°35'S, 112°12'E) at present water depth of 1367 m (Figure 4.1.7.1).

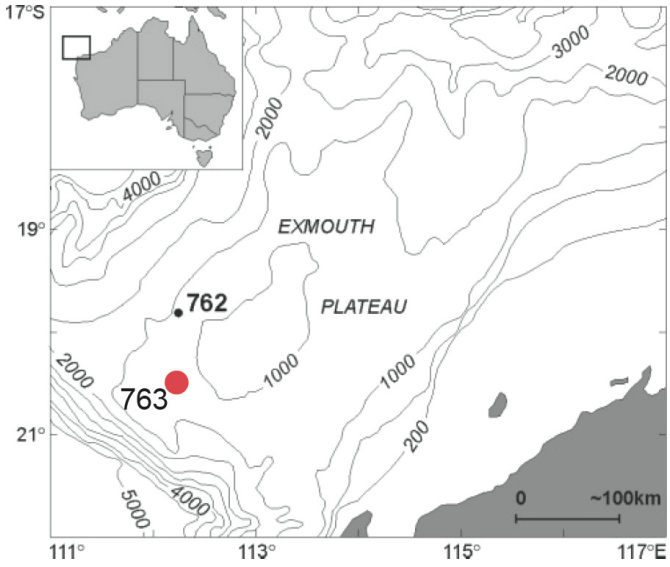

Figure 4.1.7.1 - Location of ODP Site 763. (modified after Exon et al., 1992).

A total of three holes were drilled at ODP Site 763: 21 cores were drilled in Hole A, 54 cores in Hole B and 46 cores in Hole with a recovery rate of about 80 %. The penetrated sequences extend in age from the Quaternary to early Berriasian-Tithonian (Haq et al., 1992).

Sampling: A total of 92 samples from Hole 763A were examined for calcareous nannofossil quantitative analyses, collected with a resolution of 1 sample about every 0.5 m. The considered interval spans from the Turonian to the Campanian (Russo, 2014) and includes Cores 122-763B-14X to 21X (Figure 4.1.7.2). All the studied samples were prepared as simple smear slides.

Two lithologic subunits were recognized in the studied stratigraphic interval (Subunit IIIB and IIIC; Figure 4.1.7.2). The upper Subunit IIIB consists of green-gray to light green-gray foraminifer-nannofossil chalk, the underlying Subunit IIIC consists of gray-green and green-gray color-banded nannofossil chalk with clay. The contact between Subunits IIIB and IIIC at 353.0 mbsf corresponds approximately to a condensed interval or a hiatus (Haq et al., 1992; Bralower and Sissier, 1992).

Previous studies on calcareous nannofossil assemblages at ODP Site 763 were published by Bralower and Sissier (1992). The biozonations applied to the Upper Cretaceous interval od Hole ODP 763A were those of Sissingh (1977) and Roth (1978). The interval from cores 122-763B-14X to 21X includes nannofossil zones CC18 to CC12 and NC18 to NC14 Zones, according to the FOs of *M. furcatus*, *M. staurophora*, *L. grilli*, *L. cayeuxii* and *A. parcus parcus* (Figure 4.1.7.2).

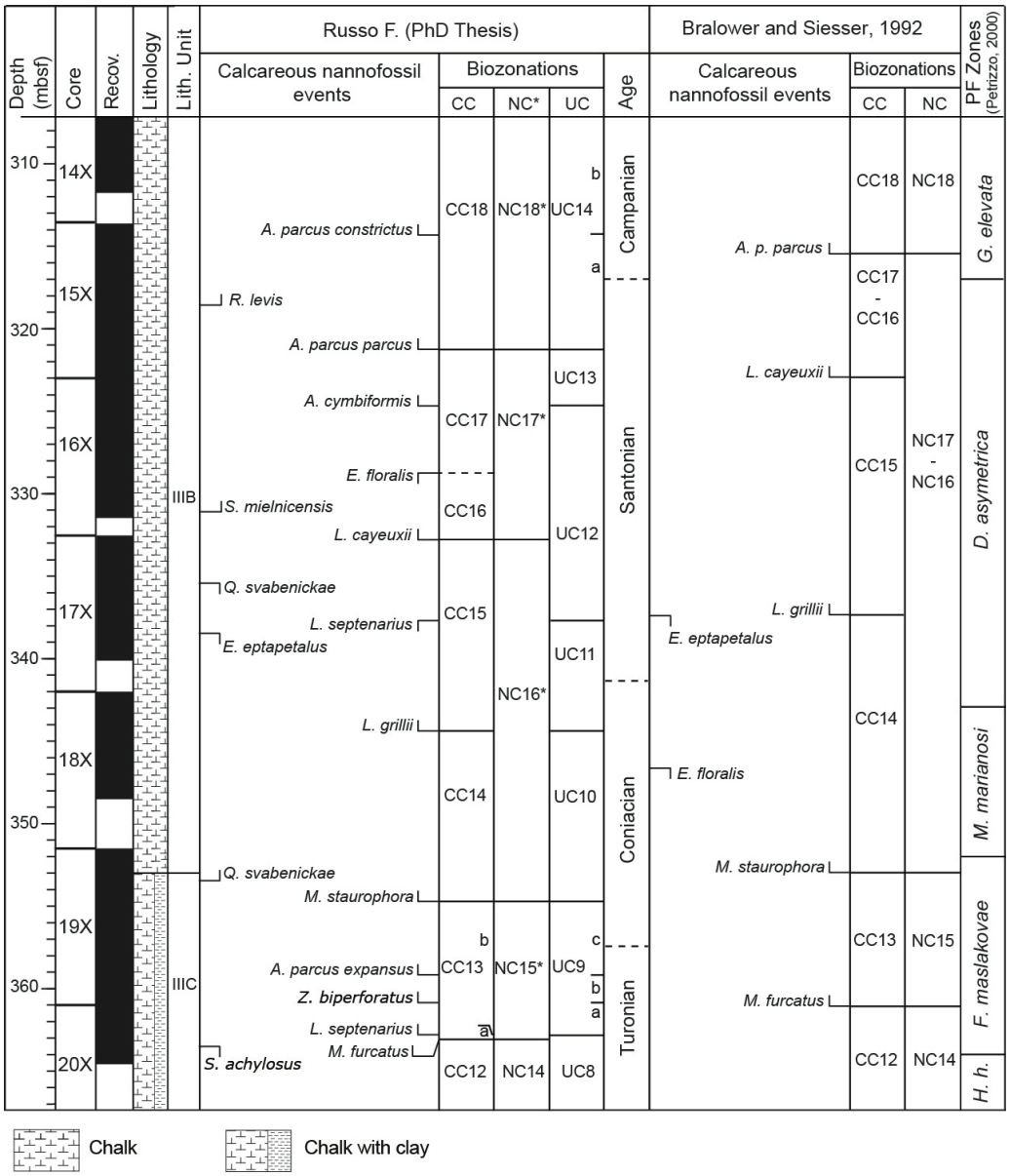

Figure 4.1.7.2 - Litho-biostratigraphic summary of ODP Site 763. Lithostratigraphy and core recovery are from Haq et al. (1992). Calcareous nannofossil biozonation reported according to Bralower and Sissier (1992) and Russo (2014).

A biostratigraphic revision of the investigated interval (cores 122-763B-14X to 21X) was carried out by Russo (2014, PhD Thesis), that refined the position of the events previously detected by Bralower and Sissier (1992) and added four new events (Figure 4.1.7.2). These last are the FOs of *L. septenarius*, *A. parcus expansus* and *A. parcus constrictus* and the LO of *L. septenarius*. According to Russo (2014) the CC18-CC12 zones of Sissingh (1977), NC18*-NC14 zones of Bralower et al. (1995) and UC8 to UC14b zones of Burnett (1998) were identified.

A summary of the analyzed sections is given in Figure 4.1.8.

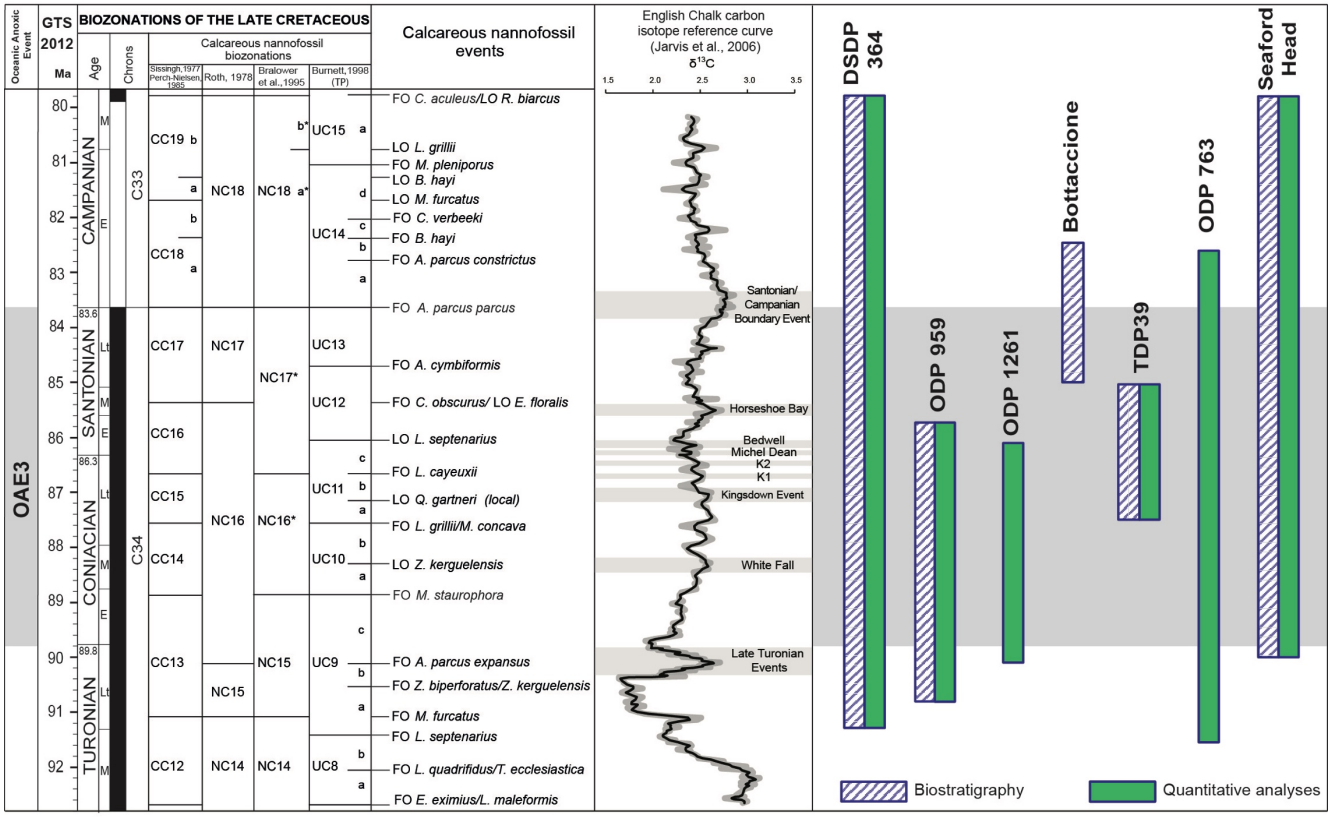

Figure 4.1.8 - Summary of the stratigraphic intervals studied in individual sections/cores.

4.2 Sample preparation techniques.

Most samples were prepared in the Micropaleontology Lab. of the Earth Sciences Department of the University of Milan, with the only exception of samples from the Seaford Head section that were processed at the Earth Sciences Department Labs of the University of Copenhagen. The rock samples were prepared for calcareous nannofossil analyses following the preparation techniques described below.

Simple smear slide (Monechi and Thierstein 1985):

a) A small amount of rock material was powdered in the agate mortar with bi-distillate water. b) Few drops of suspension was pipette up and put it on a cover slide. c) The suspension was smeared thinly across the surface of the coverslip with a toothpick and dried rapidly on a hotplate. d) The slide was covered with a cover slide, affixed with Norland Optical Adhesive and fixed for 1 minute under UV lamp.

Settling boxes (Geisen et al.,1999):

This method has the advantage to obtain a homogenous distribution of sediment on the glass slide and to gather absolute abundances since the quantity of sediment used in the procedure is known.
a) A small amount of rock is powdered in an agate mortar and weighed (ca. 0.10 to 100 mg depending on lithology and nannofossil content) using a microbalance. b) Ammoniac water is prepared using the following proportion: 0.5 ml NH3 5 % is added to 10l of demineralized water and 0.2 ml of Triton x100. The pH of the solution has to be close to 8.5.c) The vial containing the sample is half filled with ammoniac water and shaked. d) The vial goes through an ultrasonic bath for 10 seconds until all particles are in suspension. e) The suspended sample is transferred to a volumetric flask and diluted to 500 ml with ammoniac water. f) When the suspension is homogenized by ca. four inversion of the flask the content is tipped into the settling box (500 ml). g) Rapidly two glass cover slides are placed on the cylinders using a pinzette. h). They are let to settle for 24 hours and then the water is release slowly (single drops). i) When the cover slides are dry, they are mounted on a glass slides and fixed with Norland Optical Adhesive.

Samples enriched in organic matter were treated with a combined method which integrates the procedure by Shamrock et al. (2015) with the random settling technique. These samples are characterized by a high clay content, opaque mineral such as pyrite and marine-derived amorphous organic matter (AOM) which obscure individual nannofossil specimens and cause aggregations of nannofossils and background sediments.
Drop technique (Thibault and Gardin, 2006):
a) Sediments were disaggregated and 50 mg of dried sediment were weighed and suspended in 50 ml of distilled water (milliQ). b) The suspension was agitated with a magnetic stirrer for homogenization. c) a dry cover slip was weighed (0.1 mg). d) 0.75 ml of the suspension was extracted with a micropipette and dropped on a cover slip to completely cover it and paying attention to the homogeneity of smearing. d) The cover slip was weighed again to calculate the weight of the sediments obtained subtracting the weight of the dry empty cover slip to the weight after preparation.

4.3 Semiquantitative biostratigraphy.

Biostratigraphic investigations were conducted following the zonations of Sissingh (1977) as modified by Perch-Nielsen (1985), Roth (1978), Bralower et al. (1995) and Burnett (1998), therefore applying the CC, NC, NC* and UC codes, respectively. Calcareous nannofossil semiquantitative abundances were

coded as follows, after inspection of at least 6 traverses in each smear slide using a polarizing microscope at 1250X magnification.

Total abundance: Abundant (A) = 21-30 specimens in each field of view; Common (C) = 11-20 specimens in each field of view; Few (F)= 6-10 specimens in each field of view; Rare (R) = 1-5 specimens in each field of view.

Species abundance: Abundant (A) = $\geq$ 1 specimen in each field of view; Common (C) = 1 specimen in 2-10 fields of view; Few (F) = 1 specimen in 11-30 fields of view; Rare (R) = 1 specimen in > 31 fields of view.

Due to dissolution and/or overgrowth, preservation of calcareous nannofossils may vary significantly. Preservation was characterized as follows:

Good (G) if nannofossil specimens show little or no evidence of dissolution and/or overgrowth and the primary morphological characters are only slightly altered allowing species identification; moderate (M) if specimens exhibit some etching and/or overgrowth, primary morphological characters are somewhat altered allowing, however, identification at the species level; poor (P) if specimens show severe etching and/or overgrowth, primary morphological characters are obliterated, hampering identification at the species and/or even generic level.

4.4. Quantitative abundances.

The quantitative analyses were performed counting at least 300 nannofossil specimens in each slide. The following data were acquired:

Relative abundance: expressed as the percentage of the single taxon on the total nannoflora.

Absolute abundance: The total and single taxon absolute abundances are obtained from slides prepared with the settling and the drop technique and are expressed as the number of nannofossils/1 gram of sediment. The absolute abundance was calculated according to the equation of Bollmann et al. (1999):

$X = (N * V) / (M * F * A * H)$

Where X = number of coccoliths/g; N = number of coccoliths counted; V = volume of water used for dilution (500 ml); M = grams of sediment (g); F = fields of view inspected; A = surface area of one field of view; height of water column above slide (2 cm).

The diversity of calcareous nannofossil assemblages is quantified using the species richness and the Shannon Index (Shannon and Weaver, 1949). The term **species richness** is referred to the number of taxa counted in each sample.

The **Shannon index** (Shannon and Weaver, 1949) represents a diversity measurement that takes into account the number of taxa (species richness) as well as the number of individuals (heterogeneity). Highly diverse assemblages are characterized by high values of Shannon index whereas assemblages dominated by only one species have an index of 0.

The Shannon index is calculated as follow:

$$H = -\sum_{i=1}^{s} pi * lnpi$$

where H= Shannon–Wiener Diversity; s= number of species; p= proportion (n/N) of individuals of a species (n) found divided by the total number of individuals found (N).

4.5. Paleoecological indicies of Temperature and Fertility.

In this study, the temperature (TI) and a nutrient (NI) indices were calculated following the equations proposed by Bottini et al. (2015). The TI formula includes the cooler-water temperature taxa *R. parvimentatum*, *S. stradneri* and *E. floralis* and warmer-water taxa *R. asper* and *Z. diplogrammus*. However, the absence in the studied sections of *R. parvimentatum* and *S. laffittei* together with the stratigraphic distribution of *E. floralis* limit the application of the temperature index (TI) of Bottini et al. (2015). In fact, *E. floralis* becomes extinct in the middle Santonian (base of CC17 and NC17 zones) and, consequently this cool-water indicator can be used only in its stratigraphic range. According to the paleoecological affinity of nannofossil taxa the TI of Bottini et al. (2015) was modified in various ways. The second version (V.2) of the TI includes *G. segmentatum* but not *E. floralis* as cool water taxon, whereas a third version (V.3) of the TI includes *G. segmentatum* and *A. octoradiata* with both of them considered to have a cool water affinities. The last version (V.4) of the TI includes only *A. octoradiata* as cool water taxa indicator.

In this study, the TI will be therefore calculated according to the following equations:

$$\text{TI (Bottini et al., 2015)} = \frac{R.parvimentatum+S.laffittei+E.floralis}{R.parvimentatum+S.stradneri+E.floralis+R.asper+Z.diplogrammus} * 100$$

$$\text{TI (V.2)} = \frac{G.segmentatum}{G.segmentatum+R.asper+Z.diplogrammus} * 100$$

$$\text{TI (V.3)} = \frac{G.\ \text{segmentatum}+\text{A. octoradiata}}{\text{G.segmentatum+A.octoradiata+R.asper+Z.diplogrammus}} * 100$$

$$\text{TI (V.4)} = \frac{A.\ octoradiata}{A.\ octoradiata+R.asper+Z.diplogrammus} * 100$$

The NI equation is based on the higher fertility taxa *B. constans, D. ignotus* and *Z. erectus* and lower-fertility indicator *W. barnesiae*. In this study, the NI will be calculated according to Bottini et al. (2015):

$$\text{NI} = \frac{B.constans+D.ignotus+Z.erectus}{B.constans+D.ignotus+Z.erectus+W.barnesiae} * 100$$

4.6. Statistical analyses.

The quantitative data will be statistically characterized considering both the distribution of genera and species. The following parameter will be evaluated: average, minimum value, maximum value, mode, standard deviation and median.

The degree of correlation between the different genera and species will be evaluated for each section in terms of Pearson's correlation coefficients that measure the linear relationship between two data points. The Pearson's correlation (r) has a value of r = +1 with a perfect positive correlation, r = -1 with a perfect negative correlation and r = 0 when there is no linear relationship between the two variables.

Chapter 5
Results.

5.1 DSDP Site 364

5.1.1 Biostratigraphy

Calcareous nannofossils in the studied interval are abundant, with preservation that varies from good to moderate. Only cores 364-18R and 364-19R are characterized by poorly preserved assemblages.

A total of fifteen events were detected, allowing the identification, of the CC11-CC21 Zones of Sissingh (1977), NC14-NC19 Zones of Roth (1978), NC14-NC19* Zones of Bralower et al. (1995) and UC7-UC15c Zones of Burnett (1998). The results are presented in Figure 5.1.1 and the zonal and subzonal markers identified in this study are described below from the oldest to the youngest. A range chart for Site 364 is provided in the Appendix 5.

At the base of the studied succession, the presence of biostratigraphic index taxa as *Q. gartneri* and *K. magnificus* (sample 40-364-23R-4, 52-54; 649.02 mbsf) and the lack of *E. eximius* indicate the CC11, NC14 and UC7 zones. The FO of *E. eximius* in sample 40-364-23R,57-59 (646.07 mbsf) defines the base of zones CC12 and UC8. Both the FOs of *M. furcatus* and *L. septenarius* were observed in the same sample 40-364-22R-4, 77-80 (620.77 mbsf). These events define the base of CC13, NC15 and NC15* zones, whereas the base of the UC9 zone is undetermined (Figure 5.1.1). The FO of small *A. parcus expansus* in sample 40-364-22R-2, 24-27 (617.24 mbsf) marks the base of the NC15 and UC9c zone and subzone, respectively. The FO of *M. staurophora* in sample 40-364-21R-3, 121-125 (600.86 mbsf) defines the base of CC15 and UC11 zones. The FO of *L. grillii* was observed close to that of *M. concava* in samples 40-364-20R-4, 91-94 (582.91 mbsf) and 40-364-20R-4,7-10 (582.07 mbsf), respectively. The FO of *L. grillii* in sample 40-364-20R-4, 91-94 (582.91 mbsf) defines the base of zones CC15 and UC11. The LO of *L. septenarius*, in sample 40-364-19R-4, 130-132 (573,8 mbsf) allowed the identification of the UC12 zone. The LO of *E. floralis* was found in sample 40-364-20R-2, 43-46 (579.43 mbsf), but Proto Decima et al. (1974) documented the LO of *E. floralis* at a higher stratigraphic level (sample 40-364-19R-3, 33-34; 571.33 mbsf). Therefore, this last datum was considered in the synthesis scheme (Figure 5.1.1) to define zones CC17 and NC17. The FO of *A. cymbiformis* was observed in sample 40-364-17R-6, 48-51 (538.43 mbsf) where the base of the UC13 zone was placed. The FO of *A. parcus parcus* was observed in sample 40-364-16R-6, 107-112 (510.07 mbsf). However, Proto Decima et al. (1974) reported the occurrence of *A. parcus parcus* from the lowermost sample in core 40-364-16R

(364-16R, CC; 510,5 mbsf), thus this last datum was used in the synthesis scheme to define the CC18, NC18, NC18* and UC14 zones.

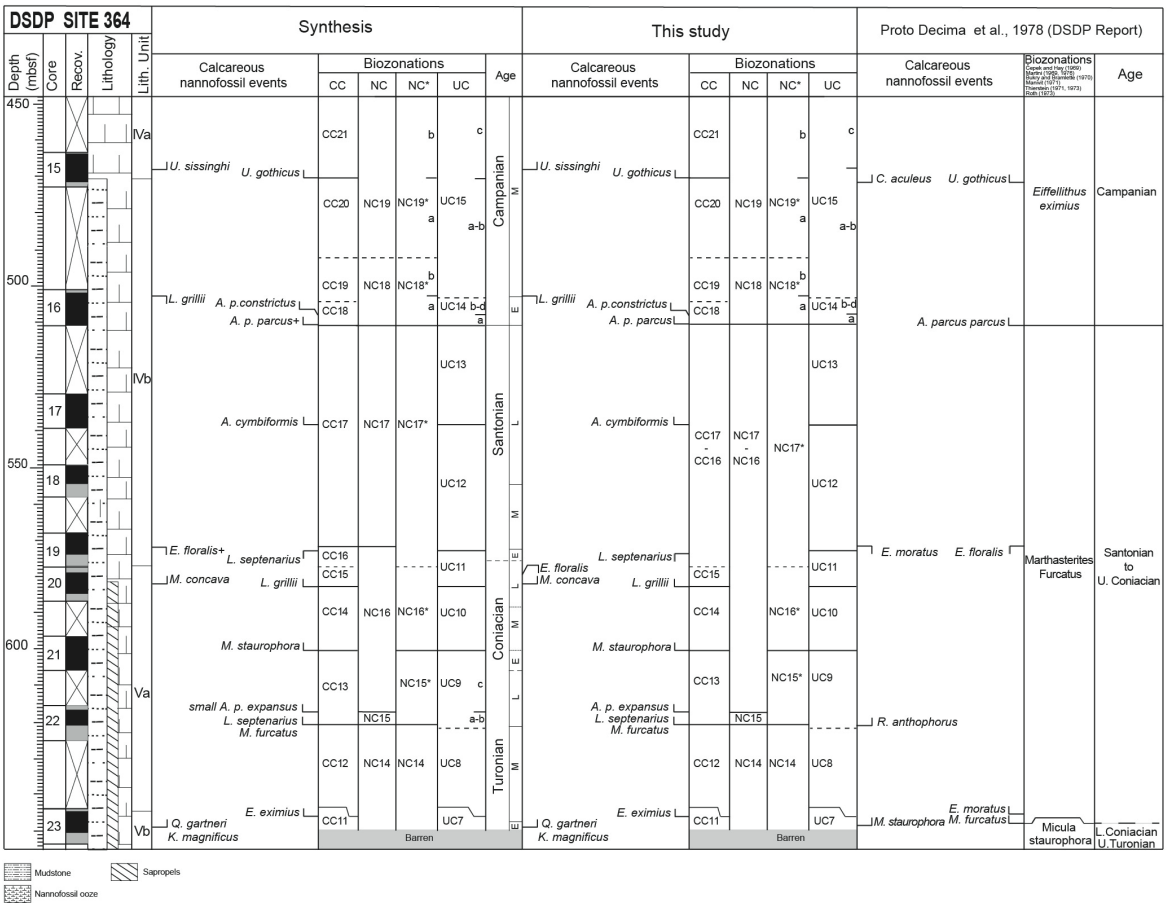

Figure 5.1.1 - DSDP Leg 40 Site 364 calcareous nannofossil biostratigraphy (this study) and comparison with previous data (Proto Decima et al., 1974). Biostratigraphic zonation: CC (Sissingh, 1977), NC (Roth,1978), NC* (Bralower 1995), and UC (Burnett 1998) are shown. The synthesis column is based on integration of data gathered in this study with those from the literature. Data from literature used for zonation in marked with asterisk (+).

The FO of *A. parcus constrictus* in sample 40-364-16R-5, 99-102; (508.49 mbsf) marks the base of the UC14b subzone. The base of zones CC20, NC19 and NC19* was not constrained (FO of *C. aculeus* and LO of *C. biarcus* not identified), whereas the FO of *U. gothicus* and *U. sissinghi* define the base of CC21, NC19b zones and the base of UC15c subzone, respectively.

According to the calcareous nannofossil biostratigraphy obtained with this study, integrated with data from Proto Decima et al. (1974), the following stage boundaries were placed:

- the Turonian/Coniacian boundary between the FO of small *A. p. expansus* and the FO of *M. staurophora*;
- the Coniacian/Santonian boundary was placed between the FO of *L. grillii* and the LO of *L. septenarius* in the upper part of the UC11 zone;

- the Santonian/Campanian boundary at the FO of *A. parcus parcus* (see discussion in Miniati et al., 2020).

5.1.2 Nannofossil paleoecology and paleoceanography

At DSDP Site 364 a total of 76 taxa were recognized. Three intervals with barren samples are present respectively in Core 40-464-23R-4 and in samples 40-364-23R-3, 137-139 (619.87 mbsf) and 40-364-21R-5, 76-78 (603.41 mbsf). The species richness of individual samples varies from a maximum of 34 (sample 40-364-20R-4, 7-10; 582.07 mbsf) to 9 (sample 40-364-21R-3, 121-125; 600.86 mbsf) with a mean of 21 species for sample (Figure 5.1.2.1). The higher values were detected in the lower Turonian (up to 33 in sample 40-364-23R-4,52-54 – 649.02 mbsf) and in the upper Turonian-Coniacian with average of 22.8 from sample 40-364-22R-1,139-141 (616.89 mbsf) to sample 40-364-19R-4,130-132 (573.8 mbsf).

The Shannon index (Figure 5.1.2.1) fluctuates around the average value of 1.8 without any significant trend. It ranges between 1 (sample 40-364-21R-3, 121-125; 600.86 mbsf) and 2.8 (sample 40-364-23R-3, 26-26; 647.26 mbsf), suggesting moderately to well diversified assemblages.

The total nannofossil abundance (number of specimens/field of view) has an average of 36. The higher values - up to 113 - are present in the lower Turonian (sample 40-364-23R-4,52-54; 649.02 mbsf) and upper Turonian-Coniacian (average of 40.7) from sample 40-364-22R-1,139-141 (616.89 mbsf) to sample 40-364-19R-4,130-132 (573.8 mbsf). The absolute abundance of calcareous nannofossils shows a similar pattern, with an average of 3.54 X 10^9 specimens/g. It ranges from a maximum of 11 X 10^9 specimens/g in the lower Turonian (sample 40-364-23R-4,52-54; 649.02 mbsf) to a minimum of 1.08 X 10^9 specimens/g in the upper Coniacian (sample 40-364-20R-3,70-74; 581.2 mbsf).

The presence of moderately to well diversified assemblages suggests that the distribution and abundance of calcareous nannofossils mainly reflect the primary ecological signal with negligible diagenetic modifications.

The descriptive statistics of calcareous nannofossil genera and species are synthesized in Tables 5.1.2.1 and 5.1.2.2. At DSDP Site 364, five genera show an average relative abundance > 3% (*Micula, Prediscosphaera, Retecapsa, Watznaueria, Zegrhabdotus*) and two genera are characterized by average relative abundance > 2% (*Eiffellithus, Marthasterites*). Genera with average relative abundance < 2% are not discussed here but their descriptive statistics are show in Tables 5.1.2.1 and 5.1.2.2.. Figure 5.1.2.1illustrates the relative abundances of genera with an average > 1%. The dominant genus is *Watznaueria* which ranges from 0% to 74% (average 45.8%). As shown in Table 5.1.2.1. *W. barnesiae*

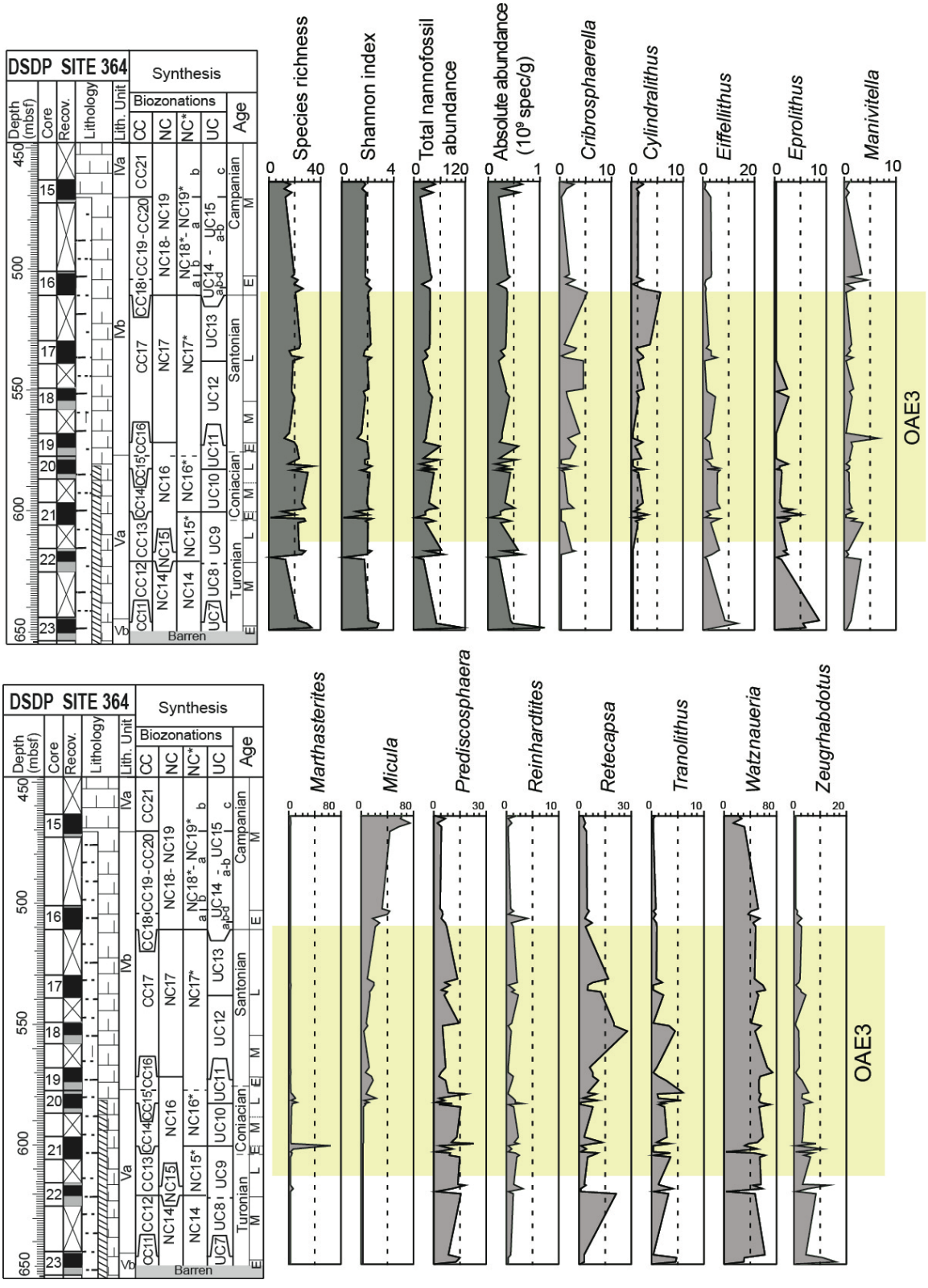

Figure 5.1.2.1 - Calcareous nannofossil data from DSPD Site 364 showing the fluctuations of species richness, Shannon index, total nannofossil abundances (n. of specimens/FOV) absolute abundances (n. of specimens/gram of sediment) and the relative abundances of genera with an average abundance >1%. The yellow band indicates the OAE3 interval.

GENUS	Average %	Minimum %	Maximum %	Mode	Standard Deviation	Median
Watznaueria	47.8	11.5	74.0	51.5	43.2	52.4
Micula	13.8	0.0	74.2	5.8	29.2	0
Prediscosphaera	7.6	0.0	22.6	6.0	31.2	2
Retecapsa	6.4	0.0	27.6	4.1	35.2	0
Zeugrhabdotus	3.3	0	15.9	2.4	44.2	0
Eiffellithus	2.8	0.0	13.2	2.4	13.2	0
Marthasterites	2.4	0.0	63.8	0.0	27.2	0
Tranolithus	1.5	0.0	5.9	0.8	41.2	0
Cribrosphaerella	1.3	0.0	5.2	1.0	9.2	0
Eprolithus	1.2	0.0	8.6	0.0	14.2	0
Cylindralithus	1.1	0.0	5.5	0.9	10.2	0
Manivitella	1.0	0.0	6.5	0.7	26.2	0
Reinhardtites	1.0	0.0	3.8	1.0	34.2	0
Lithastrinus	0.9	0.0	4.1	0.6	23.2	0
Chiastozygus	0.8	0.0	3.8	0.6	7.2	0
Uniplanarius	0.8	0.0	15.3	0.0	42.2	0
Rucinolithus	0.8	0.0	5.2	0.0	38.2	0
Microrhabdolus	0.7	0.0	3.1	0.6	28.2	0
Helicolithus	0.7	0.0	5.7	0.0	1.2	0
Biscutum	0.6	0.0	15.6	0.0	4.2	0
Rhagodiscus	0.6	0.0	3.0	0.0	36.2	0
Aspidolithus	0.5	0.0	4.8	0.0	3.2	0
Gartnerago	0.5	0.0	2.1	0.3	16.2	0
Lithraphidites	0.5	0.0	3.3	0.0	24.2	0
Stoverius	0.2	0.0	3.3	0.0	39.2	0
Flabellites	0.2	0.0	2.0	0.0	15.2	0
Quadrum	0.2	0.0	1.4	0.0	32.2	0
Radiolithus	0.1	0.0	1.4	0.0	33.2	0
Braarudosphaera	0.1	0.0	3.4	0.0	5.2	0
Ceratolithoides	0.1	0.0	2.0	0.0	8.2	0
Arkhangelskiella	0.1	0.0	1.0	0.0	2.2	0
Ahmuellerella	0.1	0.0	1.0	0.0	0.2	0
Loxolithus	0.1	0.0	1.7	0.0	25.2	0
Broinsonia	0.1	0.0	1.0	0.0	6.2	0
Amphizygus	0.05	0.0	0.7	0.0	1.2	0
Rotelapillus	0.04	0.0	1.5	0.0	37.2	0
Haqius	0.04	0.0	0.7	0.0	18.2	0
Tetrapodorhabdus	0.04	0.0	0.7	0.0	40.2	0
Corollithion	0.03	0.0	0.9	0.0	11.2	0
Kamptnerius	0.02	0.0	0.6	0.0	22.2	0
Placozygus	0.01	0.0	0.7	0.0	30.2	0
Discorhabdus	0.01	0.0	0.7	0.0	12.2	0
Grantarhabdus	0.01	0.0	0.5	0.0	17.2	0

Table 5.1.2.1 - Descriptive statistics of genera identified at DSDP Site 364.

SPECIES	Average %	Minimum %	Maximum %	Mode	Standard Deviation	Median
Ahmuellerella octoradiata	0.1	0.0	1.0	0.0	0.3	0
Amphizygus brooksii	0.05	0.0	0.7	0.0	0.2	0
Arkhangelskiella cymbiformis	0.1	0.0	1.0	0.0	0.3	0
Aspidolithus parcus constrictus	0.2	0.0	4.6	0.0	0.7	0
Aspidolithus parcus expansus	0.1	0.0	2.0	0.0	0.3	0
Aspidolithus parcus parcus	0.2	0.0	3.8	0.0	0.6	0
Biscutum constans	0.5	0.0	15.6	0.0	2.3	0
Braarudosphaera hockwoldensis	0.01	0.0	0.7	0.0	0.1	0
Braarudosphaera cf. B. bigelowii	0.02	0.0	1.0	0.0	0.1	0
Braarudosphaera turbinea	0.1	0.0	2.4	0.0	0.4	0
Broinsonia matalosa	0.1	0.0	1.0	0.0	0.2	0
Chiastozygus litterarius	0.8	0.0	3.8	0.5	1.0	0
Ceratolithoides veerbeki	0.1	0.0	1.4	0.0	0.3	0
Cribrosphaerella ehrenbergii	1.2	0.0	5.2	0.7	1.4	0
Cylindralithus biarcus	0.1	0.0	1.4	0.0	0.3	0
Cylindralithus nudus	0.7	0.0	5.5	0.0	1.0	0
Cylindralithus sculptus	0.2	0.0	2.8	0.0	0.5	0
Cylindralithus serratus	0.1	0.0	1.2	0.0	0.2	0
Corollithion signum	0.03	0.0	0.9	0.0	0.1	0
Discorhabdus ignotus	0.01	0.0	0.7	0.0	0.1	0
Eiffellithus eximius	0.9	0.0	4.9	0.5	1.2	0
Eiffellithus gorkae	0.3	0.0	2.1	0.0	0.6	0
Eiffellithus hancockii	0.0	0.0	1.0	0.0	0.1	0
Eiffellithus turriseiffelii	1.4	0.0	9.9	0.6	2.2	0
Eprolithus floralis	0.9	0.0	8.6	0.0	1.8	0
Eprolithus moratus	0.2	0.0	2.5	0.0	0.6	0
Flabellites oblongus	0.2	0.0	2.0	0.0	0.5	0
Gartnerago segmentatum	0.5	0.0	2.1	0.2	0.6	0
Grantarhabdus coronadventis	0.01	0.0	0.5	0.0	0.1	0
Haqius circumradiatus	0.04	0.0	0.7	0.0	0.1	0
Helicolithus anceps	0.5	0.0	5.7	0.0	1.1	0
Helicolithus trabeculatus	0.1	0.0	2.3	0.0	0.4	0
Kamptnerius magnificus	0.02	0.0	0.6	0.0	0.1	0
Lithastrinus grillii	0.5	0.0	4.1	0.0	0.9	0
Lithastrinus septenarius	0.3	0.0	3.2	0.0	0.8	0
Lithraphidites carniolensis	0.5	0.0	3.3	0.0	0.8	0
Loxolithus armilla	0.1	0.0	1.7	0.0	0.3	0
Manivitella pemmatoidea	1.0	0.0	6.5	0.7	1.2	0
Marthasterites furcatus	2.2	0.0	63.8	0.0	9.1	0
Microrhabdolus decoratus	0.7	0.0	3.1	0.5	0.9	0
Micula clypeata	5.2	0.0	35.8	0.9	8.6	0
Micula staurophora	7.8	0.0	44.4	3.1	10.9	0
Placozygus fibuliformis	0.0	0.0	0.7	0.0	0.1	0
Prediscosphaera columnata	4.5	0.0	16.2	3.6	4.0	0
Prediscosphaera cretacea	2.6	0.0	9.5	2.0	2.6	0

Table 5.1.2.2 - Descriptive statistics of species identified at DSDP 364.

Prediscosphaera grandis	0.1	0.0	1.7	0.0	0.3	0
Quadrum gartneri	0.2	0.0	1.4	0.0	0.3	0
Radiolithus planus	0.1	0.0	1.4	0.0	0.3	0
Reinhardtites anthophorus	0.01	0.0	0.7	0.0	0.1	0
Reinhardtites levis	0.9	0.0	3.8	0.7	0.9	0
Retecapsa angustiforata	0.0	0.0	0.7	0.0	0.1	0
Retecapsa crenulata	0.2	0.0	4.2	0.0	0.7	0
Retecapsa ficula	0.1	0.0	2.1	0.0	0.3	0
Retecapsa surirella	5.7	0.0	27.6	3.9	6.2	0
Rhagodiscus achlyostaurion	0.1	0.0	1.2	0.0	0.3	0
Rhagodiscus angustus	0.0	0.0	0.7	0.0	0.1	0
Rhagodiscus asper	0.4	0.0	3.0	0.0	0.7	0
Rhagodiscus splendens	0.04	0.0	1.0	0.0	0.2	0
Rucinolithus terebrodentarius	0.7	0.0	5.2	0.0	1.1	0
Stoverius achylosus	0.2	0.0	3.3	0.0	0.7	0
Tetrapodorhabdus decorus	0.0	0.0	0.7	0.0	0.1	0
Tranolithus gabalus	0.3	0.0	4.1	0.0	0.8	0
Tranolithus minimus	0.1	0.0	1.3	0.0	0.3	0
Tranolithus orionatus	1.1	0.0	5.9	0.6	1.3	0
Uniplanarius gothicus	0.8	0.0	15.3	0.0	2.9	0
Uniplanarius sissinghii	0.01	0.0	0.3	0.0	0.0	0
Watznaueria barnesiae	43.7	0.0	74.0	49.1	17.4	0
Watznaueria biporta	0.2	0.0	2.9	0.0	0.7	0
Watznaueria communis	0.6	0.0	10.1	0.0	1.8	0
Watznaueria ovata	0.3	0.0	6.1	0.0	1.1	0
Zeugrhabdotus bicrescenticus	0.8	0.0	2.8	0.5	0.9	0
Zeugrhabdotus diplogrammus	0.04	0.0	1.1	0.0	0.2	0
Zeugrhabdotus elegans	0.03	0.0	0.6	0.0	0.1	0
Zeugrhabdotus embergeri	0.4	0.0	3.0	0.0	0.6	0
Zeugrhabdotus erectus	1.9	0.0	15.0	0.0	3.3	0

Table 5.1.2.2 - Descriptive statistics of species identified at DSDP 364.

relative abundance > 2% (*Eiffellithus, Marthasterites*). Genera with average relative abundance < 2% are not discussed here but their descriptive statistics are show in Tables 5.1.2.1 and 5.1.2.2.. Figure 5.1.2.1 illustrates the relative abundances of genera with an average > 1%. The dominant genus is *Watznaueria* which ranges from 0% to 74% (average 45.8%). As shown in Table 5.1.2.1. *W. barnesiae* represents the most abundant species ranging from 0% to 74% (average 43.7%). Whereas, other *Watznaueria* species (*W. biporta*, *W. communis*, *W. ovata*) remain rare in the assemblage.

The second most common genus at DSDP Site 364 is *Micula* that ranges from 0% to 74.2% (average 13.2%). An increase in abundance of *Micula* is observed in in the upper Coniacian to lower Santonian (from sample 40-364-20R-4,7-10 at 581.2 mbsf to sample 40-364-19R-4,130-132 at 572.12 mbsf). This increase is followed by a decline in *Micula* in the middle Santonian. The relative abundance of *Micula* increases again reaching the maximum (74.2%) in sample 40-364-15R-3,64-67 (467.14 mbsf) in the

middle Campanian. This genus is composed by two species: *M. clypeata* that ranges from 0% to 35.8% (average 5.2 %) and *M. staurophora* that ranges from 0% to 44.4% (average 7.8 %).
The genus *Prediscosphaera* - including *P. columnata*, *P. cretacea* and *P. grandis* - ranges from 0% to 22.6% (average 7.3%). The higher relative abundances (average 12%) are recorded from the lower Turonian (sample 40-364-23R-4,52-54; 649.02 mbsf) to the upper Coniacian (sample 40-364-20R-3,70-74; 579.43 mbsf). The most abundant species is *P. columnata* ranging from 0% to 16.2% (average 4.5%), followed by *P. cretacea* that ranges from 0% to 9.5% (average 2.6%).
Genus *Retecapsa* ranges from 0% to 27.6% (average 6.1%). Two distinctive peaks in *Retecapsa* occur in the upper Turonian (21%) (sample 40-364-22R-4,77-80; 620.77 mbsf) and in the upper Santonian (27.6%) (sample 40-364-18-3,137-141; 553.37 mbsf), respectively (Figure 5.1.2.1).
Zeugrhabdotus ranges from 0% to 15.9% (average 3.1%) with the higher relative abundances recorded in the Turonian (average 7.7%). This genus is mostly composed of *Z. erectus* that ranges from 0% to 15% (average 1.9%) followed by *Z. embergeri* fluctuating from 0% to 3% (average 0.4%), *Z. bicrescenticus* ranging from 0% to 2.8% (average 0.8%), and rare *Z. diplogrammus* and *Z. elegans.*
Eiffellithus ranges from 0% to 13.2% (average 2.7 %). This genus is represented by four species: *E. eximius*, *E. gorkae*, *E. hancockii*, *E. turriseiffelii*. The most abundant species is *E. turriseiffelii* ranging from 0% to 9.9% (average 1.4%).
The genus *Marthasterites* ranges from 0% to 63.8% (average 2.3%). A distinctive peak (63.8%) occurs in sample 40-364-21R-5, 76-78 (600.86 mbsf) in the lowermost Coniacian (Figure 5.1.2.1).

The fluctuations in the NI and TI are presented in Figure 5.1.2.2. At DSDP Site 364 the NI shows the higher value of 57 at the base of the studied interval in the lower Turonian (sample 40-364-23R-4,52-54; 649.02 mbsf). The NI suddenly declines to very low values through the rest of the studied interval. Among the fertility-related taxa *Z. erectus* is the most abundant at DSDP Site 364, with an average relative abundance of 4.9 % in the lower Turonian to the lower-middle Coniacian. The presence of abundant *W. barnesiae* and the low content in high fertility taxa suggest the prevalence of oligotrophic conditions along the studied interval. Only during the Early Turonian, the relative increase of *Z. erectus* together with *B. constans* and *D. ignotus* and the decrease in *W. barnesiae* indicate more mesotrophic conditions.

The TI V.1 (Figure 5.1.2.2) shows the prevalence of cooler water conditions interrupted by short warm interval n the Turonian-lower Santonian. The TI V.2 and V.3 show a similar pattern with a short cooling in the lower Turonian and a gradual warming during the middle Turonian. The upper Turonian- lower

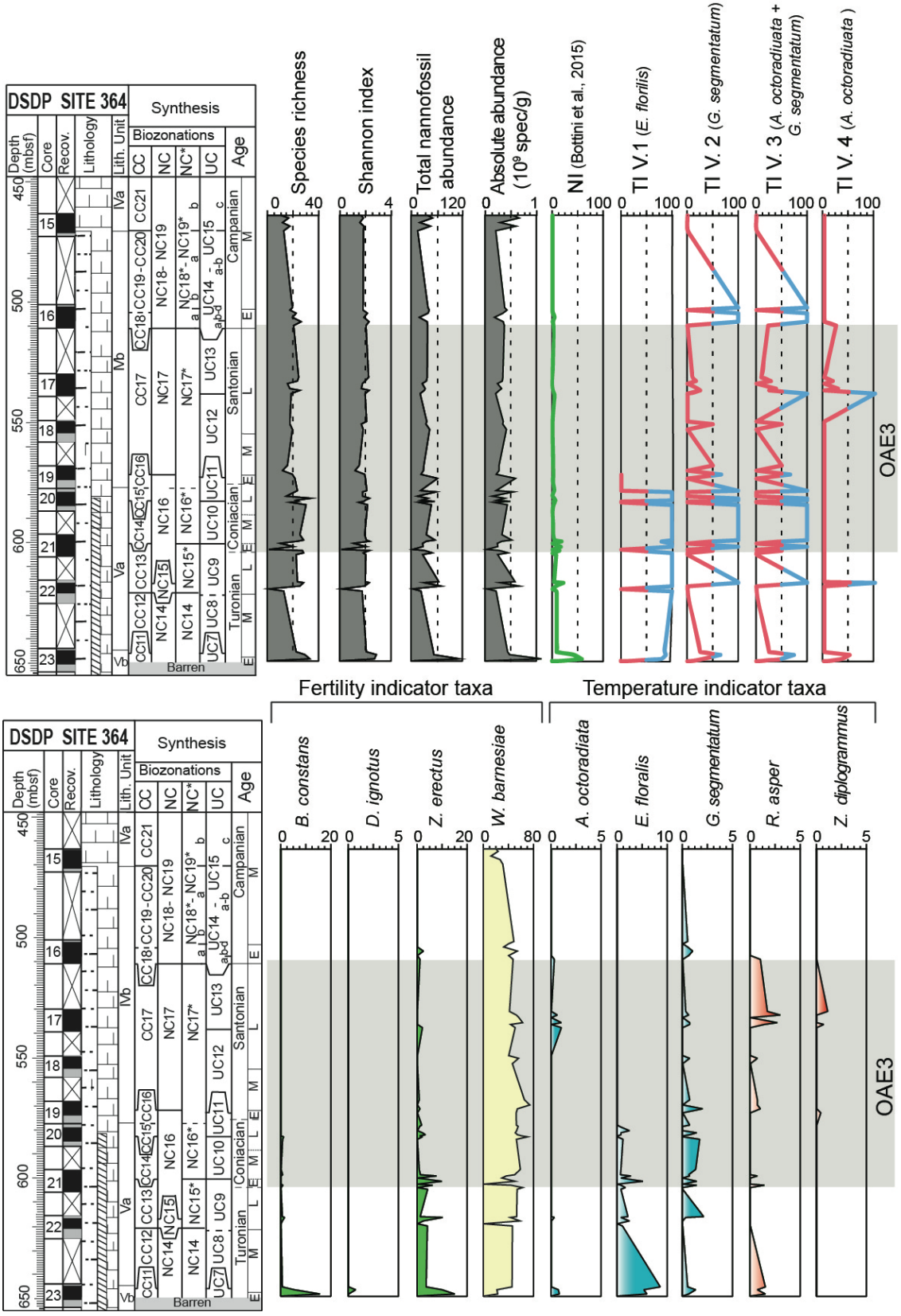

Figure 5.1.2.2 - Fluctuations of calcareous nannofossil temperature and fertility indicator taxa at DSDP Site 364. The species richness, Shannon index, total nannofossil abundances (specimens/FOV) absolute abundances (specimens/gram of sediment) are also reported. The grey band indicates the OAE3 interval.

Santonian Coniacian is characterized by an alternation between cooler and warmer water phases separated by more stable cooler conditions during the middle–upper Coniacian. This last stable cooler is well detectable in both TI V.2 and TI V.3, and also in TI V.1. During the Santonian, a change to a warmer condition occurs and only one peaks of cooling is showed by TI V.3 in the upper Santonian. According to TI V.2 and TI V.3, the early Campanian is characterized by cooler conditions with a gradual transition to a warming in the middle Campanian. Unlike the other indices, the TI V.4 shows the prevalence of warmer condition along the studied interval. This trend is interrupted by two short episodes of cooling in the upper Turonian and upper Santonian, respectively.

At DSDP Site 364 the correlation matrix doesn't support a strong correlation between the cool water taxa *A. octoradiata*, *E. floralis* and *G. segmentatum*. *E. floralis* is positively correlated with *W. communis* (0.63), *W. ovata* (0.82) and *Z. erectus* (0.66). *A. octoradiata* shows no correlation with *G. segmentatum* (0.03) and no correlation versus *E. floralis* (0.19). The latter has a very low positive correlation with *G. segmentatum* (0.25).

The Pearson's correlation coefficients can help to tests the potential affinities between the genera. A summary of the correlation matrix showing only the genera with a correlation > 0.6 (or < - 0.6) is reported in (5.1.2.3), whereas the complete matrix is provided in the Appendix (6A).

	Amphizygus	*Biscutum*	*Braarudosphaera*	*Chiastozygus*	*Ceratolithoides*	*Corollithion*	*Discorhabdus*	*Eiffellithus*	*Eprolithus*	*Haqius*	*Helenea*	*Kamptnerius*	*Lithraphidites*	*Micula*	*Placozygus*	*Prediscosphaera*	*Rotelapillus*	*Stoverius*	*Tetrapodorhabdus*	*Uniplanarius*	*Watznaueria*	*Zeugrhabdotus*
Amphizygus	1																					
Biscutum	-0.04	1																				
Braarudosphaera	-0.08	0.02	1																			
Chiastozygus	0.12	-0.13	0.31	1																		
Ceratolithoides	-0.10	0.13	**0.71**	0.36	1																	
Corollithion	0.16	**0.81**	0.02	-0.02	0.13	1																
Discorhabdus	-0.04	0.30	-0.04	-0.12	-0.05	-0.03	1															
Eiffellithus	0.09	0.33	-0.18	-0.12	-0.22	0.10	0.59	1														
Eprolithus	0.05	0.50	-0.02	-0.19	-0.10	0.37	0.33	**0.61**	1													
Haqius	**0.80**	0.24	-0.05	0.09	-0.03	0.46	-0.04	0.05	0.17	1												
Helenea	-0.05	0.43	-0.03	-0.14	-0.02	0.10	**0.99**	**0.60**	0.38	0.00	1											
Kamptnerius	-0.06	0.00	-0.06	0.20	-0.07	-0.04	-0.03	0.26	0.05	-0.06	-0.04	1										
Lithraphidites	0.34	**0.64**	-0.04	-0.05	-0.06	0.53	0.51	0.39	0.45	0.52	0.58	-0.04	1									
Micula	-0.21	-0.17	-0.02	-0.03	0.23	-0.15	-0.11	-0.44	-0.42	-0.21	-0.12	-0.15	-0.38	1								
Placozygus	-0.04	0.30	-0.04	-0.12	-0.05	-0.03	**1.00**	0.59	0.33	-0.04	**0.99**	-0.03	0.51	-0.11	1							
Prediscosphaera	0.10	0.21	-0.10	-0.20	-0.17	0.12	0.19	0.31	0.36	0.03	0.21	0.14	0.43	-0.53	0.19	1						
Rotelapillus	-0.06	**0.90**	0.03	-0.12	0.15	**0.82**	-0.03	0.17	0.55	0.24	0.11	-0.04	0.44	-0.14	-0.03	0.12	1					
Stoverius	0.04	0.42	-0.07	-0.02	-0.06	0.21	**0.65**	**0.62**	0.45	0.13	**0.67**	0.56	0.47	-0.25	**0.65**	0.32	0.21	1				
Tetrapodorhabdus	**0.61**	-0.05	-0.07	0.12	-0.08	0.21	-0.04	0.18	0.32	**0.69**	-0.04	-0.05	0.25	-0.18	-0.04	-0.04	0.12	0.02	1			
Uniplanarius	-0.08	-0.06	-0.07	-0.21	0.00	-0.06	-0.04	-0.19	-0.17	-0.08	-0.05	-0.06	-0.16	**0.60**	-0.04	-0.29	-0.05	-0.09	-0.07	1		
Watznaueria	0.18	-0.26	0.00	0.13	-0.15	-0.11	-0.21	0.11	-0.05	0.11	-0.24	0.07	-0.07	**-0.61**	-0.21	0.03	-0.16	-0.07	0.20	-0.51	1	
Zeugrhabdotus	0.07	**0.63**	0.04	-0.19	-0.02	0.46	0.30	0.48	**0.60**	0.22	0.38	-0.04	0.56	-0.50	0.30	0.55	0.50	0.32	0.06	-0.24	-0.05	1

Table 5.1.2.3 - Correlation matrix of genera detected at the DSDP Site 364. Bold light blue values correlation ≈0. 60; bold blue values correlation >0. 70.

There is a positive correlation documented for:

- *Amphizygus* versus *Haquius* (0.80) and *Tetrapodorhabdus* (0.61).
- *Biscutum* versus *Corollithion* (0.81), *Lithraphidites* (0.64), *Rotelapillus* (0.90) and *Zeugrhabdotus* (0.63).
- *Brarudosphaera* versus *Ceratolithoides* (0.71).
- *Corollithion* versus *Rotelapillus* (0.83).
- *Discorhabdus* versus *Placozygus* (1.0) and *Stoverius* (0.65).
- *Eiffellithus* versus *Eprolithus* (0.61) and *Stoverius* (0.62).
- *Eprolithus* versus *Zeugrhabdothus* (0.60).
- *Haquis* versus *Tetrapodorhabdus* (0.69).
- *Micula* versus *Uniplanariu*s (0.60).
- *Placozygus* versus *Stoverius* (0.65)
- *Micula* shows a negative correlation with *Watznaueria (-0.61)*.

Pearson's correlation coefficients were also obtained for the species detected at DSDP Site 364. A summary of the correlation matrix showing only the species with a correlation >0.6 (or < -0.6) is reported in (5.1.2.4), whereas the complete matrix is provided in the Appendix (6B). A strong correlation (>0.7) was documented for:

- *A. brooksii* versus *H. circumradiatus* (0.80) and *R. angustiforata* (0.90).
- *A. parcus constrictus* versus *L. armilla* (0.72) and *P. grandis* (.0.89)
- *A. parcus parcus* versus *B. bigelowii* (0.83) and *B. turbinea* (0.72).
- *B. constans* versus *C. signum* (0.81)
- *B. hockwoldensis* versus *M. furcatus* (0.98)
- *B. bigelowii* versus *B. turbinea* (0.89).
- *D. ignotus* versus *H. chiastia* (0.99) and *P. fibuliphormis* (1.0)
- *E. hancockii* versus *R. splendens* (0.79) and *U. sissinghii* (1.00).
- *E. floralis* versus *W. ovata* (0.82).
- *G. coronadventis* versus *H. trabeculatus* (0.85).
- *H. chiastia* versus *P. fibuliformis* (0.99).
- *M. clypeata* versus *M. staurophora* (0.84).
- *R. crenulata* versus *R. ficula* (0.77)
- *R. angustus* versus *T. decorus* (0.70) and *T. gabalus* (0.73).

	Amphizygus brooksii	*Aspidolithus parcus constrictus*	*Aspidolithus parcus parcus*	*Biscutum constans*	*Braarudosphaera hockwoldensis*	*Braarudosphaera cf. B. bigelowii*	*Braarudosphaera turbinea*	*Bronsonia matalosa*	*Ceratolithoides verbeekii*	*Cylindralithus sculptus*	*Cylindralithus serratus*	*Corollithion signum*	*Discorhabdus ignotus*	*Eiffellithus gorkae*	*Eiffellithus hancockii*	*Eiffellithus turriseiffelii*	*Eprolithus floralis*	*Gruntarhabdus coronadventis*	*Haqius circumradiatus*	*Helena chiastia*	*Helicolithus trabeculatus*	*Lithraphidites carniolensis*	*Loxolithus armilla*	*Marthasterites furcatus*	*Micula clypeata*	*Micula staurophora*	*Placozygus fibuliformis*	*Prediscosphaera grandis*	*Retecapsa angustiforata*	*Retecapsa crenulata*	*Retecapsa ficula*	*Rhagodiscus angustus*	*Rhagodiscus splendens*	*Stoverius achylosus*	*Tetrapodorhabdus decorus*	*Tranolithus gabalus*	*Tranolithus minimus*	*Uniplanarius sissinghii*	*Watznaueria communis*	*Watznaueria ovata*	*Zeugrhabdotus diplogrammus*	*Zeugrhabdotus erectus*
Amphizygus brooksii	1																																									
Aspidolithus parcus constrictus	-0.09	1																																									
Aspidolithus parcus parcus	-0.08	0.10	1																																								
Biscutum constans	-0.04	-0.07	-0.06	1																																								
Braarudosphaera hockwoldensis	-0.04	-0.04	-0.04	-0.04	1																																							
Braarudosphaera cf. B. bigelowii	-0.04	0.15	**0.83**	-0.04	-0.02	1																																					
Braarudosphaera turbinea	-0.08	0.12	**0.72**	0.05	-0.04	**0.89**	1																																				
Bronsonia matalosa	0.05	0.04	0.50	-0.06	-0.05	**0.65**	0.54	1																																			
Ceratolithoides verbeekii	-0.09	0.04	**0.60**	0.05	-0.05	0.41	0.51	0.20	1																																		
Cylindralithus sculptus	-0.10	0.08	-0.09	-0.08	-0.05	-0.05	-0.09	0.20	-0.11	1																																	
Cylindralithus serratus	-0.09	0.48	0.06	-0.07	-0.04	-0.04	-0.08	-0.09	-0.09	-0.04	1																																
Corollithion signum	0.16	-0.06	-0.05	**0.81**	-0.03	-0.03	0.05	-0.07	0.06	-0.07	-0.06	1																															
Discorhabdus ignotus	-0.04	-0.04	-0.04	0.30	-0.02	-0.02	-0.04	-0.05	-0.05	-0.05	-0.04	-0.03	1																														
Eiffellithus gorkae	0.31	-0.17	-0.15	0.56	-0.08	-0.08	0.01	-0.06	-0.11	-0.19	-0.16	0.45	0.39	1																													
Eiffellithus hancockii	-0.04	-0.04	-0.04	0.05	-0.02	-0.02	-0.04	-0.05	-0.05	-0.05	-0.04	-0.03	-0.02	0.15	1																												
Eiffellithus turriseiffelii	0.12	-0.20	-0.16	0.28	-0.05	-0.10	-0.11	-0.04	-0.16	-0.24	-0.16	0.06	0.57	0.55	0.11	1																											
Eprolithus floralis	0.07	-0.16	-0.14	0.52	-0.02	-0.08	0.04	-0.05	-0.10	-0.18	-0.15	0.38	0.36	0.47	-0.02	**0.67**	1																										
Gruntarhabdus coronadventis	-0.04	-0.04	-0.04	-0.04	-0.02	-0.02	-0.04	-0.05	-0.05	-0.05	-0.04	-0.03	-0.02	-0.08	-0.02	-0.04	-0.08	1																									
Haqius circumradiatus	**0.80**	-0.09	-0.08	0.24	-0.04	-0.04	-0.04	0.08	-0.05	-0.10	-0.08	0.46	-0.04	0.28	-0.04	0.09	0.19	-0.04	1																							
Helena chiastia	-0.05	-0.05	-0.04	0.43	-0.02	-0.02	-0.03	-0.06	-0.03	-0.06	-0.05	0.10	**0.99**	0.44	-0.02	0.57	0.41	-0.02	0.00	1																					
Helicolithus trabeculatus	0.09	-0.08	-0.07	-0.03	-0.04	-0.04	-0.07	-0.09	-0.08	-0.04	-0.08	-0.05	-0.04	-0.02	0.35	-0.01	-0.10	**0.85**	0.11	-0.04	1																				
Lithraphidites carniolensis	0.34	-0.18	-0.15	**0.64**	-0.09	-0.09	0.01	-0.07	-0.11	0.12	-0.17	0.53	0.51	**0.67**	0.09	0.38	0.42	0.08	0.52	0.58	0.15	1																			
Loxolithus armilla	-0.07	**0.72**	-0.06	-0.06	-0.04	-0.04	-0.06	0.04	-0.08	0.27	**0.63**	-0.05	-0.04	-0.14	-0.04	-0.17	-0.13	-0.04	-0.07	-0.04	-0.06	-0.11	1																		
Marthasterites furcatus	-0.01	-0.08	-0.07	-0.05	**0.98**	-0.04	-0.05	-0.06	-0.08	-0.08	-0.07	-0.04	-0.04	-0.10	-0.03	-0.01	0.02	0.01	-0.02	-0.04	-0.02	-0.09	-0.06	1																	
Micula clypeata	-0.19	0.17	0.07	-0.15	-0.09	-0.08	-0.09	-0.16	0.16	0.01	0.38	-0.13	-0.09	-0.35	-0.09	-0.35	-0.29	-0.09	-0.19	-0.11	-0.13	-0.36	0.21	-0.12	1																
Micula staurophora	-0.21	0.37	0.23	-0.18	-0.11	0.08	0.07	-0.08	0.39	-0.02	0.49	-0.15	-0.11	-0.41	-0.11	-0.41	-0.36	-0.07	-0.21	-0.13	-0.15	-0.36	0.26	-0.15	**0.84**	1															
Placozygus fibuliformis	-0.04	-0.04	-0.04	0.30	-0.02	-0.02	-0.04	-0.05	-0.05	-0.05	-0.04	-0.03	**1.00**	0.39	-0.02	0.57	0.36	-0.02	-0.04	**0.99**	-0.04	0.51	-0.04	-0.04	-0.09	-0.11	1														
Prediscosphaera grandis	-0.06	**0.89**	-0.05	-0.05	-0.03	-0.03	-0.06	-0.07	-0.07	0.05	0.41	-0.04	-0.03	-0.12	-0.03	-0.15	-0.11	-0.03	-0.06	-0.04	-0.06	-0.12	0.55	-0.05	0.09	0.28	-0.03	1													
Retecapsa angustiforata	**0.90**	-0.08	-0.07	-0.04	-0.04	-0.04	-0.07	-0.09	-0.08	-0.09	-0.07	0.19	-0.04	0.33	-0.04	0.10	0.02	-0.04	**0.66**	-0.04	0.12	0.30	-0.06	-0.03	-0.16	-0.18	-0.04	-0.05	1												
Retecapsa crenulata	-0.07	0.24	-0.06	-0.06	-0.03	-0.03	-0.06	-0.08	-0.07	0.12	0.01	-0.05	-0.03	-0.13	-0.03	-0.16	-0.12	-0.03	-0.07	-0.04	-0.04	-0.14	0.12	-0.06	0.01	0.17	-0.03	0.12	-0.06	1											
Retecapsa ficula	0.10	0.33	-0.07	-0.06	-0.04	-0.04	-0.07	-0.09	-0.08	0.08	0.09	-0.05	-0.04	-0.10	-0.04	-0.14	-0.11	-0.04	0.13	-0.04	0.01	-0.02	0.30	-0.06	-0.03	0.06	-0.04	0.28	0.13	**0.77**	1										
Rhagodiscus angustus	0.59	-0.04	-0.04	-0.04	-0.02	-0.02	-0.04	-0.05	-0.05	-0.05	-0.04	-0.03	-0.02	0.08	-0.02	0.03	-0.02	-0.02	**0.67**	-0.02	0.23	0.27	-0.04	-0.03	-0.09	-0.09	-0.02	-0.03	**0.66**	-0.03	0.25	1									
Rhagodiscus splendens	0.29	-0.07	-0.06	0.25	-0.04	-0.04	-0.04	-0.08	-0.04	-0.08	-0.07	0.17	-0.04	0.27	**0.79**	0.12	0.07	-0.04	0.41	0.00	0.40	0.35	-0.06	-0.05	-0.15	-0.17	-0.04	-0.05	0.33	-0.06	0.10	0.54	1								
Stoverius achylosus	0.04	-0.10	-0.09	0.42	-0.05	-0.05	-0.06	0.19	-0.07	-0.12	-0.10	0.21	**0.65**	0.52	-0.05	**0.67**	0.49	-0.05	0.13	**0.67**	-0.09	0.47	-0.08	-0.07	-0.22	-0.25	**0.65**	-0.07	-0.04	-0.08	-0.08	-0.05	-0.02	1							
Tetrapodorhabdus decorus	**0.61**	-0.08	-0.07	-0.05	-0.04	-0.04	-0.07	-0.09	-0.08	-0.09	-0.07	0.21	-0.04	0.17	-0.04	0.26	0.13	-0.04	**0.69**	-0.04	0.13	0.25	-0.06	-0.05	-0.16	-0.18	-0.04	-0.05	**0.69**	-0.06	0.14	**0.70**	0.35	0.02	1						
Tranolithus gabalus	0.48	-0.12	-0.11	0.29	-0.06	-0.06	0.05	-0.10	-0.09	-0.14	-0.12	0.17	0.19	0.51	0.07	0.29	0.21	-0.06	0.51	0.22	0.15	0.52	-0.10	-0.07	-0.26	-0.29	0.19	-0.09	0.56	-0.10	0.13	**0.73**	0.53	0.17	0.46	1				
Tranolithus minimus	0.44	-0.09	-0.08	0.17	-0.04	-0.04	-0.08	-0.10	-0.09	-0.10	-0.09	-0.06	**0.63**	0.42	-0.04	0.42	0.20	0.42	0.16	**0.61**	0.42	0.47	-0.07	-0.04	-0.19	-0.20	**0.63**	-0.06	0.50	-0.07	0.03	0.32	0.13	0.35	0.18	0.44	1			
Uniplanarius sissinghii	-0.04	-0.04	-0.04	0.05	-0.02	-0.02	-0.04	-0.05	-0.05	-0.05	-0.04	-0.03	-0.02	0.15	**1.00**	0.11	-0.02	-0.02	-0.04	-0.02	0.35	0.09	-0.04	-0.03	-0.09	-0.11	-0.02	-0.03	-0.04	-0.03	-0.04	-0.02	**0.79**	-0.05	-0.04	0.07	-0.04	1		
Watznaueria communis	-0.11	0.02	-0.10	0.25	-0.06	-0.06	-0.07	0.08	-0.09	0.24	-0.04	0.13	0.21	0.17	-0.06	0.43	**0.63**	-0.06	-0.04	0.24	0.01	0.10	0.07	-0.10	-0.12	-0.17	0.21	0.08	-0.10	-0.07	-0.06	-0.06	-0.03	0.34	0.33	0.00	0.06	-0.06	1	
Watznaueria ovata	0.03	-0.08	-0.07	0.50	-0.04	-0.04	-0.03	-0.09	-0.04	-0.09	-0.08	0.27	0.54	0.41	-0.04	**0.66**	**0.82**	-0.04	0.15	0.59	-0.02	0.45	-0.07	-0.07	-0.17	-0.20	0.54	-0.06	0.05	-0.06	-0.02	0.14	0.12	0.47	0.45	0.27	0.36	-0.04	**0.76**	1	
Zeugrhabdotus diplogrammus	-0.07	-0.07	-0.06	-0.06	-0.04	-0.04	-0.06	0.26	-0.08	**0.69**	-0.07	-0.05	-0.04	-0.14	-0.04	-0.17	-0.13	-0.04	-0.07	-0.04	0.08	-0.05	0.18	-0.06	-0.02	-0.08	-0.04	-0.05	-0.06	0.20	-0.04	-0.04	-0.06	-0.08	-0.06	-0.10	-0.07	-0.04	0.39	-0.07	1
Zeugrhabdotus erectus	-0.08	-0.16	-0.04	**0.70**	-0.09	0.02	0.17	-0.04	-0.02	-0.20	-0.17	0.46	0.35	0.51	0.36	0.48	**0.66**	-0.05	0.14	0.43	0.07	0.55	-0.14	-0.06	-0.35	-0.39	0.35	-0.13	-0.09	-0.14	-0.12	0.00	0.43	0.34	-0.01	0.42	0.16	0.36	0.18	0.46	-0.14	1

Table 5.1.2.4 - Correlation matrix of selected species detected at the DSDP Site 364. Bold light blue values correlation ≈0. 60; bold blue values correlation >0. 70.

- *R. splendens* versus *U sissinghii* (0.79).
- *W. communis* versus *W. ovata* (0.76)

5.1.3 The Coniacian-Santonian OAE3 at DSDP Site 364

According to the biostratigraphic results, the succession recovered at DSDP Site 364 covers all the OAE3 interval, from the Turonian/Coniacian boundary in core 40-364-21R to the Santonian/Campanian boundary in sample 40-364-16R-6, 107-112 (510.07 mbsf).

Major changes in abundance of nannolith genera *Micula* and *Marthasterites* were detected during the OAE3. These are plotted in Figure 5.1.3.1, both in terms of percentages and absolute abundances (n. specimens/gram of sediments). The holoccoccoliths *Lucianorhabdus* and *Calculites* were not observed at DSDP Site 364.

The changes in relative abundance of *Micula* are evidenced by abundant *M. staurophora* together with *M. clypeata*. A first peak is detected in sample 40-364-20R-3,70-74 (581.2 mbsf) at the top of the CC15/NC16/NC16* zones and lower UC11 zone (lower Coniacian). This is characterized by an equal relative abundance of 10.3% of both *M. staurophora* and *M. clypeata*. A second peak is present in sample 40-364-19R-4,130-132 (573.8 mbsf) at the top of the CC16/NC16/UC11 zone and lower NC17* zone (lower Santonian). This increase is mainly driven by *M. staurophora* that reaches up to 11.7% of the assemblage compared to *M. clypeata* that remains low (4.2%). This spike is also visible in terms of absolute abundances (n. specimens/gram of sediments) with an increase in *M. staurophora* (4.8 $X10^8$spec./g) and *M. clypeata* (1.2 $X10^8$ spec./g),

The middle Santonian is characterized by a general reduction in abundance of *Micula* with *M. clypeata* that becomes more abundant compare to the *M. staurophora*.

The upper Santonian is characterized by an increase in the *Micula* content with the occurrence of a distinctive peak in sample 40-364-17R-2,125-129 (533.2 mbsf) in the CC17/NC17/NC17* zones and lower UC13 zone (upper Santonian) characterized by 12.3% of *M. staurophora* and 4.8% of *M. clypeata*. Another increment in *Micula* was observed close to the Santonian/Campanian boundary (sample 40-364-16R-5,99-102; 508.49 mbsf) where *M. staurophora* and *M. clypeata* reach up to 17.1% and 9.1%, respectively. Also, the absolute abundance shows a peak of *M. staurophora* reaching $2.86X10^8$ spec./g and *M. clypeata* up to $1.52X10^8$ spec./g.

At DSDP Site 364 the maximum in *Micula* content is reached in the Campanian. Two distinctive peaks are present in the lower and in middle Campanian. The first (sample 40-364-16R-1,114-119 (502.64 mbsf) in the CC19/NC18/NC18*b and UC14bd zones where *M. staurophora* and *M. clypeata* reach

23.1% and 7%, respectively. The second peak correlates with the lower CC21/UC15c zones and NC19/NC19* zones (sample 364-40-15R-3,64-67; 467.14 mbsf) where *M. staurophora* and *M. clypeata* reach 44.4% and 29.8%, respectively.

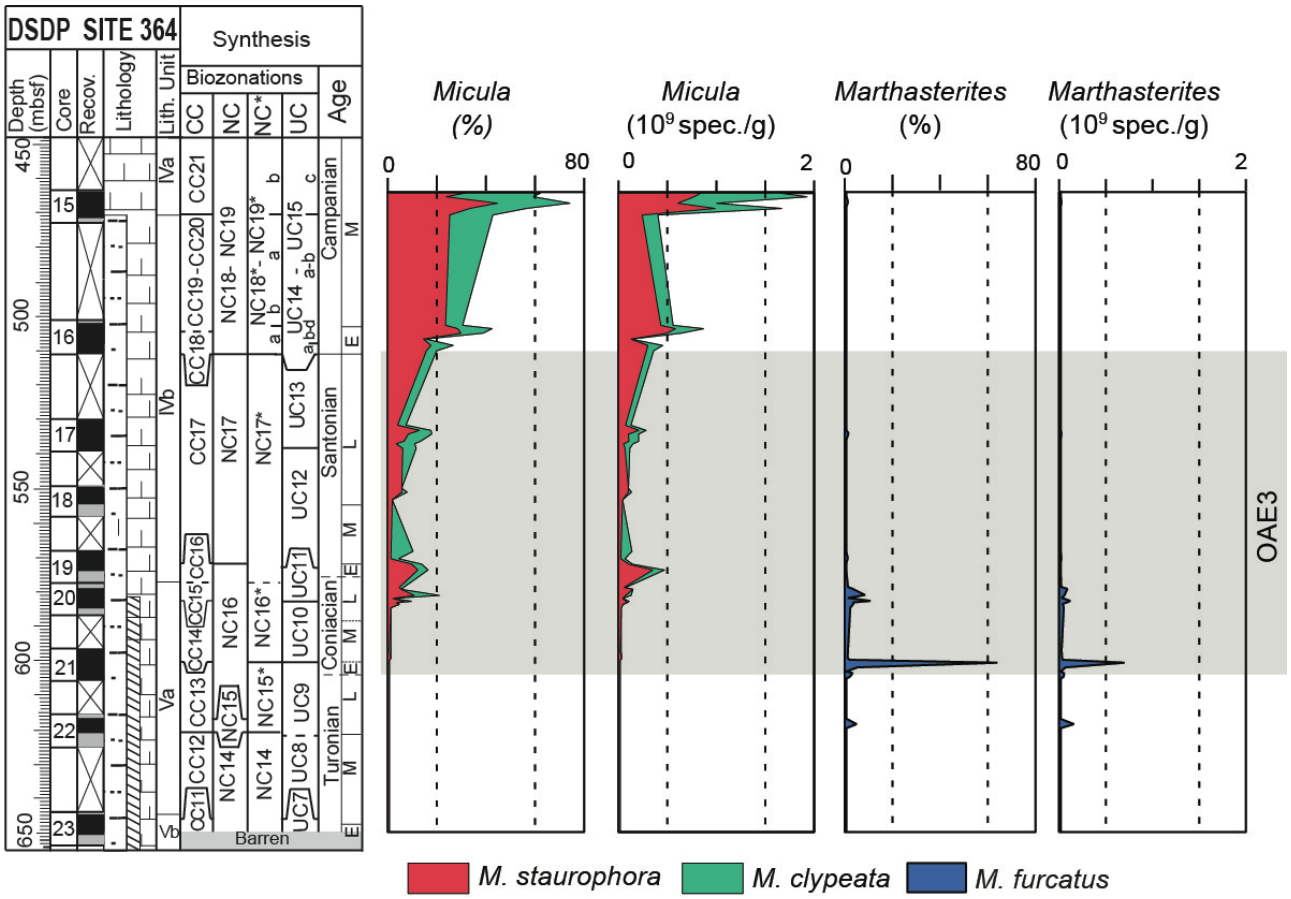

Figure 5.1.3-1 - Relative (%) and absolute (number of specimens/g of sediment) abundances of *Micula* and *Marthasterites*. The OAE3 interval is indicated by a grey band.

These spikes are also present in the absolute abundance curve, but slightly shifted compared to the relative abundance. The first peak is in sample 40-364-16R-2,61-63 (503.61 mbsf) where *M. staurophora* reaches 5.72X10^8 spec./g and *M. clypeata* 2.9X10^8 spec./g. The second spikes in sample 40-364-15R-1,70-74 (464.20 mbsf) consists of 8.3X10^8 spec./g *M. staurophora* and 8.2X10^8 spec./g *M. clypeata*.

Marthasterites is represented only by the species *M. furcatus* at DSDP 364 and three distinct spikes were detected both in terms of percentage than absolute abundances. The first is in sample 40-364-22R-3,18-21 (618.68 mbsf) in the lower CC13NC15/NC15* and UC9 zones (upper Turonian), where *Marthasterites* reaches up to 4.3% (1.43X10^8 spec./g). The second peak is the most prominent and occurs in sample 40-364-21R-3,121-125 (600.86 mbsf) corresponding to the base of CC14/NC16 and UC10

zones (lower Coniacian). Here, *M. furcatus* increases up to 63.8% (6.88X10^8 spec./g) of the assemblage. The last increment is in the CC15/NC16/NC16*and UC11 zones (upper Coniacian) (sample 40-364-20R-4,91-94, 582.91 mbsf), where *M. furcatus* reaches up to 10.2 % (1.04X10^8 spec./g) of the assemblage.

5.2 Site 959

5.2.1 Biostratigraphy

Calcareous nannofossils are generally abundant in cores 959-65R and 959-66R, but become rare in cores 959-67R and 959-68R. Also, the preservation varies along the studied interval: it is moderate in cores 959-65R and 959-66R-5 and poor in cores 959-66R-6 to 959-68R.

A total of five events were detected, allowing the identification of the CC11 and CC13-CC16 zones of Sissingh (1977), NC13 and NC16 zones of Roth (1978), NC13 and NC16*-NC17* of Bralower et al. (1995), and UC7 and –UC9-UC12 zones of Burnett (1998). The results are presented in Figure 5.2.1 and the zonal and subzonal markers identified in this study are described below from the oldest to the youngest. A range chart for Site 959 is provided in the Appendix 7.

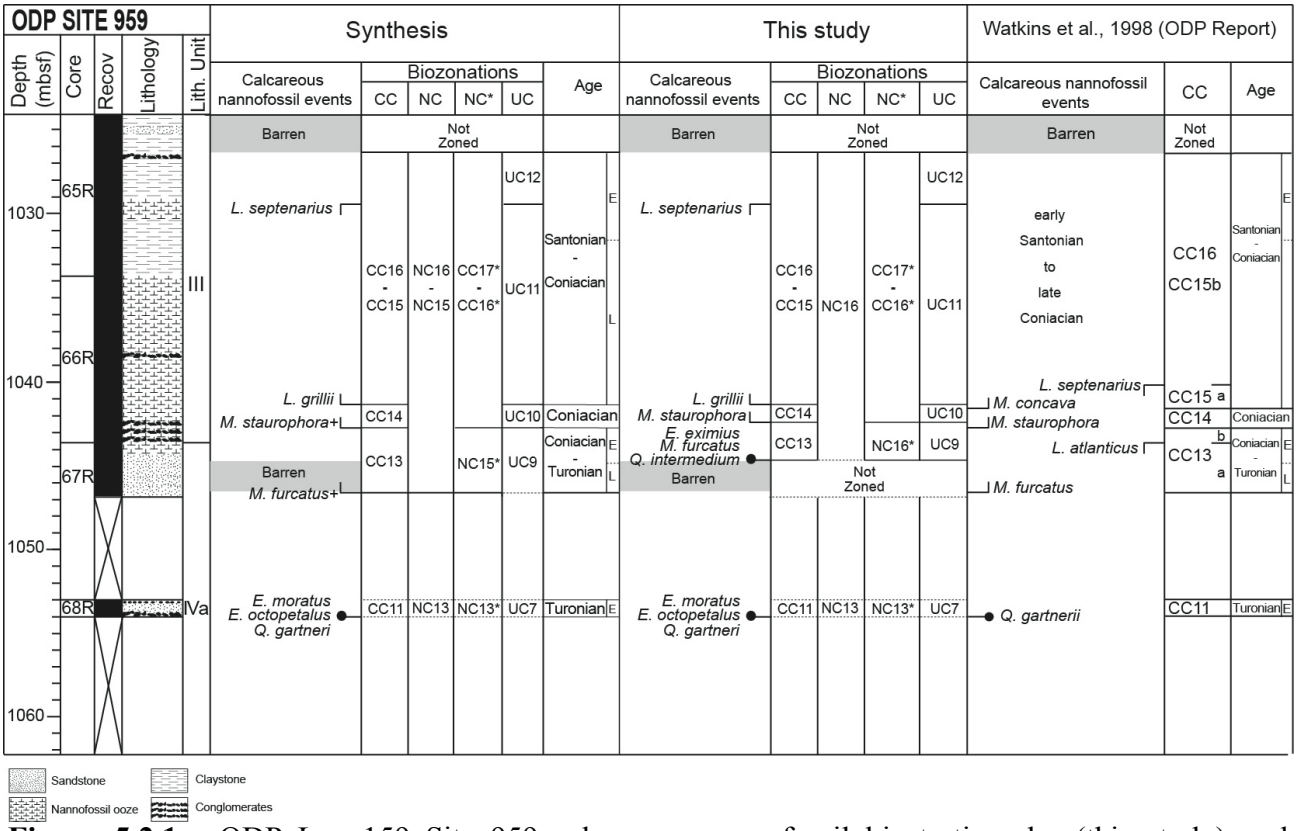

Figure 5.2.1 - ODP Leg 159 Site 959 calcareous nannofossil biostratigraphy (this study) and comparison with previous data (Watkins et al., 1998). Biostratigraphic zonation: CC (Sissingh, 1977), NC (Roth,1978), NC* (Bralower 1995), and UC (Burnett 1998) are shown. The synthesis column is based on integration of data gathered in this study with those from the literature. Data from literature used for zonation is marked with asterisk (*).

The occurrence, in sample 159-959-68R-CC, of biostratigraphic index taxa as *Q. gartneri* together with *E. moratus* and *E. octopetalus*, and the absence of *E. eximius*, indicate zones CC11, NC14 and UC7. A barren interval extends from 159-959-67R-3 to 159-959-67R-2, whereas the occurrence of *E. eximius* and M. *furcatus* in sample 159-959-67R-1, 134-137 (1044.64 mbsf) indicates the presence of CC13, NC15* and UC9 zones. Watkins et al. (1998) reported the occurrence of *M. furcatus* from a lower sample 159-959-67R-2, 105-106 (1045.9 mbsf), thus this last datum is used to define the CC13, NC15* and UC9 zones.

In this study, the FO of *M. staurophora* was detected in a sample 159-959D-66R-6, 115-119 (1042.35 mbsf) higher compared to Watkins et al. (1998) that reported the FO of *M. staurophora* from a lower sample 159-959D-66R-7, 8-11 (1042.8 mbsf). This last datum was then used to define the base of the CC14, NC16* and UC10 zones. The FO of *L. grillii* in sample 159-959D-66R-6, 4-8 (1041.24 mbsf) marks the base of the CC15 and UC11 zones, whereas the LO of *L. septenarius* in sample 159-959D-65R-4, 78-83 (1029.38 mbsf) corresponds to the base of the UC12 zone.

The calcareous nannofossil data from this study, in agreement with those of Watkins (1998) allow to constrain an early Turonian age for core 159-959-68R. An early Coniacian – late Turonian age is assigned to the interval between the FO of *M. furcatus* (1045.9 mbsf) and the FO of *M. staurophora* (1042.35 mbsf). A Coniacian age is attributed to the interval between the FO of *M. staurophora* (1042.35 mbsf) and the FO of *L. grillii* (1041.24 mbsf), whereas a late Coniacian-Santonian age is derived for the interval from the FO of *L. grillii* and the LO of *L. septenarius* (1029.38 mbsf) (Figure Figure 5.2.1).

5.2.2 Nannofossil paleoecology and paleoceanography

At ODP Site 959 a total of 79 taxa were recognized. The species richness varies from a maximum of 43 (sample 159-959-66R-5,33-38;1040.03 mbsf) to 15 (sample 159-959-65R-3,131-135;1028.41 mbsf) with a mean of 31 species for sample (Figure 5.2.2.1).

The Shannon index shows patterns similar to the species richness (Figure 5.2.2.1). The Shannon index ranges between 1.7 (sample 159-959-65R-3,131-135;1028.41 mbsf) and 3.2 (sample 159-959-66R-5,33-38;1040.03 mbsf), with an average value of 2.6, suggesting moderately to well diversified assemblages and absence of dominance of single taxa. The total nannofossil abundance (number of specimens/field of view) has a mean of 42 with the highest values reached in the middle and uppermost Coniacian (76 specimens/field of view).

The absolute abundance of calcareous nannofossils shows a similar pattern of the total nannofossil abundance with a mean of 0.83 X 10^9 specimens/g with the highest value reached in the middle and uppermost Coniacian (~1.6 X 10^9 specimens/g). The presence of moderately to well diversified

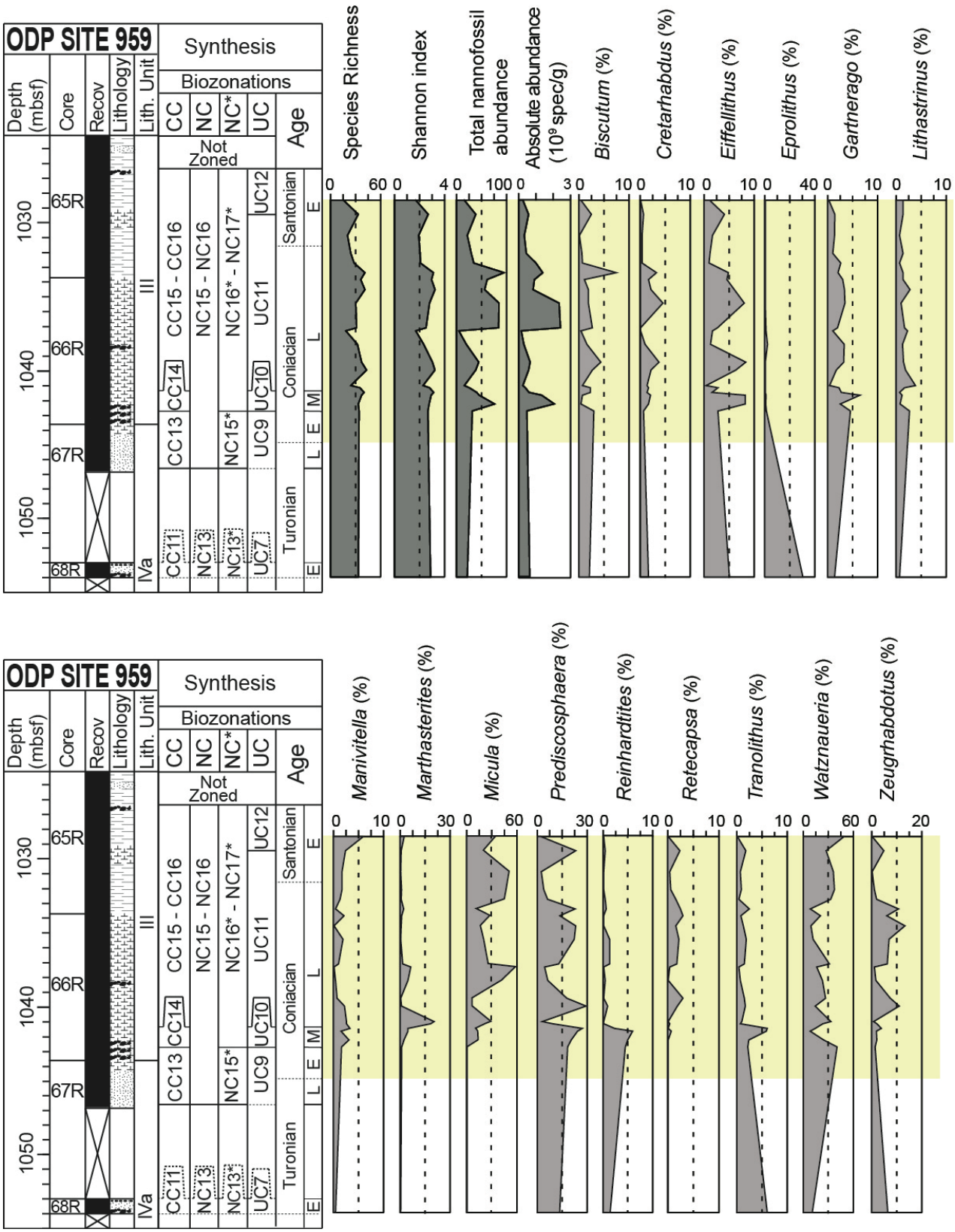

Figure 5.2.2.1 - Calcareous nannofossil data from ODP Site 959 showing the fluctuations of species richness, Shannon index, total nannofossil abundances (specimens/FOV) absolute (specimens/gram of sediment) and relative abundances of genera with an average relative abundance >1%. The yellow band indicates the OAE3 interval.

GENUS	Average %	Minimum %	Maximum %	Mode	Standard Deviation	Median
Micula	23.5	0	58.2	19.8	17	19.8
Watznaueria	23.4	7.8	48.8	23.1	11.8	23.1
Prediscosphaera	14.4	1.9	29.2	13.4	9	13.4
Gartnerago	4.6	0.3	12.8	4.4	2.9	4.4
Zeugrhabdotus	4.2	0	13.2	1.9	3.9	1.9
Eiffellithus	3.8	0.3	8.3	2.7	2.8	2.7
Marthasterites	3.2	0	20.2	0.6	5.6	0.6
Tranolithus	1.8	0	6	1.4	1.8	1.4
Biscutum	1.8	0	7.4	1.8	1.7	1.8
Eprolithus	1.7	0	30.3	0	6.6	0
Manivitella	1.7	0	5.9	1.6	1.4	1.6
Lithastrinus	1.5	0.6	3.8	1.3	0.8	1.3
Cretarhabdus	1.4	0	4.5	1.3	1.2	1.3
Reinhardites	1.1	0	5.9	0.3	1.8	0.3
Retecapsa	1.0	0	2.9	0.5	1.1	0.5
Helicolithus	0.9	0	2.6	0.7	0.8	0.7
Rhagodiscus	0.7	0	3.4	0.3	0.9	0.3
Placozygus	0.7	0	2.6	0.3	0.8	0.3
Cylindralithus	0.6	0	4.3	0.3	1	0.3
Chiastozygus	0.6	0	2.1	0.6	0.6	0.6
Loxolithus	0.5	0	1.3	0.6	0.5	0.6
Calculites	0.4	0	2.1	0	0.6	0
Broinsonia	0.4	0	3	0	0.8	0
Bukrylithus	0.3	0	1.6	0	0.5	0
Ahmuellerella	0.3	0	1.6	0	0.5	0
Corollithion	0.3	0	2.2	0	0.5	0
Rucinolithus	0.3	0	4.7	0	1	0
Microrhabdulus	0.3	0	1.4	0	0.4	0
Repagulum	0.2	0	1	0	0.3	0
Staurolithites	0.1	0	0.6	0	0.2	0
Cribrosphaerella	0.1	0	0.6	0	0.2	0
Quadrum	0.1	0	0.6	0	0.2	0
Rotelapillus	0.04	0	0.5	0	0.1	0
Discorhabdus	0.03	0	0.5	0	0.1	0
Stoverius	0.03	0	0.3	0	0.1	0
Cyclagelosphaera	0.02	0	0.5	0	0.1	0
Flabellites	0.01	0	0.3	0	0.1	0
Seribiscutum	0.01	0	0.3	0	0.1	0

Table 5.2.2.1 - Descriptive statistics of genera identified at ODP Site 959.

SPECIES	Average %	Minimum %	Maximum %	Mode	Standard Deviation	Median
Ahmuellerella octoradiata	0.3	0	1.6	0	0.5	0
Biscutum constans	1.6	0	6.3	0.6	1.5	1.2
Biscutum enormis	0.2	0	1.7	0	0.4	0
Broinsonia matalosa	0.3	0	2	0	0.6	0
Broinsonia signata	0.1	0	1.2	0	0.3	0
Bukrylithus ambiguus	0.3	0	1.6	0	0.5	0
Chiastozygus litterarius	0.6	0	2.1	0	0.6	0.6
Corollithion signum	0.3	0	2.2	0	0.5	0
Cretarhabdus conicus	1.3	0	3.7	0.3	1.1	1.3
Cretarhabdus inaequalis	0.1	0	1.2	0	0.3	0
Cretarhabdus striatus	0.1	0	0.8	0	0.2	0
Cribrosphaerella ehrenbergii	0.1	0	0.6	0	0.2	0
Cylindralithus coronatus	0.3	0	4.3	0	1	0
Discorhabdus ignotus	0.03	0	0.5	0	0.1	0
Eiffellithus eximius	2.4	0	7.4	0.3	2.3	2
Eiffellithus gorkae	0.3	0	1.2	0	0.3	0.3
Eiffellithus turriseiffellii	0.2	0	1	0	0.3	0
Eprolithus floralis	0.9	0	15.3	0	3.3	0
Eprolithus moratus	0.1	0	1.3	0	0.3	0
Eprolithus octopetalus	0.3	0	5.7	0	1.2	0
Eprolithus rarus	0.04	0	0.9	0	0.2	0
Flabellites oblongus	0.01	0	0.3	0	0.1	0
Gartnerago cf. G. coxalliae	0.03	0	0.6	0	0.1	0
Gartnerago cf. G. ponticula	0.1	0	0.9	0	0.3	0
Gartnerago cf. G. theta	0.1	0	0.7	0	0.2	0
Gartnerago obliquum	0.3	0	2.9	0	0.7	0
Gartnerago segmentatum	2.8	0	8.9	0	2.2	2.6
Grantarhabdus coronadventis	0.1	0	1.6	0	0.4	0
Helicolithus anceps	0.5	0	2.3	0.3	0.6	0.3
Helicolithus compactus	0.04	0	0.5	0	0.1	0
Helicolithus leckiei	0.0	0	0.3	0	0.1	0
Helicolithus trabeculatus	0.2	0	1.1	0	0.3	0.3
Lithastrinus grilli	0.8	0	2.7	0	0.8	0.9
Lithastrinus septenarius	0.4	0	2.6	0	0.7	0
Loxolithus armilla	0.5	0	1.3	0	0.5	0.6
Manivitella pemmatoida	1.7	0	5.9	0.3	1.4	1.6
Marthasterites crassus	0.7	0	4.1	0	1.2	0
Marthasterites furcatus	1.0	0	8.2	0	2.2	0
Microrhabdulus belgicus	0.1	0	0.8	0	0.2	0
Microrhabdulus decoratus	0.2	0	1.1	0	0.3	0
Micula adumbrata	0.5	0	1.6	0	0.6	0
Micula concava	5.0	0	14.7	0	3.8	4.7
Micula cubiformis	0.5	0	2.3	0	0.7	0.3
Micula staurophora	16.5	0	45	11.9	12.3	13
Micula swastica	1.0	0	4.6	0	1.2	0.7
Placozygus fibuliformis	0.7	0	2.6	0	0.8	0.3
Prediscosphaera columnata	0.9	0	3.4	0	0.9	0.6
Prediscosphaera cretacea	6.4	0.3	16.8	0.6	5	5
Prediscosphaera spinosa	1.0	0	3.6	0	1.1	0.7
Quadrum gartneri	0.1	0	0.6	0	0.2	0
Reinhardites antophorus	1.0	0	5.6	0	1.6	0.3
Reinhardtites levis	0.1	0	1	0	0.2	0
Repagulum parvidentatum	0.2	0	1	0	0.3	0
Retecapsa crenulata	0.4	0	2.9	0	0.8	0
Retecapsa surirella	0.6	0	2.6	0	0.8	0.3

Table 5.2.2.2 - Descriptive statistics of species identified at ODP Site 959.

Rhagodiscus angustus	0.4	0	2.1	0	0.6	0
Rhagodiscus asper	0.3	0	1.1	0	0.4	0
Rhagodiscus reniformis	0.02	0	0.5	0	0.1	0
Rotelapillus laffittei	0.04	0	0.5	0	0.1	0
Rucinolithus hayi	0.0	0	0.3	0	0.1	0
Rucinolithus terebrodntarius	0.08	0	1.7	0	0.4	0
Stoverius achylosus	0.0	0	0.3	0	0.1	0
Staurolithites crux	0.1	0	0.6	0	0.2	0
Tranolithus gabalus	0.2	0	0.8	0	0.2	0
Tranolithus orionatus	1.7	0	5.7	0.3	1.7	1.2
Watznaueria barnesiae	10.4	4.3	20.6	8.2	4.6	9.3
Watznaueria biporta	0.4	0	1.9	0	0.6	0
Watznaueria fasciata	12.3	1.6	39.9	0	9.5	10.4
Watznaueria ovata	0.3	0	0.9	0	0.3	0
Zeugrhabdotus praesigmoides	0.5	0	2.4	0	0.7	0
Zeugrhabdotus bicescenticus	0.0	0	0.3	0	0.1	0
Zeugrhabdotus diplogrammus	0.6	0	2.3	0	0.6	0.5
Zeugrhabdotus elegans	0.0	0	0.6	0	0.1	0
Zeugrhabdotus erectus	1.9	0	8.2	0	2.2	1.3
Zeugrhabdotus howei	0.3	0	2.7	0	0.7	0
Zeugrhabdotus streetiae	0.1	0	0.9	0	0.2	0
Zeugrhabdotus trivectis	0.06	0	0.6	0	0.2	0
Zeugrhabdotus xenotus	0.01	0	0.3	0	0.1	0

Table 5.2.2.2 - Descriptive statistics of species identified at ODP Site 959.

assemblages and the occurrence of *W. barnesiae* together with delicate and less diagenesis-resistant taxa such as *B. constans*, *D. ignotus* and *Z. erectus* suggest that the distribution and abundance of calcareous nannofossils mainly reflect primary ecological signals with negligible diagenetic modifications.

The descriptive statistics of calcareous nannofossil genera and species are synthesized in Tables 5.2.2.1 and 5.2.2.2. At ODP Site 959 there are seven genera with an average relative abundance > 3% (*Eiffellithus, Gartnerago, Marthasterites, Micula, Prediscosphaera, Watznaueria, Zeugrhabdotus).* Genera with average relative abundance < 2% are not discussed here but their descriptive statistics are show in Tables 5.5.2.1 and 5.5.2.2. Figure 5.2.2.1 illustrates the relative abundances of genera with an average relative abundance > 1%.

The dominant genus is *Micula* which ranges from 0% to 58.2% (average 23.5%). The higher relative abundances are recorded in the upper Coniacian and in the Coniacian/Santonian transition. As shown in Table 5.2.2.2. *M. staurophora* represents the most abundant species ranging from 0% to 45%. Another frequent *Micula* species is *M. concava* that ranges from 0% to 14.7% (average 5%). Other species of *Micula* are *M. adumbrata, M. cubiformis* and *M. swastica*.

Watznaueria is the second genus in abundance and varies from 48.8% to 7.8% (average 23.4%). This genus includes *W. barnesiae, W. biporta*, *W. fasciata* and *W. ovata*. The most abundant species are *W.*

barnesiae that ranges from 4.3% to 20.6% (average 10.4%) and *W. fasciata* that ranges from 1.6% to 39.9% (average 12.3%).
The genus *Prediscosphaera* is the third in abundance and ranges from 1.9% to 29.2% (average 14.4%). The most abundant species is *P. cretacea* ranging from 0.3% to 16.8% (average 6.4%) but also the species *P. columnata* and *P. spinosa* are present.
Gartnerago fluctuates from 0.3% to 12.8% (average 4.6 %). This genus is represented by five species: *G.* cf. *G. coxalliae, G. obliquum, G.* cf. *G. ponticula, G. segmentatum,* and *G.* cf. *theta*. The most abundant species is *G. segmentatum* ranging from 0% to 8.9% (average 2.8%).
The genus *Zeugrhabdotus* - including *Z. bicrescenticus, Z. diplogrammus, Z. elegans, Z. erectus, Z. howei, Z. streetiae, Z. trivectis and Z. xenotus*, - ranges from 0% to 13.2% (average 4.2%).
Eiffellithus varies from 0.3% to 8.3% (average 3.8 %). The genus *Eiffellithus* is mostly represented by *E. eximius* that ranges from 0% to 7.4% (average 2.4%) but also includes rare *E. gorkae* and *E. turriseiffellii*.
The genus *Marthasterites* ranges from 0% to 20.2% (average 3.2 %) and includes *M. furcatus* and *M. crassus*. A distinctive peak in *Marthasterites* occurs in the middle-late Coniacian (sample 159-959-66R-6,4-8;1041.24 mbsf).

The fluctuations in the NI and TI are presented in Figure 5.2.2.2. The NI is suggestive of moderate to relatively high surface water fertility with the higher values recorded in the upper Coniacian. Two peaks were detected in samples 159-959-66R-5,33-38 (1040.03 mbsf) and 159-959-65R-7,24-29 (1033.37 mbsf). The NI is mainly driven by the changes in abundance of *B. constans* and *Z. erectus* whereas *D. ignotus* is rare. *B. constans* ranges from 0% to 6.3% (average 1.6), *Z. erectus* ranges from 0% to 8.2% (average 1.9) whereas *D. ignotus* ranges from 0% to 0.5% (average 0.03%). The relatively high abundance of the fertility-related taxa together with a low percentage of *W. barnesiae* (average 20.6%) suggest that the investigated interval is characterized by mesotrophic conditions of surface waters.

At ODP Site 959 the TI V.1 shows the prevalence of cool conditions from the lower Turonian to the lower Coniacian interval where there is a shift to warmer waters. The TI V.2 and V.3 show an opposite scenario with warmer conditions in the lower Turonian and the prevalence of cooler surface waters in the upper Turonian-Santonian. A return to a warmer condition occur at the top of the studied interval. The TI V.4 displays generally warmer conditions throughout the studied interval with one episode of cooling in the upper Coniacian.

At ODP Site 959, the cool water taxon *A. octoradiata* is rare (average 0.3%) as well as *R. parvidentatum* (average 0.2%). *E. floralis* shows an increase in relative abundance (15.3%) in the lower Turonian

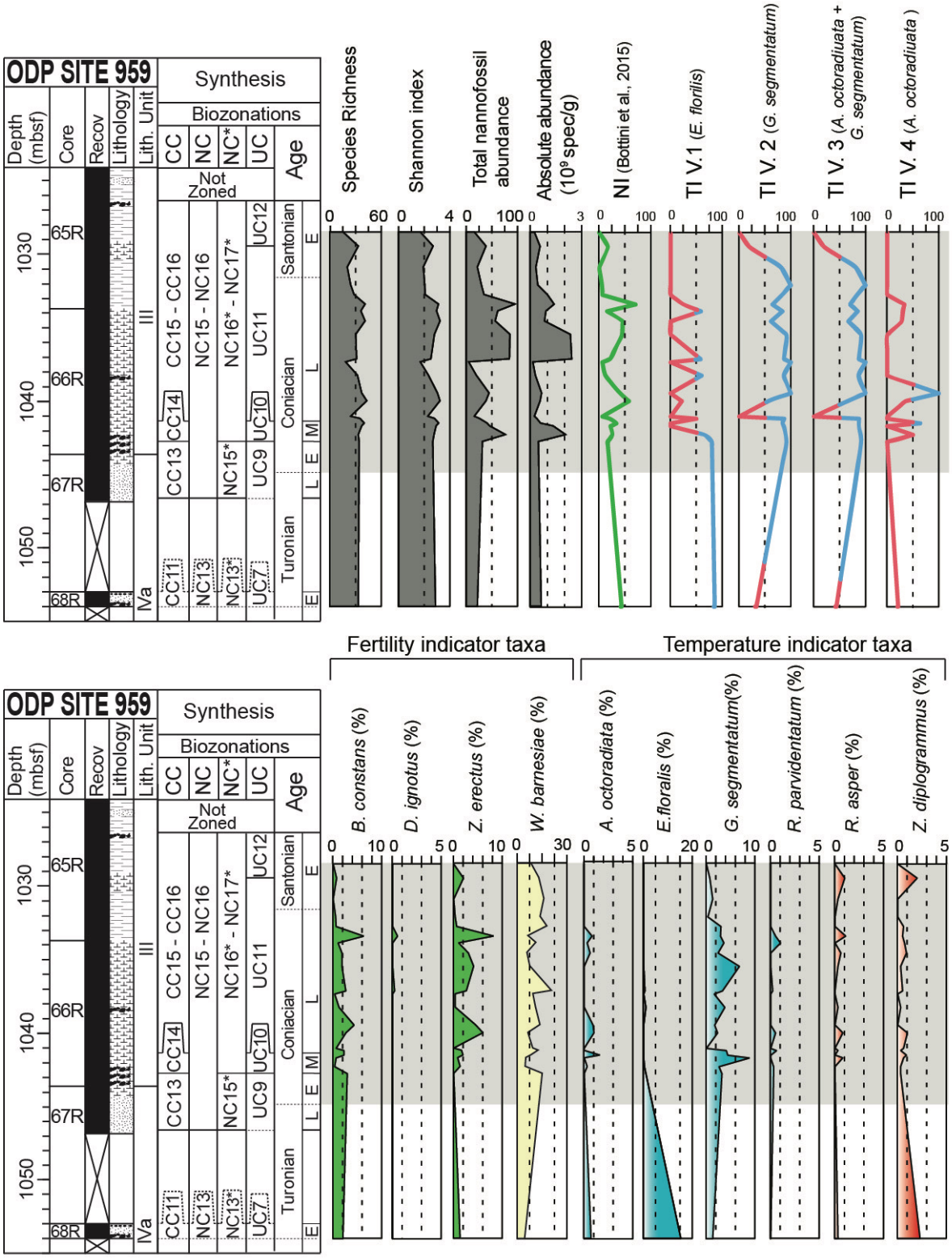

Figure 5.2.2.2 - Fluctuations of temperature and fertility related taxa at ODP Site 959. NI after Bottini et al. (2015); TI after Bottini et al. (2015); TI. V2, V3, V4 modified in this work. The species richness, Shannon index, total nannofossil abundances (n. specimens/FOV), relative abundances are also reported. The grey band indicates the OAE3 interval.

(sample 159-959-68R-CC,13-1; 1054.18 mbsf), whereas is rare in most of the studied interval. *G. segmentatum* is the most abundant cool water taxon (average 2.8%) and its highest relative abundance was observed in the upper Coniacian. Also, the warm water indicators *R. asper* and *Z. diplogrammus* occur with low abundances with an average of 0.3% and 0.6%, respectively. The correlation matrix for the species quantified at ODP Site 959 doesn't support a correlation between the cool water taxa (values around 0).

The potential affinities of genera were tested by calculating the Pearson's correlation coefficients. A summary of the correlation matrix for the genera with a correlation > 0.6 (or < - 0.6) is reported in (Table 5.2.2.3), whereas the complete matrix is provided in the Appendix (8A).
There is a positive correlation documented for:

- *Ahmuellerella* versus *Corollithion* (0.79).
- *Biscutum* versus *Discorhabdus* (0.75).
- *Broinsonia* versus *Quadrum* (0.75).
- *Bukrylithus* versus *Staurolithites* (0.83) and *Zeugrhabdotus* (0.83)
- *Cretarhabdus* versus *Eiffellithus* (0.76) and *Placozygus* (0.72).
- *Eiffellithus* versus *Prediscosphaera* (0.71).
- *Eprolithus* versus *Rucinolithus* (0.99).
- *Helicolithus* versus *Placozygus* (0.70) and *Retecapsa* (0.70).
- *Microrhabdulus* versus *Tranolithus* (0.77).
- *Placozygus* versus *Retecapsa* (0.70) and *Zeugrhabdotus* (0.73).
- *Reinhardites* versus *Stoverius* (0.80)
- *Rhagodiscus* versus *Seribiscutum* (0.72) and *Zeugrhabdotus* (0.75).
- *Rotelapillus* versus *Seribiscutum* (0.85).

And a negative correlation is present for *Micula* versus *Prediscosphaera* (-0.78) Pearson's correlation coefficients were also obtained for all species quantified at ODP Site 959. A summary of the correlation matrix showing only the species with a correlation >0.6 (or < -0.6) is reported in (Table 5.2.2.4), whereas the complete matrix is provided in the Appendix (8B). A strong correlation (>0.7) was documented for:

- *A. octoradiata* versus *C. signum* (0.79).
- *B. constans* versus *D. ignotus* (0.70), *P. fibuliformis* (0.70) and *Z. erectus* (0.81).
- *B. signata* versus *C. ehrenbergii* (0.74), *Gartnerago* cf. *G. coxalliae* (0.94), *G. obliquum* (0.72), *L. septenarius* (0.78) *Q. gartneri* (0.85) and *R. hayi* (0.94).

	Ahmuellerella	*Biscutum*	*Bronsonia*	*Bukryithus*	*Calculites*	*Chiastozygus*	*Corollithion*	*Cretarhabdus*	*Crtbrosphaerella*	*Discorhabdus*	*Eiffellithus*	*Eprolithus*	*Gartnerago*	*Helicolithus*	*Loxolithus*	*Microrhabdulus*	*Micula*	*Placozygus*	*Prediscosphaera*	*Quadrum*	*Reinhardtites*	*Retecapsa*	*Rhagodiscus*	*Rotelapillus*	*Rucinolithus*	*Stoverius*	*Serbiscutum*	*Staurolithites*	*Tranolithus*	*Watznaueria*	*Zeugrhabdotus*
Ahmuellerella	1																														
Biscutum	0.49	1																													
Bronsonia	0.25	0.21	1																												
Bukryithus	0.48	0.50	-0.13	1																											
Calculites	0.50	0.19	0.07	0.17	1																										
Chiastozygus	0.12	0.23	-0.23	0.55	0.37	1																									
Corollithion	**0.79**	0.37	0.20	0.10	**0.68**	0.18	1																								
Cretarhabdus	0.41	0.52	-0.02	**0.66**	0.35	**0.64**	0.25	1																							
Cribrosphaerella	-0.04	0.21	**0.62**	0.10	-0.16	-0.25	-0.21	-0.14	1																						
Discorhabdus	0.18	**0.75**	-0.08	0.27	-0.02	0.11	0.18	0.21	-0.11	1																					
Eiffellithus	0.28	0.29	0.00	0.59	0.34	0.46	0.01	**0.76**	0.01	0.04	1																				
Eprolithus	0.18	0.02	0.49	-0.19	-0.16	-0.24	0.00	0.02	-0.07	-0.07	0.09	1																			
Gartnerago	0.04	0.13	0.26	0.10	0.55	0.35	0.20	0.39	0.18	-0.07	0.53	-0.13	1																		
Helicolithus	0.26	**0.60**	-0.22	0.45	0.24	0.52	0.21	**0.65**	-0.10	0.43	0.54	-0.25	0.38	1																	
Loxolithus	0.36	0.43	0.03	0.04	**0.62**	0.34	0.59	0.23	0.08	0.21	0.06	-0.26	0.27	0.42	1																
Microrhabdulus	0.30	-0.13	0.24	-0.01	0.18	-0.17	0.17	0.14	-0.05	-0.14	0.41	0.42	0.32	-0.15	-0.03	1															
Micula	-0.56	-0.56	-0.55	-0.44	-0.38	-0.20	-0.34	-0.56	-0.39	-0.15	**-0.63**	-0.31	-0.41	-0.35	-0.36	-0.48	1														
Placozygus	0.50	**0.66**	0.08	**0.64**	0.38	0.41	0.23	**0.72**	0.10	0.28	0.50	0.00	0.24	**0.70**	0.30	-0.24	-0.47	1													
Prediscosphaera	**0.60**	0.50	0.27	**0.66**	0.48	0.40	0.43	0.58	0.33	0.18	**0.71**	-0.04	0.52	0.39	0.40	0.41	**-0.78**	0.43	1												
Quadrum	0.09	0.15	**0.75**	0.02	0.09	0.07	0.22	0.11	**0.62**	-0.11	-0.02	-0.07	0.39	-0.02	0.08	-0.10	-0.37	0.09	0.30	1											
Reinhardtites	0.01	-0.07	0.43	-0.11	0.17	-0.10	0.07	0.08	0.30	-0.07	0.44	0.05	**0.66**	0.03	-0.01	**0.64**	-0.48	-0.22	0.47	0.43	1										
Retecapsa	0.19	0.51	-0.34	**0.66**	0.21	0.52	0.00	0.51	0.01	0.34	0.46	-0.24	0.15	**0.70**	0.25	-0.30	-0.20	**0.70**	0.41	-0.18	-0.31	1									
Rhagodiscus	0.41	0.50	0.10	**0.68**	0.13	0.25	0.02	0.48	0.26	0.26	0.45	0.15	0.05	0.11	0.15	0.29	-0.50	0.44	0.57	-0.14	-0.09	0.34	1								
Rotelapillus	0.23	0.14	-0.04	0.51	-0.20	-0.08	-0.17	0.03	0.51	-0.09	0.19	-0.08	-0.17	-0.04	0.03	0.20	-0.24	0.11	0.44	-0.12	-0.09	0.30	**0.68**	1							
Rucinolithus	0.17	0.02	0.51	-0.20	-0.17	-0.24	-0.01	0.00	-0.04	-0.08	0.06	**0.99**	-0.13	-0.27	-0.28	0.39	-0.30	0.00	-0.05	-0.04	0.04	-0.22	0.13	-0.08	1						
Stoverius	-0.11	-0.27	-0.11	-0.14	0.15	-0.04	-0.08	0.10	-0.12	-0.10	0.53	-0.06	0.48	0.10	-0.05	**0.65**	-0.21	-0.29	0.29	-0.12	**0.80**	-0.22	-0.11	-0.10	-0.09	1					
Serbiscutum	0.35	0.11	0.03	**0.60**	-0.15	-0.03	-0.12	0.13	0.36	-0.07	0.21	-0.06	-0.11	-0.02	-0.11	0.31	-0.24	0.20	0.38	-0.09	-0.04	0.17	**0.72**	**0.85**	-0.06	-0.07	1				
Staurolithites	**0.64**	0.52	-0.08	**0.83**	0.28	0.28	0.32	**0.62**	0.02	0.20	0.39	-0.18	0.01	0.36	0.12	0.04	-0.45	**0.66**	0.50	0.02	-0.19	0.48	0.56	0.38	-0.19	-0.23	0.53	1			
Tranolithus	0.52	0.18	0.51	-0.01	0.38	-0.09	0.56	0.26	0.01	0.05	0.37	0.52	0.41	-0.03	0.17	**0.77**	**-0.62**	-0.02	0.57	0.25	**0.61**	-0.19	0.15	-0.03	0.50	0.40	0.06	1		
Watznaueria	-0.49	-0.34	-0.06	-0.44	-0.46	-0.48	-0.42	**-0.61**	0.23	-0.23	-0.57	-0.25	-0.39	-0.27	-0.29	-0.45	0.38	-0.35	**-0.64**	0.10	-0.17	-0.27	-0.54	-0.12	-0.21	-0.21	-0.18	-0.32	-0.54	1	
Zeugrhabdotus	0.58	**0.63**	0.02	**0.83**	0.41	0.54	0.26	**0.61**	0.03	0.40	0.55	0.10	0.13	0.41	0.27	0.02	-0.54	**0.73**	**0.67**	-0.10	-0.18	**0.67**	**0.75**	0.36	0.10	-0.20	0.39	**0.67**	0.15	**-0.62**	1

Table 5.2.2.3 - correlation matrix of genera detected at the ODP Site 959. Bold light blue values correlation ≈0. 60; bold blue values correlation >0. 70.

- *B. signata* versus *C. ehrenbergii* (0.74), *Gartnerago* cf. *G. coxalliae* (0.94), *G. obliquum* (0.72), *L. septenarius* (0.78) *Q. gartneri* (0.85) and *R. hayi* (0.94)
- *B. ambiguous* versus *E. gorkae* (0.70), *P. cretacea* (0.70), *P. spinosa* (0.73), *R. angustus* (0.70) and *Z. erectus* (0.84)
- *C. signum* versus *Z. xenotus* (0.87)
- *C. conicus* versus *E. eximius* (0.76) and *P. fibuliformis* (0.74).
- *C. striatus* versus *D. ignotus* (0.86) and *H. compactus* (0.78).
- *C. ehrenbergii* versus *Gartnerago cf. G. coxalliae* (0.81), *G. obliquum* (0.72) and *R. hayi* (0.81)
- *C. coronatus* versus *G. coronadventis* (0.90) and *R. levis* (0.89),
- *D. ignotus* versus *H. compactus* (0.78) and *H. trabeculatus* (0.71)
- *E. eximius* versus *H. anceps* (0.70).
- *E. gorkae* versus *P. spinosa* (0.78) and *Z. howei* (0.71)
- *E. floralis* versus *E. moratus* (1.0), *E. octopetalus* (1.0) and *R. terebrodentarius* (1.0).
- *E. rarus* versus *Z. trivectis* (0.81).
- *F. oblongus* versus *S. crux* (0.81).
- *Gartnerago* cf. *G. coxalliae* versus *G. obliquum* (0.79), *L. septenarius* (0.70), *Q. gartneri* (0.81) and *R. hayi* (1.0)
- *G. obliquum* versus *R. hayi* (0.79).
- *G. coronadventis* versus *R. levis* (0.92)
- *H. compactus* versus *R. crenulata* (0.80)
- *L. septenarius* versus *R. hayi* (0.70).
- *M. crassus* versus *M. furcatus* (0.85).
- *M. belgicus* versus *R. reniformis* (0.86) and *R. laffittei* (0.71).
- *M. decoratus* versus *S. achylosus* (0.71) and *T. orionatus* (0.74).
- *M. adumbrata* versus *M. swastica* (0.73).
- *P. fibuliformis* versus *P. spinosa* (0.77).
- *P. cretacea* versus *Z. erectus* (0.75).
- *P. spinosa* versus *Z. howei* (0.78).
- *Q. gartneri* versus *R. hayi* (0.81).
- *R. antophorus* versus *S. achylosus* (0.75)
- *R. levis* versus *S. achylosus* (0.78).
- *R. parvidentatum* versus *R. crenulata* (0.71).
- *R. angustus* versus *R. reniformis* (0.71).
- *R. reniformis* versus *R. laffittei* (0.85).
- *Z. elegans* versus *Z. howei* (0.78) and *Z. streetiae* (0.78).

Table 5.2.2.4 – correlation matrix of selected species detected at ODP Site 959. Bold light blue values correlation ≈0. 60; bold blue values correlation >0. 70.

5.2.3 The Coniacian-Santonian OAE3 at ODP Site 959

According to calcareous nannofossil biostratigraphy, the stratigraphic range of the OAE3 interval at ODP Site 959 extends from core 159-959-67R to core 159-959-65R as show in Figure 5.2.3.1 At ODP Site 959 the OAE3 was only partially recovered and its upper portion was not sampled.

Fluctuations in relative abundances of *Micula*, holoccoccoliths (*Calculites*) and *Marthasterites* were observed during the OAE3 interval as plotted in Figure 5.6.2.3. The abundance of *Micula* is characterized by three intervals of increased relative and absolute abundance. A first peak is present in middle-upper Coniacian (lower CC15-CC16/NC15-NC16/NC16*-NC17*/UC11 zone; sample 159-959-66R-5,139-142 at 1041.09 mbsf) where *Micula* reaches the 29% of the assemblage. This abundance peak is due to *M. staurophora* (22%), *M. concava* (5.4%) and rare *M. cubiformis* (1.3%) and *M. adumbrata* (0.3%). At ODP Site 959 the maximum in *Micula* was observed in the upper Coniacian (middle of CC15-CC16/NC15-NC16/NC16*-NC17*/UC11 zones; sample 159-959-66R-3,65-67 at 1037.35 mbsf) where it reaches the 58% of the assemblages. This abundance peak is characterized by *M. staurophora* (45%), *M. concava* (11%), *M. swastica* (1.6%) and *M. adumbrata* (1%).

A further interval of high abundance of *Micula* was observed in the Coniacian/Santonian transition in the upper CC15-CC16/NC15-NC16/NC16*-NC17*/UC11 zones (between sample 159-959-65R-6,111-116 at 1032.71 mbsf and sample 159-959-65R-5,72-77 at 1030.82 mbsf) with an average content in *Micula* of 47.4%. This peak consists of *M. staurophora* (31.2%), *M. concava* (10.7%), *M. swastica* (3.1%) and *M. adumbrata* (1.3%) and *M. cubiformis* (1.2%).

The *Micula* increases are also visible in the absolute abundance fluctuations, but slightly shifted compared to the relative abundances. The first peak in sample 159-959-66R-6,115-119 (1042.35 mbsf) shows a *Micula* content of 0.27 X 10^9 spec./g, with *M. staurophora* (0.17 X 10^9 spec./g), *M. concava* (0.81 X 10^9 spec./g) and *M. swastica* (0.01 X 10^9 spec./g). The second increase in abundance was detetced between sample 159-959-66R-3,44-48 (1037.14 mbsf) and sample 159-959-66R-2,25-29 (1035.45 mbsf) with a *Micula* abundance of 0.54 X 10^9 spec./g, with *M. staurophora* (0.4 X 10^9 spec./g), *M. concava* (0.14 X 10^9 spec./g) and *M. swastica* (0.003 X 10^9 spec./g).

The peak found in sample 159-959-65R-6,111-116 (1032.71 mbsf) shows a *Micula* abundance of 0.44 X 10^9 spec./g, with *M. staurophora* (0.32 X 10^9 spec./g), *M. concava* (0.09 X 10^9), *M. swastica* (0.01 X 10^9 spec./g), *M. adumbrata* (0.009 X 10^9 spec./g) and *M. cubiformis* (0.003 X 10^9 spec./g).

The holoccocoliths are represented only by *Calculites* (average 2.1%) whereas no *Lucianorhabdus* was found at ODP Site 959. Three different spikes of holoccocoliths are visible both in terms of relative abundances. The first peak was observed in the middle Coniacian CC14/UC10 zones and lower NC15-

NC16/NC15*-NC16* zones (sample 159-959-66R-6,36-40; 1041.56 mbsf) where *Calculites* reaches the 1.6% of the assemblage (0.01 X 10^9 spec./g). The second abundance maximum occurs in the upper Coniacian, upper CC15-CC16/ NC15-NC16/NC15*-NC16/ UC11 zone (sample 159-959-66R-1,83-86; 1034.53 mbsf) where the genus *Calculites* reaches the 2.2% of the assemblage (0.02 X 10^9 spec./g).

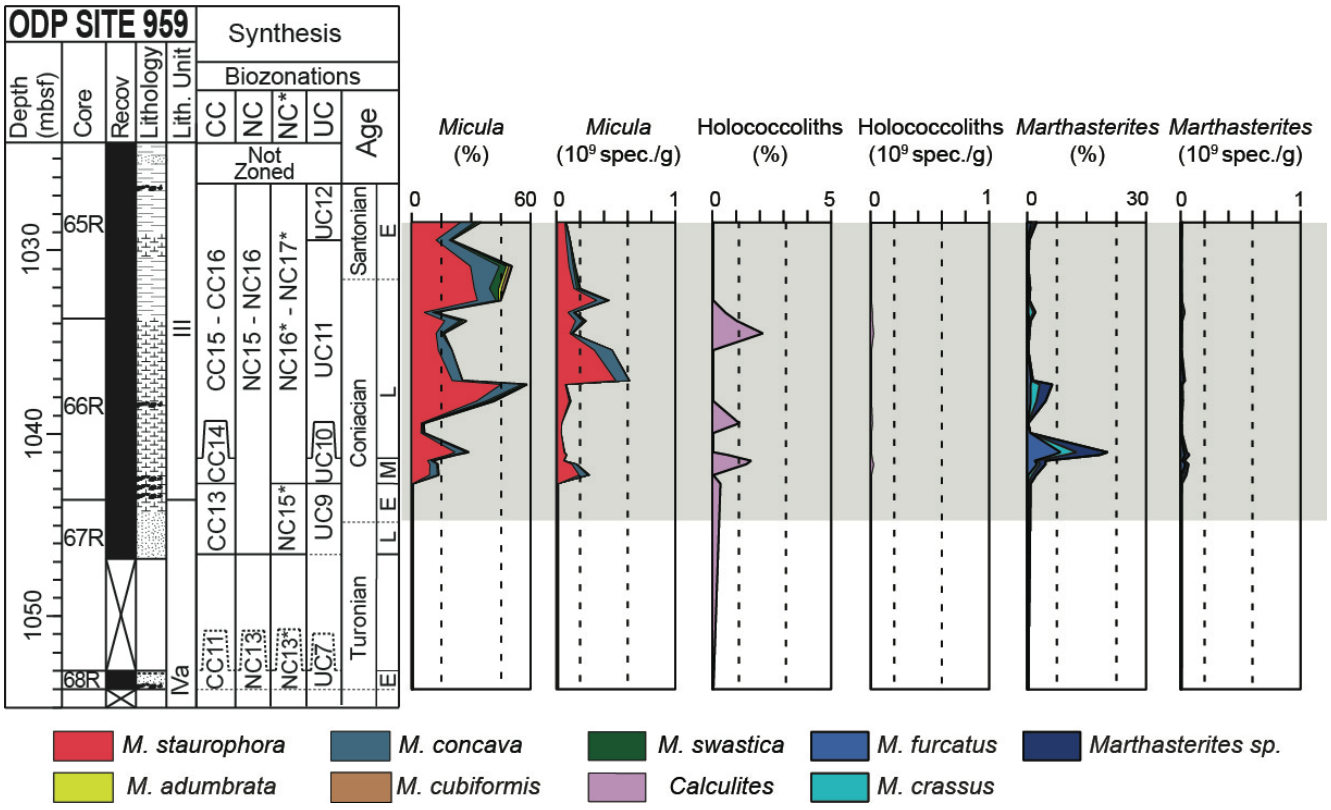

Figure 5.2.3.1 - Relative (%) and absolute abundance (number of specimens/g of sediment) of *Micula*, holococcoliths and *Marthasterites*. The OAE3 interval is indicated by a grey band.

As concern as the genus *Marthasterites* is concerned, the relative abundance curve shows two spikes, whereas no increases are show by the absolute abundance fluctuations.

The first peak is the most prominent and occurs in the CC14/UC10 zones and lower NC15-NC16/NC15*-NC16* (sample 159-959-66R-5,139-142; 1041.09 mbsf) where *Marthasterites* increases up to 20.2%, with *M. furcatus* (8.2%), *M. crassus* (4.1%) and *Marthasterites* sp.1 (7.9%). The absolute abundance shows increases slightly shifted compared to the relative abundance ones, and the highest value was observed in sample 159-959-66R, 4-8 (1041.24 mbsf) where the *Marthasterites* content is 0.06 X 10^9 spec./g, with *M. furcatus* (0.02 X 10^9), *M. crassus* (0.01 X 10^9) and *Marthasterites* sp.1 (0.03 X 10^9).The second spike occurs in the upper Coniacian CC15-CC16/ NC15-NC16/NC15*-NC16/ UC11 zones (sample 159-959-66R-3,65-67; 1037.35 mbsf), where *Marthasterites* increases up to 6.1% of the assemblages, with *Marthasterites* sp.1 (3.2%), *M. furcatus* (2.3%) and *M. crassus* (0.6%). Also in this case the absolute abundance is slightly shifted compared to the relative abundance, and the highest value

is reached in sample 159-959-66R-3, 44-48 (1037.14 mbsf) where *Marthasterites* absolute abundance is 0.03 X 10^9 spec./g, with *Marthasterites* sp.1 (0.01 X 10^9) and *M. furcatus* (0.02 X 10^9),

5.3 ODP Site 1261

5.3.1 Biostratigraphy

The biostratigraphic data available for Site ODP 1261 (Russo, 2014; Flögel et al., 2008 and Erbacher et al., 2004), were reinterpreted in this study.

Calcareous nannofossils are generally abundant to few-common, with a preservation that varies from good to moderate-poor. A total of five events were detected within the studied interval, allowing the identification of the CC12-CC16 zones of Sissingh (1977), NC14-NC16 zones of Roth (1978), NC14-NC17* of Bralower et al. (1995) and UC9-UC11c zones of Burnett (1998). Three further events were recognized and reported in Figure 5.3.1, because of their utility as biostratigraphic marker for the Turonian/Coniacian boundary interval. The results are presented in Figure 5.3.1 and the zonal and subzonal markers used in this study are described below from the oldest to the youngest. A range chart for Site 1261 is provided in the Appendix 9.

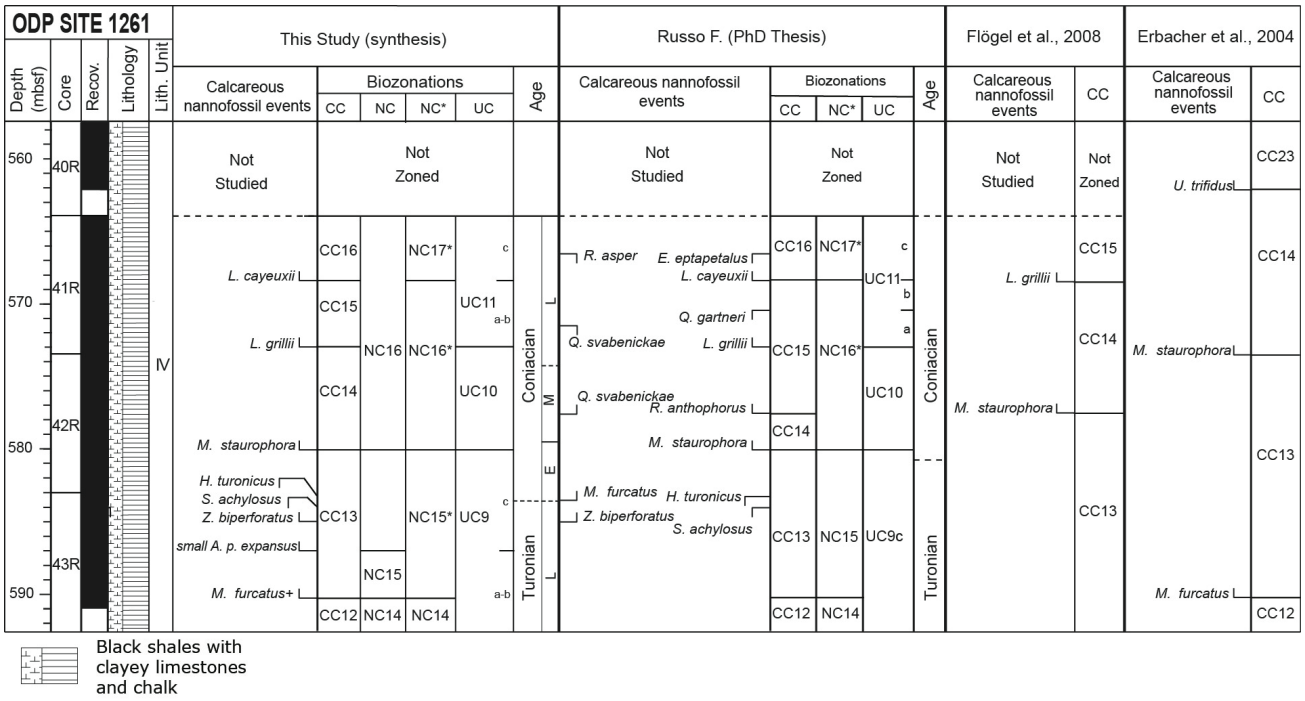

Figure 5.3.1 - ODP Leg 207 Site 1261 calcareous nannofossil biostratigraphy (this study) and comparison with previous data (Erbacher et al., 2004; Flögel et al., 2008; Russo F. PhD thesis). Biostratigraphic zonation: CC (Sissingh, 1977), NC (Roth,1978), NC* (Bralower 1995), and UC (Burnett 1998) are shown. The synthesis column is based on integration of data gathered in this study with those from the literature. Data from literature used for zonation in marked with asterisk (*).

The FO of *M. furcatus* defines the base of CC13, NC15, NC15* zones. This event was detected by Russo (2014) in sample 207-1261A-43R-1, 60-61 (583.60 mbsf) whereas Erbacher et al. (2004) found the FO of *M. furcatus* in a lower sample 207-1261A- 43R-CC,12-17 (590.10 mbsf). Thus, this last datum was used in this study (Figure 5.3.1). The FO of *A. parcus expansus* in sample 207-1261A- 43R-3,100-101 (587.0 mbsf) defines the base of zone NC16 and subzone UC9c. The FO of *M. staurophora* in sample 207-1261A-42R5, 100-101 (580.40 mbsf) marks the base of CC14, NC16, NC16* and UC10 zones. The FO of *L. grillii* was observed in sample 207-1261A-41R-7, 20-21 (573.00 mbsf) where the base of CC15 and UC11 zones was placed. The FO of *L. cayeuxii* in sample 207-1261A-41R-3, 140-141 (568.20 mbsf) defines the base of CC16 and NC17* zones.

According to calcareous nannofossil biostratigraphy (Russo, 2014; Flögel et al., 2008; Erbacher et al., 2004) revised in this study the Turonian/Coniacian boundary is placed between the FO of small *A. parcus expansus* and the FO of *M. staurophora,* below the LO of *H. turonicus* as suggested by Lees (2008).

5.3.2 Nannofossil paleoecology and paleoceanography

A total of 69 taxa were recognized in the investigated interval from ODP Site 1261. The species richness varies from a maximum of 46 in sample 207-1261-43R-1,20-21 (583. 2 mbsf) to 21 in sample 207-1261-43R-4,150-151 (589 mbsf) with a mean of 34 species for sample (Figure 5.3.2.1). The Shannon index ranges between 2.1 (24 m) and 3.3(130 m), with an average value of 2.9, suggesting well-diversified assemblages without dominance of single taxa. The total nannofossil abundance (number of specimens/field of view) varies from a maximum of 52 in sample 207-1261-41R-2,110-111 (566.4 mbsf) to 1 in sample 207-1261-43R-4,130-131 (588.8 mbsf) with a mean of 16 specimens/field of view (Figure 5.3.2.1). Higher values of total nannofossil abundance are recorded in the upper Turonian and upper Coniacian.

The presence of well-diversified assemblages and the occurrence of *W. barnesiae* together with abundant delicate and less diagenesis-resistant taxa such as *B. constans*, *D. ignotus* and *Z. erectus* suggest that the composition and abundance of calcareous nannofossils mainly reflect primary ecological signals with negligible diagenetic modifications.

The descriptive statistics of calcareous nannofossil genera and species are synthesized in Tables 5.3.2.1and 5.3.2.2. At ODP Site 1261 there are eight genera with an average relative abundance > 3% (*Biscutum, Eiffellithus*, *Microrhabdolus, Prediscosphaera, Seribiscutum, Tegumentum*, *Watznaueria* and *Zeugrhabdotus*). Further genera are characterized by average relative abundance > 2% (*Calculites*, *Staurolithites*, *Corollithion*, *Rhagosdiscus* and *Marthasterites*). Genera with average relative abundance

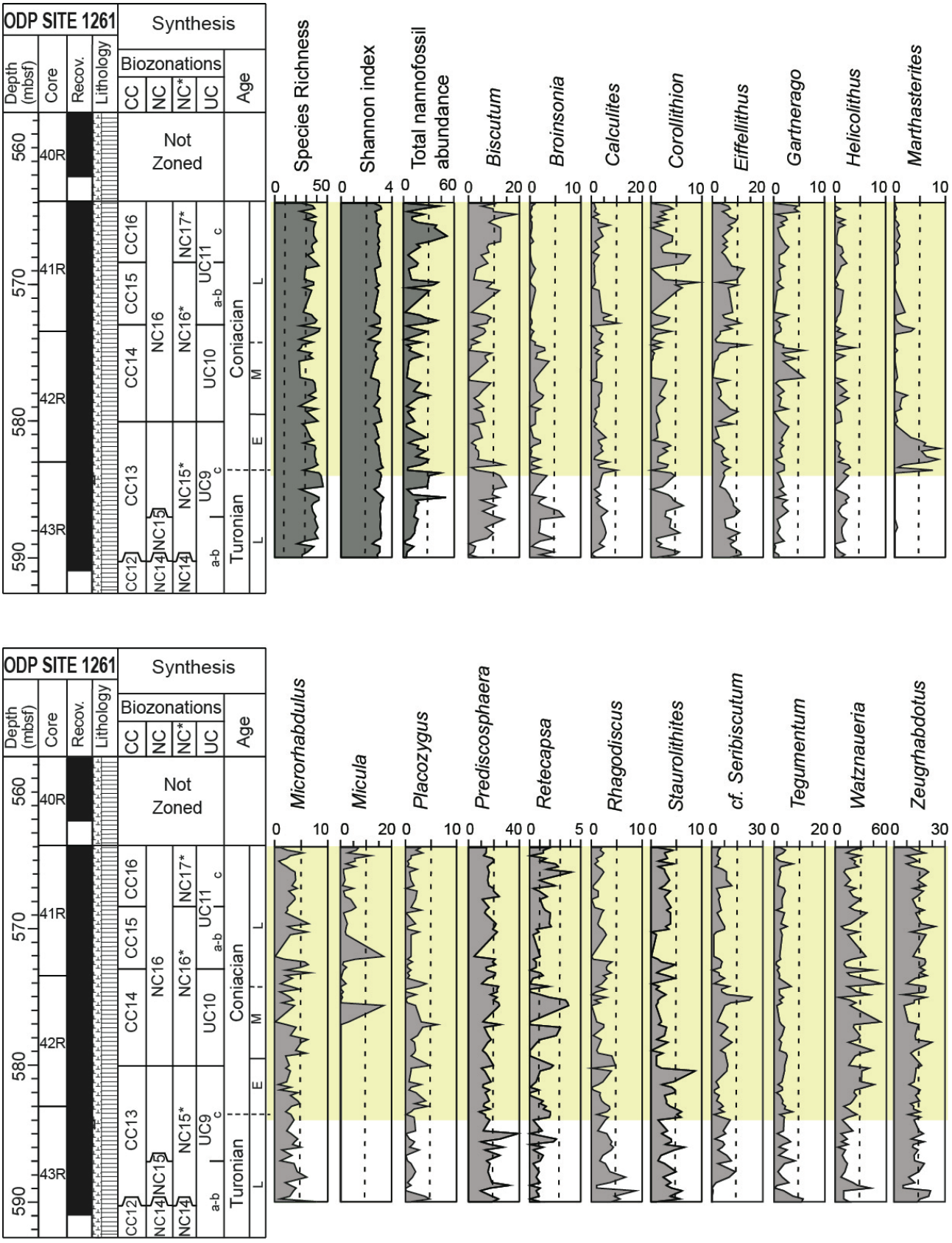

Figure 5.3.2.1 - Calcareous nannofossil data from ODP Site 1261 showing the fluctuations in species richness, Shannon index, total nannofossil abundance (specimens/FOV), absolute abundances (n. specimens/gram of sediment) and relative abundance of genera with an average relative abundance >1%. The yellow band indicates the OAE3 interval.

GENUS	Average %	Minimum %	Maximum %	Mode	Standard Deviation	Median
Watznaueria	20.5	2.3	54	17.2	11	19
Prediscosphaera	16.9	4	39	16.7	5.4	16.6
Zeugrhabdotus	13.5	4.9	23.9	17.9	4.1	13
Biscutum	6.4	0	18.7	1	4.1	6.4
Eiffellithus	5.7	0	13.9	7	3	5.8
cf. Seribiscutum	5.6	0	23.5	1	4.1	5
Tegumentum	3.1	0	11.3	2	2.1	2.9
Microrhabdulus	3.1	0	7.8	2.9	1.6	2.9
Calculites	2.9	0	10.5	2.9	2	2.9
Staurolithites	2.9	0	8.7	1	1.6	2.8
Corollithion	2.4	0	9.2	0	1.9	2.2
Rhagodiscus	2.2	0	8.7	2	1.6	2
Marthasterites	2.1	0	17.9	0	4.2	0.3
Gartnerago	1.6	0	6	1	1.2	1.3
Micula	1.5	0	16.8	0	3.2	0
Placozygus	1.5	0	6.2	1	1.3	1
Broinsonia	1.2	0	6.7	0	1.4	0.7
Retecapsa	1.1	0	4.1	0	1	1
Helicolithus	1.0	0	3.8	0	0.9	0.7
Manivitella	0.6	0	3.5	0	0.8	0.3
Lithastrinus	0.6	0	12.9	0	1.6	0
Discorhabdus	0.6	0	2.3	0	0.6	0.3
Eprolithus	0.4	0	5	0	0.8	0
Cylindralithus	0.4	0	2.9	0	0.5	0.3
Cribrosphaerella	0.3	0	2	0	0.5	0
Rotelapillus	0.2	0	1.6	0	0.4	0
Quadrum	0.2	0	2	0	0.4	0
Kamptnerius	0.1	0	2.9	0	0.4	0
Radiolithus	0.1	0	2.3	0	0.4	0
Loxolithus	0.1	0	2	0	0.3	0
Ahmuellerella	0.1	0	2	0	0.3	0
Chiastozygus	0.1	0	3	0	0.4	0
Nephrolithus	0.1	0	1	0	0.2	0
Aspidolithus	0.1	0	1	0	0.2	0
Cretarhabdus	0.05	0	1	0	0.2	0
Braarudosphaera	0.05	0	1	0	0.2	0
Liliasterites	0.04	0	1	0	0.1	0
Lucianorhabdus	0.02	0	0.3	0	0.1	0
Bukryaster	0.01	0	0.3	0	0.1	0
Stoverius a	0.01	0	0.3	0	0.1	0
Tetrapodorhabdus	0.01	0	0.3	0	0.1	0

Table 5.3.2.1 - Descriptive statistics of genera identified at ODP Site 1261.

SPECIES	Average %	Minimum %	Maximum %	Mode	Standard Deviation	Median
Ahmuellerell a octoradiata	0.1	0	2	0	0.3	0
Biscutum constans	6.4	0	18.7	1	4.1	6.4
Broinsonia matalosa	1.2	0	6.7	0	1.4	0.7
Aspidolithus parcus espansus	0.1	0	1	0	0.2	0
Braarudosphaera bigelowii	0.05	0	1	0	0.2	0
Bukryaster hayi	0.01	0	0.3	0	0.1	0
Chiastozygus platyrhethus	0.1	0	3	0	0.4	0
Corollithion signum	2.2	0	9.2	0	1.9	2
Corollithion exiguum	0.2	0	2	0	0.4	0
Cribrosphaerella ehrenbergii	0.3	0	2	0	0.5	0
Cretarhabdus conicus	0.05	0	1	0	0.2	0
Cylindralithus biarcus	0.4	0	2.9	0	0.5	0.3
Discorhabdus ignotus	0.6	0	2.3	0	0.6	0.3
Eiffellithus eximius	2.8	0	12	1	2.5	2
Eiffellithus gorkae	1.7	0	6.3	0	1.5	1.6
Eiffellithus turriseiffelii	1.1	0	8.5	0	1.5	0.7
Eprolithus floralis	0.4	0	5	0	0.8	0
Gartnerago obliquum	0.5	0	2	0	0.5	0.3
Gartnerago segmentatum	1.0	0	5	0	1.0	0.7
Grantarhabdus coronadventis	0.1	0	1.9	0	0.3	0
Helicolithus compactus	0.03	0	0.3	0	0.1	0
Helicolithus trabeculatus	0.9	0	3.8	0	0.9	0.7
Helicolithus turonicus	0.01	0	0.7	0	0.1	0
Kamptnerius magnificus	0.1	0	2.9	0	0.4	0
Lithastrinus grillii	0.1	0	2	0	0.3	0
Lithastrinus septenarius	0.5	0	12.9	0	1.6	0
Liliasterites angularis	0.04	0	1	0	0.1	0
Loxolithus armilla	0.1	0	2	0	0.3	0
Lucianorhabdus cayeuxii	0.02	0	0.3	0	0.1	0
Manivitella pemmatoidea	0.6	0	3.5	0	0.8	0.3
Marthasterites furcatus	2.1	0	17.9	0	4.2	0.3
Microrhabdulus belgicus	0.3	0	2	0	0.5	0
Microrhabdulus decoratus	2.8	0	7.8	2.9	1.5	2.8
Micula staurophora	1.5	0	16.8	0	3.2	0
Micula concava	0.02	0	0.7	0	0.1	0
Nephrolithus frequens	0.1	0	1	0	0.2	0
Placozygus fibuliformis	1.5	0	6.2	1	1.3	1
Prediscosphaera columnata	10.2	2	26	9.7	3.9	9.7
Prediscosphaera cretacea	0.4	0	4	0	0.6	0.3
Prediscosphaera ponticula	4.2	0.9	11.3	3	2.2	4
Prediscosphaera spinosa	2.1	0	10.3	1	1.6	1.9
Quadrum gartneri	0.1	0	2	0	0.4	0
Quadrum intermedium	0.003	0	0.3	0	0.0	0
Quadrum svabenikae	0.003	0	0.3	0	0.0	0

Table 5.3.2.2 -Descriptive statistics of species identified at ODP 1261.

Radiolithus planus	0.1	0	2.3	0	0.4	0
Retecapsa angustiforata	0.1	0	1.4	0	0.2	0
Retecapsa crenulata	0.3	0	2	0	0.5	0
Retecapsa ficula	0.3	0	2.7	0	0.6	0
Retecapsa surirella	0.5	0	3	0	0.7	0
Rhagodiscus angustus	0.9	0	3.2	0	0.9	0.7
Rhagodiscus plebeius	0.8	0	3.9	0	0.8	0.7
Rhagodiscus splendens	0.6	0	2.9	0	0.6	0.3
Rotelapillus crenulatus	0.2	0	1.6	0	0.4	0
Staurolithites laffittei	2.9	0	8.7	1	1.6	2.8
Stoverius achylosus	0.01	0	0.3	0	0.1	0
Tegumentum stradneri	1.0	0	3.4	0	0.8	0.9
Tegumentum orionatus	2.2	0	8.5	1	1.8	1.9
Tetrapodorhabdus decorus	0.01	0	0.3	0	0.1	0
Watznaueria barnesiae	17.2	2.3	51	10.6	9.5	14.5
Watznaueria biporta	2.0	0	15.6	0	3.1	0.6
Watznaueria fossacincta	1.3	0	6.9	0	1.3	1
Zeugrhabdotus bicrescenticus	0.8	0	3.8	0	0.9	0.3
Zeugrhabdotus biperforatus	0.7	0	3.6	0	0.7	0.6
Zeugrhabdotus diplogrammus	0.9	0	3.8	0	0.8	0.7
Zeugrhabdotus embergeri	0.04	0	2	0	0.2	0
Zeugrhabdotus erectus	9.3	2	21.8	6	3.7	8.9
Zeugrhabdotus kerguelenensis	0.2	0	3.8	0	0.6	0
Zeugrhabdotus noeliae	0.1	0	4.6	0	0.6	0
Zeugrhabdotus scutula	1.5	0	5.2	0	1.2	1.2

Table 5.3.2.2 - Descriptive statistics of species identified at ODP 1261.

< 2% are not discussed here but their descriptive statistics is shown in Tables 5.4.3.1 and 5.4.3.2. Figure 5.3.2.1illustrates the relative abundances of genera with an average > 1%. The dominant genus is *Watznaueria* which ranges from 2.3% to 54% (average 20.5%). The higher relative abundances are recorded in the middle Coniacian, whereas in the upper Turonian this genus is less abundant. As shown in Table 5.4.3.2 *W. barnesiae* represents the most abundant species ranging from 2.3% to 51%. Other *Watznaueria* species are *W. biporta* and *W. fossacinta*.

The second most abundant genus is *Prediscosphaera* which fluctuates from 4% to 39% (average 16.9%). The maximum relative abundance is reached in the uppermost Turonian. This genus is represented by four species: *P. columnata*, *P. cretacea*, *P. ponticula* and *P. spinosa*. The most abundant species is *P. columnata* ranging from 2% to 26% (average 10.2%).

The genus *Zeugrhabdotus* ranges from 4.9% to 23.9% (average 13.5%). The most abundant *Zeugrhabdotus* species is *Z. erectus* varying between 2% to 21.8% (average 9.3%). Many other species of *Zeugrhabdotus* were detected at ODP Site 1261: *Z. bicrescenticus*, *Z. biperforatus*, *Z. diplogrammus*, *Z. embergeri*, *Z. kerguelenensis*, *Z. noeliae* and *Z. scutula*.

Genus *Biscutum* ranges from 0% to 18.7% (average 6.4%). The higher relative abundances are recorded in the upper Turonian (from sample 207-1261-43R-4,110-111 at 588.6 mbsf to sample 207-1261-43R-1,80-81 at 583.8 mbsf) and in the upper Coniacian (from sample 207-1261-41R-2,150-151 at 566.8 mbsf to 207-1261-41R-1,20-21 at 564 mbsf). *Eiffellithus* ranges from 0% to 13.9% (average 5.7%). This genus includes *E. eximius* that varies from 0% to 12%(average 2.8%), *E. gorkae* that ranges from 0% to 6.3% (average 1.7%) and *E. turriseiffelii* that ranges from 0% to 8.5% (average 1.1%).

The genus *Seribiscutum* fluctuates from 0% to 23.5% (average 5.6%) and shows a distinctive peak in the middle Coniacian (sample 207-1261-42R-2,10-11; 575 mbsf).

The genus *Microrhabdulus* ranges from 0% to 7.8% (average 3.1%) and includes the species *M. belgicus* and *M. decoratus*.

Tegumentum ranges from 0% to 11.3% (average 3.1%), with higher relative abundances recorded in the upper Turonian. The genus *Tegumentum* is composed of *T. stradneri* that ranges from 0% to 3.4% (average 1%) and *T. orionatus* that ranges from 0% to 8.5% (average 2.2%).

The genus *Calculites* ranges from 0% to 10.5% (average 3.1%). The maximum content in *Calculites* was reached in two distinctive peaks, respectively in the uppermost Turonian and in the upper Coniacian.

Staurolithites varies from 0% to 8.7 % (average 2.9%), whereas *Corollithion* ranges from 0% to 9.2% (average 2.4%). Genus *Rhagosdiscus* ranges from 0% to 8.7 % (average 2.2%) and includes *R. angustus* that ranges from 0% to 3.2% (average 0.9%), *R. plebeius* that ranges from 0% to 3.9% (average 0.8%) and *R. splendens* that ranges from 0% to 2.9% (average 0.6%)

The genus *Marthasterites* ranges from 0% to 17.9 % (average 2.1%) of the assemblages and is represented only by the species *M. furcatus*. In the uppermost Turonian-early Coniacian a peak of 12% was detected.

The fluctuations in the NI and TI are presented in Figure 5.3.2.2. At ODP Site 1261 the NI values show relatively high values throughout the studied section with an average of 50 and reaching a maximum of 88. The NI is mainly driven by the high content in *B. constans* and *Z. erectus* that occur with an average relative abundance of 6.4% and 9.3%, respectively. The fertility related *D. ignotus* is, instead, relatively rare (average 0.6%). The relatively high content of high fertility taxa together with a low content of *W. barnesiae* (average 20.5%) suggest that the investigated interval is characterized by meso-eutrophic condition of surface waters.

ODP Site 1261 the TI V.1 shows the prevalence of warmer water conditions interrupted by cooling interludes, with the most extended of them in the upper Coniacian (Figure 5.3.2.2). The TI V.2 and V.3

have a similar trend showing longer episodes of cooling in the upper Turonian and middle and upper Coniacian. The TI V.4 index shows the prevalence of warmer water conditions interrupted only by a few cooling interludes.

At ODP Site 1261, the cool water taxa as *A. octoradiata* and *E. floralis* are rare with an average content respectively of 0.1% and 0.4% of the assemblages. *G. segmentatum* have a higher relative abundance and ranges from 0% to 5 % (average 1%), and show a peak of increase in the middle and the upper Coniacian. Also, the warm water indicator, *Z. diplogrammus* occur with low abundances and ranges from 0% to 3.8 % (average 0.9%).

The correlation matrix for the ODP Site 1261 doesn't support a correlation among the cool water taxa (values around 0) suggesting that they change independently of one another.

The Pearson's correlation coefficients for the genera detected at the ODP Site 1261 documented only a positive correlation with *Lithastrinus* that exhibits a positive correlation with *Radiolithus* (0.62). The complete correlation matrix is provided in the Appendix (10A). Correlation coefficients were also obtained for all species detected at ODP Site 1261 (Appendix 10B). A correlation was documented for:

- *L. septenarius* versus *R. planus* (0.60)
- *Q. svabenike* versus *R. angustiforata* (0.61)
- *M. furcatus* versus *W. biporta* (0.60)

5.3.3 The Coniacian-Santonian OAE3 at ODP Site 1261

According to calcareous nannofossil biostratigraphy, the stratigraphic range of the OAE3 interval at ODP Site 1261 extends from Core 207-1261-43R but the studied interval only extends up to the upper Coniacian (Core 207-1261-41R) as show in Figure 5.3.2.3.

Significant fluctuations in relative abundance of genera *Micula* and *Marthasterites* and of holoccoccoliths (*Lucianorhabdus* and *Calculites*) were detected (Figure 5.3.2.3).

The genus *Micula* ranges from 0% to 16.8 % (average 1.5%) and includes *M. concava* and *M. staurophora*. Distinctive increases in relative abundance of *Micula* are recognized at ODP Site 1261: the first peak in the CC14/UC10 zones and lower NC16* zone in the middle Coniacian (sample 207-1261-42R-2,70-71; 575.6 mbsf). Here, *M. staurophora* reaches the 16.8% of the assemblage. A second spike occurs in the CC15/UC11a-b zones and upper NC16* zone in the upper Coniacian (sample 207-1261-41R-6,70-71; 572 mbsf). Also in this sample *M. staurophora* reaches a value of 16.8%. A further increase is documented in the CC16/NC17*zones and UC11c subone in the upper Coniacian (sample 207-1261-41R-1, 80-; 564.6 mbsf), where *M. staurophora* shows a relative abundance of 11.7%.

Holoccocoliths are mostly composed of *Calculites* (average 2.9%) and rare *Lucianorhabdus* (average 0.02%). A first peak in holoccocolith relative abundance occurs in the CC13/NC15*/UC9c zones (Turonian/Coniacian boundary) where *Calculites* reaches a value of 10%. A second spike is present in CC15/UC11a-b zone and upper NC16* zone in the upper Coniacian (sample 207-1261-41R-6,150-151; 572.8 mbsf) where *Calculites* represents the 10.5% of the assemblage. A further maximum was observed is in the CC16/NC17*zones and UC11c subzone in the upper Coniacian (sample 207-1261-41-2,30-31; 565.6 mbsf).

The genus *Marthasterites* shows two distinct intervals of higher relative abundance: the first was observed in the CC13/NC15*zones and UC9c subzone in the Turonian/ Coniacian boundary interval, with three distinctive spikes reaching 15% (sample 207-1261-43R-1,60-61 at 583.6 mbsf), 17.2% (sample 207-1261-42R-7,40-41 at 582.8 mbsf) and 17.9% (sample 207-1261-43R-6,110-111 at 582 mbsf), respectively.

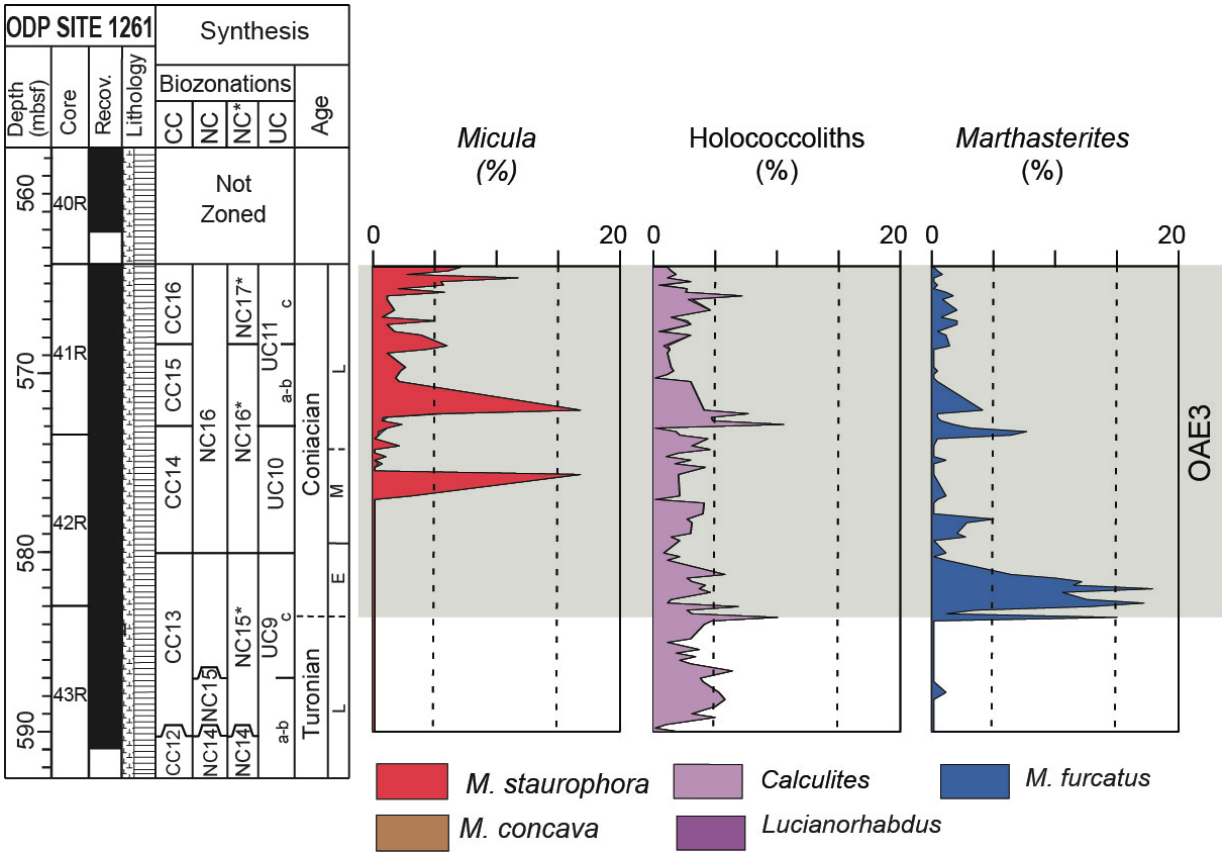

Figure 5.3.2.3 - Relative (%) and absolute (number of specimens/g of sediment) abundances of *Micula*, holococcoliths and *Marthasterites*. The OAE3 interval is indicated by the grey band.

The second increase in relative abundance was detected in the upper Coniacian (CC15/NC16* and UC11a-b subzone) where *Marthasterites* reaches the 7.6% of the assemblage in sample 207-1261-41R-7,40-41 (573.2 mbsf).

5.4 Seaford Head

5.4.1 Biostratigraphy

The preservation of calcareous nannofossil assemblages in the studied interval is moderate, with specimens that exhibit overgrowth rather than etching. However, although the primary morphological characters are somewhat altered, the identification at the species level was in most cases possible. The biostratigraphy scheme followed in this study includes the one by Fritsen et al. (2000). This zonation is originated from that of Burnett (1998), with some revision based on the investigation carried out in the North Sea chalk and circum North Sea Basin outcrop sections.

The total nannofossil abundance varies from rare in the first 26 m becoming few to common in the upper part of the studied interval. The zonal and subzonal markers identified are described from the oldest to the youngest (Figure 5.4.1) A range chart for Seaford Head is provided in the Appendix 11.

The results of this study are compared to that of Hampton (2007) who also studied the Seaford Head section. Fifteen events, including zonal and subzonal markers, were detected allowing the identification of the CC13-CC18, NC16-NC18, NC15*-NC18*, UC9c-UC14 zones and UC9* –UC14* zones of Fritsen et al. (2000). Other two events were recognized and reported in Figure 5.4.1 because of their utility as biostratigraphic marker for the Turonian/Coniacian boundary interval.

small *A. parcus expansus* and *L. septenarius* are present from the lowermost analyzed sample, thus the base of the section lies in the CC13, NC15, UC9c, UC9* zones. *M. quasihoschulzii* has its FO at 8 m and the last occurrence (LO) of *H. turonicus* at 12 m, although this species was found in only two samples in the studied interval.

The FO of *M. staurophora* was observed at 26 m where the base of CC14, NC16, NC16*, UC10, UC10 zones was placed. The FO of *L. grillii* lies at 36 m and defines the base of the CC15 UC11and UC11* zones. At Seaford Head, *M. concava* is extremely rare and observed only in two samples (at 40 and 42 m). The FO of *L. cayeuxii* at 48 m defines the base of the CC16, NC17* zones and UC11c subzone.

In the Seaford Head section *E. floralis* is found to be continuous in the association up to 40 m. After that level, it is found discontinuously up to 82.09 m where it become extinct. Accordingly, these events where respectively label the Last Common Occurrence (LCO) and the LO of *E. floralis*. The LO of *E. floralis* defines the base of the CC17 and NC17 zones.

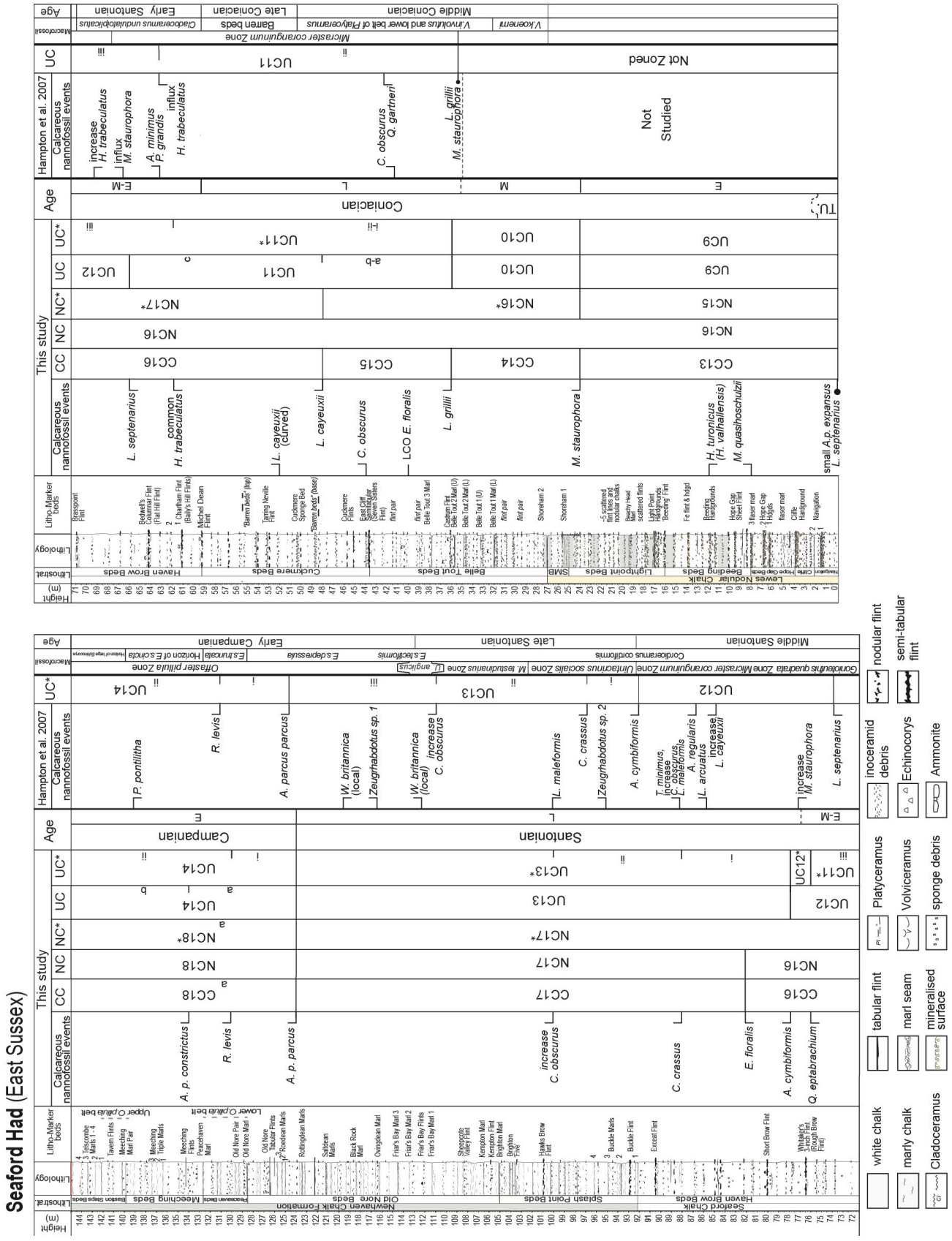

Figure 5.4.1 - Calcareous nannofossil biostratigraphy of Seaford Head section (this study) compared with previous data of Hampton et al. (2007). Biostratigraphic zonation: CC (Sissingh, 1977), NC (Roth,1978), NC* (Bralower 1995), and UC (Burnett 1998) are shown. Macrofossil biostratigraphy is after Mortimore (1986).

H. trabeculatus was recorded as common between 48 m and 66 m, the end of common *H. trabeculatus* marks the base of UC11*iii. The LO of *L. septenarius* was observed at 66 m where the base UC12 Zone was placed.

The LO of *Q. eptabrachium* at 76 m marks the base of UC12* zone. The FO of *A. cymbiformis* lies at 78 m and defines the base of the UC13 and UC13* zones. The FO of *C. crassus* at 88 m define the base of the UC13i subzone, whereas the increase in abundance of *C. obscurus* marks the base of UC13ii subzone. The FO of *A. parcus parcus* was observed at 124 m where the base of CC18, NC18, NC18*, UC14 zones was placed. The FO of *R. levis* at 130 m marks the base of UC14i subzone whereas the FO *A. parcus contrictus* at 134 define the base of UC14b subzone.

According to the calcareous nannofossil biostratigraphy data from this study and the macrofossil zonation from Hampton et al. (2007) the following stage boundaries were placed:

- the Turonian/Coniacian boundary cannot be determined precisely. According to Lees (2008) the Turonian/Coniacian boundary lie between the FO of *A. parcus expansus* and the FO of *M. staurophora*. The presence of small *A. parcus expansus* at the base of the section, followed by two events considered to occur in the early Coniacian (Burnet,1997; Lees, 2008) as the FO of *M. quasihoschulzii* and the LO of *H. turonicus* respectively at 8 m and 12m suggest that the lower part of the section includes only the topmost Turonian or otherwise belongs entirely to the Coniacian. For this reason, the Turonian/Coniacian boundary is indicated with a dashed line in figure 5.4.1.
- The Coniacian/Santonian boundary corresponds to the FO of the inoceramid *Cladoceramus undulatoplicatus* as defined in the GSSP reference section of Olazagutia (Lamolda et al., 2014).
- The Santonian/Campanian boundary corresponds to the FO of *A. parcus parcus*, that is used to approximate the base of the Campanian (Miniati et al., 2020). However, this event lies about 11 m above the LO of *Marsupites testudinarius* that represents the event traditionally used in southern England to place the Santonian/Campanian boundary as reported by Hampton et al. (2007).

5.4.2 Nannofossil paleoecology and paleoceanography

In the Seaford Head section a total of 128 taxa were recognized. The species richness of individual samples varies from a maximum of 53 (94.09 m) to 25 (50 m) with a mean of 39 species for sample (Figure 5.4.3.1). The lower values of species richness are present in the uppermost Turonian-lower Coniacian, with an average of 30, whereas the higher values (average of 44) are present in the upper Santonian-lower Campanian. The Shannon index and the total nannofossil abundance show patterns similar to the species richness (Figure 5.4.3.1). The Shannon index ranges between 1.4 (24 m) and 3.1 (130 m), with an average value of 2.3, suggesting a moderately to well diversified assemblages and

absence of dominance of single taxa. The total nannofossil abundance (number of specimens/field of view) has low values in the upper Turonian – Coniacian (~4 specimens/field of view) and increases in the Santonian (~10 specimens/field of view).

The absolute abundance of calcareous nannofossils have an average of 0.37 X 10^9 specimens/g. It ranges from a minimum of 0.06X 10^9 specimens/g in the lower Coniacian to a maximum of 1.33X10^9 specimens/g in the late Santonian.

The presence of moderately to well diversified assemblages and the occurrence of *W. barnesiae* together with delicate and less diagenesis-resistant taxa such as *B. constans*, *D. ignotus* and *Z. erectus* suggest that the distribution and abundance of calcareous nannofossils reflect mainly the primary ecological signal with negligible diagenetic modifications.

The descriptive statistics of calcareous nannofossil genera and species are synthesized in Tables 5.4.3.1 and 5.4.3.2. In the Seaford Head section, there are seven genera with an average relative abundance > 3% (*Biscutum, Eiffellithus, Lucianorhabdus, Micula, Prediscosphaera, Retecapsa, Watznaueria*). Further genera are characterized by average relative abundance > 2% (*Calculites, Helicolithus, Tranolithus*). Genera with average relative abundance < 2% are not discussed here but their descriptive statistics are show in Tables 5.4.3.1 and 5.4.3.2. Figure 5.4.3.1illustrates the relative abundances of genera with an average > 1%.

The dominant genus is *Watznaueria* which ranges from 22.2% to 73.4% (average 47.7%). The higher relative abundances are recorded in the uppermost Turonian – lower Santonian interval, whereas a decrease was observed in the upper Santonian-lower Campanian. As shown in Figure Figure 5.4.3.1. *W. barnesiae* represents the most abundant species ranging from 21.2% to 69.7%. Another frequent *Watznaueria* species is *W. communis* that ranges from 0% to 8.8% (average 2.2%).

The genus *Prediscosphaera* is the second in abundance and ranges from 2.9% to 21.7% (average 10.6%). High abundance of *Prediscosphaera* (>10%) of the assemblage occurs from the upper Santonian upwards (Figure 5.4.2.1). This genus is represented by six species: *P. columnata*, *P. cretacea*, *P. desiderograndis*, *P. grandis*, *P. ponticula* and *P. spinosa*. The most abundant species is *P. cretacea* ranging from 2.9% to 19.5% (average 9.3%).

Lucianorhabdus ranges from 0.3% to 11.4% (average 5.7 %). Low relative abundances of *Lucianorhabdus* occur in the uppermost Turonian – lower Coniacian (average 1.2%) whereas higher relative abundances are recorded from the lower Coniacian to the lower Campanian (average 6.4%). Four different species of *Lucianorhabdus* were detected at Seaford Head: *L. arcuatus; L. cayeuxii*; *L. maleformis*; *L. quadrifidus*. The most abundant species are *L. cayeuxii* that ranges from 0% to 5,7% (average 1.2%), and *L. maleformis* that ranges from 0% to 5,8% (average 2.4%).

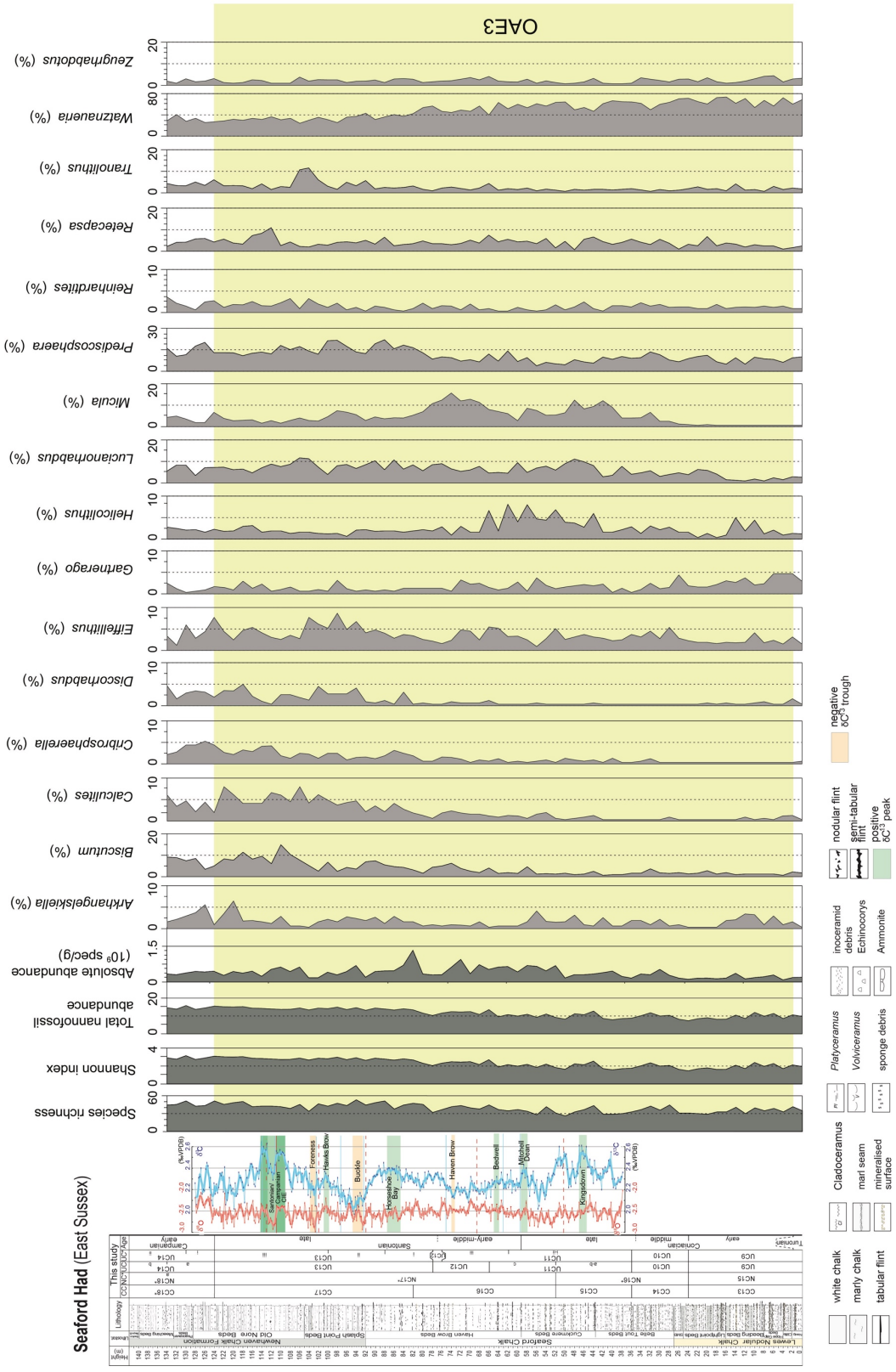

Figure 5.4.2.1 - Calcareous nannofossil data from the Seaford Head section showing the fluctuations of species richness, Shannon index, total nannofossil abundances (specimens/FOV) absolute abundances (specimens/gram of sediment) and the relative abundances of genera with an average abundance >1%. The isotopes record after Thibault et al. (2016). Yellow band indicates the OAE3 interval.

SPECIES	Average %	Minimum %	Maximum %	Median	Standard Deviation	Mode
Ahmuellerella octoradiata	0.2	0.0	1.3	0.0	0.4	0.0
Ahmuellerella regularis	0.2	0.0	2.5	0.0	0.5	0.0
Amphizygus brooksii brooksii	0.1	0.0	1.0	0.0	0.2	0.0
Amphizygus brooksii nanus	0.02	0.0	0.3	0.0	0.1	0.0
Amphizygus minimus	0.2	0.0	1.3	0.0	0.3	0.0
Arkhangelskiella confusa	1.3	0.0	5.1	1.3	1.1	0.3
Arkhangelskiella cymbiformis	0.1	0.0	1.9	0.0	0.3	0.0
Aspidolitus enormis	0.4	0.0	2.4	0.0	0.7	0.0
A.parcus expansus	0.1	0.0	1.3	0.0	0.2	0.0
A.parcus parcus	0.02	0.0	0.9	0.0	0.1	0.0
Biscutum hattneri	0.00	0.0	0.3	0.0	0.0	0.0
Biscutum constans	3.3	0.0	14.7	2.0	3.1	0.6
Biscutum coronum	0.02	0.0	0.6	0.0	0.1	0.0
Biscutum magnum	0.01	0.0	0.3	0.0	0.1	0.0
Biscutum melaniae	0.02	0.0	0.6	0.0	0.1	0.0
Braarudosphaera bigelowii	0.3	0.0	1.8	0.3	0.4	0.0
Broinsonia signata	0.2	0.0	1.2	0.0	0.3	0.0
Bukrylithus ambiguus	0.00	0.0	0.3	0.0	0.0	0.0
Calculites obscurus	1.5	0.0	7.9	0.3	2.0	0.0
Calculites ovalis	0.4	0.0	1.6	0.3	0.5	0.0
Calculites percernis	0.05	0.0	1.0	0.0	0.2	0.0
Chiastozygus bifarius	0.03	0.0	0.3	0.0	0.1	0.0
Chiastozygus fessus	0.4	0.0	3.0	0.0	0.7	0.0
Chiastozygus litterarius	0.05	0.0	0.9	0.0	0.2	0.0
Chiastozygus spissus	0.02	0.0	0.6	0.0	0.1	0.0
Cribrosphaerella circula	0.00	0.0	0.3	0.0	0.0	0.0
Cribrosphaerella ehrenbergii	1.1	0.0	5.1	0.6	1.3	0.0
Cyclagelosphaera margerelii	0.01	0.0	0.3	0.0	0.1	0.0
Cylindralithus biarcus	0.1	0.0	1.6	0.0	0.3	0.0
Cylindralithus coronatus	0.03	0.0	0.6	0.0	0.1	0.0
Cylindralithus crassus	0.04	0.0	0.6	0.0	0.1	0.0
Cylindralithus nudus	0.1	0.0	0.6	0.0	0.1	0.0
Cylindralithus sculptus	0.04	0.0	0.6	0.0	0.1	0.0
Cylindralithus serratus	0.04	0.0	0.3	0.0	0.1	0.0
Cretarhabdus conicus	0.04	0.0	0.6	0.0	0.1	0.0
Discorhabdus ignotus	0.9	0.0	7.9	0.3	2.0	0.0
Eiffellithus angustus	0.04	0.0	0.6	0.0	0.1	0.0
Eiffellithus casolus	0.1	0.0	1.2	0.0	0.3	0.0
Eiffellithus collis	0.1	0.0	1.3	0.0	0.2	0.0
Eiffellithus digitatus	0.01	0.0	0.6	0.0	0.1	0.0
Eiffellithus eximius	1.8	0.3	5.3	1.6	0.9	1.3
Eiffellithus gorkae	0.1	0.0	0.6	0.0	0.1	0.0
Eiffellithus nudus	1.0	0.0	5.4	0.7	1.0	0.6
Eiffellithus turriseiffelii	0.1	0.0	0.9	0.0	0.2	0.0
Eprolithus floralis	0.3	0.0	2.6	0.0	0.6	0.0
Eprolithus moratus	0.02	0.0	0.3	0.0	0.1	0.0
Gartnerago obliquum	0.01	0.0	0.6	0.0	0.1	0.0
Gartnerago segmentatum	1.5	0.0	4.5	1.1	1.1	0.3
Grantarhabdus coronadventis	0.1	0.0	0.7	0.0	0.2	0.0
Grantarhabdus diversum	0.00	0.0	0.3	0.0	0.0	0.0
Haqius circumradiatus	0.03	0.0	0.3	0.0	0.1	0.0
Helicolithus compactus	0.04	0.0	0.6	0.0	0.1	0.0
Helicolithus trabeculatus	0.8	0.0	6.0	0.2	1.4	0.0
Helicolithus turonicus	0.01	0.0	0.3	0.0	0.1	0.0
Helicolithus amceps	1.3	0.0	4.2	1.2	0.9	1.3
Lithastrinus grillii	0.5	0.0	2.0	0.2	0.6	0.0
Lithastrinus septenarius	0.2	0.0	1.6	0.0	0.4	0.0
Lithraphidites carniolensis	0.4	0.0	2.4	0.3	0.5	0.0
Loxolithus armilla	0.3	0.0	1.5	0.3	0.4	0.0
Lucianorhabdus arcuatus	0.1	0.0	0.9	0.0	0.2	0.0
Lucianorhabdus cayeuxii	1.4	0.0	6.0	1.0	1.6	0.0
Lucianorhabdus maleformis	2.4	0.0	5.8	2.2	1.6	1.9
Lucianorhabdus quadrifidus	0.4	0.0	1.9	0.3	0.5	0.0
Manivitella pemmatoidea	0.3	0.0	1.3	0.3	0.3	0.0

Table 5.4.2.1 - Descriptive statistics of genera identified at Seaford Head section.

GENUS	Average %	Minimum %	Maximum %	Mode	Standard Deviation	Median
Watznaueria	47.7	22.2	73.4	15.5	55.8	48.5
Prediscosphaera	10.6	2.9	21.7	4.6	8.8	9.6
Lucianorhabdus	5.7	0.3	11.4	2.8	4.2	5.8
Micula	4.3	0.0	15.5	3.8	0.0	3.5
Retecapsa	3.4	0.0	10.6	1.9	2.9	3.2
Biscutum	3.4	0.0	14.7	3.2	0.6	2
Eiffellithus	3.3	0.6	8.6	1.7	2.6	2.9
Helicolithus	2.2	0.0	8.0	1.7	1.3	1.6
Tranolithus	2.0	0.0	11.3	2.0	1.0	1.3
Calculites	2.0	0.0	7.9	2.2	0.0	1.2
Gartnerago	1.5	0.0	4.5	1.1	0.3	1.2
Zeugrhabdotus	1.5	0.0	3.9	1.0	0.3	1.3
Arkhangelskiella	1.4	0.0	6.3	1.3	0.3	1.3
Cribrosphaerella	1.1	0.0	5.1	1.3	0.0	0.6
Reinhardtites	1.1	0.0	3.4	0.8	0.6	1
Discorhabdus	0.9	0.0	4.8	1.3	0.0	0.3
Nannoconus	0.7	0.0	5.1	1.1	0.0	0.3
Placozygus	0.7	0.0	2.7	0.6	0.0	0.6
Lithastrinus	0.7	0.0	2.2	0.6	0.3	0.6
Aspidolitus	0.5	0.0	2.7	0.7	0.0	0.2
Cylindralithus	0.5	0.0	2.5	0.5	0.0	0.3
Chiastozygus	0.5	0.0	3.0	0.8	0.0	0
Quadrum	0.5	0.0	2.9	0.6	0.0	0.3
Ahmuellerella	0.4	0.0	3.1	0.7	0.0	0
Lithraphidites	0.4	0.0	2.4	0.5	0.0	0.3
Amphizygus	0.3	0.0	2.3	0.5	0.0	0
Eprolithus	0.3	0.0	2.7	0.7	0.0	0
Manivitella	0.3	0.0	1.3	0.3	0.0	0.3
Braarudosphaera	0.3	0.0	1.8	0.4	0.0	0.3
Microrhabdulus	0.3	0.0	2.2	0.5	0.0	0
Loxolithus	0.3	0.0	1.5	0.4	0.0	0.3
Broinsonia	0.2	0.0	1.2	0.3	0.0	0
Kamptnerius	0.2	0.0	1.3	0.3	0.0	0
Staurolithites	0.2	0.0	1.3	0.3	0.0	0
Grantarhabdus	0.1	0.0	0.7	0.2	0.0	0
Rhagodiscus	0.1	0.0	0.7	0.2	0.0	0
Rotelapillus	0.1	0.0	1.9	0.3	0.0	0
Rucinolithus	0.1	0.0	1.0	0.2	0.0	0
Cretarhabdus	0.04	0.0	0.6	0.1	0.0	0
Tetrapodorhabdus	0.04	0.0	0.6	0.1	0.0	0
Haqius	0.03	0.0	0.3	0.1	0.0	0
Micrantholithus	0.03	0.0	0.6	0.1	0.0	0
Cyclagelosphaera	0.01	0.0	0.3	0.1	0.0	0
Tegumentum	0.01	0.0	0.3	0.1	0.0	0
Bukrylithus	0.004	0.0	0.3	0.0	0.0	0
Lapideacassis	0.004	0.0	0.3	0.0	0.0	0
Radiolithus	0.004	0.0	0.3	0.0	0.0	0

Table 5.4.2.2 - Descriptive statistics of species identified at Seaford Head

Micrantholithus quasihoschulzi	0.03	0.0	0.6	0.0	0.1	0.0
Microrhabdulus decoratus	0.3	0.0	2.2	0.0	0.5	0.0
Micula adumbrata	0.2	0.0	1.6	0.0	0.3	0.0
Micula concava	0.01	0.0	0.3	0.0	0.1	0.0
Micula cubiformis	0.1	0.0	1.0	0.0	0.2	0.0
Micula swastica	0.2	0.0	1.6	0.0	0.4	0.0
Micula staurophora	3.9	0.0	14.0	3.2	3.4	0.0
Nannoconus elongatus	0.02	0.0	0.3	0.0	0.1	0.0
Nannoconus multicadus	0.05	0.0	1.2	0.0	0.2	0.0
Nannoconus truitti frequens	0.2	0.0	1.5	0.0	0.4	0.0
Nannoconus truitti trutti	0.01	0.0	0.3	0.0	0.1	0.0
Nannoconus truitti rectangular	0.2	0.0	2.4	0.0	0.4	0.0
Placozygus fibuliformis	0.7	0.0	2.7	0.6	0.6	0.0
Placozygus spiralis	0.01	0.0	0.3	0.0	0.1	0.0
Prediscosphaera columnata	0.9	0.0	2.4	0.6	0.7	0.3
Prediscosphaera cretacea	9.3	2.9	19.5	8.0	4.4	15.8
Prediscosphaera desiderogran	0.1	0.0	1.8	0.0	0.3	0.0
Prediscosphaera grandis	0.04	0.0	0.6	0.0	0.1	0.0
Prediscosphaera ponticula	0.1	0.0	1.3	0.0	0.2	0.0
Prediscosphaera spinosa	0.1	0.0	1.3	0.0	0.3	0.0
Quadrum eneabrachium	0.02	0.0	0.3	0.0	0.1	0.0
Quadrum eptabrachium	0.1	0.0	1.0	0.0	0.2	0.0
Quadrum intermedium	0.00	0.0	0.3	0.0	0.0	0.0
Quadrum gartnerii	0.3	0.0	2.1	0.0	0.5	0.0
Radiolithus planus	0.00	0.0	0.3	0.0	0.0	0.0
Retecapsa angustiforata	0.1	0.0	1.2	0.0	0.3	0.0
Retecapsa crenulata	1.4	0.0	4.7	1.3	1.1	0.6
Retecapsa ficula	0.5	0.0	5.6	0.3	0.9	0.0
Retecapsa octofenestrata	0.4	0.0	2.3	0.0	0.5	0.0
Retecapsa schizobrachiata	0.00	0.0	0.3	0.0	0.0	0.0
Retecapsa surirella	0.2	0.0	1.3	0.0	0.3	0.0
Rhagodiscus achlyostaurion	0.01	0.0	0.3	0.0	0.1	0.0
Rhagodiscus angustus	0.00	0.0	0.3	0.0	0.0	0.0
Rhagodiscus asper	0.00	0.0	0.3	0.0	0.0	0.0
Rhagodiscus plebeius	0.1	0.0	0.7	0.0	0.2	0.0
Rhagodiscus splendens	0.02	0.0	0.3	0.0	0.1	0.0
Reinhardtites anthophorus	1.1	0.0	3.0	0.9	0.7	0.6
Reinhardtites levis	0.04	0.0	0.9	0.0	0.2	0.0
Rotelapillus crenulatus	0.1	0.0	1.9	0.0	0.3	0.0
Rucinolithus hayi	0.1	0.0	1.0	0.0	0.2	0.0
Staurolithites imbricartus	0.01	0.0	0.3	0.0	0.1	0.0
Staurolithites laffittei	0.1	0.0	1.3	0.0	0.3	0.0
Staurolithites mielnicensis	0.00	0.0	0.3	0.0	0.0	0.0
Tetrapodorhabdus decorus	0.04	0.0	0.6	0.0	0.1	0.0
Tranolithus gabalus	0.04	0.0	0.3	0.0	0.1	0.0
Tranolithus orionatus	1.9	0.0	11.3	1.3	1.9	0.6
Tranolithus minimus	0.1	0.0	1.3	0.0	0.3	0.0
Tegumentum stradneri	0.01	0.0	0.3	0.0	0.1	0.0
Kamptnerius magnificus	0.2	0.0	1.3	0.0	0.3	0.0
Watznaueria barnesiae	45.1	21.2	69.7	46.2	14.9	32.8
Watznaueria biporta	0.2	0.0	1.0	0.0	0.2	0.0
Watznaueria britannica	0.00	0.0	0.3	0.0	0.0	0.0
Watznaueria communis	2.2	0.0	8.1	2.0	1.5	1.6
Watznaueria manivitiae	0.2	0.0	1.3	0.0	0.3	0.0
Watznaueria ovata	0.1	0.0	0.9	0.0	0.2	0.0
Zeugrhabdotus bifarius	0.1	0.0	0.6	0.0	0.1	0.0
Zeugrhabdotus biperforatus	0.3	0.0	1.6	0.2	0.4	0.0
Zeugrhabdotus bicrescenticus	0.01	0.0	0.9	0.0	0.1	0.0
Zeugrhabdotus diplogrammus	0.7	0.0	3.0	0.6	0.6	0.3
Zeugrhabdotus elegans	0.02	0.0	0.3	0.0	0.1	0.0
Zeugrhabdotus embergeri	0.03	0.0	0.3	0.0	0.1	0.0
Zeugrhabdotus erectus	0.2	0.0	1.3	0.0	0.4	0.0
Zeugrhabdotus praesigmoides	0.1	0.0	0.6	0.0	0.1	0.0
Zeugrhabdotus scutula	0.04	0.0	1.0	0.0	0.2	0.0

Table 5.4.2.2 - Descriptive statistics of species identified at Seaford Head.

The genus *Micula* - including *M. adumbrata*, *M. concava*, *M. cubiformis*, *M. swastica* and *M. staurophora* - ranges from 0% to 15.5%(average 4.3%). Distinctive increases of *Micula* are recognized in the Seaford Head section: a first peak is present in the middle Coniacian at 32 m (6.2%), then two maxima occur in the upper Coniacian and middle-upper Santonian, respectively (Figure 5.4.2.1). The first from 40m to 50m (average 9.2%) and the second from 62m to 80m (average 10%).The most abundant species is *M. staurophora* with relative abundances ranging from 0% to 14% (average 3.9%) with highest values in the upper Coniacian (average 8.2%) and in the lower-middle Santonian (average 11.3%).

Retecapsa ranges from 0% to 10.6% (average 3.4%) of the assemblage. A distinctive peak in *Retecapsa* occurs at 112 m (10.6%) close to the Santonian/Campanian boundary (Figure 5.4.2.1). The genus *Retecapsa* is mostly composed by *R. crenulata* that ranges from 0% to 4.7% (average 1.4%) and *R. ficula* that ranges from 0% to 5.6% (average 0.5%), but also includes rare *R. octofenestrata*, *R. schizobrachiata* and *R. surirella*.

The genus *Biscutum* ranges from 0% to 14.6% (average 3.38%). Within this genus *B. constans* is the most abundant species, ranging from 0% to 13.4% (average 2.8%). The highest abundance of *B. constans* was recorded in the uppermost Santonian (Figure 5.4.2.1). Other species of *Biscutum* are: large *B. constans*, *B. hattneri*, *B. coronum*, *B. magnum* and *B. melaniae*.

Genus *Eiffellithus,* ranging from 0.6% to 8.6% (average 3.3%), includes *E. angustus*, *E. casolus*, *E. collis*, *E. digitatus*, *E. eximius*, *E. gorkae*, *E. turriseiffelii* and *E. nudus.* A maximum of *Eiffellithus* occurs in the middle-upper Santonian from 94.09m to 104.9m (average 6.4%). The most abundant *Eiffellithus* species are *E. eximius* that ranges from 0.3% to 5.3% (average 1.7%) and *E. nudus* that ranges from 0% to 5.4% (average 1%).

Helicolithus ranges from 0% to 8% (average 2.2%) of the assemblage. A distinctive maximum of genus *Helicolithus* occurs in the upper Coniacian – lower Santonian, from 44m to 62.09m (average 5.1%). This genus includes *H. anceps* that ranges from 0% to 4.2% (average 1.3%), *H. trabeculatus* that ranges from 0% to 6% (average 0.8%) and less abundant *H. turonicus* (average 0.3%). A distinctive maximum of *Helicolithus* occurs in the upper Coniacian – lower Santonian from 44m to 62.09m (average 5.1%).

The genus *Calculites* ranges from 0% to 7.9% (average 2%) of the assemblage. This genus is rare in the lower part of the section but increases in the upper Santonian (average 4.3%). Within this genus *C. obsurus* is the most abundant species, ranging from 0% to 7.9% (average 2.8%). Other species of *Calculites* are: *C. ovalis* and *C. pernicensis*.

Genus *Tranolithus,* includung *T. gabalus*, *T. minimus* and *T. orionatus*, ranges from 0% to 11.3% (average 2%). A distinctive peak in *Tranolithus* occurs in the upper Santonian between 104.09 and

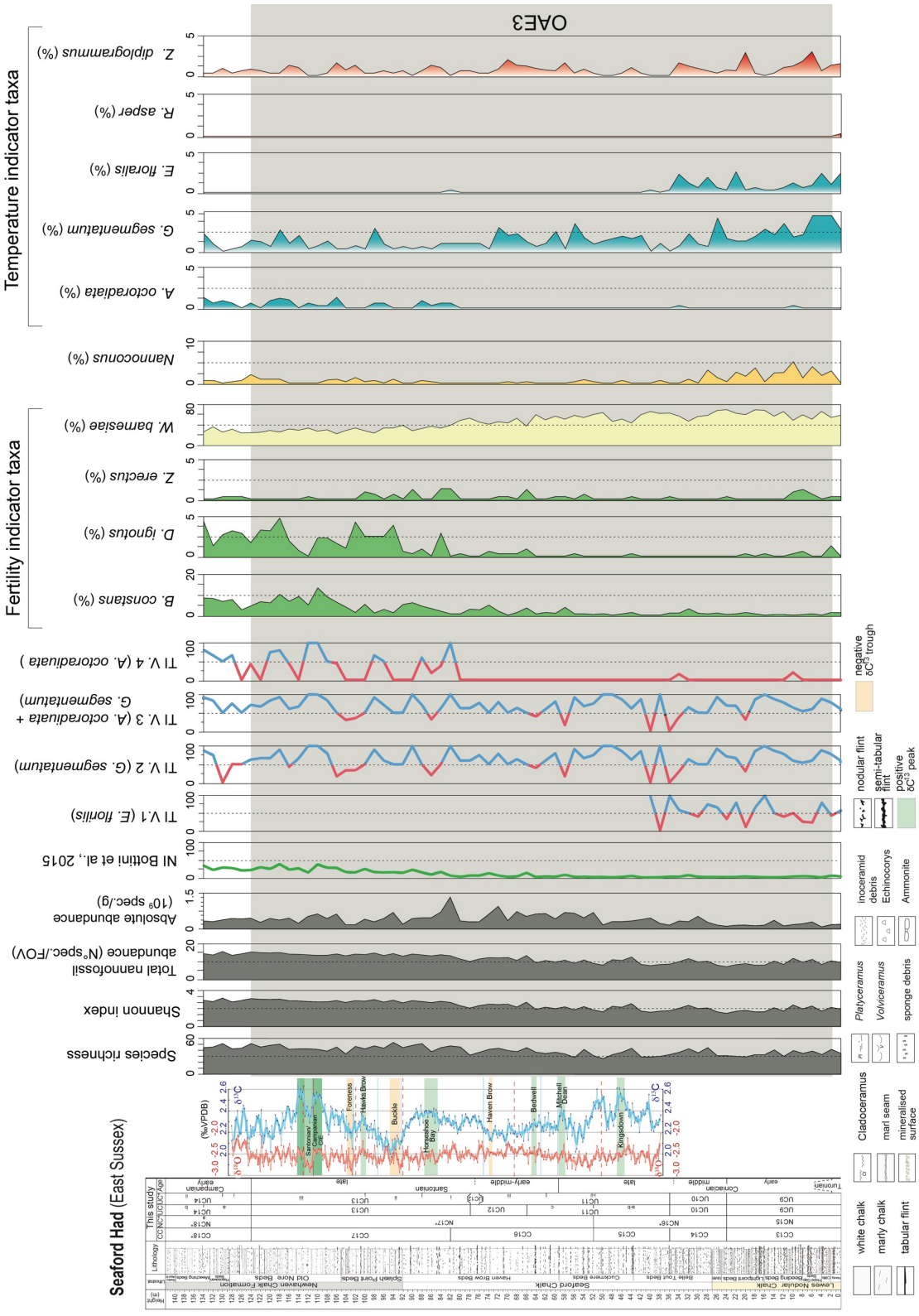

Figure 5.4.2.2 - Fluctuations of calcareous nannofossil temperature and fertility indicator taxa at Seaford Head section. Nutrient index (NI) after Bottini et al. (2015); Temperature index (TI) after Bottini et al. (2015) and modified here (V2, V, V4). The species richness, Shannon index, total nannofossil abundances (specimens/FOV) absolute abundances (specimens/gram of sediment) are also reported. The grey band indicates the OAE3 interval.

106m, reaching a relative abundance of 11.3% of the assemblages. This peak coincides with the maximum of *T. orionatus* in the assemblages.

The fluctuations in the NI and TI are presented in Figure 5.4.2.2. At Seaford Head the NI values remain close to zero from the base to the lower-middle Santonian (ca. 64m), then a moderate increase (up to 37) indicates a progressively higher fertility in the upper Santonian-lower Campanian. The increase in the NI is mainly driven by the increase in relative abundance of *B. constans* and *D. ignotus* together with a reduction of *W. barnesiae*. It is worth mentioning that *Z. erectus* considered the most fertility-related taxon, shows relative low abundances throughout the investigated interval suggesting mesotrophic (but not eutrophic) conditions.

In the Seaford Head section the TI indices 1, 2 and 3 show a similar trend (Figure 5.4.2.2), with the prevalence of cool water conditions interrupted by a few interludes of warming. More instable surface water temperature is reflected by the TI 1, with a more frequent alternation between cooler and warmer water condition in the uppermost Turonian-lower Coniacian. An opposite result was achieved with the TI. 4 that shows the prevalence of warm water conditions along the studied interval. Only from the late Santonian, this trend is interrupted by short cooling episodes.

However, at Seaford Head section the correlation matrix doesn't support a strong correlation between the cool water taxa *A. octoradiata*, *E. floralis* and *G. segmentatum*. *A. octoradiata* is positively correlated with *T. minimus* (0.61) and have a negative correlation with *W. barnesiae* (-0.61). It shows a low negative correlation versus *E. floralis* (-0.20) and *G. segmentatum* (-0.18), whereas these last have a low positive correlation (0.30).

The potential affinities of genera were tested by calculating the Pearson's correlation coefficients. A summary of the correlation matrix showing only the genera with a correlation > 0.6 (or < - 0.6) is reported in (Table 5.4.3.3), whereas the complete matrix is provided in the Appendix (12A).

There is a positive correlation documented for

- *Ahmuellerella* versus *Biscutum* (0.62), *Calculites* (0.64), *Cribrosphaerella* (0.83), *Discorhabdus* (0.69)
- *Amphizygus* versus *Discorhabdus* (0.61), *Staurolithites* (0.64)
- *Aspidolithus* versus *Calculites* (0.60)
- *Biscutum* versus *Calculites* (0.73), *Cribrospharella* (0.64), *Discorhabdus* (0.61) and *Staurolithites* (0.66)
- *Calculites* versus *Cribrospharella* (0.66) and *Discorhabdus* (0.73).

  All these genera show a negative correlation with *Watznaueria*.

Pearson's correlation coefficients were also obtained for all species detected at Seaford Head. A summary of the correlation matrix showing only the species with a correlation >0.6 (or < -0.6) is reported

	Ahmuellerella	Amphizygus	Aspidolitus	Biscutum	Calculites	Cribrosphaerella	Discorhabdus	Prediscosphaera	Staurolithites	Watznaueria
Ahmuellerella	1									
Amphizygus	0.57	1								
Aspidolitus	0.40	0.43	1							
Biscutum	**0.62**	0.57	0.50	1						
Calculites	**0.64**	0.55	**0.60**	**0.73**	1					
Cribrosphaerella	**0.83**	0.58	0.48	**0.64**	**0.66**	1				
Discorhabdus	**0.69**	**0.61**	0.47	**0.61**	**0.73**	0.57	1			
Prediscosphaera	0.54	0.50	0.51	0.55	0.59	0.56	0.54	1		
Staurolithites	0.59	**0.64**	0.21	**0.66**	0.53	0.56	0.52	0.49	1	
Watznaueria	**-0.75**	**-0.62**	**-0.60**	-0.76	**-0.83**	**-0.78**	**-0.72**	**-0.76**	**-0.60**	1

Table 5.4.2.3 - Correlation matrix of genera detected at the Seaford Head. Bold light blue values correlation ≈0. 60; bold blue values correlation >0. 70.

in (Table 5.4.2.4), whereas the complete matrix is provided in the Appendix (12B). A strong correlation (>0.7) was documented for:

- *A. regularis* versus *C. ehrenbergii* (0.78)
- *B. constans* versus *C. obscurus* (0.73)
- *B. hattneri* versus *B. magnum* (0.72) and *R. angustus* (1).
- *B. melaniae* versus *R. hayi* (0.71).
- *C. obscurus* versus *D. ignotus* (0.75) and *L. cayeuxii* (0.79),
- *C. circula* versus *R. ficula* (0,71).
- *C. ehrenbergii* versus *L. cayeuxii* (0.78)
- *E. digitatus* versus *Z. bicrescenticus* (1.0)
- *W. barnesiae* a negative correlation versus *B. constans* (-0.76), *C. ehrenbergii* (-0.77), *D. ignotus* (-0.72), *L. cayeuxii* (-0.79) and *P. cretacea* (-0.80).

	Ahmuellerella octoradiata	*Ahmuellerella regularis*	*Amphicyxus brooksi nanus*	*Amphicyxus minimus*	*Arkhangelskiella cymbiformis*	*Aspidolitus enormis*	*A.parcus parcus*	*Biscutum hatteri*	*Biscutum constans*	*Biscutum coronum*	*Biscutum magnum*	*Biscutum melaniae*	*Calculites obscurus*	*Chiastozygus litterarius*	*Cribrosphaerella circula*	*Cribrosphaerella ehrenbergii*	*Cylindralithus crassus*	*Discorhabdus ignotus*	*Eiffellithus gorkae*	*Eiffellithus collis*	*Eiffellithus digitatus*	*Helicolithus turonicus*	*Lucianorhabdus cayeuxii*	*Namocons multicadus*	*Nannoconus truitti rectangularis*	*Predicosphaera cretacea*	*Predicosphaera desiderogrundis*	*Predicosphaera spinosa*	*Quadrum intermedium*	*Reticapsa angustiforata*	*Reticapsa fjcula*	*Rhagodiscus angustus*	*Rhagodiscus asper*	*Ructinolithus hayi*	*Staurolithites laffittei*	*Tranolithus minimus*	*Watznaueria barnesiae*	*Watznaueria biporta*	*Watznaueria britannica*	*Zeugrhabdotus bicrescenticus*
Ahmuellerella octoradiata	1																																							
Ahmuellerella regularis	0.33	1																																						
Amphicyxus brooksi nanus	0.4	0.14	1																																					
Amphicyxus minimus	0.45	0.35	0.14	1																																				
Arkhangelskiella cymbiformis	0.38	0.35	0.31	0.44	0.38	1																																		
Aspidolitus enormis	0.38	0.32	0.17	0.4	0.35	1																																		
A.parcus parcus	0.02	0.13	0.04	0.25	0.39	0.08	1																																	
Biscutum hatteri	0.25	0.02	0.48	0.15	**0.82**	0.27	0.02	1																																
Biscutum constans	0.56	0.44	0.46	0.5	0.25	0.53	0.2	0.1	1																															
Biscutum coronum	0.24	0.14	0.3	0.32	**0.81**	0.18	**0.61**	**0.68**	0.26	1																														
Biscutum magnum	0.13	0.08	0.33	0.28	**0.86**	0.22	**0.64**	**0.72**	0.17	**0.94**	1																													
Biscutum melaniae	0.55	0.23	0.06	0.38	0.15	0.17	0.04	0.03	0.35	0.07	0.04	1																												
Calculites obscurus	0.59	0.52	0.42	0.59	0.46	**0.6**	0.4	0.24	**0.73**	0.47	0.45	0.31	1																											
Chiastozygus litterarius	0.11	0.08	0.08	0.03	0	0.1	0.17	0.04	0.18	0.09	0.11	0.08	0.05	1																										
Cribrosphaerella circula	0.14	0.1	0.03	0.04	0.04	0.02	0.02	0.01	0.09	0.03	0.02	0.03	0.24	0.04	1																									
Cribrosphaerella ehrenbergii	0.56	**0.78**	0.26	0.48	0.37	0.47	0.16	0.07	**0.63**	0.19	0.14	0.31	**0.67**	0.2	0.27	1																								
Cylindralithus crassus	0.23	0.3	0.06	0.36	0.37	**0.63**	0.06	0.27	0.19	0.14	0.16	0.14	0.33	0.04	0.05	0.31	1																							
Discorhabdus ignotus	0.58	0.54	0.31	**0.63**	0.41	0.5	0.22	0.2	0.59	0.41	0.3	0.39	**0.75**	0.03	0.09	0.57	0.42	1																						
Eiffellithus gorkae	0.05	0.05	0.11	0.27	0.13	0.29	0.07	0.05	0.13	0.01	0.08	0.01	0.07	0.07	0.05	0.02	0.41	0.26	1																					
Eiffellithus collis	0.34	0.07	0.03	0.29	0.01	0.41	0.22	0.05	0.27	0.16	0.13	0.19	0.32	0.03	0.05	0.16	0.03	0.37	0.32	1																				
Eiffellithus digitatus	-0.07	-0.06	-0.03	-0.07	-0.04	0.03	-0.02	-0.01	0.01	-0.03	-0.02	-0.03	-0.09	-0.04	-0.01	-0.08	-0.05	-0.01	0.44	0.24	1																			
Helicolithus turonicus	0.1	0.09	0.04	0.1	0.05	0.12	0.03	0.02	0.13	0.04	0.03	0.04	0.13	0.06	0.02	0.13	0.07	0.12	0.08	0.08	-0.09	1																		
Lucianorhabdus cayeuxii	0.51	**0.66**	0.28	0.41	0.31	0.44	0.26	0.09	**0.66**	0.24	0.2	0.19	**0.79**	0.17	0.18	**0.78**	0.28	0.55	0	0.14	0.09	0.16	1																	
Namocons multicadus	0.08	0.16	0.07	0.08	0.03	0.18	0.04	0.03	0.1	0.01	0.05	0.01	0.12	0.58	0.03	0.03	0.1	0.02	0.07	0.04	-0.03	0.05	0.07	1																
Namocons truitti rectangularis	0.01	0.17	0.08	0.03	0.16	0.05	0.06	0.19	0.18	0.06	0.09	0.13	0.02	**0.64**	0.07	0.07	0.12	0.13	0.01	0.14	-0.07	0.09	0.07	0.05	1															
Predicosphaera cretacea	0.51	0.47	0.35	0.47	0.21	**0.63**	0.06	0.08	**0.61**	0.1	0.11	0.1	**0.63**	0.07	0.03	**0.62**	0.35	0.59	0.21	0.24	-0.03	0.15	0.07	0.09	0.14	0.35	1													
Predicosphaera desiderogrundis	0.1	0.05	0.11	0.27	0.09	0.44	0.07	0.05	0.19	0.05	0.07	0.01	0.08	0.07	0.05	0.06	0.51	0.1	**0.61**	0.2	-0.05	0.07	0.1	0.1	0.12	0.42	0.11	1												
Predicosphaera spinosa	0.56	0.14	0.02	0.39	0.04	0.47	0.04	0.07	0.39	0.12	0.1	0.45	0.35	0.18	0.07	0.33	0.15	0.41	0.03	**0.61**	-0.07	0.1	0.25	**0.77**	0.59	0.05	0.05	0.07	1											
Quadrum intermedium	0.03	0.06	0.03	0.07	0.04	0.08	0.02	0.01	0.11	0.03	0.02	0.03	0.09	**0.67**	0.01	0.11	0.05	0.06	0.05	0.05	-0.01	0.02	0.11	0.09	0.03	0.31	0.15	0.01	0.06	1										
Reticapsa angustiforata	0.23	0.2	0.25	0.38	0.56	0.3	0.45	0.37	0.34	**0.61**	**0.62**	0.06	0.42	0.01	0.23	0.36	0.23	0.33	0.32	0.29	0.48	0.08	0.26	0.02	0.05	0.32	0.06	0.13	0.03	0.4	1									
Reticapsa fjcula	0.36	0.56	0.02	0.29	0.18	0.28	0.12	0.03	0.36	0.04	0.05	0.26	0.46	0.1	**0.71**	**0.68**	0.21	0.18	0.01	0.05	0.01	0.1	0.51	0.03	0.19	0.08	0.05	0.07	0.01	0.37	0.03	1								
Rhagodiscus angustus	0.25	0.02	0.48	0.15	**0.82**	0.27	0.02	**1**	0.1	**0.68**	**0.72**	0.03	0.24	0.04	0.01	0.07	0.27	0.2	0.05	0.05	-0.01	**0.68**	0.11	0.06	0.02	0.16	0.08	0.26	0.05	0.06	0.07	0.01	1							
Rhagodiscus asper	0.07	0.06	0.03	0.07	0.04	0.08	0.02	0.01	0.08	0.03	0.02	0.03	0.09	0.04	0.01	0.08	0.05	0.09	0.05	0.05	-0.01	0.68	0.11	0.06	0.02	0.16	0.08	0.26	0.05	0.12	0.31	0.18	0.05	1						
Ructinolithus hayi	0.37	0.41	0.02	0.39	0.34	0.29	0.02	0.18	0.26	0.15	0.1	**0.71**	0.37	0.06	0.05	0.4	0.28	0.4	0.05	0.04	-0.05	0.07	0.39	0.01	0.02	0.54	0.12	0.21	0.06	0.31	0.28	0.08	0.06	0.01	1					
Staurolithites laffittei	0.43	0.46	**0.65**	0.48	0.26	0.26	0.05	0.08	**0.64**	0.12	0.1	0.03	0.54	0.13	0.07	0.55	0.26	0.49	0.03	0.04	-0.06	0.08	0.5	0.02	0.04	0.44	0.04	0.17	0.06	0.29	0.33	0.23	0.08	0.25	0.58	1				
Tranolithus minimus	**0.61**	0.56	0.54	0.27	0.44	0.37	0.28	0.23	0.56	0.37	0.31	0.19	**0.66**	0.1	0.06	**0.62**	0.29	0.59	0.04	0.2	-0.06	0.01	**0.7**	0.03	0.03	**-0.8**	0.25	0.44	0.03	0.43	0.46	0.14	0.11	0.31	0.58	0.58	1			
Watznaueria barnesiae	**-0.61**	**-0.61**	0.31	0.59	0.36	**-0.63**	0.19	0.14	**-0.76**	0.27	0.22	0.28	**-0.81**	0.09	0.1	**-0.77**	0.39	**-0.72**	0.23	0.32	-0.07	0.2	**-0.79**	0.14	0.07	0.11	0.14	0.1	0.08	0.04	0.11	0.08	0.22	0.25	0.23	0.19	0.16	1		
Watznaueria biporta	0.09	0.28	0.16	0.01	0.19	0.1	0.1	0.08	0.29	0.13	0.11	0.15	0.29	0.03	0.08	0.23	0.05	0.18	0.27	0.19	0.07	0.21	0.29	0.34	0.24	0.06	0.05	0.25	0.01	0.06	0.25	0.01	0.01	0.05	0.18	0.2	0.18	0.08		
Watznaueria britannica	0.12	**0.61**	-0.03	0.03	0.09	-0.08	-0.02	-0.01	0.05	-0.03	-0.02	-0.03	0.01	-0.04	-0.01	0.29	-0.05	0.07	-0.05	0.09	-0.02	0.20	0.34	0.24	0.06	-0.05	0.07	-0.01	-0.06	0.25	-0.01	-0.01	-0.05	0.18	0.20	-0.18	-0.08	-0.08	1	
Zeugrhabdotus bicrescenticus	-0.07	-0.06	-0.03	-0.07	-0.04	0.03	-0.02	-0.01	0.01	-0.03	-0.02	-0.03	-0.09	-0.04	-0.01	-0.08	-0.05	-0.01	0.44	0.24	**1.00**	-0.02	-0.09	-0.03	-0.07	-0.03	-0.05	-0.07	-0.01	0.48	0.01	-0.01	-0.01	-0.05	0.18	0.25	-0.06	-0.06	-0.07	0.07	-0.01	1

Table 5.4.2.4 - correlation matrix of selected species detected at the Seaford Head. Bold light blue values correlation ≈0. 60; bold blue values correlation >0. 70.

5.4.3 The Coniacian-Santonian OAE3 at Seaford Head

The stratigraphic range of the OAE3 interval at Seaford Head extends from the base of the section up to 124 m as show in Figure 5.4.3.1. According to the biostratigraphic results the first meters of the section already belong to Coniacian or topmost Turonian. This uncertainty in the placing the Turonian/Coniacian boundary is marked by a question marks in Figure 5.4.3.1.

As concern the changes observed in the calcareous nannofossil assemblages, a distinctive characteristic of this interval are the fluctuations in abundances of nannoliths of genus *Micula* and that of holoccoccoliths that includes the genera *Lucianorhabdus* and *Calculites*. These are plotted in Figure 5.4.3.1, both in terms of percentage and absolute abundances (specimens/gram of sediments).

The observed changes in abundance of *Micula* show a similar pattern of variation between percentage and absolute abundances with *M. staurophora* (in reed) as dominant species of this group. A first peak is present at 32 m (middle Coniacian) at the top of the CC14/UC10 zones and lower NC16* zone, characterized by an increase of *M. staurophora* up to 6.2% (0.18 $X10^8$ spec./g) of the assemblage. The interval from 42 m to 58m (late Coniacian) show three distinctive spikes. Two of them occur in the upper CC15/NC16* zones and UC11a-b subzones with the first peak characterized by an increment of *M. staurophora* (9.9%; 0.37 $X10^8$ spec./g) together with *M. cubiformis* (1%; 0.04 $X10^8$ spec./g), rare *M. adumbrata* (0.3%;0.01$X10^8$) and *M. concava* (0.3%;0.01$X10^8$ spec./g), and the second, show an increment of *M. staurophora* (10.2%; 3$X10^7$ spec./g) together with *M. swastica* (1.6%; 4.6$X10^6$ spec./g). The third spike occur the lower CC16/NC17* zones, UC11c subzones and show an increment of *M. staurophora* (6.8%;0.44$X10^8$) together with *M. adumbrata* (1.6%; 0.02$X10^8$ spec./g).

At Seaford Head the maximum in *Micula* content was reached, in the upper CC16/UC12 zones, lower NC17* zone (early-middle Santonian) with *M. staurophora* (14%;0.84$X10^8$ spec./g) together with that *M. adumbrata* (0.6%;0.04$X10^8$) and *M. swastica* (0.6%;0.04$X10^8$ spec./g).

Other two increments in *Micula* was observed occur respectively in the CC17/UC13 zones and upper NC17* zone (late Santonian), where *M. staurophora* reach up to 7% (0.2$X10^8$ spec./g) of the assemblage and at the base of CC18/NC18* and UC14* zones (Santonian/Campanian boundary) where *M. staurophora* reach up to 6.2% (0.27$X10^8$ spec./g) of the assemblage.

As concern the change in Holococcoliths content, these show a general increase from the bottom to the top of the section (Figure 5.4.3.3). This long-term increase can be subdivided in four intervals of increase in abundance well detectable both in terms of percentage than absolute abundances. The first interval ranges from the base up to 16m and is restricted to the CC13/NC15 UC9 zones (early Coniacian). It is

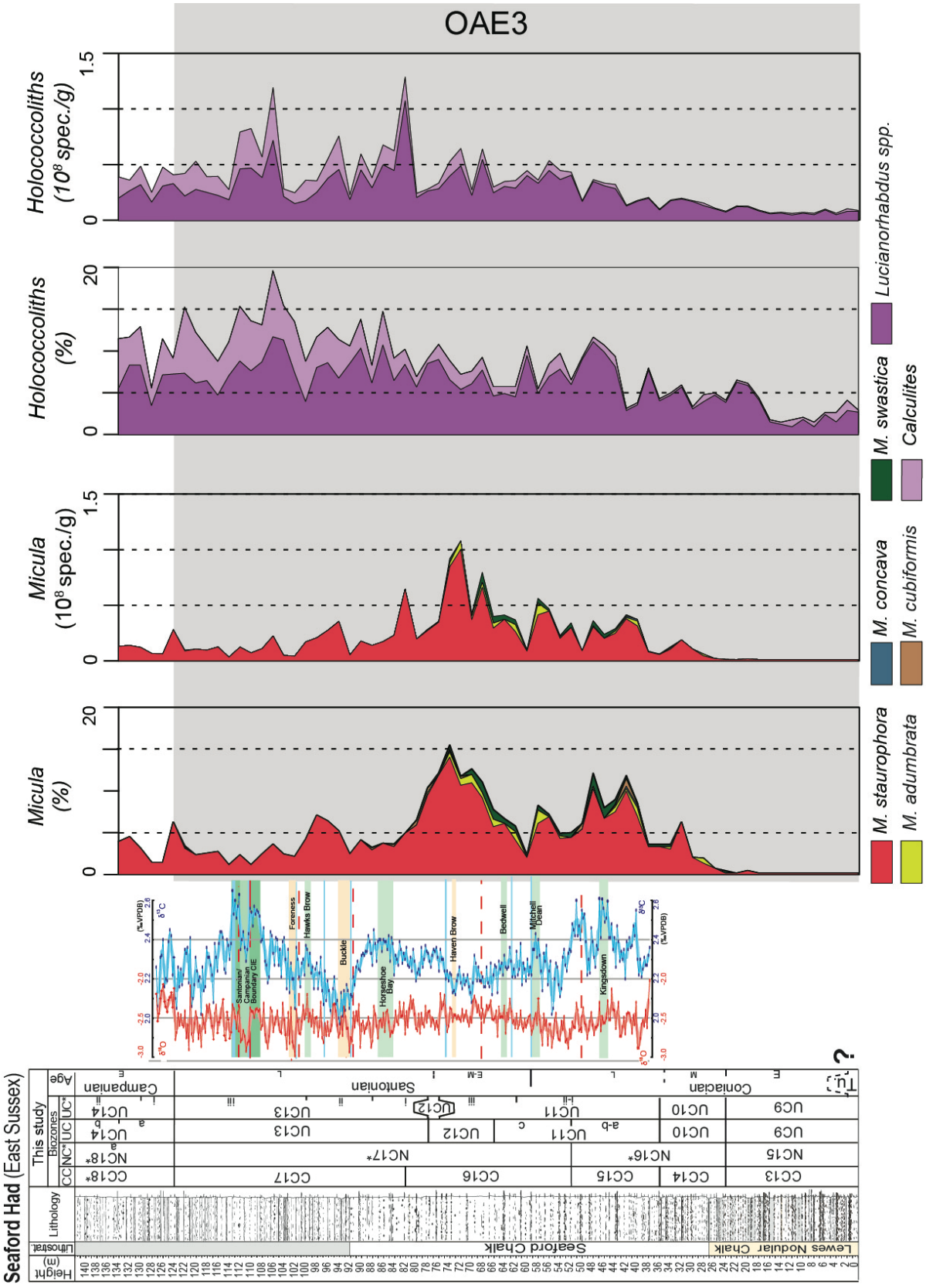

Figure 5.4.3.1 - Relative (%) and absolute abundance (number of specimens/g of sediment) of *Micula* and Holococcoliths. The OAE3 interval is indicated by a grey band.

characterized by a low content of *Lucianorhabdus* (1.2%; 0.02X10^8 spec./g) and a rare *Calculites* (0.3%; 0.004X10^8 spec./g). The second interval range from 16 to 42m and include the top of the CC13/NC15/ UC9 zones up to lower CC15/UC11zones and top NC16* zone (middle- late Coniacian). In this interval, holococcoliths are almost entirely composed of *Lucianorhabdus* (4.1%; 0.1X10^8 spec./g). The third interval range from 42 m to 82m include the CC15-16, top od NC16* and the lower NC17* and the UC11 to lower CC13 zones (late Coniacian - middle Santonian). Here, both *Lucianorhabdus* (6.7%; 0.3X10^8 spec./g) and *Calculites* (1%; 0.05X10^8 spec./g) increase in abundance. The last interval reaches the top of the section and include the CC17-18/UC13-14a and the upper NC17*and NC18*a subzones (late Santonian-early Campanian). In this range, the Holococcoliths reach the higher abundance both in terms of *Lucianorhabdus* (7.2%; 3.1X10^7 spec./g) than *Calculites* (4.2%; 0.18X10^8 spec./g). This interval, is characterized, in terms of absolute abundances by two prominent peaks respectively at 82m (1.3X10^8 spec./g) and 106m (1.2X10^8 spec./g). It also important to notice that at Seaford Head, the maximum abundance of Holococcoliths during the late Santonian-early Campanian correspond to a general low content in *Micula* in the assemblages.

5.5 Tanzania TD39

5.5.1 Biostratigraphy

In the TDP39 the Nangurukuru Formation is characterized by abundant and nicely to moderately preserved calcareous nannofossils whereas in the Lindi Formation the assemblages are generally rare and moderately preserved.

A total of four events were detected within the studied interval, allowing the identification, of the CC15-CC17 zones of Sissingh (1977), NC16-NC17 zones of Roth (1978), NC16*-NC17* zones of Bralower et al. (1995) and UC11-UC12 zones of Burnett (1998). The results are presented in Figure 5.5.1 and the zonal and subzonal markers used are described from the oldest to the youngest. A range chart for TDP39 is provided in the Appendix 13.

L. grilli and *M. staurophora* are present from the lowermost analyzed sample, thus the base of the section lies in the CC15, NC16, NC16*, UC11 zones. *L. grillii* becomes continuous (FCO = first common occurrence in figure 5.5.1) from meter 56.56 close to the position were Jiménez Berrocoso et al. (2015) placed the first occurrence of *L. grillii* (53.05 m).

The FO of *L. cayeuxii* was found at 66.56 m and defines the base of the CC16, NC17* Zones and UC11c subzones. The LO of *L. septenarius* was found at 24.56 m, whereas Jiménez Berrocoso et al. (2015) reported the LO of *L. septenarius* from 21.05 m. This last datum was then used for defining the base of

the UC12 zone. The FO of *C. obscurus* lies at 4.51 m, close to the top of the section, where the base. the CC17 and NC17 zones was placed.

According to calcareous nannofossil biostratigraphy the Coniacian/Santonian boundary is placed between the FO of *L. cayeuxii* and LO of *L. septenarius*. Otherwise, Petrizzo et al. (2017) considered the first occurrence of the planktonic foraminifera *G. linneiana* as a most reliable marker for the Coniacian/Santonian boundary at TDP39 because this event is placed 10 cm above the FO of *C. undulatoplicatus* at Olazagutia section (Lamolda et al., 2014).

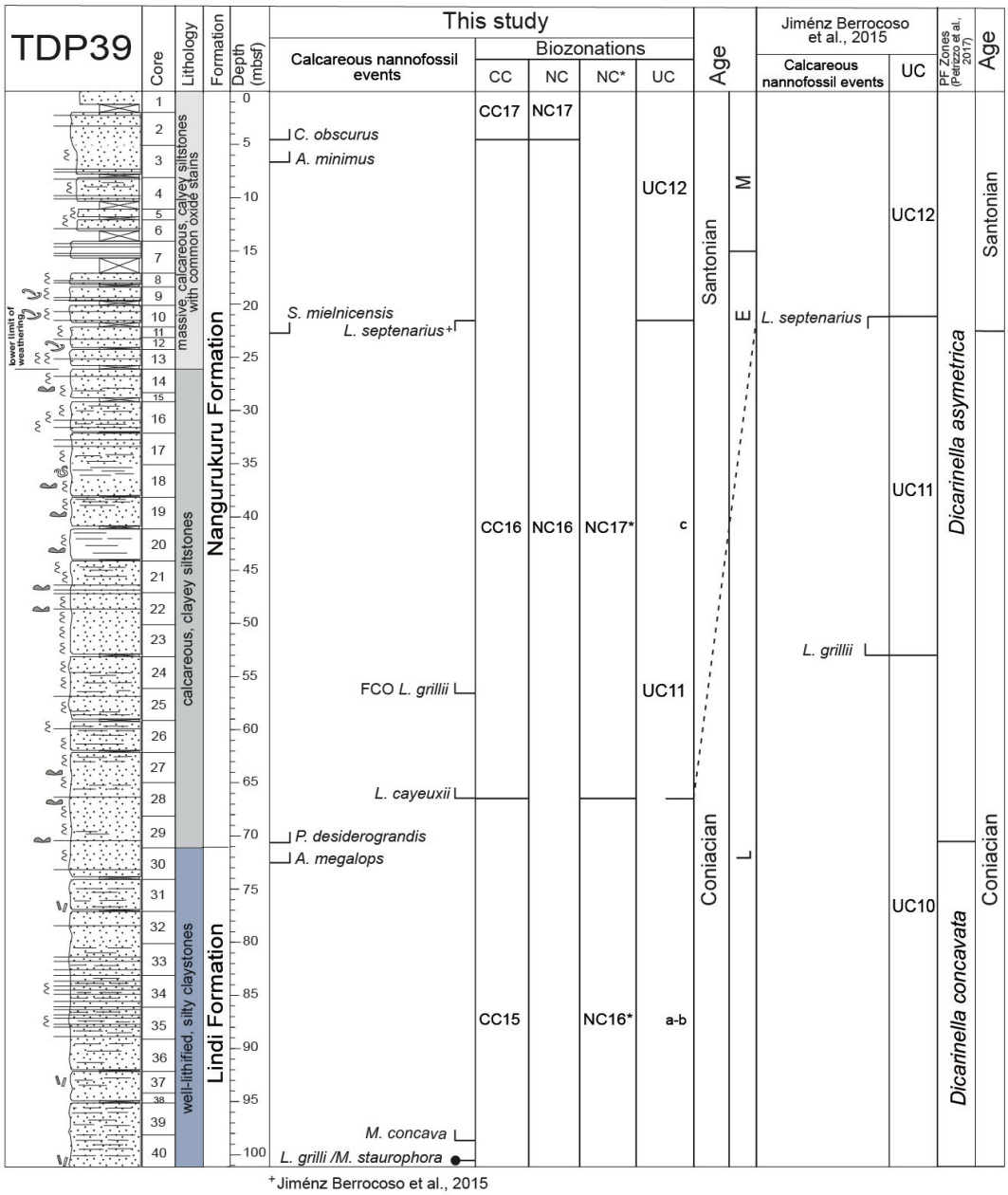

Figure 5.5.1 - TDP39 calcareous nannofossil biostratigraphy (this study) and comparison with previous data of Jiménez-Berrocoso et al. (2015). Biostratigraphic zonation: CC (Sissingh, 1977), NC (Roth,1978), NC* (Bralower 1995), and UC (Burnett 1998) are shown. Data from literature used for zonation in marked with asterisk (*). FCO (first common occurrence).

5.5.2 Nannofossil paleoecology and paleoceanography

At site TDP39 a total of 118 taxa were recognized. The species richness varies from a maximum of 53 (94.09 m) to 25 (96.56 m) with a mean of 45 species for sample (Figure 5.5.2.1). The species richness shows minor changes along the studied interval.

The Shannon index ranges between 2 and 3 with an average value of 2.8, suggesting well-diversified assemblages and absence of dominance of single taxa. The total nannofossil abundance (number of specimens/field of view) has low values in the Lindi Formation (average of 6 specimens/field of view) and increases in the Nangurukuru Formation (average of 28 specimens/field of view) with a maximum of 86 specimens/field of view at 40.56m.

The absolute abundance of calcareous nannofossils have an average of 1.93 X 10^7 specimens/g three intervals were distinguished. The lower part of the studied interval (Lindi Formation) is characterized by low abundances with an average of 0.9 X 10^7 specimens/g. In the second interval between 70.56m and 20.56m the absolute abundance has an average of 2.49 X 10^7 specimens/g. The upper part of the studied section, from 20.56m to the top, shows a decline in the absolute abundance with an average value of 1.75 X 10^7 specimens/g. There is a good correspondence between the changes observed in the absolute abundances and the $CaCO_3$ (Fig. 5.5.2.2): lower values in $CaCO_3$ correspond to low absolute abundances in the Lindi Formation.

The presence at TDP39 of well diversified assemblages and the occurrence of *W. barnesiae* together with delicate and diagenesis-prone taxa such as *B. constans*, *D. ignotus* and *Z. erectus* also in the Lindi Formation, suggest that the composition and abundance of calcareous nannofossil assemblages mainly reflect primary ecological signals with negligible diagenetic modifications.

The descriptive statistics of calcareous nannofossil genera and species are synthesized in Tables 5.5.2.1 and 5.5.2.2. At TDP39 eight genera have an average relative abundance > 3% (*Cribrosphaerella*, *Eiffellithus*, *Marthasterites*, *Prediscosphaera*, *Retecapsa*, *Tranolithus*, *Watznaueria*, *Zeugrhabdotus*). Further genera are characterized by average relative abundance > 2% (*Biscutum, Chiastozygus, Discorhabdus, Lithastrinus*). Genera with average relative abundance < 2% are not discussed here but their descriptive statistics is shown in Tables 5.5.2.1 and 5.5.2.2. Figure 5.5.2.1 illustrates the relative abundances of all genera with an average > 1%. The dominant genus is *Watznaueria* which ranges from 15.1% to 50.2% (average 30%). *W. barnesiae* represents the most abundant species fluctuating from 14.2% to 49.9% (average 29.4%). Other species of *Watznaueria* are *W. biporta*, *W. communis*, *W. ovata* and *W. quadriradiata*.

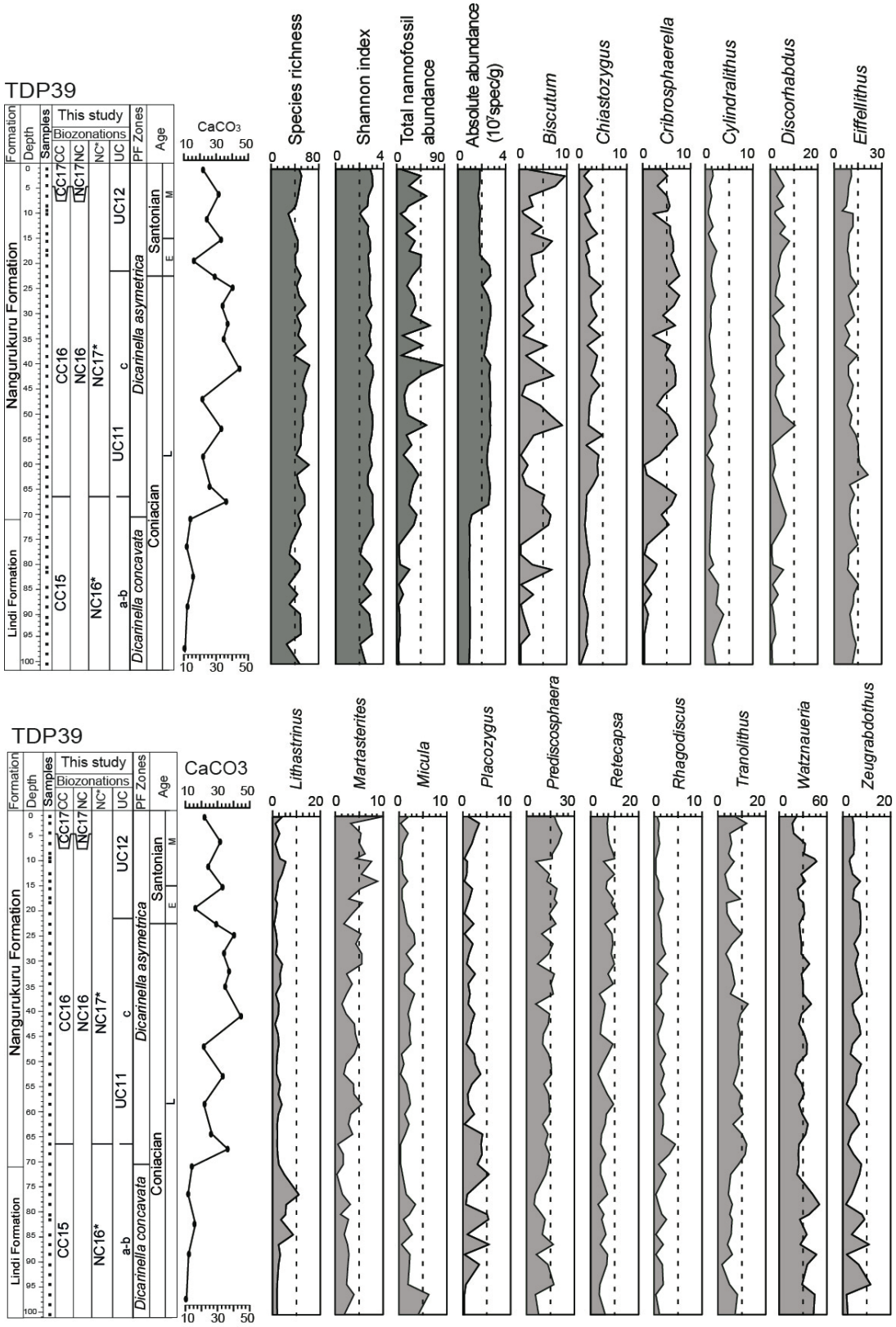

Figure 5.5.2.1 - Calcareous nannofossil data from the TDP39 showing the fluctuations of species richness, Shannon index, total nannofossil abundances (specimens/FOV), absolute (n. specimens/gram of sediment) and relative abundances of genera with an average relative abundance >1%.

GENUS	Average %	Minimum %	Maximum %	Mode	Standard Deviation	Median
Watznaueria	30.0	15.1	50.2	28.5	8	27
Prediscosphaera	12.6	3.8	21.8	13.2	4.4	13.7
Eiffellithus	10.3	4.2	21.0	9.6	3	8.2
Tranolithus	6.4	1.0	12.3	5.8	2.7	3.9
Retecapsa	6.2	2.6	11.1	6.2	2.2	9.2
Zeugrabdothus	4.8	0.6	11.3	4.2	2.4	4.2
Cribrosphaerella	4.1	0.0	7.6	5.0	2.5	0
Martasterites	3.4	0.0	9.9	3.2	2	5.4
Discorhabdus	2.8	0.0	10.1	2.4	2.3	1.5
Biscutum	2.8	0.0	9.6	2.4	2.6	0
Lithastrinus	2.3	0.0	10.7	1.8	1.9	1.3
Chiastozygus	2.1	0.0	4.7	1.8	1.1	1.2
Placozygus	1.6	0.0	5.3	1.2	1.5	0
Loxolithus	1.6	0.2	5.0	1.3	1.2	0.8
Micula	1.4	0.0	6.1	1.3	1.2	0
Cylindralithus	1.2	0.0	3.6	1.1	0.7	0.9
Rhagodiscus	1.1	0.0	4.2	1.1	0.9	0
Manivitella	0.8	0.0	3.2	0.8	0.6	0.8
Helicolithus	0.7	0.0	4.7	0.4	0.9	0
Eprolithus	0.5	0.0	5.4	0.0	1.2	0
Tegumentum	0.3	0.0	2.0	0.3	0.4	0
Corollithion	0.3	0.0	2.2	0.2	0.5	0
Microrhabdulus	0.3	0.0	1.3	0.2	0.3	0
Radiolithus	0.3	0.0	0.9	0.2	0.3	0
Tetrapodorhabdus	0.2	0.0	1.8	0.0	0.4	0
Amphizygus	0.2	0.0	2.9	0.0	0.5	0
Ahmuellerella	0.2	0.0	2.5	0.0	0.5	0
Rucinolithus	0.2	0.0	0.6	0.0	0.2	0
Braarudosphaera	0.1	0.0	2.5	0.0	0.4	0
Flabellites	0.1	0.0	1.1	0.0	0.2	0
Lucianorhabdus	0.1	0.0	0.7	0.0	0.2	0
Calculites	0.1	0.0	1.0	0.0	0.2	0
Cretarhabdus	0.1	0.0	0.6	0.0	0.2	0
Arkhangelskiella	0.1	0.0	0.7	0.0	0.2	0
Quadrum	0.1	0.0	0.6	0.0	0.2	0
Lithraphidites	0.1	0.0	0.7	0.0	0.2	0
Staurolitithes	0.1	0.0	0.6	0.0	0.2	0
Unipolanarius	0.1	0.0	0.7	0.0	0.2	0
Bukrylithus	0.1	0.0	0.8	0.0	0.2	0
Stoverius	0.1	0.0	0.8	0.0	0.2	0
Gartnerago	0.05	0.0	1.1	0.0	0.2	0
Grantarhabdus	0.04	0.0	0.4	0.0	0.1	0
Nannoconus	0.03	0.0	0.4	0.0	0.1	0
Reinhardtites	0.03	0.0	0.3	0.0	0.1	0
Broinsonia	0.02	0.0	0.6	0.0	0.1	0
Prolatipatella	0.02	0.0	0.3	0.0	0.1	0
Owenia	0.01	0.0	0.4	0.0	0.1	0
Axopodorhabdus	0.01	0.0	0.2	0.0	0	0
Haqius	0.01	0.0	0.2	0.0	0	0

Table 5.5.2.1 - Descriptive statistics of genera identified at TDP39.

SPECIES	Average %	Minimum %	Maximum %	Mode	Standard Deviation	Median
Amphizygus brooksii brooksii	0.1	0.0	0.6	0.0	0.1	0.0
Amphizygus brooksii nanus	0.01	0.0	0.2	0.0	0.0	0.0
Amphizygus megalops	0.03	0.0	0.5	0.0	0.1	0.0
Amphizygus minimus	0.1	0.0	2.3	0.0	0.4	0.0
Ahmuellerella octoradiata	0.2	0.0	2.4	0.0	0.5	0.0
Ahmuellerella regularis	0.004	0.0	0.2	0.0	0.0	0.0
Arkhangelskiella confusa	0.1	0.0	0.7	0.0	0.2	0.0
Axopodorhabdus albianus	0.008	0.0	0.2	0.0	0.0	0.0
Biscutum constans	2.8	0.0	9.6	2.4	2.6	0.0
Bukrylithus ambiguus	0.1	0.0	0.8	0.0	0.2	0.0
Braarudosphaera	0.1	0.0	2.5	0.0	0.4	0.0
Broinsonia matalosa	0.006	0.0	0.3	0.0	0.0	0.0
Broinsonia signata	0.01	0.0	0.3	0.0	0.1	0.0
Calculites maghredaswampensis	0.03	0.0	0.5	0.0	0.1	0.0
Calculites ovalis	0.03	0.0	0.6	0.0	0.1	0.0
Calculites pernicensis	0.04	0.0	0.5	0.0	0.1	0.0
Chiastozygus amphipons	0.1	0.0	1.1	0.0	0.2	0.0
Chiastozygus bifarius	0.4	0.0	2.0	0.3	0.5	0.0
Chiastozygus litterarius	1.1	0.0	3.0	1.0	0.7	0.7
Chiastozygus platyrhetus	0.01	0.0	0.3	0.0	0.1	0.0
Corollithion signum	0.2	0.0	1.6	0.0	0.3	0.0
Corollithion madagaskarensis	0.1	0.0	1.5	0.0	0.3	0.0
Cretarhabdus conicus	0.1	0.0	0.6	0.0	0.2	0.0
Cretarhabdus striatus	0.01	0.0	0.3	0.0	0.1	0.0
Cribrosphaerella ehrenbergii	4.1	0.0	7.6	5.0	2.5	0.0
Cylindralithus biarcus	0.3	0.0	2.2	0.0	0.5	0.0
Cylindralithus coronatus	0.1	0.0	1.1	0.0	0.2	0.0
Cylindralithus nudus	0.1	0.0	1.3	0.0	0.3	0.0
Cylindralithus sculptus	0.03	0.0	0.5	0.0	0.1	0.0
Cylindralithus serratus	0.1	0.0	1.1	0.0	0.2	0.0
Discorhabdus ignotus	2.8	0.0	10.1	2.4	2.3	1.5
Eiffellithus angustus	0.2	0.0	0.8	0.0	0.2	0.0
Eiffellithus casolus	0.7	0.0	2.0	0.6	0.5	0.3
Eiffellithus collis	0.4	0.0	1.6	0.3	0.5	0.0
Eiffellithus digitatus	0.05	0.0	0.3	0.0	0.1	0.0
Eiffellithus eximius	5.1	1.7	9.3	4.9	1.8	3.4
cf. Eiffellithus eximius	0.6	0.0	2.5	0.5	0.5	0.3
Eiffellithus gorkae	0.1	0.0	1.4	0.0	0.2	0.0
Eiffellithus nudus	0.7	0.0	2.5	0.5	0.8	0.0
Eiffellithus keio	0.03	0.0	0.5	0.0	0.1	0.0
Eiffellithus turriseiffelii	0.6	0.0	1.8	0.5	0.5	0.0
Eprolithus floralis	0.4	0.0	5.4	0.0	1.0	0.0
Eprolithus moratus	0.1	0.0	3.5	0.0	0.5	0.0
Flabellites oblongus	0.1	0.0	1.1	0.0	0.2	0.0
Grantarhabdus coronadventis	0.04	0.0	0.4	0.0	0.1	0.0
Gartnerago segmentatum	0.02	0.0	0.3	0.0	0.1	0.0
Gartnerago obliquum	0.02	0.0	1.1	0.0	0.2	0.0
Haqius circumrtadiatus	0.008	0.0	0.2	0.0	0.0	0.0
Helicolithus compactus	0.006	0.0	0.3	0.0	0.0	0.0
Helicolithus trabeculatus	0.2	0.0	1.3	0.0	0.3	0.0
Helicolithus anceps	0.5	0.0	4.5	0.2	0.8	0.0
Lithastrinus grillii	0.6	0.0	5.0	0.2	1.1	0.0
Lithastrinus septenarius	1.6	0.0	10.7	1.3	2.1	0.0
Lithraphidites carniolensis	0.1	0.0	0.7	0.0	0.2	0.0
Loxolithus armilla	1.6	0.2	5.0	1.3	1.2	0.8
Lucianorhabdus cayeuxii	0.0	0.0	0.3	0.0	0.1	0.0
Lucianorhabdus maleformis	0.1	0.0	0.7	0.0	0.2	0.0
Microrhabdulus decoratus	0.2	0.0	0.8	0.0	0.2	0.0
Microrhabdulus undosus	0.1	0.0	1.0	0.0	0.2	0.0

Table 5.5.2.2 - Descriptive statistics of species identified at TDP39.

Manivitella pemmatoidea	0.8	0.0	3.2	0.8	0.6	0.8
Martasterites crassus	0.01	0.0	0.4	0.0	0.1	0.0
Martasterites furcatus	3.4	0.0	9.9	3.2	2.1	5.4
Micula adumbrata	0.0	0.0	0.6	0.0	0.1	0.0
Micula concava	0.1	0.0	1.4	0.0	0.2	0.0
Micula cubiformis	0.03	0.0	0.8	0.0	0.1	0.0
Micula staurophora	1.2	0.0	6.1	1.0	1.1	0.0
Nannoconus truitti	0.004	0.0	0.2	0.0	0.0	0.0
Owenia hillii	0.01	0.0	0.4	0.0	0.1	0.0
Placozygus fibuliformis	1.6	0.0	5.3	1.2	1.5	0.0
Prediscosphaera columnata	2.9	0.0	6.5	2.9	1.7	3.3
Prediscosphaera cretacea	9.4	1.7	18.9	9.0	4.2	15.6
Prediscosphaera disdeograndis	0.01	0.0	0.3	0.0	0.1	0.0
Prediscosphaera ponticula	0.1	0.0	0.8	0.0	0.2	0.0
Prediscosphaera spinosa	0.2	0.0	1.3	0.0	0.3	0.0
Prolatipatella multicarinata	0.02	0.0	0.3	0.0	0.1	0.0
Quadrum gartnerii	0.1	0.0	0.6	0.0	0.2	0.0
Radiolithus	0.3	0.0	0.9	0.2	0.3	0.0
Reinhardtites anthophorus	0.03	0.0	0.3	0.0	0.1	0.0
Retecapsa angustiforata	1.2	0.0	4.1	1.1	0.9	0.8
Retecapsa crenulata	1.3	0.0	4.8	1.3	0.8	1.0
Retecapsa surirella	0.5	0.0	2.7	0.4	0.6	0.0
Retecapsa ficula	0.5	0.0	2.5	0.3	0.6	0.0
Retecapsa octofenestrata	0.3	0.0	2.7	0.0	0.5	0.0
Retecapsa schizobrachiata	0.006	0.0	0.3	0.0	0.0	0.0
Rhagodiscus achlyostaurion	0.1	0.0	0.5	0.0	0.1	0.0
Rhagodiscus angustus	0.4	0.0	1.5	0.4	0.4	0.0
Rhagodiscus asper	0.1	0.0	0.7	0.0	0.2	0.0
Rhagodiscus plebeius	0.02	0.0	0.4	0.0	0.1	0.0
Rhagodiscus reniformis	0.4	0.0	1.9	0.3	0.5	0.0
Rhagodiscus splendens	0.1	0.0	0.8	0.0	0.2	0.0
Rucinolithus terebrodentarius	0.2	0.0	0.6	0.0	0.2	0.0
Staurolithites flavus	0.01	0.0	0.2	0.0	0.0	0.0
Stoverius achylosus	0.1	0.0	0.8	0.0	0.2	0.0
Tegumentum stradneri	0.3	0.0	2.0	0.3	0.4	0.0
Tetrapodorhabdus decorus	0.2	0.0	1.8	0.0	0.4	0.0
Tranolithus gabalus	0.1	0.0	0.9	0.0	0.2	0.0
Tranolithus macleodiae	0.8	0.0	5.5	0.4	1.1	0.0
Tranolithus orionatus	5.5	0.5	11.5	5.2	2.3	4.4
Uniplanarius gothicus	0.05	0.0	0.7	0.0	0.1	0.0
Uniplanarius sissinghii	0.03	0.0	0.6	0.0	0.1	0.0
Watznaueria barnesiae	29.4	14.2	49.9	27.7	8.1	29.8
Watznaueria biporta	0.1	0.0	0.6	0.0	0.1	0.0
Watznaueria communis	0.3	0.0	1.2	0.2	0.4	0.0
Watznaueria ovata	0.1	0.0	0.8	0.0	0.2	0.0
Watznaueria quadriradiata	0.008	0.0	0.2	0.0	0.0	0.0
Zeugrhabdotus acanthus	0.1	0.0	0.7	0.0	0.2	0.0
Zeugrhabdotus biperforatus	0.2	0.0	1.7	0.0	0.3	0.0
Zeugrhabdotus bicrescenticus	0.02	0.0	0.2	0.0	0.1	0.0
Zeugrhabdotus blowii	0.3	0.0	2.2	0.0	0.5	0.0
Zeugrhabdotus diplogrammus	1.5	0.0	5.6	1.4	1.1	1.3
Zeugrhabdotus elegans	0.3	0.0	1.6	0.3	0.4	0.0
Zeugrhabdotus embergeri	0.2	0.0	1.1	0.0	0.2	0.0
Zeugrhabdotus erectus	0.9	0.0	5.8	0.5	1.3	0.0
Zeugrhabdotus kerguelenensis	0.004	0.0	0.2	0.0	0.0	0.0
Zeugrhabdotus scutula	0.03	0.0	0.5	0.0	0.1	0.0
Zeugrhabdotus praesigmoides	0.2	0.0	1.1	0.0	0.3	0.0
Zeugrabdothus sp. 2	0.004	0.0	0.2	0.0	0.0	0.0
Zeugrabdothus sp. 1	1.1	0.0	3.8	0.8	1.0	0.3

Table 5.5.2.2 - Descriptive statistics of species identified at

The genus *Prediscosphaera* ranges from 3.8% to 21.8% (average 12.6%) and includes *P. columnata*, *P. cretacea*, *P. desiderograndis*, *P. ponticula* and *P. spinosa*. The most abundant species is *P. cretacea* ranging from 1.7% to 18.9% (average 9.4%).

The third most abundant genus is *Eiffellithus* fluctuating from 4.2% to 21% (average 10.3%); it includes *E. angustus*, *E. casolus*, *E. collis*, *E. digitatus*, *E. eximius*, *E. gorkae*, *E. nudus, E. keio and E. turriseiffelii*. The most abundant *Eiffellithus* species is *E. eximius* that ranges from 1.7% to 9.3% (average 5.1%).

The genus *Tranolithus* ranges from 1% to 12.3% (average 6.4%). Higher abundance of *Tranolithus* occurs from 70.56m to 38.56m with an average of 8.9%. The most abundant species is *T. orionatus* that varies from 0.5% to 11.5% (average 5.5%).

Retecapsa ranges from 2.6% to 11.1% (average 6.2%). This genus is represented by six species: *R. angustiforata*, *R. crenulata*, *R.* surirella, *R. ficula*, *R. octofenestrata*, *R. schizobrachiata*. The most abundant species are *R. angustiforata* that ranges from 0% to 4,1% (average 1.2%), and *R. crenulata maleformis* that ranges from 0% to 4,8% (average 1.3%).

Zeugrhabdotus ranges from 0.6% to 11.3% (average 4.8%) and includes *Z. acanthus*, *Z. biperforatus*, *Z. bicrescenticus*, *Z. blowii*, *Z. diplogrammus*, *Z. elegans*, *Z. embergeri, Z. erectus, Z. kerguelenensis, Z. scutula, Z. praesigmoides, Zeugrhabdotus* sp. 1 and *Zeugrhabdotus* sp. 2. The most abundant *Zeugrhabdotus* species is *Z. diplogrammus* that ranges from 0.3% to 5.6% (average 1.5%).

Genus *Cribrosphaerella* ranges from 0% to 7.6% (average 4.1%). This genus is rare in the Lindi Formation, but increases from 72.56m in the Nangurukuru Formation.

Genus *Marthasterites* ranges from 0% to 9.9% (average 3.4%) showing a gradual increase through the studied interval reaching up the 7.5% of the assemblage at 10.1m in the middle Santonian.

Biscutum ranges from 0% to 9.6% (average 2.8%), whereas *Discorhabdus* ranges from 0% to 10.1 % (average 2.8%).

The genus *Lithastrinus* varies between 0% and 10.7% (average 2.3%). The highest relative abundance of genus *Lithastrinus* was recorded between 84.56m and 74.56min the upper Coniacian (Lindi Formation). This genus includes *L. grillii* that ranges from 0% to 5% (average 0.6%) and *L. septenarius* that range from 0% to 10.7% (average 1.6%).

Chiastozygus ranges from 0% to 4.7% (average 2.1%) and includes *C. amphipons*, *C. bifarius, C. litterarius*, *C. platyrhetus*.

The fluctuations in the NI and TI indices are presented in Figure 5.5.2.2. At TDP39 the NI ranges from 0 to 55 (average 19). The highest values of the NI occur between 81.56m and 52.56m. The variations observed in the NI index are mostly related to changes in the relative abundance of *B. constans* and *D. ignotus* together with a reduction of *W. barnesiae. Z. erectus, instead,* is relatively rare (average 0.9%)

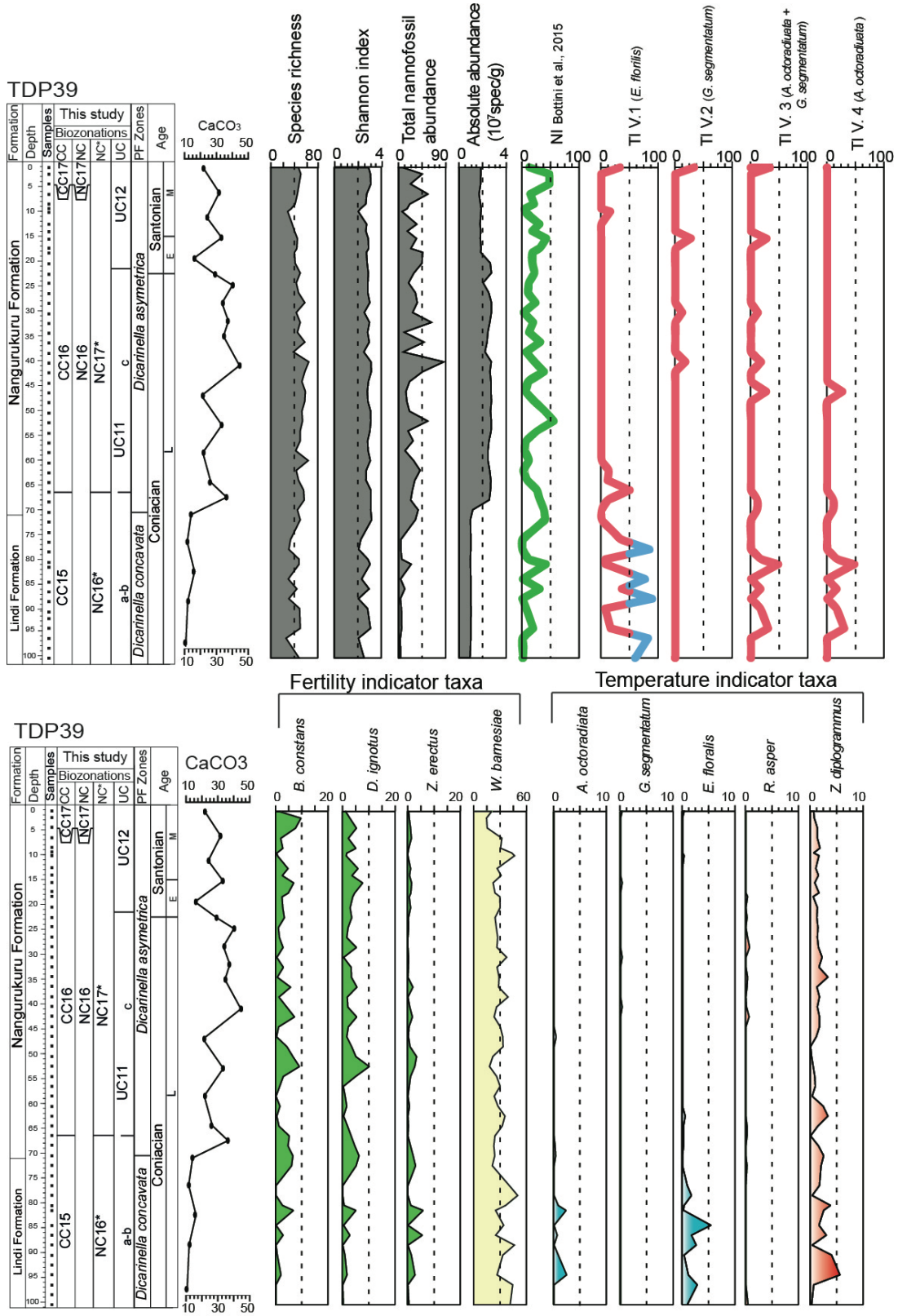

Figure 5.5.2.2 - Fluctuations of calcareous nannofossil temperature and fertility taxa TDP39. Nutrient Index (NI) after Bottini et al. (2015); Temperature Index (TI) after Bottini et al. (2015) and modified V.2, V.3, V.4. The species richness, Shannon index, total nannofossil abundance (n. specimens/FOV), absolute abundance (n. specimens/gram of sediment) are also reported.

) in the studied interval suggesting mesotrophic (but not eutrophic) conditions.

At TDP39 all the TI indices show the prevalence of warm water conditions throughout the lower part of the studied interval (between the base and 78.56m in the Lindi Formation). At TDP 39

the cool water taxa *A. octoradiata* (average 0.2%), *E. floralis* (average 0.4%) and *G. segmentatum* (average 0.02%) are quite rare, whereas the warm water *Z. diplogrammus* is more abundant (average 1.5%). The correlation matrix for species detected at TDP39 doesn't show a linear correlation between the supposed temperature-related taxa.

The potential affinities of genera were tested by calculating the Pearson's correlation coefficients. A summary of the correlation matrix showing only the genera with a correlation > 0.6 (or < - 0.6) is reported in (Table 5.5.2.3), whereas the complete matrix is provided in the Appendix (14A).

There is a positive correlation documented for *Biscutum* versus *Discorhabdus* (0.81) while a negative correlation is present for *Watznaueria* versus *Biscutum* (-0.73) and *Prediscosphaera* (-0.73).

	Biscutum	*Braarudosphaera*	*Discorhabdus*	*Helicolithus*	*Nannoconus*	*Prediscosphaera*	*Stoverius*	*Watznaueria*
Biscutum	1							
Braarudosphaera	0.28	1						
Discorhabdus	**0.81**	0.35	1					
Helicolithus	0.00	**0.63**	0.08	1				
Nannoconus	0.22	0.51	0.27	0.35	1			
Prediscosphaera	0.52	0.34	0.51	0.30	0.28	1		
Stoverius	0.27	0.43	0.30	0.41	**0.61**	0.23	1	
Watznaueria	**-0.73**	0.42	**-0.66**	0.15	0.24	**-0.73**	0.25	1

Table 5.5.2.3 - correlation matrix of genera detected TDP39. Bold light blue = values correlation ≈0. 60; bold blue values = correlation >0. 70.

Pearson's correlation coefficients were also obtained for all species detected at TDP39. A summary of the correlation matrix showing only the species with a correlation >0.6 (or < -0.6) is reported in (Table 5.5.2.4), whereas the complete matrix is provided in the Appendix (14B). A strong correlation (>0.7) was documented for:

- *A. brooksii nanus* versus *Zeugrabdothus* sp. 2 (0.70).
- *B. constans* versus *D. ignotus* (0.81).
- *C. striatus* versus *M. adumbrata* (0.91).
- *C. serratus* versus *T. macleodiae* (0.71).

	Amphizygus brooksii nanus	*Amphizygus minimus*	*Ahmuellerella octoradiata*	*Ahmuellerella regularis*	*Biscutum constans*	*Braarudosphaera bigelowii*	*Broinsonia matalosa*	*Broinsonia signata*	*Calculites ovalis*	*Calculites perniciensis*	*Chiastozygus amphipons*	*Corollithion madagaskarensis*	*Cretarhabdus conicus*	*Cretarhabdus striatus*	*Cribrosphaerella ehrenbergii*	*Cylindralithus nudus*	*Cylindralithus serratus*	*Discorhabdus ignotus*	*Eiffellithus keio*	*Eprolithus floralis*	*Eprolithus moratus*	*Helicolithus amceps*	*Lithastrinus grillii*	*Lucianorhabdus cayeuxii*	*Microrhabdulus undosus*	*Martasteritles furcatus*	*Micula adumbrata*	*Nannoconus truitti*	*Owenia hillii*	*Placozygus fibuliformis*	*Predicosphaera disdiagrandis*	*Predicosphaera spinosa*	*Retecapsa ficula*	*Retecapsa schizobrachiata*	*Rhagodiscus angustus*	*Stoverius achylosus*	*Tetrapodorhabdus decorus*	*Tranolithus macleodae*	*Watznaueria barnesae*	*Watznaueria quadriradiata*	*Zeugrhabdotus diplogrammus*	*Zeugrhabdotus erectus*	*Zeugrhabdotus kerguelenensis*	*Zeugrhabdotus sp. 2*
Amphizygus brooksii nanus	1																																											
Amphizygus minimus	-0.05	1																																											
Ahmuellerella octoradiata	-0.07	-0.07	1																																										
Ahmuellerella regularis	-0.03	-0.03	**0.63**	1																																									
Biscutum constans	0.24	0.17	0.08	0.21	1																																							
Braarudosphaera bigelowii	-0.07	-0.08	0.29	0.02	-0.28	1																																						
Broinsonia matalosa	-0.03	0.16	-0.05	-0.02	0.26	-0.05	1																																					
Broinsonia signata	-0.04	0.11	0.32	0.54	0.33	-0.03	**0.83**	1																																				
Calculites ovalis	-0.05	-0.06	-0.09	-0.04	0.10	-0.01	-0.04	-0.05	1																																			
Calculites perniciensis	-0.08	-0.09	0.12	-0.06	-0.10	0.20	-0.06	-0.08	-0.03	1																																		
Chiastozygus amphipons	0.10	-0.01	-0.17	-0.08	0.21	-0.15	0.23	0.14	0.32	-0.07	1																																	
Corollithion madagaskarensis	0.22	0.02	-0.11	-0.07	0.37	-0.17	-0.07	-0.10	0.42	-0.08	0.11	1																																
Cretarhabdus conicus	0.00	**0.61**	-0.15	-0.09	0.18	-0.21	0.34	0.24	-0.12	-0.03	0.26	-0.08	1																															
Cretarhabdus striatus	-0.04	-0.05	-0.07	-0.03	-0.22	0.07	-0.03	-0.04	-0.05	-0.08	-0.12	-0.10	-0.12	1																														
Cribrosphaerella ehrenbergii	0.22	0.00	-0.31	-0.10	-0.46	-0.54	-0.07	-0.12	0.16	-0.26	0.12	0.06	-0.20	1																														
Cylindralithus nudus	-0.10	-0.05	-0.12	-0.07	0.17	-0.15	-0.07	-0.10	-0.07	-0.04	-0.11	-0.15	-0.10	0.36	1																														
Cylindralithus serratus	0.19	0.41	-0.14	-0.08	0.57	-0.10	0.10	0.04	0.24	-0.03	0.31	0.17	0.48	-0.12	0.15	0.09	1																												
Discorhabdus ignotus	0.35	-0.07	-0.01	0.14	**0.81**	-0.35	0.15	0.20	0.04	-0.19	0.15	0.32	0.01	-0.22	0.56	0.23	0.30	1																												
Eiffellithus keio	-0.07	-0.08	**0.60**	0.25	-0.04	0.22	-0.05	0.10	-0.10	-0.06	-0.13	-0.12	-0.10	0.25	-0.17	-0.03	-0.13	-0.08	1																										
Eprolithus floralis	-0.08	-0.05	0.07	-0.03	-0.35	0.41	-0.06	-0.07	0.08	-0.02	0.01	-0.17	-0.21	0.10	**-0.60**	-0.20	-0.20	-0.41	-0.02	1																								
Eprolithus moratus	-0.04	-0.06	-0.02	-0.19	0.17	-0.02	-0.03	0.02	-0.07	-0.06	-0.08	-0.09	**0.69**	-0.12	0.13	-0.42	-0.24	-0.09	-0.21	-0.06	0.25	1																						
Helicolithus amceps	-0.12	-0.12	0.23	0.09	-0.11	**0.75**	0.03	0.03	-0.06	0.23	-0.22	0.12	-0.22	0.13	-0.42	0.09	0.04	-0.24	-0.11	-0.09	0.19	0.27	1																					
Lithastrinus grillii	-0.06	0.35	-0.18	-0.09	-0.02	-0.18	0.22	0.14	-0.16	-0.19	-0.19	-0.17	0.28	-0.12	0.09	0.04	-0.02	0.08	-0.15	0.00	0.19	-0.10	-0.17	1																				
Lucianorhabdus cayeuxii	0.21	0.24	-0.07	-0.05	0.36	-0.13	0.55	0.43	-0.10	0.07	0.19	-0.10	**0.64**	-0.07	0.01	-0.09	0.52	0.22	-0.01	-0.14	0.06	-0.12	0.11	-0.15	1																			
Microrhabdulus undosus	-0.09	0.06	-0.14	-0.06	-0.04	-0.15	-0.06	-0.09	-0.11	-0.14	-0.16	-0.11	-0.10	-0.09	0.24	**0.63**	-0.12	0.07	-0.09	-0.17	-0.07	-0.19	0.11	-0.15	1																			
Martasteritles furcatus	-0.16	0.39	-0.20	-0.06	-0.20	-0.24	0.12	0.07	-0.16	-0.24	-0.25	-0.36	0.28	0.07	0.11	0.11	-0.04	-0.03	0.01	-0.19	-0.03	-0.29	**0.70**	0.05	0.15	1																		
Micula adumbrata	-0.05	-0.05	-0.07	-0.03	-0.22	0.01	-0.03	-0.05	-0.06	-0.09	-0.08	-0.08	-0.06	**0.91**	-0.21	-0.11	-0.04	-0.21	0.31	0.02	0.40	0.03	-0.14	-0.08	-0.10	0.10	1																	
Nannoconus truitti	-0.03	-0.03	-0.05	-0.02	-0.15	**0.80**	-0.02	-0.03	-0.04	0.22	-0.08	0.18	-0.09	-0.03	-0.24	-0.07	0.04	-0.17	-0.05	0.08	-0.02	**0.71**	-0.06	-0.05	-0.06	-0.13	-0.03	1																
Owenia hillii	-0.04	-0.04	-0.01	-0.03	0.22	-0.07	-0.03	-0.04	**0.61**	-0.08	0.18	0.51	-0.12	-0.04	0.12	-0.10	0.29	0.15	-0.07	-0.06	-0.04	0.18	-0.12	-0.07	-0.09	-0.27	-0.05	-0.03	1															
Placozygus fibuliformis	0.17	0.02	0.31	0.34	0.55	-0.21	0.06	0.24	0.08	0.20	0.08	0.42	0.05	-0.14	0.13	-0.08	0.20	0.36	-0.05	-0.17	-0.15	0.09	-0.30	0.22	-0.23	-0.47	-0.10	-0.15	0.22	1														
Predicosphaera disdiagrandis	-0.04	-0.04	0.00	-0.03	-0.21	-0.07	-0.03	-0.04	-0.05	-0.08	-0.12	-0.04	0.07	0.57	-0.03	-0.10	0.02	-0.15	0.31	-0.08	-0.03	-0.10	-0.04	0.15	-0.09	0.16	**0.70**	-0.03	-0.04	-0.12	1													
Predicosphaera spinosa	0.25	0.00	0.04	0.08	0.59	-0.18	0.51	0.47	0.08	-0.19	0.17	0.19	0.11	-0.15	0.34	-0.05	0.18	**0.67**	0.02	-0.24	-0.11	-0.06	0.12	0.29	-0.11	-0.05	-0.17	-0.11	0.31	0.21	-0.15	1											
Retecapsa ficula	-0.06	0.47	-0.21	-0.08	0.52	-0.27	0.30	0.21	0.29	-0.26	0.24	0.19	0.41	-0.13	0.41	0.12	0.56	0.26	-0.07	-0.32	-0.14	-0.24	0.13	0.26	0.06	0.05	-0.08	-0.08	0.34	0.20	-0.12	0.39	1										
Retecapsa schizobrachiata	-0.03	-0.03	-0.05	-0.02	-0.09	-0.05	-0.02	-0.03	-0.04	-0.06	**0.60**	-0.07	0.17	-0.03	0.03	-0.07	-0.08	-0.07	-0.05	-0.06	-0.02	-0.03	-0.09	-0.05	-0.06	-0.16	-0.03	-0.02	-0.03	-0.08	-0.03	-0.11	-0.13	1									
Rhagodiscus angustus	0.42	-0.18	0.06	0.16	0.40	-0.26	0.05	0.13	0.23	-0.04	0.14	**0.61**	-0.15	-0.20	0.35	0.16	0.11	0.37	-0.05	-0.30	-0.17	-0.09	-0.28	0.05	0.07	-0.41	-0.17	-0.14	0.39	0.58	-0.11	0.27	0.14	-0.14	1								
Stoverius achylosus	-0.07	-0.07	0.06	-0.05	-0.27	0.43	-0.05	-0.07	0.05	**0.62**	-0.05	-0.05	-0.13	-0.07	-0.37	-0.17	0.02	-0.30	-0.12	0.04	-0.05	0.47	-0.18	-0.12	-0.14	-0.22	-0.03	**0.58**	0.08	-0.02	-0.07	-0.15	-0.11	-0.05	-0.09	1							
Tetrapodorhabdus decorus	-0.07	0.35	-0.18	-0.08	-0.13	-0.04	0.09	0.03	-0.10	-0.22	-0.19	-0.15	0.08	**0.63**	-0.01	0.01	-0.06	-0.09	0.09	0.01	0.33	-0.09	0.36	-0.09	-0.05	0.46	**0.60**	-0.08	-0.12	-0.24	0.41	0.02	0.12	-0.08	-0.31	-0.20	1						
Tranolithus macleodae	0.24	0.37	-0.19	-0.10	**0.69**	-0.26	-0.04	-0.09	0.15	-0.12	0.25	0.24	0.30	-0.09	0.45	0.24	**0.71**	0.41	-0.10	-0.27	-0.12	-0.25	-0.10	0.34	0.02	-0.20	-0.09	-0.10	0.23	0.32	-0.05	0.21	**0.63**	0.01	0.26	-0.19	-0.04	1					
Watznaueria barnesae	-0.19	-0.33	-0.08	-0.09	**-0.74**	0.40	-0.26	-0.26	-0.03	0.22	-0.14	-0.34	-0.24	0.18	-0.53	-0.15	-0.43	**-0.65**	-0.12	0.41	0.41	0.29	0.07	-0.27	-0.04	0.01	0.05	0.21	-0.14	-0.47	-0.06	-0.50	-0.54	0.17	-0.44	0.23	0.00	-0.57	1				
Watznaueria quadriradiata	-0.04	0.33	-0.07	-0.03	0.20	-0.07	-0.03	-0.04	-0.05	0.11	-0.03	0.22	-0.14	-0.04	0.03	-0.02	0.36	-0.05	-0.07	-0.06	-0.04	-0.03	-0.08	0.50	-0.09	-0.02	-0.05	-0.03	-0.04	-0.08	-0.04	-0.08	0.24	-0.03	-0.07	-0.07	0.44	-0.16	1				
Zeugrhabdotus diplogrammus	-0.08	-0.16	**0.64**	0.13	-0.13	0.06	-0.03	0.05	-0.24	0.24	-0.10	-0.08	-0.21	-0.22	-0.33	-0.08	-0.25	-0.12	0.28	0.02	-0.17	0.10	-0.23	-0.21	-0.06	-0.21	-0.17	-0.17	-0.08	0.21	-0.16	-0.08	-0.36	0.03	0.08	0.18	-0.32	-0.31	-0.03	-0.08	1		
Zeugrhabdotus erectus	0.08	-0.08	**0.61**	0.55	0.52	0.02	0.01	0.31	-0.10	0.00	-0.11	0.16	-0.13	-0.15	-0.02	-0.04	0.03	0.45	0.21	-0.06	-0.12	0.20	-0.19	-0.01	-0.07	-0.26	-0.15	-0.06	-0.01	**0.62**	-0.13	0.23	-0.03	-0.10	0.24	-0.10	-0.24	0.08	-0.40	-0.09	0.31	1	
Zeugrhabdotus kerguelenensis	-0.03	-0.03	-0.05	-0.02	-0.09	-0.05	-0.02	-0.03	-0.04	0.22	-0.08	-0.07	0.34	-0.03	-0.01	-0.07	-0.08	-0.07	-0.05	-0.03	-0.02	0.04	-0.09	0.35	-0.06	0.00	-0.03	-0.02	-0.03	0.21	-0.03	-0.11	-0.13	-0.02	0.05	-0.05	-0.08	-0.04	0.05	**0.70**	-0.01	-0.08	1
Zeugrhabdotus sp. 2	**0.70**	-0.03	-0.05	-0.02	0.00	-0.05	-0.02	-0.03	-0.04	-0.06	-0.08	0.27	-0.09	-0.03	0.15	-0.07	-0.08	0.02	-0.05	-0.06	-0.02	-0.08	0.01	-0.05	-0.06	-0.09	-0.03	-0.02	-0.03	0.06	-0.03	0.13	-0.08	-0.02	0.39	-0.05	-0.01	0.09	-0.06	-0.03	0.01	-0.08	-0.02	1

Table 5.5.2.4 – correlation matrix of selected species detected at the TDP39. Bold light blue values correlation ≈0. 60; bold blue values correlation >0. 70.

- *H. anceps* versus *N. truittii* (0.71)
- *L. grillii* versus *M. furcatus* (0.70)
- *M. adumbrata* versus *P. desiderograndis* (0.70)
- *W. quadriradiata* versus *Z. kerguelenensis* (0.70)
- *W. barnesiae* has a negative correlation with *B. constans* (-0.74).

5.5.3 The Coniacian-Santonian OAE3 at TDP39

According to the biostratigraphic results, the TDP39 section covers only partially the OAE3 interval as this site extends from the upper Coniacian (CC15//NC16/NC16* zones and UC11a-b subzones) to the middle Santonian (CC17/NC17/NC17*/UC12 zones). Significant changes in abundances of *Micula,* holoccoccoliths (*Lucianorhabdus, Calculites, Owenia*) and *Marthasterites* were observed (Figure 5.5.3.1) both for relative (%) and absolute abundances (n. specimens/gram of sediments).

The genus *Micula* ranges from 0% to 6.1 % (average 1.4%) and includes *M. adumbrata*, *M. concava*, *M. cubiformis* and *M. staurophora*. The latter is the dominant species (Fig. 5.5.3.1). In terms of *Micula* relative abundance, the higher value (6.1%) was observed at 96.56m in the CC15/NC16* zones and UC11a-b subzone. The absolute abundance showshigh values in two intervals in the CC16/NC17* zones, UC11c subzone. The first extends from 62.56m to 56.56m and is characterized by *M. staurophora* (1.3%; $0.33X10^6$), *M. adumbrata* (1.5%; $0.37X10^6$), *M. concava* (1.6%;$0.38X10^6$) and *M. cubiformis* (1.7%;$0.4X10^6$). The second maximum extends from 46.56m to 26.56m and is characterized by *M. staurophora* (1.8%;$0.44X10^6$), *M. adumbrata* (average 1.8%; $0.44X10^6$); *M. concava* (1.9%;$0.48X10^6$) and *M. cubiformis* (2%;$0.5X10^6$).

Holococcolith are quite rare at TDP39 as they never reach more than 2% of the assemblage. The maximum in relative and absolute abundance is at 66.56m with an increase of *Lucianorhabus* (0.7%; 0.2 X 10^6), *Calculites* (1%; 0.25 X 10^6) and *Owenia* (0.4%; 0.1 X 10^6). This peak corresponds to a level where genus *Micula* becomes rare in the assemblage.

The observed changes in abundance of *Marthasterites* show a similar pattern for percentages and absolute abundances. This genus is mainly composed of *M. furcatus* (average 3.4%) and rare *M. crassus* (average 0.01%). The interval from the base of the studied section to 66.56m, corresponding to the CC15/NC16* zones and UC11a-b subzone (upper Coniacian), shows the lowest *Marthasterites* abundance recorded at TDP39 (average 1.8%; 0.17 X 10^6). The *Marthasterites* content shows a gradual increase from the upper Coniacian (CC16/NC17*zones and UC11c) to the middle Santonian (CC17/NC17/UC12 zones) where it reaches the maximum abundances (9.9%;1.77 X 10^6).

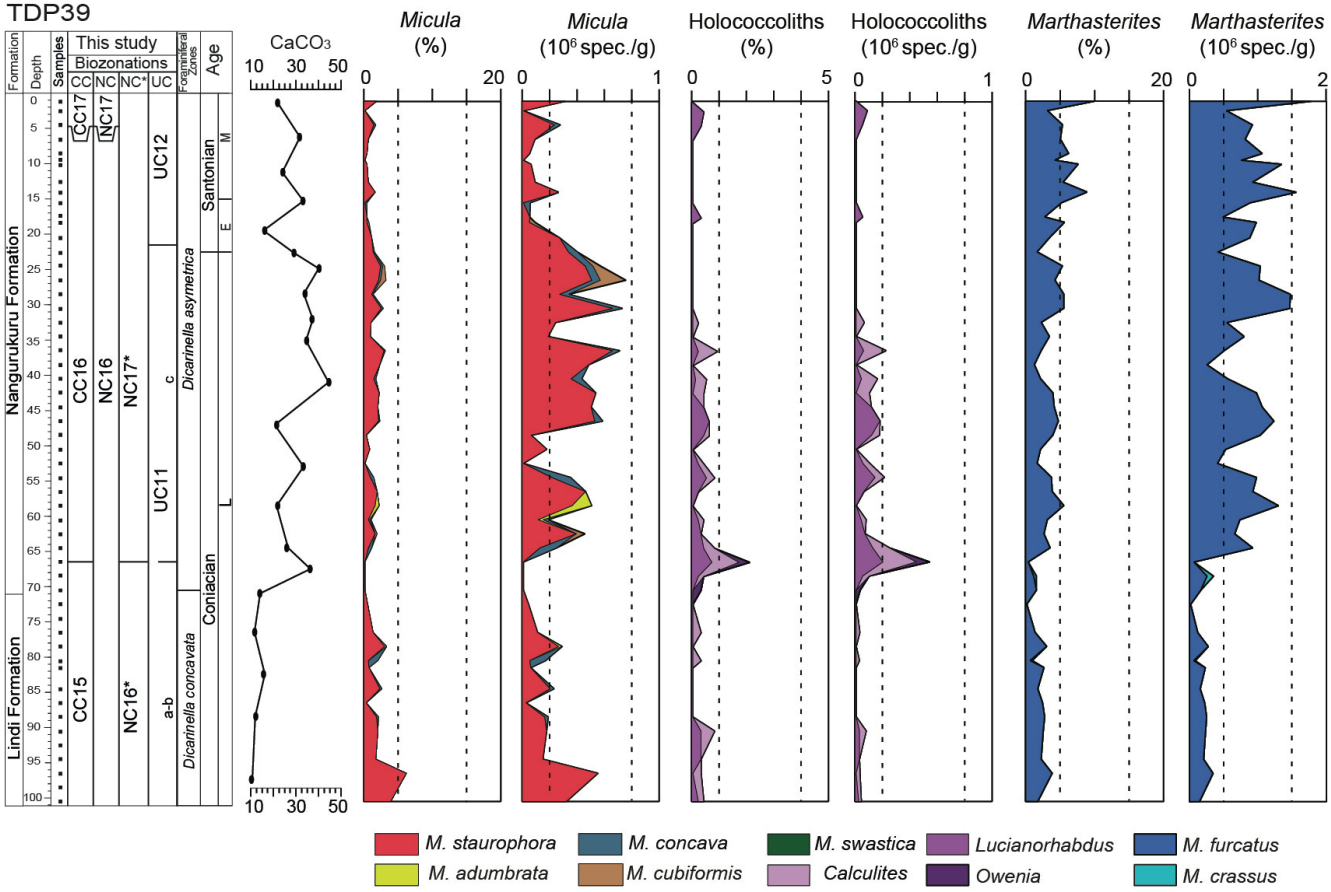

Figure 5.5.3.1 - Relative (%) and absolute (number of specimens/g of sediment) abundance of *Micula*, holococcoliths and *Marthasterites*.

5.6 ODP Site 763

5.6.1 Biostratigraphy

The biostratigraphic data available for Site ODP 763 (Russo, 2014; Bralower and Siesser, 1992), were reinterpreted in this study. In the investigated interval, calcareous nannofossils are generally common to few, with a preservation that varies from moderate-good to moderate. A total of eleven events were detected by Russo (2014), allowing the identification of the CC12-CC18 zones of Sissingh (1977), NC14-NC18 zones of Roth (1978), NC14-NC18* zones of Bralower et al. (1995) and UC8-UC14b zones of Burnett (1998). The results are presented in Figure 5.6.1 and zonal and subzonal markers used in this study are described from the oldest to the youngest. A range chart for Site 763 is provided in the Appendix 15.

The FO of *M. furcatus* defines the base of CC13, NC15, NC15* zones. This event was detected by Russo (2014) in sample 122-763B-20X-2, 56-58 (363.06 mbsf). The FO of *L. septenarius* in sample 122-763B-20X-2, 40-42 (362.92 mbsf) defines the base of CC13b subzone and UC9 zone. The FO of *Z.*

biperforatus in sample 122-763B-19X-CC, 15-17 (560.97 mbsf) define the base of the NC16 zone and UC9b subzones. Russo (2014) placed the FO of *A. parcus expansus* (<8 μm) in sample 122-763B-19X-5, 140-142 (358.92 mbsf). However, the taxonomic concept of *A. parcus expansus* applied in this study is different from that of Russo (2014). In fact, the photo of *A. parcus expansus* (<8μm) showed in Plate 1, fig. F of Russo (2014) illustrate a specimen having a monocyclic margin, that resemble that of *Arkhangelskiella* confusa. For this reason, the FO of *A. parcus expansus* in not reported here in the synthesis scheme.

The FO of *M. staurophora* in sample 122-763B-19X-3, 20-22 (354.72 mbsf) indicate the zone CC14, NC16* and UC10.The FO of *L. grillii* was observed in sample 122-763-18X-2, 70-72 (344.22 mbsf) where the base of CC15 and UC11 zones was placed. The LO of *L. septenarius* in sample 122-763B-17X-4, 86-88 (337.28 mbsf) corresponds to the base of the UC12 zone, whereas the FO of *L. cayeuxii* in sample 122-763B-17X-1, 19-21 (332.71 mbsf) defines the base of CC16 and NC17* zones. The LO of *E. floralis* in sample 122-763B-16X-4,139-141 (328.91 mbsf) marks the base of the CC17 and NC17 Zones.

The FO of *A. cymbiformis* was observed in sample 122-763B-16-2,16-18 (324.68 mbsf) where the base of the UC13 zone was placed. The FO of *A. parcus parcus* was observed in sample 122-763B-15-6,10-12 (321.12 mbsf) and defines the base of CC18, NC18, NC18* and UC14 zones, whereas the FO of *A. parcus constrictus* in sample 122-763B-15X-1,86-88 (314.38 mbsf) marks the base of the subzone UC14b.

According to calcareous nannofossil biostratigraphic data (Russo, 2014; Bralower and Siesser, 1992) and revised in this study the following stage boundaries were placed:

- the Turonian/Coniacian boundary between the FO of *Z. biperforatus* and the FO of *M. staurophora* in the *F. maslakovae* planktonic foraminiferal zone according to Lees (2008) and Walaszczyk et al. (2010);
- the Coniacian/Santonian boundary between the FO of *L. grillii* and the LO of *L. septenarius* in the *D. asymetrica* planktonic foraminiferal zone. The FO of *L. cayeuxii* represents the last nannofossil event of the Coniacian (Lamolda et al., 2014), however, at ODP Site 763, the FO of *L. cayeuxii*, was found to occur at a higher stratigraphic level (122-763B-17X-1, 19-21; 332.71 mbsf);
- the Santonian/Campanian boundary at the FO of *A. parcus parcus* (see discussion in Miniati et al., 2020).

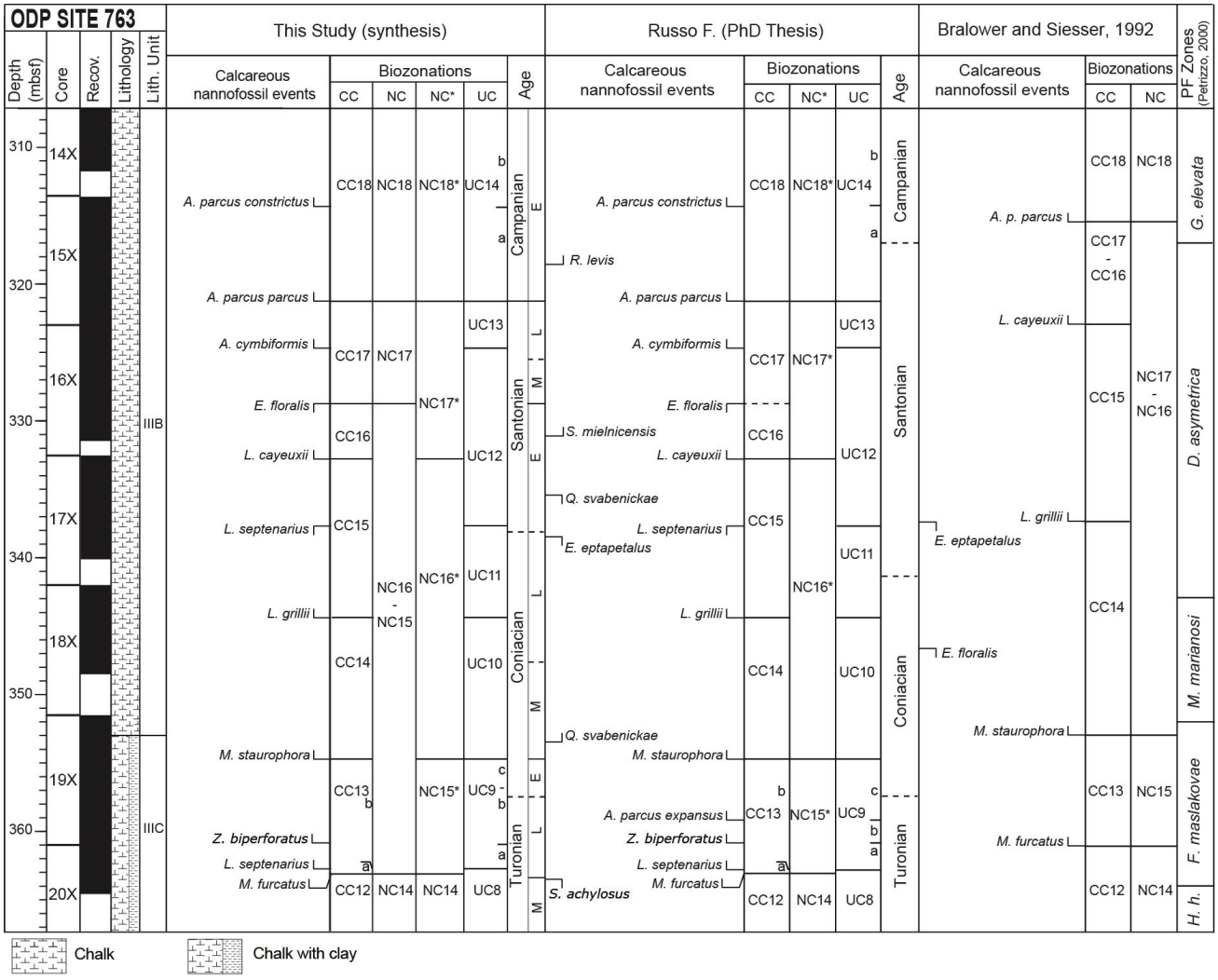

Figure 5.6.1 - ODP Leg 122 Site 763 calcareous nannofossil biostratigraphy (Russo, 2014; Bralower and Sissier, 1992). Biostratigraphic zonation: CC (Sissingh, 1977), NC (Roth,1978), NC* (Bralower 1995), and UC (Burnett 1998) are shown.

5.6.2 Nannofossil paleoecology and paleoceanography.

At ODP Site 763 a total of 66 taxa were recognized. Except for a barren sample (122-763B-18X-CC,26-28; 348.28 mbsf), the species richness varies from a maximum of 35.6 (sample 122-763B-19X-6,10-12; 359.78 mbsf) to 2.1 (sample 122-763B-15X-5,140-142;320.92 mbsf) with a mean of 12.4 species for sample (Figure 5.6.2.1).

The Shannon index shows a pattern similar to the species richness (Figure 5.6.2.1) and ranges between 1 (sample 122-763B-17X-5,10-12; 338.62 mbsf) and 2.3 (sample 122-763B-15X-CC,11-13; 322.93 mbsf), with an average value of 1.7, suggesting moderately diversified assemblages and absence of dominance of single taxa.

The total nannofossil abundance (number of specimens/field of view) fluctuates around the average value of 18 specimens/field of view, with the maximum recorded in the upper Turonian (27 specimens/field of view) and the minimum in the lower Santonian (7 specimens/field of view).

The presence of moderately to well diversified assemblages and the occurrence of *W. barnesiae* together with delicate and less diagenesis-resistant species such as *B. constans*, suggest that the composition and abundance of calcareous nannofossils mainly reflect primary ecological signal with negligible diagenetic modifications.

The descriptive statistics of calcareous nannofossil genera and species are synthesized in Tables 5.6.2.1 and 5.6.2.2. At ODP Site 763, there are four genera with an average relative abundance > 2% (*Eiffellithus*, *Micula*, *Prediscosphaera, Retecapsa, Watznaueria*). Genera with average relative abundance < 2% are not discussed here but their descriptive statistics are show in Tables 5.6.2.1. Figure 5.6.2.1 illustrates the relative abundances of genera with an average > 1%.

The dominant genus is *Watznaueria* fluctuating from 0% to 77.2% (average 57%). *W. barnesiae* represents the most abundant species ranging from 0% to 76.2%. Other rare *Watznaueria* species are *W. biporta, W. fossacinta* and *W. manivitiae.*

The genus *Micula* is the second in abundance and ranges from 0% to 42.4% (average 11.5%). At ODP Site 763 a first peak (17.3%) is present in the middle Coniacian (sample 122-763B-19X-2,26-28; 353.28 mbsf), followed by two maxima of 42.4% (sample 122-763B-18X-3,96-98; 345.98 mbsf) and 41.6% (sample 122-763B-18X-1, 76-78; 342.78 mbsf) in the upper Coniacian. Other two spikes are present at the Coniacian/Santonian boundary and in the lower Santonian with relative abundances of 36.6% (sample 122-763B-17X-4,140-14; 338.43 mbsf and 33.3% (sample122-763B-17X-3, 86-88; 336.38 mbsf). Another increase up to 23% occurs in the lower Campanian (sample 122-763B-15X-2, 26-28; 315.28 mbsf).

The third most abundant genus is *Prediscosphaera* that ranges from 0% to 28.1% (average 9.6%). A peak of 26.9% is present in the lower Santonian (sample 122-763B-17X-2, 89.91; 334.91 mbsf), whereas a maximum of 17.2% occurs in the upper Santonian-lower Campanian. Three different species of *Prediscosphaera* were detected at ODP Site 763: *P. cretacea*, *P. columnata* and *P. grandis.* The most abundant species are *P. cretacea* that ranges from 0% to 17% (4.4%) and *P. columnata* that ranges from 0% to 21.6% (4.5%).

The genus *Retecapsa* ranges from 0% to 17.2% (average 3.8 %). Higher relative abundances occur in the lower Turonian (sample 122-763B-20X-2, 40-; 362.92 mbsf), lower Santonian (sample 122-763B-17X-1,136-; 333.88 mbsf) and uppermost Santonian (Core 122-763B-15X section 6). Genus *Retecapsa* is represented by *R. surirella* that ranges from 0.7% to 14% (average 3.1%), *R. crenulata* that ranges

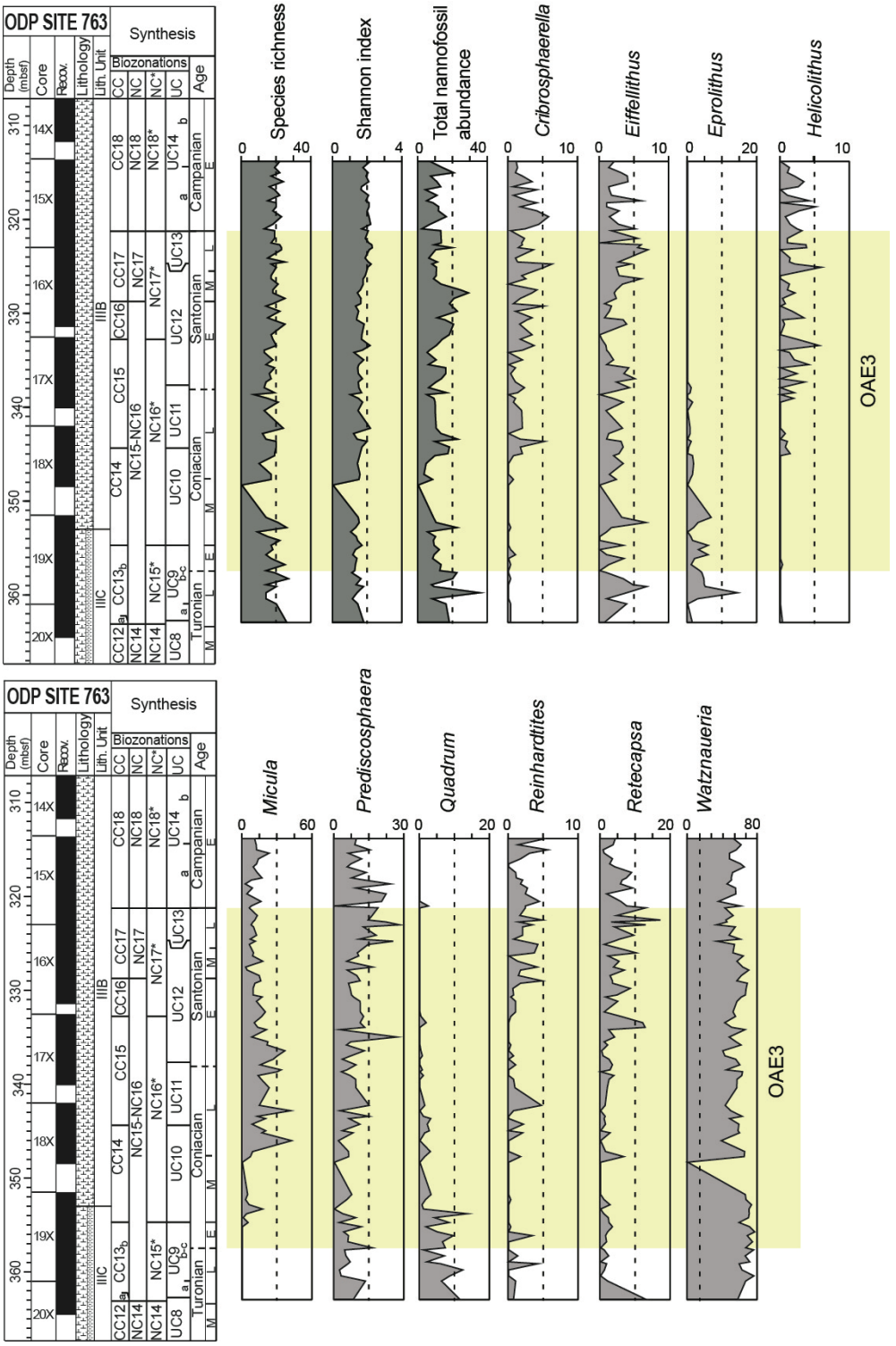

Figure 5.6.2.1 - Calcareous nannofossil data from the ODP Site 763 showing the fluctuations in species richness, Shannon index, total nannofossil abundance (n. specimens/FOV) absolute abundance (n. specimens/gram of sediment) and the relative abundance of genera with an average relative abundance >1%. The yellow band indicates the OAE3 interval.

GENUS	Average %	Minimum %	Maximum %	Mode	Standard Deviation	Median
Watznaueria	57.0	0	77.2	65.1	12	58
Micula	11.5	0	42.4	0	9.6	10.2
Prediscosphaera	9.6	0	28.1	7.1	6.2	8.2
Retecapsa	3.7	0	17.2	0	3.7	2.6
Eiffellithus	2.5	0	7	1	1.8	2.4
Quadrum	1.7	0	13.6	0	3.1	0
Cribrosphaerella	1.6	0	6.3	0	1.6	1
Reinhardtites	1.3	0	5.6	0	1.5	0.7
Helicolithus	1.1	0	5.9	0	1.5	0.3
Eprolithus	1.0	0	14.4	0	2.2	0
Marthasterites	0.9	0	8.2	0	1.6	0
Biscutum	0.8	0	7	0	1.3	0
Microrhabdulus	0.8	0	5.2	0	1	0.3
Aspidolithus	0.6	0	8.5	0	1.2	0
Zeugrhabdotus	0.6	0	5.4	0	1	0
Lithastrinus	0.5	0	3.6	0	0.7	0.3
Manivitella	0.5	0	3.2	0	0.7	0
Arkhangelskyella	0.4	0	5.1	0	0.9	0
Cylindralithus	0.4	0	2.1	0	0.6	0
Grantarhabdus	0.4	0	2.3	0	0.6	0
Tranolithus	0.4	0	3.5	0	0.7	0
Broinsonia	0.4	0	1.9	0	0.5	0
Tetrapodorhabdus	0.2	0	1.4	0	0.3	0
Chiastozygus	0.2	0	1.8	0	0.4	0
Ahmuellerella	0.1	0	1.4	0	0.3	0
Rotelapillus	0.1	0	1.4	0	0.3	0
Lithraphidites	0.1	0	1.4	0	0.3	0
Lucianorhabdus	0.1	0	1	0	0.2	0
Kamptnerius	0.1	0	1.1	0	0.2	0
Haqius	0.1	0	1.4	0	0.2	0
Corollithion	0.1	0	2.4	0	0.3	0
Flabellites	0.1	0	1.3	0	0.2	0
Rhagodiscus	0.1	0	3	0	0.4	0
Bukrylithus	0.04	0	1	0	0.2	0
Rucinolithus	0.04	0	1	0	0.2	0
Loxolithus	0.03	0	0.7	0	0.1	0
Calculites	0.02	0	1	0	0.1	0
Repagulum	0.00	0	0.3	0	0	0

Table 5.6.2.1 - Descriptive statistics of genera identified at ODP Site 763.

SPECIES	Average %	Minimum %	Maximum %	Mode	Standard Deviation	Median
Ahmuellerella octoradiata	0.1	0	1.4	0	0.3	0
Arkhangelskyella cymbiformis	0.4	0	5.1	0	0.9	0
Aspidolithus enormis	0.02	0	0.7	0	0.1	0
Aspidolithus furtivus	0.05	0	1.3	0	0.2	0
Aspidolithus parcus constrictus	0.02	0	1.1	0	0.1	0
Aspidolithus parcus expansus	0.4	0	7.8	0	1.1	0
Aspidolithus parcus parcus	0.1	0	1.4	0	0.3	0
Biscutum constans	0.6	0	7	0	1.3	0
Biscutum large	0.1	0	1.7	0	0.3	0
Broinsonia matalosa	0.4	0	1.9	0	0.5	0
Broinsonia signata	0.02	0	1.4	0	0.2	0
Bukrylithus ambiguus	0.04	0	1	0	0.2	0
Calculites sp.	0.02	0	1	0	0.1	0
Chiastozygus litterarius	0.2	0	1.8	0	0.4	0
Corollithion signum	0.1	0	2.4	0	0.3	0
Cribrosphaerella ehrenbergii	1.6	0	6.3	0	1.6	1
Cylindralithus nudus	0.4	0	2.1	0	0.5	0
Cylindralithus sculptus	0.04	0	2	0	0.2	0
Eiffellithus eximius	1.4	0	6.3	0	1.8	0.9
Eiffellithus gorkae	0.2	0	4.1	0	0.6	0
Eiffellithus turriseiffelii	0.9	0	4.8	0	1.3	0
Eprolithus floralis	0.9	0	14.4	0	2.2	0
Eprolithus eptapetalus	0.1	0	1.7	0	0.3	0
Flabellites oblongus	0.1	0	1.3	0	0.2	0
Gartnerago segmentatum	0.4	0	2.3	0	0.6	0
Grantarhabdus coronadventis	0.03	0	1	0	0.1	0
Haqius circumradiatus	0.1	0	1.4	0	0.2	0
Helicolithus anceps	1.0	0	5.6	0	1.4	0
Helicolithus trabeculatus	0.1	0	3.7	0	0.5	0
Kamptnerius magnificus	0.1	0	1.1	0	0.2	0
Lithastrinus grillii	0.4	0	3.6	0	0.7	0
Lithastrinus septenarius	0.1	0	1.7	0	0.3	0
Lithraphidites carniolensis	0.1	0	1.4	0	0.3	0
Loxolithus armilla	0.03	0	0.7	0	0.1	0
Lucianorhabdus cayeuxii	0.1	0	1	0	0.2	0
Lucianorhabdus maleformis	0.02	0	0.7	0	0.1	0
Manivitella pemmatoidea	0.5	0	3.2	0	0.7	0
Marthasterites furcatus	0.9	0	8.2	0	1.6	0
Microrhabdulus decoratus	0.8	0	5.2	0	1	0.3
Micula cubiformis	0.8	0	10.5	0	2	0
Micula staurophora	10.7	0	42.4	0	9.8	8.7
Prediscosphaera cretacea	4.4	0	17	0	4.1	3.5
Prediscosphaera columnata	4.5	0	21.6	0	4	3.1
Prediscosphaera grandis	0.8	0	8.4	0	1.9	0
Quadrum gartneri	0.6	0	9.1	0	1.6	0
Quadrum intermedium	0.7	0	8.9	0	1.9	0
Quadrum octobrachium	0.3	0	4.8	0	0.9	0
Reinhardtites anthophorus	0.5	0	4.7	0	0.9	0
Reinhardtites levis	0.8	0	4.2	0	1.2	0

Table 5.6.2.2 - Descriptive statistics of species identified at ODP Site 763.

Repagulum parvidentatum	0.004	0	0.3	0	0	0
Retecapsa angustiforata	0.03	0	1.7	0	0.2	0
Retecapsa crenulata	0.6	0	6.5	0	1.1	0
Retecapsa surirella	3.1	0	14	0	2.9	2.4
Rhagodiscus asper	0.1	0	3	0	0.4	0
Rotelapillus coronatus	0.1	0	1.4	0	0.3	0
Rucinolithus terebrodentarius	0.04	0	1	0	0.2	0
Tetrapodorhabdus decorus	0.2	0	1.4	0	0.3	0
Tranolithus gabalus	0.04	0	1	0	0.2	0
Tranolithus orionatus	0.3	0	3.5	0	0.7	0
Watznaueria barnesiae	55.0	0	76.2	58.3	12.4	56.6
Watznaueria biporta	0.4	0	2.8	0	0.8	0
Watznaueria fossacincta	0.4	0	2.4	0	0.6	0
Watznaueria manivitiae	1.2	0	8.6	0	2.2	0
Zeugrhabdotus bicrescenticus	0.2	0	2.4	0	0.5	0
Zeugrhabdotus embergeri	0.2	0	3.4	0	0.5	0
Zeugrhabdotus scutula	0.1	0	1.7	0	0.4	0

Table 5.6.2.2: Descriptive statistics of species identified at ODP Site 763.

from 0% to 6.5%(average 0.8%) and less abundant *R. angustiforata*.

Eiffellithus ranges from 0% to 7% (average 2.5%) and *E. eximius* is the most abundant species, ranging from 0% to 6.3% (average 1.4%). Other species of *Eiffellithus* are *E. gorkae* and *E. turriseiffelii.*

The fluctuations in the NI and TI are presented in Figure 5.6.2.2. At ODP Site 763 the NI values remain close to zero throughout the studied interval. A very minor increase (up to 9) occurs in the lower Campanian. The high fertility taxa *D. ignotus* and *Z.* erectus are absent and only *B. constans* occurs but with low abundances (average 0.6%). Thus, the presence of scarce high fertility taxa together with abundant *W. barnesiae* suggest the prevalence of oligotrophic conditions in the studied interval.

At ODP Site 763 the TI V.1 shows unstable conditions with an alternation of brief cooler and warmer episodes (Figure 5.6.2.2). However, intervals of more stable temperature are present in the upper Turonian-lower Coniacian with the prevalence of cooler waters and in the upper Coniacian and lower Santonian with warmer conditions.

The TI V.2 and TIV. 3 show a similar trend (Figure 5.6.2.2) also characterized by a high frequency alternations of short cooler and warmer episodes. More stable warmer temperature can be found in the middle-upper Coniacian and in the uppermost-lowermost Campanian, whereas periods of stable cooler waters occur in the upper Coniacian and lower Santonian. On the contrary, the TI V.4 shows the presence of stable warmer temperature during the lower Turonian-lower Santonian and only from the middle Santonian a change to unstable conditions with short cooler and warmer episodes (Figure 5.6.2.2).

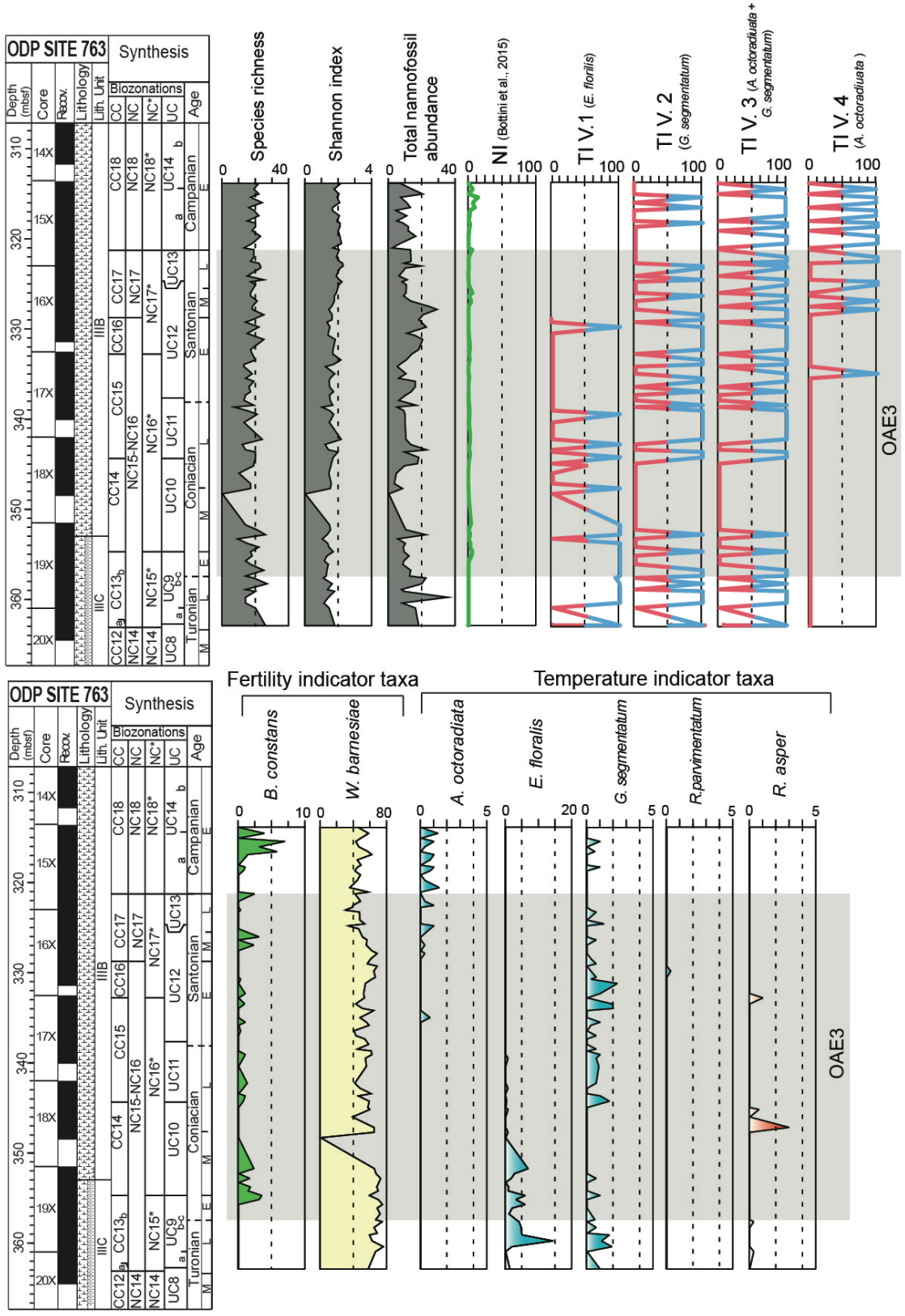

Figure 5.6.2.2 - Fluctuationsin calcareous nannofossil temperature and fertility indicator taxa at ODP Site 763. Nutrient Index (NI) after Bottini et al. (2015); Temperature Index (TI) after Bottini et al. (2015) and modified V.2, V.3, V.4. The species richness, Shannon index, total nannofossil abundance (n. specimens/FOV), absolute abundance (n. specimens/gram of sediment) are also reported. The grey band indicates the OAE3 interval.

At ODP Site 763 the temperature indicator taxa show relatively low abundances. *A. octoradiata* ranges from 0% to 1.4%(average 0.1%), *G. segmentatum* ranges from 0% to 2.3%(average 0.4%), *R. parvimentatum* ranges from 0% to 0.3 %(average 0.004%) while *R. asper* ranges from 0% to 3 %(average 0.1%). The only exception is the cooler water indicator *E. floralis* that ranges from 0% to 14.4%(average 0.9%).

The Pearson's correlation coefficients calculated for all the genera detected at ODP Site 763 don't support the existence of any linear correlation. However, the correlation matrix obtained for all species detected at ODP Site 763 shows the existence of a linear correlation between some taxa. A summary showing only the species with a correlation >0.6 (or < -0.6) is reported in Appendix (16A), whereas the complete matrix is provided in the Appendix (16B). A strong correlation (>0.7) was documented for:

- *A. parcus expansus* versus *B. ambiguus* (0.70)
- *B. signata* versus *R. asper* (0.90)
- *G. coronadventis* versus *R. parvidentatum* (0.72)

	Aspidolithus enormis	*Aspidolithus parcus expansus*	*Broinsonia signata*	*Bukrylithus ambiguus*	*Corollithion signum*	*Cylindralithus sculptus*	*Eprolithus floralis*	*Eprolithus eptapetalus*	*Grantarhabdus coronadventis*	*Haqius circumradiatus*	*Lithastrinus septenarius*	*Loxolithus armilla*	*Prediscosphaera grandis*	*Quadrum gartneri*	*Repagulum parvidentatum*	*Retecapsa crenulata*	*Retecapsa surirella*	*Rhagodiscus asper*	*Rucinolithus terebrodentarius*	*Watznaueria manivitiae*
Aspidolithus enormis	1																			
Aspidolithus parcus expansus	0.33	1																		
Broinsonia signata	0.35	0.37	1																	
Bukrylithus ambiguus	0.28	**0.70**	0.35	1																
Corollithion signum	0.37	0.33	0.46	0.31	1															
Cylindralithus sculptus	0.36	0.40	0.44	0.35	**0.65**	1														
Eprolithus floralis	0.35	0.25	0.35	0.25	**0.62**	0.42	1													
Eprolithus eptapetalus	0.44	0.20	**0.62**	0.19	0.30	0.34	0.22	1												
Grantarhabdus coronadventis	0.31	0.31	0.38	0.30	0.39	0.39	0.31	0.22	1											
Haqius circumradiatus	0.25	0.24	**0.68**	0.23	0.28	0.32	0.25	0.43	0.33	1										
Lithastrinus septenarius	0.35	0.21	0.37	0.21	0.58	0.45	0.39	**0.63**	0.30	0.24	1									
Loxolithus armilla	**0.62**	0.35	0.32	0.24	0.33	0.32	0.29	0.28	0.27	0.23	0.19	1								
Prediscosphaera grandis	0.17	0.49	0.23	0.35	0.19	0.34	0.11	0.07	0.18	0.16	0.09	0.13	1							
Quadrum gartneri	0.32	0.21	0.29	0.20	**0.63**	0.31	**0.69**	0.21	0.33	0.41	0.41	0.28	0.08	1						
Repagulum parvidentatum	0.38	0.40	0.45	0.37	0.42	0.47	0.37	0.30	**0.72**	0.34	0.32	0.34	0.26	0.32	1					
Retecapsa crenulata	0.29	0.23	0.29	0.20	0.32	0.33	0.20	0.16	**0.69**	0.21	0.17	0.23	0.20	0.22	0.42	1				
Retecapsa surirella	0.15	0.36	0.20	0.23	0.17	0.19	0.03	-0.02	0.39	0.05	0.03	0.16	0.30	0.06	0.36	**0.65**	1			
Rhagodiscus asper	0.45	0.41	**0.90**	0.35	0.41	0.44	0.35	0.58	0.39	**0.68**	0.33	0.37	0.23	0.30	0.46	0.28	0.22	1		
Rucinolithus terebrodentarius	0.28	0.44	0.35	**0.60**	0.33	0.36	0.30	0.20	0.30	0.24	0.22	0.29	0.18	0.22	0.37	0.20	0.19	0.41	1	
Watznaueria manivitiae	0.12	0.37	0.18	0.35	0.13	0.26	0.07	0.00	0.12	0.16	0.03	0.07	**0.67**	0.05	0.21	0.17	0.31	0.17	0.13	1

Table 5.6.2.3: correlation matrix of species detected ODP Site 763. Bold light blue = values correlation ≈0. 60; bold blue values = correlation >0. 70.

5.6.3 The Coniacian-Santonian OAE3 at ODP Site 763

The stratigraphic succession investigated at ODP 763 extends from the middle Turonian to the lower Campanian thus include all the OAE3 interval (from sample 122-763-19X-5,12-14 at 357.64 mbsf to sample 122-763B-15-6,10-12 at 321.12 mbsf).

The calcareous nannofossil assemblages across the OAE3 interval are characterized by significant fluctuations in abundance of *Micula*, *Marthasterites* and holoccoccoliths that include the genera *Lucianorhabdus* and *Calculites*. These are plotted in Figure 5.6.2.3 in terms of relative abundances (%). The observed changes in relative abundance of *Micula* show that *M. staurophora* represents the dominant species of this genus up to the upper Santonian where also the *M. cubiformis* shows an increase in abundance. A first peak is present in the middle Coniacian (sample 122-763B-19X-2,26-28; 353.28 mbsf), characterized by an increase of *M. staurophora* up to 17.3% of the assemblage. The maximum relative abundance of *Micula* was observed in the upper Coniacian-lower Santonian, with four discrete spikes. The first is in the upper Coniacian at the top of the CC14/UC10 zones and lower NC16* zone (sample 122-763B-18X-3,96-98; 345.98 mbsf) and is characterized by an increase of *M. staurophora* up to 42.4% of the assemblage. The second peak was also detected in the upper Coniacian in the lower CC15/UC11 zones and NC16* zone (sample 122-763B-18X-1, 76-78; 342.78 mbsf) and is marked by an increase of *M. staurophora* up to 41.6% of the assemblage. The third peak was observed in the CC15/NC16* zones and topmost UC11 zone, close to the Coniancian/Santonian boundary (sample 122-763B-17X-4,140-142; 338.43 mbsf) with *M. staurophora* increasing up to 36.6% of the assemblage. The last spike was detected in the lower Santonian in the upper CC15/UC12 zones and lower UC12 zone (sample122-763B-17X-3, 86-88; 336.38 mbsf), with *M. staurophora* reaching 33.3% of the assemblage. In the Santonian, the relative abundance of *Micula* remains quite high fluctuating around the average value of 11.2%. From the uppermost Santonian there is a relative increase of *M. cubiformis* that reaches the 10.5% of the assemblage in sample 122-763B-15X-6, 92-94 (321.94 mbsf). Another spike occurs in the CC18/NC18/NC18* and upper UC14a subzone (lower Campanian) (sample 122-763B-15X-2, 26-28; 315.28 mbsf) where *M. staurophora* reaches the 23% of the assemblage.

ODP Site 763 is characterized by a low abundance of holococcoliths with *Lucianorhabdus* and *Calculites* that never reach more than the 1% and 1.4% of the assemblage, respectively. Genus *Lucianorhabdus* is more abundant in the middle-upper Santonian (CC17/NC17/NC17* zone and UC12/UC13 zones) whereas *Calculites* increases in abundance in the lower Campanian (CC18/NC18/NC18* and upper UC14a subzone).

As far as genus *Marthasterites* is concerned, only the species *M. furcatus* is present at ODP Site 763, showing two distinct intervals of increase in relative abundance. The first ranges from the upper Turonian to the lower-middle Coniacian and is marked by an average abundance of 1.5%. At the Turonian/Coniacian boundary a spike of *M. furcatus* of 8.2% of the assemblage was detected in the CC13b/NC15*/UC9b-c zones (sample 122-763-19X-5,12-14 at 357.64 mbsf).

A second interval of higher *Marthasterites* abundance ranges from the upper Coniacian to the lower Santonian showing an average relative abundance of 2.4%. Two spikes occur in the upper Coniacian and in the lower Santonian, respectively, with values of 5.4% (sample 122-763B-18X-3,96-98; 345.98 mbsf) and 6.8% (sample 122-763B-17X-3,140-142; 336.92 mbsf).

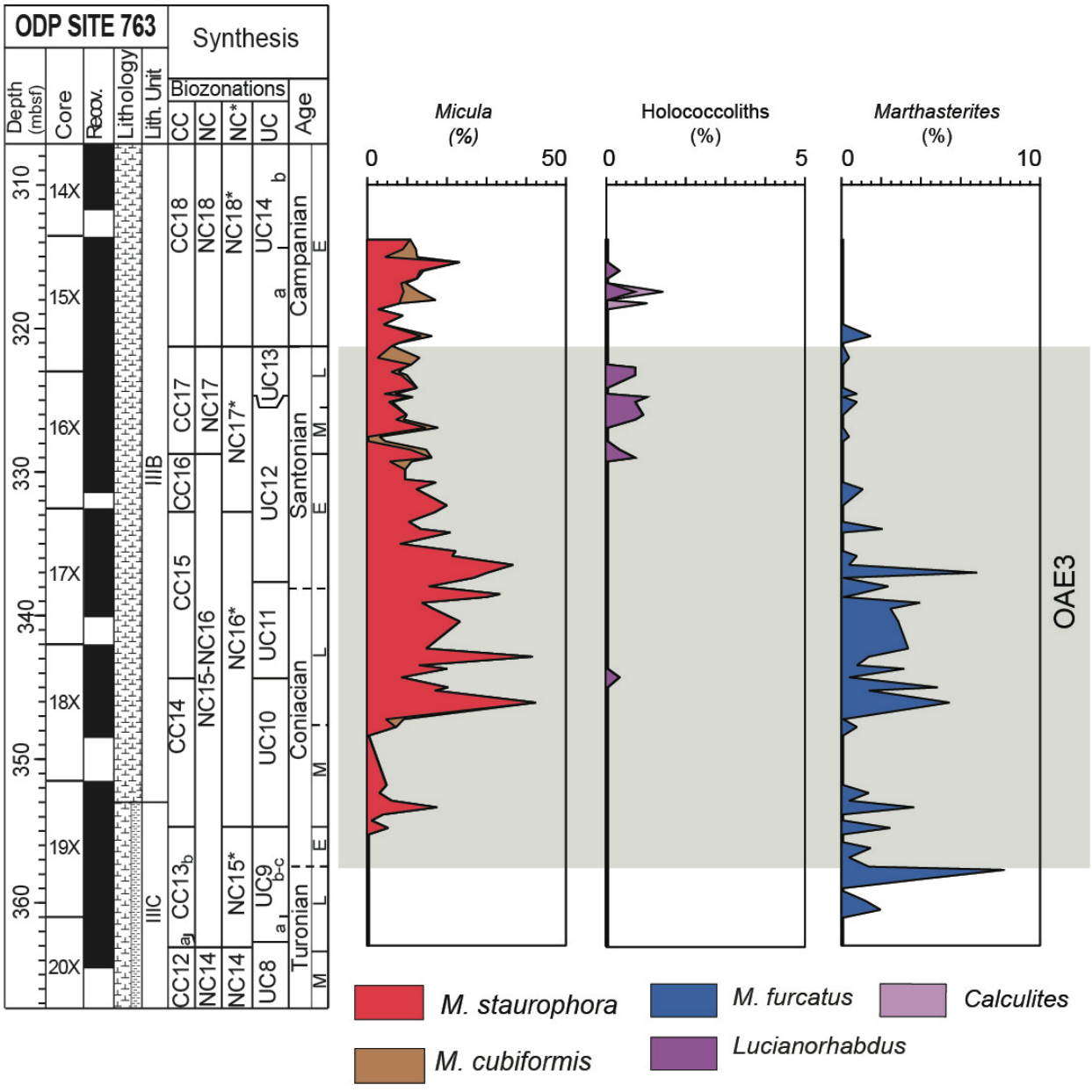

Figure 5.6.2.3 -Relative abundance of *Micula*, holococcoliths and *Marthasterites* at ODP Site 763.

Chapter 6
Discussion

6.1 Changes of surface-water fertility during the Coniacian-Santonian OAE3

Figure 6.1.1 synthetizes the variations in the NI quantified for each studied site/section calibrated against the chronostratigraphy based on calcareous nannofossil biozonation (see Chapter 2) and the C stable isotope curve of Jarvis et al. (2006) within the framework of the timescale by Gradstein et al. (2012). The calcareous nannofossil NIs are plotted using the same scale, with lowest values indicating low fertility of surface waters and highest values corresponding to relatively high trophic conditions. It is worth mentioning that calcareous nannoplankton (coccolithophore algae) have oligotrophic affinity with a few taxa supporting or taking advantage of meso-eutrophic conditions. Instead, when really eutrophic levels prevail, diatoms become dominant and coccolithophores are outnumbered. Thus, the NI can only trace fluctuations between oligotrophic to meso(-eu) trophic conditions, but not the highest fertility of surface waters (see discussion in Erba, 2004).

The comparison of data obtained at individual sites shows significant disparities, with differences both in terms of magnitude and time distribution of nutrients during OAE3. Moreover, the fertility-related taxa that concur in the estimate of the NI, show variable abundance at individual sites.

At Seaford Head low values of NI are reconstructed from the base of the OAE3 interval up to the lower-middle Santonian, and a moderate increase occurs in the upper Santonian-lower Campanian (NI up to 37). This NI variations are mainly related to changes in the relative abundance of *B. constans* and *D. ignotus* while *Z. erectus* remains quite rare through the studied interval. Therefore, at Seaford Head oligotrophy prevailed across OAE3 with a relative increase to mesotrophic conditions in the late part of this event and the immediately following interval.

The highest NI values reconstructed in this study are reached in the equatorial central Atlantic ODP Sites 1261 (values between 40 and 70) in the upper Turonian-Coniacian interval. Here, the NI is mainly controlled by the variation in abundance of *B. constans* and *Z. erectus*, whereas *D. ignotus* is rare. This suggests the permanence of meso-eutrophic conditions of surface waters.

At ODP Site 959 in the northern South Atlantic, the NI shows low-medium values (around 25), with two increases to relatively high values in the upper Coniacian and close to the Coniacian/Turonian boundary. As for ODP Site 1261, *B. constans* and *Z. erectus* are the most abundant fertility-related species whereas *D. ignotus* is rare. Overall the trophic level was intermediate though the studied interval.

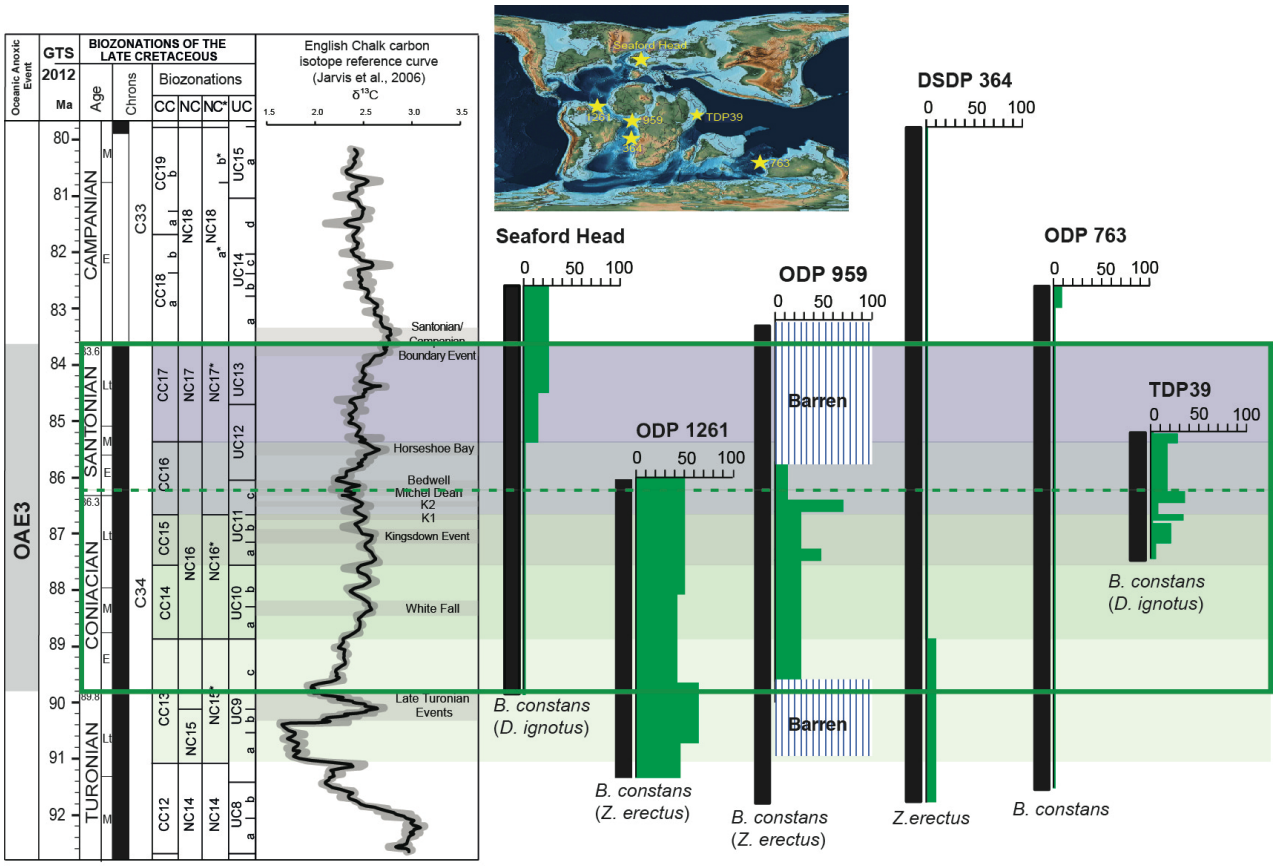

Figure 6.1.1 - Changes in the nutrient index across OAE3 in the studied sections. Calcareous nannofossil biozonation of Sissingh (1977) CC, Roth (1978) NC, Bralower et al. (1995) NC* and Burnett (1998) UC. The C stable isotope curve is after Jarvis et al. (2006) and the numerical ages are based on the timescale of Gradstein et al. (2012).

At ODP Site 364 in the South Atlantic the NI is low (values around 15) in the interval preceding OAE3 and its lowermost part (Figure 6.1.1) and then close to zero through OAE3 and in the following interval. Thus, at this location oligotrophic conditions prevailed during the OAE3 as documented by rare fertility-related taxa, although *Z. erectus* is more abundant than *B. constants* and *D. ignotus*.

The NI obtained for ODP Site 763 shows extremely low values (close to zero) due to rare *B. constans* and the absence of *D. ignotus* and *Z. erectus*. Therefore, this location was characterized by oligotrophic conditions before, during and after OAE3.

At TDP39 the NI shows fluctuations around intermediate values (5-30) in the upper Coniacian – middle Santonian interval suggesting oligotrophic to mesotrophic conditions. At TDP 39 *B. constans* and *D. ignotus* are common, whereas *Z. erectus* remains rare.

The variations of the NI obtained here document the absence of common patterns. Conversely, each site is characterized by specific values and changes that indicate local rather than regional-global patterns in fertility across OAE3. The higher NI values observed at the equatorial Atlantic Site 1261 and northern

South Atlantic ODP Site 959 can be explained by the prolonged upwelling conditions in these areas. The abundance of the fertility-related taxa *B. costans* and *Z. erectus* at these sites further suggest high nutrient conditions typical of upwelling zones at both locations (Roth and Krumbach, 1986)

At Demerara Rise the strength of the upwelling system was controlled by shifts in the position of the ITCZ due to changes in the insolation (Hofmann and Wagner, 2011). Whereas the nutrient availability in the west Africa region was also linked to chemical weathering and freshwater runoff from the African continent during periods of maximum insolation (Beckmann et al., 2005a, b). The climatic fluctuations modulated by precession and eccentricity drove the deposition of black shales both in the Deep Ivorian Basin (ODP Site 959) and at Demerara Rise (ODP Site 1261).

DSDP Site 364, located along the western African margin south of ODP Site 959, evidently was characterized by oligotrophic conditions, although sedimentation is dominated by black shale deposition. Here, possibly the absence of nutrient recycling associated to runoff/river discharge was not active because of the tropical paleolocation outside an upwelling system.

The literature was inspected relative to nannofossil assemblages in sections/sites covering the OAE3 interval to reconstruct paleofertility conditions and changes in a variety of settings of both hemispheres. Quantitative and semiquantitative data are available from the Tethys and surrounding area (Razmjooei et al., 2020; Al Rawahi and Dunkley Jones, 2019), the Basque Cantabrian area (Melinte and Lamolda, 2002), the Atlantic Ocean (Guerra et al., 2012; Linnert et al., 2011), the Western Interior Seaway (De Gama et al., 2014; Blair and Watkins, 2009), the Indian Ocean (Watkins and Guerra, 2020) (Figure 6.1.2 and 6.1.3)

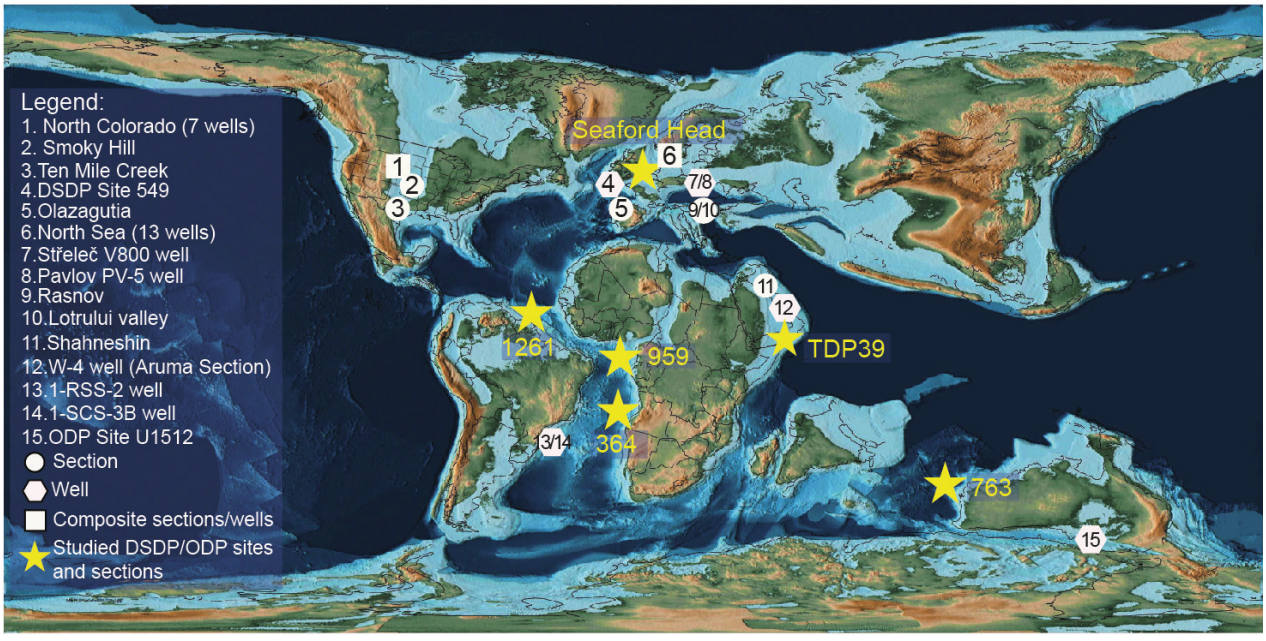

Figure 6.1.2 - Location of sections/sites covering the OAE3 interval both from this study and literature. Paleogeographic reconstruction at 90 Ma (PALEOMAP PaleoAtlas; Scotese, 2016).

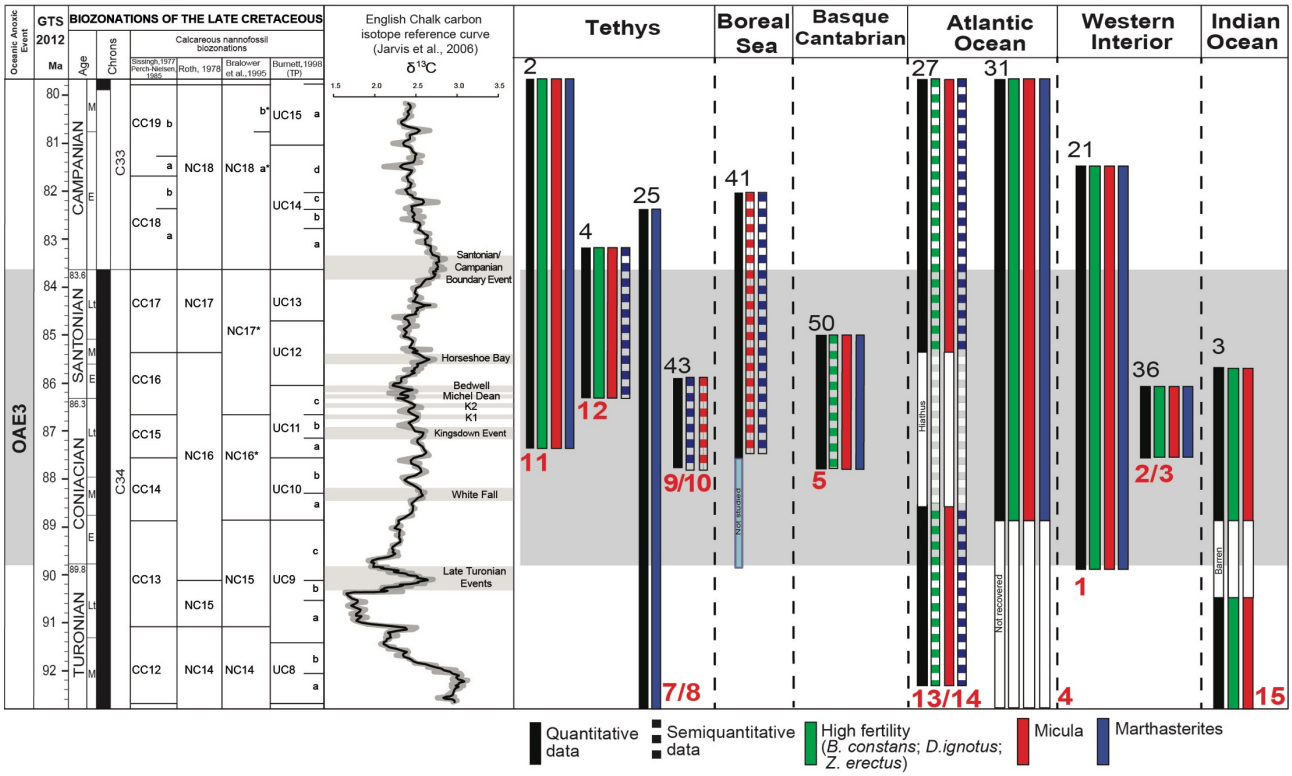

Figure 6.1.3 - Stratigraphic distribution of sections with calcareous nannofossil quantitative (solid line) and semiquantitative (dashed line) data across OAE3 from literature. In green fertility taxa (*B. constans, D. ignotus* and *Z. erectus*), in red *Micula* and in blu *Marthasterites*. Calcareous nannofossil biozonations after Sissingh (1977) CC, Roth (1978) NC, Bralower et al. (1995) NC* and Burnett (1998) UC. The C stable isotope curve is after Jarvis et al. (2006) and the numerical ages are based on the timescale of Gradstein et al. (2012). Black numbers refer to papers reported in Appendix 4, red numbers refer to Figure 6.1.2.

In the Shahneshin section (Zagros Basin), Razmjooei et al. (2020) document rare *B. constans* and *Z. erectus* while *D. ignotus* is absent in the late Coniacian to Maastrichtian interval. Thus, fertility was suppressed across OAE3 and in the following interval.

Melinte and Lamolda (2002) studied nannofossil assemblages of the upper Coniacian-lower Santonian interval of the Olazagutia section in the Basque Cantabrian basin, reporting rare *B. constans, D. ignotus* and *Z. erectus* as a result of low fertility.

At DSDP Site 549 on the Goban Spur (North Atlantic), *B. constans, D. ignotus* and *Z. erectus* increase in relative abundance from ca. 1% to ca. 5 % in the Coniacian-Santonian (Linnert et al., 2011) implying a minor increase in trophic conditions across OAE3.

Guerra et al. (2012) investigated three wells in the Pelotas Basin facing the South Atlantic Ocean: The studied sections cover the upper Albian-Maastrichtian interval that results devoid of the fertility-related *B. constans, D. ignotus* and *Z. erectus.*

A few sites were characterized in the Western Interior Seaway by De Gama et al. (2014) and Blair and Watkins (2009). The investigation of seven wells in Colorado (De Gama et al., 2014) showed generally rare *Biscutum* and *Zeugrhabdotus* in the Coniacian-lower Campanian interval, with distinctive peaks of *Biscutum* (ca. 20%) and of *Zeugrhabdotus* (ca. 20%) in the middle-upper Santonian (UC12-UC13) corresponding to the upper part of OAE3. Blair and Watkins (2009) studied the Coniacian/Santonian boundary interval in the Ten Mile Creek and Smoky Hill sections documenting quite different fertility conditions at the two localities. In fact, high relative abundances of *Biscutum* (10-15%) and *Discorhabus* (4-8.5%), but rare *Zeugrhabdotus* (0-0.2 %) were observed at Ten Mile Creek, while *Zeugrhabdotus* is relatively abundant (6.5-21 %) at Smoky Hill where *Biscutum* (0-3%) and *Discorhabus* (2.5-6-5%) are less frequent.

Al Rawahi and Dunkley Jones (2019) investigated the Aruma section in Oman and reported relatively high abundances for *B. constans* (10-20%) and *D. ignotus* (10-30%) in the Coniacian-Maastrichtian interval, with maximum values in the UC 12-UC 13 Zones /Santonian). At this location, however, Z. erectus shows relative abundance of 3-4%. Thus, a general mesotrophy characterized the area, but meso-eutrophic conditions were not reached.

Watkins and Guerra (2020) report relative abundances of 5-10% and 10-15 % for *Biscutum* and *Zeugrhabdotus*, respectively, in the Turonian interval at IODP Site U1512 in the Great Australian Bight. Both genera decrease to 2% and 5%, respectively, in the Coniacian-Santonian interval suggesting a lowering of fertility during OAE3.

The integration of the results of my investigation with literature data confirms that OAE3 was not characterized by a global fertilization episode and that fertility remained suppressed with the exception of upwelling areas as illustrated in figures 6.1.4 to 6.1.8. As shown by the time-slices corresponding to Zones CC 13 (Figure 6.1.4), CC14 (Figure 6.1.5), CC15 (Figure 6.1.6), CC16 (Figure 6.1.7) and CC17 (Figure 6.1.8), meso-eutrophic conditions characterized only ODP Site 1261 on Demarara Rise in the equatorial upwelling belt of the Central Atlantic Ocean. At ODP Site 959 in the northern South Atlantic Ocean, mesotrophic, but not eutrophic, conditions prevailed across OAE3, with higher fertility during the late Coniacian to early middle Santonian time interval.

During the late Coniacian meso-eutrophy was reached also in the southern part of the Western Interior Seaway and on the eastern African margin at tropical latitudes (Figure 6.1.5). As far as the Western Interior Seaway is concerned, meso-eutrophic conditions characterized the north Colorado area in the middle-late Santonian corresponding to the final part of OAE3 (Figure 6.1.8).

The Tethyan area, the Boreal Realm-North Sea, Oman, and the Southern Ocean remained in oligotrophic conditions during the entire OAE3 interval as well as in the preceding and following intervals.

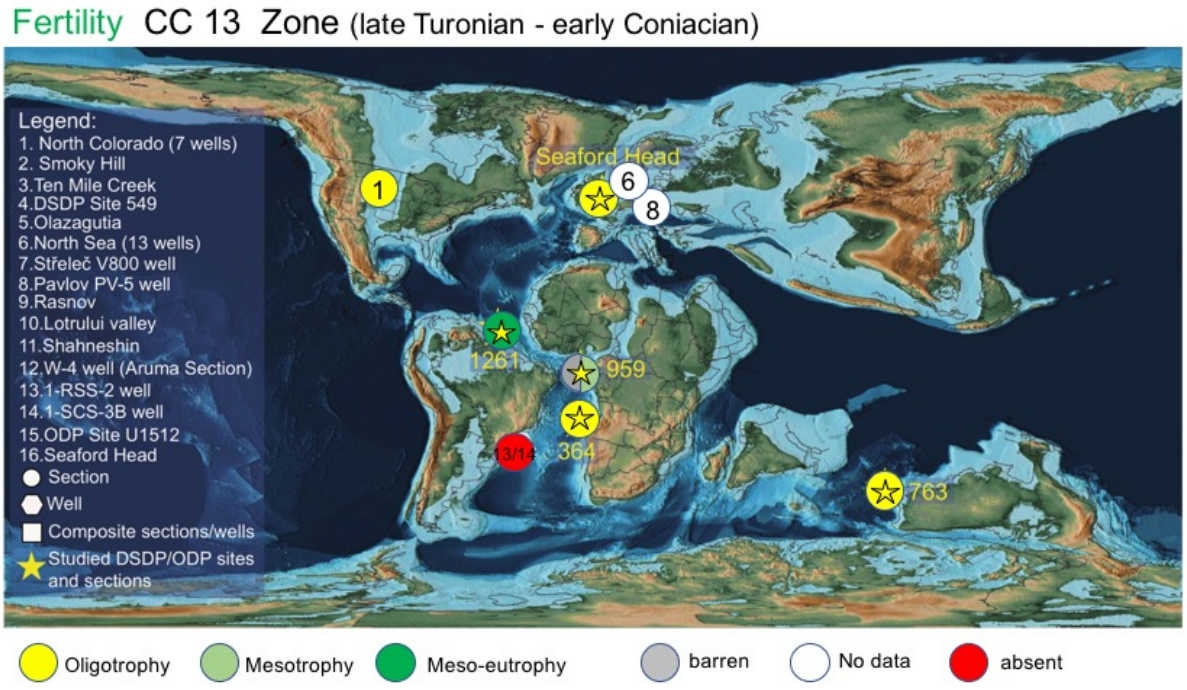

Figure 6.1.4 - Paleogeographic reconstruction showing the distribution of fertility in the CC13 Zone (late Turonian – early Coniacian).

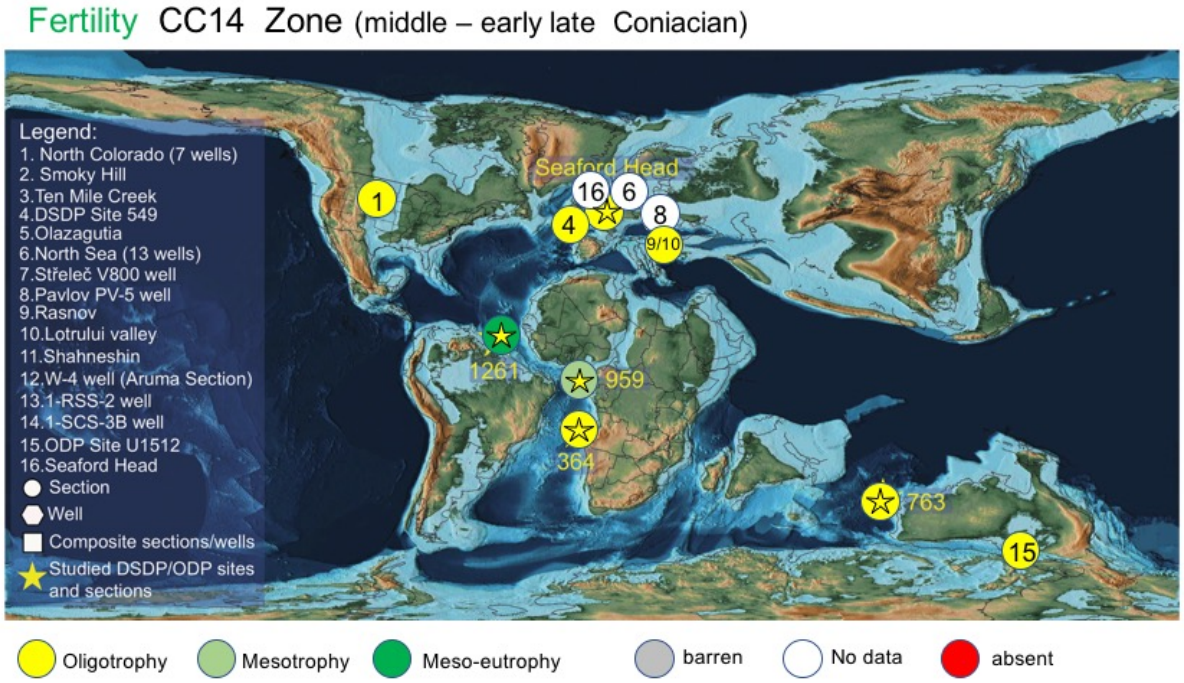

Figure 6.1.5 - Paleogeographic reconstruction showing the distribution of fertility in the CC14 Zone (middle –early late Coniacian).

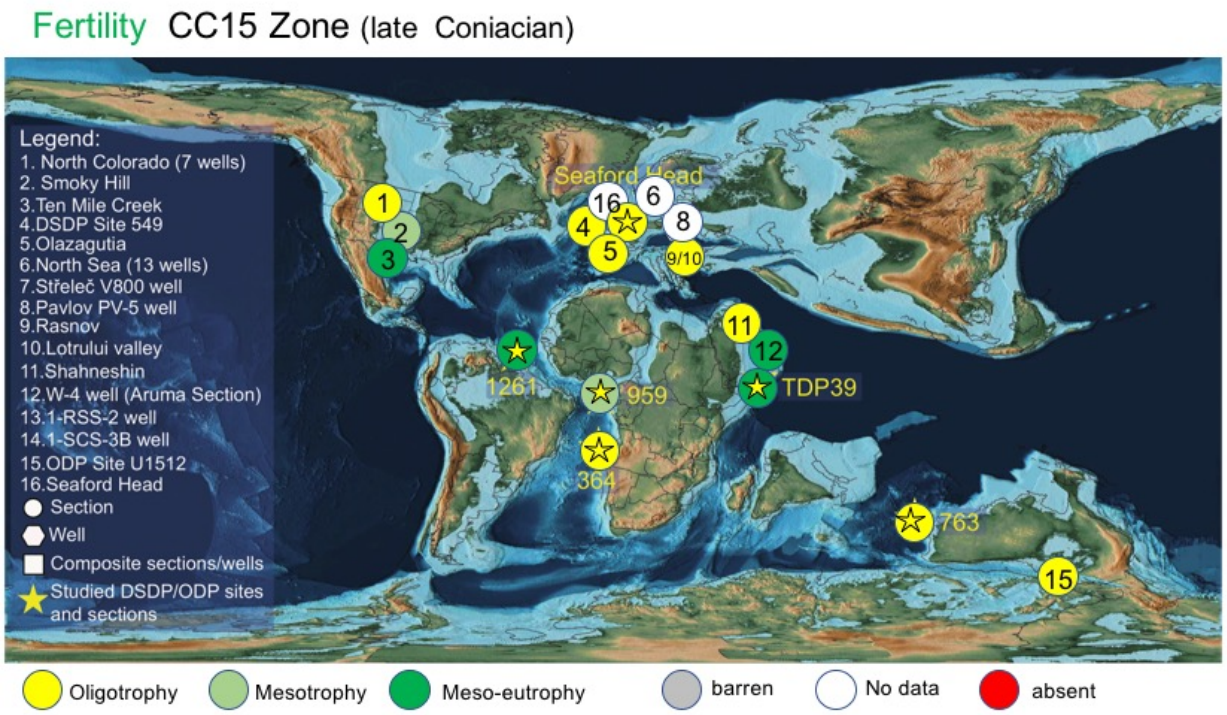

Figure 6.1.6 - Paleogeographic reconstruction showing the distribution of fertility in the CC15 Zone (late Coniacian).

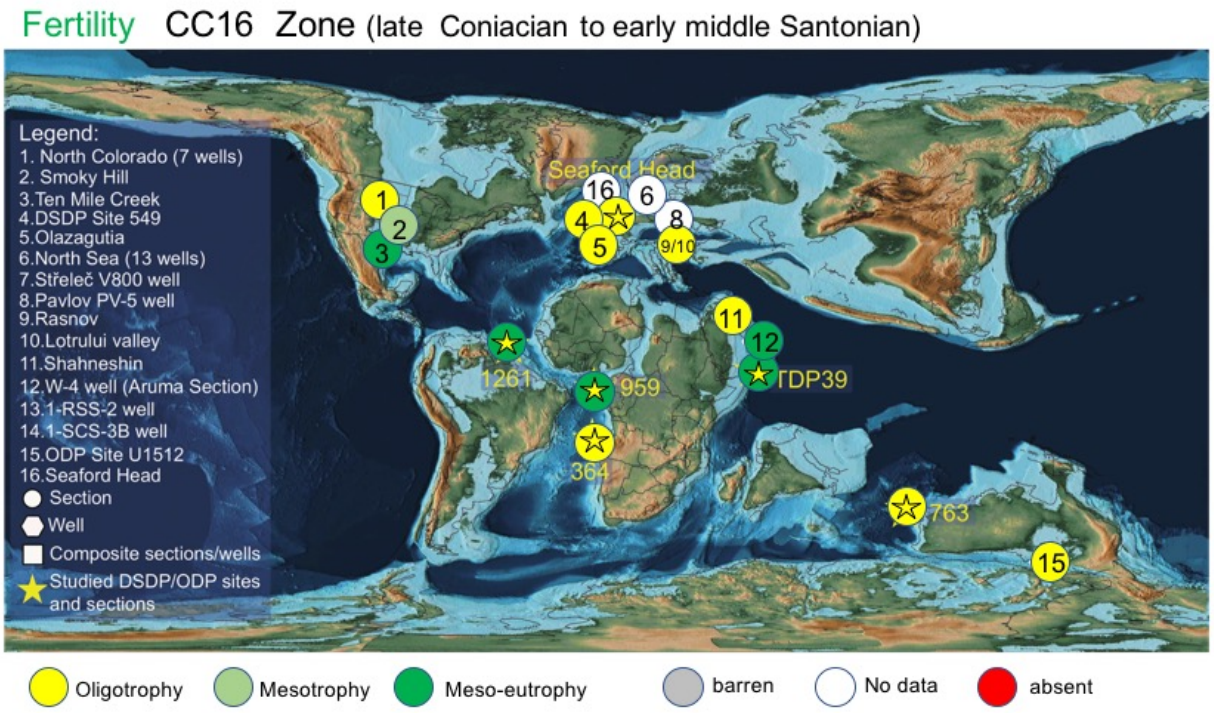

Figure 6.1.7 - Paleogeographic reconstruction showing the distribution of fertility in the CC16 Zone (late Coniacian to early middle Santonian).

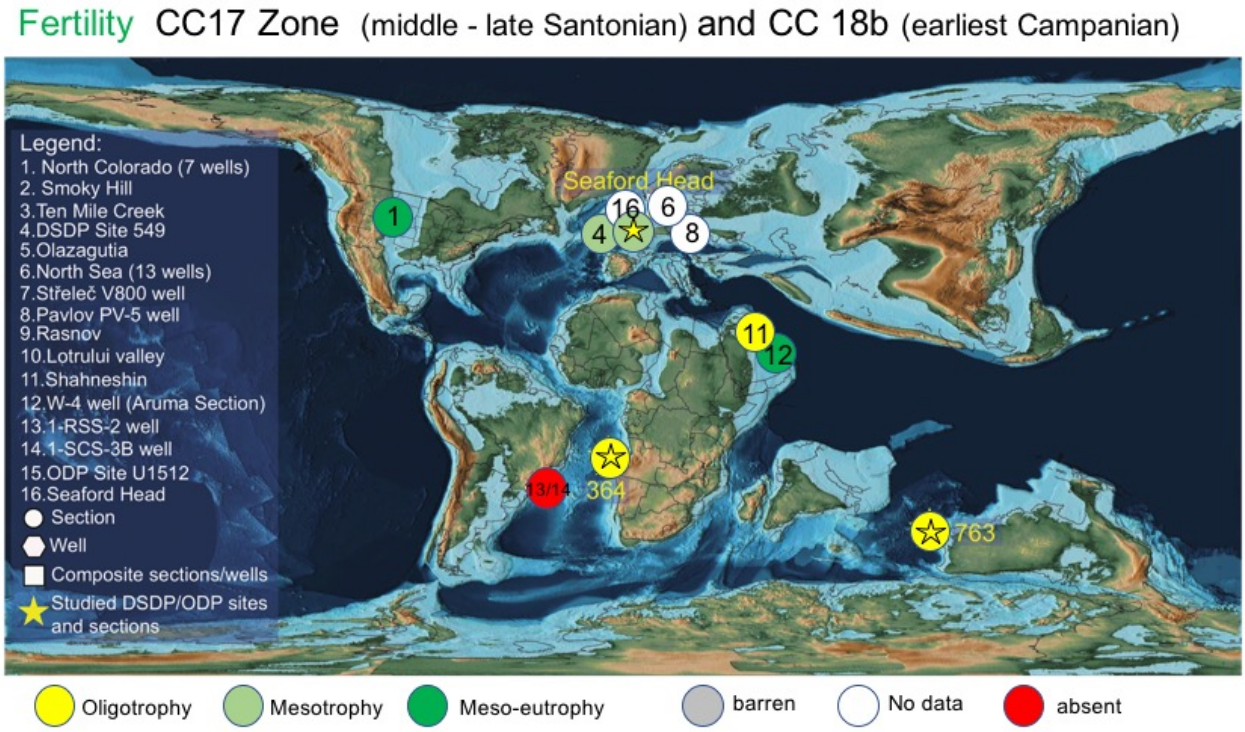

Figure 6.1.8 - Paleogeographic reconstruction showing the distribution of fertility in the CC17 Zone (middle – late Santonian) and CC18 (earliest Campanian).

6.2 Abundance changes of genera *Micula* and *Marthasterites* across the Coniacian-Santonian OAE3.

The quantitative analyses conducted in this study point out a significant change in the calcareous nannofossil assemblages across OAE3. In particular, relatively large fluctuations of genera *Micula* and *Marthasterites* were detected in the Coniacian-Santonian interval as illustrated in Figure 6.2.1. Each studied site/section is calibrated using a chronostratigraphy based on calcareous nannofossil biozonation (see Chapter 2) and the C stable isotope curve of Jarvis et al. (2006) within the framework of the timescale by Gradstein et al. (2012).

The changes in abundance of genera *Micula* and *Marthasterites* show several peaks during the OAE3 that are correlatable between the different areas. Two distinct abundance peaks of *Marthasterites* were detected in the early middle phases of OAE3, although with different values at the various investigated sites. The first peak occurs at the Turonian/Coniacian boundary (CC13; UC9c) at ODP Site 1261 (16%), DSDP Site 364 (60%), and Site ODP 763 (8%) (Figure 6.2.1). Only two investigated sections don't show this increment: the Turonian/Coniacian boundary interval at ODP Site 959 is barren of calcareous

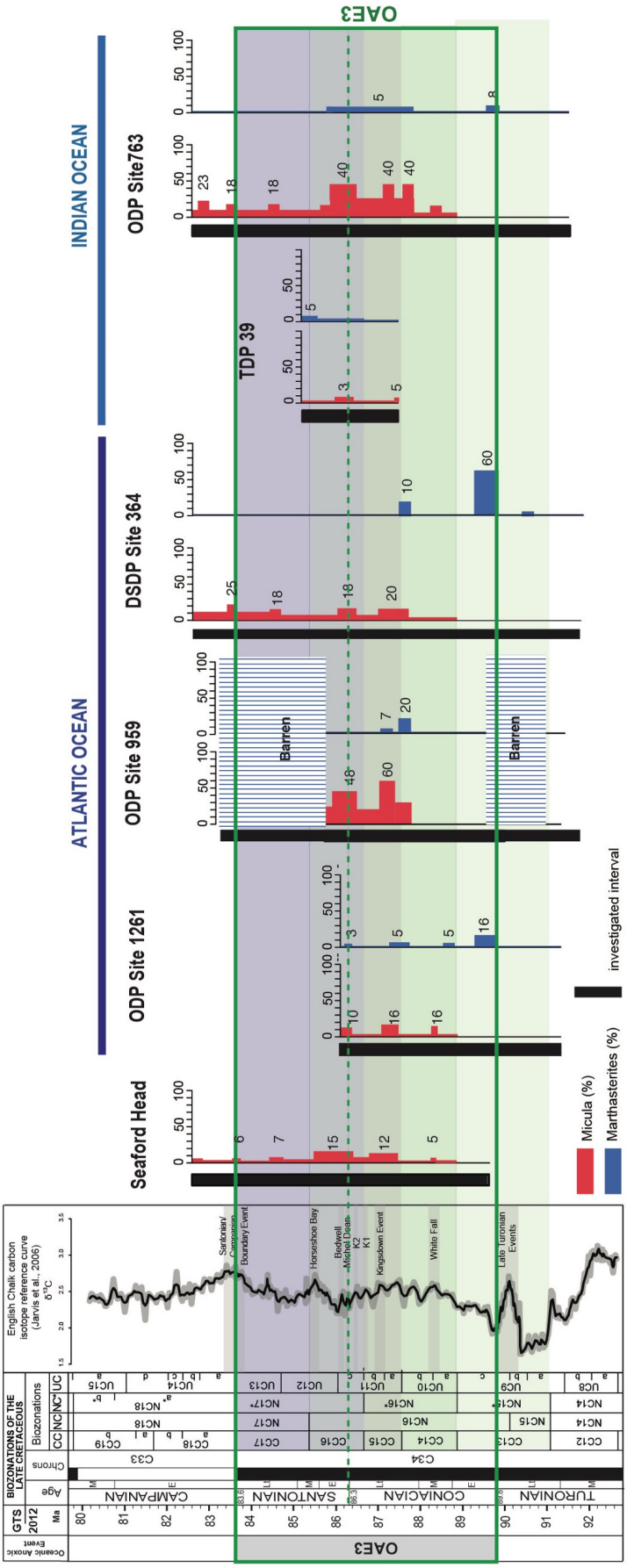

Figure 6.2.1: Changes in percentage of genera *Micula* and *Marthasterites* across OAE3 in the studied sections. Calcareous nannofossil biozonats after Sissingh (1977) CC, Roth (1978) NC, Bralower et al. (1995) NC* and Burnett (1998) UC , C stable isotope curve is after Jarvis et al. (2006) and the numerical ages are based on the timescale of Gradstein et al. (2012).

nannofossils while *Marthasterites* doesn't occur at Seaford Head, as previously reported also by Hampton et al. (2007).

A second abundance increase in relative abundance of *Marthasterites* was observed in the CC14/CC15 zonal boundary interval (early late Coniacian) with values lower than the first abundance peak at all sites: 5% at ODP Site 1261, 20% at ODP Site 959, 10% at DSDP Site 364. At ODP Site 763 a longer interval of increased relative abundance of *Marthasterites* (5%) spans the upper CC14-CC15-CC16 zones without a distinctive peak.

Literature data in general confirm the occurrence of two *Marthesterites* abundance peaks during OAE3. Exceptions are: the Ten Mile Creek and Smoky Hill section with rare *Marthesterites* (Blair and Watkins, 2009), DSDP Sites 549 with extremely rare *M. simplex* (31-Linnert et al., 2011), the Olazagutia section (Melinte and Lamolda, 2002) and the Shahneshin section (Zagros Basin) where this genus is very rare and discontinuous (Razmjooei et al., 2020), the Aruma Section in Oman yielding extremely rare *M. furcatus* (Al Rawahi and Dunkley Jones, 2019), the Pelotas Basin with absent to sparse *M. furcatus* (Guerra et al., 2012). At ODP Site U1512,Watkins and Guerra (3-2020) describe a barren interval within the CC13 Zone that might correspond to the Turonian/Coniacian Boundary and the "*Marthasterites* abundance peak 1".

Figures 6.2.2 and 6.2.3 illustrate the occurrence of the "*Marthasterites* abundance peak 1" and "abundance peak 2" in a paleogeographic context.

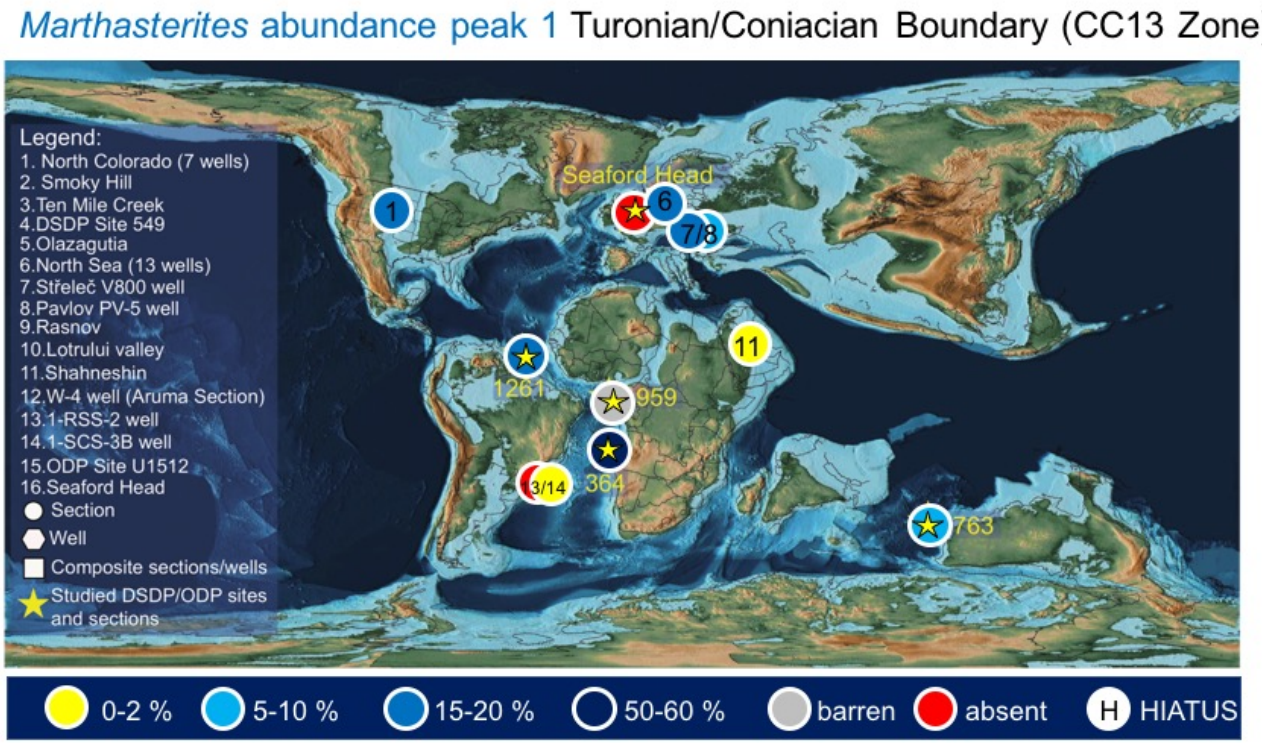

Figure 6.2.2 - Paleogeographic reconstruction showing the distribution of *M. furcatus* during the "*Marthasterites* abundance peak 1" in the CC13 Zone (Turonian/Coniacian Boundary).

The peak in relative abundance at the onset of OAE3 (Turonian/Coniacian boundary) was recorded in most investigated basins suggesting widespread peculiar paleoceanographic conditions.

The "*Marthasterites* abundance peak 2" across the CC14/CC15 zonal boundary (late Coniacian) is everywhere less prominent. In the Rasnov and Lotrului Valley sections, *M. furcatus* is common in this time interval, but the "*Marthesterites* abundance peak 1" interval was not investigated (Melinte and Lamolda, 2007).

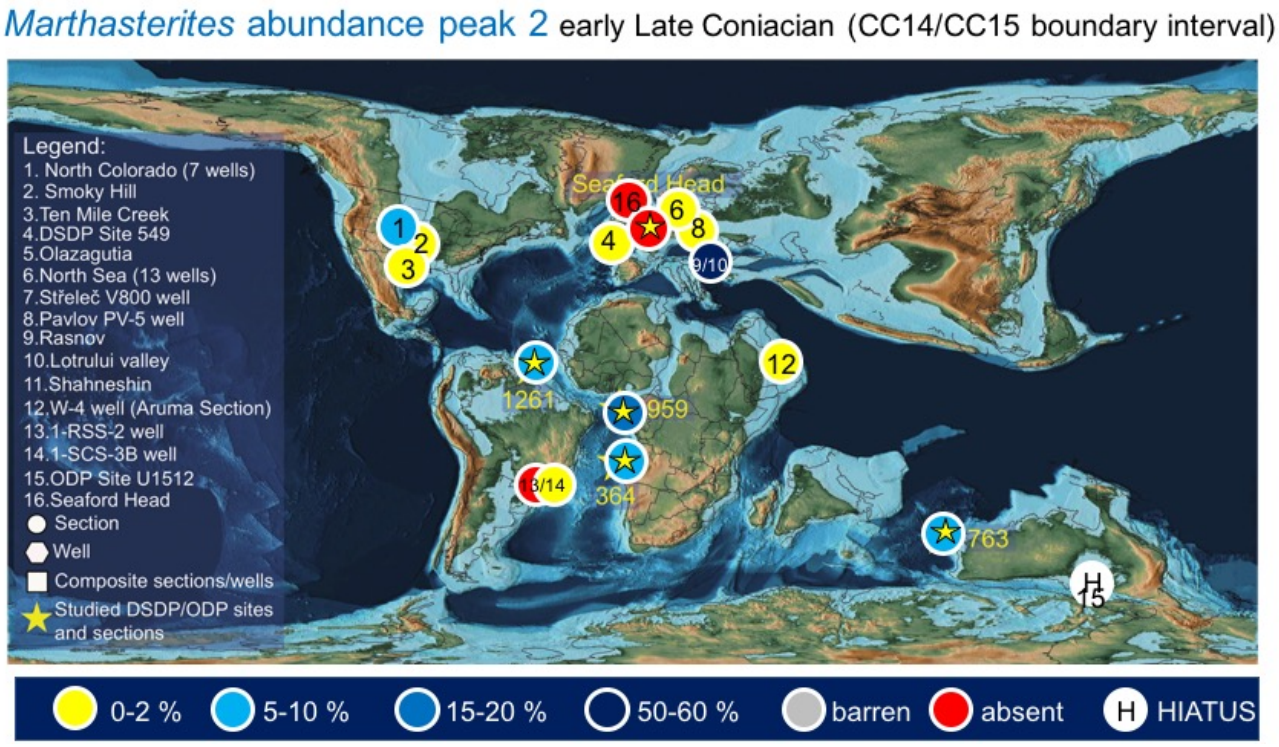

Figure 6.2.3 - Paleogeographic reconstruction showing the distribution of *M. furcatus* during the "*Marthasterites* abundance peak 2" in the CC14/CC15 Zone (early Late Coniacian).

As far as the genus *Micula* is concerned, five distinct peaks in abundance of *M. staurophora* were observed in the OAE3 interval of the sites/sections studied here (Figure 6.2.1); these are reproducible at all studied sites although with differences in the magnitude of increment. The first abundance peak occurs in the middle Coniacian (CC14 zone) at Seaford Head (5%), ODP Site 1261 (16%) and ODP Site 763 (17%). The CC15 zone (late Coniacian) is marked by a second abundance peak in *Micula* that was observed in all the sites/sections studied, again with variable values as follows: 12% at Seaford Head, 16% at ODP Site 1261, 60% at ODP Site 95, 20% at DSDP Site 364, 5% at TDP39 and 40% at ODP Site 763. This "abundance peak 2" corresponds to the maximum increase in *Micula* abundance detected in this study. The third abundance peak is characterized by another significant increase in *Micula* that occurs in the lower CC16 Zone across the Coniacian/Santonian boundary. As the previous "abundance

peak 2", it was observed at all studied sites/sections: Seaford Head (15%), ODP Site 1261 (10%), ODP Site 959 (48%), DSDP Site 364 (18%), TDP39 (3%) and ODP Site 763 (40%).

A fourth abundance peak in *Micula* was detected in the middle part of the CC17 Zone (late Santonian) at Seaford Head (7%), DSDP Site 364 (18%) and ODP Site 763 (40%). At ODP Site 959 the stratigraphic interval equivalent to the CC17 zone is barren of calcareous nannofossils.

The youngest peak ("abundance peak 5") corresponds to the CC17/CC18 zonal boundary (Santonian/Campanian boundary) and was observed at Seaford Head (6%), DSDP Site 364 (25%) and ODP Site 763 (18%).

The changes in abundance of genera *Micula* - essentially *M. staurophora* - are synchronous at the different sites and evidence repetitive short increases within OAE3, suggesting paleoenvironmental changes at global scale. Indeed, literature inspection (Figure 6.1.2) revealed that the same "abundance peaks" of *Micula* occurred synchronously in different basins and paleoceanography settings (Figures 6.2.4-6.2.5-6.2.6-6.2.7 and 6.2.8).

The only exception is the Pelotas Basin where *M. staurophora* is rare and discontinuous through the Coniacian-Santonian interval (Guerra et al., 2012). Also, in the Western Interior Seaway *Micula* is never common, but minor increases were reported for the "abundance peak 3" interval (Blair and Watkins, 2009). As previously observed, the highest relative abundances characterized the *Micula* "abundance peak 2" and "abundance peak 3" of late Coniacian and early Santonian age, respectively, at global scale (Figures 6.2.5 and 6.2.6). Thus, the middle part of OAE3 was marked by peculiar oceanographic conditions triggering anomalous abundances of *Micula* nannoliths for almost 2 millions years delimitated by discrete peaks (*Micula* "abundance peak 2" and "abundance peak 3"). It is worth noticing that this prolonged *Micula* climax started immediately after the *Marthasterites* "abundance peak 2", perhaps suggesting even more stressing environmental conditions in the core of OAE3.

Although the *Micula* "abundance peak 5" is of limited amplitude, this increase in relative abundance is recorded at very widespread (virtually global) scale (Figure 6.2.8) at the Santonian/Campanian boundary, somehow closing OAE3.

Despite the wide distribution of *M. staurophora* (*Micula decussata* of some authors) in Upper Cretaceous assemblages, its paleoecological affinity is not understood yet. Hill (1975) and Thierstein (1980, 1981) considered *M. staurophora* a highly solution-resistant species generally used to test the preservation degree of the nannofossil assemblage. Thus, the documented "abundance peaks" of *M. staurophora* were sometimes interpreted as dissolution artefact resulting from elimination of delicate and dissolution-prone forms (Eshet and Almogi-Labin, 1996).

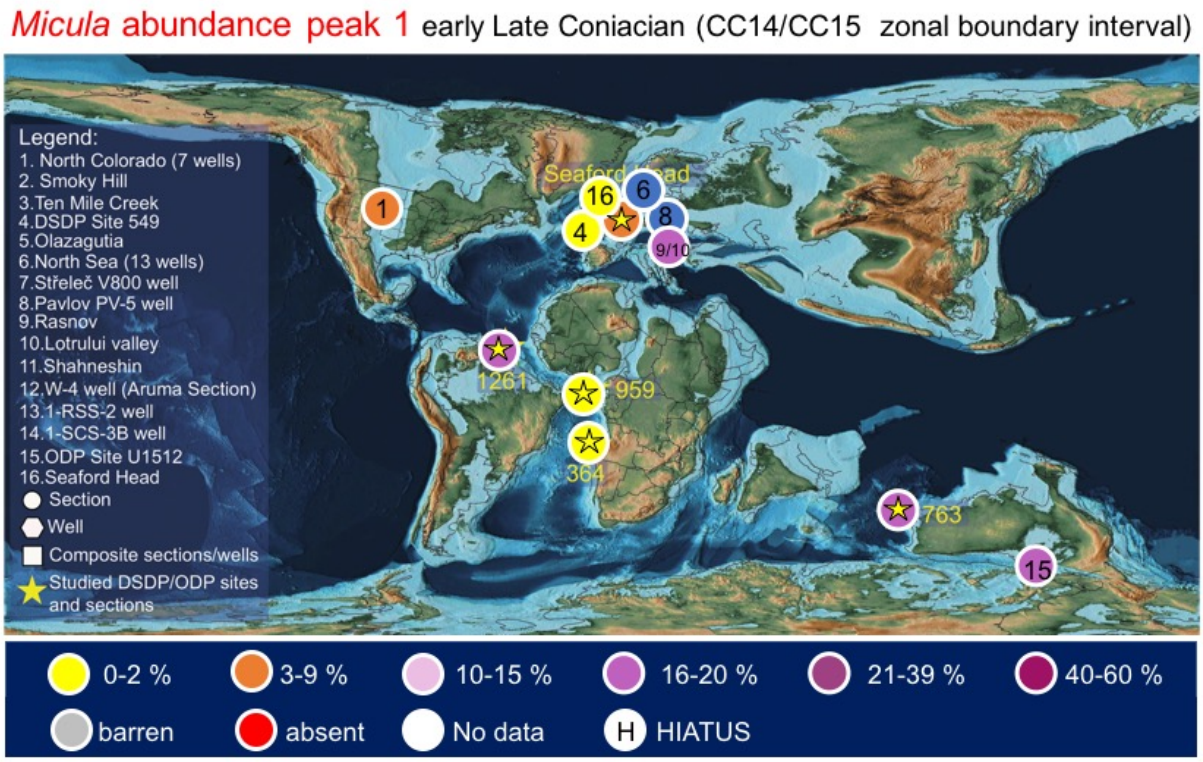

Figure 6.2.4 - Paleogeographic reconstruction showing the distribution of *M. staurophora* abundances during the "*Micula* abundance peak 1" in the CC14/CC15 Zone (early late Coniacian).

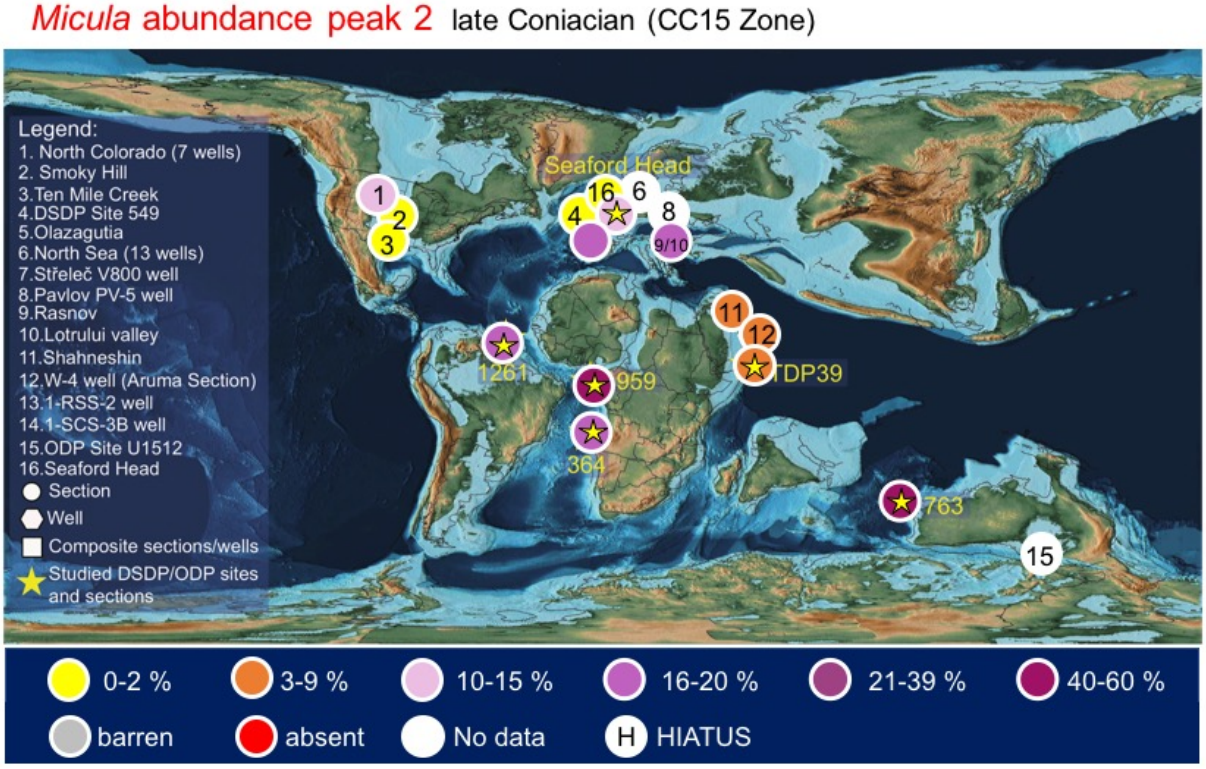

Figure 6.2.5 - Paleogeographic reconstruction showing the distribution of *M. staurophora* abundances during the "*Micula* abundance peak 2" in the CC14/CC15 Zone (early late Coniacian).

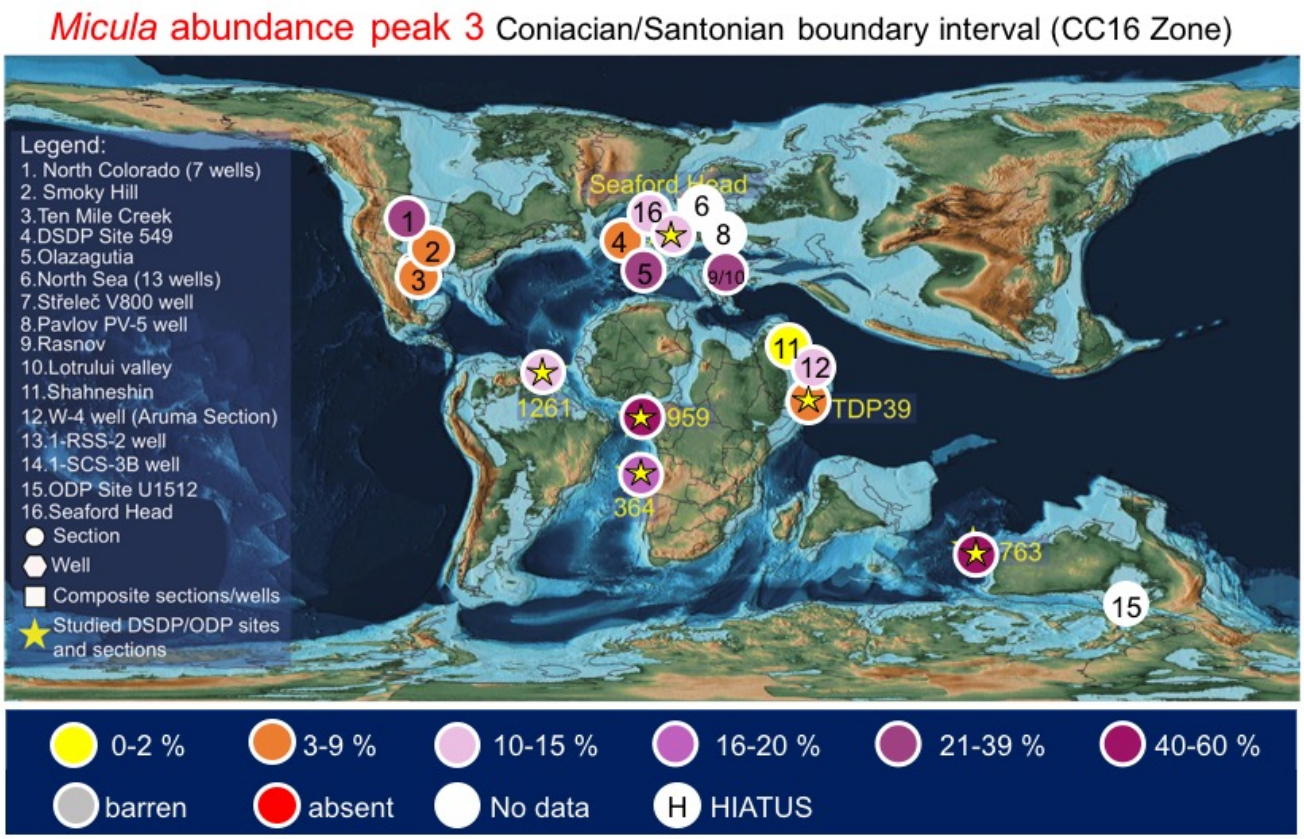

Figure 6.2.6 - Paleogeographic reconstruction showing the distribution of *M. staurophora* abundances during the "*Micula* abundance peak 3" in the CC16 Zone (Coniacian/Santonian boundary).

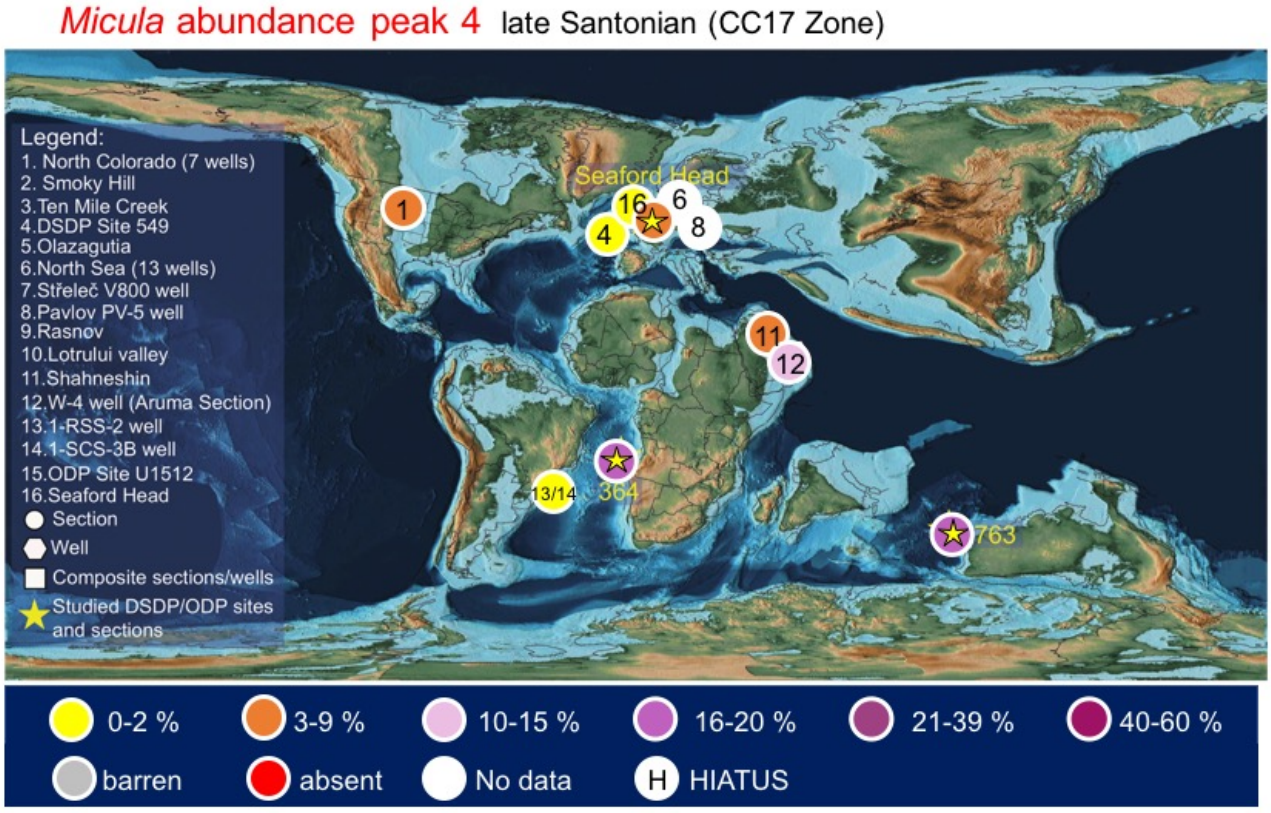

Figure 6.2.7 - Paleogeographic reconstruction showing the distribution of *M. staurophora* abundances during the "*Micula* abundance peak 4" in the CC17 Zone (late Santonian).

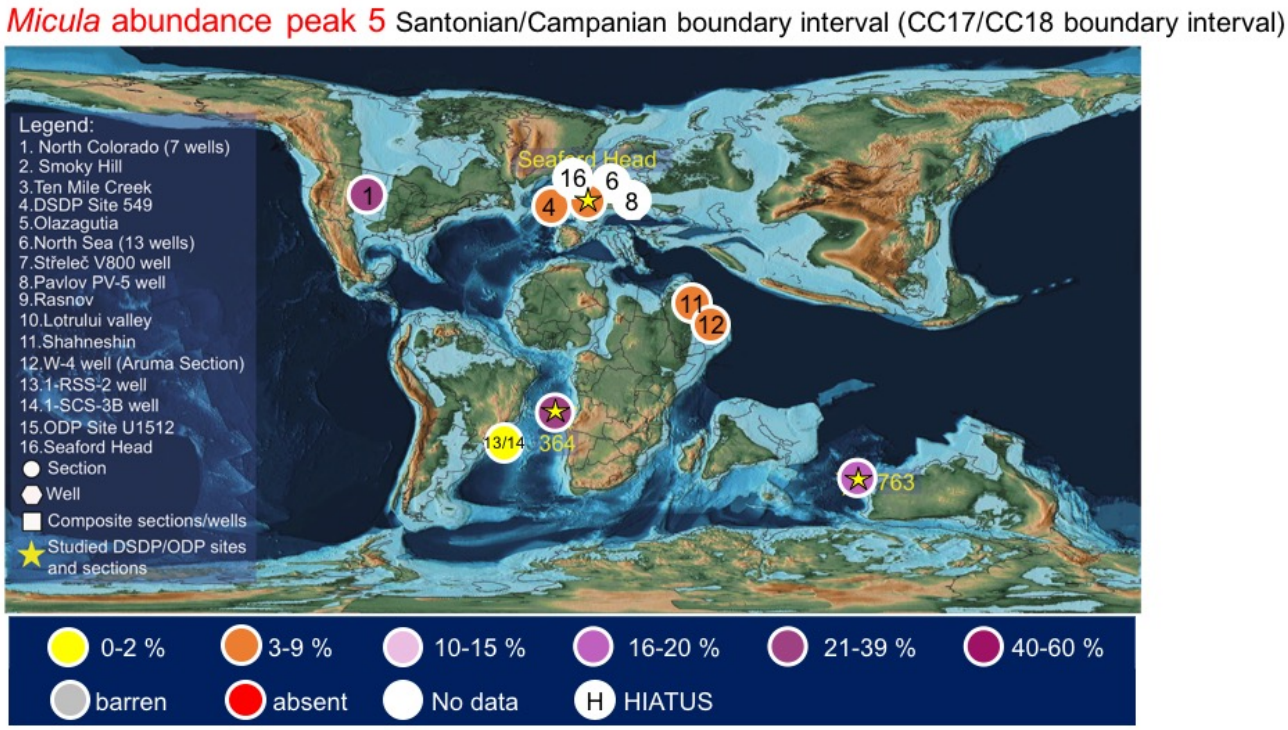

Figure 6.2.8 - Paleogeographic reconstruction showing the distribution of *M. staurophora* abundances during the "*Micula* abundance peak 5" in the CC17 Zone (Santonian/Campanian boundary).

High abundances of *M. staurophora* named "*M. staurophora* blooms" (Tantaway, 2003; Tantaway et al., 2009), were recognized in numerous localities during Late Maastrichtian in the Atlantic Ocean (Thierstein, 1981; Watkins and Self-Trail, 2005; Thibault and Gardin, 2006;Mandur and El Ashwah, 2015), North Sea (Sheldon et al., 2010) and Tethys Ocean (Eshet et al., 1992; Eshet and Almogi-Labin, 1996; Gardin and Monechi, 1998; Gardin, 2002; Tantawy, 2003; Thibault et al.,2016), both from shallow- to deep-water environments. However, in the literature different paleoecological affinities are reported for *M. staurophora*. Henriksson and Malmgren (1997) and Lees (2002) considered *M. staurophora* a cosmopolitan taxon, that occurs abundantly at tropical latitudes. A warm-water affinity was proposed by Thibault and Gardin (2006) and Sheldon (2010). Conversely, some authors consider *M. staurophora* a cooler water taxon (Thierstein, 1976; Wind 1979; Doevon, 1983; Watkins and Self-Trail, 2005; Mandur and El Ashwah, 2015). According to Watkins and Self-Trail (2005) *M. staurophora* exhibits high abundances at high latitudes with a preference for nearshore localities. High abundances of *M. staurophora* was also associated with low-nutrient and highly-stressed environmental conditions (Eshet et al., 1992; Tantaway, 2003 and Thibault and Gardin, 2006). Hewaidy et al. (2019) suggested different fertility relationships for individual *Micula* species in the Campanian-Maastrichtian interval of Egypt. Specifically, while *M. concava* is considered a k-strategists, all other species including *M. staurophora* were used as r-strategists.

In conclusion, the paleoecological affinity of *Micula* and specifically *M. staurophora* has not been uniquely resolved, since abundance peaks have been registered at coastal or more open ocean locations, in warm or cool waters and under oligotrophic to eutrophic conditions. Therefore, the significance of individual "*Micula* abundance peak " and of the climax in the middle part of OAE3 remains unexplained although stressful paleoenvironmental conditions must have controlled calcareous nannoplankton at global scale, perhaps favoring the most resilient taxa.

Different ecological interpretations have been suggested also for the genus *Marthasterites,* whose ecological preferences are still unknown. Increases in abundance of *Marthasterites* were interpreted by Švábenická and Bubík (2014) as the result of both a decrease in surface water temperature and sea-level fluctuations producing more nearshore conditions. Otherwise, Bergen and Sikora (1999) associated the abundance of *Marthasterites* to changes in surface water fertility, although not explaining in which direction (toward lower or higher fertility).

As discussed for the *Micula* abundance peaks , the significance of the *Marthasterites* abundance peaks remains to be explored and understood. However, it is factual to note that the onset of OAE3 coincides with a major increase in abundance (and locally dominance) of *M. furcatus* suggesting the rapid establishment of new and peculiar paleoceanographic conditions at widespread to global scale.

Chapter 7

Conclusions

This PhD thesis presents a study of calcareous nannofossil biostratigraphy and abundance patterns of sections/sites during the late Turonian-early Campanian time interval (Upper Cretaceous) including the OAE3 of Coniacian-Santonian age. The investigation was conducted on DSDP/ODP sites from the equatorial and south Atlantic Ocean: ODP Site 1261 (Demerara Rise), ODP Site 959 (Ivory Coast–Ghana), and DSDP Site 364 (Angola Basin). The study was extended to higher latitudes in the Anglo-Paris Basin (Seaford Head section) and Indian Ocean (Tanzania TDP 39 and ODP Site 763) in order to reconstruct supra-regional changes.
The achieved results and interpretations can be summarized as follows:

- The four standards biozonation schemes available for the Upper Cretaceous (Sissingh,1977; Roth. 1978; Bralower et al., 1995; Burnett, 1998) were successfully applied in this study leading to a robust **biostratigraphic characterization** of the studied successions.
  A total of 15 zonal and 3 subzonal markers were recognized, allowing the identification respectively of the CC11-CC21 Zones of Sissingh (1977), NC13-NC19 Zones of Roth (1978), NC13*-NC19* Zones of Bralower et al. (1995) and UC7-UC15 Zones of Burnett (1998).
  The zonation of Sissingh (1977) and Burnett (1998) have a comparable biostratigraphic resolution for the Coniacian-Santonian interval, whereas a lower resolution is achieved with the Roth (1978) and Bralower et al. (1995) zonations. This is probably due to the integration of many of the Sissingh (1977) and Perch-Nielsen (1985) events in the Burnett (1998) scheme for the Tethyan Province. Three zonal events introduced by the Burnett (1998) Zonation were widely recognized in this study as the FO of *L. septenarius*, LO of *L. septenarius* and the FO of *A. cymbifomis*. Whereas, many of the Burnett's subzonal events were not identified in the studied site/sections apart from the FO *A.p. constrictus*.
  However, only the zonation of Sissingh (1977) as modified by Perch-Nielsen (1985) is proved to be fully applicable for supra-regional correlations of sites and sections situated in different oceanic basins and a variety of depositional settings.

- The **quantitative analyses of calcareous nannofossil assemblages** allowed the reconstruction of the temperature (TI) and nutrient (NI) indices during the late Turonian- early Campanian. In addition to the TI and NI of Bottini et al. (2015) three modification of the TI were applied. No significant changes in the TI were observed in the studied successions, perhaps due to unresolved unambiguous temperature-related nannofossil taxa in the Late Cretaceous. Another explanation might reside on the fact that only minor temperature changes characterized the OAE3 interval at mid-low latitudinal localities. The literature survey confirmed the absence of systematic temperature changes in the late Turonian-early Campanian time interval.

  The NI displays different values in the studied basins, although local rather than global pictures were reconstructed. The data available in the literature also shows trophic levels and their evolution cannot be reproduced even on a regional scale: In particular, OAE3 was not characterized by a global fertilization episode; conversely, fertility remained globally suppressed with the exception of upwelling areas characterized by meso-eutrophic conditions also in the interval preceding and following OAE3.
- The quantitative analyses carried out in this study were used to derive **relative and absolute abundances of nannofossil taxa**. These two different quantifications of calcareous nannofloras are generally in good agreement. The Pearson's correlation confirmed the relationship of *B. constans, D. ignotus* and *Z. erectus* with higher fertility in the Late Cretaceous. Other correlations were extracted, although the paleoecological affinities remain to be explored.

- The quantitative analyses conducted in this study pointed out **significant changes in the calcareous nannofossil assemblages across OAE3.** In fact, relatively large fluctuations of genera *Micula* and *Marthasterites* were detected in the Coniacian-Santonian interval. These abundance increases were labelled "abundance peaks" recognized in all the studied sections/sites as well as at location described in the literature, even if with different value of abundance.

  The ***Micula* (*M. staurophora*) and *Marthasterites (M. furcatus)* "abundance peaks"** have been numbered as synthetized in Figure 7.1. The "*Marthasterites* abundance peak 1" (CC13) marks the onset of OAE3, whereas the "*Marthasterites* abundance peak 2" (CC14/CC15 zones) occurs in the middle of the event. The peak in relative abundance at the onset of OAE3 (Turonian/Coniacian boundary) was recorded in most investigated basins suggesting widespread peculiar paleoceanographic conditions. The "*Marthasterites* abundance peak 2" across the CC14/CC15 zonal boundary (late Coniacian) is everywhere less prominent.

As far as the genus *Micula* is concerned, five distinct peaks in abundance of *M. staurophora* were observed in the OAE3 interval (Figure 7.1) at all the sites/sections studied here and reported in the literature, although with differences in the magnitude of increment.

The *Micula* "abundance peak 1" occurs in the middle Coniacian (CC14 zone) and correlates with the "Withe Fall" isotopic excursion (Figure 7.1.). The "*Micula* abundance peak 2" is late Coniacian in age and matches with the "Kingsdown isotopic event" (Figure 7.1). The "*Micula* abundance peak 3" occurs in the lower CC16 Zone across the Coniacian/Santonian boundary. The "*Micula* abundance peak 2" and "abundance peak 3" are characterized by the highest relative abundances of *M. staurophora* in the middle part of OAE3 at global scale. The "*Micula* abundance peak 4" was detected in the middle part of the CC17 Zone (late Santonian): this level coincides with a positive isotopic excursion between the "Horseshoes Bay" and the "Santonian/Campanian boundary event". The younger abundance peak ("*Micula* abundance peak 5") marks the end of the OAE3 interval close to the CC17/CC18 zone (Santonian/Campanian boundary) and the "Santonian/Campanian boundary event" isotopic excursion Figure 7.1.).

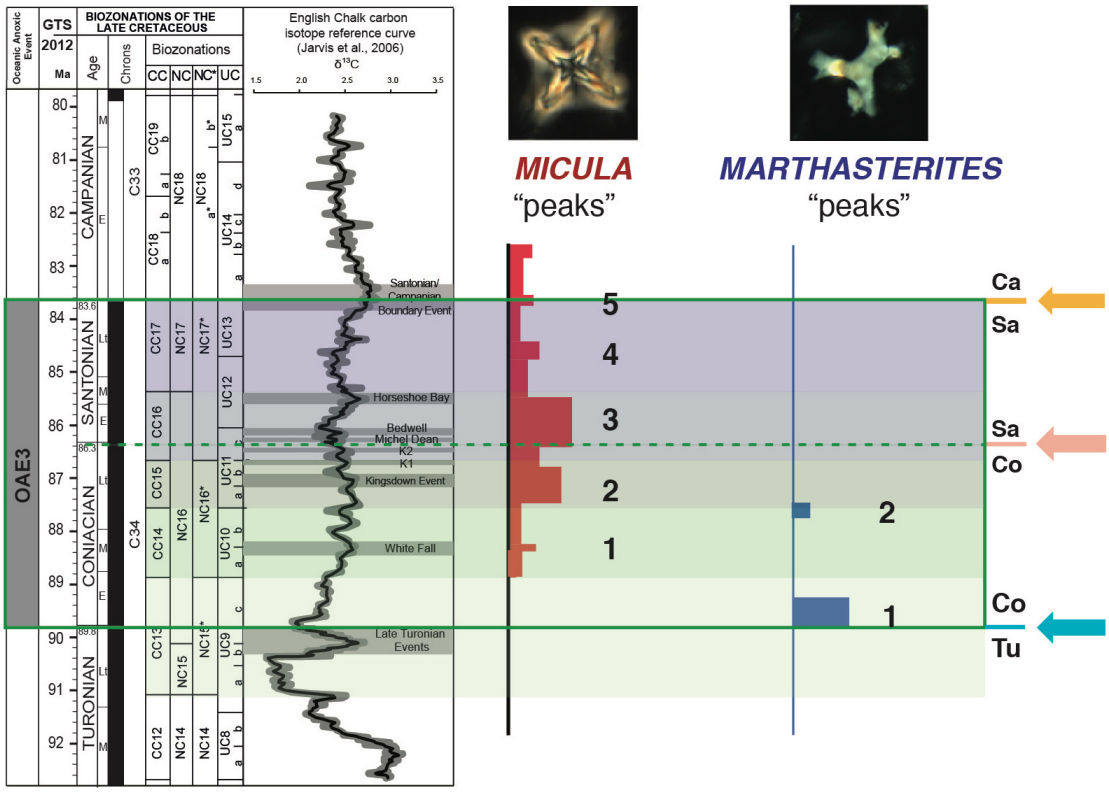

Figure 7.1 - Micula and Marthasterites "abundance peaks" events across the OAE3 interval. Calcareous nannofossil biozonation of Sissingh (1977) CC, Roth (1978) NC, Bralower etal. (1995) NC* and Burnett (1998) UC. The C stable isotope curve is after Jarvis et al.2006) and the numerical ages are based on the timescale of Gradstein et al. (2012).

- **The paleoecological affinity** of *Micula* and specifically *M. staurophora* as well as that of genus *Marthasterites* remains unexplained. Specifically, despite the wide distribution of *M. staurophora* in Upper Cretaceous assemblages, its paleoecological affinity is not understood yet, since "abundance peaks" of this taxon have been recorded at coastal or more open ocean locations, in warm or cool waters and under oligotrophic to eutrophic conditions. Different ecological interpretations have been suggested for the genus *Marthasterites,* whose ecological preferences is still unknown, because increases in abundance of *M. furcatus* were interpreted as possibly linked to nearshore conditions and/or fertility changes.

- The **nannofossil-based paleoceanography of OAE3** derives from profound changes in the assemblages during the Coniacian-Santonian. As far as fertility patterns are concerned, the fertility-related nannofossil taxa and the NI indicate that OAE3 was not characterized by a global fertilization episode and that, conversely, fertility remained suppressed with the exception of upwelling areas. The **onset of OAE3** coincides with a major increase in abundance (and locally dominance) of *M. furcatus* suggesting the rapid establishment of new and peculiar paleoceanographic conditions at widespread to global scale. Individual *Micula* "abundance peaks" and particularly the abundance climax in the **middle part of OAE3** can be related to **stressful paleoenvironmental conditions that must have controlled calcareous nannoplankton at global scale, perhaps favoring the most resilient taxa**.

- **The *Marthasterites* and *Micula* "abundance peaks" can also represent useful events complementing biostratigraphic characterization**, especially as far as the Turonian/Coniacian, Coniacian/Santonian and Santonian/Campanian boundaries are concerned. This particularly relevant for the Turonian/Coniacian and Coniacian/Santonian boundaries, both lacking specific calcareous nannofossil biohorizons.

  The **Turonian/Coniacian boundary** is not ratified yet and the proposed marker is the FO of inoceramid *Cremnoceramus deformis erectus*, which appearance datum is reported between the FO of small *A. parcus expansus* and the FO of *M. staurophora* in the CC13 Zone. The first abundance peak of *M. furcatus* ("*Marthasterites* abundance peak 1") in the CC13 zone seems a global additional event useful to identify the base of the Coniacian. It is worth noticing that the abundance peak in *Marthasterites* observed in the Bohemian basin in the CC13 zone is very close to the FO of *C. deformis erectus* and, thus, to the Turonian/Coniacian boundary (Švábenická and Bubík, 2014).

The **GSSP for the base of the Santonian** was defined at the Olazagutia section (North Spain) and is marked by the FO of inoceramid *Platyceramus undulatoplicatus* (Lamolda et al., 2014), which appearance datum is reported between the FO *L. cayeuxii* and the LO *L. septenarius*. An increase of *Micula* was reported in the Global Stratotype Section and Point (GSSP) section of Olazagutia just below the FO of *P. undulatoplicatus* (Melinte and Lamolda,2002). This increase in abundance of M. staurophora correlates with the "*Micula* abundance peak 3" identified at global scale in this study and, therefore, may represent an additional nannofossil event useful to approximate the base of Santonian.

The Bottaccione section (central Italy) has been selected as a candidate for the Campanian GSSP. The proposed marker is the base of magnetochron C33r that according to Miniati et al. (2020) lies close to FO of *Aspidolithus parcus parcus*. Another event has been recognized in this study in order to approximate the Santonian/Campanian boundary is the "*Micula* abundance peak 5" at the end of the OAE3 interval. This increase in abundance of *M. staurophora* was found across the CC17/CC18 zonal boundary and, consequently, the **Santonian/Campanian boundary** at global scale.

In conclusion, this thesis characterized for the first time OAE3 in terms of changes in the calcareous nannofossil assemblages. Taking advantage of a detailed biostratigraphic characterization of sites and sections, the different abundance peaks of *Micula* and *Marthasterites* detected in this study were traced at global scale in a variety of basins and paleoceanographic settings. Although the paleoecology of genera *Micula* and *Marthasterites* remains to be fully exploited and understood, their "abundance peaks" unequivocally denote that OAE3 started during a time of particular environmental stress inducing anomalous abundances of *M. furcatus*. The most altered paleoceanographic conditions were reached in the core of OAE3 with the synchronous maximum abundance (climax) of *M. staurophora*. The termination of OAE3 coincides with a late *Micula* increase in abundance ("abundance peak 5") although of minor entity.

In addition to their value for paleoenvironmental reconstructions, the Micula and Marthasterites "abundance peaks" turned out to be extremely useful for the implementation of the biostratigraphic characterization of the Turonian/Coniacian, Coniacian/Santonian and Santonian/Campanian boundaries and might be introduced as additional events in future nannofossil zonations for the Late Cretaceous.

References

Al Rawahi, Z., Dunkley Jones, T., 2019. Calcareous nannofossil assemblages of the Late Cretaceous Fiqa Formation, north Oman. Journal of *Micropalaeontology*.38, 25–54.

Alvarez, W. And Montanari, A., 1988. The Scaglia limestone (Late Cretaceous–Oligocene) in the northeastern Apennines carbonate sequence: stratigraphic context and geological significance. In: Premoli Silva I., Coccioni R., Montanari A. (Ed.). *The Eocene–Oligocene boundary in the Marche–Umbria basin (Italy)*. 1, 13-29. Industrie Grafiche F.lli Aniballi, Ancona.

Alvarez, W., Arthur, M.A., Fischer, A.G., Lowrie, W., Napoleone, G., Premoli Silva, I., Roggenthen W.M., 1977.Upper Cretaceous–Paleocene magnetic stratigraphy at Gubbio, Italy. Type section for the Late Cretaceous-Paleocene geomagnetic reversal time scale. *Geological Society of America Bulletin*. 88, 383-389.

Arthur, M.A. and Fischer, A.G., 1977. Upper Cretaceous–Paleocene magnetic stratigraphy at Gubbio, Italy I. Lithostratigraphy and sedimentology. Geological Society of America Bulletin. 88, 367-371.

Arthur M.A. and Schlanger S.O., 1979. Cretaceous "oceanic anoxic events" as causal factors in development of reef-reservoired giant oil fields. *AAPG Bulletin*. 63, 870-885.

Arthur M.A., Jenkyns H.C., Brumsack H.J., Schlanger S.O.,1990. Stratigraphy, geochemistry, and paleoceanography of organic-carbon-rich Cretaceous sequences. In Ginsburg R.N. and Beaudoin B. (Eds), Cretaceous Resources, Events and Rhythms, NATO ASI Series, 304, 75-119.

Arthur, M.A., Premoli Silva, I., 1982. Development of widespread organic carbon-rich strata in Mediterranean Tethys. In: Schlanger, S.O., Cita, M.B. (Eds.), *Nature and Origin of Cretaceous Carbon-rich Facies*. 7-54.

Aubry, M. P., 2013. Cenozoic Coccolithophores: Braarudosphaerales. Micropaleontology Press, American Museum of Natural History, New York. 1-336.

Bauer, J., Marzouk, A.M., Steuber, T., Kuss, J., 2001. Lithostratigraphy and biostratigraphy of the Cenomanian–Santonian strata of Sinai, Egypt. *Cretaceous Research*. 22, 497–526.

Beckmann, B., Wagner, T., Hofmann, P., 2005a. Linking Coniacian–Santonian (OAE3) black-shale deposition to African climate variability: a reference section from the eastern tropical Atlantic at orbital time scales (ODP site 959, off Ivory Coast and Ghana). SEPM Special Publications.82, 125–143.

Beckmann, B., Flögel, S., Hofmann, P., Schulz, M., Wagner, T., 2005b. Mid-Cretaceous African climate development and implications for the marine carbon cycle. *Nature*. 437, 241–244.

Bergen, J. A.,1994. Berriasian to early Aptian calcareous nannofossils from the Vocontian Trough (SE France) and Deep Sea Drilling Site 534: new nannofossil taxa and a summary of low-latitude biostratigraphic events. *Journal of Nannoplankton Research*. 16(2), 59-69.

Bergen, J.A., Sikora, P.J., 1999. Microfossil diachronism in southern Norwegian North Sea chalks: Valhall and Hod fields. *Geological Society London*, *Special Publications*. 152 (1), 85–111.

Black M., 1971a. Coccolitbs of the Speeton Clay and Sutterby Mari. *Procedings Yorkshire geological Society*. 38, 381-424.

Black, M.,1968. Taxonomic problems in the study of coccoliths. *Palaeontology*. 11,793-813.

Blair, S. A. & Watkins, D. K.,2009. High-resolution calcareous nannofossil biostratigraphy for the Coniacian/Santonian Stage boundary, Western Interior Basin. *Cretaceous Research*. 30(2), 367-384.

Boersma, A., 1984. Cretaceous-Tertiary planktonic foraminifers from the Southeastern Atlantic. Walvis Ridge area. DSDP Leg 74: *Initial Reports Deep Sea Drilling Project*. 74. p. 501 - 523.

Bolli, H. M., Ryan W. B. F. et al., 1978. Initial Reports of the Deep Sea Drilling Project*,* 40. U.S. Government Printing Office, Washington. 1079 pp.

Bottini, C., Erba, E., Tiraboschi, D., Jenkyns, H. C., Schouten, S., Sinninghe Damsté, J. S., 2015. Climate variability and ocean fertility during the Aptian Stage. *Climate of the Past*. 11, 383–402.

Boudreaux, J. E. and Hay, W. W., 1969. Calcareous nannoplankton and biostratigraphy of the late Pliocene-Pleistocene-Recent sediments in the Submarex cores. *Revista Española de Micropaleontología*. 1(3), 249-292.

Bown, P. R. and Young, J. R., 1998. Introduction - calcareous nannoplankton biology. In: Bown, P. R. (Eds.), Calcareous Nannofossil Biostratigraphy. British Micropalaeontological Society Publication Series, London. 1-15.

Bown, P. R. and Young, J. R., 1997. Mesozoic calcareous nannoplankton classification. *Journal of Nannoplankton Research*. 19(1), 21-36.

Bralower, T.J., 1988. Calcareous nannofossil biostratigraphy and assemblages of the Cenomanian–Turonian boundary interval: implications for the origin and timing of oceanic anoxia. *Paleoceanography* 3, 275–316.

Bralower, T. J. and Bergen, J. A., 1998. Cenomanian-Santonian calcareous nannofossil biostratigraphy of a transect of cores drilled across the Western Interior Seaway. *In*, Dean, W. E. & Arthur, M. A. (eds) Stratigraphy and paleoenvironments of the Cretaceous Western Interior Seaway. *SEPM Concepts in Sedimentology and Paleontology*.

Bralower, T.J., Siesser, W.J., 1992. Cretaceous calcareous nannofossil biostratigraphy of Sites 761, 762 and 763, Exmouth and Wombat Plateaus, northwest Australia. In: von Rad, U., Haq, B. U., et al. (Eds.), Proceedings of the Ocean Drilling Program, Scientific Results. College Station Ocean Drilling Program, Texas.122, 529-556.

Bralower, T.J., Leckie, R.M., Sliter, W.V., Thierstein, H.R., 1995. An integrated Cretaceous microfossil biostratigraphy. In: Berggren, W.A., Kent, D.V., Aubry, M.-P., Hardenbol, J. (Ed.), Geochronology, Time Scales and Global Stratigraphic Correlation. Society of Economic Paleontologists and Mineralogists, Special Publication.54, 65-79.

Bralower, T. J., Monechi, S., Thierstein, H. R., 1989. Calcareous nannofossil zonation of the Jurassic-Cretaceous boundary interval and correlation with the geomagnetic polarity timescale. *Marine Micropaleontology*. 14, 153-235,

Bramlette, M. N. & Martini, E.,1964. The great change in calcareous nannoplankton fossils between the Maestrichtian and Danian. *Micropaleontology*. 10(2), 291-322.

Bristow, C.R., Mortimore, R.N., Wood, C.J., 1997. Lithostratigraphy for mapping the Chalk of southern England. *Proceedings of the Geologists' Association 108*. 293-315.

Bukry, D., 1973a. Low-latitude coccolith biostratigraphic zonation, In: Edgar, N. T., Saunders, J. B., et al. (Eds.), Initial Reports of the Deep Sea Drilling Project. U.S. Government Printing Office Washington. 15, 685-703.

Bukry, D., 1973b. Phytoplankton stratigraphy, Deep Sea Drilling Project Leg 20, Western Pacific Ocean. In: Heezen, Bruce C, Mac Gregor, Ian D., et al.,(Eds.) Initial Reports of the Deep Sea Drill-ing Project. U.S. Government Printing Office, Washington. 20,307-317.

Bukry, D., and Bramlette, M.N., 1970. Coccolith Age Determina-tions, Leg 3, Deep Sea Drilling Project. In: Maxwell, A. E. et al.,1970 (Eds). Initial Reports of the Deep Sea Drilling Project. U.S. Government Printing Office, Washington.3,589-611.

Bukry, D.,1969. Upper Cretaceous coccoliths from Texas and Europe. *University of Kansas Paleontological Contributions, Articles. 51 (Protista 2)*. 1-79.

Burnett, J.A., 1988. North-west European Late Cretaceous calcareous nannofossils: Biostratigraphy and selected evolutionary lineages. *Ph.D. Thesis*, University College London.

Burnett J., 1990. A new nannofossil zonation scheme for the Boreal Campanian. INA Newsletter. 12. 67-70.

Burnett, J.A., 1996. Nannofossils and Upper Cretaceous (sub-)stage boundaries - state of the art. *Journal of Nannoplankton Research*, 18, 23-32

Burnett, J. A., 1997. New species and new combinations of Cretaceous nannofossils and a note on the origin of *Petrarhabdus* (Deflandre) Wise and Wind. *Journal of Nannoplankton Research*. 19, 133-146.

Burnett, J. A., and Whitham, F., 1999. Correlation between the nannofossil and macrofossil biostratigraphies and the lithostratigraphy of the Upper Cretaceous of NE England. *Proceedings of the Yorkshire Geological Society*, *52*(4), 371-38.

Burnett, J.A., Hancock, J.M., Kennedy, W.J., Lord, A.R., 1992a. Macrofossil, planktonic foraminiferal and nannofossil zonation at the Campanian/Maastrichtian boundary. *Newsletters on Stratigraphy*, 27, 157-172.

Burnett, J.A., Kennedy, W.J., Ward, P.D., 1992b. Maastrichtian nannofossil biostratigraphy in the Biscay region (south western France, northern Spain). *Newsletters on Stratigraphy*, 26, 145-155.

Burnett, J.A., Whitham, F., 1999. Correlation between the nannofossil and macrofossil biostratigraphies and the lithostratigraphy of the Upper Cretaceous of NE England. *Proceedings of the Yorkshire Geological Society*, 52, 371-381.

Cavalier-Smith, T., 1981. Eukaryote kingdoms: seven or nine?*BioSystems*. 10, 93-114.

Cavalier-Smith, T., 1986. The Kingdom Chromista: Origins and systematics. *Progress in Phycological Research*. 4, 309-344.

Čepek, P., Hay, W.W., 1969. Calcareous nannoplankton and biostratigraphic subdivision of the Upper Cretaceous. *Gulf Coast Association of Geological Societies* .19, 323-336.

Cetean, C.G., Bălc, R., Kaminski, M.A., Filipescu, S., 2011. Integrated biostratigraphy and palaeoenvironments of an upper Santonian – upper Campanian succession from the southern part of the Eastern Carpathians, Romania. *Cretaceous Research.* 32, 575–590.

Chave, A. D., 1984. Lower Paleocene-Upper Cretaceous magnetic stratigraphy from Sites 525.527.528 and 529. DSDP leg 74: Initial Reports of the Deep Sea Drilling Project. U.S. Government Printing Office, Washington.74. p. 525-531.

Coccioni, R. and Premoli Silva, I., 2015. Revised upper Albian-Maastrichtian planktonic foraminiferalbiostratigraphy and magnetostratigraphy of the classical Tethyan Gubbio section (Italy). *Newsletters on Stratigraphy*.48 (1), 47-90.

Corbett, M. J. and Watkins, D. K., 2014. Cenomanian through basal Coniacian Calcareous Nannofossil biostratigraphy of the Mancos Shale reference section, Mesa Verde National Park, CO. *Stratigraphy*. 11(1),97-108.

Cresta, S., Monechi, S., Parisi G., 1989. Stratigrafia del Mesozoico e Cenozoico nell'area Umbro–Marchigiana. *Memorie descrittive della Carta Geologica d'Italia*. 39, 185.

Crux, J. A., 1982. Upper Cretaceous (Cenomanian to Campanian) calcareous nannofossils. In, Lord, A. R. (ed.) A Stratigraphical Index of Calcareous Nannofossils. British Micropalaeontological Society Series. Ellis Horwood, Chichester. 81-135.

Crux, J.A., 1982. Upper Cretaceous (Cenomanian to Campanian) calcareous nannofossils. In: Lord, A.R. (Eds.), A Stratigraphical Index of Calcareous Nannofossils. *British Micropalaeontological* Society Series. Ellis Horwood Limited, Chichester.81-135.

Da Gama, R. O., Lutz, B., Desjardins, P., Thompson, M., Prince, I., Espejo, I., 2014. Integrated paleoenvironmental analysis of the Niobrara Formation: Cretaceous Western Interior Seaway, northern Colorado. *Palaeogeography, Palaeoclimatology, Palaeoecology*.413, 66-80.

Davis, C., Pratt, L., Sliter, W., Mompart, L., Murat, B.,1999. Factors influencing organic carbon and trace metal accumulation in the upper Cretaceous La Luna Formation of the western Maracaibo Basin, Venezuela, in The Evolution of Cretaceous Ocean/Climate Systems, Barrera E. and Johnson C. (Eds.), *Geological Society of America*. 332, 203– 230.

De Romero, L. M., Truskowski, I. M., Bralower, T. J., Bergen, J. A., Odreman, O., Zachos, J. C., & Galea-Alvarez, F. A., 2003. An integrated calcareous microfossil biostratigraphic and carbon-isotope stratigraphic framework for the La Luna Formation, western Venezuela. *Palaios*, *18*(4-5), 349-366.

Dean, W. E., Arthur, M. A., Stow, D. A. V.,1984. Origin and geochemistry of Cretaceous deep-sea black shales and multicolored claystones, with emphasis on Deep Sea Drilling Project Site 530, southern Angola Basin. Initial Report of Deep Sea Drilling Project. U.S. Government Printing Office, Washington. 75, 819– 844.

Dean, W.E., Arthur, M.A., 1998. Cretaceous Western Interior Seaway Continental Scientific Drilling project: an overview. In: Dean, W.E., Arthur, M.A. (Eds.), Stratigraphy and Paleoenvironments of the Cretaceous Western Interior Seaway. *SEPM Concepts in Sedimentology and Paleontology*. 6, 1–10

Deflandre, G. and Fert, C.,1954. Observations sur les coccolithophoridés actuels et fossiles en microscopie ordinaire et électronique. *Annales de Paléontologie*. 40,115-176.

Deflandre, G.,1959. Sur les nannofossiles calcaires et leur systématique. *Revue de Micropaléontologie*. 2, 127-152.

Doeven, P.H., 1983.Cretaceous nannofossil stratigraphy and paleoecology of the Canadian Atlantic Margin. *Bulletin of the Geulugical Survey of Canada*. 356, 1-70.

Dubicka, Z., Jurkowska, A., Thibault, N., Razmjooei, M.J., Wójcik, K., Gorzelak, P., Felisiak, I., 2017. An integrated stratigraphic study across the Santonian/Campanian boundary at Bocieniec, southern Poland: A new boundary stratotype candidate. *Cretaceous Research*. 80, 61–85.

Erba, E., 1992. Calcareous nannofossil distribution in pelagic rhythmic sediments (Aptian-Albian Piobbico core, central Italy). *Rivista italiana di paleontologia e stratigrafia*. 97, 455-484.

Erba E., 1994. Nannofossils and superplumes: the early Aptian nannoconid crisis. *Paleoceanography.* 9, 483-501.

Erba E., 2004. Calcareous nannofossils and Mesozoic oceanic anoxic events. *Marine Micropaleontology*, 52,85-106.

Erba, E., Bottini, C., Faucher, G., Gambacorta, G., Visentin, S., 2019. The response of calcareous nannoplankton to Oceanic Anoxic Events: The Italian pelagic record. *Bollettino della Società Paleontologica Italiana*, 58(1), 52.

Erba, E., Duncan, R. A., Bottini, C., Tiraboschi, D., Weissert, H., Jenkyns, H. C., Malinverno, A., 2015. Environmental consequences of Ontong Java Plateau and Kerguelen Plateau volcanism. *The origin, evolution, and environmental impact of oceanic large igneous provinces.* Geological Society of America Special Paper.511, 271-303.

Erbacher J., Thurow J. & Littke R., 1996. Evolution patterns of radiolaria and organic matter variations: A new approach to identify sea-level changes in mid-Cretaceous pelagic environments. *Geology*. 24, 499-502.

Erbacher, J., Friedrich, O., Wilson, P.A., Birch, H., Mutterlose, J., 2005. Stable organic carbon isotope stratigraphy across Oceanic Anoxic Event 2 of Demerara Rise, western tropical Atlantic. *Geochemistry, Geophysics, Geosystems.* 6.

Erlich, R. N., Palmer-Koleman, S. E., Antonieta Lorente, M., 1999. Geochemical characterization of oceanographic and climatic changes recorded in upper Albian to lower Maastrichtian strata, western Venezuela. *Cretaceous Research*. 20, 547– 581.

Eshet, Y, and Almogi-Labin, A., 1996. Calcareous nannofossils as paleoproductivity indicators in Upper Cretaceous organic-rich sequences in Israel. *Mar Micropaleontol*ogy. 29,37–61.

Eshet, Y, Moshkovitz, S, Habib, D, Benjamini, C, Magaritz, M., 1992. Calcareous nannofossil and dinoflagellate stratigraphy across the Cretaceous/Tertiary boundary at Hor Hahar, Israel. Marine Micropaleontology. 18,199–228

Exon, N. F., Haq, B. U., & Von Rad, U.,1992. Exmouth Plateau revisited: scientific drilling and geological framework. In: von Rad, U., Haq, B. U., et al. (Eds.), Proceedings of the Ocean Drilling Program, Scientific Results. College Station Ocean Drilling Program, Texas. 122. 3-20.

Farhan, A. J., Burnett, J. A., Bown, P. R., Lord, A. R., 1994. Holococcoliths from the Upper Cretaceous of Alabama and Mississippi (USA). *Cahiers de Micropaléontologie*. 9, 57-73.

Faris, M., Jaff, R.B.N., Farouk, S., 2019. Calcareous nannofossil biostratigraphy and bio-events of the Coniacian–lower Campanian succession in the Kurdistan region, northeastern Iraq. *Arabian Journal of Geosciences*. 12, 153.

Farouk, S., Ahmad, F., Powell, J.H., Marzouk, A.M., 2016. Integrated microfossil biostratigraphy, facies distribution, and depositional sequences of the upper Turonian to Campanian succession in northeast Egypt and Jordan. *Facies*. 62, 8.

Farouk, S., Faris, M., 2012. Late Cretaceous calcareous nannofossil and planktonic foraminiferal bioevents of the shallow-marine carbonate platform in the Mitla Pass, west central Sinai, Egypt. *Cretaceous Research*. 33, 50–65.

Farouk, S., Faris, M., Elamri, Z., Ahmad, F., Wagreich, M., 2018. Tethyan plankton bioevents calibrated to stable isotopes across the upper Santonian–lower Campanian transition in north-western Tunisia. *Cretaceous Research*. 85, 128–141.

Fischer, A. G., and Arthur, M. A., 1977. Secular variations in the pelagic realm. *Society* of *Economic Paleontologists* and *Mineralogists Special Publication.25*, 19-50.

Flögel, S., Beckmann, B., Hofmann, P., Bornemann, A., Westerhold, T., Norris, R. D., Wagner, T., 2008. Evolution of tropical watersheds and continental hydrology during the Late Cretaceous greenhouse; impact on marine carbon burial and possible implications for the future. *Earth and Planetary Science Letters*.274(1-2), 1-13.

Forchheimer, S., 1972. Scanning electron microscope studies of Cretaceous coccoliths from the Köpingsberg Borehole No. 1, SE Sweden. *Sveriges Geologiska Undersökning, Series C*. #668.65,1-141.

Friedrich, O., and Erbacher, J., 2006. Benthic foraminiferal assemblages from Demerara Rise (ODP Leg 207, western tropical Atlantic): possible evidence for a progressive opening of the Equatorial Atlantic Gateway. *Cretaceous Research*. 27(3), 377-397.

Fritsen, A., Bailey, H.W., Gallagher, L.T., Hampton, M.J. et al. (12 other authors), 2000. A joint Chalk Stratigraphic Framework. JCR Symposium, Brighton, 21-24 March 2000. 1-2, 206.

Galbrun, B., 1992. Magnetostratigraphy of Upper Cretaceous and Lower Tertiary sediments. Sites 761 and 762. Exmouth Plateau. Northwest Australia. In: von Rad, U., Haq, B. U., et al., 1992 (Eds.), Proceedings of the Ocean Drilling Program Scientific Results. College Station Ocean Drilling Program, Texas. 122,699-716

Gale, A.S., Kennedy, W.J., Burnett, J.A., Caron, M., Kidd, B.E., 1996. The Late Albian to Early Cenomanian succession at Mont Risou near Rosans (Drome, SE France): an integrated study (ammonites, inoceramids, planktonic foraminifera, nannofossils, oxygen and carbon isotopes). *Cretaceous Research,* 17*,* 515-606.

Gale, A. S., Kennedy, W. J., Lees, J. A., Petrizzo, M. R., & Walaszczyk, I., 2007. An integrated study (inoceramid bivalves, ammonites, calcareous nannofossils, planktonic foraminifera, stable carbon isotopes) of the Ten Mile Creek section, Lancaster, Dallas County, north Texas, a candidate Global boundary Stratotype Section and Point. *Acta Geologica Polonica*. 57, 113-160.

Gallagher, S. J., Taylor, D., Apthorpe, M., Stilwell, J. D., Boreham, C. J., Holdgate, G. R., Quilty, P. G., 2005. Late Cretaceous dysoxia in a southern high latitude siliciclastic succession, the Otway Basin, southeastern Australia. *Palaeogeography, Palaeoclimatology, Palaeoecology*. *223(*3-4) 317-348

Gardet, M., 1955. Contribution à l'étude des coccolithes des terrains néogènes de l'Algérie. *Publications du Service de la Carte Géologique de l'Algérie (Nouvelle Série)*. 5, 477-550.

Gartner Jr., S., 1968. Coccoliths and Related Calcareous Nannofossil from Upper Cretaceous Deposits of Texas and Arkansas, 48. *University of Kansas Paleontological Contributions*, 48, 1-56.

Gardin, S., 2002. Late Maastrichtian to early Danian calcareous nannofossils at Elles (northwest Tunisia). A tale of one million years across the K/T boundary. *Palaeogeography, Palaeoclimatology, Palaeoecology*. 2756, 1–21.

Gardin, S., and Monechi, S., 1998. Palaeoecological change in middle to low latitude calcareous nannoplankton at the Cretaceous/Tertiary boundary. *Bulletin de la Société géologique de France*. *169*(5), 709-723.

Gardin, S., Del Panta, F., Monechi, S., Pozzi, M.,2001. A Tethyan reference record for the Campanian and Maastrichtian stages: The Bottaccione section (Central Italy); review of data and new calcareous nannofossil results. In: G.S. Odin (Ed.) - The Campanian–Maastrichtian Stage Boundary. *Developments in Palaeontology and Stratigraphy*, Elsevier. 19, 745-757.

Geisen, M., Bollmann, J., Herrle, J. O., Mutterlose, J., Young, J. R., 1999. Calibration of the random settling technique for calculation of absolute abundances of calcareous nannoplankton. *Micropaleontology*.437-442.

Gradstein, F.M., Ogg, J.G., Schmitz, M.D., Ogg, G.M., 2012.The Geologic Time Scale 2012. *Elsevier*, Oxford, UK. 1144.

Guerra, R. do M., Tokutake, L.R., Fauth, G., 2012. Cretaceous calcareous nannofossils from Pelotas Basin, Brazil: Biostratigraphic and paleoecological inferences. *Journal of South American Earth Sciences*. 36, 55–71.

Hampton, M. J., Bailey, H. W, Gallagher, L. T., Mortimore, R. N., Wood, C. J., 2007. The biostratigraphy of Seaford Head, Sussex, southern England; an international reference section for the basal boundaries for the Santonian and Campanian Stages in chalk facies. *Cretaceous Research*. 28, 43–60.

Hancock, J. M., Gale, A. S., 1996. The Campanian stage. In: F. Rawson et al., (Ed.). Proceedings, "Second International Symposium on Cretaceous Stage Boundaries", Brussels, September 1995. *Bull. de l'Institut Royal des* Sciences *Naturelles de Belgique.*66, (Supplement), 103–109.

Haq, B.U., Boyd, R.L., Exon, N.F., von Rad, U., 1992. Evolution of the central Exmouth Plateau: a post-drilling perspective. In: von Rad, U., Haq, B.U., et al. (Eds.), Proceedings of the Ocean Drilling Program, Scientific Results. College Station Ocean Drilling Program, Texas. 122, 801-808.

Hardas, P., Mutterlose, J., 2006. Calcareous nannofossil biostratigraphy of the Cenomanian/Turonian boundary interval of ODP Leg 207 at the Demerara Rise. *Revue de Micropaléontologie*. 49, 165–179.

Henriksson, A.S., Malmgren, B.A., 1997. Biogeographic and Ecologic Patterns in calcareous nannoplankton in the Atlantic and Pacific Oceans during the Terminal Cretaceous. *Studia Geologica Salmanticensia*. 33, 17–40.

Hattner, J. G. and Wise, S. W., 1980. Upper Cretaceous calcareous nannofossil biostratigraphy of South Carolina. *South Carolina Geology*. 24,41-117.

Hattner, J. G., Wind, F. H. and Wise, S. W.,1980. The Santonian-Campanian boundary: comparison of nearshore-offshore calcareous nannofossil assemblages. *Cahiers de Micropaléontologie*. 3,9-26.

Herrle, J.O., 2003. Reconstructing nutricline dynamics of mid-Cretaceous oceans: evidence from calcareous nannofossils from the Niveau Paquier black shale (SE France*)*. *Marine Micropaleontology* 47, 307–321.

Herrle, J.O., Pross, J., Friedrich, O., Hemleben, Ch., 2003. Short-term environmental changes in the Cretaceous Tethyan Ocean: micropalaeontological evidence from the Early Albian Oceanic Anoxic Event 1b. *Terra Nova*. 15, 14–19.

Hewaidy, A. G. A., Mandur, M. M., Farouk, S., El Agroudy, I. S., 2019. Upper Campanian-Maastrichtian calcareous nannoplankton biostratigraphy and paleoecology in Wadi Qena, Eastern Desert, Egypt. *Arabian Journal of Geosciences*. *12*(11), 366.

Hibberd, D.J., 1976. The ultrastructure and taxonomy of the Chrysophyceae and Prymnesiophyceae (Haptophyceae): a survey with some new observations on the ultrastructure of the Chrysophyceae. *Botanical Journal of the Linnaen Society*, 72, 55-80.

Hoffmann, N.,1970. Taxonomische Untersuchungen an Coccolithen aus der Kreide Norddeutchlands anhand elektronenmikroskopischer Aufnamen. *Hercynia*. 7(1-3),163-198.

Hofmann, P., and Wagner, T., 2011. ITCZ controls on Late Cretaceous black shale sedimentation in the tropical Atlantic Ocean. *Paleoceanography* 26 (4).

Hofmann, P., Beckmann, B., Wagner, T., 2003. A millennial- to centennial-scale record of African climate variability and organic carbon accumulation in the Coniacian-Santonian eastern tropical Atlantic (ODP Site 959, off Ivory Coast/Ghana). *Geology*. 31(2), 135–138.

Howe, R.W., Sikora, P.J., Gale, A.S., Bergen, J.A., 2007. Calcareous nannofossil and planktonic foraminiferal biostratigraphy of proposed stratotypes for the Coniacian/Santonian boundary: Olazagutía, northern Spain; Seaford Head, southern England; and Ten Mile Creek, Texas, USA. *Cretaceous Research*. 28, 61–92.

Hu, X., Jansa, L., Wang, C., Sarti, M., Bak, K., Wagreich, M., Sotak, J., 2005. Upper Cretaceous oceanic red beds (CORBs) in the Tethys: occurrences, lithofacies, age, and environments. *Cretaceous Research*. *26*(1), 3-20.

Huber, B. T., 1990. Maastrichtian planktonic foraminifera biostratigraphy of the Maud Rise (Weddell Sea. Antarctica): ODP Leg 113 holes 689B and 690C. *Proceedings Ocean Drilling Program Scientific Results*. Ocean Drilling Program College Station, Texas. 113,489-513.

Huber, B. T., 1991. Planktnic foraminifer biostratigraphy of Campanian-Maastrichtiansediments from ODP Leg 114 sites 698 and 700, southern Atlantic Ocean. *Proceedings Ocean Drilling Program Scientific Results*. Ocean Drilling Program College Station, Texas. 114, 281-297.

Jarvis I., Mabrouk A., Moody R.T.J., Cabrera S.D., 2002. Late Cretaceous (Campanian) carbon isotope events, sea-level change and correlation of the Tethyan and Boreal realms. *Palaeogeography, Palaeoclimatology, Palaeoecology*, 188: 215-248.

Jarvis, I., Gale, A. S., Jenkyns, H. C., Pearce, M. A., 2006. Secular variation in Late Cretaceous carbon isotopes: A new δ13C carbonate reference curve for the Cenomanian–Campanian (99.6–70.6 Ma). *Geological Magazine*.143, 561–608.

Jenkyns, H.C.,1980. Cretaceous anoxic events: from continents to oceans. *Journal of the Geological Society of London*.137.171–188.

Jenkyns, H.C., 1985. The Early Toarcian and Cenomanian-Turonian anoxic events in Europe: comparisons and contrasts. *Geologische Rundschau*.74, 505–518.

Jenkyns, H.C., 1988. The Early Toarcian (Jurassic) Anoxic Event: stratigraphic, sedimentary and geochemical evidence. *American Journal of Science*. 288, 101–151

Jenkyns, H.C., 2003. Evidence for rapid climate change in the Mesozoic-Palaeogene greenhouse world. *Philosophical Transactions of the Royal Society A: Mathematical, Physical and Engineering Sciences*. 361, 1885–1916.

Jenkyns H.C., 2010. Geochemistry of oceanic anoxic events. *Geochemistry, Geophysics, Geosystems,* 11.

Jenkyns H.C., Gale A.S. and Corfield R.M., 1994. Carbon- and oxygen-isotope stratigraphy of the English Chalk and Italian Scaglia and its palaeoclimatic significance. *Geological Magazine*.131, 1-34.

Jeremiah, J., 1996. A proposed Albian to Lower Cenomanian nannofossil biozonation for England and the North Sea Basin. *Journal of Micropalaeontology*. 15,97-129.

Jimenez Berrocoso, A., Huber, B.T., MacLeod, K.G., Petrizzo, M.R., Lees, J.A., Wendler, I., Coxall, H., Mweneinda, A.K., Falzoni, F., Birch, H., Haynes, S.J., Bown, P.R., Robinson, S.A. and Singano, J.M., 2015. Lithostratigraphy, biostratigraphy and chemostratigraphy of Upper Cretaceous and Paleogene sediments from southern Tanzania: Tanzania Drilling Project Sites 36 to 40. Journal of *African Earth Sciences.*101, 282–308.

Kennedy, W.J., Hansotte, M., Bilotte, M., Burnett, J., 1992. Ammonites and Nannofossils from the Campanian of Nalzen (Ariège, France). *Geobios*, 25, 2, 263-278.

King, C., Bailey, H. W., Burton, C. A., King, A. D., 1989. Cretaceous of the North Sea. In: Jenkins, D. G. and Murray, J. W. (Eds.), Stratigraphical Atlas of Fossil Foraminifera (2nd edn). Ellis Horwood, Chichester. 372-417.

Kita, Z.A., Watkins, D.K., Sageman, B.B., 2017. High-resolution calcareous nannofossil biostratigraphy of the Santonian/Campanian Stage boundary, Western Interior Basin, USA. *Cretaceous Research*. 69, 49–55.

Lamolda, M. A., and Hancock, J. M.,1996. The Santonian stage and substages. In: F. Rawson et al., (Ed.). Proceedings, "Second International Symposium on Cretaceous Stage Boundaries", Brussels, September 1995. *Bull. de l'Institut Royal des* Sciences *Naturelles de Belgique.*66, (Supplement), 95–102.

Lamolda, M. A., Paul, C. R. C., Peryt, D., & Pons, J. M., 2014. The global boundary stratotype and section point (GSSP) for the base of the Santonian Stage," Cantera de Margas", Olazagutia, northern Spain. *Episodes*, 37, 2-13.

Larson, R.L. and Erba, E., 1999. Onset of the mid-Cretaceous greenhouse in the Barremian–Aptian: Igneous events and the biological, sedimentary and geochemical responses. *Paleoceanography*. 14(6), 663-678.

Leckie R.M., Bralower T.J. and Cashman R., 2002. Oceanic anoxic events and plankton evolution: Biotic response to tectonic forcing during the mid-Cretaceous. *Paleoceanography*, 17: PA000623.

Lees, J.A., 2002. Calcareous nannofossil biogeography illustrates paleoclimate change in the Late Cretaceous Indian Ocean. *Cretaceous Research.* 23, 537–634.

Lees, J. A., 2007. New and rarely reported calcareous nannofossils from the Late Cretaceous of coastal Tanzania: outcrop samples and Tanzania Drilling Project Sites 5, 9 and 15. *Journal of Nannoplankton Research*. 29(1),39-65.

Lees, J.A., 2008. The calcareous nannofossil record across the Late Cretaceous Turonian/Coniacian boundary, including new data from Germany, Poland, the Czech Republic and England. *Cretaceous Research*. 29, 40–64.

Lees, J. A. and Bown, P. R., 2005. Upper Cretaceous calcareous nannofossil biostratigraphy, ODP Leg 198 (Shatsky Rise, Northwest Pacific Ocean). In: Bralower, T.J., Premoli Silva, I., and Malone, M.J. (Eds.), *Proceedings of the Ocean Drilling Program, Scientific Results.* College Station, Ocean Drilling Proigram, Texas.198, 1-60.

Lees, J. A. and Bown, P. R., 2016. New and intriguing calcareous nannofossils from the Turonian (Upper Cretaceous) of Tanzania. *Journal of Nannoplankton Research*. 36(1),83-95.

Linnert, C. and Mutterlose, J., 2009. Biometry of the Late Cretaceous *Arkhangelskiella* group: ecophenotypes controlled by nutrient flux. *Cretaceous Research*. 30, 1193-1204.

Linnert, C., Mutterlose, J., Herrle, J.O., 2011. Late Cretaceous (Cenomanian–Maastrichtian) calcareous nannofossils from Goban Spur (DSDP Sites 549, 551): Implications for the palaeoceanography of the proto North Atlantic. *Palaeogeography, Palaeoclimatology, Palaeoecology*. 299, 507–528.

Locklair, R., Sageman, B., Lerman, A., 2011. Marine carbon burial flux and the carbon isotope record of Late Cretaceous (Coniacian–Santonian) Oceanic Anoxic Event III. Sediment. Geol. 235, 38–49.

Mandur, M. M., and El Ashwah, A. A. 2015. Calcareous nannofossil biostratigraphy and paleoecology of the Maastrichtian in the western coast of the Gulf of Suez, Egypt. *Arabian Journal of Geosciences*. *8*(5), 2537-2550.

Manivit, H., 1971. Nannofossiles calcaires du Cretacé francais (Aptien-Maestrichtien). Essai de biozonation appuyée sur les stratotypes: Thesis Facult. Sci. Orsay, 1-187.

Manivit, H., 1972. Les nannofossiles du Cretace. (Aptien-Turonien inclus). Mem. B.R.G.M., Fr., 77, p. 165-169.

Manivit, H., 1984. Palcogene and Upper Cretaceous calcareous nannofossilsfrom DSDP Leg 74: Initial Reports of the Deep Sea Drilling Project. U.S. Government Printing Office, Washington.74, p. -175- 501.

Manivit, H., Perch-Nielsen K., Prins, B., and Verbeek, J. W.,1977. Mid-Cretaceous calcareous nannofossil biostratigraphy. *Proc. Koninkl. Nederl. Akad. Wehettschappen,* Amsterdam. B80, 3, 169-181.

Maron, M. and Muttoni, G. (accepted) - A detailed record of the C34n/C33r magnetozone boundary for the definition of the base of the Campanian Stage at the Bottaccione section (Gubbio, Italy). *Newsletters on Stratigraphy*.

Martinez, J. I., 2003. The paleoecology of Late Cretaceous upwelling events from the upper Magdalena Basin, Colombia. *Palaios*.*18*(4-5), 305-320.

Martini, E., 1961. Nannoplankton aus dem Tertiär und der obersten Kreide von SW-Frankreich. *Senckenbergiana Lethaea*. 42, 1-32.

Martini, E., 1969. Nannoplankton aus dem Latdorf (locus typicus) und weltweite Parallelisierungen im oberen Eozan und unteren Oligozan: Senckenberg. *Lethaea*. 50, 117-159.

Martini, E., 1976. Cretaceous to Recent nannoplankton from the central Pacific Ocean (DSDP Leg 33). In: Schlanger, S. O., Jackson, E. D., et al. (Eds) Initial Reports of the Deep Sea Drilling Project. U.S. Government Printing Office, Washington.33, 383-424.

Martini, E. and Stradner, H., 1960. *Nannotetraster*, eine stratigraphisch bedeutsame neue Discoasteridengattung. *Erdoel-Zeitschrift*. 76(8), 266-270.

März, C., Beckmann, B., Franke, C., Vogt, C., Wagner, T., Kasten, S., 2009. Geochemical environment of the Coniacian–Santonian western tropical Atlantic at Demerara Rise. *Palaeogeography, Palaeoclimatology, Palaeoecology*. 273, 286–301.

März, C., Poulton S. W., Beckmann B., Küster K., Wagner, T., Kasten, S., 2008. Redox sensitivity of P cycling during marine black shale formation. *Geochimica* et *Cosmochimica Acta*. 72(15), 3703–3717.

Mascle, J., Lohmann, G.P., Clift, P.D., et al., 1996. Initial Reports of the Ocean Drilling Program 159. College Station Ocean Drilling Program, Texas.159, 616.

Melinte-Dobrinescu, M.C., 2010. Lithology and biostratigraphy of Upper Cretaceous marine deposits from the Haţeg region (Romania): Palaeoenvironmental implications. *Palaeogeography, Palaeoclimatology, Palaeoecology*. 293, 283–294.

Melinte, M. C., and Lamolda, M. A., 2002. Calcareous nannofossils around the Coniacian/Santonian boundary interval in the Olazagutia section (N. Spain*)*. In: Wagreich, M. (Eds.). Aspects of Cretaceous Stratigraphy and Paleobiogeography. Proceedings of the 6'h International Cretaceous Symposium Vienna, 2000. 351-364.

Melinte, M.C., and Lamolda, M.A., 2007. Calcareous nannofossil biostratigraphy of the Coniacian/Santonian boundary interval in Romania and comparison with other European regions. *Cretaceous Research*. 28, 119–127.

Miniati, F., Petrizzo, M.R., Falzoni, F., Erba, E., 2020.Calcareous plankton biostratigraphy of the Santonian-Campanian boundary interval in the Bottaccione Section (Umbria-Marche Basin, Central Italy). *Rivista Italiana di Paleontoleontologia e Stratigrafia*. 126(3), 771-789.

Mohler, H.P., 1966. Stratigraphische Untersuchungen in den Giswiler Klippen (Prealpes Medianes) und ihrer helvetisch- ultrahelvetischen Unterlage. Beiträge zur Geologischen Karte der Schweiz. 129,15-84.

Monechi, S.,1977. Upper Cretaceous and Early Tertiary nannoplankton from Scaglia Umbra Formation (Gubbio, Italy). *Rivista Italiana di Paleontologia e Stratigrafia*. 83, 759-802.

Monechi, S. and Pirini Radrizzani, C., 1975. Nannoplankton from Scaglia Umbra Formation (Gubbio) at the Cretaceous-Tertiary boundary. *Rivista Italiana di Paleontologia e Stratigrafia*. 81, 85-96.

Monechi, S., and Thierstein, H., 1985. Late Cretaceous-Eocene Nannofossil And Magnetostratigraphic Correlations Near Gubbio, Italy. *Marine Micropaleontology*. 9, 419-440.

Monechi, S., Bleil U., Backman J., 1985. Magnetobiochronology of Late Cretaccous-Paleogene and late Cenozoic pelagic sedimentary sequences from the Northwest Pacific (Deep Sea Drilling Project Leg 86. Site 577). In: Heath, G. R., Burckle, L. H., et al., 1985 (Eds.), Initial Reports of the Deep Sea Drilling Project. U.S. Government Printing Office, Washington. 86, 787-798.

Mortimore, R.N., 1986. Stratigraphy of the Upper Cretaceous White Chalk of Sussex. *Proceedings of the Geologists' Association 97*.97-139.

Mortimore, R.N., Pomerol, B., 1987. Correlation of the Upper Cretaceous White Chalk (Turonian to Campanian) in the Anglo-Paris Basin. *Proceedings of the Geologists' Association 98*. 97-143.

Mortimore, R.N., Wood, C.J., Gallois, R.W., 2001. British Upper Cretaceous Stratigraphy. In: *Geological Conservation Review Series*. Joint Nature Conservation Committee, Peterborough. 23.558.

Napoleone, G., Premoli Silva I., Heller F., Cheli P., Corezzi S., Fischer, A.G.,1983.-Eocene magnetic stratigraphy at Gubbio, Italy, and its implications for Paleogene geochronology. *Geological Society of America Bulletin*. 94, 181-191.

Noël, D., 1959. Étude de coccolithes du Jurassique et du Crétacé inférieur. *Publications du Service de la Carte Géologique de l'Algérie (Nouvelle Série) Bulletin*. 20, 155-196

Noël, D., 1969. *Arkhangelskiella* (coccolithes Crétacés) et formes affines du Bassin de Paris. *Revue de Micropaléontologie*. 11,191-204.

Noël, D., 1970. *Coccolithes Crétacés: La Craie Campanienne du Bassin de Paris.* Éditions du Centre National de la Recherche Scientifique, Paris.

Obradovich, J.D., 1993. A Cretaceous time-scale. In: Caldwell, W. G. E. and Kauffman, E. G., (Eds.), Evolution of the Western Interior Basin: St. Johns. *Geological Association of Canada Special Paper*.39, 379-396.

Parente, M., Frijia, G., Di Lucia, M., Jenkyns, H. C., Woodfine, R. G., Baroncini, F., 2008. Stepwise extinction of larger foraminifers at the Cenomanian-Turonian boundary: A shallow-water perspective on nutrient fluctuations during Oceanic Anoxic Event 2 (Bonarelli Event). *Geology*. 36(9), 715-718.

Perch-Nielsen, K., 1972. Remarks on the Late Cretaceous to Pleistocene coccoliths from the North Atlantic. In: Laughton, A. S., Berggren, W. A., et al. (Eds.). Initial Reports of the Deep Sea Drilling Project. U.S. Government Printing Office, Washington.12, 1003-1069.

Perch-Nielsen, K., 1973. Neue Coccolithen aus dem Maastrichtien von Danemark, Madagaskar und Agypten. *Bulletin of the Geological Society of Denmark*. 22,306-333.

Perch-Nielsen, K., 1977. Albian to Pleistocene Calcareous Nannofossils from the Western South Atlantic, DSDP Leg 39. In: Supko, P.R., Perch-Nielsen, K, et al. (Eds.). Initial Reports of the Deep Sea Drilling Project. U.S. Government Printing Office, Washington 39, 699-823.

Perch-Nielsen, K., 1979. Calcareous nannofossils from the Cretaceous between the North Sea and the Mediterranean. In: Wiedmann, J. (Eds.), Aspekte der Kreide Europas. International Union of Geological Sciences. A6, 223–272.

Perch-Nielsen, K., 1983. Recognition of Cretaceous stage boundaries by means of calcareous nannofossils. In T. Birkelund, R. Bromley, W.K. Christensen, E. Hakansson and F. Surlyk (Eds.). Symposium on Cretaceous stage boundaries. Copenhagen.152-156

Perch-Nielsen, K., 1984. Validation of new combinations. *INA Newsletter*. 6(1), 42-46.

Perch-Nielsen, K.,1985. Mesozoic calcareous nannofossils. In: Bolli, H.M., Saunders, J.B., Perch-Nielsen, K. (Eds.), *Plankton Stratigraphy*. Cambridge University Press, Cambridge. 329–427.

Perch-Nielsen, K., 1986. New Mesozoic and Paleogene calcareous nannofossils. *Eclogae Geologicae Helvetiae*. 79(3), 835-847.

Perez-Infante, J., Farrimond, P., & Furrer, M., 1996. Global and local controls influencing the deposition of the La Luna Formation (Cenomanian-Campanian), western Venezuela. *Chemical Geology*.130, 271-288.

Persico, D. and Villa, G., 2002. Problematic side views of *Eprolithus*: Comparison with *Micula decussata*. *Journal of Nannoplankton Research*. 24(1), 15-25.

Petrizzo, M. R., Jiménez Berrocoso, Á., Falzoni, F., Huber, B. T., Macleod, K. G., 2017. The Coniacian–Santonian sedimentary record in southern Tanzania (Ruvuma Basin, East Africa): Planktonic foraminiferal evolutionary, geochemical and palaeoceanographic patterns. *Sedimentology*. 64(1), 252-285.

Pletsch, T., Erbacher, J., Holbourn, A.E.J., Kuhnt, W., Moullade, M., Oboh-Ikuenobe, F.E., So¨d-ing, E., and Wagner, T., 2001, Cretaceousopening history of the equatorial Atlanticgateway: The view from the west African con-tinental margin (ODP Leg 159). *Journal of South American Earth Sciences*. 14. 147–174.

Poore, R. Z., Tauxe L., Percival S. F. Jr., LaBrecque J. L., Wright R., Petersen N. P., Smith, C. S., Tucker P., Hsu, K. J., 1983. Late Cretaceous-Cenozoic magnetostratigraphic and biostratigraphic correlations of the South Atlantic Ocean: DSDP Leg 73. *Palaeogeography Palaeoclimatology Palacoccology*. 42,127- 149.

Pospichal, J.J., and Wise, S.W., Jr., 1990. Calcareous nannofossils across the K/T boundary, ODP Hole 690C, Maud Rise, Weddell Sea. In: Barker, P.F., Kennett, J.P., et al.(Eds.), Proceedings of the Ocean Drilling Program. Scientific Results. College Station Ocean Drilling Program, Texas. 113, 515–532.

Postuma, J.A., 1971. Manual of plantonic Foraminifera. Elseviers Publishing Company, Amsterdam. 1-420.

Premoli Silva, I., 1977. Upper Cretaceous-Paleocene magnetic stratigraphy at Gubbio, Italy II. Biostratigraphy. *Geological Society of America Bulletin* .88: 371-374.

Premoli Silva, I. and Sliter, W.V., 1995. Cretaceous planktonic foraminiferal biostratigraphy and evolutionary trends from the Bottaccione section, Gubbio, Italy. *Palaeontographia Italica* .82,1-85.

Prins, B., 1971. Speculations on relations, evolution and stratigraphic distribution of discoasters. *In*, Farinacci, A. (Eds.) Proceedings of the Second Planktonic Conference Roma *1970.* Edizioni Tecnoscienza, Rome. 2, 1017-1037.

Proto Decima, F., Medizza, F., Todesco, L., 1978. Southeastern Atlantic Leg 40 calcareous nannofossils. In: Bolli, H.M., Ryan, W.B.F., et al. (Eds.). Initial Reports of the Deep Sea Drilling Project. U.S. Government Printing Office, Washington 40, 571-634.

Püttmann, T., Linnert, C., Dölling, B., & Mutterlose, J., 2018. Deciphering Late Cretaceous (Cenomanian to Campanian) coastline dynamics in the southwestern Münsterland (northwest Germany) by using calcareous nannofossils: Eustasy vs local tectonics. *Cretaceous Research*. *87*, 174-184.

Radomski A., 1967. Some stratigraphical units based on nannoplankton in the Polish Outer Carpathians. *X Europejskie Kolokwium Mikropaleontologiczne w Polsce*.5, 385-393.

Razmjooei, M.J., Thibault, N., Kani, A., Mahanipour, A., Boussaha, M., Korte, C., 2014. Coniacian – Maastrichtian calcareous nannofossil biostratigraphy and carbon-isotope stratigraphy in the Zagros Basin (Iran): consequences for the correlation of Late Cretaceous Stage Boundaries between the Tethyan and Boreal realms. *Newsletters on Stratigraphy*. 47, 183–209.

Razmjooei, M.J., Thibault, N., Kani, A., Dinarès-Turell, J., Pucéat, E., Shahriari, S., Radmacher, W., Jamali, A.M., Ullmann, C.V., Voigt, S., Cocquerez, T., 2018. Integrated bio- and carbon-isotope stratigraphy of the Upper Cretaceous Gurpi Formation (Iran): A new reference for the eastern Tethys and its implications for large-scale correlation of stage boundaries. *Cretaceous Research*. 91, 312–340.

Razmjooei, M.J., Thibault, N., Kani, A., Dinarès-Turell, J., Pucéat, E., Chin, S., 2020a. Calcareous nannofossil response to Late Cretaceous climate change in the eastern Tethys (Zagros Basin, Iran). *Palaeogeography*, *Palaeoclimatology, Palaeoecology*. 538, 109418.

Razmjooei, M.J., Thibault, N., Kani, A., Ullmann, C.V., Jamali, A.M., 2020b. Santonian-Maastrichtian carbon-isotope stratigraphy and calcareous nannofossil biostratigraphy of the Zagros Basin: Long-range correlation, similarities and differences of carbon-isotope trends at global scale. *Global* and *Planetary Change*.184, 103075.

Reinhardt, P., 1965. Neue Familien für fossile Kalkflagellaten (Coccolithophoriden, Coccolithineen). *Monatsberichte der Deutschen Akademie der Wissenschaften zu Berlin*. 7,30-40.

Reinhardt, P., 1966. Zur Taxonomie und Biostratigraphie des fossilen Nannoplanktons aus dem Malm, der Kreide und dem Alttertiär Mitteleuropas. *Freiberger Forschungshefte*. C196, 5-109.

Rey, O., Simo, J. A., Lorente, M. A., 2004.A record of long- and short-term environmental and climatic change during OAE3: La Luna Formation, Late Cretaceous (Santonian-early Campanian), Venezuela. *Sedimentary Geology*.170, 85–105.

Robaszynski, F. and Caron, M., 1995. Foraminiferes planctoniques du Cretace; commentaire de la zonation Europe-Mediterranee. *Bulletin de la Société géologique de France*, 166, 6, 681-692.

Robaszynski, F., Caron, M., Dupuis, C., Amédro, F., Gonzalez Donoso, J.-M., Linares, D., Hardenbol, J., Gartner, S., Calandra, F., Deloffre, R., 1990. A tentative integrated stratigraphy in the Turonian of Central Tunisia: Formations, zones and sequential stratigraphy in the Kalaat Senan area. Bulletin du *Centre* de recherches Elf *Exploration Production Elf-Aquitaine*, 14, 213-384.

Rood, A. P., Hay, W. W., Barnard, T., 1971. Electron Microscope Studies of Oxford Clay Coccoliths. *Eclogae Geologicae Helvetiae*. 64,245-272.

Rood, A. P., Hay, W. W., Barnard, T., 1973. Electron microscope studies of Lower and Middle Jurassic coccoliths. *Eclogae Geologicae Helvetiae*. 66, 365-382.

Roth, P.H., 1973. Calcareous nannofossils. In: Winterer, E.L., Ewing, J.I., et al., (Eds.). Initial Reports of the Deep Sea Drilling Project. U.S. Government Printing Office, Washington. 17, 695–795.

Roth, P.H., 1978. Cretaceous nannoplankton biostratigraphy and oceanography of the northwestern Atlantic Ocean. In: Benson, W.E., Sheridan, R.E., et al., (Eds.), Initial Reports of the Deep Sea Drilling Project. U.S. Government Printing Office, Washington.44, 731–759.

Roth, P. H., and Bowdler J. L., 1981. Middle Cretaceous calcareous nannoplankton biogeography and oceanography of the Atlantic Ocean, *SEPM Special Publication*, 32, 517-546.

Roth, P.H., and Krumbach, K.R., 1986. Middle Cretaceous calcareous nannofossil biogeography and preservation in the Atlantic and Indian oceans: Implications for paleoceanography. *Marine Micropaleontology.* 10, 235–266.

Roth, P.H., and Thierstein, H., 1972. Calcareous nannoplankton: Leg 14 of the Deep Sea Drilling Project. In: Hayes, D.E., Pimm, A.C., et al. (Eds.). Initial Reports of the Deep Sea Drilling Project. U.S. Government Printing Office, Washington. 14, 421-485.

Russo, F., 2014. Calcareous nannofossil revised biostratigra-phy of the latest Albian-earliest Campanian time interval (late Cretaceous). PhD thesis, Università degli Studi di Milano.

Rutledge, D. and Bown, P. R., 1996. New names for old: taxonomic clarification of some Early Cretaceous nannofossil marker-species. *Journal of Nannoplankton Research*. 18(2), 53-59.

Sachse, V.F., Littke, R., Jabour, H., Schümann, T., Kluth, O., 2012. Late Cretaceous (Late Turonian, Coniacian and Santonian) petroleum source rocks as part of an OAE, Tarfaya Basin, Morocco. *Marine and Petroleum Geology*. 29, 35–49.

Schlanger, S.O. and Jenkyns, H.C.,1976. Cretaceous oceanic anoxic events: causes and consequences. *Geologie en Mijnbouw*.55, 179–194.

Scotese, C. R., 2016. PALEOMAP PaleoAtlas for GPlates and the PaleoData plotter program. Technical Report· February 2016, DOI: 10.13140/RG.2.2.34367.0016

Shamrock, J. L., Muñoz, E. J., Carter J. H., 2015. An improved sample preparation technique for calcareous nannofossils in organic-rich mudstones. *Journal of Nannoplankton Research*. 35, 101-110.

Shannon, C.E., Weaver, W., 1949. The Mathematical Theory of Communication. University of Illinois Press, Urbana. 125.

Sheldon, E., Ineson, J., Bown, P., 2010. Late Maastrichtian warming in the Boreal Realm: calcareous nannofossil evidence from Denmark. *Palaeogeography, Palaeoclimatology, Palaeoecology*. 295, 55-75.

Shumenko, S. I., 1968. Coccolithophorids as revealed by electron microscope. *Paleontologicheskiy Zhurnal*. 4, 464-470.

Sikora, P. J., Howe, R. W., Gale, A. S., & Stein, J. A.,2004. Chronostratigraphy of proposed Turonian-Coniacian (Upper Cretaceous) stage boundary stratotypes: Salzgitter-Salder, Germany, and Wagon Mound, New Mexico, USA. *Geological Society, London, Special Publications*, *230*(1), 207-242.

Singano, J.M., 2015. The Lindi Formation (upper Albian–Coniacian) and Tanzania Drilling Project Sites 36–40 (Lower Cretaceous to Paleogene): Lithostratigraphy, biostratigraphy and chemostratigraphy. *Journal of African Earth Sciences*.101, 282–308.

Sissingh, W., 1977. Biostratigraphy of Cretaceous calcareous nannoplankton. *Geologie en Mijnbouw*. 65, 37-65.

Sissingh, W., 1978. Microfossil biostratigraphy and stage-stratotypes of the Cretaceous. *Geologie* en *Mijnbouw*. 57, 433–440.

Sissingh, W.,1977. Biostratigraphy of Cretaceous calcareous nannoplankton. *Geologie en Mijnbouw*. 56, 37–65.

Sliter, W. V., 1992. Cretaceous planktonic foraminiferal biostratigraphy and palcoceanographic events in the Pacific Ocean with emphasis on indurated sediment. In: lshizaki. K. and Saito. T., (Ed.) Century of Japanese Micropaleomology, Tokyo. Terra Scientific Publishing Compant. 281-299.

Sliter, W.V.,1989. Biostratigraphic zonation for Cretaceous planktonic foraminifers examined in thin sections. *Journal of Foraminiferal Research*. 19, 1-19.

Stover, L. E., 1966. Cretaceous coccoliths and associated nannofossils from France and the Netherlands. *Micropaleontology*. 12(2), 133-167.

Stradner, H. & Steinmetz, J., 1984. Cretaceous calcareous nannofossils from the Angola Basin, Deep Sea Drilling Project Site 530. In: Hay, W.W., Sibuet, J.-C, et al., (Eds.), Initial Reports of the Deep Sea Drilling Project. U.S. Government Printing Office, Washington. 75, 565-649.

Stradner, H., 1961. Vorkommen von Nannofossilien im Mesozoikum und Alttertiär. *Erdoel-Zeitschrift*. 77(3), 77-88.

Stradner, H., 1962. Über neue und wenig bekannte Nannofossilien aus Kreide und Alttertiär. *Verhandlungen der Geologischen Bundesanstalt (Wien)*. 2, 363-377.

Stradner, H., 1963. New contributions to Mesozoic stratigraphy by means of nannofossils. Proceedings of the Sixth World Petroleum Congress. Section 1 Paper 4,167-183.

Stradner, H., and Steinmetz, J., 1984. Cretaceous calcareous nannofossils from the Angola Basin, Deep Sea Drilling Project Site 530. In: Hay, W.W., Sibuet, J.-C., et al. (Eds.). *Initial Reports of the Deep Sea Drilling Project.* U.S. Government Printing Office, Washington.75, 565-649.

Švábenická, L., 2012. Nannofossil record across the Cenomanian-Coniacian interval in the Bohemian Cretaceous Basin and Tethyan foreland basins (Outer Western Carpathians), Czech Republic. *Geologica Carpathica*.63, 201-217.

Švábenická, L., and Bubík, M., 2014. Biostratigraphical correlations of the calcareous nannofossil Marthasterites furcatus in the Bohemian Cretaceous Basin and Outer Flysch Carpathians, Czech Republic. *Cretaceous Research*. 51, 386-398.

Tantawy, A.A.A.M., 2003. Calcareous nannofossil biostratigraphy and paleoecology of the CretaceouseTertiary transition in the central Eastern Desert of Egypt. *Marine Micropaleontology*. 47, 323-356.

Tantawy, A. A. A., Keller, G., Pardo, A., 2009. Late Maastrichtian volcanism in the Indian Ocean: effects on calcareous nannofossils and planktic foraminifera. *Palaeogeography, Palaeoclimatology, Palaeoecology*. *284*(1-2), 63-87.

Tauxe, L., Tucker P., Petersen N. P., LaBrecque J. L., 1983. The magnetostratigraphy of leg 73 sediments: *Palaeogeography, Palacoclimalology, Palaeoecology*. 42. p. 65-90.

Tessin, A., Schröder-Adams, C., Elderbak, K., Sheldon, N.D., Hendy, I., 2019. Local versus seaway-wide trends in deoxygenation in the Late Cretaceous Western Interior Seaway. *GSA Bulletin*. 131, 1017–1030.

Thibault, N., 2010. Calcareous nannofossils from the boreal Upper Campanian- Maastrichtian chalk of Denmark. *Journal of Nannoplankton Research*. 31, 39-56.

Thibault, N., and Gardin, S., 2006. Maastrichtian calcareous nannofossil biostratigraphy and paleoecology in the Equatorial Atlantic (Demerara Rise, ODP Leg 207 Hole 1258A). *Revue de Micropaléontologie.* 49.199–214.

Thibault, N., Jarvis, I., Voigt, S., Gale, A. S., Attree, K., Jenkyns, H. C., 2016a. Astronomical calibration and global correlation of the Santonian (Cretaceous) based on the marine carbon isotope Record. *Paleoceanography*. 31, 847–865.

Thibault, N., Galbrun, B., Gardin, S., Minoletti, F., Le Callonnec, L., 2016b. The end-Cretaceous in the southwestern Tethys (Elles, Tunisia): orbital calibration of paleoenvironmental events before the mass extinction. *International Journal of Earth Sciences*.*105*(3), 771-795.

Thierstein, H.R.,1973. Lower Cretaceous calcareous nannoplankton biostratigraphy. *Abhandlungen der Geologischen Bundesandsalt*. 29, 1-52.

Thierstein, H. R., 1974. Calcareous nannoplankton - Leg 26, Deep Sea Drilling Project. In Davies, T. A., Luyendyk, B. P.,et al.,(Eds.), Initial Reports of the Deep Sea Drilling Project. U.S. Government Printing Office, Washington.26, 619-66

Thierstein, H. R., 1976. Mesozoic calcareous nannoplankton biostratigraphy of marine sediments. *Marine Micropaleontology*. 1,325-362.

Thierstein, H.R., 1981. Late Cretaceous nannoplankton and the change at the Cretaceous–Tertiary boundary. In: Warme, J.E., Douglas, R.G., Winterer, E.L. (Eds.), The Deep Sea Drilling Project: a decade of progress. *SEPM Special Publication*. Tulsa. 32. 355–394.

Tremolada, F., 2002. Aptian to Campanian calcareous nannofossils biostratigraphy from the Bottaccione section, Gubbio, central Italy. *Rivista Italiana di Paleontologia*

Varol, O., 1989. Quantitative analysis of the *Arkhangelskiella cymbiformis* group and its biostratigraphical usefulness in the North Sea area. *Journal of Micropalaeontology*. 8, 131-134.

Varol, O., 1991. New Cretaceous and Tertiary Calcareous Nannofossils. *Neues Jahrbuch für Geologie und Paläontologie, Abhandlungen*. 182, 211-237.

Varol, O., 1992. Taxonomic revision of the Polycyclolithaceae and its contribution to Cretaceous biostratigraphy. *Newsletters on Stratigraphy*. 27,93-127

Vekshina, V. N.,1959. Coccolithophoridae of the Maastrichtian deposits of the West Siberian lowlands. *Trudyi Instituta Geologii i Geogiziki, Sibiriskoe Otlodelenie, Akademiya Nauk SSSR (Nauka) Moscow*. 2,56-81.

Verbeek, J. W., 1976. Upper Cretaceous nannoplankton zonation in a composite section near El Kef, Tunisia. *Proceedings of the Koninklijke Nederlandse Akademie van Wetenschappen*. 79,129-148.

Verbeek, J. W., 1977. Calcareous nannoplankton biostratigraphy of Middle and Upper Cretaceous deposits in Tunisia, southern Spain and France. *Utrecht Micropaleontological Bulletin*. 16, 1-157.

Wagner, T., Sinninghe Damsté, J.S., Hofmann, P., Beckmann, B., 2004. Euxinia and primary production in Late Cretaceous eastern equatorial Atlantic surface waters fostered orbitally driven formation of marine black shales: euxinia Cretaceous. *Paleoceanography*.19.3.

Wagreich, M., 2009. Coniacian-Santonian oceanic red beds and their link to Oceanic Anoxic Event 3, in: Cretaceous Oceanic Red Beds: Stratigraphy, Composition, Origins, and Paleoceanographic and

Paleoclimatic Significance. In.: Hu, X., Wang, C., Scott, R. W., Wagreich, M., and Jansa, L. (Eds.), SEPM Special publications. 91, 235–242.

Wagreich, M., 2012. " OAE 3"-regional Atlantic organic carbon burial during the Coniacian-Santonian. *Climate of the Past*. 8(5), 1447.

Wagreich, M., Summesberger, H., Kroh, A., 2010. Late Santonian bioevents in the Schattau section, Gosau Group of Austria – implications for the Santonian–Campanian boundary stratigraphy. *Cretaceous Research*. 31, 181–191

Walaszczyk, I., Lees, J. A., Peryt, D., Cobban, W. A., & Wood, C. J., 2012. Testing the congruence of the macrofossil versus microfossil record in the Turonian–Coniacian boundary succession of the Wagon Mound–Springer composite section (NE New Mexico, USA). *Acta Geologica Polonica*.62, 581-594.

Wang, C. and HU, X., 2005.Cretaceous world and oceanic red beds: *Earth Science Frontiers*.12, 11–21.

Wang, C., Hu, X., Huang, Y., Wagreich, M., Scott, R., Hay, W., 2011. Cretaceous oceanic red beds as possible consequence of oceanic anoxic events. *Sedimentary Geology*. 235, 27–37

Watkins, D. K., 1992. Upper Cretaceous nannofossils from Leg 120, Kergeulen Plateau, Southern Ocean. In: Wise, S.W., Jr., Schlich, R., et al., 1992 (Eds.), Proceedings of the Ocean Drilling Program, Scientific Results. College Station Ocean Drilling Program, Texas. 120,343-370.

Watkins, D. K. and Bergen, J. A., 2003. Late Albian adaptive radiation in the calcareous nannofossil genus *Eiffelithus*. *Micropaleontology*. 49(3),231-252.

Watkins, D.K., Wise, S.W., Jr., Pospichal, J.J., Crux, J., 1996. Upper Cretaceous calcareous nannofossil biostratigraphy and paleoceanography of the Southern Ocean. In: Moguilevsky, A., and Whatley, R. (Ed.), *Microfossils and Oceanic Environments.* Aberystwyth Press, University of Wales.355-381.

Watkins, D.K., Shafik, S., Shin, I., 1998. Calcareous nannofossils from the Cretaceous of the Deep Ivorian Basin. In: Mascle, J., Lohmann, G.P., and Moullade, M. (Eds.). Proceedings of the Ocean Drilling Program, Scientific Results. College Station Ocean Drilling Program, Texas.159, 319-333.

Watkins, D.K., Self-Trail, J.M., 2005. Calcareous nannofossil evidence for the existenc of the Gulf Stream during the late Maastrichtian. *Paleoceanography*.20

Weissert H. and Erba E., 2004. Volcanism, CO2 and palaeoclimate: A Late Jurassic–Early Cretaceous carbon and oxygen isotope record. *Journal of the Geological Society*, 161: 695-702.

Weissert H., Lini A., Föllmi K.B., Kuhn O., 1998. Correlation of Early Cretaceous carbon isotope stratigraphy and platform drowning events: a possible link?. *Palaeogeography, Palaeoclimatology, Palaeoecology,* 137:,189-203.

Wind, F. H., 1979. Maestrichtian-Campanian nannoflora provinces of the southern Atlantic and Indian oceans, in Deep Sea Drilling Results in the Atlantic Ocean: Continental Margins and Paleoenvironment. M. Talwani, W. W. Hay, and W. B. F. Ryan (Eds.), Maurice Ewing Ser. AGU, Washington, D. C., 3,123 – 137.

Wise, S. W., 1983. Mesozoic and Cenozoic calcareous nannofossils recovered by DSDP Leg 71 in the Falkland Plateau region, Southwest Atlantic Ocean.In: Ludwig, W. J., Krasheninnikov, V. A., et al., Initial Reports of the Deep Sea Drilling Project. U.S. Government Printing Office. 71,481-550.

Wise, S. W. and Wind, F. H., 1977. Mesozoic and Cenozoic calcareous nannofossils recovered by DSDP Leg 36 drilling on the Falkland Plateau, south-west Atlantic sector of the Southern Ocean. In:

Barker, P. F., Dalziel, I.W.D. et al., 1976 (Eds.). InitialReports of the Deep Sea Drilling Project. U.S. Government Printing Office, Washington.36, 269-492.

Wolfgring, E., Wagreich, M., Dinarès-Turell, J., Yilmaz, I.O., Böhm, K., 2018. Plankton biostratigraphy and magnetostratigraphy of the Santonian–Campanian boundary interval in the Mudurnu–Göynük Basin, northwestern Turkey. *Cretaceous Research*. 87, 296–311.

Worsley, T.R., 1971. Calcareous nannofossil zonation of Upper Jurassic and Lower Cretaceous sediments from the Western Atlantic. *Proceedings II Planktonic Conference* (Roma, 1970), p. 1301-1322.

Wyton, J., Bown, P. R., and Bailey, H., 2007. Palaeoecological trends in Turonian-Coniacian (Late Cretaceous) calcareous nannofossils from Chalk Group sections, SE England. *Journal of Nannoplankton Research*. 29, 31-37.

Young, J. R. and Bown, P. R., 1997. Proposals for a revised classification system for calcareous nannoplankton. *Journal of Nannoplankton Research*. 19, 15-47.

Appendix 1

Systematic Paleontology

Kingdom **CHROMISTA** Cavalier-Smith, 1981
Division (Phylum) **HAPTOPHYTA** Hibberd *ex* Cavalier-Smith, 1986
Class **PRYMNESIOPHYCEAE** Hibberd, 1976
Subclass **PRYMNESIOPHYCIDAE** Cavalier-Smith, 1986

This chapter is dedicated to the taxonomic analysis and discussion of genera used as markers in Upper Cretaceous biozonations (Sissing, 1977 as modified by Perch-Nielsen, 1985; Roth, 1978; Bralower at al., 1995 and Burnett, 1998), specifically for the Turonian – Campanian time interval.

Heterococcoliths

Order Arkhangelskiales
Bown & Hampton in Young and Bown (1997)

This order includes placoliths composed by 3 -5 tiers or "shields". The central area can be filled by different structures such as: transverse bars, proximal net, axial or near-axial crosses and perforate plates with axial sutures. The order *Arkhangelskiales* comprises two families, *Arkhangelskiellaceae* and *Kamptneriaceae*. Figure 1 illustrates the main criteria used in this study to distinguish the different genera within this order.

Family Arkhangelskiellaceae Bown & Hampton, 1997 *in* Bown & Young, 1997

Tiered coccoliths with the rim that is bright under cross polarized light. The rim can be monocyclic (*Arkhangelskiella*) or bicyclic (*Aspidolithus*; *Broinsonia*; *Thiersteinia)*. The central area is spanned by axial crosses and/or perforated plates.

Genus ***Arkhangelskiella*** Vekshina, 1959
Type-species: *Arkhangelskiella cymbiformis* Vekshina, 1959

Family	*Arkhangelskiellaceae*				*Kamptneriaceae*	
Genera	*Arkhangelskiella*	*Aspidolithus*	*Broinsonia*	*Thiersteinia*	*Gartnerago*	*Kamptnerius*
Shape	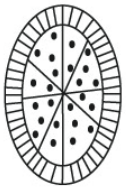	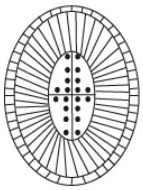	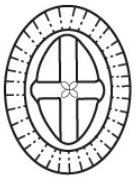	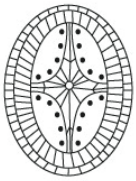		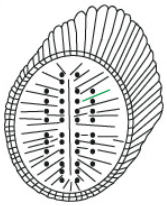
Margin	Monocyclic (Radial)	Bicyclic (Radial)	Bicyclic (Radial)	Bicyclic (Radial)	Tricyclic (Tilted)	Tricyclic
Cross	No	No	Yes	Yes	No	No
Plates	Yes	Yes	No	Yes	Yes	Yes
Perforations	Yes	Yes	No	Yes	Yes	Yes
Flange	No	No	No	No	No	Yes

Figure 1 - The different genera belonging to Arkhangelskiales and their main characteristics.

Description: Elliptical coccolith with a monocyclic rim and a central area filled by perforated plates divided into four segments aligned with the major and minor axes. Each of the four segments is in turn subdivided in two wedge-shaped portions of different size. The larger of each quarter show strong birefringence with a characteristic pattern that resembles the blades of a windmill.

Remarks: At polarizing light microscope *Arkhangelskiella* shows a bright unicycle rim. In proximal view a discontinuity line between the distal shield (wider) and the proximal shield (smaller) is sometimes appreciable.

In the past, the number of plate pores was used to distinguish between *A. cymbiformis* and *A. specillata* (Veskhina, 1959; Prins and Sissingh, 1977; Perch-Nielsen, 1985). However, the perforations are visible only in well-preserved specimens, hampering discrimination between these two species. More recently, Varol (1989) suggested to use the rim width to discriminate between the different species of *Arkhangelskiella*. He distinguished three different morphotypes of *A. cymbiformis* termed as follow: var. N (rim width < 2µm), var. NT (rim width 1-1.5 µm) and var. W (rim width ≥2 µm).

Burnett (1997) separated these same species according to the rim width and coccolith dimensions as follows: *A. confusa (*rim width 1-1.5 µm; length <8 µm); *A. cymbiformis* (rim width <1µm; length >8 µm) and *A. maastrichtiensis* (rim width >1.5µm; length >10 µm). Subsequently, Thibault (2010) emended Varol's definitions with the introduction of a new morphotype. He distinguished between var. N (rim width <1.5µm; length 6-8.5 µm); var. SW (rim width >1.5µm; length 8.5-11 µm); var. W *(*rim

width >1.7µm; length >11 µm) var. NT *(*rim width <1.5µm; length <11 µm; rim width <1.7µm; length 11 µm to 14.5 µm). According to Thibault (2010) this last morpohotype could correspond to *A. specillata* due to the presence of a wide central area and a thin rim.

In contrast, Linnert & Mutterlose (2009) found difficult to discriminate between the different group of *A. cymbiformis* and suggested that all specimens are part of a continuous morphometric cluster belonging to *A. cymbiformis.*

A taxonomic revision of this genus should include specimens from the entire stratigraphic range, in order to evaluate its evolution thought time. In this this work I follow the subdivision of Burnett (1997) as summarized in Figure 2.

Arkhangelskiella	SEM-LM (not in scale)	Schematic sketch	Dimensions	Rim/Margin	Stratigraphic Range
A. confusa	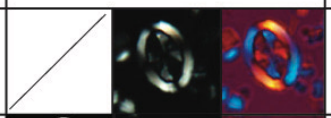		L < 8 µm	< 1.5 µm	Coniacian Maastrichtian
A. cymbiformis	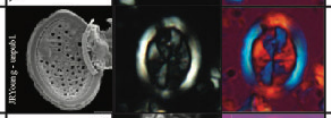		L >8 µm	< 1.5 µm	Campanian Maastrichtian
A. maastrichtiensis	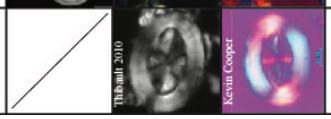		L > 10 µm	> 1.5 µm	Campanian Maastrichtian

Figure 2 - *Arkhangelskiella* species: LM and SEM images, diagnostic features. Some photos are from Nannotax3 website (http://www.mikrotax.org/Nannotax3) and Thibault (2010)

Arkhangelskiella confusa Burnett, 1997

Description: A species of *Arkhangelskiella* with a total length of the coccolith < 8 µm and a margin/rim width < 1.5 µm.

Remarks: *A. confusa* is considered here as a synonymous of *A. cymbiformis* var. N of Varol (1989) and *A. cymbiformis* var. N of Thibault (2010).

Size: length 5.5 -7 µm; width 4-5 µm.

Arkhangelskiella cymbiformis Vekshina, 1959

Description: A species of *Arkhangelskiella* with a total length of the coccolith > 8 µm and a margin/rim width < 1.5 µm.

Remarks: *A. cymbiformis* is considered here as a synonymous of *A. specillata* of Vekshina (1959) and *A. cymbiformis* var NT of Varol (1989).

Size: length 8-10 μm; width 6-7 μm.

Arkhangelskiella maastrichtiensis Burnett, 1997

Description: A large species of *Arkhangelskiella* with a total length of the coccolith > 11 μm and e wide margin/rim width > 1.5 μm.

Remarks: *A. maastrichtiensis* is considered here as a synonymous of *A cymbiformis* var. W of Varol (1989) and *A cymbiformis* var. W of Thibault (2010).

Size length >10μm; width 8 μm.

The following description of genus *Aspidolithus* and that of species *Aspidolithus parcus constrictus*, *A. parcus expansus* and *A. parcus parcus* are taken from Miniati et al., 2020 reported in Appendix (23)

Genus **Aspidolithus** Noël, 1969

Type-species: *Aspidolithus angustus* Noël, 1969.

Description: Elliptical coccolith with a tired bicyclic rim and a central area filled by perforated plates with axial sutures. At polarizing light microscope, the inner and outer cycles of the rim are visible in distal view, whereas in proximal view only the outer cycle in visible. At crossed nicols, the inner cycle appears brighter than the outer cycle.

Remarks. In this work, we follow Lauer (1974), Prins in Perch Nielsen (1979) and Perch-Nielsen (1985) and, accordingly, genus *Aspidolithus* is differentiated from genus Broinsonia due to the presence of plates instead of a cross in the central area. Within the *Aspidolithus* lineage, the subsequent appearances of *A. parcus expansus*, *A. parcus parcus* and *A. parcus constrictus* are marked by a gradual reduction of the central area/margin ratio as described by Wise (1983).

The differences between the genus *Aspidolithus* and *Broinsonia* are showed in Figure 3. The main characters useful for distinguishing the different species of *Aspidolithus parcus* at light microscope (LM) are illustrated in Figure 4.

Aspidolithus enormis Shumenko, 1968

Description: Medium-sized *Aspidolithus* with a thin outer distal cycle and a wider and brighter inner cycle. The central area is filled by imperforated plates with axial sutures. At LM the outer rim appears thinner and less birefringent compared to the thicker and brighter inner cycle.

Remarks: *A. enormis* is generally assigned to genus *Broinsonia*, but in this work, I prefer to include *A.*

enormis in the *Aspidolithus* group due to the presence of plates instead of a cross in the central area. *A. enormis* is considered here as a synonymous of *Aspidolithus angustus of* Noel (1969) and *Broinsonia bevieri* of Bukry (1969).

Size: lenght 7-8µm; width 5 µm.

	Family	Arkhangelskiellaceae	
	Genus	*Aspidolithus*	*Broinsonia*
	Schematic sketch (not in scale)	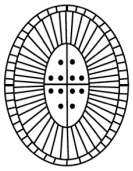	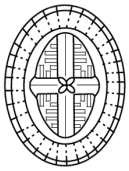
	Margin	Bicyclic (Radial)	Bicyclic (Radial)
Central area structures	Cross	No	Yes
	Plates	Yes	No
	Perforations	Yes	No

Figure 3 - Illustration of diagnostic characters (distal view) for separating genera *Aspidolithus* and *Broinsonia* (after Miniati et al., 2020).

Aspidolithus parcus constrictus (Hattner et al.,1980) Perch-Nielsen, 1984

1980 *Broinsonia parca constricta* – Hattner, Wind and Wise, p. 23; Plate 2, Figs 1-3, 5-8.

1984 *Aspidolithus parcus constrictus* – Perch-Nielsen, p. 43.

Remarks: A subspecies of Aspidolithus parcus with a small central area spanned by a perforated plate divided by axial sutures. One to three perforations per quadrants lie parallel to the major axis. The width of the central area is small compared to the shield margin and have a width equivalent or less than the shield margin (b/a ratio ≤1). *A. parcus constrictus* evolved during the early Campanian from *A. parcus parcus* and represents the youngest subspecies in the *Aspidolithus* lineage.
Specimens with the same b/a ratio but a total length <10 µm were considered as "small" A. parcus constrictus by Gardin et al. (2001). Wolfgring et al. (2018), instead, considered small the specimens with a total length <9 µm. Both papers outline an increase in size in younger levels.
In the studied Bottaccione section (Miniati et al., 2020) *A. parcus constrictus* specimens display a total length varying between 8 and 10.3 µm with no correlation with the stratigraphic position.

Aspidolithus parcus expansus (Wise and Watkins in Wise, 1983) Perch-Nielsen, 1984

1983 *Broinsonia parca expansa* – Wise and Watkins in Wise, p. 506; plate 9, Figs. 1-5; plate 10, Figs. 5-9; Plate 11, Figs. 1-9.

1984 *Aspidolithus parcus expansus* – Perch-Nielsen, p. 43.

Remarks: A subspecies of *Aspidolithus parcus* with a wide central area spanned by a perforated plate divided by axial sutures. Central area perforations lie parallel to the ellipse axes. The width of the central area is approximately twice or more than twice the width of the shield margin (the b/a ratio is ≥2). *A. parcus expansus* represents the oldest subspecies belongings to the *Aspidolithus parcus* lineage starting in the late Santonian (Wise 1983; Perch-Nielsen 1985). Specimens with this b/a ratio but a total length <10 μm or <9 μm were considered as "small" *A. parcus expansus* by Gardin et al (2001) and Wolfgring et al. (2018), respectively. The specimens observed in the studied Bottaccione section have a length variable between 9 and 12.3 μm. In the lowermost part of the subspecies range (latest Santonian) specimens are rather small (coccolith length of 10–10.2 μm) and co-occur with "small" *A. parcus expansus* (coccolith length varying between 9 and 9.9 μm) from just prior to the Santonian-Campanian boundary. The coccolith length increases in the earliest Campanian as testified by presence of some relatively large specimens (total length of 11–12.3 μm) together with small specimens (length varying between 9.5 and 9.9 μm) through the rest of the studied interval.

Corbett et al. (2014) use the FO of *Broinsonia furtiva* instead of FO of *Aspidolithus/Broinsonia parcus expansus* as biostratigraphic markers for the UC9c subzone (late Turonian-Coniacian). The specimens documented by Corbett et al. (2014) as *Broinsonia furtiva* show the occurrence of an evident cross in its central area (Plate 2, figure E) without the presence of visible plates. Thus, the assignment to *Broinsonia* instead to Aspidolithus was in this case correct.

However, the specimens observed in this study from the late Turonian-Coniacian assemblages are ultrastructurally similar to diagnostic description of *A. parcus parcus* but are definitively smaller and with a thinner outer cycle compared to Santonian – Campanian specimens. Moreover, the late Turonian-Coniacian "*A. p expansus"* is found to be rarer and discontinuous, whereas the Santonian –Campanian larger (= normal) specimens are more abundant and continuous in the assemblages. For example, in the Seaford Head section, the late Turonian – Coniacian *A. p. expansus* specimens are of about 8.5-9.5 μm in length and show a thinner outer cycle compared to the Santonian –Campanian *A. p expansus* specimens that are of about 10 μm length with a thicker outer cycle.In this study, the specimens of *A. p expansus* with a length <10 μm was termed as "small *A. p expansus*" and distinguished from the larger (= normal) of *A. p expansus* with a length >10 μm.

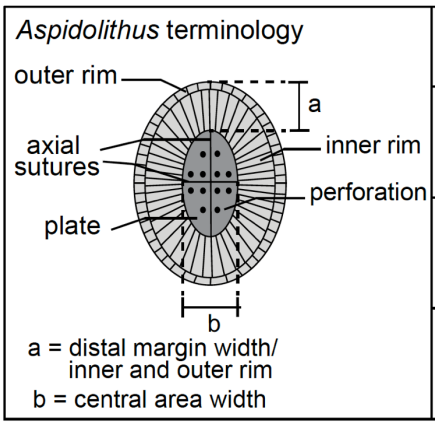

Aspidolithus parcus subspecies	Schematic sketch (not in scale)	central area (b) / distal margin (a) ratio	Dimensions holotype (µm) length	width
A. parcus constrictus		b/a ≤ 1	10.6	8.3
A. parcus expansus		b/a ≥ 2	9.5	6.2
A. parcus parcus		1<b/a<2	12.2	9.4

Figure 4 - Schematic morphological characters (distal view) and their terminology of Aspidolithus specimens. Aspidolithus parcus subspecies are typified by the b (central area width)/a (distal margin width) ratio. The dimensions of length and width of the holotypes are reported (after Miniati et al., 2020).

Aspidolithus parcus parcus (Stradner, 1963) Noël, 1969

1963 *Arkhangelskiella parca* – Stradner, p. 10; Plate 1, Figs. 3, 3a.

1969 *Aspidolithus parcus* – Noël, p. 196; Plate 1, Figs. 3, 4.

Remarks. A subspecies of *Aspidolithus parcus* with a central area spanned by a perforated plate divided by axial sutures. Central area perforations lie parallel to the ellipse axes. The width of the central area is approximately between one to two times the width of the shield margin (b/a ratio between 1 and 2). In the latest Santonian, *A. parcus parcus* evolved from *A. parcus expansus* with a reduction of the central area width. Specimens with this b/a ratio but a total length <10 µm were considered as "small" *A. parcus parcus* by Gardin et al. (2001); Wolfgring et al. (2018), instead, considered small the specimens with total length <9 µm. Both studies outline an increase in size upwards. In the studied Bottaccione section *A. parcus parcus* specimens have a length varying between 9.5 and 11.8 µm, with a general increase in coccolith length upwards in analogy to previous records (Gardin et al. 2001; Wolfgring et al. 2018). However, in the lowermost part of its range (latest Santonian), the coccolith length varies between 10 µm and 10.2 µm, thus, within the size range of *A. parcus parcus* (≥10 µm, following Gardin et al. 2001) although very close to the lower limit of size range. A single specimen with total length of 9.6 µm (small *A. parcus parcus*) was observed in this interval. A minor increase in length size (10.5–11.7 µm) of *A. parcus parc*us coccoliths is observed in the lower Campanian; these specimens co-occur with small *A. parcus parcus* coccoliths with length varying from 8.4 to 9.9 µm.

Genus ***Broinsonia*** Bukry, 1969

Type-species: *Broinsonia dentata* Bukry, 1969

Description: Elliptical coccolith with a tired bicyclic rim and a central area spanned by an axial cross. The arms of the cross are parallel to the major and the minor axes of the ellipse and divide the central area into empty quadrants that can be filled by lateral bars or a net/grill. At LM, in distal view an inner and an outer cycle are visible in the rim. In proximal view only the outer cycle is visible.

Remarks: In poorly preserved specimens at LM the central area structures can be obliterated by overgrowth and appear like plates, while the bars and grill appear as a perforation. The main character useful for distinguishing the different species of *Broinsonia* at LM are showed in Figure 5.

Broinsonia dentata Bukry, 1969

Description: a species of *Broinsonia* having the central area quadrants characterized by the presence of bars (processes). The single bars arise from the arms of the cross and goes toward the rim. The number of bars in each quadrant is 4 to 6.

Size: length 6-10 µm; width 7 µm.

Broinsonia ethmoquadrata Bukry, 1969

Description: a species of *Broinsonia* having the central area quadrants characterized by the presence of a grill/or net.

Size: length 5-7 µm; width 7 µm.

Broinsonia	SEM-LM (not in scale)	Schematic sketch	Diagnostic features	Stratigraphic Range
B. dentata	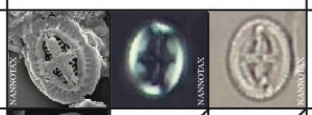		axial cross with lateral bars.	Campanian
B. ethmoquadrata			axial cross with net.	Campanian
B. furtiva			axial cross with lateral bars that simulate perforatins.	Turonian Santonian
B. matalosa	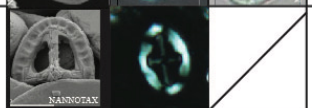		axial cross with open quadrants thicker margin compare to *B. signata*. The cross is composed of two pieces easily recognizable in LM image.	Valanginian Campanian
B. signata			axial cross with open quadrants,each bar of the cross is composed of two pieces easily recognizable in LM image.	Aptian Maastrichtian
B. verecundia			small (<6µm) elongate species with lozenge-like central body and lateral bars.	Campanian Maastrichtian

Figure 5 - *Broinsonia* species: LM and SEM images and their diagnostic features. Some photos are from Nannotax3 and Calcite Palace website (http://www.mikrotax.org/Nannotax3),Wise and Wind (1977) and Noël (1969).

Broinsonia furtiva (Bukry, 1969) Hattner, Wind and Wise 1980

Description: Species of *Broinsonia* whit a central area spanned by an axial cross parallel to the axes of the ellipse dividing the central area in four empties quadrants. These last are filled by lateral bars that can eventually join together to simulate perforations. The thickness of the bars depends to the degree of preservation.

Size: length 7µm; width 5.5 µm.

Broinsonia matalosa (Stover, 1966) Burnett in Gale et al., 1996

Description: a species of *Broinsonia* whit a central area spanned by an axial cross and wide-open quadrants. At the center of the cross a spine or boss can be present. The tips of the cross expand at the rim. A band of variable width surrounds the central area next to the rim, it is generally narrower at the expanded ends of the crossbars. At LM, under cross nicols, the cross appears composed of two pieces with different crystallographic orientation.

Size: length 7-11 µm; width 6-9 µm.

Broinsonia signata (Noël, 1969) Noël, 1970

Description: a species of *Broinsonia* with a central area spanned by an axial cross and open quadrants. As in *B. matalosa*, a band of variable width surrounds the central area next to the rim. It is generally narrower at the expanded ends of the crossbars.

Remarks: Compared to *B. matalosa*, in *B. signata* the quadrants are less opened due to the greater thickness of the central area band.

Size: length 5-9 µm; width 7 µm.

Broinsonia verecundia Wind and Wise in Wise and Wind, 1977

Description: Small *Broinsonia* (generally less than 4 µm) characterized by the presence of platform, instead of a cross, in the central area. The platform is connected to the rim by four larger axial/sub-axial bars and smaller spines.

Size: length 5-6 µm; width 3-4 µm width.

Genus ***Thiersteinia*** Wise and Watkins in Wise, 1983

Type species: *Thiersteinia ecclesiastica* Wise and Watkins *in* Wise, 1983

Description: Elliptical coccolith with a tired bicyclic rim (similar to *Aspidolithus*) and a perforated central area. The central area is spanned by a cross, with the arms parallel to the major and minor axes of the ellipse (Figure 1). The cross supports a spine composed of thin, lath-like crystals.

Thiersteinia ecclesiastica Wise and Watkins *in* Wise, 1983

Description: a species of *Thiersteinia that shows, in cross nicols, a high birefringent cross when rotated* of 22.5° to the polarizing direction and low birefringence when rotated of 22.5° to the opposite direction. Parallel to the major and minor axes of the crossbar, 3 to 5 perforations are presents. The outer distal margin is about 1/3 to 1/4 wider than the inner distal margin. The width of the central area is about 2.5 times the width of the distal margin (b/a ratio= 2.5).

Size: length 8-10 µm; width 6-8µm.

Family Kamptneriaceae Bown and Hampton, 1997 *in* Bown and Young, 1997

Coccoliths composed of a three-tiered rim and a central area. The rim appears, at cross polarized light, composed of a narrow dark outer cycle, a characteristic bright median cycle and a dark inner cycle. The central area is spanned by transverse bar, crossbars or plate, usually perforated that appear dark at light microscope (LM).

Genus ***Gartnerago*** Bukry, 1969

Gartnerago	SEM-LM (not in scale)	Schematic sketch	Diagnostic features	Stratigraphic Range
G. clarusora	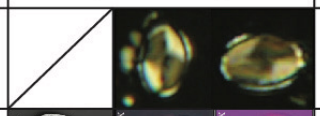		Central area filled by four equal size plates separated by axial suture. The shiled have a low birefringence compere to the more bright median cycle.	Turonian Santonian
G. costatum			G. costatum differs from G. segmentatum in having a single row of perforations along either side of the axials sutures	Santonian Campanian
G. magaritatus			The central plate of G. magaritatus contain an axial cross slightly offset from the major axies.	Coniacian Santonian
G. obliquum	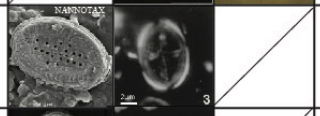		Narrow rim and a broad central area, filled with a plate with pores(~>10 in each quadrant). The plate is crossed by sutures, the transverse of which is slightly oblique.	Cenomanian Coniacian
G. segmentatum	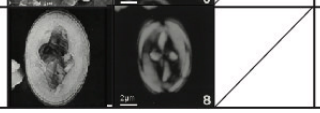		Central area filled with plate separated by axial sutures.*G. segmentatum* is the only species belongings to this group to have an imperforate plate.	Cenomanian Maastrichtian

Figure 6 - *Gartnerago* species: LM and SEM images, their diagnostic features. Photos are from Nannotax3 and Calcite Palace websites, Blair and Watkins (2009), Burnett (1998) and Thierstein (1974).

Type species: *Gartnerago segmentatum* (Stover, 1966)

Desciption: Elliptical coccolith composed of a set of 4 to 5 appressed rim tiers and a central area covered by plates. The shield is convex and divided into quadrants by subaxial sutures. Aligned to the subaxial sutures a row of perforations is presents. The sutures between the elements of the rims are inclined as show in Figure 1. At LM, *Gartnerago* shows a distinctive tricyclic rim shape with a dark outer-cycle, a characteristic bright median cycle and a dark inner cycle.

Remarks: *Gartnerago* differs from the other genera of Arkhangelskiellids in having a great number of elements for each tier separated by inclined sutures. At LM *Gartnerago* is less birefringent compared to *Aspidolithus* and *Broinsonia*. Compared to *Kamptnerius*, *Gartnerago* lacks a flange. The main characters useful for distinguish the different species of *Gartnerago* at LM are illustrated in Figure 6.

Gartnerago segmentatum (Stover, 1966) Thierstein, 1974

Description: a species of *Gartnerago* with a medium width rim and a central area filled by an imperforated plate. The sutures are aligned with the major axes of the ellipse. At cross-polarized light, at about 45°, the central area is divided into eight radially arranged, wedge-shaped blocks alternatively light and dark. The orientation of the bright wedges is to the right when the distal side is observed, and to the left when viewed proximally.

Remarks: *G. segmentatum* is the only species belonging to this genus to have an imperforated plate.

Size: length 9-12 μm; width: 4.0 μm.

Gartnerago obliquum (Stradner, 1963) Noël, 1970

Description: a species of *Gartnerago* with a narrow rim and a large central area filled by a plate with numerous perforations. The plate is crossed by sutures, one of them is parallel to the main axis of the ellipse while the other is slightly oblique.

At cross-polarized light, at about 45°, the central area is divided into eight radially arranged, wedge-shaped blocks alternatively bright and dark.

Remaks: *G. obliquum* differs from *G. segmetatum* in having an oblique suture.

Size: length 6-13 μm.

Gartnerago clarusora Varol, 1991

Description: a species of *Gartnerago* with a central area spanned by four equally sized plates separated by axial sutures. At LM, *G. clarusora shows the characteristic* tricyclic rim shape of *Gartnerago* with a dark outer-cycle, a strongly birefringence median cycle and a dark inner cycle.

Remaks: *G. clarusora* was documented by Varol (1991) in Turonian sediments of South America. More recently, Blair and Watkins (2009) found rare specimens of *G. clarusora* in Coniacian-Santonian sediments of the Western Interior Basin.
Size: length 4-6 μm.

Gartnerago margaritatus Blair and Watkins, 2009
Description: a species of *Gartnerago* with a narrow rim, and a central plate that contains a thin axial cross. The crossbars are slightly offset from the major and minor axes of the coccolith. At LM the proximal rim appears very thin and dark, whereas the median cycle is very bright. The distal rim is low birefringent in LM.
Remaks: *G. margaritatus* was described by Blair and Watkins (2009) from Coniacian-Santonian sediments of the Western Interior Basin. *G. marginatus* differs from other species of *Gartnerago* due to the reduced dimensions and the presence of an axial cross.
Size: length 5.5 μm; width 4 μm.

Gartnerago costatum (Gartner, 1968) Bukry, 1969
Description: a species of *Gartnerago* with a narrow rim and a broad central area. A row of perforations is present along the longitudinal and transversal sutures of the central area. When view in cross-polarized light, at about 45°, the central area is divided into eight radially arranged, wedge-shaped blocks alternatively light and dark. When *G. costatum is* observed in distal view the light wedge-shaped blocks are on the right of the axial suture, the opposite when it is observed in proximal view (Smith, 1981).
Remaks: *G. costatum* differs from *G. segmentatum* in having a single row of perforations along either side of the longitudinal and transversal sutures of the central area (Smith, 1981).
Size: length 7-12 μm.

Genus ***Kamptnerius*** Deflandre, 1959
Type-species: *Kamptnerius magnificus* Deflandre, 1959
Description: Elliptical placoliths with a rim composed by three cycles and a perforated central area. Sutures are present across the central area. At LM the rim appears with a diagnostic pattern: a narrow dark outer-cycle, a bright median-cycle and a dark inner-cycle. Also, the central plate appears dark at LM. An asymmetrical flange develops in continuity with the distal cycle of the rim, it is composed by elongated narrow elements (Figure 1).

Kamptnerius magnificus Deflandre, 1959

Description: a species of *Kamptnerius* characterized by a wide central area, three narrow rim cycles and a broad asymmetrical flange. The central area is concave with a medial suture along the main axis of the ellipse.

Remarks: The different specimens observed show a variable length of the flange. The flange can be larger or smaller than the length of the coccolith. In poorly preserved specimens the flange can be broken or absent.

Size: length 8-20 μm; width 8-12 μm.

Order Eiffellithales

Rood, Hay & Barnard, 1971

This order includes elliptical muroliths with a high wall-like rim composed by two cycles (V-unit and R-unit) and a central area spanned by different structures. The distal/outer cycle (V-unit) consists of clockwise imbricated elements. However, these features are distinguishable only in SEM images. The term loxolith is applied to this rim structure (Bown, 1987).

Family Chiastozygaceae (Rood, Hay and Barnard, 1973) Varol and Girgis, 1994

Unicyclic or bicyclic loxoliths characterized by a variably-developed proximal/inner cycle and a central area spanned by crossbars with an axial, non-axial or diagonal disposition, or a single transverse bar formed by fused bars.

Genus ***Amphizygus*** Bukry, 1969

Type species*: Amphizygus brooksii*

Description: Muroliths composed by a bicyclic rim, and a central area spanned by a traverse bar. The second cycle of the rim is visible only in proximal view while in distal view the rim appears monocyclic. The traverse bar, supporting a central stem, is made of rods that continue around the inner edge of the rim and ring the central area delineating two circular perforation. At LM, *Amphizygus* show general low birefringence with a characteristic yoke cycle of elements that surround the central openings.

Remarks: The different species of *Amphizygus* are distinguished at LM mainly according to the width of their perforations. Other useful criteria are the thickness and the optical behaviour of the proximal and distal rims, and the diameter of the specimens as show in Figure 6.

Amphizygus brooksii brooksii Bukry, 1969

Description: a subspecies of *A. brooksii* with a bicyclic rim, a central area with two perforations and a transverse bar. At LM, the rim appears monocyclic in distal view while bicyclic in proximal view. The two perforations have a distinctive yoke-cycles and traverse that can support a stem.

Remarks: *A. brooksii brooksii* differs from *A brookssi nanus* for its wider perforations that occupy about the 30% of the total coccolith width.

Size: length maximum 8μm.

Amphizygus brooksii nanus Bukry 1969

Description: a subspecies of *A. brooksii* with reduced perforations, equivalent to about 15% of the total length of the coccolith.

Size: length 8-9 μm.

Amphizygus megalops Blair & Watkins 2009

Description: a species of *Amphizygus* with a bicyclic rim, and a central area occupied by two symmetrical openings and a transverse bar. The distal rim is narrow (<1 μm) and with low birefringence at crossed nicols. The proximal rim is thin and birefringent at crossed nicols. The circular openings (perforations) are wide and cover about 42% of the total coccolith width. The transverse bar is composed of four elements and support a central knob or short spine.

Remarks: *A. megalops* differs from other *Amphizygus* species due to the size of the openings, the thickness of the distal and proximal cycles and the birefringence of the proximal cycle.

A. megalops is considered a synonymous of *Gartnerago coxalliae* by Lees (2017). However, according to the original description of Blair & Watkins (2009) in *A. megalops* the rim is bicyclic as in *Amphyzygus* and not tricyclic as in *Gartnerago*. Thus, in this study *A. megalops* is included in *Amphizygus* and not in *Gartnerago*. The FO of *A. megalops* was reported close to the Coniacian/Santonian stage boundary in the Western Interior Basin by Blair & Watkins (2009).

Size: length 6 μm; width 4 μm.

A. minimus Bukry, 1969

Description: Small *Amphizygus* with a maximum length of 4.6 μm. No evidence of a stem is present on the traverse bar. In *A. minimus* the central perforations are equivalent to about 12% of the total length of the coccolith.

Remarks: At LM, with parallel nicols, the two perforations in the central area are well identifiable.

Size: length 4-6 μm.

Genus ***Zeugrhabdotus*:**

Type species*: Zeugrhabdotus erectus* (Deflandre *in* Deflandre & Fert, 1954) Reinhardt, 1965

Description: Muroliths composed by a distal and a proximal rim and a variably constructed transverse bar with a spine. The transverse bar is surrounded by two openings which can be filled by a net. The net is only visible at electron microscope and in well preserved material. The distal rim can be wider than the proximal rim, thus at LM, the different species of *Zeugrhabdotus* can appear as monocyclic or bicyclic. The bicyclic specimens show a distinct dark outer/distal rim and a brighter internal/proximal rim at crossed nicols.

Remarks: According to Nannotax website the different species of *Zeugrhabdotus can be discriminated according to the following features: Rim structure* (*unicylic* or *bicyclic*); *Size* (smaller and larger species); *Bar structure: a)* divided longitudinally; b) split perpendicular to length; c) complex (more elaborate) structures. Bars can also show low birefringence wen the coccolith is at 0° or at 45° position.

Zeugrhabdotus acanthus Reinhardt, 1965

Description: a species of *Zeugrhabdotus* composed by a bicyclic rim and a central area spanned by a traverse bar. The inner rim is brighter than the outer one. The traverse bar is composed by numerous calcite crystals and is slightly flaring when meets the rim showing a X-shape.

Size: length 5-8 μm.

Zeugrhabdotus blowii Lees, 2007

Description: a small *Zeugrhabdotus* species with a monocyclic rim and a bar composed by two separate elements. The rim and the bar have a low birefringence, this last becomes extinct at 0˚ whereas at 45° the bar and the rim have the same birefringence.

Remarks: *Z. blowii* differs from other *Zeugrhabdotus* species for the extinction pattern of the bar goes into extinction at 0˚.

Size: length: 3.5 μm; width 2.6 μm.

Zeugrhabdotus erectus (Deflandre, 1954) Manivit (1971) emend. Bralower et al.,1989

Description: a small species of *Zeugrhabdotus* with a narrow rim and a central area spanned by a lath-shaped bar that supports a spine. At LM, the bar is more birefringent than the rim, that shows a monocyclic extinction pattern.

Size: length 3-5 μm.

Zeugrhabdotus noeliae Rood et al., 1971

Description: a small species of *Zeugrhabdotus* with a relatively broad bicyclic rim and small central openings. The central area is spanned by a traverse bar composed of few elements (at least four). The diameter of the central openings is about 1/3 the diameter of the coccolith.

Remarks: *Z. noeliae* differs from *Z. erectus* in having a traverse bar composed of few crystals. Also, the proportions of the central openings are different in the two species. In *Z. noeliae* the central openings are 1/3 or less the width of the coccolith, while in *Z. erectus* the openings are more than 2/3 the width of the coccolith.

Size: length 2.9 μm; width 1.8 μm.

Zeugrhabdotus bicrescenticus (Stover, 1966) Burnett *in* Gale et al., 1996

Description: a species of *Zeugrhabdotus with a broad monocyclic rim and* a narrow central area. The central area is almost filled by a broad bipartite traverse bar.

Remarks: *Z. bicrescenticus* differs from *Z. diplogrammus* in having a broad bipartite traverse bar which occupies almost completely the central area.

Size: length 6-8 μm; width 4.5-6 μm.

Zeugrhabdotus diplogrammus (Deflandre *in* Deflandre & Fert, 1954) Burnett *in* Gale et al., 1996

Description: a species of *Zeugrhabdotus with a monocyclic rim and a central area spanned by a bipartite traverse bar. At LM the bar is darkest at 60°.*

Size: length 4-8 μm; width ≈ 5 μm.

Zeugrhabdotus *elegans* (Gartner 1968) Bukry 1969

Description: a species of *Zeugrhabdotus* with a central area spanned by a bar composed of at least four small calcite crystals giving a granular appearance. At LM, the rim extinction pattern is monocyclic with the bars becoming dark at 45°.

Remarks: In this study, I used the name *Z. elegans* instead of *Z. howei* as this last was defined later by Bown *in* Kennedy et al. (2000). Moreover, *Z. howei* has the same morphology of *Z. elegans* (Kennedy et al., 2000).

Size: length 6.0 μm; width 4.0 μm.

Zeugrhabdotus biperforatus (Gartner, 1968) Burnett, 1997

Description: a species of *Zeugrhabdotus* with a broad rim composed of strongly imbricated elements. The central area is nearly closed and spanned by a bipartite traverse bar defining two small openings on

either side of the crossbar. The traverse bar consists of numerous calcite elements and may be surmounted by a stem. At LM, the rim extinction pattern is monocyclic with bright bars under cross nicols.

Remarks: *Z. biperforatus* differs from the other *Zeugrhabdotus* due to strong imbrication of the elements that give rise to the highly inclined sutures of the rim.

Size: length 8-10 μm.

Zeugrhabdotus kerguelenensis Watkins, 1992

Description: a species of *Zeugrhabdotus* with a broad rim and large short stem. At LM, the rim extinction pattern is monocyclic. The large stem is supported by a bridge parallel to the minor axis and visible only in proximal view. In distal view, the stem composed by numerous spirally arranged calcite prisms, fills the central area. The lath length decreases distally, resulting in a conical stem.

Remarks: *Z. kerguelenensisis* differs from *Z. embergeri* in having a large and wide stem that fills almost entirely the central area. *Z. embergeri* is also characterized by a diamond-shaped traverse bar.

Size: length 8-11 μm; width 4-7 μm.

Zeugrhabdotus embergeri (Noël, 1959) Perch-Nielsen, 1984

Description: a species of *Zeugrhabdotus with a wide rim and a* large, diamond-shaped transverse bar and small to no perforations occupy the central area. At LM, *Z. embergeri* exhibits a bicyclic rim extinction pattern with the inner cycle brighter than the outer cycle.

Remarks: *Z. embergeri* evolved from *Z. erectus* with an increase of rim and a change in the shape of the traverse bar, from lath-shaped in *Z. erectus* to diamond-shaped in *Z. embergeri* (Thierstein, 1976; Wind, 1978; Roth, 1983; Casellato, 2010). According to Bralower et al. (1989) *Z. embergeri* differs from *Z. erectus* due to: 1) maximum diameter > 8 μm in *Z. embergeri*. 2) width of the central area > ¼ of the maximum diameter in *Z. embergeri*.

Size: length 8-14 μm.

Zeugrhabdotus praesigmoides Burnett, 1997

Description: a species of *Zeugrhabdotus* with a small open central area spanned by a traverse bar composed of small blocks with a sigmoidal appearance. At LM, the rim extinction pattern is bicyclic, with a low birefringent outer rim and high birefringent inner rim. The opposite quadrants of the inner rim go into extinction together during rotation.

Remarks: Z. *praesigmoides* differs from *Z. sigmoides* in having smaller dimensions and a broader inner cycle.

Size: length 5-9 μm.

Zeugrhabdotus scutula (Bergen, 1994) Rutledge & Bown, 1996

Description: a species of *Zeugrhabdotus* with a narrow rim and a central traverse bar that supports a distal boss. The central area is filled by numerous calcite elements parallel to the minor axis of the murolith. The central area is greater than half the murolith width. At LM, the rim extinction pattern is monocyclic. When the specimen is oriented at 45° to the polarizing direction, the bar is divided by a longitudinal extinction line. Instead, when the specimen is oriented parallel to the polarizing direction a brightly birefringent, elongated, diamond-shaped figure is observed on the central portion of the bar.

Zeugrhabdotus sigmoides (Bramlette & Martini, 1964) Bown & Young, 1997

Description: a species of *Zeugrhabdotus* with a wide central area spanned by an arched bar that supports a short stem. At LM, *Z. sigmoides* exhibits a bicyclic rim extinction pattern with a narrow inner cycle that appears bright in cross polarized light. The inner cycle is broad where the bar meets the rim. At LM, the two calcite segments that form the traverse bar show a sigmoid curvature due to the different orientation of the crystals.

Size: length 9-11 μm.

Zeugrhabdotus simplex Lees, 2007

Description: a species of *Zeugrhabdotus* with a narrow rim and a *wide* central area spanned by a simple thin bar. At LM, *Z. simplex exhibits a bicyclic rim extinction pattern. The bar shows a crystallographic uniform behaviour.*

Size: length 8 μm; width 6 μm.

***Zeugrhabdotus* sp. 1**

Description: a species of *Zeugrhabdotus* composed by a monocyclic rim and a central area spanned by a traverse bar. The bar is thick and occupies most of the central area leaving only two small openings. The traverse bar consists of four elliptical crystals that are bright at LM, in crossed nicols. The crystals surround an opening in the center of the bar.

Size: length 7.5 – 8.7 μm; width 5.3 - 6 μm.

Occurrence: *Zeugrhabdotus* sp. 1 was found in the Coniacian-Santonian interval of Tanzania (TDP39).

Zeugrhabdotus trivectis Bergen, 1994

Description: medium-sized species of *Zeugrhabdotus with a well-developed* inner/proximal rim cycle and a central area spanned by a transverse bar. The bar arises from the inner margin and is broad at the junction with the latter. The bar consists of two or three element bundles oriented at slightly oblique angles to each other. At LM, *Z. trivectis* exhibits a bicyclic rim extinction pattern and the inner cycle is brighter than the outer cycle.
Remarks: *Z. trivectis* differs from *Z. xenotus* because it lacks a X-shaped bridge.
Size: length 5-6 μm.

Family Eiffellithaceae Reinhardt, 1965

Muroliths (loxoliths) with a narrow outer rim (distal cycle) and a wide inner rim (proximal cycle). The central area is wide and spanned by axial or diagonal, symmetric or asymmetric cross-bars.

Genus ***Eiffellithus*** Reinhardt, 1965
type species*: Eiffellithus turriseiffelii* (Deflandre,1954) Reihardt,1965
Description: Loxolith coccoliths with an elliptical shape composed by an outer rim and an inner rim consisting of overlapping plates (inner plates Figure 7A). The plates are crossed by four cross-bars that support a large stem. These inner plates can fill the central area or join to create an elliptical opening (Figure 8A). The crossbars are composed of thin, lath-like crystallites with a median extinction line. The cross-bar terminations have different shapes according to the different species of *Eiffellithus*. They can be pointed to blunt, forked, bifurcated or trifurcated (Figure 7B). When present, the central stem appears solid or as a small circular opening, when absent, a prominent square or diamond-shaped opening is present in the cross base (Shamrock and Watkins, 2009). At LM, in cross-polarized light, the central area plates appear more birefringent than the outer rim.
Remarks: The genus *Eiffellithus* originated from *Vakshinella angusta* (Stover 1966) Verbeek, 1977 in the late Albian, giving rise to one of the most important group of calcareous nannofossils in Upper Cretaceous assemblages, both in term of abundance and geographical distribution (Shamrock and Watkins, 2009). These characteristics combined with a rapid evolution and a high dissolution resistance make *Eiffellithus* species good biostratigraphic markers. Both *E. turriseiffelii* and *E. eximius* are biostratigraphically used in many zonation schemes (Sissingh,1977; Roth, 1978; Burnett, 1998*)*. Recently, a taxonomic review of thegenus Eiffelithus was conducted by Watkins and Bergen (2003) and Shamrock and Watkins (2009). Shamrock and Watkins (2009) mainly focus on Upper Cretaceous assemblages with the introduction of six new species, a revised and more precise stratigraphic

distribution and evolutionary patterns for all Upper Cretaceous lineages. According *to* Shamrock and Watkins (2009) the Turonian-Santonian represents one of the interval with an important turnover of Eiffellithus species, associated with an increase in abundance. These modifications could be related to the environmental changes in sea-level, surface water temperature, nutrient availability and water stratification (Shamrock and Watkins, 2009).

In this study, I follow the new taxonomic subdivision proposed by Shamrock and Watkins (2009): the main features used in this study to distinguish the different species of *Eiffellithus* are summarized in Figure 8. The shape of the central cross (angular orientation, cross-bar ration, termination morphology, central openings) represent the main diagnostic feature.

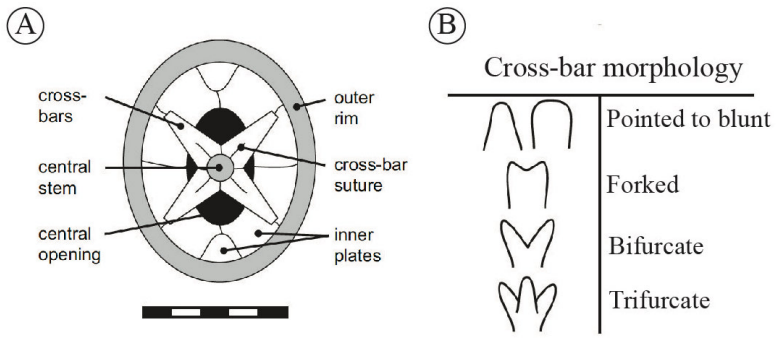

Figure 7 - A: General structures and terminology of *Eiffellithus*. B: Cross-bar morphology. (after Shamrock and Watkins, 2009)

Eiffellithus angustus (Bukry, 1969) Shamrock and Watkins, 2009

Description: a species of *Eiffellithus* of medium to large size, with a central area occupied by an asymmetrical diagonal cross. The midline of the larger cross-bar falls 20°– 44° of the longitudinal axis of the ellipse. A large diamond-shaped opening is present at the center of the crossbars that rises above the plane of the coccolith. The cross-bar is composed by the union of four "C"-shaped crystal each made of curved lath-like elements. The central area is not completely closed by back plates and a wide elliptical opening in the center of the coccolith is present.

Remarks: *E. angustus* differs from *E. eximius* in having a greater length and a broader and more robust crossbar. Compared to *E. eximius*, the crossbar of *E. angustus* shows prominent sutures along their length, with bifurcations on all four terminations.

Size: length 7.4 - 14 µm; width 5.7 - 9.2 µm.

Eiffellithus casolus Shamrock in Shamrock and Watkins, 2009

Description: a species of *Eiffellithus* of small to medium size, with a stem base composed by lath-like elements that form a four disjunct cross-bars. The cross-bar terminations are pointed and form a symmetrical diagonal cross aligned 45°–60° to the longitudinal axis of the coccolith. An elliptical opening that can occupsy about 50% of the longitudinal axes is present at the center of the back plates.

Remarks: Overgrowth of the back plates can refill the central area opening that appears closed. *E. casolus* differs from *E. turriseiffelii* by its smaller size.
Size: length 4.4 < 8.0 μm; width 3.3–6.1 μm.

Eiffellithus collis Hoffmann, 1970
Description: a species of *Eiffellithus* of small size, with a central area occupied by a symmetrical diagonal cross. The midline of the larger cross-bar falls 45°– 60° of the longitudinal axis of the ellipse. A square-shaped opening is present at the center of the cross. The cross-bars are composed of lath-like elements that form four, roughly triangular cross-bars, with pointed terminations. The central area is not completely closed by back plates and a small opening is present.
Remarks*: E. collis* differs from *E. casolus* in having a more elliptical shape and more pointed cross terminations.
Size: length 5.6 μm; width 3.4 μm.

Eiffellithus digitatus Shamrock in Shamrock and Watkins, 2009
Description: a species of *Eiffellithus* of medium to large size, with a central area occupied by an asymmetrical diagonal cross. The midline of the larger cross-bar falls 20°– 44° of the longitudinal axis of the ellipse. A square-shaped opening is present at the center of the cross. The cross-bars are composed of lath-like crystallites of irregular shape and size, with bifurcated to trifurcated cross-bar terminations. The central area is not completely closed by back plates and an elliptical opening can occupy > 50% of the longitudinal axes.
Remarks: *E. digitatus* differs from *E. keio* in having an asymmetrical cross and a different orientation of the axial cross. *E. digitatus* differs from *E. perch-nielseniae* in having a more ornate distal morphology of the cross-bars with bifurcated to trifurcated terminations.
Size: length 7.7–12 μm; width 5.7–10.2 μm.

Eiffellithus eximius (Stover, 1966) Shamrock and Watkins, 2009
Description: a species of *Eiffellithus* of medium to large size with a central area occupied by a symmetrical to slightly asymmetrical axial cross that spans most of the length of the coccolith. The cross-bars are composed of lath-like elements tapering towards the rim. The cross-bar terminal morphology is pointed to blunt, or weakly bifurcated. A circular stem can be present and appears dark in cross-polarized light. When absent, the stem base contains a large opening through which the back plates that fill the central area can be seen.

Remarks: In contrast to what reported by Shamrock and Watkins (2009), in this study I include in *E. eximius* only specimens with a cross-bar aligned with the longitudinal axis of the coccolith (0°-5°). The specimens with a cross-bar orientation within 5° to 20° were included in *E.* cf. *E. eximius*. Whereas the specimens with a cross-bar that falls at 20° to 44° along the longitudinal axis of the coccolith were included in *E. perch-nielseniae*.
Size: length 7.3 -10.4 μm; width 5.2-7.8μm.

Eiffellithus gorkae Reinhardt, 1965

Description: a species of *Eiffellithus* of small to medium size with a nearly cubic stem base and an opened central area. No free lengths of the cross-bars are present and the stem base appears as a small diagonal cross isolated in the center of the coccolith.
Remarks*:* *E. gorkae* differs from *E. casolus* due to lacking of a free-length of the cross-bars.
E. gorkae is indicated by many authors as present in the middle late Albian trough Maastrichtian calcareous nannofossil associations. According to Shamrock and Watkins (2009) the stratigraphic distribution of *E. gorkae* should be confined to the late Campanian – Maastrichtian. This different distribution is most probably related to a different taxonomic interpretation.
Size: length 5-9 μm.

Eiffellithus keio Shamrock in Shamrock and Watkins, 2009
Eiffellithus turriseiffelii A, Perch-Nielsen 1985, Figure 12
Description: a species of *Eiffellithus* of medium to large size, with a central area occupied by a symmetrical diagonal cross. The midline of the larger cross-bar falls ≥45° of the longitudinal axis of the ellipse. A square-shaped opening is present at the center of the cross. The cross distal terminations can be bifurcated or trifurcated, with commonly both lobate and highly forked forms. Sometimes the cross can appear slightly asymmetrical due to high variability of the distal terminations both between specimens and within individual specimens.
Remarks: *E. keio* differs from *E. turriseiffelii* in having bifurcated or trifurcated cross termination instead that blunt, pointed, or weakly forked cross terminations as in *E. turriseiffelii. E. keio* differs from *E. casolus* in having larger size and more complex cross terminations.
Size: length 7.3–11.3 μm; width 5.3–9.5 μm.

Eiffellithus lindiensis Lees, 2007

Description: a species of *Eiffellithus* of small size with a central cross aligned to the main axes if the coccolith. The cross-bars have pointed to blunt terminations and the central area is completely closed by back plates.

Remarks: *E. lindiensis* differs from *E. nudus* in having sub-parallel cross bars with pointed terminations. *E. lindiensis* also lacks a stem in the center of the cross and an opening in the central area.

Size: length 3-5 μm; width 3 μm.

Eiffellithus nudus Shamrock in Shamrock and Watkins, 2009

Description: a species of *Eiffellithus* of small to medium size, with a central area occupied by an asymmetrical diagonal cross. The axial cross is composed by lath-like elements tapering towards the rim with pointed to blunt terminations. The cross is aligned within 20° of the longitudinal axes of the coccolith. The extinction line divides the cross into four cross-bars. A knob-like stem can be present in the center of cross.

Remarks: *E. nudus* differs from *E. eximius* and *E. angustus* in having a small size and for the lack of distal bifurcations.

Size: length 5.5–7.0 μm; width 4.3–5.5 μm.

Eiffellithus parallelus Perch-Nielsen, 1973

Description: a species of *Eiffellithus* of medium to large size, with a central area occupied by a symmetrical diagonal cross. The midline of the larger cross-bar falls 45°-60° of the longitudinal axis of the ellipse. A square-shaped opening is present in the center of the cross. The cross is composed by lath-like elements that form four crossbars. The crossbars show prominent axial suture with distal terminations highly forked.

Remarks*:* *E. parrallelus* differs from *E. phantasma* in having a different orientation of the axial cross (diagonal) and a symmetrical crossbar.

Size: length 5–12 μm.

Eiffellithus perch-nielseniae Shamrock in Shamrock and Watkins, 2009

Eiffellithus turriseiffelii (Deflandre) Reinhardt, Gartner 1968, pl. 22, Figure 4; pl. 24 Figure 2; pl. 26, Figure 4.

Description: a species of *Eiffellithus* of medium to large size, with a central area occupied by an asymmetrical diagonal cross. The midline of the larger cross-bar falls 20°– 44° of the longitudinal axis

of the ellipse. A square-shaped opening is present in the center of the cross. The cross-bars are composed of lath-like elements that form four, roughly triangular cross-bars, with pointed to blunt or bifurcated terminations. The central area is not completely closed by back plates and an elliptical opening that can occupy > 50% of the longitudinal axes is present. In well-preserved specimens, the central cross contains a square-shaped opening.

Remarks: *E. perch-nielseniae* differs from *E. turriseifelii* in having an asymmetrical diagonal cross.

Size: length 6.6–10.3 μm; width = 5.2–7.6 μm.

Eiffellithus phantasma Shamrock in Shamrock and Watkins, 2009

Description: a species of *Eiffellithus* of medium to large size with a central area occupied by an asymmetrical cross. The midline of the larger cross-bar falls 20°– 44° of the longitudinal axis of the

ellipse. The cross-bars are composed of lath-like elements with tapered to blunt or weakly forked cross-bar terminations. The central area is completely closed by back plates that converge behind the central cross. At crossed-polarized light the overall appearance of the central area plates is faint.

Remarks: According to Shamrock and Watkins (2009) *E. panthasma* is the ancestor of *E. parallelus*.

Size: length 5.6–8.4 μm; width 4.1–6.1 μm.

Eiffellithus pospichalii Burnett, 1997

Description: a species of *Eiffellithus* of large size, with a central area occupied by a broad and thick symmetrical diagonal cross with bunt distal terminations. The midline of the larger cross-bar falls 45° of the longitudinal axis of the ellipse. The central area is completely closed by back plates. Size: length 11.3; width 7.8μm.

Eiffellithus turriseiffelii (Deflandre *in* Deflandre & Fert, 1954) Shamrock and Watkins, 2009

Description: a species of *Eiffellithus* of large size with a central area occupied by an asymmetrical diagonal cross. The midline of the larger cross-bar falls 45°– 60° of the longitudinal axis of the ellipse. A square-shaped opening is present in the center of the cross. The cross-bars are composed of lath-like elements with tapered to blunt cross-bar terminations. Small extinction lines run parallel to the axes of the coccolith and divide the central cross into four units that appear roughly triangular under cross-polarized light. The central area is not completely closed by back plates and an elliptical opening can occupy > 50% of the longitudinal axis.

Eiffellithus	LM (not in scale)	Schematic sketch	Central cros fetures				Dimensions(μm)			Remarks (this study)
			angular orientation	cross-bars ratio	termination morfology	central opening	length	width	eccentricity	
E. eximius			sub-parallel (~10°)	asymmetrical elongate (>1,25)	pointed to blunt weakly clavate		7.3-10.4	5.2-7.8	1.23-1.47	*cf E. eximius:* cross sligtly rotated from the axial position of about 20°
E. lindiensis			sub-parallel (~10°)	asymmetrical	pointed to blunt		4.4	3.08		
E. angustus	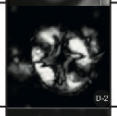		axial (<20°)	asymmetrical elongate (>1,25)	bifurcate trifurcate	diamond -shaped	7.4-14	5.7-9.2	1.15-1.45	
E. nudus	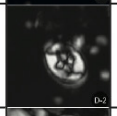		axial (<20°)	elongate (>1,25)	pointed to blunt forked		< 5 5-8	4.3-5.5	1.3-134 1.5-1.7	
E. digitatus	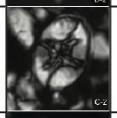		intermediate (20°-40°)	asymmetrical elongate (>1,25)	bifurcate trifurcate	square -shaped	5-8 8-12	5.7-10.2	1.1-1.2 1.3-1.4	
E. perch-nielseniae	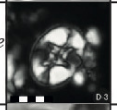		intermediate (20°-40°)	asymmetrical elongate (>1,25)	pointed to blunt, forked	square -shaped	6.6-10.3	5.2-7.6	1.2-1.46	
E. phantasma			intermediate (20°-40°)	asymmetrical elongate (>1,25)	pointed to blunt or forked		5 - 12	4.1 - 6.1	1.1-1.4	
E. casulus			diagonal (45°-60°)	equant (~1)	pointed to blunt		4.4-<8.0	3.3-6.1	1.21-1.50	
E. collis			diagonal (45°-60°)	equant (~1)	pointed to blunt		5.6	3.4		*E. collis* differs from *E. casolus* in having a more elliptical shape and more pointed cross termination
E. gorkae	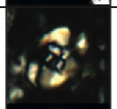		diagonal (45°-60°)	equant (~1)	pointed to blunt	cross isolated in centre of coccolith	5-9			
E. keio	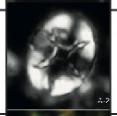		diagonal (45°-60°)	equant (~1)	bifurcate trifurcate	square -shaped	7.3-11.3	5.3-9.5	1.15-1.42	
E. parallelus			diagonal (45°-60°)	equant (~1)	forked, prominent suture	square -shaped	5-12		1.1-1.4	
E. pospichalii	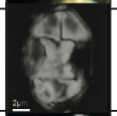		diagonal (45°)	equant (~1)	blunt		11.3	7.8		
E. turriseiffelii			diagonal (45°-60°)	equant (~1)	pointed to blunt	square -shaped	≥8.0-11.5	5.6-8.3	1.22-1.47	

Figure 8 - Upper Cretaceous *Eiffellithus* species. This scheme is re-elaborated after Shamrock and Watkins (2009). Photos are from Nannotax3 website (http://www.mikrotax.org/Nannotax3), Shamrock and Wtkins (2009), Watkins and Bergen (2003) and Burnett (1998). Schematic sketch this study and Shamrock and Wtkins (2009).

Remarks: *E. turriseiffelii* differs from *E. keio* in having tapered to blunt cross-bar terminations in contrast to the highly ornate, bifurcated to trifurcated terminations of *E. keio*. *E. turriseiffelii* differs from *E. parallelus* in having the cross divided in four triangular elements with less evident extinction lines. In the former the cross has parallel lamellae with marked extinction line

Size: length ≥ 8.0–11.5 μm; width 5.6–8.3 μm.

Order Stephanolithiales

Bown and Young, 1997

Muroliths composed by an outer cycle (V-units) and an inner cycle (R-units) giving a bicyclic appearance in cross-polarized light. The term "*protolith"* is applied to this rim structure (Bown, 1987). The outer cycle is composed of non-imbricating elements with sutures that appear vertical or near-vertical in side view.

Family **Stephanolithiaceae**

Black, 1968

Protoliths with a rim with a proximal/inner cycle (R-unit) weakly-developed or vestigial. The central area is spanned by one to numerous bars.

Genus ***Cylindralithus*** Bramlette and Martini, 1964

Type species: *Cylindralithus serratus* Bramlette and Martini, 1964

Description: Cylindrical forms with the elements of the outer/distal cycle (wall) relatively high and in vertical position. At LM, in top view this species appears as a serrate ring, with the elements of wall showing a high birefringence. The central area can be vacant or spanned by bars.

Remarks: *Cylindralithus* differs from the other genera of the family Stephanolithiaceae, in having a circular outline and a high wall; the central area can be spanned by 4 bars. Also, *Rotelapillus* is a circular to elliptical coccolith but the central area is spanned by 6 to 8 bars. *Stoverius* has a lower wall with a rcircular to elliptical outline. *Cylindralithus biarcus* was included by Lees and Bown (2005) in *Rotelapillus,* whereas Perch-Nielsen (1985) included *Cylindralithus biarcus* in *Stoverius* together with *Cylindralithus coronatus*. This classification is not followed here and all the mentioned species are included in *Cylindralithus*. The diagnostic characters useful for distinguishing the different species of *Cylindralithus* at LM are showed in Figure 9.

Cylindralithus biarcus Bukry, 1969

Description: a species of *Cylindralithus* with a wall composed by columnar elements. The wall flares out toward the distal and proximal openings *forming a dentate margin in proximal* and distal views. A X-shaped crossbar is present at the proximal termination with two acute and two obtuse angles, respectively, delieating two large and two small openings.

Size: Maximum diameter 7.2 µm

Cylindralithus coronatus Bukry, 1969

Description: a species of *Cylindralithus* with a wall composed by columnar elements. The wall flares out toward the distal and proximal openings forming a dentate margin in proximal and distal views.
At the proximal termination a cross is present with the bars that meet at 90° making four openings of the same width.

Remarks: *C. coronatus* differs from *C. biarcus* in having a symmetrical cross in the proximal ending.

Size: Maximum diameter 6.7 µm.

Cylindralithus nudus Bukry, 1969

Description: *C. nudus* represents the only species of *Cylindralithus* with an elliptical shape. The wall is composed by serrated columnar elements that flare out toward the distal and proximal openings. The central opening las any cross structure.

Size: Maximum diameter 5.6 µm.

Cylindralithus sculptus Bukry, 1969

Description: a species of *Cylindralithus* with a serrate outline. The wall is composed only by few thick elements (9 or 10). No bars are present in the proximal ending that remains vacant. At LM, in proximal view the central area seems closed, whereas in distal view the central area appears narrow and surrounded by *a* large and birefringent edge.

Size: Maximum diameter 5.2 µm.

Cylindralithus serratus Bramlette & Martini, 1964

Cylindralithus crassus Stover, 1966

Description: a species of *Cylindralithus* with a wall composed by columnar elements that taper toward the proximal ending. A dentate margin is present in the proximal side that appear partially closed. The central area is open even if reduced in width.

Size: Diameter 6-8 μm.

Cylindralithus	**LM** (not in scale)	Schematic sketch	Shape	Central area
C. biarcus	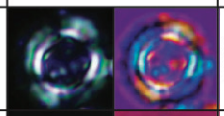		circular	Open and spanned by a X-shaped cross
C. coronatus	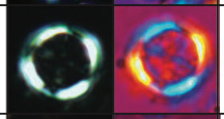	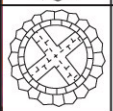	circular	Open and spanned by a cross
C. nudus	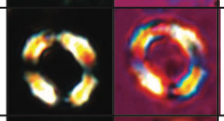	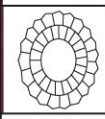	elliptical	Open with an elliptical shape
C. sculptus	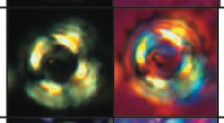	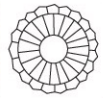	circular	Reduced in width, almost completly closed
C. serratus	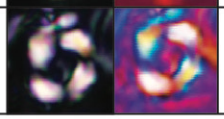	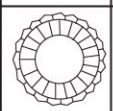	circular	Open with a circular shape

Figure 9 - *Cylindralithus* species: LM images, their diagnostic features.

Holococcoliths

These coccoliths are characterized exclusively by simple euhedral crystals. The holococcolith morphologies show a less well-defined division between rim and central-area structures probably due to the consistent use of identical building blocks (Bown and Young, 1998).

Family **Calyptrosphaeraceae**

Boudreaux & Hay, 1969

A morphological taxonomic grouping which embraces coccolithophores secreting holococcoliths (Bown and Young, 1997).

Genus *Calculites* Prins and Sissingh in Sissingh, 1977

Type species: *Calculites obscurus* (Deflandre, 1959) Prins and Sissingh in Sissingh, 1977

Description: Elliptical holoccoliths composed of a narrow rim and a broad wall consisting of several blocks that can be continuous or divided by sutures. A short process can be present in the center of the holoccoliths. At LM, the entire holoccolith is bright in cross polarized light in plain view, but the rim is not always recognizable. The main characters useful for distinguishing the different species of *Calculites* at LM are showed in Figure 10.

Calculites axosuturalis Bergen in Bralower and Bergen, 1998

Calculites maghredaswampensis Lees, 2007

Description: a species of *Calculites* composed by a wall divided into four quadrants by irregular sutures that are nearly aligned with the ellipse axes. A circular pore may be present in the center of the holococcolith. At LM, this species shows a weak gray birefringence in plain view with the extinction lines kinked near the central pore. With the axes rotated, the extinction lines become sigmoidal X-shaped across the holoccolith.

Size: length 6-9 μm; width 4 μm.

Calculites obscurus (Deflandre, 1959) Prins and Sissingh in Sissingh, 1977

Description: a species of *Calculites* composed by a narrow rim and four blocks divided by sutures. The sutures are diagonally oriented relative to the main axes of the ellipse. These can converge towards the center of the ellipse or have a "V" shape and be joined by a suture placed parallel to the major axis (Figure 12, Sissingh, 1977).

Remarks: The rim is not always detectable at LM. At crossed-nicols the blocks are darker when oriented parallel to the nicols, whereas they are bright and the sutures well defined when oriented at 45°. *C. obscurus* differs from *C. ovalis* due to the different orientations of the sutures. Thierstein (1976) considered the FO of *C. obscurus* together with *C. ovalis* a good marker for the Coniacian/Santonian boundary. According to Thierstein (1976) *C. obscurus* is rare in tropical seas while increases at high paleolatitude with preferences for marginal and epicontinental seas.

Size: length 6-7 μm; width 4.5-5 μm.

Calculites ovalis (Stradner, 1963) Prins & Sissingh in Sissingh, 1977

Description: a species of *Calculites* composed by a narrow rim and four blocks divided by sutures. At LM, under crossed polarized nicols, when the axes of the ellipse are aligned with the nicols the extinction lines coincide with the axes of the ellipse. With the ellipse axes are at 45°, the extinction lines are almost diagnonal relative to axes.

Remarks: *C. ovalis* is sometimes considered a synonymous of *C. obscurus* (Thierstein, 1976; Crux, 1982; Melinte and Lamolda, 2002).

Size: length 5-7μm; width 4 μm.

Calculites percernis Jeremiah, 1996

Description: a species of *Calculites* composed by a narrow rim, a wall composed of a limited number of calcite blocks and a central pore. At LM, in crossed polarized nicols, when the axes of the ellipse are aligned with the nicols the extinction lines lie on the principal axes of the ellipse. With the axes rotated at 45° the extinction line does not intersect, but form two arches in the acute ends of the ellipse.

Size: length 3-5 µm; width 4 µm.

Calculites	LM (not in scale)	Schematic sketch 0°	Schematic sketch 45°	Rim	Pore	Sutures 0°	Sutures 45°
C. axosuturalis	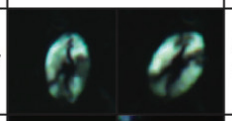			Absent	Present	Kinked	Sigmoidal X- shaped
C. obscurus	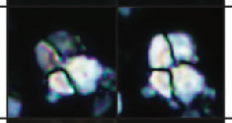			Present	Absent	V- shaped	V- shaped
C. ovalis	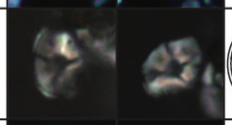			Present	Present	Alligned to the main axes	Ruotated
C. pernicensis				Present thin	Present	Alligned to the main axes	Two arches at the ends of the ellipse

Figure 10 - *Calculites species*: LM images, diagnostic features.

Genus ***Lucianorhabdus*** Deflandre, 1959

Type species: *Lucianorhabdus cayeuxii* Deflandre, 1959

Description: Holococcoliths made of a proximal disc and a stem. The proximal shield includes a rim and a proximal plate composed of four distinct blocks. The stem develops from the proximal shield with a variable height and shape: it can be straight, curved or bulbous with a ridged or pitted surface. A plug is present at the top of the spine that is visible at crossed nicols due to different crystallographic orientation compared to the stem. In some specimens, the plug can be absent. An extinction line, of variable width bisects the holococcolith in two parts.

Remarks: Figure 11 illustrates the diagnostic criteria used in this study to distinguish the different species within this genus. According to Perch-Nielsen (1985) the use of quartz plate is sometimes necessary to discriminate between *Lucianorhabdus* species as show in Figure 11.

Lucianorhabdus cayeuxii Deflandre, 1959

Description: a species of *Lucianorhabdus* with a short and narrow proximal shield and a thin or absent rim. The stem can be straight or arcuate. A wide extinction line bisects the whole holococcoliths. The plug is minute or absent.

Remarks: In poorly preserved material it is difficult to distinguish between *L. cayeuxii* and *L. maleformis*. In these cases, to make use of *L. cayeuxii,* only the arcuate forms have to been used as a a biostratigraphic marker (Crux, 1982).
Size: length 10–30 μm.

Lucianorhabdus arcuatus Forchheimer, 1972
Description: a species of *Lucianorhabdus* with a short and narrow proximal shield and a thin or absent rim. The diameter of the basal shield is equal to the width of the stem. The stem is massive and curved at 90° at the top. A wide extinction line, bisects the holococcolith in two parts.
Remarks: *L. arcuatus* differs from *L. quadrifidus* in having a curved and slender process and a proximal shield with a diameter equal to the width of the process.
Size: Length 10–20 μm.

Lucianorhabdus compactus (Verbeek, 1976) Lees, 2007
Description: a species of *Lucianorhabdus* with a wide, elliptical proximal shield. The proximal shield and the rim are composed of four distinct crystallographic units. At LM a wide extinction line bisects the holococcolith in two parts. At crossed nicols the plug is bright due to the different crystallographic orientation. At LM, with the quartz lamina, an opposite pattern of interference colors is visible between the four elements of the proximal shield, respectively at 0° and 45° to the nicols (Figure 11). The plug and the stem appear dark at 0° whereas the plug is yellow and the stem is blue at 45° to the nicols (Perch-Nielsen, 1985).
Size: length 6–10 μm.

Lucianorhabdus inflatus Perch-Nielsen & Feinberg in Perch-Nielsen, 1986
Description: a species of *Lucianorhabdus* with a short and narrow proximal plate and an inflated stem. The stem is wider in the lower third or half of its length and more tapered towards its distal end.
Size: Length 10-20 μm.

Lucianorhabdus maleformis Reinhardt, 1966
Description: a species of *Lucianorhabdus* with a thick and wide proximal shield and a thin rim. The proximal disc forms an angle of about 120° with the stem. The stem is straight and massive. Although the stem is generally reduced, its height can be variable. The plug is well developed and, at LM, is bright in crossed nicols. At LM, with the quartz lamina, half of the disc and stem (longitudinally) appear blue

and the opposite half yellow, the plug is dark. When rotated at 45° the entire stem appears blue whereas the plug is yellow (Perch-Nielsen, 1985).

Remarks: *L. maleformis* differs from *L. cayeuxii* in having a large proximal shield and a well-developed plug. At LM, with the quartz lamina, at 45° all the stem appears blue whereas the plug is yellow. Conversely, *L. maleformis* shows the same interference pattern at 0° and at 45°.

Size: length 10-20 μm.

Lucianorhabdus quadrifidus Forchheimer, 1972

Description: a species of *Lucianorhabdus* with a thick and wide proximal disc and a prominent rim. The plug is well developed and wider than the stem, that is massive and straight. At LM, with the quartz lamina, half of the proximal shield and the stem (longitudinally) appears blue and the opposite half yellow, the plug is dark. When rotated at 45° the entire stem appears blue whereas the plug is yellow (Perch-Nielsen, 1985).

Remarks: *L. quadrifidus* differs from other species of the genus by the large plug wider than the stem.

Size: length 8-16 μm.

Lucianorhabdus cubiterminalis Farhan et al., 1994

Description: a species of *Lucianorhabdus* with a cube shaped shield and a curved stem. The rim is absent and the plug is reduced or absent.

Remarks: *L. cubiterminalis* differs from other species of the genus by the cube shaped proximal shield.

Size: length 30-34 μm.

Lucianorhabdus lageniformis Farhan et al., 1994

Description: Species of *Lucianorhabdus* with an inflated, bulbous, hollow distal stem which has a highly perforated proximal surface. The proximal shield is short and narrow, whereas the proximal plate is absent. No plug is present at the top of the stem.

Remarks: *L. lageniformis* differs from *L. windii* in having a more bulbous and spherical shape of the stem.

Size: length 30-34 μm

.

Lucianorhabdus windii Hattner & Wise, 1980

Description: a species of *Lucianorhabdus* with a curved bulb-like process whose outer surface is covered by honeycomb-like ridges. The proximal rim is short and narrow, whereas the rim is absent. No plug is present at the top of the stem. **Size:** length 15-30 μm.

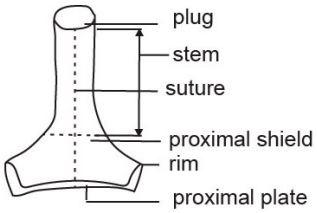

Lucianorhabdus	LM (not in scale)	Cross Nicols	λ plate 0°	λ plate 45°	proximal disc	rim	stem	plug	suture	Stratigraphic Range
L. cayeuxii	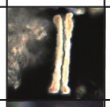	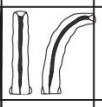		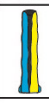	short and narrow	thin or absent	strenght or curved	reduced or absent	wide	Coniacian-Maastrichtian
L. compactus	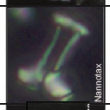				thick and wide	prominent	strenght and shorther	distinctive at NX	wide	Albian - Turonian
L. arcuatus			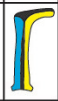		short and narrow	thin or absent	curved at ≈ 90°	distinctive at NX	wide	Coniacian-Maastrichtian
L. maleformis					thick and wide	thin	strenght and shorther	distinctive at NX	narrow	Turonian-Maastrichtian
L. inflatus					short and narrow	absent	influted	absent	wide	Campanian
L. quadrifidus			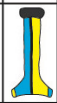		thick and wide	prominent	strenght	distinctive wider than stem	narrow	Turonian-Maastrichtian
L. windii	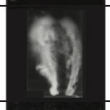				short and narrow	absent	curved bulbous	absent	wide	Campanian-Maastrichtian
L. lageniformis	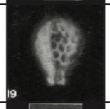				short and narrow	absent	spherical bulbous	absent	wide	Campanian
L. cubiterminalis	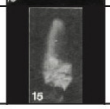				cube shaped	absent	curved	reduced	narrow	Campanian-Maastrichtian

Figure 11 - Terminology used in the description of *Lucionorhabdus* species: LM images, their diagnostic features. Some photos form Nannotax3 website (http://www.mikrotax.org/Nannotax3), Burnett (1998), Farha et al. (1994); Pospichal and Wise (1990).

Nannoliths

Nannoliths include calcareous nannofossils that lack the typical features of heterococcoliths or holococcoliths. Nannoliths represent a heterogeneous group with a wide range of shapes that make this group of uncertain systematic affinity (Bown and Young, 1998).

Order Braarudosphaerales

Bown and Hampton in Young and Bown (1997)

Family **Braarudosphaeraceae**

(Aubry, 2013) Lees and Bown (2016)

Nannoliths composed of multiple layers of thin elements. The elements are thin or flat, equidimensional, triangular or squared to trapezoid, but sometimes with scalloped outer edges. The elements can be placed next to each other or overlapped. The nannolith shape can be pentagonal to circular and ranges from relatively flat to very tall.

Bukryaster Prins, 1971

Description: Pentaliths with a proximal column having a stellate shape and composed by curved elements. The elements are divided by deep sutures that go to the edges of the pentagon. The distal part is reduced and composed only of dextrally oriented ridges with a star-shape.

Bukryaster hayi: (Bukry, 1969) emended by Prins and Sissingh in Sissingh, 1977

Description: a species of *Bukryaster* with 5 thin straight tapering rays with a clockwise imbrication. Five small rods form a star in the center. In well preserved specimens the rays can be bifurcated at the tips.

Family Polycyclolithaceae

(Forchheimer, 1972) Varol, 1992

Description: Nannoliths composed of two wall cycles and a central area. The elements in each cycle of the wall are either vertical, inclined or imbricated. The central area may be closed, open and vacant, or spanned by a diaphragm-like structure. The diaphragm, which is made up of dextrally imbricated elements, is single- or multi-tiered. Each cycle contains the same number of elements in the shape of a ray, petal or brick. At LM, these nannoliths appear birefringent with the individual elements of the wall cycles that extinguish separately when the specimens are rotated under crossed nicols.

Remarks: In this study I included in the Polycyclolithaceae (Forchheimer, 1972) the genus *Micula* as reported by Perch-Nielsen (1985) and Lees and Bown (2005). However, in the emendation of the group made by Varol (1992), the genus *Micula* was considered a "related form" but not conform to his definition of Polycyclolithaceae.

According to Varol, 1989 the different genera that belongs to Polycyclolithaceae can be distinguished according to the presence or absence of a diaphragm, the size of the diaphragm and the shape of the wall elements (Figure 12).

Eprolithus has a wide diaphragm and a petal-like element of the wall. Other Polycyclolithaceae have instead ray-like wall elements as *Lithastrinus, Quadrum* and*Uniplanarius*, whereas pyramidal shaped wall elements are present in *Micula.*

Lithastrinus differs from *Eprolithus* by having a smaller central area and diaphragm. The rays are more twisted in *Lithastrinus* compared to *Eprolithus*. Moreover, the rays of *Lithastrinus* protrude from the proximal and the distal ends instead of a continuous ridge between layers as in *Eprolithus* (Corbett and Watkins, 2014). *Lithastrinus* differs from *Uniplanarius* in having more than four elements in each cycle of the wall.

The forms assigned to *Quadrum* and *Micula* differs from the other Polycyclolithaceae because have no diaphragm. *Micula* differs from *Quadrum* in having each cycle of the wall is made up of four imbricated elements. According to Crux (1982), *Micula* evolves from *Quadrum* after a gradual rotation in the opposite direction of the upper and lower elements of the wall.

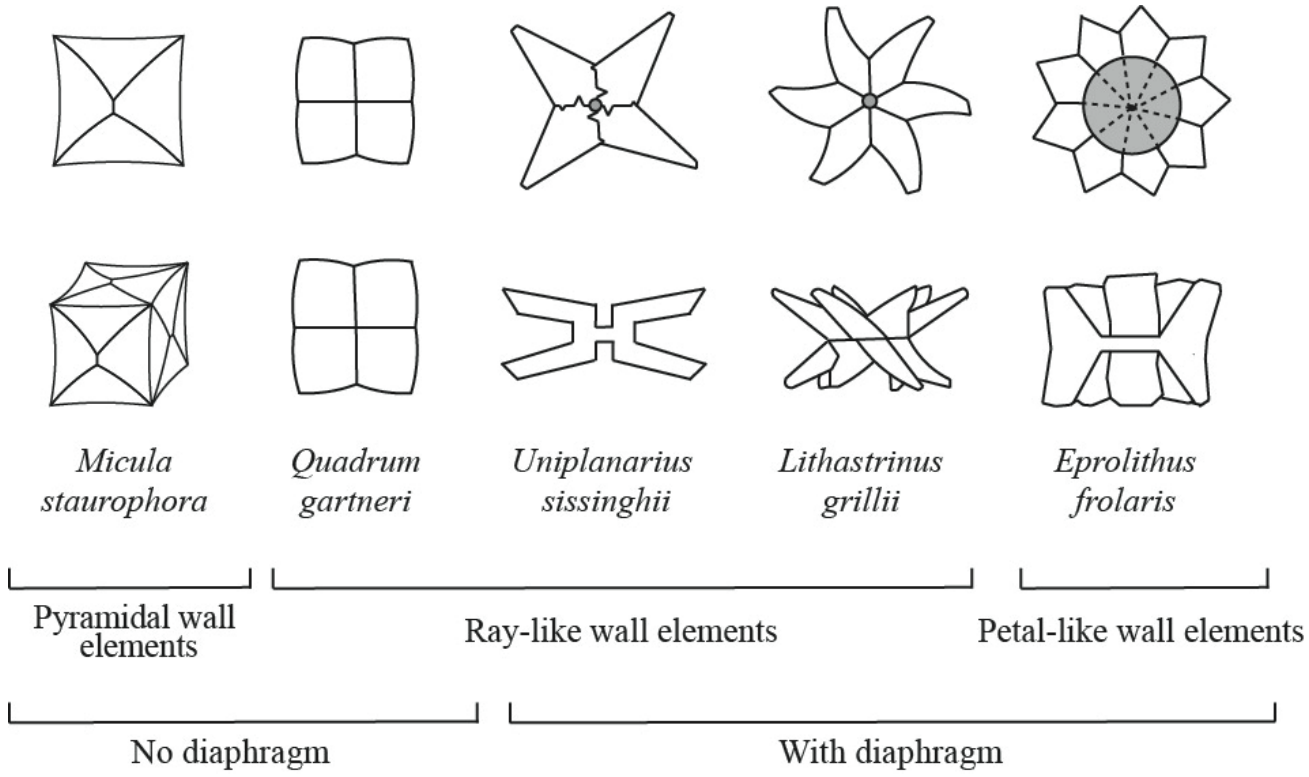

Figure 12 - Summary of the Polycyclolithaceae discussed in this section (modified after Varol, 1992).

Genus ***Eprolithus*** (Stover, 1966) Varol,1992

Type species: *Lithastrinus floralis* Stradner, 1962

Description: Polycyclolith composed by a wall with two cycles of five to nine petal-like elements that surround a central depression. A narrowing is present at the mid height of the wall where the two cycles are joined and a median diaphragm extends into the central depression (Figure 13). Along the diaphragm the cycles of the wall are slightly twisted. At LM, in side view, the diaphragm and the central depression connecting the two cycles is visible with a characteristic "H" or "X" shape. A reduction of the number of in each cycle of the wall took place through time.

Remarks: The different species of *Eprolithus* are distinguished by the number of elements in each cycle of the wall (Varol, 1992; Figure 15).

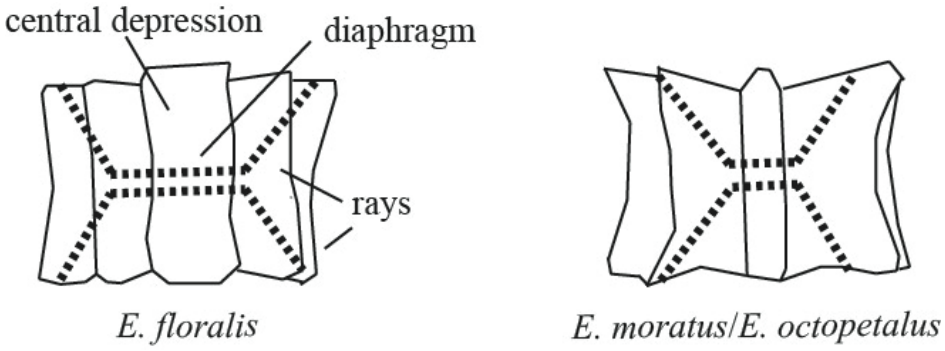

Figure 13 - Schematic 3D sketch showing the morphology of *Eprolithus* (after Corbet and Watkins, 2014).

Eprolithus floralis (Stradner, 1962) Stover, 1966

Description: a species of *Eprolithus* with nine petal-like elements in each cycle of the wall. The two cycles are coupled in the middle of the central depression by the diaphragm consisting of nine overlapping lath-shaped elements.

Size: diameter 3-9 μm.

Eprolithus octopetalus Varol, 1992

Description: a species of *Eprolithus* with eight petal-like elements in each cycle of the wall. The two cycles are coupled in the middle of the central depression by the diaphragm consisting of eight overlapping lath-shaped elements.

Size: diameter 3-9 μm.

Eprolithus moratus (Stover) Burnett, 1998

Description: a species of *Eprolithus* with seven petal-like elements in each cycle of the wall that surround a wide central depression. The two cycles form a continuous ridge between the two cycles. The cycles are coupled in the middle of the central depression by the diaphragm consisting of seven overlapping lath-shaped elements (Corbett and Watkins, 2014).

Size: diameter 7-11 μm.

Eprolithus	**LM** (not in scale)	Schematic sketch	Diagnostic features
E. floralis	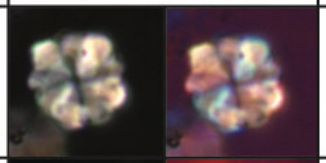		9 wall-elements.
E. octopetalus	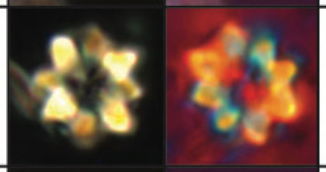	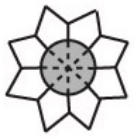	8 wall-elements.
E. moratus	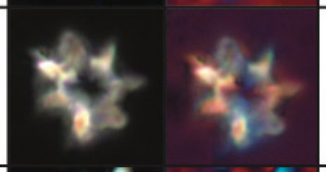		7 wall-elements.
E. rarus	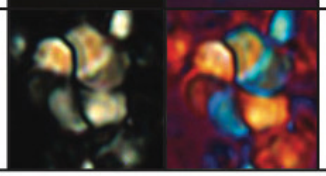		6 wall-elements.

Figure 14 - The species of *Eprolithus*: LM images, diagnostic features.

Eprolithus rarus Varol, 1992

Description: a species of *Eprolithus* with six petal-like elements in each cycle of the wall that surround a small central depression. The two cycles are coupled in the middle of the central depression by the diaphragm consisting of six overlapping lath-shaped elements.

Size: diameter 7-11 μm.

Genus ***Lithastrinus*** (Stradner, 1962) Varol, 1992

Type species: ***Lithastrinus grillii*** Stradner, 1962

Description: Polycyclolith composed by a wall with two twisted cycles made of five to seven ray-like elements around a central depression. The central depression is narrow and hold a small to medium

diaphragm from where two cycles of the wall join. The rays are straight or slightly curved and project from the proximal and distal ends of each wall element. The ray's length is always longer on one side (proximal?) compare to the other (distal?). At LM, the central area is bright due to the thickness of the wall elements and spin slightly when focusing along the diaphragm. In poorly preserved specimens, when the rays are broken, a rounded outline of the elements around the diaphragm is visible (Corbett and Watkins, 2014). The different species of *Lithastrinus* are distinguished according to the number of rays (Figure 15), the number of rays decreases with time.

Remarks: According to Corbett and Watkins (2014), *Lithastrinus* (*L. septenarius*) evolve from *Eprolithus* (*E. moratus*) in the late Turonian.

Lithastrinus	**LM** (not in scale)	Schematic sketch	Diagnostic features
L. grillii			6 ray-like elements.
L. septenarius	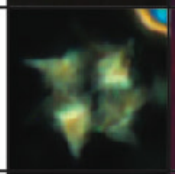		7 ray-like elements.
L. pentabrachiatus	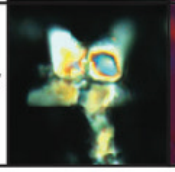		5 ray-like elements.

Figure 15 - The species of *Lithastrinus*: LM images, diagnostic features.

Lithastrinus grillii Stradner, 1962

Description: a species of *Lithastrinus* composed by two cycles of six ray-like elements around a central depression/ diaphragm. The cycles are connected by a small diaphragm made of overlapping lath-shaped elements.

Size: diameter 7-11 µm.

Lithastrinus septenarius (Forchheimer, 1972) Corbett and Watkins, 2014

Description: a species of *Lithastrinus* composed by two cycles of seven twisted ray-like elements around a central depression/diaphragm. The cycles are connected by a small diaphragm made of overlapping lath-shaped elements.

Remarks: *L. septenarius* differs from *E. moratus* in having a reduced central area/diaphragm and the non-continuous development of the rays between the proximal and the distal cycle.
Size: diameter 5-10 μm.
Lithastrinus pentabrachius Varol, 1992

Description: a species of *Lithastrinus* composed by two cycles of five twisted ray-like elements around a central depression/diaphragm. The cycles are connected by a small diaphragm made of overlapping lath-shaped elements.
Size: diameter 5-15 μm.

-Genus ***Micula*** Vekshina, 1959

Type species: *Micula staurophora* (Gardet, 1955) Stradner, 1963
Description: Cubic nannoliths composed by two or one cycle of four pyramidal/blocky elements each. The elements are joined along sutures that always turn in one direction on each side, pointing toward the corners of the cube. The elements may protrude slightly away from the edges of the cube. No diaphragm is present (Figure 16A). At LM, in cross polarized light, all the elements are bright when the specimen is parallel to the polarizing directions and darker when rotated of 45° from this position.
Remarks: The evolution of the *Micula* lineage is characterized by the elements to increasingly protrude beyond the periphery of the cube. With time Micula also show a trend toward a reduction of the size of the elements of the upper cycle and an increase in size of those of the lower cycle.
The optical behaviour of *Micula* (e.i. *M. staurophora*) in side view can resemble that of an *Eprolithus* side view. Especially, *E. octopetalus* and *E. moratus* show rectangular side view crossed by an X as

in *Micula*. At LM under cross nicols and quartz lamina, *Micula* shows the first and the third quadrant blue and the second and fourth yellow (Moshkovitz and Osmond, 1989; Figure 16B). According to Persico and Villa (2002) a similar pattern is not visible in *Eprolithus* side-views, in which the interference colours vanish from the center toward the wall (Figure 15B). The main characters useful for distinguish the different species of *Micula* at LM are showed in Figure 17.

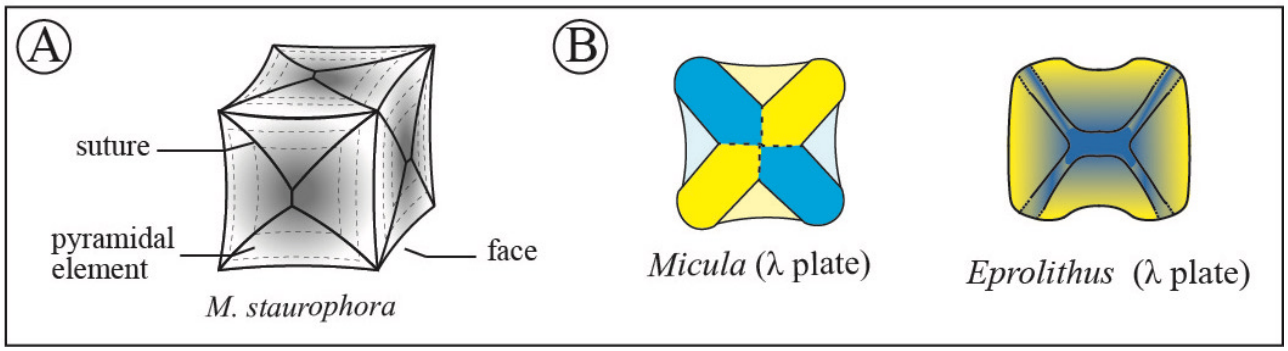

Figure 16 - A) Schematic 3D sketch showing the morphology of *Micula.* B) Comparison of *Micul*a and *Eprolithus* side view with the quartz plate.

Micula adumbrata Burnett, 1997

Description: a small species composed by two cycles, each consisting of four equally sized pyramidal blocks. The sutures between the blocks are less marked compared to other species of *Micula*.

Remarks: According to Burnett (1997) *M. adumbrata* can represent the ancestral form of *M. staurophora* that originated from *Quadrum*. *M. adumbrata* differs from *M. staurophora* for its small dimensions and a less evident and wide diagonal cross.

Size: length 4-6 μm.

Micula clypeata Lees and Bown, 2005

Description: a species of *Micula* that appears to be composed of a single cycle of four elements joined along uneven sutures that bend sharply at their ends. A distinctive raised circular area, equal in diameter to the width of the nannolith, lies above the level of the main structure. A narrow zone of darker birefringence lies along each of the suture lines and broadens toward the corners.

Remarks: *M. clypeata* differs from *M. praemurus* in having a square shape and more complex sutures.

Size: length 5.5-6.5 μm.

Micula concava (Stradner *in* Martini and Stradner, 1960) Verbeek, 1976

Description: a species of *Micula* composed by two cycles, each consisting of four equal-sized pyramidal blocks. The elements are joined along sutures; face and sides of the cube are concave and corners protrude outward as "rays". At LM, *M. concava* shows an evident cross along the diagonal sutures. A further small cross superimposed to the main one is sometimes visible.

Remarks: *M. concava* differs from *M. staurophora* for its deeply concave sides and the protruding corners. In *M. concava*, the sutures are slightly shifted from the corners of the cube compared to *M. sturophora*.

Size: length 5-7 μm.

Micula cubiformis Forchheimer, 1972

Description: a species of *Micula* composed by two cycles each consisting of four equal-sized pyramidal blocks. The corners of the cube are square or rounded and a central depression is present in each face. At LM, a small cross can be present in the middle of the central depression. The latter can be included or extend beyond the periphery of the depression. At LM, under crossed polarized light, two additional sutures are parallel to the outline and crossing in the center of the nannolith are visible.

Remarks: *M. cubiformis* differs from *M. staurophora* in having a small dimension and a face of the cube characterized by square or rounded corners with a central depression in the middle. The sutures parallel to the sides are well recognizable at LM under crossed nicols in *M. cubiformis*, whereas are less evident in *M. staurophora* and absent in *M. concava*.

Size: length 3-6 μm.

Micula murus (Martini, 1961) Bukry, 1973b

Description: a species of *Micula* composed by an upper cycle reduced in extension and a lower cycle consisting of elongated elements. Each cycle twists in opposite directions. The elements protrude significantly away from the edges of the cube.

Remarks: At LM *M. murus* differs from *M. swastica* having the elements that protrude away from the edges of the cube, whereas, *M. swastica* show a general square shape.

Size: length 5-9 μm.

Micula praemurus (Bukry, 1973b) Stradner and Steinmetz, 1984

Description: a species of *Micula* composed of only a single cycle of four elements; it is a flat nannolith characterized by a circular outline. The elements meet along “S” shaped sutures that intersect in the center. At LM, the four quadrants become extinct contemporaneously during the rotation of the specimen relative to the cross-polarization.

Remarks: *M. preamurus* differs from *M. premolisilvae* in having a circular outline.

Size: length 5-8 μm.

Micula premolisilvae Lees and Bown, 2005

Description: a flat species of *Micula* composed of only a single cycle of four elements with a square to cruciform shape. The elements are separated by slightly curved sutures. At LM, the entire nannolith goes into extinction when rotated at 45°relative to the direction of cross-polarization.

Remarks: *M. premolisilvae* differs from *M. praemurus* in having a square to cruciform outline.

Size: length 5-8 μm.

Micula	**LM** (not in scale)	Schematic sketch	Diagnostic features	Stratigraphic Range
M. adumbrata	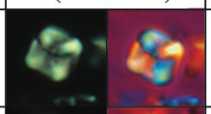		Small Micula with poorly marked diagonal cross.	late Turonian-Coniacian
M. staurophora	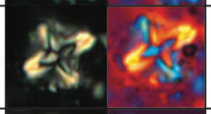		Micula of a compac cube shape with a well evident diagonal cross pointing toward the corner of the cube.	mid Turonian-late Maastrichtian
M. concava	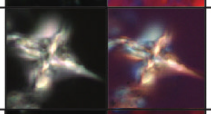		Micula with concave sides and corners that protrude away as rays protruting. Suture slyglty rotated from the corners	Coniacian - Maastrichtian
M. cubiformis	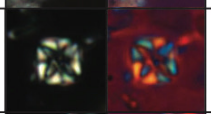		Micula with a central depression in each face of the cube. A cross is present in the depression that can be included or extended beyond peryphery of the depression.	Coniacian - Maastrichtian
M. swastica	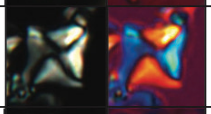		*Micula* with a sutures between triangular elements hving a swastica pattern.	Coniacian - Maastrichtian
M. murus	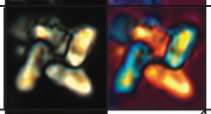		*Micula* with a upper cycle reduce in extenction and a lower cycle of elongate elements.The lower cycle elements protrude from the edges of the cube.	late Maastrichtian
M. prinsi			*Micula* with one one cycle that is reduced/relict and one cycle cycle of four rays with cross shape that extend well beyound the edge of the cube.	late Maastrichtian
M. clypeata	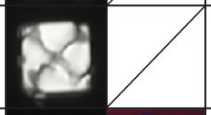		*Micula* with only a sigle cyle of four element. The elemetsmeet along sutures that curves at their ends. A zone ofdarker birifrangent is visible around the sutures broader at the cornes.	Campanian-late Maastrichtian
M. praemurus	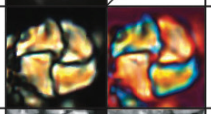		*Micula* with only a sigle cyle of four element having a flat and cricular shape. The elemets joint along S-shaped sutures.	Campanian-late Maastrichtian
M. premolisivae	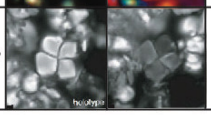		Flat Micula composed of only a sigle cyle of four elements with a square to cruciform shape. The elemets joint slightly curved sutures.	late Campanian-late Maastrichtian

Figure 17 - *Micula* species: LM images, their diagnostic features. Some photos are from Lees and Bown (2005).

Micula prinsii

Perch-Nielsen, 1979

Description: species of *Micula* composed by four elongated elements (arms)These are long and slightly curved and protrude well away from the edges of the cube. The arms meet tangentially in the middle of the nannolith and their ends can be rounded of or bifurcated.

Remarks: *M. prinsii* evolve from *M. murus* after the reduction of one cycle. According to Perch-Nielsen,1985 *M. prinsii* differs from *M. murus* having more taper elements compare to *M. murus*.
Size: length 4-9 μm.

Micula staurophora (Gardet, 1955) Stradner, 1963
Description: a species of *Micula* composed by two cycles each consisting of four equal-sized pyramidal blocks. The faces of the cube are concave and the elements are joined along sutures that point toward the corners of the cube. At LM, *M. staurophora* shows an evident diagonal cross along the sutures.
Remarks: In well preserved specimens superimposed to the main cross a further small cross is visible. At LM with the quartz lamina, the small superimposed cross shows an opposite interference color pattern compared to the main one (Figure 16). M. *M. staurophora is considered here as a synonymous of Micula decussata* Vekshina (1959).
Size: length 3-8 μm.

Micula swastica Stradner & Steinmetz, 1984
Description: a species of *Micula* composed by two cycles each consisting of four equal-sized pyramidal blocks. The elements have a triangular shape and are separated by sutures showing a swastika pattern. Elements of the cycles may protrude slightly from the edge of the cube.
Remarks: According to Lees and Bown (2005), *M. swastika* gave rise to *M. murus* through the reduction of one of the cycles.
Size: length 4-9 μm.

Genus ***Quadrum*****:**

Type species: Quadrum gartneri Prins & Perch-Nielsen *in* Manivit et al., 1977
Description: Polycycloliths with wall formed of two cycles of four to nine non-imbricated elements. The elements join in the center of the nannolith leaving no central opening or diaphragm. The cycles of the wall are moderately twisted along their joining surface.
Remarks: The shape of *Quadrum* nannoliths range between cubiform to stellate. When cubiform, the elements are joined along sutures that go out to the mid-point of the cube edges. In the stellate specimens, the sutures are sharper and the elements have a closer arrangement.
A different optical behaviour allows to distinguish between *Quadrum* and *Micula*. At LM under crossed nicols and quartz lamina, *Quadrum* specimens show the first and the third quadrants yellow and the

second and fourth blue, whereas an opposite pattern is visible in *Micula* (Moshkovitz and Osmond, 1989) (Figure 18). The diagnostic characters useful for distinguish the different *Micula* species at LM are synthetized in Figure 19.

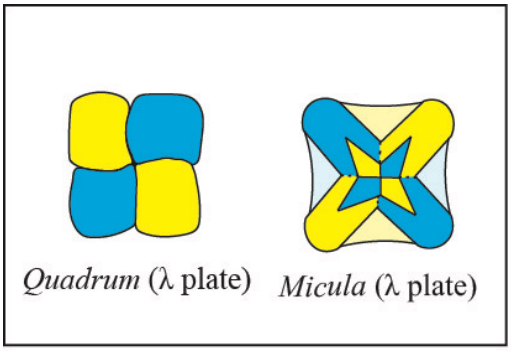

Figure 18 - Comparison of *Quadrum* and *Micula* colors interference pattern with the quartz lamina.

Quadrum	**LM** (not in scale)	Schematic sketch	Diagnostic features	Stratigraphic Range
Q. gartneri			Quadrum with 4 wall-cycle elements.	Turonian-Maastrichtian
Q. svabenickae			Quadrum with a central depression and thick outer corner. A structure, that appear dark at cross nicols, with a shape that resamble a cross is situated in the central depression.	Coniacian-Maastrichtian
Q. intermedium			Quadrum with four large wall-cycle elements alternating with one to three smaller wall-cycle elements.	Cenomanian - Coniacian
Q. eptabrachium			*Quadrum* with 7 elements per cycle	Turonian - Santonian
Q. octobrachium			*Quadrum* with 8 elements per cycle	Turonian
Q. enebrachium			*Quadrum* with 9 elements per cycle	Middle Albian-Santonian
Q. giganteum			Large (>10 µm) *Quadrum* with 9 elements per cycle	Turonian

Figure 19 - The species of *Quadrum*: LM images, their diagnostic features. Pothos of *Q. octobrachium* from Varol (1992).

Quadrum eneabrachium Varol, 1992

Description: a species of *Quadrum* composed of two cycles each consisting of nine ray-like elements.

Size: 3-5 µm.

Quadrum eptabrachium Varol, 1992

Description: A species of *Quadrum* composed of two cycles each consisting of seven ray-like elements.

Size: 3-6 µm.

Quadrum gartneri Prins & Perch-Nielsen *in* Manivit et al., 1977

Description: a species of *Quadrum* composed of two cycles each consisting of four cubic elements separated by sutures parallel to the nannolith outline. The corners of each cube can be slightly protruding from the corners making the cube slightly constricted in the middle. At LM, Q. gartneri behaves like a holococcolith and is entirely bright or dark during rotation.

Remarks: *Q. gartneri* differs from *U. gothicus* in having sutures between the elements with a straight instead of a scalloped profile (Figure 20).

Size: 3-6 μm.

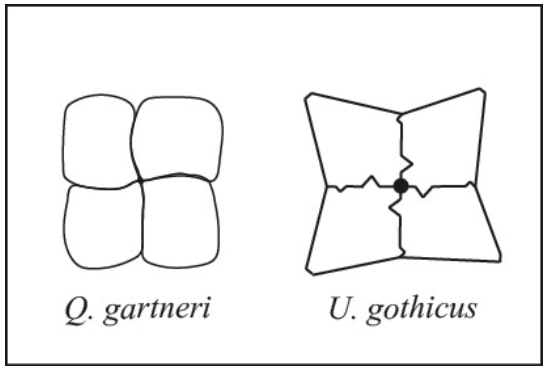

Figure 20 - Comparison of *Q. gartneri* characterized by straight sutures with *U. gothicus* characterized by scalloped sutures (Watkins, personal communication).

Quadrum giganteum Varol, 1992

Description: A large species (>10 μm) of *Quadrum* composed of two cycles each consisting of nine ray-like elements.

Remarks: *Q. giganteum* differs from *Q. eneabrachium* in having a large dimension.

Size: 10-14 μm.

Quadrum intermedium Varol,1992

Description: a species of *Quadrum* having four large elements of equal size that alternate with small ray-like elementsthat may be 1-3 in number.

Size: 4-6 μm.

Quadrum octobrachium Varol, 1992

Description: a species of *Quadrum* composed of two cycles each consisting of eight ray-like elements.

Size: 3-5 μm.

Quadrum svabenickae Burnett, 1997

Description: a species of *Quadrum* composed of two cycles each consisting of four ray-like elements. A depression is present in the center of each cycle whereas the edges appear thickened.

Remarks: In several specimens, the depression hosts a structure with a cross shape that appears dark under crossed nicols.

Size: 5-8 μm.

Nannoliths incertae sedis

Genus ***Ceratolithoides*****:**

Description: Nannoliths consisting of a base surmounted by a cone. The base is forms by two horns of different cristallographic orientation, whereas the cone has numerous faces divided by sutures. The shape of the nannolith can be conical, arrowed-shaped or horse-shaped.

Remarks: This group of calcareous nannofossils has been revisited by Burnett (1997) with the introduction of many new species. The study was based on different ODP/DSDP sites from the Indian Ocean at high latitudes. This genus appeared in the early Campanian and evolved through the Campanian - late Maastrichtian time interval. Burnett (1997) identified four different groups of *Ceratolithoides* according to their morphology:

Group I (*Ceratolithoides* sp.; *C. verbekii*) characterized by the presence of more than two horns and little or no distinction between the base and the cone.

Group II (*C. aculeus*; *C. brevicornis*) characterized by an arrowed shape, a very short internal horn length, and a distinct base and cone.

Group III (*C. arcuatus*; *C. quasiarcuatus*; *C. sesquipedalis*) characterized by slender horns forming an ≈90° angle, a very short internal horn length, and a cone completely free of the horns.

Group IV (*C. indiensis*; C. *longissimus*; *C. prominens*; *C. ultimus*) with cone entirely or partially enclosed by the horn.

In this chapter I report only the description of species used as biostratigraphic marker, or that first occur in the early Campanian. The terminology used for the description is illustrated in Figure 21.

Ceratolithoides aculeus (Stradner, 1961) Burnett, 1997

Description: a medium to large species of *Ceratolithoides* with an arrowhead shape. The base and the cone is distinct with a base/cone ratio of 1:1. The internal horn length is short with an inter-horn angle of ≈ 90°. The base may be composed of two or four horns.

Size: 6.7-7.4 µm.

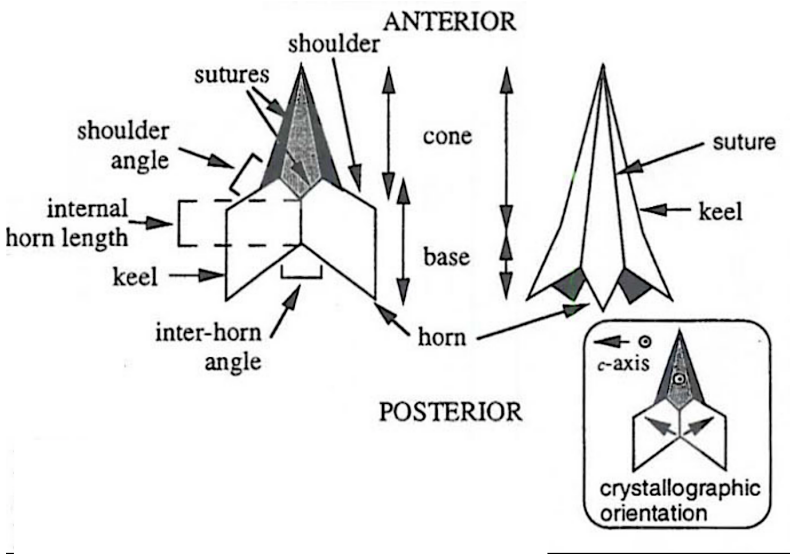

Figure 21- *Ceratolithoides* morphology and terminology (after Burnett, 1997).

Ceratolithoides arcuatus Prins & Sissingh in Sissingh, 1977

Description: a small to medium species of *Ceratolithoides* with a horseshoe shape. The cone is small and the base consist of two long, curving horns. The base cone ratio is 3:1 with a short internal horn length. The inter-horn angle is > 90° (obtuse).

Size: 4.4-4.5 µm.

Ceratolithoides indiensis Burnett, 1997

Description: a medium species of *Ceratolithoides* with a cone almost entirely enclosed between the horns.

The cone is broad and bright at LM with an obtuse inter-horn angle. The internal horn length is short and the base/cone ratio is 2:1.

Size: 6.5 µm.

Ceratolithoides kamptneri Bramlette & Martini, 1964

Description: Small to medium *Ceratolithoides* with a reduced or absent cone and two elongated, slender horns. The inter-horn angle ≈90° with a very short internal horn length.

Size: 4.4 µm.

Ceratolithoides quasiarcuatus Burnett, 1997

Description: Medium to large *Ceratolithoides* with a subhorse shoe shape. The cone is small with a pointed apex, and forms a distinct, obtuse shoulder angle with the base. The base consists of with two elongated, slender, curving horns. The base/cone ratio is 2:1 with an internal horn length very short. The inter-horn angle ≈90°.

Remarks: C. *quasiarcuatus* differs from *C. arcuatus* in having a longer and pointed cone, a inter-horn angle of ≈90° and a different base/cone ratio.

Size: 6.5 μm.

Ceratolithoides verbeekii Perch-Nielsen, 1979

Description: Species of *Ceratolithoides* with a base made of six horns and a high horn. A continues ridge from each horn form the high cone.

Size: 5.7-6.8 μm.

Marthasterites Deflandre, 1959

Type species: *Marthasterites furcatus* (Deflandre in Deflandre and Fert, 1954) Deflandre, 1959

Description: Nannolith composed three branches/rays of equal length. The branches are straight or slightly arched and lies on the same plane, they can have rounded of forked lobes terminations (Figure 22). The angle between the branches is often at about 120°. At LM, *Marthasterites* is low birefringent.

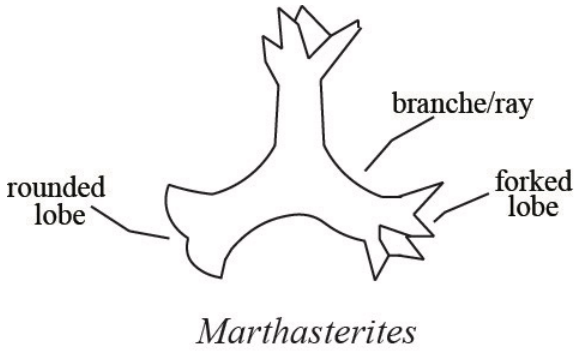

Figure 22 - *Marthasterites* morphology and terminology.

Marthasterites crassus (Deflandre, 1959) Burnett, 1997

Description: a species of *Marthasterites* having thick and short branches with forked lobe terminations.

Size: 4-8 μm.

Marthasterites furcatus (Deflandre in Deflandre & Fert, 1954) Deflandre, 1959

Description: a species of *Marthasterites* composed by three branches of about equal length with forked lobe terminations.
Size: 5-16 μm.

Marthasterites simplex (Bukry, 1969) Burnett, 1997
Description: a species of *Marthasterites* composed by three branches of about equal length with rounded lobe terminations.
Remarks: *M. simplex* is similar to *M. furcatus* but lacks the forked terminations in its branches.
Size: 5-8 μm.

Marthasterites inconspicuus Deflandre, 1959
Description: Species of *Marthasterites* composed by three short branches of about equal length, giving a general shape of a triangle with concave sides to the nannolith. No branches terminations are present.
Size: 3-5 μm.

Appendix 2

Taxonomic list

Calcareous nannofossil species identified in this study are here listed following genera and species alphabetical order. References to original descriptions are not given.

Genus: *Ahmuellerella* Reinhardt, 1964

A. octoradiata (Górka, 1957) Reinhardt & Górka, 1967

A. regularis (Górka, 1957) Reinhardt & Górka, 1967

Genus: *Amphizygus* Bukry, 1969

A. brooksii brooksii Bukry, 1969

A. brooksii nanus Bukry, 1969

A. megalops Blair & Watkins 2009

A. minimus Bukry, 1969

Genus: *Arkhangelskiella* Vekshina, 1959

A. confusa Burnett (1997)

A. cymbiformis Vekshina, 1959

Genus: *Aspidolithus* Noël, 1969

A. enormis (Shumenko, 1968) Manivit, 1971

A. parcus constrictus (Hattner et al., 1980) Perch-Nielsen, 1984

A. parcus expansus (Wise & Watkins in Wise, 1983) Perch-Nielsen, 1984

A. parcus parcus (Stradner, 1963) Noël, 1969

Genus: *Axopodorhabdus* Wind & Wise in Wise & Wind, 1977

A. albianus (Black, 1967) Wind & Wise in Wise & Wind, 1977

Genus: *Biscutum* Black in Black & Barnes, 1959

B. constans (Górka, 1957) Black in Black and Barnes, 1959

B. coronum Wind & Wise in Wise & Wind 1977

B. ellipticum (Górka, 1957) Grün in Grün and Allemann, 1975

B. hattneri Wise, 1983

B. magnum Wind & Wise in Wise & Wind, 1977

B. melaniae (Górka, 1957) Burnett, 1997

Genus: *Braarudosphaera* Deflandre, 1947

B. bigelowii (Gran & Braarud, 1935) Deflandre, 1937

Genus: *Broinsonia* Bukry, 1969

B. ethmoquadrata Bukry, 1969

B. furtiva Bukry, 1969 emend Hattner, Wind & Wise 1980

B. matalosa (Stover, 1966) Burnett in Gale et al., 1996

B. signata (Noël, 1969) Noël, 1970

Genus: *Bukrylithus* Black, 1971

B. ambiguus Black, 1971

B. hayi (Bukry, 1969) Prins & Sissingh in Sissingh, 1977

Genus: *Calculites* Prins & Sissingh in Sissingh, 1977

C. maghredaswampensis Lees, 2007

C. obscurus (Deflandre, 1959) Prins & Sissingh in Sissingh, 1977

C. ovalis (Stradner, 1963) Prins & Sissingh in Sissingh, 1977

C. percensis Jeremiah, 1996

Genus: *Chiastozygus* Gartner, 1968

C. amphipons (Bramlette & Martini, 1964) Gartner, 1968

C. bifarius Bukry, 1969

C. fessus Stover, 1966

C. litterarius (Górka, 1957) Manivit, 1971

C. platyrhethus Hill, 1976

C. spissus Bergen in Bralower & Bergen, 1998

C. trabalis (Górka, 1957) Burnett, 1997

Genus: *Corollithion* Stradner, 1962

C. exiguum Stradner, 1961

C. madagaskarensis Perch-Nielsen, 1973

C. signum Stradner, 1963

Genus: *Cretarhabdus* Bramlette & Martini, 1964

C. conicus Bramlette & Martini, 1964

C. inaequalis Crux, 1987

C. striatus (Stradner, 1963) Black, 1973

Genus: *Cribrosphaerella* Deflandre in Piveteau, 1952

C. ehrenbergii (Arkhangelsky, 1912) Deflandre in Piveteau, 1952

C. circula (Risatti, 1973) Lees, 2007

Genus: *Cyclagelosphaera* Noël, 1965

C. margerelii Noël, 1965

C. reinhardtii (Perch-Nielsen, 1968) Romein, 1977

C. rotaclypeata Bukry, 1969

Genus: *Cylindralithus* Bramlette & Martini, 1964

C. asymmetricus Bukry 1969

C. biarcus Bukry, 1969

C. coronatus Bukry, 1969

C. crassus Bramlette & Martini, 1964

C. nudus Bukry, 1969

C. sculptus Bukry, 1969

C. serratus Bramlette & Martini, 1964

Genus: *Discorhabdus* Noël, 1965

D. ignotus (Górka, 1957) Perch-Nielsen, 1968

Genus: *Eiffellithus* Reinhardt, 1965

E. angustus (Bukry, 1969) Shamrock in Shamrock & Watkins, 2009

E. casolus Shamrock in Shamrock and Watkins, 2009

E. collis Hoffmann, 1970

E. digitatus Shamrock in Shamrock and Watkins, 2009

E. eximius (Stover, 1966) Shamrock and Watkins, 2009

E. gorkae Reinhardt, 1965

E. keio Shamrock in Shamrock and Watkins, 2009

E. nudus Shamrock in Shamrock and Watkins, 2009

E. perch-nielseniae Shamrock in Shamrock & Watkins, 2009

E. turriseiffelii (Deflandre *in* Deflandre & Fert, 1954) Shamrock and Watkins, 2009

Genus: *Eprolithus* Stover, 1966

E. moratus Varol, 1992

E. floralis (Stradner, 1962) Stover, 1966

E. octopetalus Varol, 1992

E. rarus Varol, 1992

Genus: *Flebellites* Thierstein, 1973

F. oblongus (Bukry, 1969) Crux in Lord, 1982

Genus: *Gartnerago* Bukry, 1969

G. coxalliae Lees, 2007

G. ponticula Bown & Hampton *in* Bown, 2005

G. obliquum Stradner, 1963

G. segmentatum (Stover, 1966) Thierstein, 1974

G. theta (Black in Black & Barnes, 1959) Jakubowski, 1986

Genus: *Grantarhabdus* Black, 1971

G. coronadventis (Reinhardt, 1966) Grün in Grün and Allemann, 1975

Genus: *Haqius* Roth, 1978

H. circumradiatus (Stover, 1966) Roth, 1978

Genus: *Helenea* Worsley, 1971

H. chiastia Worsley, 1971

Genus: *Helicolithus* Noël, 1970

H. anceps (Górka, 1957) Nöel, 1970

H. compactus (Bukry, 1969) Varol & Girgis, 1994

H. trabeculatus (Górka, 1957) Verbeek, 1977

H. turonicus Varol & Girgis, 1994

Genus: *Kamptnerius* Deflandre, 1959

K. magnificus Deflandre, 1959

Genus: *Lepideacassis* Black, 1971

L. bispinosa (Perch-Nielsen, in Perch-Nielsen & Franz, 1977) Burnett 1997

L. cornuta (Forchheimer & Stradner, 1973) Wind & Wise *in* Wise & Wind, 1977

L. mariae (Black, 1971) Wind & Wise in Wise & Wind, 1977

Genus: *Liliasterites* Stradner & Steinmetz, 1984

L. angularis Svabenicka & Stradner in Stradner & Steinmetz, 1984

Genus: *Lithastrinus* Stradner, 1962

L. grillii Stradner, 1962

L. pentabrachiatus Varol, 1992

L. septenarius Forchheimer, 1972

Genus: *Lithraphidites* Deflandre, 1963

L. carniolensis Deflandre, 1963

Genus: *Loxolithus* Noël, 1965

L. armilla (Black in Black & Barnes, 1959) Noel, 1965

Genus: *Lucianorhabdus* Deflandre, 1959

L. arcuatus Forchheimer, 1972

L. cayeuxii Deflandre, 1959

L. maleformis Reinhardt, 1966

L. quadrifidus Forchheimer, 1972

Genus: *Manivitella* Thierstein, 1971

M. pemmatoidea (Deflandre in Manivit, 1965) Thierstein, 1971

Genus: *Marthasterites* Deflandre, 1959

M. crassus (Deflandre, 1959) Burnett, 1997

M. furcatus (Deflandre in Deflandre & Fert 1954) Deflandre, 1959

M. simplex (Bukry, 1969) Burnett, 1997

Genus: *Microrhabdulus* Deflandre, 1959

M. quasihoschulzii Burnett, 1997

M. belgicus Hay & Towe, 1963

M. decoratus Deflandre, 1959

M. undosus Perch-Nielsen, 1973

Genus: *Micula* Vekshina, 1959

M. adumbrata Burnett, 1997

M. concava (Stradner in Martini & Stradner, 1960) Verbeek, 1976

M. cubiformis Forchheimer, 1972

M. staurophora (Gardet, 1955) Stradner, 1963

M. swastica Stradner & Steinmetz, 1984

Genus: *Nannoconus* Kamptner, 1931

N. elongatus Brönnimann, 1955

N. farinaceae Bukry, 1969

N. multicadus Deflandre & Deflandre-Rigaud, 1959

N. truitti frequens Deres and Achéritéguy, 1980

N. truitti rectangularis Deres and Achéritéguy, 1980

N. trutti truitti Brönnimann, 1955

Genus: *Orastrum* Wind & Wise in Wise & Wind, 1977

O. robinsonii Lees, 2007

Genus: *Owenia* Crux, 1991

O. hillii Crux, 1991

Genus: *Petrarhabdus* Wind & Wise in Wise, 1983

P. copulatus (Deflandre, 1959) Wind & Wise in Wise, 1983

Genus: *Placozygus* Hoffman, 1970

P. fibuliformis (Reinhardt, 1964) Hoffman, 1970

P. spiralis **(**Bramlette & Martini, 1964) Hoffmann, 1970

Genus: *Prediscosphaera* Vekshina, 1959

P. columnata (Stover, 1966) Perch-Nielsen, 1984

P. cretacea (Arkhangelsky, 1912) Gartner, 1968

P. desiderograndis Blair & Watkins 2009

P. grandis Perch-Nielsen, 1979

P. ponticula (Bukry, 1969) Perch-Nielsen, 1984

P. spinosa (Bramlette & Martini 1964) Gartner 1968

Genus: *Prolatipatella* Gartner, 1968

P. multicarinata Gartner, 1968

Genus: *Quadrum* Prins & Perch-Nielsen in Manivit et al., 1977

Q. eneabrachium Varol, 1992

Q. eptabrachium Varol, 1992

Q. gartneri Prins & Perch-Nielsen in Manivit et al., 1977

Q. giganteum Varol, 1992

Q. intermedium Varol, 1992

Q. octobrachium Varol, 1992

Q. svabenickae Burnett, 1997

Genus: *Radiolithus* Stover, 1966

R. planus Stover, 1966

Genus: *Reinhardtites* Perch-Nielsen, 1968

R. anthophorus (Deflandre, 1959) Perch-Nielsen, 1968

R. levis Prins & Sissingh in Sissingh, 1977

Genus: *Repagulum* Forchheimer, 1972

R. parvidentatum (Deflandre & Fert, 1954) Forchheimer, 1972

Genus: *Retecapsa* Black, 1971

R. angustiforata Black, 1971

R. crenulata (Bramlette & Martini, 1964) Grün in Grün and Allemann, 1975

R. ficula (Stover, 1966) Burnett, 1997

R. octofenestrata Bown *in* Bown & Cooper, 1998

R. schizobrachiata (Gartner, 1968) Grün in Grün and Allemann, 1975

R. surirella (Deflandre & Fert, 1954) Grün in Grün and Allemann, 1975

Rhabdolithus aquitanicus Manivit 1971

Genus: *Rhagodiscus* Reinhardt, 1967

R. achlyostaurion (Hill, 1976) Doeven, 1983

R. angustus (Stradner, 1963) Reinhardt, 1971

R. asper (Stradner, 1963) Reinhardt, 1967

R. plebeius Perch-Nielsen, 1968

R. reniformis Perch-Nielsen, 1973

R. splendens (Deflandre, 1953) Verbeek, 1977

Genus: *Rotelapillus* Noël, 1973

R. crenulatus (Stover, 1966) Perch-Nielsen, 1984

R. laffittei Noël 1957

Genus: *Rucinolithus* Stover, 1966

R. hayi Stover, 1966

R. terebrondentarius Applegate et al. in Covington & Wise, 1987

R. terebrondentarius youngii Tremolada & Erba (2002)

Genus: *Seribiscutum* Filewicz et al. *in* Wise & Wind, 1977

S. primitivum (Thierstein, 1974) Filewicz et al. *in* Wind & Wise 1983

Genus: *Staurolithites* Caratini, 1963

S. crux (Deflandre & Fert, 1954) Caratini, 1963

S. dicandidula Bergen in Bralower & Bergen, 1998

S. ellipticus (Gartner, 1968) Lambert, 1987

S. flavus Burnett, 1997

S. halfanii Lees, 2007

S. imbricatus (Gartner, 1968) Burnett, 1997

S. laffittei Caratini, 1963

S. mielnicensis (Górka 1957) Crux, 1982

S. minutus Burnett, 1997

Genus: *Stoverius* Perch-Nielsen, 1984

S. achylosus (Stover, 1966) Perch-Nielsen, 1984

Genus: *Tegumentatum* Thierstein in Roth & Thierstein, 1972

T. stradneri Thierstein in Roth & Thierstein, 1972

Genus: *Tetrapodorhabdus* Black, 1971

T. decorus (Deflandre in Deflandre & Fert, 1954) Wind & Wise in Wise & Wind, 1977

Genus: *Tranolithus* Stover, 1966

T. gabalus Stover, 1966

T. minimus (Bukry, 1969) Perch-Nielsen, 1984

T. orionatus Reinhardt, 1966

T. salillum (Noel, 1965) Crux, 1981

Genus Uniplanarius Hattner & Wise, 1980

U. gothicus (Deflandre, 1959) Hattner & Wise, in Wind & Wise 1983

U. sissinghii (Perch-Nielsen, 1986) Farhan 1987

Genus: *Watznaueria* Reinhardt, 1964

W. barnesiae (Black, 1959) Perch-Nielsen, 1968

W. biporta Bukry, 1969

W. britannica (Stradner, 1963) Reinhardt, 1964

W. fossacinta (Black, 1971) Bown in Bown & Cooper, 1989

W. manivitiae Bukry, 1973

W. ovata Bukry, 1969

W. quadriradiata Bukry, 1969

Genus: *Zeugrhabdotus* Reinhardt, 1965

Z. acanthus Reinhardt, 1965

Z. bicrescenticus (Stover, 1966) Burnett in Gale et al., 1996

Z. biperforatus (Gartner, 1968) Burnett, 1997

Z. blowii Lees, 2007

Z. diplogrammus (Deflandre in Deflandre & Fert, 1954) Burnett in Gale et al., 1996

Z. embergeri (Noël, 1958) Perch-Nielsen, 1984

Z. erectus (Deflandre in Deflandre & Fert, 1954) Reinhardt, 1965

Z. howei Bown in Kennedy et al., 2000

Z. kerguelensis Watkins, 1992

Z. noeliae Rod, Hay & Barnard, 1971

Z. praesigmoides Burnett, 1997

Z. scutula (Bergen, 1994) Rutledge & Bown, 1996

Z. sigmoides (Bramlette & Sullivan, 1961) Bown & Young, 1997

Z. streetiae Bown *in* Kennedy et al., 2000

Z. trivectis Bergen, 1994

Appendix 3
Plates

PLATE 1

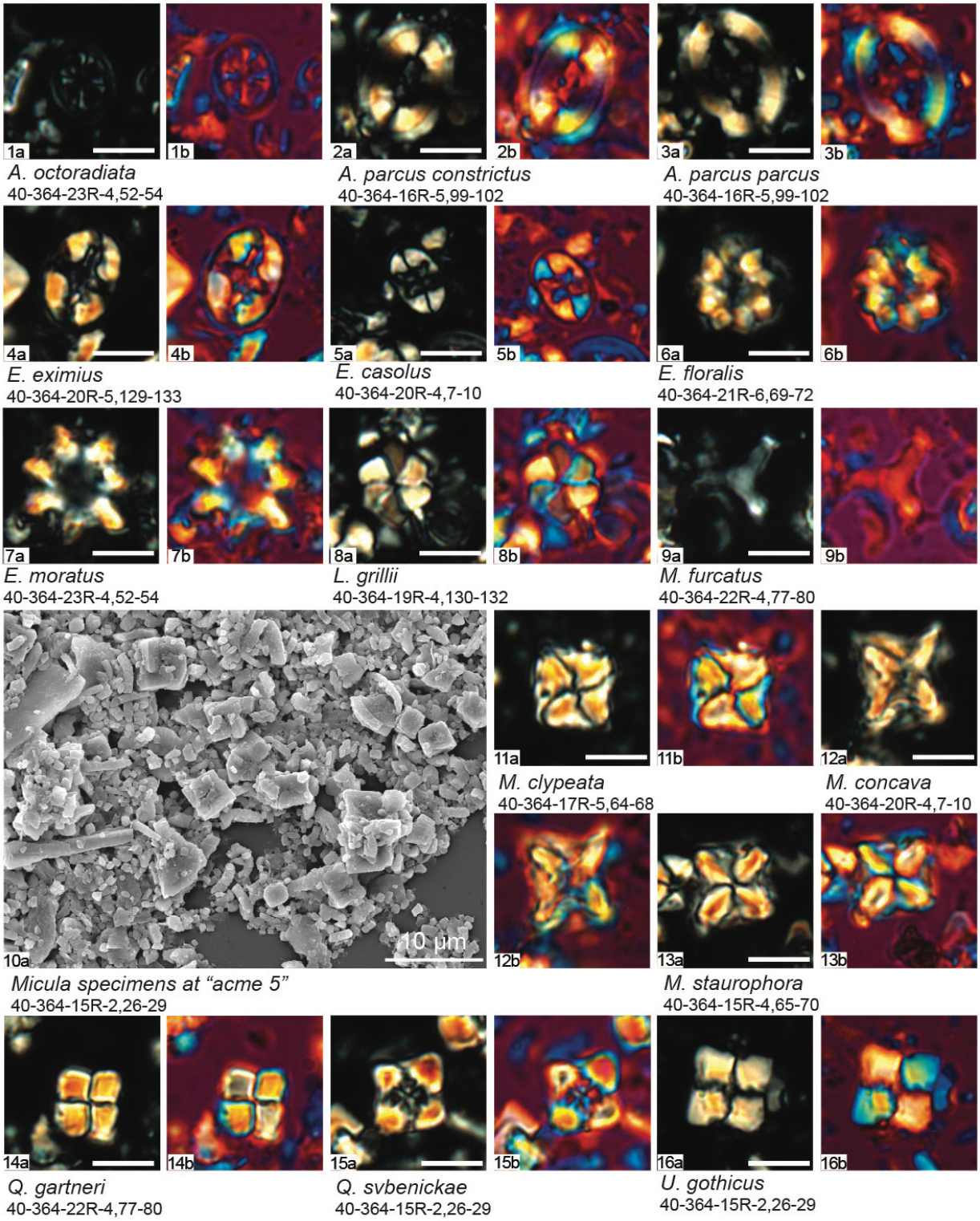

PLATE 2

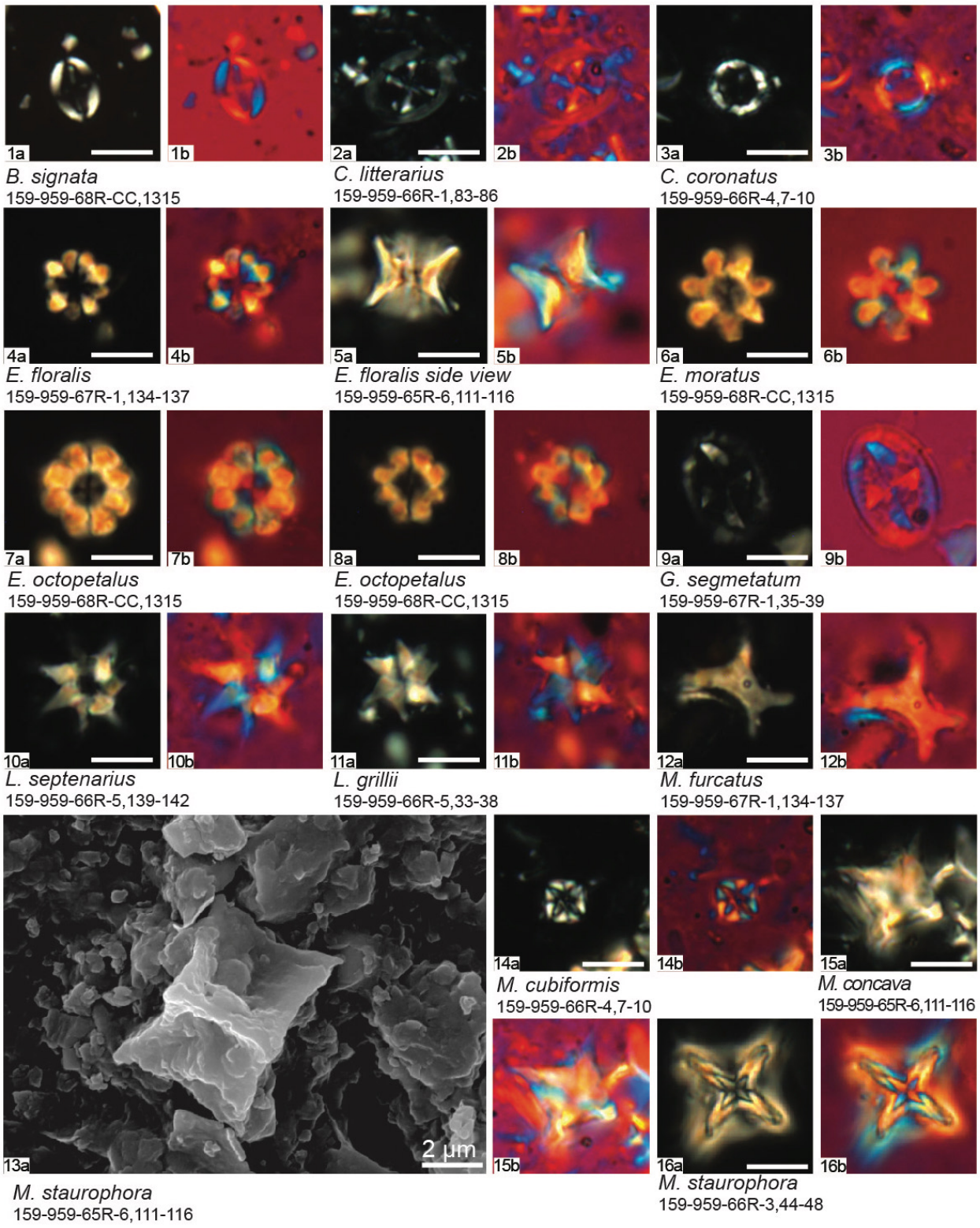
5 µm
1a
1b
B. signata
159-959-68R-CC,1315
2a
2b
C. litterarius
159-959-66R-1,83-86
3a
3b
C. coronatus
159-959-66R-4,7-10
4a
4b
E. floralis
159-959-67R-1,134-137
5a
5b
E. floralis side view
159-959-65R-6,111-116
6a
6b
E. moratus
159-959-68R-CC,1315
7a
7b
E. octopetalus
159-959-68R-CC,1315
8a
8b
E. octopetalus
159-959-68R-CC,1315
9a
9b
G. segmetatum
159-959-67R-1,35-39
10a
10b
L. septenarius
159-959-66R-5,139-142
11a
11b
L. grillii
159-959-66R-5,33-38
12a
12b
M. furcatus
159-959-67R-1,134-137
13a
2 µm
M. staurophora
159-959-65R-6,111-116
14a
M. cubiformis
159-959-66R-4,7-10
14b
15a
M. concava
159-959-65R-6,111-116
15b
16a
16b
M. staurophora
159-959-66R-3,44-48

PLATE 3

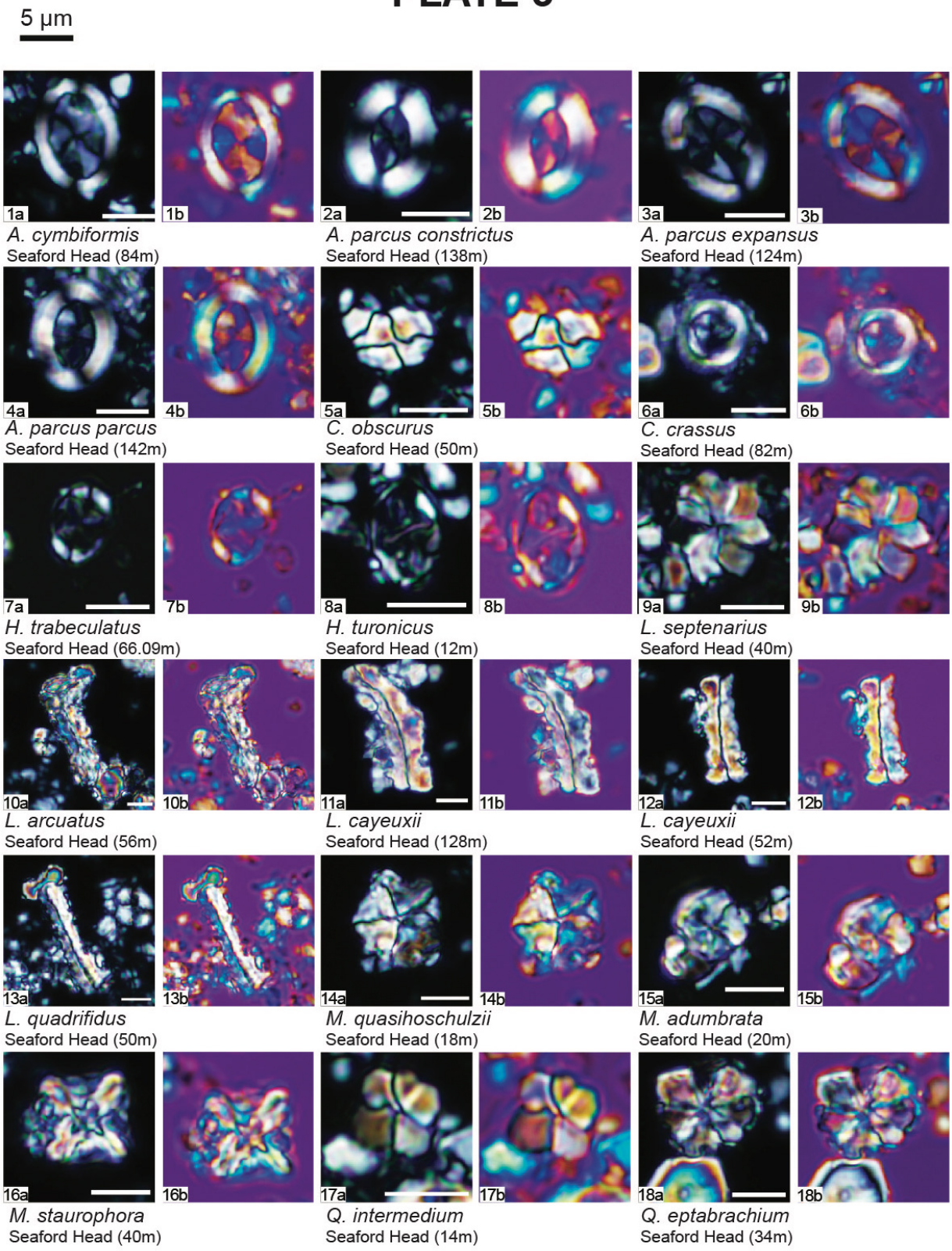
5 µm
1a
1b
A. cymbiformis
Seaford Head (84m)
2a
2b
A. parcus constrictus
Seaford Head (138m)
3a
3b
A. parcus expansus
Seaford Head (124m)
4a
4b
A. parcus parcus
Seaford Head (142m)
5a
5b
C. obscurus
Seaford Head (50m)
6a
6b
C. crassus
Seaford Head (82m)
7a
7b
H. trabeculatus
Seaford Head (66.09m)
8a
8b
H. turonicus
Seaford Head (12m)
9a
9b
L. septenarius
Seaford Head (40m)
10a
10b
L. arcuatus
Seaford Head (56m)
11a
11b
L. cayeuxii
Seaford Head (128m)
12a
12b
L. cayeuxii
Seaford Head (52m)
13a
13b
L. quadrifidus
Seaford Head (50m)
14a
14b
M. quasihoschulzii
Seaford Head (18m)
15a
15b
M. adumbrata
Seaford Head (20m)
16a
16b
M. staurophora
Seaford Head (40m)
17a
17b
Q. intermedium
Seaford Head (14m)
18a
18b
Q. eptabrachium
Seaford Head (34m)

PLATE 4

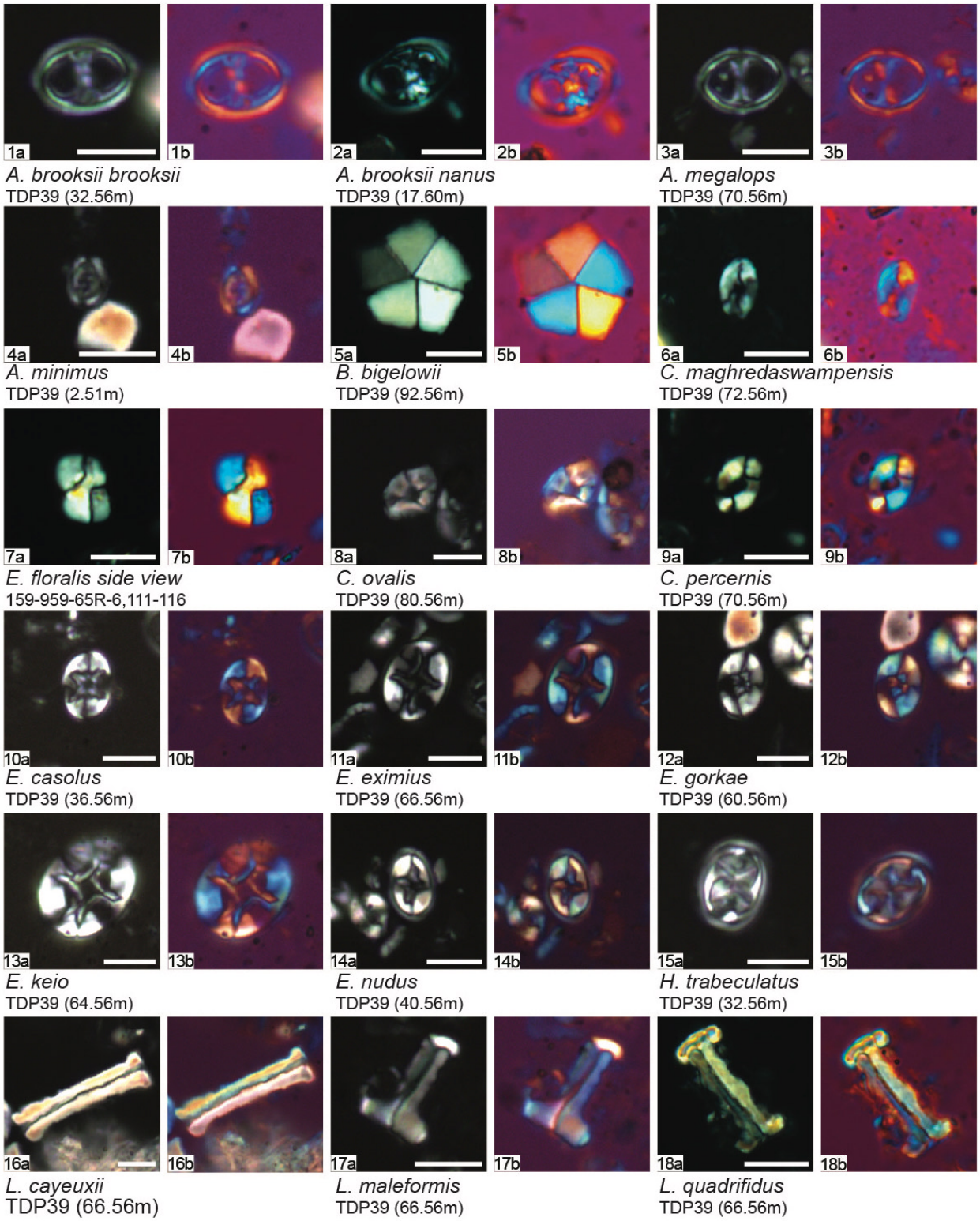
5 µm
1a
1b
A. brooksii brooksii
TDP39 (32.56m)
2a
2b
A. brooksii nanus
TDP39 (17.60m)
3a
3b
A. megalops
TDP39 (70.56m)
4a
4b
A. minimus
TDP39 (2.51m)
5a
5b
B. bigelowii
TDP39 (92.56m)
6a
6b
C. maghredaswampensis
TDP39 (72.56m)
7a
7b
E. floralis side view
159-959-65R-6,111-116
8a
8b
C. ovalis
TDP39 (80.56m)
9a
9b
C. percernis
TDP39 (70.56m)
10a
10b
E. casolus
TDP39 (36.56m)
11a
11b
E. eximius
TDP39 (66.56m)
12a
12b
E. gorkae
TDP39 (60.56m)
13a
13b
E. keio
TDP39 (64.56m)
14a
14b
E. nudus
TDP39 (40.56m)
15a
15b
H. trabeculatus
TDP39 (32.56m)
16a
16b
L. cayeuxii
TDP39 (66.56m)
17a
17b
L. maleformis
TDP39 (66.56m)
18a
18b
L. quadrifidus
TDP39 (66.56m)

PLATE 5

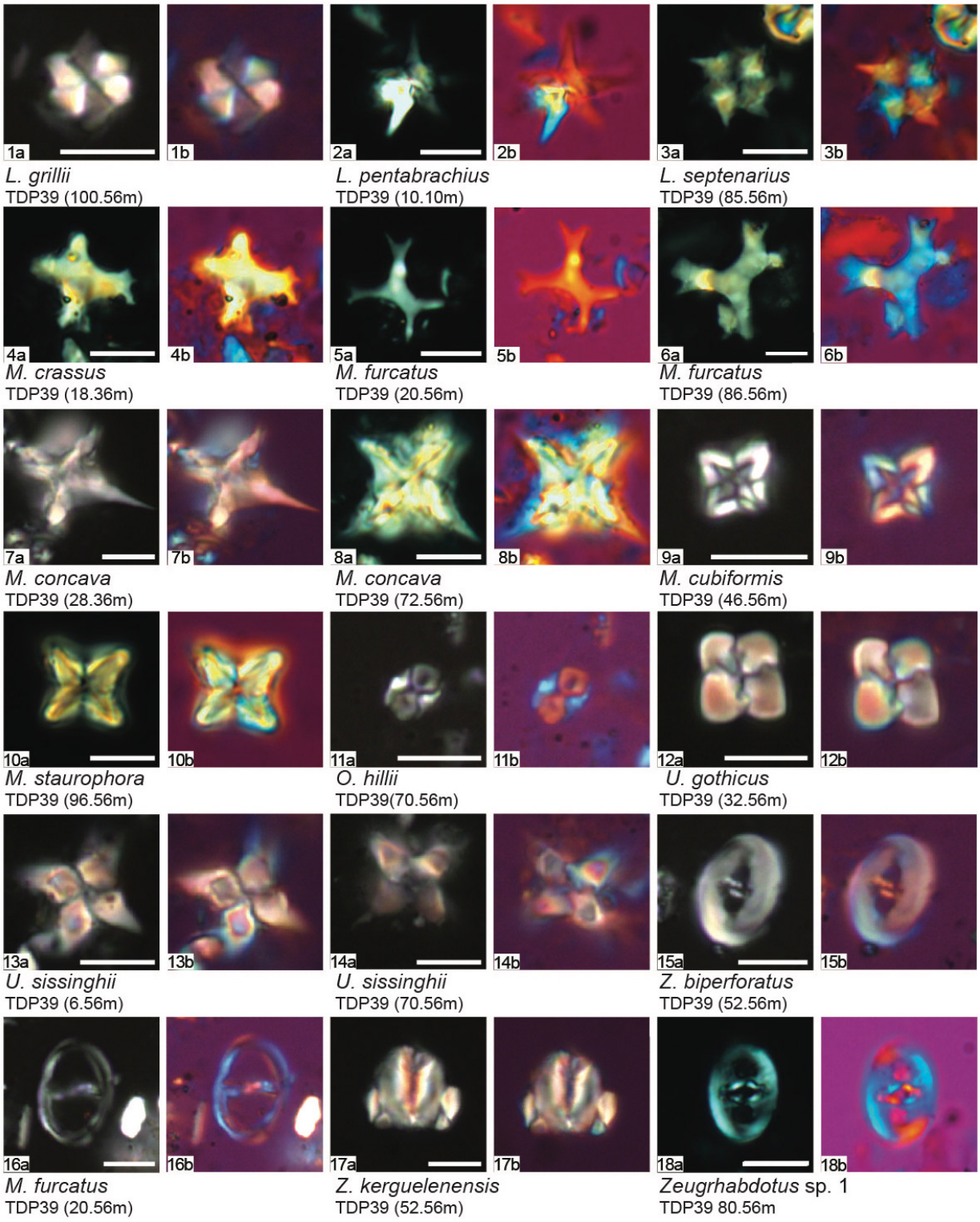
5 µm
1a
1b
2a
2b
3a
3b
L. grillii
TDP39 (100.56m)
L. pentabrachius
TDP39 (10.10m)
L. septenarius
TDP39 (85.56m)
4a
4b
5a
5b
6a
6b
M. crassus
TDP39 (18.36m)
M. furcatus
TDP39 (20.56m)
M. furcatus
TDP39 (86.56m)
7a
7b
8a
8b
9a
9b
M. concava
TDP39 (28.36m)
M. concava
TDP39 (72.56m)
M. cubiformis
TDP39 (46.56m)
10a
10b
11a
11b
12a
12b
M. staurophora
TDP39 (96.56m)
O. hillii
TDP39(70.56m)
U. gothicus
TDP39 (32.56m)
13a
13b
14a
14b
15a
15b
U. sissinghii
TDP39 (6.56m)
U. sissinghii
TDP39 (70.56m)
Z. biperforatus
TDP39 (52.56m)
16a
16b
17a
17b
18a
18b
M. furcatus
TDP39 (20.56m)
Z. kerguelenensis
TDP39 (52.56m)
Zeugrhabdotus sp. 1
TDP39 80.56m

Appendix 4

Table of papers with biostratigraphic and paleocological data for the Turonian-Campanian interval.

№	PAPER	Realm	Basin	Section	Time interval studied	Methodology	TAXONOMY	BIOSTRATIGRAPHY	Plates	Range chart	PALEOENVIRONMENT	PALEOECOLOGY	Morphometrics	Principal component analyses	Cluster Analyses	New bioevents	Lithostratigraphy	Ammonite stratigraphy	Foraminiferal stratigraphy	Inoceramids bivalves	Calcareous	Echinoids	Paleoecology/O xygen proxies	Chemo stratigraphy (C-O isotopes)	Magneto stratigraphy	Cicle stratigraphy
1	**Razmjoo et al., (2020a)**	Tethys	Zagros Basin (Iran)	Bevan	L.Santonian-Selandian	Semi-quantitative	NO	YES	YES	YES	YES	NO	NO	NO	NO	NO	YES	NO	NO	NO	NO	NO	NO	YES	NO	NO
2	**Razmjoo et al., (2020b)**	Tethys	Zagros Basin (Iran)	Shahneshin	L. Coniacian - Maastrichtian	Quantitative	NO	NO	YES	YES	YES	NO	NO	NO	NO	NO	NO	NO	YES	NO	NO	NO	NO	NO	NO	NO
3	**Watkins and Mann Guerra (2020)**	Great Australian Bight	Australian-Antarctic Basin	IODP Site U1512	E. Turonian-M. Santonian	Quantitative	NO	YES	NO	NO	YES	YES	NO	YES (DCA)	NO	NO	NO	NO	NO	NO	NO	NO	NO	NO	NO	NO
4	**Al Hawali and Dorobek Jones (2019)**	Tethys	Arauma (Oman)	9 wells from Fiqra formation	L. Coniacian- E. Campanian	Quantitative (cascading count)	YES	YES	YES	NO	YES	YES	NO	NO	NO	NO	NO	NO	NO	NO	NO	NO	NO	NO	NO	NO
5	**Faris et al., (2019)**	Tethys	Kurdistan (Iraq)	Dokan	Coniacian -L. Campanian	Semi-quantitative/ Quantitative	NO	YES	YES	YES	NO	NO	NO	NO	NO	NO	NO	NO	NO	NO	NO	NO	NO	NO	NO	NO
6	**Pérez Panera et al., (2019)**	South America	Magdalena Valley Basin (Colombia)	Well	Turonian-L. Campanian	Semiquantitative	NO	YES	YES	NO	NO	NO	NO	NO	NO	YES	NO	NO	NO	NO	NO	NO	NO	NO	NO	NO
7	**Farouk et al., (2018)**	Tethys	Carbonate platform system	Ain Zeuddes section	L. Santonian/E. Campanian	Qualitative	NO	YES	YES	NO	NO	NO	NO	NO	NO	YES	NO	NO	YES	NO	NO	NO	NO	YES	NO	NO
8	**Pittmann et al., (2018)**	Boreal Sea	Mississauga Basin	6 wells -Baltic area	Coniacian-Campanian	Semiquantitative	NO	YES	YES	NO	YES	NO	NO	NO	NO	YES	NO	NO	NO	NO	NO	NO	NO	YES	NO	NO
9	**Razmjoo et al., (2018)**	Tethys	Zagros Basin (Iran)	Shahneshin section	Coniacian-Maastrichtian	153 samples processed; abundance&2 counted 300 specimens	NO	YES	YES	NO range chart in Razmjoo et al., (2018)	NO	NO	NO	NO	NO	NO	YES	NO	YES	NO	NO	NO	NO	YES	YES	NO	NO
10	**Wolfgring et al., (2018)**	Tethys	Thethys (Northern Alps)	Perdaun section (Gosau Group)	L. Santonian/E. Campanian	Semiquantitative	NO	YES	YES	NO	NO	NO	NO	NO	NO	NO	YES	NO	YES	NO	NO	NO	NO	NO	YES (+ C45Y3 SR87/SR86)	YES	YES
11	**Dubicka et al., (2017)**	Boreal Sea	Polish epicontinental sea	Bocieniec	L. Santonian/E. Campanian	Semiquantitative	NO	YES	YES	YES	NO	NO	NO	NO	NO	NO	NO	NO	YES (+ benthic)	NO	YES	NO	YES	YES	YES	NO
12	**Farouk et al., (2017)**	Tethys	North- central Tunisia	Jbil- Gabel Imaidda Jguem Sidab El Kef	L. Coniacian/E. Santonian	Semiquantitative	NO	YES	YES	NO	NO	NO	NO	NO	NO	NO	YES	YES	YES	YES	NO	NO	NO	NO	NO	NO	NO
13	**Kita et al., (2017)**	North America	Western Interior	Smoky Hill- Armstrong Aragas 12-8	L. Santonian/E. Campanian	Semi-quantitative - absence/ presence	NO	YES	YES	NO	NO	NO	NO	NO	NO	NO	YES	NO	NO	NO	NO	NO	NO	NO	NO	YES (pers. communication)	NO
14	**Wolfgring et al., (2017)**	Tethys	Maiolica Gyronk (Turkey)	Composite section	L. Santonian/E. Campanian	Qualitative	NO	YES	YES	NO	NO	NO	NO	NO	NO	NO	YES	NO	NO	NO	NO	NO	NO	NO	NO	YES	YES
15	**Farouk et al.,(2016)**	Tethys	North Egypt and Jordan Basin	Gebel Qabaliat, Gebel Nataruk,Ras el Gifa (Sinai); Jordan,Kraik, Wadi Musib, Wadi El Hafar (Jordan)	L. Turonian - Campanian	Semiquantitative	NO	YES	YES	YES	NO	NO	NO	NO	NO	NO	YES	NO	YES	NO	NO	NO	NO	NO	NO	NO	NO	NO
16	**Jiménez Berrocoso et al., 2015**	Indian Ocean	Mandawa and Rovuma Basin	TDP39	Middle Coniacian -Early Maastrichtian	Semiquantitative	NO	YES	NO	NO	NO	NO	NO	NO	NO	NO	YES	NO	YES	NO	NO	NO	NO	NO	YES	NO	NO
17	**Bruce and Watkins (2014)**	Atlantic Ocean; North America; Indian Ocean	Western Interior, Gulf of Mexico, Blake Nose, Atlantic Plains, Angola Basin	Washington Co., KS, Smoky Hill Sites(SH); DSDP Site 95; ODP Site 1049A/1050C; ODP Leg 150;DSDP Leg 71;DSDP Leg 26	L.A.Basin- Maastrichtian	Biometric	YES	YES	NO	YES	NO	NO	YES	NO	NO	NO	NO	NO	NO	NO	NO	NO	NO	NO	NO	NO	NO	NO
18	**Corbett and Watkins (2016)** a	North America	Western Interior	Mesa Verde National Park	Coniacian - E. Campanian	Semiquantitative	YES	YES	YES	NO	NO	NO	NO	NO	NO	NO	NO	NO	NO	NO	NO	NO	NO	NO	NO	NO	NO
19	**Corbett and Watkins (2016)** b	Atlantic Ocean; North America	Western Interior, Gulf of Mexico, Blake Nose, Atlantic Plains, Angola Basin	ODP Site 95(H); Sites 1275B and 1256C; Kast Beach Core hole NH-C; Cretaceous Rock Outcrops Mesa Verde National Park, Colorado	E. Turonian/E. Santonian	Biometric	YES	YES	NO	NO	YES	YES	NO	NO	YES	NO	NO	NO	NO	NO	NO	NO	NO	NO	NO	NO	NO	NO
20	**Corbett et al., (2014)**	North America	Western Interior	Mesa Verde National Park,Rock Canyon & Hwy 90 composite	L. Coniacian/E. Campanian	Quantitative (cascading count)	NO	YES	YES	NO	NO	NO	NO	NO	NO	NO	NO	NO	NO	NO	NO	NO	NO	NO	NO	NO	NO	NO
21	**Da Gama et al., 2014**	North America	Western Interior	7 wells (Nobrara Fm.)	L. Turonian - E. Campanian	Quantitative (cascading count)	NO	YES	YES	YES	NO	NO	NO	NO	NO	NO	YES	NO	YES	NO	NO	NO	YES	NO	NO	NO	NO
22	**Lamolda et al.(2014)**	Basque-Cantabrian	Navarro-Cantabrian Platform	Olazagutia	E. Coniacian/E. Santonian	Qualitative	NO	YES	NO	NO	YES	NO	NO	NO	NO	NO	YES	YES	YES	YES	YES	YES	NO	YES	YES	NO	NO
23	**Lamolda et al., (2014)**	Atlantic Ocean	Celtic Sea	DSDP Site 549	Coniacian - Maastrichtian	Biometric	NO	NO	YES	NO	YES	YES	YES	NO	YES	NO	NO	NO	NO	NO	NO	NO	NO	NO	NO	NO	NO
24	**Razmjoo et al., (2014)**	Tethys	Zagros Basin (Iran)	Shahneshin section	Coniacian-Maastrichtian	153samples processed; abundance&2 counted 300 specimens	NO	YES	YES	YES	NO	NO	NO	NO	NO	NO	YES	NO	YES	NO	NO	NO	NO	YES	NO	NO	NO
25	**Sabelnikk and Babik (2014)**	Tethys	Bohemian and Outer Flysch Carpathians	Quarry: Rhaetic (Opletaly Member) borehole: Bh-2010/4 ; Sedlova Skála; Stráský VRT0004; Malý	M. Turonian-L.Coniacian	Semiquantitative and Quantitative	NO	YES	YES	YES	YES	NO	NO	NO	NO	NO	YES	NO	YES	NO	NO	NO	NO	NO	NO	NO	NO	NO
26	**Farouk and Faris (2012)**	Tethys	West Central Sinai	Mitla Pass section (Sinai)	Coniacian-Middle Campanian	Semiquantitative	NO	YES	YES	NO	NO	NO	NO	NO	NO	NO	YES	NO	YES	NO	NO	NO	NO	NO	NO	NO	NO
27	**Guerra et al., (2012)**	Atlantic Ocean	Pelotas Basin (Brazil)	3 wells	L.Albian/E. Cretaceous-Maastrichtian	Semiquantitative/ Quantitative	NO	YES	YES	YES	NO	NO	NO	NO	NO	NO	YES	NO	NO	NO	NO	NO	NO	NO	NO	NO	NO
28	**Svabenická (2012)**	Tethys	Bohemian Cretaceous Basin	Outcrops and boreholes	Coniacian-Cenomanian	Semi-quantitative	NO	YES	NO	YES	NO	NO	NO	NO	NO	NO	YES	NO	NO	NO	NO	NO	NO	NO	NO	NO	NO
29	**Wahnsiedler et al., (2012)**	North America	Western Interior	Wagon Mound - Springer (USA)	Turonian/Coniacian	Semiquantitative	NO	YES	NO	YES	NO	NO	NO	NO	NO	NO	NO	NO	YES	NO	NO	NO	NO	NO	NO	NO	NO
30	**Cetean et al., (2011)**	Tethys	Eastern Carpathians	Ialoz Valley section	L. Santonian/E. Campanian	Semiquantitative	NO	YES	NO	NO	NO	NO	NO	NO	NO	NO	NO	NO	YES (+ benthic)	NO	NO	NO	NO	NO	NO	NO	NO
31	**Linnert et al., (2011)**	Atlantic Ocean	Celtic Sea	DSDP Site 549-551	Coniacian-Maastrichtian	Quantitative	NO	YES	YES	YES	NO	YES	NO	NO	NO	NO	NO	NO	NO	NO	NO	NO	NO	NO	NO	NO	NO
32	**Mellere-Dabrowska and Bujtar (2010)**	Tethys	South Carpathians	Hateg region (Romania)	Coniacian-Campanian	Semiquantitative	NO	YES	YES	NO	NO	NO	NO	NO	NO	NO	NO	NO	NO	NO	NO	NO	NO	NO	NO	NO	NO
33	**Wagreich et al., (2010)**	Tethys	Thethys (Northern Alps)	St Hauig area (Gosau Formation)	L. Coniacian/ Campanian	Semiquantitative	NO	YES	YES	NO	NO	NO	NO	NO	NO	NO	YES	YES	YES	NO (in Pflug et al., 1973; Sissingh, 1977)	NO	NO	NO	YES	YES	NO	NO
34	**Wahnsiedler et al., (2010)**	Boreal Sea	Central Europe Basin system	Schatma section (Gosau Group)	Upper Santonian	Semiquantitative	NO	YES	NO	NO	NO	NO	NO	NO	NO	NO	YES	YES	YES	YES	NO	NO	NO	NO	YES (+SR87/SR86)	NO	NO
35	**Wahnsiedler et al., (2010)**	Boreal Sea	Central Europe Basin system	Salzgitter-Salder (Germany); Stupa Nadbrzezhna (Poland)	Turonian/Coniacian	Semiquantitative	NO	YES	NO	NO	NO	NO	NO	NO	NO	NO	YES	YES	YES	YES	NO	NO	NO	NO	YES	NO	NO
36	**Blair and Watkins (2009)**	North America	Western Interior	Ten Mile Creek / Locality 13	E. Coniacian/E. Santonian	Qualitative and Quantitative	NO	YES	NO	NO	NO	NO	NO	NO	NO	NO	YES	NO	NO	YES	NO	NO	NO	NO	NO	NO	NO
37	**Skupinski and Wildeis (2009)**	North America; Atlantic Ocean	Western Interior, Gulf of Mexico; Blake Nose	Washington Co., KS, Smoky Hill Sites(SH); DSDP Site 95; ODP Site 1049A/1050C	Coniacian-Maastrichtian	Quantitative	YES	NO	YES	NO	YES	YES	YES	NO	NO	NO	YES	NO	NO	NO	NO	NO	NO	NO	NO	NO	NO	NO
38	**Gale et al., (2008)**	North America	Western Interior	Wandaville	E. Santonian/E. Campanian	Semiquantitative	NO	YES	YES	NO	NO	NO	NO	NO	NO	NO	YES	YES	YES	YES	NO	NO	NO	NO	YES(Milner and Kirkland, 2006)	NO	NO
39	**Ifrim (2008)**	Boreal Sea	Central Europe Basin system; Baltic-Mazhkiel Basin	Salzgitter-Salder Quarry-Stupa Nadbrzezhna (Poland); Rüthen-Kallenhardt quarries Sinsen	Turonian/Coniacian	Semiquantitative	NO	YES	NO	YES	NO	NO	NO	NO	NO	NO	YES	NO	YES	NO	NO	NO	NO	NO	NO	NO	NO	NO
40	**Gale (2007)**	North America	Western Interior	Ten Mile Creek	E. Coniacian/E. Santonian	Semiquantitative	NO	YES	YES	YES	NO	NO	NO	NO	NO	NO	YES	YES	YES	YES	NO	NO	NO	NO	YES	NO	NO

Appendix 5
Range chart of DSDP Site 364

Full range chart of nannofossil taxa recognized at **DSDP Site 364** is available upon request. Semi-quantitative abundance of all taxa detected are reported, as well as total abundance and preservation of calcareous nannofossils in each studied sample.

Total abundance: Abundant (A) = 21-30 specimens in each field of view; Common (C) = 11-20 specimens in each field of view; Few (F)= 6-10 specimens in each field of view; Rare (R) = 1-5 specimens in each field of view.

Species abundance: Abundant (A) = $\geq$ 1 specimen in each field of view; Common (C) = 1 specimen in 2-10 fields of view; Few (F) = 1 specimen in 11-30 fields of view; Rare (R) = 1 specimen in > 31 fields of view.

Preservation was characterized as follows:

Good (G) if nannofossil specimens show little or no evidence of dissolution and/or overgrowth and the primary morphological characters are only slightly altered allowing species identification;

Moderate (M) if specimens exhibit some etching and/or overgrowth, primary morphological characters are somewhat altered allowing, however, identification at the species level;

Poor (P) if specimens show severe etching and/or overgrowth, primary morphological characters are obliterated, hampering identification at the species and/or even generic level

Appendix 6A
Correlation matrix of genera – DSDP 364

The quantitative data used to produce this matrix are available upon request

	Ahmuellerella	*Amphizygus*	*Arkhangelskiella*	*Aspidolithus*	*Biscutum*	*Braarudosphaera*	*Broinsonia*	*Chiastozygus*	*Ceratolithoides*	*Cribrosphaerella*	*Cylindralithus*	*Corollithion*	*Discorhabdus*	*Eiffellithus*	*Eprolithus*	*Flabellites*	*Gartnerago*	*Grantarhabdus*	*Haqius*	*Helicolithus*	*Kamptnerius*	*Lithastrinus*
Ahmuellerella	1																					
Amphizygus	-0.11	1																				
Arkhangelskiella	0.21	-0.11	1																			
Aspidolithus	-0.13	-0.08	0.34	1																		
Biscutum	0.24	-0.04	-0.09	-0.11	1																	
Braarudosphaera	-0.08	-0.08	0.45	0.52	0.02	1																
Broinsonia	-0.12	0.05	0.27	0.29	-0.06	0.57	1															
Chiastozygus	0.14	0.12	0.25	0.48	-0.13	0.31	0.23	1														
Ceratolithoides	0.01	-0.10	0.29	0.49	0.13	**0.71**	0.38	0.36	1													
Cribrosphaerella	0.19	-0.07	0.31	0.29	-0.18	-0.12	-0.05	0.35	0.11	1												
Cylindralithus	0.04	-0.18	-0.03	0.24	-0.21	-0.13	-0.03	0.26	0.12	0.32	1											
Corollithion	0.09	0.16	-0.07	-0.07	**0.81**	0.02	-0.07	-0.02	0.13	-0.19	-0.16	1										
Discorhabdus	0.37	-0.04	-0.05	-0.08	0.30	-0.04	-0.05	-0.12	-0.05	-0.14	-0.14	-0.03	1									
Eiffellithus	0.11	0.09	-0.26	-0.27	0.33	-0.18	-0.07	-0.12	-0.22	-0.33	-0.24	0.10	0.59	1								
Eprolithus	0.05	0.05	-0.23	-0.26	0.50	-0.02	-0.09	-0.19	-0.10	-0.37	-0.21	0.37	0.33	**0.61**	1							
Flabellites	0.03	0.12	-0.16	-0.19	0.25	-0.11	0.15	-0.27	-0.10	-0.29	-0.27	0.07	0.33	0.38	0.38	1						
Gartnerago	0.03	0.20	-0.09	0.15	0.11	0.10	0.19	0.22	-0.06	-0.03	0.04	-0.04	0.20	0.43	0.22	-0.05	1					
Grantarhabdus	-0.05	-0.04	-0.05	0.00	-0.04	-0.04	-0.05	-0.12	-0.05	0.01	0.16	-0.03	-0.02	-0.11	-0.09	0.09	-0.12	1				
Haqius	-0.05	**0.80**	-0.10	-0.12	0.24	-0.05	0.08	0.09	-0.03	-0.08	-0.25	0.46	-0.04	0.05	0.17	0.21	0.05	-0.04	1			
Helicolithus	-0.05	0.04	-0.20	-0.21	-0.03	-0.09	0.07	-0.25	-0.17	-0.12	0.00	-0.08	0.01	0.28	0.13	0.10	0.05	0.20	0.02	1		
Kamptnerius	-0.08	-0.06	-0.08	-0.04	0.00	-0.06	0.16	0.20	-0.07	0.15	-0.14	-0.04	-0.03	0.26	0.05	0.05	0.28	-0.03	-0.06	-0.12	1	
Lithastrinus	0.08	-0.15	0.08	0.05	-0.16	0.04	0.11	0.11	-0.17	0.17	0.21	-0.17	-0.12	0.01	-0.11	-0.22	0.53	-0.12	-0.18	0.12	0.11	1
Lithraphidites	0.20	0.34	-0.21	-0.20	**0.64**	-0.04	-0.07	-0.05	-0.06	-0.09	-0.19	0.53	0.51	0.39	0.45	0.33	0.09	0.08	0.52	0.12	-0.04	-0.16
Loxolithus	-0.09	-0.07	-0.09	0.45	-0.06	-0.06	0.04	-0.03	-0.08	0.11	0.18	-0.05	-0.04	-0.17	-0.15	-0.11	-0.06	-0.04	-0.07	-0.11	-0.05	-0.01
Manivitella	-0.24	-0.07	0.02	0.05	-0.11	-0.09	-0.14	-0.06	-0.21	0.01	-0.05	-0.07	-0.04	-0.15	-0.13	0.02	-0.13	-0.06	-0.08	-0.16	-0.02	-0.05
Marthasterites	-0.09	-0.01	-0.08	-0.11	-0.05	0.14	-0.06	-0.11	-0.08	-0.22	-0.16	-0.04	-0.04	-0.09	0.05	-0.05	-0.12	0.01	-0.02	-0.06	-0.05	-0.15
Microrhabdolus	0.01	0.00	-0.22	0.00	0.05	-0.12	-0.11	0.07	-0.14	-0.01	0.25	-0.09	0.10	0.37	0.21	0.04	0.49	0.20	-0.11	0.22	0.16	0.33
Micula	-0.08	-0.21	0.18	0.22	-0.17	-0.02	-0.12	-0.03	0.23	0.09	0.15	-0.15	-0.11	-0.44	-0.42	-0.31	-0.33	-0.09	-0.21	-0.32	-0.15	-0.23
Placozygus	0.37	-0.04	-0.05	-0.08	0.30	-0.04	-0.05	-0.12	-0.05	-0.14	-0.14	-0.03	**1.00**	0.59	0.33	0.33	0.20	-0.02	-0.04	0.01	-0.03	-0.12
Prediscosphaera	0.01	0.10	-0.17	-0.22	0.21	-0.10	0.05	-0.20	-0.17	-0.05	0.01	0.12	0.19	0.31	0.36	0.25	0.18	0.06	0.03	0.45	0.14	0.05
Quadrum	-0.05	0.37	-0.22	-0.20	0.01	0.01	-0.13	-0.10	-0.19	-0.18	-0.16	-0.02	0.20	0.25	0.30	0.09	0.10	0.12	0.44	0.23	0.07	-0.20
Radiolithus	-0.08	0.11	-0.15	-0.04	0.31	-0.08	-0.14	0.08	-0.05	-0.22	-0.01	0.36	-0.06	0.27	0.24	0.08	0.10	0.54	0.10	0.06	0.11	-0.26
Reinhardtites	0.10	0.29	0.17	0.24	-0.20	0.42	0.41	0.25	0.30	-0.04	0.06	-0.04	-0.16	-0.09	-0.07	0.08	0.10	0.30	0.26	0.19	0.04	0.06
Retecapsa	-0.03	0.01	-0.05	-0.12	-0.15	-0.16	-0.08	0.14	-0.17	0.20	0.09	-0.08	-0.10	-0.11	-0.08	-0.04	-0.06	-0.15	-0.03	-0.10	0.06	0.13
Rhagodiscus	0.45	0.14	-0.25	-0.20	0.45	-0.14	-0.01	0.05	-0.01	-0.03	0.03	0.34	0.03	0.22	0.26	0.06	0.32	-0.10	0.23	0.02	0.08	0.11
Rotelapillus	0.11	-0.06	-0.07	-0.10	**0.90**	0.03	-0.06	-0.12	0.15	-0.18	-0.18	**0.82**	-0.03	0.17	0.55	0.19	0.03	-0.03	0.24	-0.08	-0.04	-0.16
Rucinolithus	-0.22	-0.06	-0.13	-0.28	-0.15	-0.10	0.17	-0.11	-0.22	-0.03	-0.03	-0.11	-0.10	-0.13	-0.07	-0.08	-0.18	0.08	-0.04	0.11	-0.14	-0.04
Stoverius	0.21	0.04	-0.12	-0.15	0.42	-0.07	0.19	-0.02	-0.06	-0.11	-0.30	0.21	**0.65**	**0.62**	0.45	0.36	0.37	-0.05	0.13	-0.11	0.56	0.00
Tetrapodorhabdus	-0.10	**0.61**	-0.09	-0.10	-0.05	-0.07	-0.09	0.12	-0.08	-0.04	-0.21	0.21	-0.04	0.18	0.32	0.04	0.10	-0.04	**0.69**	0.05	-0.05	-0.15
Tranolithus	0.10	0.29	-0.20	-0.27	0.34	-0.15	0.12	-0.10	-0.18	-0.08	-0.15	0.16	0.28	0.33	0.21	0.40	0.24	0.07	0.36	0.41	-0.09	0.01
Uniplanarius	-0.10	-0.08	-0.08	0.04	-0.06	-0.07	-0.09	-0.21	0.00	-0.19	0.00	-0.06	-0.04	-0.19	-0.17	-0.12	-0.23	-0.04	-0.08	-0.14	-0.06	-0.23
Watznaueria	0.00	0.18	0.03	-0.06	-0.26	0.00	0.13	0.13	-0.15	0.07	-0.12	-0.11	-0.21	0.11	-0.05	0.12	0.15	0.15	0.11	0.09	0.07	0.31
Zeugrhabdotus	0.24	0.07	-0.17	-0.22	**0.63**	0.04	0.00	-0.19	-0.02	-0.26	-0.15	0.46	0.30	0.48	**0.60**	0.38	0.25	0.04	0.22	0.45	-0.04	-0.06

	Lithraphidites	*Loxolithus*	*Manivitella*	*Marthasterites*	*Microrhabdolus*	*Micula*	*Placozygus*	*Prediscosphaera*	*Quadrum*	*Radiolithus*	*Reinhardtites*	*Retecapsa*	*Rhagodiscus*	*Rotelapillus*	*Rucinolithus*	*Stoverius*	*Tetrapodorhabdus*	*Tranolithus*	*Uniplanarius*	*Watznaueria*	*Zeugrhabdotus*
Lithraphidites	1																				
Loxolithus	-0.11	1																			
Manivitella	-0.09	0.04	1																		
Marthasterites	-0.09	-0.06	0.01	1																	
Microrhabdolus	0.12	-0.07	-0.18	-0.05	1																
Micula	-0.38	0.25	-0.07	-0.14	-0.34	1															
Placozygus	0.51	-0.04	-0.04	-0.04	0.10	-0.11	1														
Prediscosphaera	0.43	-0.07	-0.03	-0.18	0.20	-0.53	0.19	1													
Quadrum	0.38	0.14	-0.03	0.22	0.12	-0.21	0.20	0.22	1												
Radiolithus	0.19	-0.10	-0.06	0.04	0.38	-0.24	-0.06	0.03	0.11	1											
Reinhardtites	0.04	-0.11	-0.20	-0.12	0.17	-0.20	-0.16	0.15	0.09	0.22	1										
Retecapsa	-0.04	0.01	0.22	-0.21	0.01	-0.26	-0.10	0.18	-0.14	-0.16	-0.05	1									
Rhagodiscus	0.27	-0.08	-0.12	-0.14	0.15	-0.28	0.03	0.14	0.05	0.16	0.08	0.06	1								
Rotelapillus	0.44	-0.05	-0.08	-0.05	-0.04	-0.14	-0.03	0.12	-0.05	0.36	-0.18	-0.13	0.48	1							
Rucinolithus	-0.05	-0.10	0.18	-0.02	-0.13	-0.21	-0.10	0.00	-0.09	-0.08	-0.11	0.11	-0.14	-0.13	1						
Stoverius	0.47	-0.08	-0.10	-0.07	0.18	-0.25	**0.65**	0.32	0.15	0.06	-0.06	-0.16	0.16	0.21	-0.18	1					
Tetrapodorhabdus	0.25	-0.06	-0.02	-0.05	-0.18	-0.18	-0.04	-0.04	0.48	0.12	0.12	0.02	0.14	0.12	-0.08	0.02	1				
Tranolithus	0.42	-0.17	-0.04	-0.13	0.08	-0.45	0.28	0.33	0.23	0.12	0.11	0.23	0.19	0.20	0.19	0.21	0.12	1			
Uniplanarius	-0.16	-0.03	-0.16	-0.07	-0.23	**0.60**	-0.04	-0.29	-0.13	-0.11	-0.09	-0.17	-0.19	-0.05	-0.19	-0.09	-0.07	-0.23	1		
Watznaueria	-0.07	-0.17	0.15	-0.16	0.12	**-0.61**	-0.21	0.03	-0.08	0.12	0.21	0.07	0.10	-0.16	0.36	-0.07	0.20	0.04	-0.51	1	
Zeugrhabdotus	0.56	-0.18	-0.17	-0.08	0.33	-0.50	0.30	0.55	0.32	0.34	0.14	-0.12	0.30	0.50	-0.05	0.32	0.06	0.52	-0.24	-0.05	1

Appendix 6B
Correlation matrix of species -DSDP Site 364

The quantitative data used to produce this matrix are available upon request

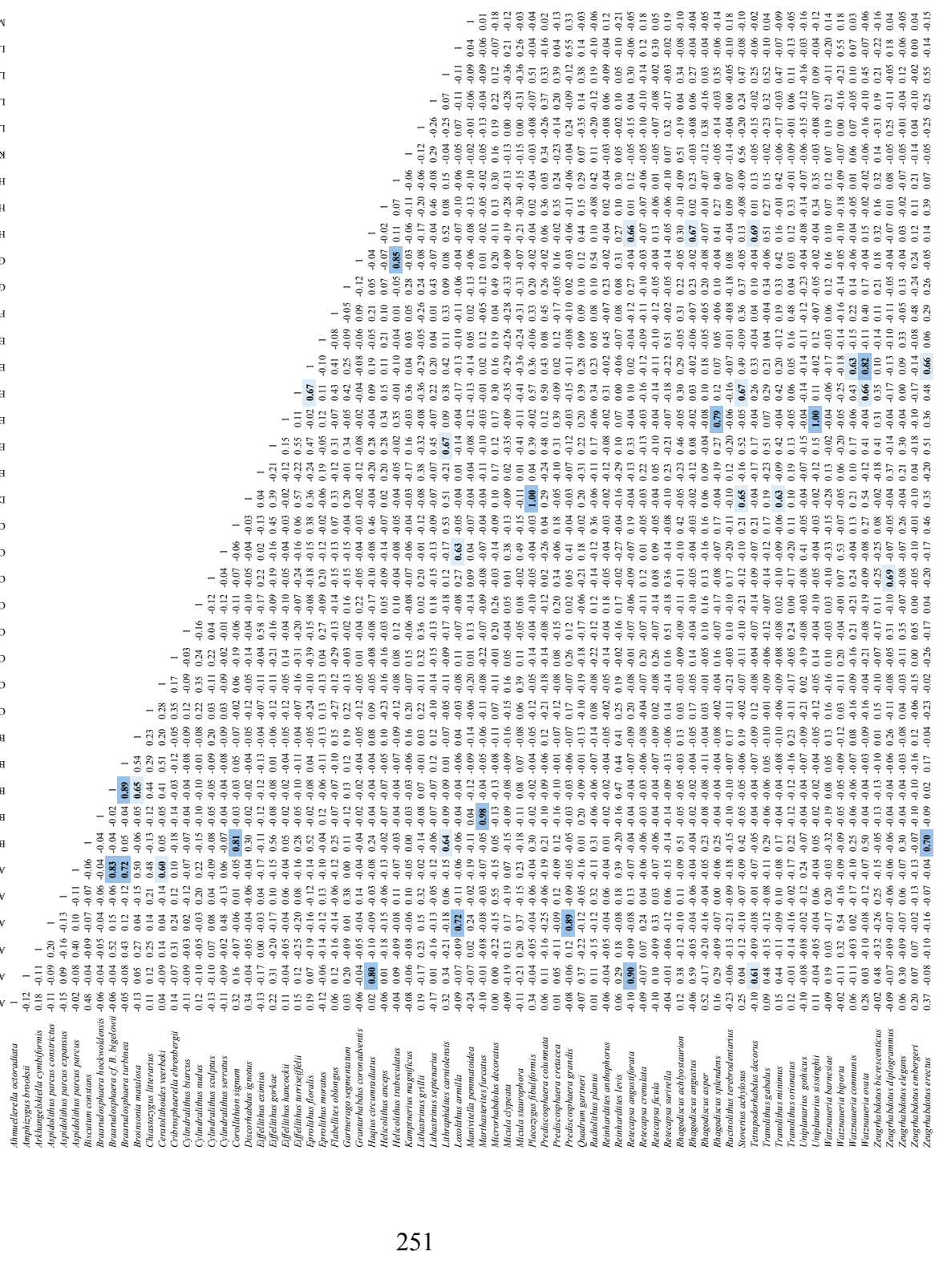

	Marthasterites furcatus	Microrhabdolus decoratus	Micula clypeata	Micula staurophora	Placozygus fibuliformis	Prediscosphaera columnata	Prediscosphaera cretacea	Prediscosphaera grandis	Quadrum gartneri	Radiolithus planus	Reinhardtites anthophorus	Reinhardtites levis	Reticapsa angustiforata	Reticapsa crenulata	Reticapsa ficula	Reticapsa surirella	Rhagodiscus achlyostaurion	Rhagodiscus angustus	Rhagodiscus asper	Rhagodiscus splendens	Rucinolithus terebrodentarius	Stoverius achylosus	Tetrapodorhabdus decorus	Tranolithus gabalus	Tranolithus minimus	Tranolithus orionatus	Uniplanarius gothicus	Uniplanarius sissinghii	Watznaueria barnesiae	Watznaueria biporta	Watznaueria communis	Watznaueria ovata	Zeugrhabdotus bicrescenticus	Zeugrhabdotus diplogrammus	Zeugrhabdotus elegans	Zeugrhabdotus embergeri	Zeugrhabdotus erectus
Marthasterites furcatus	1																																				
Microrhabdolus decoratus	-0.05	1																																			
Micula clypeata	-0.12	-0.32	1																																		
Micula staurophora	-0.15	-0.33	**0.84**	1																																	
Placozygus fibuliformis	-0.04	0.10	-0.09	-0.11	1																																
Prediscosphaera columnata	-0.13	0.18	-0.46	-0.54	0.29	1																															
Prediscosphaera cretacea	-0.16	0.15	-0.26	-0.28	-0.05	0.28	1																														
Prediscosphaera grandis	-0.05	-0.11	0.09	0.28	-0.03	-0.18	-0.06	1																													
Quadrum gartneri	0.22	0.12	-0.19	-0.21	0.20	0.23	0.11	-0.13	1																												
Radiolithus planus	0.04	0.38	-0.23	-0.24	-0.06	0.02	0.04	-0.09	0.11	1																											
Reinhardtites anthophorus	0.01	0.22	-0.09	-0.11	-0.02	0.08	-0.05	-0.03	0.20	0.24	1																										
Reinhardtites levis	-0.12	0.15	-0.23	-0.15	-0.16	0.16	0.07	-0.15	0.07	0.19	-0.04	1																									
Reticapsa angustiforata	-0.03	-0.05	-0.16	-0.18	-0.04	0.05	0.10	-0.05	0.35	0.15	-0.04	0.16	1																								
Reticapsa crenulata	-0.06	-0.18	0.01	0.17	-0.03	-0.12	-0.09	0.12	-0.14	-0.10	-0.03	-0.08	-0.06	1																							
Reticapsa ficula	-0.06	-0.17	-0.03	0.06	-0.04	-0.07	-0.01	0.28	0.04	-0.11	-0.04	-0.05	0.13	**0.77**	1																						
Reticapsa surirella	-0.20	0.04	-0.25	-0.27	-0.10	0.25	0.03	-0.07	-0.13	-0.15	0.10	-0.06	0.06	-0.11	-0.02	1																					
Rhagodiscus achlyostaurion	-0.04	0.20	-0.21	-0.24	-0.05	0.35	-0.01	-0.07	0.03	0.34	-0.05	0.10	0.21	-0.08	-0.09	-0.04	1																				
Rhagodiscus angustus	-0.03	-0.13	-0.09	-0.09	-0.02	0.00	-0.12	-0.03	0.50	-0.06	-0.02	0.07	**0.66**	-0.03	0.25	0.07	-0.05	1																			
Rhagodiscus asper	-0.12	0.08	-0.12	-0.17	0.06	0.02	-0.02	-0.12	-0.13	0.04	0.20	0.00	-0.14	-0.13	-0.14	0.11	-0.02	-0.08	1																		
Rhagodiscus splendens	-0.05	0.05	-0.15	-0.17	-0.04	0.12	0.27	-0.05	0.43	0.00	-0.04	0.06	0.33	-0.06	0.10	-0.04	0.05	0.54	-0.06	1																	
Rucinolithus terebrodentarius	-0.02	-0.13	-0.15	-0.24	-0.10	-0.10	0.17	-0.14	-0.09	-0.08	-0.01	-0.11	-0.08	0.03	0.08	0.10	-0.17	-0.01	-0.07	-0.08	1																
Stoverius achylosus	-0.07	0.18	-0.22	-0.25	**0.65**	0.52	-0.14	-0.07	0.15	0.06	-0.05	-0.06	-0.04	-0.08	-0.08	-0.14	0.41	-0.05	0.02	-0.02	-0.18	1															
Tetrapodorhabdus decorus	-0.05	-0.18	-0.16	-0.18	-0.04	0.01	-0.09	-0.05	0.48	0.12	-0.04	0.12	**0.69**	-0.06	0.14	0.00	-0.09	**0.70**	0.02	0.35	-0.08	0.02	1														
Tranolithus gabalus	-0.07	0.01	-0.26	-0.29	0.19	0.37	0.15	-0.09	0.57	0.07	0.21	0.06	0.56	-0.10	0.13	0.00	0.15	**0.73**	0.01	0.53	-0.06	0.17	0.46	1													
Tranolithus minimus	-0.04	0.20	-0.19	-0.20	**0.63**	0.26	0.10	-0.06	0.31	0.29	-0.04	0.07	0.50	-0.07	0.03	-0.10	0.18	0.32	-0.07	0.13	-0.09	0.35	0.18	0.44	1												
Tranolithus orionatus	-0.11	0.05	-0.33	-0.33	0.10	0.26	-0.07	-0.09	-0.12	0.04	0.10	0.05	-0.17	0.08	0.08	0.29	0.14	-0.05	0.02	-0.02	0.29	0.09	-0.16	0.04	-0.01	1											
Uniplanarius gothicus	-0.07	-0.23	**0.62**	0.55	-0.04	-0.28	-0.17	-0.06	-0.14	-0.11	-0.04	-0.09	-0.07	-0.06	-0.07	-0.16	-0.09	-0.04	-0.15	0.02	-0.06	-0.18	-0.09	-0.07	-0.11	-0.08	-0.20	1									
Uniplanarius sissinghii	-0.03	0.17	-0.09	-0.11	-0.02	0.12	0.39	-0.03	0.20	-0.06	-0.02	0.07	-0.04	-0.03	-0.04	-0.07	-0.05	-0.02	-0.08	**0.79**	-0.06	-0.05	-0.04	0.07	-0.04	-0.05	-0.04	1									
Watznaueria barnesiae	-0.13	0.11	-0.56	-0.55	-0.28	-0.04	0.10	-0.16	-0.10	0.09	-0.03	0.25	0.15	0.05	0.05	0.08	-0.02	0.05	0.06	-0.07	0.39	-0.15	0.12	-0.09	-0.06	0.11	-0.47	-0.04	1								
Watznaueria biporta	-0.09	-0.18	0.46	0.50	-0.05	-0.26	-0.12	0.36	0.09	-0.15	-0.05	-0.23	-0.09	0.31	0.07	-0.17	-0.12	-0.05	-0.19	-0.08	-0.24	-0.12	-0.09	-0.14	-0.11	-0.18	-0.02	-0.05	-0.29	1							
Watznaueria communis	-0.10	0.08	-0.12	-0.17	0.21	0.24	-0.09	0.08	0.01	0.11	-0.06	-0.16	-0.10	-0.07	-0.06	-0.03	0.05	-0.06	0.37	-0.03	-0.09	0.34	0.33	0.00	0.06	-0.11	-0.10	-0.06	-0.17	-0.07	1						
Watznaueria ovata	-0.07	-0.01	-0.17	-0.20	0.54	0.28	-0.12	-0.06	0.26	0.19	-0.04	-0.19	0.05	-0.06	-0.02	-0.15	0.11	0.14	0.27	0.12	-0.17	0.47	0.45	0.27	0.36	0.03	-0.07	-0.04	-0.25	-0.10	**0.76**	1					
Zeugrhabdotus bicrescenticus	-0.03	0.20	-0.34	-0.39	-0.02	0.20	0.22	-0.19	0.23	0.39	-0.02	0.36	0.48	0.02	0.11	-0.21	0.23	0.20	-0.15	0.34	0.25	0.11	0.28	0.27	0.32	0.14	-0.24	0.31	0.37	-0.32	-0.13	-0.04	1				
Zeugrhabdotus diplogrammus	-0.06	0.04	-0.02	-0.08	-0.04	0.05	0.13	-0.05	-0.15	-0.10	-0.04	0.07	-0.06	0.20	0.20	0.26	-0.08	-0.04	0.30	-0.06	0.18	-0.08	-0.06	-0.10	-0.07	-0.03	-0.07	-0.04	-0.05	-0.09	-0.09	-0.07	-0.07	1			
Zeugrhabdotus elegans	-0.05	0.09	-0.16	-0.17	-0.04	0.11	0.09	-0.05	-0.15	0.20	-0.04	-0.08	0.34	-0.06	-0.06	0.33	0.45	-0.04	-0.03	0.02	-0.06	0.00	-0.06	0.14	0.31	0.22	-0.07	-0.04	-0.05	-0.09	-0.01	0.06	0.11	-0.06	1		
Zeugrhabdotus embergeri	-0.07	-0.04	-0.24	-0.21	-0.10	0.22	-0.06	0.05	-0.10	0.08	-0.10	0.16	0.00	-0.04	0.08	0.29	-0.07	0.07	-0.04	0.09	-0.12	0.01	-0.07	0.02	0.48	-0.17	-0.10	0.22	-0.05	-0.09	-0.12	0.10	0.08	-0.04	1		
Zeugrhabdotus erectus	-0.06	0.31	-0.35	-0.39	0.35	0.48	0.29	-0.13	0.32	0.24	0.18	0.00	-0.09	-0.14	-0.12	-0.13	0.25	0.00	0.12	0.43	-0.15	0.34	-0.01	0.42	0.16	0.23	-0.16	0.36	-0.23	-0.19	0.18	0.46	0.10	-0.14	0.08	-0.01	1

Appendix 7
Range chart of ODP Site 959

Full Range chart of nannofossil taxa recognized at **ODP Site 959** is available upon request. Semi-quantitative abundance of all taxa detected are reported, as well as total abundance and preservation of calcareous nannofossils in each studied sample.

Total abundance: Abundant (A) = 21-30 specimens in each field of view; Common (C) = 11-20 specimens in each field of view; Few (F)= 6-10 specimens in each field of view; Rare (R) = 1-5 specimens in each field of view.

Species abundance: Abundant (A) = $\geq$ 1 specimen in each field of view; Common (C) = 1 specimen in 2-10 fields of view; Few (F) = 1 specimen in 11-30 fields of view; Rare (R) = 1 specimen in > 31 fields of view.

Preservation was characterized as follows:

Good (G) if nannofossil specimens show little or no evidence of dissolution and/or overgrowth and the primary morphological characters are only slightly altered allowing species identification;

Moderate (M) if specimens exhibit some etching and/or overgrowth, primary morphological characters are somewhat altered allowing, however, identification at the species level;

Poor (P) if specimens show severe etching and/or overgrowth, primary morphological characters are obliterated, hampering identification at the species and/or even generic level

Appendix 8A
Correlation matrix of genera – ODP Site 959

The quantitative data used to produce this matrix are available upon request

	Ahmuellerella	*Biscutum*	*Broinsonia*	*Bukrylithus*	*Calculites*	*Chiastozygus*	*Corollithion*	*Cretarhabdus*	*Cribrosphaerella*	*Cyclagelosphaera*	*Cylindralithus*	*Discorhabdus*	*Eiffellithus*	*Eprolithus*	*Flabellites*	*Gartnerago*	*Helicolithus*	*Lithastrinus*	*Loxolithus*	*Manivitella*
Ahmuellerella	1																			
Biscutum	0.49	1																		
Broinsonia	0.25	0.21	1																	
Bukrylithus	0.48	0.50	-0.13	1																
Calculites	0.50	0.19	0.07	0.17	1															
Chiastozygus	0.12	0.23	-0.23	0.55	0.37	1														
Corollithion	**0.79**	0.37	0.20	0.10	**0.68**	0.18	1													
Cretarhabdus	0.41	0.52	-0.02	**0.66**	0.35	**0.64**	0.25	1												
Cribrosphaerella	-0.04	0.21	**0.62**	0.10	-0.16	-0.25	-0.21	-0.14	1											
Cyclagelosphaera	-0.15	0.11	-0.12	0.17	-0.15	0.05	-0.12	-0.26	-0.09	1										
Cylindralithus	-0.11	-0.13	0.05	0.09	-0.14	0.20	-0.18	0.12	0.18	-0.03	1									
Discorhabdus	0.18	**0.75**	-0.08	0.27	-0.02	0.11	0.18	0.21	-0.11	0.33	-0.09	1								
Eiffellithus	0.28	0.29	0.00	0.59	0.34	0.46	0.01	**0.76**	0.01	-0.10	0.39	0.04	1							
Eprolithus	0.18	0.02	0.49	-0.19	-0.16	-0.24	0.00	0.02	-0.07	-0.04	-0.13	-0.07	0.09	1						
Flabellites	0.30	0.34	-0.12	0.26	0.25	0.01	0.15	0.42	-0.09	-0.05	-0.15	-0.07	0.37	-0.06	1					
Gartnerago	0.04	0.13	0.26	0.10	0.55	0.35	0.20	0.39	0.18	-0.07	0.19	-0.07	0.53	-0.13	0.13	1				
Helicolithus	0.26	**0.60**	-0.22	0.45	0.24	0.52	0.21	**0.65**	-0.10	0.01	0.12	0.43	0.54	-0.25	0.51	0.38	1			
Lithastrinus	-0.18	0.03	0.10	0.05	0.09	-0.11	-0.21	-0.07	0.30	0.04	0.00	-0.02	-0.20	-0.24	-0.01	-0.12	-0.23	1		
Loxolithus	0.36	0.43	0.03	0.04	**0.62**	0.34	0.59	0.23	0.08	-0.16	-0.06	0.21	0.06	-0.26	0.04	0.27	0.42	0.16	1	
Manivitella	-0.05	-0.33	-0.11	-0.16	-0.14	-0.12	0.01	-0.21	0.05	-0.13	0.11	-0.27	-0.19	-0.25	-0.18	-0.29	-0.14	-0.10	0.02	1
Marthasterites	-0.20	-0.14	-0.13	-0.34	-0.02	-0.04	0.02	-0.07	-0.19	-0.08	-0.08	-0.09	-0.34	-0.13	-0.13	-0.20	-0.22	0.52	0.30	0.19
Microrhabdulus	0.30	-0.13	0.24	-0.01	0.18	-0.17	0.17	0.14	-0.05	-0.03	0.10	-0.14	0.41	0.42	-0.14	0.32	-0.15	-0.20	-0.03	0.07
Micula	-0.56	-0.56	-0.55	-0.44	-0.38	-0.20	-0.34	-0.56	-0.39	0.02	-0.21	-0.15	**-0.63**	-0.31	-0.24	-0.41	-0.35	-0.03	-0.36	-0.01
Placozygus	0.50	**0.66**	0.08	**0.64**	0.38	0.41	0.23	**0.72**	0.10	-0.20	-0.12	0.28	0.50	0.00	0.59	0.24	**0.70**	0.11	0.30	-0.38
Prediscosphaera	**0.60**	0.50	0.27	**0.66**	0.48	0.40	0.43	0.58	0.33	-0.04	0.29	0.18	**0.71**	-0.04	0.08	0.52	0.39	-0.12	0.40	-0.09
Quadrum	0.09	0.15	**0.75**	0.02	0.09	0.07	0.22	0.11	**0.62**	-0.09	0.23	-0.11	-0.02	-0.07	-0.09	0.39	-0.02	0.11	0.08	0.10
Reinhardites	0.01	-0.07	0.43	-0.11	0.17	-0.10	0.07	0.08	0.30	0.01	0.55	-0.07	0.44	0.05	-0.14	**0.66**	0.03	-0.15	-0.01	0.09
Repagulum	0.11	0.28	0.02	0.21	0.09	0.36	-0.02	0.16	0.16	0.03	0.05	0.28	0.16	-0.14	-0.13	0.09	0.52	0.04	0.50	0.07
Retecapsa	0.19	0.51	-0.34	**0.66**	0.21	0.52	0.00	0.51	0.01	0.15	-0.16	0.34	0.46	-0.24	0.41	0.15	**0.70**	-0.07	0.25	-0.27
Rhagodiscus	0.41	0.50	0.10	**0.68**	0.13	0.25	0.02	0.48	0.26	-0.13	-0.14	0.26	0.45	0.15	-0.02	0.05	0.11	0.14	0.15	-0.23
Rotelapillus	0.23	0.14	-0.04	0.51	-0.20	-0.08	-0.17	0.03	0.51	-0.07	-0.02	-0.09	0.19	-0.08	-0.07	-0.17	-0.04	0.06	0.03	0.12
Rucinolithus	0.17	0.02	0.51	-0.20	-0.17	-0.24	-0.01	0.00	-0.04	-0.06	-0.16	-0.08	0.06	**0.99**	-0.06	-0.13	-0.27	-0.25	-0.28	-0.24
Stoverius	-0.11	-0.27	-0.11	-0.14	0.15	-0.04	-0.08	0.10	-0.12	-0.07	0.57	-0.10	0.53	-0.06	-0.07	0.48	0.10	-0.23	-0.05	0.13
Seribiscutum	0.35	0.11	0.03	**0.60**	-0.15	-0.03	-0.12	0.13	0.36	-0.05	-0.08	-0.07	0.21	-0.06	-0.05	-0.11	-0.02	0.10	-0.11	0.07
Staurolithites	**0.64**	0.52	-0.08	**0.83**	0.28	0.28	0.32	**0.62**	0.02	0.07	-0.12	0.20	0.39	-0.18	0.53	0.01	0.36	0.25	0.12	-0.13
Tranolithus	0.52	0.18	0.51	-0.01	0.38	-0.09	0.56	0.26	0.01	-0.05	0.03	0.05	0.37	0.52	-0.05	0.41	-0.03	-0.33	0.17	-0.07
Watznaueria	-0.49	-0.34	-0.06	-0.44	-0.46	-0.48	-0.42	**-0.61**	0.23	0.15	-0.05	-0.23	-0.57	-0.25	0.06	-0.39	-0.27	0.12	-0.29	0.50
Zeugrhabdotus	0.58	**0.63**	0.02	**0.83**	0.41	0.54	0.26	**0.61**	0.03	0.11	-0.05	0.40	0.55	0.10	0.18	0.13	0.41	0.08	0.27	-0.39

	Marthasterites	*Microrhabdulus*	*Micula*	*Placozygus*	*Prediscosphaera*	*Quadrum*	*Reinhardites*	*Repagulum*	*Retecapsa*	*Rhagodiscus*	*Rotelapillus*	*Rucinolithus*	*Stoverius*	*Seribiscutum*	*Staurolithites*	*Tranolithus*	*Watznaueria*	*Zeugrhabdotus*
Marthasterites	1																	
Microrhabdulus	0.11	1																
Micula	0.12	-0.48	1															
Placozygus	-0.33	-0.24	-0.47	1														
Prediscosphaera	-0.32	0.41	**-0.78**	0.43	1													
Quadrum	-0.13	-0.10	-0.37	0.09	0.30	1												
Reinhardites	-0.12	**0.64**	-0.48	-0.22	0.47	0.43	1											
Repagulum	0.09	-0.01	-0.23	0.30	0.20	-0.02	-0.01	1										
Retecapsa	-0.40	-0.30	-0.20	**0.70**	0.41	-0.18	-0.31	0.36	1									
Rhagodiscus	-0.07	0.29	-0.50	0.44	0.57	-0.14	-0.09	0.25	0.34	1								
Rotelapillus	-0.16	0.20	-0.24	0.11	0.44	-0.12	-0.09	0.18	0.30	**0.68**	1							
Rucinolithus	-0.15	0.39	-0.30	0.00	-0.05	-0.04	0.04	-0.14	-0.22	0.13	-0.08	1						
Stoverius	0.00	**0.65**	-0.21	-0.29	0.29	-0.12	**0.80**	-0.01	-0.22	-0.11	-0.10	-0.09	1					
Seribiscutum	-0.11	0.31	-0.24	0.20	0.38	-0.09	-0.04	0.28	0.17	**0.72**	**0.85**	-0.06	-0.07	1				
Staurolithites	-0.04	0.04	-0.45	**0.66**	0.50	0.02	-0.19	0.02	0.48	0.56	0.38	-0.19	-0.23	0.53	1			
Tranolithus	-0.12	**0.77**	**-0.62**	-0.02	0.57	0.25	**0.61**	-0.15	-0.19	0.15	-0.03	0.50	0.40	-0.03	0.06	1		
Watznaueria	0.05	-0.45	0.38	-0.35	**-0.64**	0.10	-0.17	-0.14	-0.27	-0.54	-0.12	-0.21	-0.21	-0.18	-0.32	-0.54	1	
Zeugrhabdotus	-0.36	0.02	-0.54	**0.73**	**0.67**	-0.10	-0.18	0.26	**0.67**	**0.75**	0.36	0.10	-0.20	0.39	**0.67**	0.15	**-0.62**	1

Appendix 8B
Correlation matrix of species – ODP Site 959

The quantitative data used to produce this matrix are available upon request

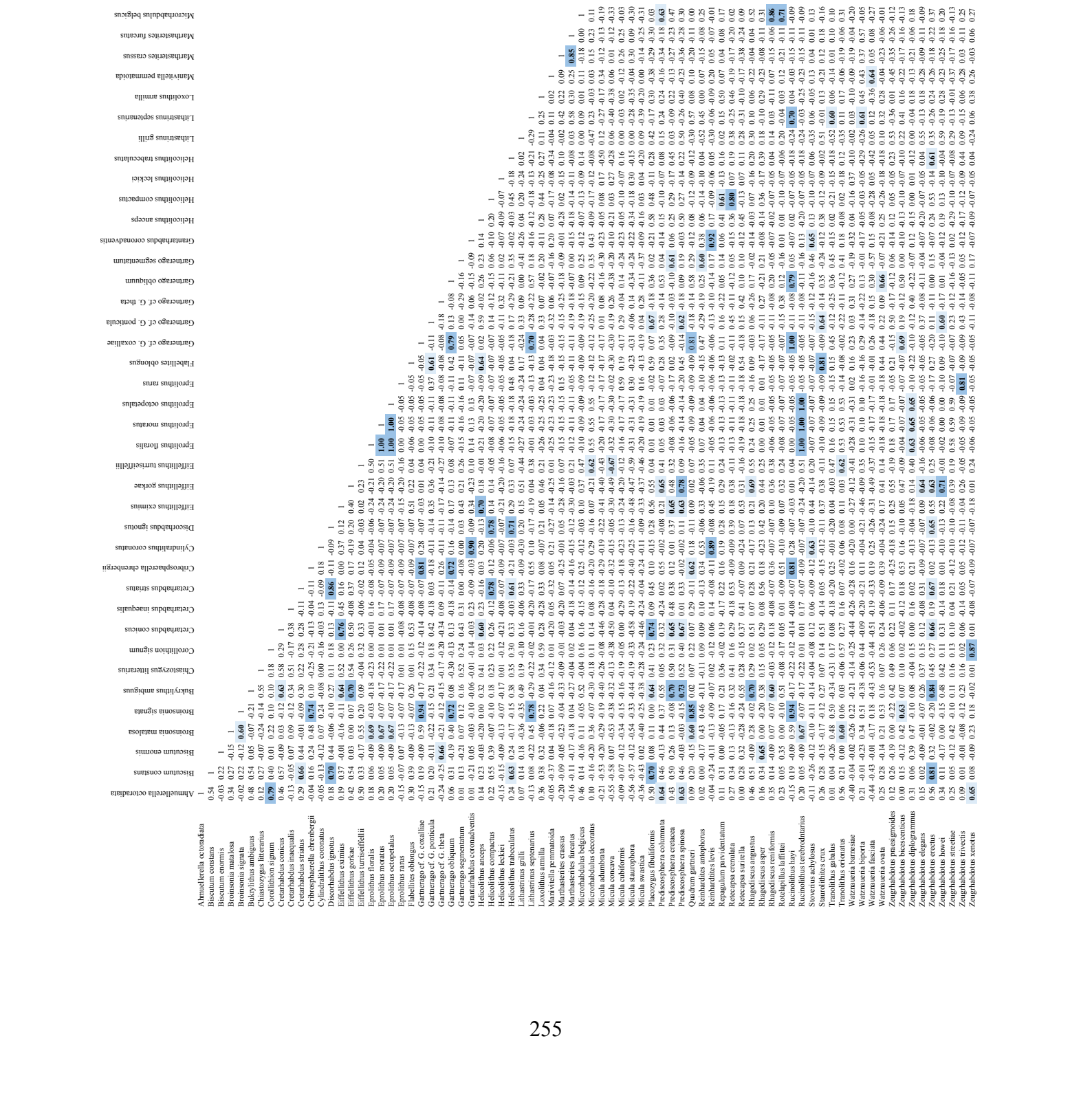

	Microrhabdulus decoratus	Micula adumbrata	Micula concava	Micula cubiformis	Micula staurophora	Micula swastica	Placozygus fibuliformis	Prediscosphaera columnata	Prediscosphaera cretacea	Prediscosphaera spinosa	Quadrum gartneri	Reinhardtites anthophorus	Reinhardtites levis	Repagulum parvidentatum	Retecapsa crenulata	Retecapsa surirella	Rhagodiscus angustus	Rhagodiscus asper	Rhagodiscus reniformis	Rotelapillus laffittei	Rucinolithus hayi	Rucinolithus terebrodontarius	Stoverius achylosus	Staurolithites crux	Tranolithus gabalus	Tranolithus orionatus	Watznaueria barnesiae	Watznaueria biporta	Watznaueria fasciata	Watznaueria ovata	Zeugrhabdotus praesigmoides	Zeugrhabdotus biscocenticus	Zeugrhabdotus diplogrammus	Zeugrhabdotus elegans	Zeugrhabdotus erectus	Zeugrhabdotus howei	Zeugrhabdotus streetiae	Zeugrhabdotus trivectis	Zeugrhabdotus xenotus
Microrhabdulus decoratus	1																																						
Micula adumbrata	-0.26	1																																						
Micula concava	-0.35	**0.66**	1																																				
Micula cubiformis	-0.24	0.13	0.18	1																																			
Micula staurophora	-0.37	0.58	**0.79**	0.38	1																																		
Micula swastica	-0.32	**0.73**	**0.69**	0.51	**0.65**	1																																	
Placozygus fibuliformis	-0.30	-0.24	-0.41	0.03	-0.48	-0.24	1																																
Prediscosphaera columnata	-0.09	-0.40	**-0.68**	-0.10	**-0.60**	-0.48	0.50	1																															
Prediscosphaera cretacea	0.17	-0.53	-0.39	-0.40	**-0.61**	-0.52	0.39	0.33	1																														
Prediscosphaera spinosa	-0.11	-0.21	-0.42	-0.22	-0.53	-0.32	**0.77**	**0.63**	0.53	1																													
Quadrum gartneri	-0.12	-0.19	-0.29	-0.25	-0.36	-0.32	0.09	0.32	0.20	-0.04	1																												
Reinhardtites anthophorus	**0.63**	-0.33	-0.39	-0.40	-0.49	-0.39	-0.21	0.19	0.39	-0.02	0.48	1																											
Reinhardtites levis	0.52	-0.18	-0.09	-0.22	-0.19	-0.09	-0.25	-0.15	0.15	0.02	-0.11	0.57	1																										
Repagulum parvidentatum	-0.11	0.02	-0.02	-0.09	-0.26	-0.11	0.30	0.16	0.14	0.25	-0.02	-0.02	0.07	1																									
Retecapsa crenulata	-0.26	0.22	0.01	-0.13	-0.16	0.02	**0.61**	0.18	0.20	0.57	-0.19	-0.25	-0.14	**0.71**	1																								
Retecapsa surirella	-0.28	-0.34	-0.03	-0.11	-0.16	-0.19	0.34	0.13	0.43	0.31	-0.05	-0.15	-0.17	-0.20	-0.12	1																							
Rhagodiscus angustus	-0.01	-0.46	-0.54	-0.04	-0.49	-0.40	0.49	**0.63**	0.41	0.48	-0.06	-0.15	-0.20	0.27	0.22	0.13	1																						
Rhagodiscus asper	0.10	-0.40	-0.15	-0.11	-0.36	-0.15	0.23	0.18	**0.63**	0.28	-0.21	0.06	-0.07	0.09	0.24	0.23	0.45	1																					
Rhagodiscus reniformis	-0.12	-0.17	-0.25	0.09	-0.23	-0.19	0.20	**0.62**	0.33	0.28	-0.09	-0.03	-0.06	0.28	0.13	0.10	**0.71**	0.33	1																				
Rotelapillus laffittei	-0.17	-0.24	-0.17	-0.01	-0.25	-0.16	0.11	0.52	0.36	0.22	-0.12	-0.09	-0.09	0.18	0.06	0.33	0.54	0.52	**0.85**	1																	
Rucinolithus hayi	-0.12	-0.17	-0.30	-0.17	-0.31	-0.19	0.07	0.35	-0.09	-0.14	**0.81**	0.47	-0.06	0.11	-0.11	-0.18	-0.03	-0.17	-0.05	-0.07	1																
Rucinolithus terebrodontarius	0.55	-0.17	-0.30	-0.17	-0.31	-0.19	0.01	0.03	-0.06	-0.14	-0.09	0.04	-0.06	-0.13	-0.11	-0.18	0.25	0.01	-0.05	-0.07	-0.05	1															
Stoverius achylosus	**0.71**	-0.16	-0.11	-0.25	-0.21	-0.13	-0.29	-0.15	0.28	0.03	-0.12	**0.75**	**0.87**	-0.01	-0.16	-0.14	-0.23	0.11	-0.07	-0.10	-0.07	-0.07	1														
Staurolithites crux	-0.12	-0.19	-0.30	0.20	-0.19	-0.20	0.57	0.31	-0.08	0.53	-0.15	-0.25	-0.11	-0.23	0.04	0.35	0.21	-0.13	-0.09	-0.12	-0.09	-0.09	-0.12	1													
Tranolithus gabalus	0.51	-0.12	-0.25	-0.15	-0.26	-0.20	-0.14	0.15	0.07	-0.10	0.38	**0.64**	0.04	-0.12	-0.31	-0.13	-0.11	0.02	-0.15	-0.21	0.45	0.15	0.36	0.00	1												
Tranolithus orionatus	**0.74**	-0.35	-0.52	-0.35	**-0.62**	-0.45	0.00	0.26	0.52	0.17	0.21	0.59	0.21	-0.15	-0.12	-0.09	0.10	0.25	-0.01	-0.01	-0.02	0.53	0.38	-0.14	0.43	1											
Watznaueria barnesiae	-0.53	0.19	0.36	0.26	0.39	0.31	-0.16	-0.09	-0.45	-0.30	0.08	-0.26	-0.36	-0.02	-0.13	0.32	-0.37	-0.38	-0.21	-0.11	0.23	-0.31	-0.41	0.01	-0.05	-0.50	1										
Watznaueria biporta	0.13	0.11	-0.24	-0.01	-0.17	-0.26	-0.18	0.09	-0.28	-0.19	0.41	0.05	-0.20	0.25	-0.02	-0.48	-0.08	-0.38	-0.16	-0.22	0.29	0.10	-0.23	-0.07	0.25	0.19	0.03	1									
Watznaueria fasciata	-0.21	0.44	0.27	0.19	0.27	0.37	-0.35	-0.27	**-0.64**	-0.49	0.04	-0.09	0.10	-0.18	-0.32	-0.20	-0.39	-0.45	-0.12	-0.09	0.26	-0.17	-0.04	-0.01	-0.16	-0.46	0.29	0.13	1								
Watznaueria ovata	-0.28	-0.08	-0.35	0.18	-0.29	0.09	0.33	0.46	0.00	0.29	0.48	0.01	-0.23	-0.07	-0.16	0.22	0.20	-0.12	0.02	0.03	0.44	-0.18	-0.27	0.39	0.27	-0.04	0.23	0.21	0.04	1							
Zeugrhabdotus praesigmoides	-0.15	-0.15	-0.18	-0.22	-0.15	-0.15	0.41	0.22	0.10	0.55	-0.13	-0.21	-0.19	0.00	0.30	0.29	0.26	-0.05	-0.15	-0.21	-0.15	0.17	-0.22	0.38	-0.26	0.00	0.12	-0.27	-0.35	0.07	1						
Zeugrhabdotus biscocenticus	-0.17	-0.16	-0.31	-0.25	-0.29	-0.15	0.24	0.47	-0.04	0.30	0.53	0.23	-0.09	-0.01	0.10	-0.20	0.22	0.02	-0.07	-0.10	**0.69**	-0.07	-0.11	0.20	0.21	-0.06	0.00	0.09	0.02	0.48	0.35	1					
Zeugrhabdotus diplogrammus	0.38	-0.35	-0.35	-0.34	-0.47	-0.39	0.05	0.29	0.27	0.14	-0.08	0.05	-0.10	-0.01	0.08	0.09	0.31	0.44	0.16	0.42	-0.10	**0.65**	-0.07	-0.13	-0.05	0.57	-0.28	0.08	-0.35	-0.17	0.15	0.01	1				
Zeugrhabdotus elegans	-0.12	-0.06	-0.14	-0.17	-0.09	-0.02	0.26	0.30	0.04	0.55	-0.09	-0.15	-0.06	-0.13	0.25	-0.09	0.34	0.20	-0.05	-0.07	-0.05	-0.07	0.36	-0.15	-0.06	-0.24	-0.16	-0.24	0.23	**0.63**	**0.69**	0.12	1				
Zeugrhabdotus erectus	-0.19	-0.48	-0.38	-0.15	-0.50	-0.37	**0.68**	0.40	**0.75**	**0.62**	-0.07	-0.12	-0.09	0.29	0.42	0.46	**0.66**	0.59	0.43	0.38	-0.20	-0.06	-0.13	0.20	-0.25	0.16	-0.27	-0.32	-0.53	0.08	0.26	-0.06	0.13	0.12	1		
Zeugrhabdotus howei	-0.18	0.05	-0.22	-0.12	-0.24	-0.07	0.54	0.54	0.12	**0.78**	-0.17	-0.23	-0.13	0.31	**0.62**	-0.04	0.53	0.18	0.32	0.23	-0.10	0.00	-0.15	0.37	-0.22	-0.09	-0.26	-0.11	-0.32	0.17	**0.60**	0.49	0.21	**0.78**	0.27	1	
Zeugrhabdotus streetiae	0.25	-0.15	-0.30	-0.25	-0.26	-0.13	0.22	0.27	-0.01	0.36	-0.12	-0.10	-0.09	-0.19	0.13	-0.19	0.43	0.17	-0.07	-0.10	-0.07	0.59	-0.10	0.24	-0.03	0.28	-0.38	-0.07	-0.30	0.07	**0.62**	0.51	0.51	**0.78**	0.05	**0.63**	1
Zeugrhabdotus trivectis	-0.20	-0.24	-0.18	0.47	0.12	0.05	0.18	0.34	0.01	0.19	-0.15	-0.17	-0.11	-0.05	0.07	-0.15	0.31	0.24	0.36	0.27	-0.09	-0.09	-0.12	0.05	-0.26	-0.15	-0.17	-0.27	-0.17	-0.05	0.16	0.20	0.03	0.36	0.09	0.38	0.24	1
Zeugrhabdotus xenotus	0.08	0.06	-0.20	-0.07	-0.17	-0.19	-0.11	0.25	0.18	0.13	0.36	0.16	-0.06	-0.13	-0.11	-0.18	-0.16	-0.17	-0.05	-0.07	-0.05	-0.05	-0.07	-0.09	0.15	0.53	-0.11	0.55	-0.22	0.23	-0.15	-0.07	0.12	-0.05	0.00	-0.10	-0.07	-0.09	1

Appendix 9
Range chart of ODP Site 1261

Full range chart of nannofossil taxa recognized at **ODP Site 1261** is available upon request. Semi-quantitative abundance of all taxa detected are reported, as well as total abundance and preservation of calcareous nannofossils in each studied sample.

Total abundance: Abundant (A) = 21-30 specimens in each field of view; Common (C) = 11-20 specimens in each field of view; Few (F)= 6-10 specimens in each field of view; Rare (R) = 1-5 specimens in each field of view.

Species abundance: Abundant (A) = $\geq$ 1 specimen in each field of view; Common (C) = 1 specimen in 2-10 fields of view; Few (F) = 1 specimen in 11-30 fields of view; Rare (R) = 1 specimen in > 31 fields of view.

Preservation was characterized as follows:

Good (G) if nannofossil specimens show little or no evidence of dissolution and/or overgrowth and the primary morphological characters are only slightly altered allowing species identification;

Moderate (M) if specimens exhibit some etching and/or overgrowth, primary morphological characters are somewhat altered allowing, however, identification at the species level;

Poor (P) if specimens show severe etching and/or overgrowth, primary morphological characters are obliterated, hampering identification at the species and/or even generic level

Appendix 10A
Correlation matrix of genera – ODP Site 1261

The quantitative data used to produce this matrix are available upon request

	Ahmuellerella	Biscutum	Broinsonia	Aspidolithus	Braarudosphaera	Bukryaster	Calculites	Chiastozygus	Corollithion	Cribrosphaerella	Cretarhabdus	Cylindralithus	Discorhabdus	Eiffellithus	Eprolithus	Gartnerago	Helicolithus	Kamptnerius	Lithastrinus	Liliasterites	Loxolithus
Ahmuellerella	1																				
Biscutum	-0.19	1																			
Broinsonia	-0.08	-0.09	1																		
Aspidolithus	-0.07	0.12	0.14	1																	
Braarudosphaera	-0.06	0.01	-0.11	0.04	1																
Bukryaster	-0.07	0.04	0.24	0.03	-0.05	1															
Calculites	-0.09	0.10	0.00	0.10	-0.06	0.03	1														
Chiastozygus	-0.08	-0.02	0.07	0.13	-0.05	-0.06	0.08	1													
Corollithion	0.09	0.29	0.03	0.09	-0.10	0.04	-0.07	0.06	1												
Cribrosphaerella	-0.04	-0.16	-0.13	-0.06	-0.05	-0.05	0.26	-0.05	-0.19	1											
Cretarhabdus	-0.11	0.25	0.21	0.18	-0.08	0.21	0.00	0.04	-0.07	-0.09	1										
Cylindralithus	0.25	-0.04	0.05	-0.07	-0.14	0.01	-0.09	-0.03	0.04	-0.19	-0.04	1									
Discorhabdus	-0.09	0.38	-0.03	0.11	-0.12	0.09	0.16	0.01	0.11	-0.07	0.26	0.16	1								
Eiffellithus	-0.09	-0.07	0.17	-0.19	-0.19	-0.05	-0.03	0.05	0.14	-0.14	-0.08	0.10	0.16	1							
Eprolithus	-0.04	-0.20	0.21	-0.10	0.08	-0.05	0.00	0.59	0.10	-0.05	-0.07	-0.01	-0.06	0.15	1						
Gartnerago	-0.03	-0.11	-0.01	-0.09	-0.07	0.00	-0.07	-0.13	-0.17	-0.25	-0.12	-0.10	-0.21	-0.13	-0.22	1					
Helicolithus	0.11	0.05	0.25	0.14	-0.15	0.07	0.06	0.05	0.26	-0.06	0.09	0.16	0.12	0.13	0.08	-0.09	1				
Kamptnerius	0.07	-0.20	0.05	-0.10	-0.09	-0.02	-0.06	-0.03	-0.05	0.10	-0.05	-0.06	-0.03	0.12	0.15	0.06	0.01	1			
Lithastrinus	-0.03	-0.14	-0.05	-0.02	-0.07	-0.04	0.01	0.00	-0.07	0.00	-0.09	0.04	0.09	0.11	0.21	-0.11	-0.10	-0.08	1		
Liliasterites	0.20	0.14	-0.15	-0.07	-0.07	-0.05	-0.09	-0.06	0.22	-0.11	-0.03	-0.09	0.15	0.02	-0.01	-0.03	-0.01	-0.05	-0.04	1	
Loxolithus	0.09	-0.05	0.18	0.18	-0.09	0.12	0.10	-0.01	0.02	0.10	-0.07	0.04	0.08	0.06	-0.03	-0.01	0.21	0.00	0.03	0.05	1
Lucianorhabdus	-0.04	0.20	-0.18	-0.10	-0.07	-0.05	-0.20	-0.07	0.01	-0.13	0.02	-0.01	0.09	0.01	-0.12	0.02	0.02	-0.08	-0.01	0.16	-0.09
Manivitella	0.04	0.12	-0.33	-0.21	0.12	-0.04	-0.04	-0.17	0.02	-0.12	0.11	-0.13	0.08	-0.05	-0.09	0.08	-0.19	-0.10	-0.04	0.32	-0.04
Marthasterites	0.10	-0.25	-0.15	0.28	0.00	0.00	0.20	-0.11	-0.15	0.34	0.02	-0.05	-0.11	-0.25	-0.16	-0.08	-0.02	-0.09	-0.01	-0.09	-0.01
Microrhabdulus	-0.01	0.05	0.01	-0.06	-0.16	-0.14	0.07	0.14	0.16	0.00	-0.11	0.05	0.08	0.16	-0.01	-0.17	-0.03	-0.20	0.09	-0.03	-0.04
Micula	-0.06	0.11	-0.17	-0.16	-0.04	-0.09	-0.12	-0.14	-0.11	0.12	0.03	-0.24	0.02	-0.06	-0.15	0.11	-0.23	-0.10	0.12	0.20	0.00
Nephrolithus	-0.09	0.04	0.18	0.21	-0.02	0.11	0.29	0.14	0.07	-0.01	0.02	0.26	0.13	0.06	0.05	0.07	0.15	0.03	-0.12	-0.09	0.08
Placozygus	-0.02	-0.15	-0.03	0.09	0.05	-0.06	-0.24	-0.11	0.12	0.09	0.14	-0.06	-0.06	-0.21	-0.07	-0.02	0.02	0.05	-0.11	-0.01	0.02
Prediscosphaera	-0.21	0.10	0.11	-0.10	-0.04	-0.01	-0.16	-0.03	0.05	-0.21	-0.09	0.11	-0.14	0.11	-0.16	0.04	0.06	-0.21	-0.24	-0.12	-0.30
Quadrum	-0.14	0.01	0.05	-0.03	0.24	0.04	0.05	-0.03	-0.16	-0.02	0.02	-0.06	-0.11	-0.17	0.20	0.14	-0.09	0.13	-0.09	-0.11	-0.04
Radiolithus	-0.13	-0.24	-0.04	-0.09	-0.05	-0.06	-0.06	0.47	0.08	-0.05	-0.10	0.01	-0.10	0.21	0.55	-0.18	-0.19	-0.08	**0.62**	-0.07	-0.04
Retecapsa	-0.02	0.29	-0.03	-0.05	0.01	0.09	0.01	-0.06	-0.09	-0.08	0.08	-0.09	0.11	-0.12	-0.18	0.03	0.04	-0.07	-0.11	0.05	0.08
Rhagodiscus	0.08	0.08	0.12	0.01	-0.04	-0.10	0.02	0.07	0.16	-0.10	0.00	0.36	0.09	0.30	0.21	-0.28	0.13	-0.01	0.42	-0.19	-0.04
Rotelapillus	-0.04	0.06	-0.03	-0.07	-0.13	-0.08	-0.15	-0.14	0.00	0.04	0.07	-0.11	-0.08	0.00	0.01	0.03	0.04	-0.02	0.03	0.06	-0.20
Staurolithites	0.24	-0.03	-0.12	0.01	-0.15	-0.07	0.15	0.06	0.26	-0.08	-0.12	0.38	0.01	0.07	0.17	0.04	0.21	-0.05	0.12	-0.03	0.07
cf. Seribiscutum	-0.06	0.20	0.17	0.01	0.18	0.06	0.03	-0.11	-0.05	-0.02	0.13	-0.01	0.03	-0.20	-0.21	0.06	0.04	0.12	-0.22	-0.11	0.04
Stoverius a	0.07	0.01	0.02	0.03	-0.05	-0.04	0.04	-0.01	-0.09	0.01	0.06	0.13	0.02	-0.16	-0.08	-0.09	0.00	-0.06	-0.03	-0.05	-0.02
Tegumentum	0.06	-0.06	0.38	-0.04	0.13	0.11	-0.13	-0.07	0.20	-0.15	0.11	0.04	-0.05	0.17	0.22	-0.10	0.26	0.12	0.09	-0.04	0.06
Tetrapodorhabdus	-0.07	-0.09	-0.05	0.03	-0.05	0.31	0.00	-0.06	0.02	0.12	-0.06	-0.07	0.05	0.01	-0.11	-0.07	0.12	0.04	-0.02	-0.05	0.18
Watznaueria	0.12	-0.50	-0.19	-0.05	0.12	-0.03	-0.14	0.07	-0.47	0.15	-0.10	-0.14	-0.20	-0.29	0.07	0.21	-0.30	0.18	-0.10	0.06	0.04
Zeugrhabdotus	0.08	0.14	-0.11	0.00	-0.06	0.04	-0.07	-0.22	0.27	-0.08	-0.04	0.06	-0.02	0.08	-0.14	-0.27	0.06	-0.08	0.21	-0.04	-0.03

	Lucianorhabdus	Manivitella	Marthasterites	Microrhabdulus	Micula	Nephrolithus	Placozygus	Prediscosphaera	Quadrum	Radiolithus	Retecapsa	Rhagodiscus	Rotelapillus	Staurolithites	cf. Seribiscutum	Stoverius a	Tegumentum	Tetrapodorhabdus	Watznaueria	Zeugrhabdotus
Lucianorhabdus	1																			
Manivitella	0.06	1																		
Marthasterites	-0.07	-0.14	1																	
Microrhabdulus	-0.03	-0.12	0.05	1																
Micula	0.18	0.41	-0.14	-0.21	1															
Nephrolithus	-0.11	-0.11	0.06	0.00	-0.19	1														
Placozygus	-0.13	0.06	0.10	-0.10	-0.04	-0.14	1													
Prediscosphaera	0.10	-0.17	-0.25	0.17	-0.12	0.13	-0.14	1												
Quadrum	-0.06	0.27	-0.19	-0.21	0.26	0.06	0.08	-0.07	1											
Radiolithus	-0.08	-0.12	-0.10	-0.03	0.10	-0.09	-0.05	-0.14	-0.12	1										
Retecapsa	0.13	-0.04	-0.15	0.00	0.15	-0.12	-0.06	0.01	-0.12	-0.06	1									
Rhagodiscus	-0.17	-0.16	-0.14	0.27	-0.35	0.04	0.10	0.05	-0.03	0.25	-0.17	1								
Rotelapillus	0.27	0.08	0.18	0.10	-0.02	-0.14	0.05	0.03	-0.10	-0.01	0.00	-0.06	1							
Staurolithites	-0.07	-0.16	0.14	0.00	-0.28	-0.01	-0.08	-0.14	-0.15	0.22	0.02	0.30	0.00	1						
cf. Seribiscutum	-0.05	-0.17	-0.22	0.11	-0.17	0.10	-0.09	0.13	-0.06	-0.25	0.34	-0.05	-0.09	-0.13	1					
Stoverius a	-0.05	-0.12	0.19	0.10	-0.09	-0.08	0.28	-0.02	-0.07	-0.06	0.09	0.14	-0.02	-0.11	0.12	1				
Tegumentum	-0.03	-0.15	-0.16	-0.10	-0.23	-0.16	0.22	-0.09	0.04	0.08	0.07	0.29	0.12	0.14	-0.10	0.02	1			
Tetrapodorhabdus	-0.05	-0.02	-0.08	0.07	-0.08	-0.08	0.22	0.13	-0.07	-0.06	-0.02	-0.03	-0.13	0.00	0.01	-0.04	-0.10	1		
Watznaueria	-0.04	0.16	0.13	-0.35	0.16	-0.14	0.10	-0.40	0.22	-0.02	-0.21	-0.46	-0.16	-0.22	-0.33	-0.06	-0.21	-0.01	1	
Zeugrhabdotus	0.04	-0.05	-0.11	0.12	-0.23	-0.11	-0.03	0.10	-0.31	0.09	0.02	0.27	0.19	0.08	0.14	-0.01	0.10	0.06	-0.51	1

Appendix 10B
Correlation matrix of species – ODP Site 1261

The quantitative data used to produce this matrix are available upon request

	Nephrolithus frequens	*Placozygus fibuliformis*	*Prediscosphaera columnata*	*Prediscosphaera cretacea*	*Prediscosphaera ponticulata*	*Prediscosphaera spinosa*	*Quadrum gartneri*	*Quadrum intermedium*	*Quadrum svabenikae*	*Radiolithus planus*	*Retecapsa angustiforata*	*Retecapsa crenulata*	*Retecapsa ficula*	*Retecapsa surirella*	*Rhagodiscus angustus*	*Rhagodiscus plebeius*	*Rhagodiscus splendens*	*Rotelapillus crenulatus*	*Staurolithites laffitei*	*Stoverius achylosus*	*Tegumentum stradneri*	*Tegumentum orionatus*	*Tetrapodorhabdus decorus*	*Watznaueria barnesiae*	*Watznaueria biporta*	*Watznaueria fossacincta*	*Zeugrhabdotus bicrescenticus*	*Zeugrhabdotus biperforatus*	*Zeugrhabdotus diplogrammus*	*Zeugrhabdotus embergeri*	*Zeugrhabdotus erectus*	*Zeugrhabdotus kerguelenensis*	*Zeugrhabdotus noeliae*	*Zeugrhabdotus scutula*
Nephrolithus frequens	1																																	
Placozygus fibuliformis	-0.14	1																																
Prediscosphaera columnata	0.07	-0.16	1																															
Prediscosphaera cretacea	0.05	-0.03	0.17	1																														
Prediscosphaera ponticulata	0.02	0.08	0.30	0.08	1																													
Prediscosphaera spinosa	0.23	-0.17	0.05	0.09	-0.09	1																												
Quadrum gartneri	0.07	0.08	-0.09	0.11	-0.07	-0.02	1																											
Quadrum intermedium	-0.05	0.10	-0.03	0.03	0.27	0.14	-0.04	1																										
Quadrum svabenikae	-0.05	-0.07	-0.03	-0.02	-0.14	0.20	-0.04	-0.01	1																									
Radiolithus planus	-0.09	-0.05	-0.14	-0.15	0.08	-0.18	-0.11	-0.04	-0.04	1																								
Retecapsa angustiforata	-0.14	-0.15	-0.01	-0.13	-0.04	0.11	-0.11	-0.03	**0.61**	0.20	1																							
Retecapsa crenulata	-0.16	0.00	-0.01	-0.09	-0.18	-0.13	-0.15	-0.06	-0.06	-0.01	-0.12	1																						
Retecapsa ficula	-0.08	-0.07	0.03	-0.09	0.02	0.35	-0.08	-0.01	0.46	-0.03	0.41	-0.06	1																					
Retecapsa surirella	0.05	0.02	-0.06	0.01	-0.13	0.37	-0.01	0.19	-0.08	-0.14	-0.20	-0.14	0.07	1																				
Rhagodiscus angustus	0.12	0.06	-0.04	0.17	0.16	-0.14	0.04	-0.11	-0.07	0.12	-0.21	0.00	-0.09	0.05	1																			
Rhagodiscus plebeius	-0.03	0.00	0.12	0.14	0.15	-0.06	-0.09	-0.07	0.09	0.24	-0.08	-0.07	-0.09	-0.11	0.23	1																		
Rhagodiscus splendens	-0.03	0.17	-0.14	-0.03	0.14	-0.11	0.00	0.01	0.02	0.15	0.14	-0.19	-0.02	-0.06	0.15	0.16	1																	
Rotelapillus crenulatus	-0.14	0.05	0.10	0.07	-0.06	-0.08	-0.11	-0.07	0.22	-0.01	0.13	-0.02	0.16	-0.17	-0.13	0.06	-0.05	1																
Staurolithites laffitei	-0.01	-0.08	-0.23	-0.04	0.13	-0.07	-0.14	-0.09	-0.01	0.22	0.07	0.05	-0.10	0.05	0.35	0.05	0.20	0.00	1															
Stoverius achylosus	-0.08	0.28	0.00	0.07	0.00	-0.09	-0.07	-0.02	-0.02	-0.06	0.02	0.02	0.03	0.12	0.06	0.18	0.03	-0.02	-0.11	1														
Tegumentum stradneri	-0.09	0.12	-0.14	-0.04	0.13	-0.17	-0.19	0.04	0.05	0.04	0.00	0.14	-0.07	0.03	0.19	0.17	0.25	0.09	0.32	0.22	1													
Tegumentum orionatus	-0.14	0.20	-0.05	-0.05	0.12	-0.21	0.12	0.18	-0.07	0.07	-0.14	0.17	-0.06	0.05	0.24	0.05	0.09	0.10	0.01	-0.08	0.11	1												
Tetrapodorhabdus decorus	-0.08	0.22	0.07	0.01	0.23	-0.06	-0.07	-0.02	-0.02	-0.06	-0.06	-0.07	-0.05	0.09	-0.05	0.03	-0.04	-0.13	0.00	-0.04	-0.17	-0.03	1											
Watznaueria barnesiae	-0.15	0.04	-0.22	-0.16	-0.25	-0.25	0.29	-0.10	-0.09	0.01	0.09	0.02	-0.16	-0.16	-0.40	-0.29	-0.14	-0.16	-0.24	-0.13	-0.15	-0.12	-0.02	1										
Watznaueria biporta	0.02	0.19	-0.33	0.07	-0.16	0.04	-0.09	-0.03	-0.07	-0.09	-0.09	-0.16	-0.17	-0.09	-0.11	-0.13	-0.18	0.01	0.00	0.13	0.02	-0.19	-0.03	0.17	1									
Watznaueria fossacincta	-0.13	0.12	-0.11	-0.02	-0.13	-0.01	0.10	0.19	-0.11	-0.08	-0.09	-0.12	-0.12	0.23	-0.26	-0.24	-0.09	-0.23	-0.13	0.06	-0.11	-0.18	0.16	0.37	0.19	1								
Zeugrhabdotus bicrescenticus	-0.08	-0.04	-0.02	-0.14	-0.11	-0.05	-0.04	-0.02	0.20	-0.12	0.04	0.04	0.06	-0.06	-0.15	-0.30	0.07	0.15	-0.08	-0.11	-0.05	0.07	-0.14	0.10	-0.15	-0.05	1							
Zeugrhabdotus biperforatus	0.04	-0.15	-0.16	0.08	-0.11	-0.14	-0.05	-0.11	-0.06	0.18	-0.20	0.17	-0.09	0.10	0.50	0.19	0.13	-0.11	0.12	-0.16	0.17	0.24	-0.13	-0.17	-0.20	-0.22	0.21	1						
Zeugrhabdotus diplogrammus	0.02	-0.05	-0.22	0.11	-0.05	-0.07	-0.08	0.22	-0.02	-0.04	0.01	-0.17	0.02	0.00	0.04	0.01	-0.22	-0.04	-0.09	-0.03	-0.15	0.05	-0.05	0.01	0.17	-0.13	-0.12	0.00	1					
Zeugrhabdotus embergeri	0.02	0.11	0.01	-0.08	-0.17	-0.03	-0.04	-0.02	-0.02	-0.04	-0.05	0.35	-0.07	-0.07	0.10	-0.13	-0.13	-0.09	-0.15	-0.03	0.09	-0.14	-0.03	0.18	-0.01	-0.04	0.04	0.18	-0.08	1				
Zeugrhabdotus erectus	-0.05	0.03	-0.01	0.10	0.15	0.08	-0.27	0.05	0.22	0.10	0.18	-0.09	0.20	-0.06	0.01	0.35	0.16	0.23	0.21	0.03	0.05	0.03	0.08	-0.55	-0.11	0.13	-0.02	0.08	0.01	-0.17	1			
Zeugrhabdotus kerguelenensis	-0.09	0.24	0.02	0.07	-0.03	-0.09	-0.11	0.02	-0.03	-0.10	-0.09	0.02	-0.13	0.11	0.04	-0.06	-0.04	-0.10	0.05	0.02	0.08	0.07	0.48	-0.01	0.13	0.24	-0.02	0.08	-0.07	-0.05	-0.02	1		
Zeugrhabdotus noeliae	-0.07	-0.18	0.17	0.04	0.12	-0.09	-0.06	-0.02	-0.02	-0.02	-0.05	-0.09	-0.09	-0.11	0.07	0.06	-0.12	0.02	-0.12	-0.03	-0.06	-0.08	-0.03	0.04	-0.11	0.04	-0.02	-0.04	0.07	-0.03	0.02	-0.05	1	
Zeugrhabdotus scutula	-0.10	-0.08	0.29	-0.01	0.28	0.04	-0.12	0.22	-0.13	0.06	-0.08	-0.04	-0.03	-0.04	-0.15	0.47	0.00	0.01	-0.26	0.04	-0.10	0.08	-0.01	-0.05	-0.20	-0.08	-0.18	-0.06	0.07	-0.12	0.15	-0.15	0.10	1

Appendix 11
Range chart of Seaford Head

Full range chart of nannofossil taxa recognized at **Seaford Head** is available upon request. Semi-quantitative abundance of all taxa detected are reported, as well as total abundance and preservation of calcareous nannofossils in each studied sample.

Total abundance: Abundant (A) = 21-30 specimens in each field of view; Common (C) = 11-20 specimens in each field of view; Few (F)= 6-10 specimens in each field of view; Rare (R) = 1-5 specimens in each field of view.

Species abundance: Abundant (A) = $\geq$ 1 specimen in each field of view; Common (C) = 1 specimen in 2-10 fields of view; Few (F) = 1 specimen in 11-30 fields of view; Rare (R) = 1 specimen in > 31 fields of view.

Preservation was characterized as follows:

Good (G) if nannofossil specimens show little or no evidence of dissolution and/or overgrowth and the primary morphological characters are only slightly altered allowing species identification;

Moderate (M) if specimens exhibit some etching and/or overgrowth, primary morphological characters are somewhat altered allowing, however, identification at the species level;

Poor (P) if specimens show severe etching and/or overgrowth, primary morphological characters are obliterated, hampering identification at the species and/or even generic level

Appendix 12A
Correlation matrix of genera - Seaford Head

The quantitative data used to produce this matrix are available upon request

	Ahmuellerella	Amphizygus	Arkhangelskiella	Aspidolitus	Biscutum	*Braarudosphaera*	*Broinsonia*	*Bukrylithus*	Calculites	Chiastozygus	*Cribrosphaerella*	*Cyclagelosphaera*	Cylindralithus	Cretarhabdus	Discorhabdus	Eiffellithus	Eprolithus	Gartnerago	Grantarhabdus	*Haqius*	Helicolithus	Lapideacassis	Lithastrinus	*Lithraphidites*
Ahmuellerella	1																							
Amphizygus	0.57	1																						
Arkhangelskiella	0.32	0.28	1																					
Aspidolitus	0.40	0.43	0.45	1																				
Biscutum	**0.62**	0.57	0.22	0.50	1																			
Braarudosphaera	0.25	0.14	0.08	0.05	0.07	1																		
Broinsonia	0.02	-0.04	0.10	0.15	-0.02	0.11	1																	
Bukrylithus	-0.08	-0.08	-0.08	-0.04	0.09	0.00	-0.08	1																
Calculites	**0.64**	0.55	0.34	**0.60**	**0.73**	0.24	0.12	0.01	1															
Chiastozygus	-0.35	-0.36	0.14	-0.32	-0.47	-0.14	0.15	-0.08	-0.45	1														
Cribrosphaerella	**0.83**	0.58	0.36	0.48	**0.64**	0.23	-0.07	0.01	**0.66**	-0.46	1													
Cyclagelosphaera	0.29	0.45	0.24	0.17	0.23	0.07	-0.11	-0.02	0.10	-0.11	0.41	1												
Cylindralithus	0.10	0.11	0.10	0.31	0.17	0.15	-0.11	0.02	0.18	-0.24	0.21	0.09	1											
Cretarhabdus	-0.10	-0.10	-0.18	-0.11	-0.03	-0.10	-0.03	-0.05	-0.04	-0.04	-0.08	-0.07	-0.01	1										
Discorhabdus	**0.69**	**0.61**	0.39	0.47	**0.61**	0.37	0.23	-0.03	**0.73**	-0.34	0.57	0.27	0.14	-0.13	1									
Eiffellithus	0.41	0.31	-0.02	0.20	0.18	0.48	0.01	-0.09	0.35	-0.28	0.38	0.09	0.27	-0.19	0.44	1								
Eprolithus	-0.28	-0.31	-0.18	-0.33	-0.36	-0.11	0.33	-0.06	-0.40	0.34	-0.37	-0.09	-0.11	0.01	-0.31	-0.25	1							
Gartnerago	-0.25	-0.31	-0.06	-0.36	-0.34	-0.09	0.44	-0.13	-0.34	0.46	-0.37	-0.20	-0.27	0.11	-0.18	-0.24	0.38	1						
Grantarhabdus	-0.01	-0.09	0.00	0.04	0.03	-0.14	-0.08	-0.09	-0.13	0.03	-0.02	0.15	-0.07	-0.21	-0.11	-0.09	0.01	0.04	1					
Haqius	-0.20	-0.19	-0.08	-0.21	-0.17	-0.12	-0.14	0.39	-0.22	0.09	-0.14	-0.05	0.09	0.02	-0.20	-0.10	-0.01	-0.21	-0.22	1				
Helicolithus	-0.17	-0.21	-0.02	-0.12	-0.13	-0.18	-0.16	-0.11	-0.22	0.14	-0.19	-0.04	-0.03	-0.01	-0.20	0.02	-0.22	-0.04	0.01	-0.01	1			
Lapideacassis	0.10	0.06	-0.01	-0.04	-0.06	0.40	0.17	-0.01	0.09	-0.08	0.10	-0.02	-0.13	-0.05	0.14	0.39	-0.06	0.15	-0.09	-0.04	-0.09	1		
Lithastrinus	0.10	0.24	-0.11	-0.02	0.20	0.24	-0.13	0.29	0.11	-0.25	0.20	0.07	0.29	0.01	0.12	0.27	-0.23	-0.03	-0.26	0.06	0.05	0.13	1	
Lithraphidites	0.37	0.31	0.18	0.26	0.46	0.19	0.03	0.12	0.30	-0.28	0.45	0.29	0.24	-0.05	0.35	0.06	-0.22	-0.15	0.02	0.01	-0.13	-0.02	0.19	1
Loxolithus	0.10	-0.01	0.07	-0.12	-0.03	0.03	0.19	-0.10	0.02	0.27	0.11	0.01	-0.15	-0.07	0.02	0.00	0.18	0.21	0.05	-0.12	-0.18	0.11	-0.13	-0.16
Lucianorhabdus	0.26	0.26	-0.02	0.41	0.36	0.08	-0.32	0.02	0.47	-0.42	0.38	-0.02	0.18	0.00	0.15	0.27	-0.48	-0.41	0.03	-0.26	-0.01	0.09	0.20	0.18
Manivitella	-0.32	-0.34	-0.13	-0.26	-0.22	-0.15	0.07	-0.12	-0.28	0.36	-0.28	-0.17	-0.32	0.27	-0.37	-0.19	0.20	0.12	-0.11	0.26	0.16	0.00	-0.19	-0.23
Micrantholithus	-0.17	-0.17	-0.19	-0.20	-0.16	0.16	-0.12	-0.03	-0.23	0.14	-0.18	-0.05	-0.09	0.46	-0.17	-0.15	0.13	0.23	-0.12	-0.08	-0.07	-0.03	0.01	-0.13
Microrhabdulus	0.24	0.38	-0.06	0.35	0.28	0.00	0.01	0.08	0.27	-0.18	0.35	-0.05	0.02	0.02	0.18	0.14	-0.18	-0.26	-0.03	-0.03	-0.18	-0.07	0.07	0.23
Micula	-0.17	-0.16	-0.15	-0.03	-0.08	0.05	-0.29	0.36	-0.10	-0.21	-0.07	-0.10	0.11	-0.22	-0.16	0.10	-0.40	-0.19	-0.09	0.14	0.23	0.09	0.38	0.05
Nannoconus	-0.04	-0.16	0.05	-0.25	-0.26	-0.07	0.26	-0.08	-0.19	0.47	-0.23	-0.09	-0.15	0.30	-0.05	-0.06	0.46	0.43	0.02	-0.09	-0.10	-0.01	-0.26	-0.18
Placozygus	0.06	0.19	0.11	-0.02	0.05	-0.04	0.36	-0.13	0.22	0.12	0.00	0.03	0.00	-0.04	0.27	0.04	0.09	0.12	0.02	-0.09	-0.18	-0.07	-0.19	-0.09
Prediscosphaera	0.54	0.50	0.22	0.51	0.55	0.22	0.12	-0.05	0.59	-0.39	0.56	0.13	0.18	-0.12	0.54	0.41	-0.24	-0.44	-0.02	-0.15	-0.24	0.28	0.09	0.20
Quadrum	-0.43	-0.42	0.04	-0.27	-0.44	-0.14	0.03	-0.03	-0.46	0.51	-0.44	-0.13	-0.15	0.03	-0.40	-0.41	0.26	0.31	-0.04	0.11	0.08	-0.09	-0.24	-0.31
Radiolithus	-0.08	-0.08	-0.13	-0.09	-0.09	0.00	-0.08	-0.01	-0.11	0.13	-0.11	-0.02	0.02	-0.05	-0.09	-0.12	0.41	-0.02	-0.09	-0.04	-0.16	-0.01	-0.07	-0.09
Retecapsa	0.19	0.23	-0.01	0.03	0.18	0.15	-0.25	-0.07	0.16	-0.23	0.33	0.09	-0.03	0.10	0.01	0.14	-0.33	-0.34	-0.24	0.03	0.19	0.00	0.18	0.10
Rhagodiscus	0.24	0.28	0.17	0.16	0.12	0.08	0.19	-0.07	0.26	-0.04	0.17	0.32	0.10	-0.15	0.43	0.27	0.06	-0.17	0.05	-0.09	0.04	-0.07	-0.20	-0.02
Reinhardtites	0.46	0.22	-0.03	0.16	0.33	0.19	0.18	0.02	0.32	-0.14	0.27	-0.08	0.14	-0.14	0.34	0.29	-0.05	-0.08	-0.03	-0.04	-0.21	0.13	0.06	0.13
Rotelapillus	0.17	0.14	0.11	0.39	0.18	-0.02	-0.13	-0.04	0.21	-0.20	0.26	0.03	0.18	-0.08	0.18	0.09	-0.11	-0.18	0.10	-0.10	-0.14	-0.04	0.04	0.16
Rucinolithus	0.48	0.34	0.27	0.24	0.29	0.06	0.07	-0.05	0.32	-0.22	0.40	0.09	0.26	-0.14	0.39	0.12	-0.19	-0.09	-0.15	-0.12	0.01	-0.05	0.31	0.15
Staurolithites	0.59	**0.64**	0.22	0.21	**0.66**	0.17	-0.09	-0.06	0.53	-0.31	0.56	0.48	-0.09	0.04	0.52	0.27	-0.26	-0.25	0.07	-0.16	-0.19	0.19	0.05	0.30
Tetrapodorhabdus	0.09	0.29	0.08	0.19	0.00	0.06	0.15	-0.04	0.12	0.04	0.11	-0.06	-0.05	-0.03	0.20	0.19	-0.09	-0.01	-0.13	0.16	-0.07	-0.04	0.06	-0.13
Tranolithus	0.50	0.33	0.03	0.23	0.41	0.03	0.08	0.00	0.54	-0.28	0.42	0.13	0.13	0.18	0.43	0.36	-0.22	-0.29	-0.12	-0.08	-0.12	-0.06	0.00	0.12
Tegumentum	-0.04	-0.11	0.13	0.11	0.00	0.07	0.25	-0.02	0.03	0.23	0.00	-0.03	0.27	-0.07	0.04	0.03	0.03	0.14	0.01	-0.05	-0.09	-0.02	-0.06	0.07
Kamptnerius	-0.15	-0.03	-0.06	-0.12	-0.13	0.00	0.00	-0.07	-0.11	0.10	-0.23	-0.10	-0.24	-0.09	-0.08	-0.02	0.11	-0.07	0.06	0.07	0.05	-0.07	-0.02	0.05
Watznaueria	**-0.75**	**-0.62**	-0.31	**-0.60**	**-0.76**	-0.30	-0.04	-0.04	**-0.83**	0.45	**-0.78**	-0.21	-0.27	0.10	**-0.72**	-0.57	0.50	0.42	0.10	0.23	0.06	-0.19	-0.31	-0.39
Zeugrhabdotus	-0.01	-0.09	-0.20	-0.10	-0.10	-0.01	0.28	0.00	-0.08	0.17	-0.03	0.04	-0.06	0.12	-0.04	0.17	0.20	0.17	0.10	-0.19	-0.01	0.05	0.14	0.01

	Loxolithus	Lucianorhabdus	*Manivitella*	*Micrantholithus*	*Microrhabdulus*	Micula	Nannoconus	Placozygus	Prediscosphaera	Quadrum	*Radiolithus*	Retecapsa	Rhagodiscus	Reinhardtites	*Rotelapillus*	*Rucinolithus*	Staurolithites	*Tetrapodorhabdus*	Tranolithus	Tegumentum	Kamptnerius	Watznaueria	Zeugrhabdotus
Loxolithus	1																						
Lucianorhabdus	-0.21	1																					
Manivitella	0.32	-0.35	1																				
Micrantholithus	0.01	-0.14	0.17	1																			
Microrhabdulus	-0.08	0.27	-0.12	-0.13	1																		
Micula	-0.38	0.34	-0.23	-0.12	-0.01	1																	
Nannoconus	0.36	-0.43	0.35	0.22	-0.18	-0.48	1																
Placozygus	0.35	-0.31	0.06	-0.14	0.00	-0.44	0.32	1															
Prediscosphaera	0.11	0.27	-0.16	-0.24	0.39	-0.13	-0.19	0.14	1														
Quadrum	0.23	-0.47	0.34	0.20	-0.29	-0.10	0.29	0.03	-0.48	1													
Radiolithus	0.11	0.01	0.00	-0.03	-0.07	-0.14	0.21	-0.13	-0.03	0.17	1												
Retecapsa	-0.04	0.13	0.15	-0.11	0.14	0.07	-0.31	-0.04	0.15	-0.24	-0.10	1											
Rhagodiscus	0.13	-0.22	-0.16	-0.15	0.02	-0.24	0.01	0.31	0.10	-0.13	-0.07	0.00	1										
Reinhardtites	-0.04	0.14	-0.19	0.00	0.15	-0.13	0.06	0.18	0.22	-0.18	-0.08	-0.05	0.18	1									
Rotelapillus	0.07	0.14	-0.17	-0.08	0.32	-0.06	-0.18	-0.03	0.40	-0.19	-0.04	0.01	-0.08	-0.11	1								
Rucinolithus	-0.14	0.10	-0.34	-0.10	0.03	-0.05	-0.12	0.07	0.11	-0.24	-0.05	0.16	0.29	0.35	-0.04	1							
Staurolithites	0.06	0.30	-0.13	-0.14	0.08	-0.17	-0.11	0.07	0.49	-0.36	-0.06	0.11	0.11	0.22	0.07	0.00	1						
Tetrapodorhabdus	0.37	-0.02	0.11	-0.09	0.40	-0.10	0.14	0.04	0.15	-0.09	-0.04	-0.07	0.13	-0.09	0.23	-0.06	-0.02	1					
Tranolithus	-0.03	0.36	-0.21	-0.17	0.23	-0.14	0.00	0.09	0.42	-0.34	0.01	-0.06	0.11	0.22	0.07	0.07	0.48	0.14	1				
Tegumentum	0.30	-0.19	0.08	-0.05	-0.11	-0.10	0.22	0.02	0.14	0.04	-0.02	-0.13	0.04	-0.05	0.12	-0.07	-0.09	0.17	0.04	1			
Kamptnerius	-0.20	-0.06	-0.05	-0.10	0.05	0.03	0.13	0.09	-0.08	-0.05	0.06	0.06	-0.21	0.03	0.04	-0.10	-0.01	-0.11	-0.07	-0.10	1		
Watznaueria	0.00	-0.54	0.31	0.28	-0.38	-0.10	0.25	-0.05	**-0.76**	0.56	0.13	-0.27	-0.16	-0.34	-0.27	-0.32	**-0.60**	-0.16	-0.58	-0.06	0.10	1	
Zeugrhabdotus	0.29	-0.14	0.12	0.02	0.13	-0.06	0.19	0.08	0.08	-0.05	-0.06	-0.06	0.10	-0.09	0.09	-0.03	-0.11	0.18	0.14	0.26	0.01	-0.07	1

Appendix 12B
Correlation matrix of species - Seaford Head

The quantitative data used to produce this matrix are available upon request

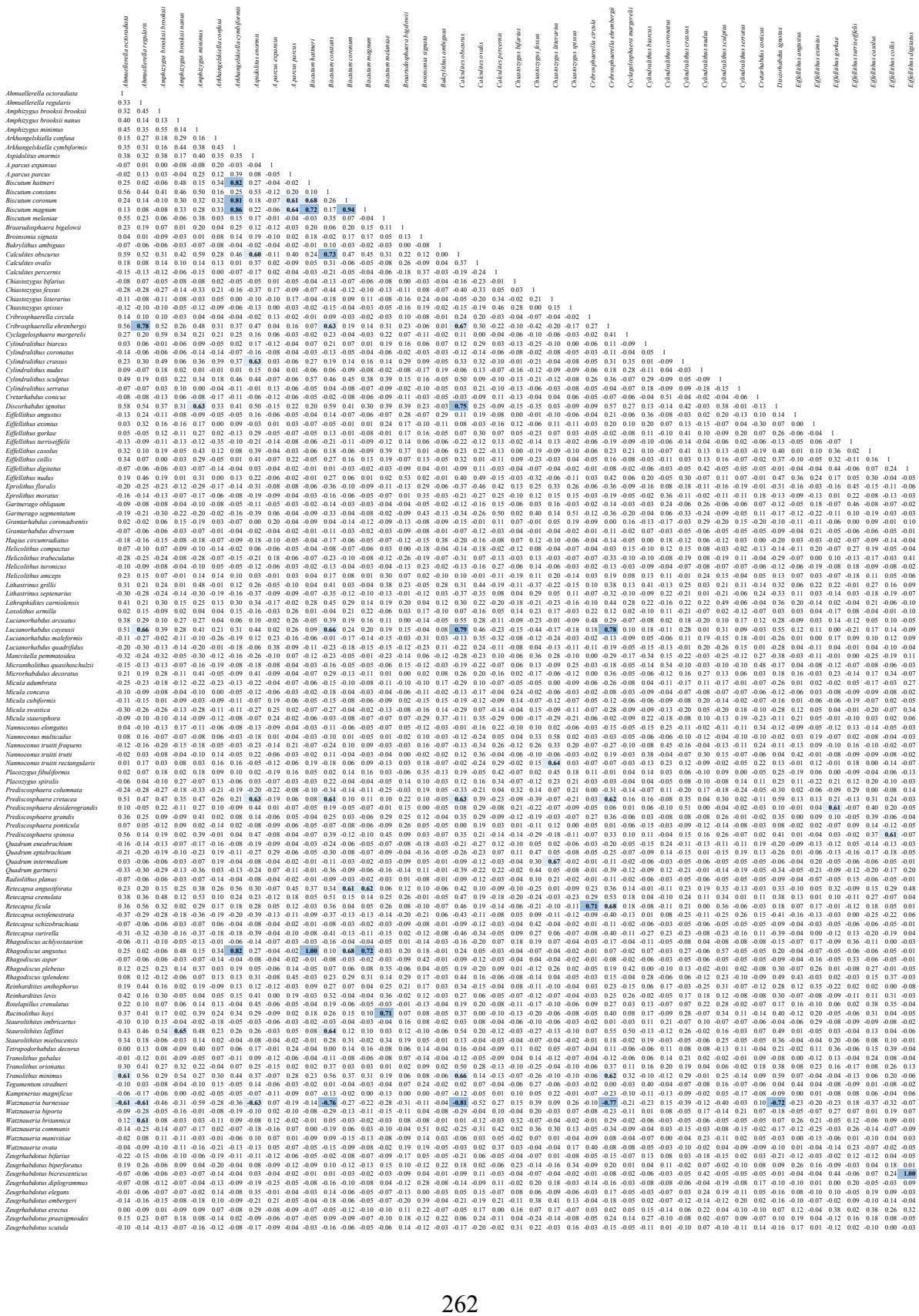

	Prediscophaera desideregrandis	*Prediscophaera grandis*	*Prediscophaera ponticula*	*Prediscophaera spinosa*	*Quadrum enatbrachium*	*Quadrum equibrachium*	*Quadrum intermedium*	*Quadrum garnieri*	*Radiolithus planus*	*Retecapsa angustiforata*	*Retecapsa crenulata*	*Retecapsa ficula*	*Retecapsa octofenestrata*	*Retecapsa schizobrachiata*	*Retecapsa surirella*	*Rhagodiscus achlyostaurion*	*Rhagodiscus angustus*	*Rhagodiscus asper*	*Rhagodiscus plebeius*	*Rhagodiscus splendens*	*Reinhardtites anthophorus*	*Reinhardtites levis*	*Rotelapillus crenulatus*	*Rucinolithus hayi*	*Sisyrolithites imbricatus*	*Sisyrolithites laffitei*	*Sisyrolithites mielnicensis*	*Terrapodorhabdus decorus*	*Tranolithus gabalus*	*Tranolithus orionatus*	*Tranolithus minimus*	*Tegumentum stradneri*	*Kamptnerius magnificus*	*Watznaueria barnesiae*	*Watznaueria biporta*	*Watznaueria britannica*	*Watznaueria communis*	*Watznaueria manivitiae*	*Watznaueria ovata*	*Zeugrhabdotus bifarius*	*Zeugrhabdotus biperforatus*	*Zeugrhabdotus hexaescenticus*	*Zeugrhabdotus diplogrammus*	*Zeugrhabdotus elegans*	*Zeugrhabdotus embergeri*	*Zeugrhabdotus erectus*	*Zeugrhabdotus praesigmoides*	*Zeugrhabdotus scutula*
Prediscosphaera spinosa	-0.01	-0.13	-0.18	-0.06	-0.09	-0.06	1																																										
Quadrum cneatbrachium	0.15	-0.24	-0.14	0.01	-0.27	-0.08	0.41	1																																									
Quadrum cphatbrachium	0.13	-0.16	-0.20	-0.03	-0.23	-0.07	0.40	0.54	1																																								
Quadrum intermedium	-0.29	0.06	0.16	-0.01	0.13	-0.09	-0.23	-0.24	-0.24	1																																							
Quadrum parmeri	-0.07	-0.03	-0.05	-0.01	0.07	-0.01	-0.06	-0.12	0.02	0.15	1																																							
Radiolithus planus	-0.31	0.11	0.12	0.04	0.29	0.05	-0.21	-0.26	-0.26	0.24	0.04	1																																						
Retecapsa angustiforata	-0.12	-0.06	-0.09	-0.03	-0.02	-0.03	-0.02	-0.11	-0.07	0.07	0.56	0.23	1																																					
Retecapsa crenulata	-0.07	-0.03	-0.05	-0.01	-0.01	-0.01	0.37	0.05	-0.03	-0.09	-0.01	-0.08	-0.03	1																																			
Retecapsa ficula	0.00	-0.01	-0.16	-0.05	-0.05	-0.05	0.13	0.17	0.17	-0.22	-0.05	-0.17	-0.09	-0.05	-0.05	1																																		
Retecapsa octofenestrata	0.32	-0.07	-0.10	-0.03	-0.09	-0.03	0.16	0.08	0.01	-0.18	-0.03	-0.16	-0.05	-0.03	-0.03	0.01	1																																	
Retecapsa schizobrachiata	0.07	0.01	-0.18	-0.03	-0.11	-0.07	-0.04	0.12	0.16	-0.18	0.08	-0.13	0.13	-0.08	-0.13	0.09	0.09	1																																	
Retecapsa surirella	0.49	-0.06	-0.08	-0.08	-0.03	-0.14	-0.03	-0.10	0.05	0.13	-0.15	-0.03	-0.13	-0.05	-0.03	-0.03	0.00	0.29	0.11	1																															
Rhagodiscus achlyostaurion	0.42	-0.09	-0.12	-0.04	-0.17	-0.04	0.06	0.04	0.25	-0.22	-0.04	-0.19	-0.07	-0.04	-0.04	-0.10	0.12	-0.11	-0.01	1																															
Rhagodiscus angustus	-0.10	-0.05	-0.07	-0.02	-0.06	-0.02	-0.08	0.01	-0.07	-0.01	-0.02	-0.11	-0.04	-0.02	-0.02	-0.05	0.32	0.02	0.30	0.31	-0.03	1																													
Rhagodiscus asper	0.21	-0.14	-0.19	-0.06	-0.30	-0.06	0.31	0.37	0.28	-0.34	-0.06	-0.30	-0.10	0.08	-0.06	0.18	0.01	0.17	0.01	0.07	-0.01	-0.08	1																											
Rhagodiscus plebeius	-0.07	-0.03	-0.05	-0.01	-0.08	-0.01	0.08	0.04	0.05	-0.01	0.06	0.33	0.04	0.14	-0.04	-0.04	-0.15	0.09	-0.15	0.23	0.10	0.38	0.25	-0.14	-0.06	0.40	0.38	0.02	0.15	0.02	-0.06	-0.03	-0.04	1															
Rhagodiscus splendens	0.19	-0.10	0.15	-0.04	-0.09	-0.04	0.05	-0.03	-0.01	0.06	0.33	0.04	0.14	-0.04	-0.04	-0.15	0.09	-0.15	-0.08	0.23	0.10	0.38	0.05	0.25	-0.09	0.58	0.21	-0.01	-0.01	-0.13	-0.05	-0.15	-0.08	-0.04	1													
Reinhardtites anthophorus	0.18	-0.10	-0.13	-0.06	-0.31	0.02	0.16	0.16	0.11	-0.26	-0.08	-0.33	-0.15	0.02	-0.06	0.12	0.08	0.22	0.07	0.06	0.06	0.40	0.38	0.02	0.15	0.02	0.15	0.02	0.09	0.13	0.25	1																
Reinhardtites levis	0.17	-0.14	-0.20	-0.06	-0.29	-0.06	0.29	0.30	0.33	-0.32	-0.06	-0.28	-0.11	0.23	0.08	0.10	0.23	0.10	0.38	0.05	0.25	-0.09	0.58	0.21	-0.01	-0.01	-0.13	0.46	1																			
Tegumentum stradneri	0.01	-0.05	-0.07	-0.02	0.09	-0.02	-0.08	-0.03	-0.07	-0.07	-0.02	-0.11	-0.04	-0.02	-0.02	-0.07	0.34	-0.04	-0.04	0.13	-0.07	-0.03	-0.08	-0.02	0.16	-0.06	0.05	-0.09	1																			
Kamptnerius magnificus	-0.05	-0.09	0.06	0.45	-0.10	0.07	-0.09	-0.01	-0.12	0.19	-0.07	0.07	-0.03	0.07	-0.07	-0.23	-0.01	0.05	-0.12	0.05	-0.09	0.10	-0.03	-0.07	-0.10	0.05	-0.07	-0.08	-0.10	1																		
Watznaueria barnesiae	-0.44	0.41	0.25	0.03	0.48	0.14	-0.43	-0.55	-0.46	0.46	0.09	0.51	0.17	-0.14	0.11	-0.12	-0.30	-0.32	-0.23	-0.27	-0.31	-0.09	-0.58	-0.17	-0.17	0.05	-0.53	-0.58	-0.08	0.09	1																	
Watznaueria biporta	0.10	-0.11	0.24	-0.08	0.17	-0.08	-0.04	-0.10	-0.11	0.01	-0.08	0.08	-0.05	-0.08	0.22	-0.17	-0.16	-0.31	-0.14	0.33	-0.25	0.00	-0.23	-0.08	0.32	0.11	-0.11	-0.19	-0.01	-0.17	0.16	1																
Watznaueria britannica	0.07	-0.03	-0.05	-0.01	-0.08	-0.01	-0.06	0.00	0.25	-0.09	-0.01	-0.08	-0.03	-0.01	-0.01	0.15	-0.03	0.25	-0.03	-0.04	-0.05	-0.02	0.18	-0.01	0.25	-0.04	0.21	0.20	-0.02	-0.07	-0.18	-0.08	1															
Watznaueria communis	-0.15	-0.05	0.02	0.20	0.44	-0.02	-0.08	-0.13	-0.21	-0.12	0.00	0.10	0.16	0.00	0.50	-0.06	-0.02	-0.09	-0.02	-0.08	-0.16	-0.01	-0.16	0.09	0.05	0.04	-0.25	-0.11	0.13	0.13	0.30	0.30	-0.11	1													
Watznaueria manivitiae	0.16	-0.09	-0.07	-0.09	0.19	-0.09	-0.15	0.00	-0.04	-0.14	0.28	0.03	0.20	-0.09	0.26	-0.06	-0.05	0.02	0.22	-0.05	-0.06	-0.04	-0.06	-0.09	-0.06	-0.03	-0.08	0.01	-0.04	-0.20	-0.02	0.09	0.13	0.25	1											
Watznaueria ovata	-0.05	-0.12	-0.08	-0.05	0.02	-0.05	-0.04	0.01	0.20	-0.05	-0.05	0.00	0.18	-0.05	-0.05	-0.13	0.12	0.13	0.06	-0.05	-0.02	0.09	-0.13	-0.05	-0.15	-0.08	-0.20	-0.12	-0.08	0.27	0.11	-0.08	-0.05	0.27	-0.15	1									
Zeugrhabdotus bifarius	0.02	-0.11	-0.10	-0.05	0.04	-0.05	-0.02	-0.09	-0.08	0.06	-0.05	0.16	-0.08	-0.05	0.21	-0.04	-0.10	-0.21	-0.08	-0.12	-0.03	-0.07	-0.04	-0.05	-0.13	0.07	-0.06	-0.16	-0.07	-0.03	0.07	0.13	-0.05	0.15	0.02	0.13	1								
Zeugrhabdotus biperforatus	0.15	0.14	-0.16	-0.09	-0.15	-0.09	-0.14	-0.15	0.01	-0.23	0.01	-0.14	0.09	-0.09	-0.09	0.12	-0.02	0.26	0.00	0.04	0.05	0.03	0.11	0.01	0.09	-0.16	0.33	0.16	0.02	-0.22	-0.12	-0.09	0.29	-0.22	0.10	-0.14	-0.27	1							
Zeugrhabdotus hexaescenticus	-0.07	-0.03	-0.05	-0.01	0.20	-0.01	0.48	0.04	0.01	0.06	-0.01	0.04	-0.03	-0.01	-0.01	-0.05	-0.03	-0.08	-0.03	-0.04	-0.05	-0.02	-0.06	-0.01	-0.04	0.13	-0.06	-0.02	-0.02	-0.07	-0.07	-0.01	-0.09	0.03	-0.05	-0.05	-0.05	0.01	1						
Zeugrhabdotus diplogrammus	-0.02	-0.10	-0.16	0.09	0.07	-0.02	-0.12	0.14	-0.06	0.10	0.04	-0.02	0.12	-0.08	0.15	0.10	-0.14	-0.11	-0.09	-0.17	0.03	-0.02	-0.15	-0.08	0.15	-0.20	0.08	0.02	0.25	0.03	0.05	0.08	0.02	0.24	0.07	0.07	0.25	-0.01	0.09	1					
Zeugrhabdotus elegans	0.06	-0.08	-0.11	-0.03	-0.06	-0.03	0.07	-0.02	0.18	-0.10	0.42	-0.12	0.20	-0.03	-0.03	-0.11	-0.07	-0.02	-0.06	0.34	-0.11	-0.05	-0.01	-0.03	0.04	0.25	-0.02	0.00	-0.05	-0.03	-0.15	-0.03	-0.03	-0.07	0.26	-0.12	-0.11	0.09	-0.03	-0.04	1				
Zeugrhabdotus embergeri	-0.17	-0.09	0.29	0.38	0.03	-0.04	-0.14	-0.14	-0.14	-0.02	-0.02	-0.04	0.00	-0.07	-0.04	0.38	-0.02	-0.08	-0.08	-0.07	-0.10	-0.02	-0.05	-0.15	-0.04	0.02	-0.11	-0.08	-0.10	0.24	0.04	0.11	0.19	-0.04	0.38	0.14	-0.14	0.11	-0.23	-0.04	0.23	-0.09	1		
Zeugrhabdotus erectus	0.17	-0.11	-0.08	0.23	0.11	-0.07	0.16	0.02	0.02	-0.03	-0.07	-0.19	-0.13	-0.07	0.03	0.03	0.12	-0.18	-0.08	0.51	-0.13	-0.10	-0.04	-0.07	0.27	0.02	-0.05	-0.16	0.27	0.18	-0.18	0.30	-0.07	0.14	-0.05	-0.01	-0.02	-0.06	0.32	0.11	0.22	0.12	1		
Zeugrhabdotus praesigmoides	0.18	-0.12	-0.11	-0.05	-0.23	-0.05	-0.03	0.00	0.07	-0.04	-0.05	-0.26	-0.09	-0.05	-0.05	0.06	0.03	0.03	-0.09	0.12	-0.04	-0.07	0.29	-0.05	0.00	0.05	0.22	0.20	-0.07	0.07	-0.27	-0.05	0.45	-0.17	-0.03	0.01	0.18	0.20	-0.05	0.01	0.01	-0.01	0.09	1	
Zeugrhabdotus scutula	-0.15	-0.08	0.19	-0.03	0.04	-0.03	-0.12	0.08	-0.12	-0.14	-0.03	0.32	0.26	-0.03	-0.03	0.04	-0.07	0.05	-0.06	-0.08	-0.10	-0.05	-0.13	-0.03	-0.09	-0.10	-0.18	-0.13	-0.05	0.03	0.14	0.09	-0.03	0.10	-0.08	0.28	0.08	0.12	-0.03	0.16	-0.08	-0.08	0.02	-0.11	1

Appendix 13
Range chart of TDP39

Full range chart of nannofossil taxa recognized at **TDP39** is available upon request. Semi-quantitative abundance of all taxa detected are reported, as well as total abundance and preservation of calcareous nannofossils in each studied sample.

Total abundance: Abundant (A) = 21-30 specimens in each field of view; Common (C) = 11-20 specimens in each field of view; Few (F)= 6-10 specimens in each field of view; Rare (R) = 1-5 specimens in each field of view.

Species abundance: Abundant (A) = $\geq$ 1 specimen in each field of view; Common (C) = 1 specimen in 2-10 fields of view; Few (F) = 1 specimen in 11-30 fields of view; Rare (R) = 1 specimen in > 31 fields of view.

Preservation was characterized as follows:

Good (G) if nannofossil specimens show little or no evidence of dissolution and/or overgrowth and the primary morphological characters are only slightly altered allowing species identification;

Moderate (M) if specimens exhibit some etching and/or overgrowth, primary morphological characters are somewhat altered allowing, however, identification at the species level;

Poor (P) if specimens show severe etching and/or overgrowth, primary morphological characters are obliterated, hampering identification at the species and/or even generic level

Appendix 14A
Correlation matrix of genera - TDP39

The quantitative data used to produce this matrix are available upon request

	Amphizygus	*Ahmuellerella*	*Arkhangelskiella*	*Axopodorhabdus*	*Biscutum*	*Bukrylithus*	*Braarudosphaera*	*Broinsonia*	*Calculites*	*Chiastozygus*	*Corollithion*	*Cretarhabdus*	*Cribrosphaerella*	*Cylindralithus*	*Discorhabdus*	*Eiffellithus*	*Eprolithus*	*Flabellites*	*Grantarhabdus*	*Gartnerago*	*Haqius*	*Helicolithus*	*Lithastrinus*	*Lithraphidites*	*Loxolithus*
Amphizygus	1																								
Ahmuellerella	0.01	1																							
Arkhangelskiella	0.02	0.16	1																						
Axopodorhabdus	0.03	0.06	0.46	1																					
Biscutum	0.04	0.09	0.09	0.04	1																				
Bukrylithus	0.05	0.11	0.33	0.04	0.25	1																			
Braarudosphaera	0.06	0.28	0.18	0.07	0.28	0.12	1																		
Broinsonia	0.07	0.17	0.13	0.04	0.31	0.06	0.04	1																	
Calculites	0.08	0.05	0.23	0.48	0.14	0.09	0.01	0.10	1																
Chiastozygus	0.09	0.19	0.04	0.07	0.25	0.15	0.37	0.03	0.07	1															
Corollithion	0.10	0.27	0.32	0.23	0.38	0.07	0.01	0.08	0.21	0.18	1														
Cretarhabdus	0.11	0.17	0.14	0.05	0.09	0.13	0.18	0.28	0.11	0.16	0.25	1													
Cribrosphaerella	0.12	0.31	0.24	0.05	0.46	0.23	0.54	0.10	0.08	0.17	0.18	0.01	1												
Cylindralithus	0.13	0.15	0.07	0.03	0.02	0.09	0.24	0.18	0.15	0.35	0.01	0.10	0.21	1											
Discorhabdus	0.14	0.01	0.04	0.04	**0.81**	0.24	0.35	0.19	0.03	0.06	0.36	0.06	0.56	0.11	1										
Eiffellithus	0.15	0.09	0.04	0.25	0.37	0.14	0.09	0.13	0.08	0.30	0.10	0.06	0.40	0.06	0.42	1									
Eprolithus	0.16	0.03	0.17	0.07	0.36	0.12	0.40	0.07	0.06	0.27	0.16	0.08	0.59	0.23	0.42	0.22	1								
Flabellites	0.17	0.09	0.03	0.12	0.23	0.03	0.14	0.07	0.03	0.03	0.04	0.10	0.21	0.12	0.13	0.36	0.17	1							
Grantarhabdus	0.18	0.28	0.00	0.13	0.05	0.14	0.30	0.07	0.05	0.13	0.39	0.08	0.24	0.25	0.08	0.13	0.05	0.23	1						
Gartnerago	0.19	0.09	0.02	0.05	0.01	0.21	0.09	0.05	0.08	0.02	0.09	0.19	0.14	0.18	0.12	0.18	0.10	0.16	0.10	1					
Haqius	0.20	0.06	0.29	0.48	0.14	0.04	0.07	0.04	0.48	0.09	0.18	0.01	0.06	0.03	0.04	0.04	0.07	0.37	0.08	0.05	1				
Helicolithus	0.21	0.20	0.06	0.00	0.00	0.16	**0.63**	0.03	0.05	0.30	0.29	0.14	0.30	0.11	0.08	0.03	0.15	0.25	0.44	0.13	0.09	1			
Lithastrinus	0.22	0.01	0.16	0.08	0.33	0.11	0.09	0.02	0.06	0.08	0.10	0.06	0.45	0.15	0.35	0.23	0.45	0.24	0.00	0.01	0.10	0.00	1		
Lithraphidites	0.23	0.09	0.06	0.24	0.36	0.02	0.17	0.09	0.38	0.05	0.35	0.01	0.27	0.06	0.26	0.18	0.18	0.19	0.10	0.20	0.12	0.04	0.22	1	
Loxolithus	0.24	0.22	0.11	0.06	0.25	0.20	0.40	0.00	0.08	0.30	0.20	0.31	0.52	0.22	0.31	0.15	0.54	0.26	0.28	0.14	0.03	0.44	0.23	0.10	1
Lucianorhabdus	0.25	0.05	0.11	0.36	0.14	0.05	0.01	0.10	0.45	0.10	0.07	0.26	0.07	0.20	0.01	0.13	0.17	0.09	0.07	0.16	0.48	0.01	0.26	0.06	0.17
Microrhabdulus	0.26	0.21	0.15	0.10	0.06	0.05	0.23	0.19	0.08	0.06	0.15	0.03	0.26	0.05	0.12	0.28	0.23	0.23	0.15	0.05	0.03	0.24	0.15	0.11	0.22
Manivitella	0.27	0.16	0.18	0.05	0.39	0.17	0.31	0.06	0.00	0.05	0.26	0.24	0.46	0.03	0.47	0.24	0.39	0.13	0.04	0.05	0.18	0.23	0.48	0.17	0.24
Martasterites	0.28	0.19	0.04	0.18	0.20	0.25	0.24	0.10	0.37	0.27	0.35	0.30	0.11	0.29	0.03	0.09	0.17	0.08	0.37	0.32	0.14	0.37	0.08	0.22	0.30
Micula	0.29	0.06	0.17	0.16	0.49	0.06	0.43	0.01	0.09	0.16	0.24	0.05	0.33	0.10	0.53	0.28	0.47	0.16	0.03	0.10	0.22	0.17	0.06	0.07	0.32
Nannoconus	0.30	0.00	0.02	0.14	0.22	0.08	0.51	0.07	0.37	0.34	0.05	0.24	0.35	0.43	0.27	0.16	0.42	0.21	0.31	0.10	0.14	0.35	0.07	0.03	0.52
Owenia	0.31	0.01	0.34	0.55	0.22	0.05	0.07	0.04	0.44	0.15	0.48	0.13	0.12	0.04	0.15	0.03	0.06	0.12	0.08	0.05	0.55	0.22	0.07	0.44	0.17
Placozygus	0.32	0.32	0.21	0.16	0.55	0.02	0.21	0.17	0.28	0.26	0.36	0.00	0.13	0.17	0.36	0.23	0.20	0.03	0.20	0.13	0.16	0.24	0.05	0.15	0.13
Prediscosphaera	0.33	0.03	0.31	0.01	0.52	0.34	0.34	0.27	0.10	0.14	0.16	0.19	0.45	0.07	0.51	0.45	0.46	0.17	0.11	0.13	0.02	0.30	0.48	0.13	0.33
Prolatipatella	0.34	0.08	0.03	0.27	0.12	0.09	0.09	0.05	0.08	0.25	0.08	0.05	0.09	0.09	0.02	0.04	0.10	0.03	0.03	0.07	0.05	0.06	0.06	0.05	0.02
Quadrum	0.35	0.01	0.17	0.11	0.13	0.14	0.31	0.10	0.09	0.09	0.07	0.15	0.06	0.13	0.15	0.15	0.22	0.06	0.04	0.13	0.11	0.14	0.17	0.11	0.10
Radiolithus	0.36	0.17	0.20	0.12	0.06	0.07	0.15	0.25	0.29	0.06	0.12	0.05	0.11	0.23	0.15	0.19	0.24	0.04	0.08	0.11	0.04	0.08	0.02	0.24	0.01
Reinhardtites	0.37	0.11	0.13	0.07	0.01	0.05	0.02	0.07	0.16	0.01	0.09	0.05	0.08	0.03	0.08	0.11	0.07	0.13	0.14	0.10	0.07	0.10	0.20	0.08	0.09
Retecapsa	0.38	0.25	0.03	0.11	0.29	0.04	0.22	0.01	0.40	0.23	0.38	0.03	0.20	0.09	0.14	0.08	0.31	0.18	0.20	0.22	0.08	0.39	0.02	0.23	0.23
Rhagodiscus	0.39	0.23	0.40	0.43	0.34	0.10	0.12	0.03	0.46	0.11	0.52	0.22	0.27	0.13	0.27	0.08	0.27	0.14	0.18	0.18	0.48	0.06	0.33	0.20	0.00
Rucinolithus	0.40	0.09	0.12	0.04	0.21	0.21	0.20	0.10	0.07	0.02	0.04	0.18	0.39	0.02	0.16	0.35	0.32	0.12	0.01	0.16	0.06	0.18	0.44	0.13	0.39
Staurolitithes	0.41	0.26	0.00	0.02	**0.66**	0.11	0.14	0.50	0.04	0.22	0.10	0.20	0.06	0.18	0.49	0.25	0.16	0.07	0.00	0.12	0.11	0.15	0.15	0.20	0.03
Stoverius	0.42	0.05	0.04	0.19	0.27	0.09	0.43	0.06	0.34	0.11	0.05	0.15	0.37	0.40	0.30	0.24	0.01	0.18	0.41	0.09	0.06	0.41	0.06	0.08	0.22
Tegumentum	0.43	0.01	0.34	0.01	0.24	0.42	0.20	0.15	0.00	0.02	0.08	0.07	0.28	0.06	0.31	0.30	0.30	0.02	0.09	0.10	0.01	0.16	0.28	0.02	0.20
Tetrapodorhabdus	0.44	0.18	0.09	0.12	0.13	0.35	0.04	0.06	0.26	0.07	0.22	0.29	0.01	0.24	0.09	0.03	0.15	0.02	0.19	0.21	0.12	0.16	0.14	0.14	0.10
Tranolithus	0.45	0.20	0.21	0.34	0.15	0.09	0.10	0.12	0.19	0.19	0.00	0.39	0.14	0.06	0.07	0.24	0.13	0.15	0.04	0.14	0.27	0.03	0.25	0.28	0.13
Unipolanarius	0.46	0.03	0.04	0.09	0.20	0.15	0.35	0.08	0.15	0.23	0.02	0.01	0.24	0.02	0.21	0.03	0.08	0.03	0.03	0.12	0.09	0.08	0.00	0.10	0.14
Watznaueria	0.47	0.07	0.34	0.11	**-0.73**	0.31	0.42	0.26	0.00	0.05	0.40	0.16	0.53	0.04	**-0.66**	0.14	0.50	0.11	0.02	0.05	0.03	0.15	0.39	0.26	0.25
Zeugrhabdotus	0.48	0.53	0.05	0.15	0.29	0.01	0.12	0.02	0.11	0.06	0.41	0.32	0.14	0.13	0.34	0.12	0.29	0.04	0.15	0.08	0.23	0.06	0.23	0.12	0.12

	Lucianorhabdus	*Microrhabdulus*	*Manivitella*	*Martasterites*	*Micula*	*Nannoconus*	*Owenia*	*Placozygus*	*Prediscosphaera*	*Prolatipatella*	*Quadrum*	*Radiolithus*	*Reinhardtites*	*Retecapsa*	*Rhagodiscus*	*Rucinolithus*	*Staurolitithes*	*Stoverius*	*Tegumentum*	*Tetrapodorhabdus*	*Tranolithus*	*Unipolanarius*	*Watznaueria*	*Zeugrhabdotus*
Lucianorhabdus	1																							
Microrhabdulus	0.11	1																						
Manivitella	0.08	0.15	1																					
Martasterites	0.19	0.25	0.07	1																				
Micula	0.11	0.16	0.34	0.05	1																			
Nannoconus	0.16	0.14	0.16	0.27	0.41	1																		
Owenia	0.30	0.09	0.16	0.27	0.24	0.17	1																	
Placozygus	0.15	0.19	0.23	0.46	0.44	0.02	0.22	1																
Prediscosphaera	0.05	0.38	0.45	0.16	0.49	0.28	0.04	0.25	1															
Prolatipatella	0.10	0.40	0.02	0.03	0.10	0.09	0.05	0.13	0.08	1														
Quadrum	0.05	0.15	0.26	0.11	0.12	0.17	0.11	0.14	0.10	0.14	1													
Radiolithus	0.08	0.11	0.10	0.35	0.28	0.18	0.20	0.02	0.21	0.02	0.18	1												
Reinhardtites	0.02	0.16	0.06	0.18	0.39	0.10	0.07	0.04	0.02	0.09	0.08	0.02	1											
Retecapsa	0.19	0.43	0.07	0.44	0.11	0.17	0.23	0.44	0.21	0.33	0.08	0.32	0.11	1										
Rhagodiscus	0.40	0.08	0.39	0.41	0.32	0.07	0.36	0.56	0.25	0.03	0.18	0.13	0.13	0.25	1									
Rucinolithus	0.10	0.24	0.22	0.13	0.06	0.21	0.08	0.10	0.42	0.00	0.13	0.17	0.24	0.10	0.11	1								
Staurolitithes	0.07	0.06	0.20	0.19	0.25	0.13	0.06	0.48	0.35	0.05	0.25	0.02	0.11	0.28	0.15	0.14	1							
Stoverius	0.27	0.12	0.35	0.23	0.20	**0.61**	0.08	0.02	0.23	0.01	0.12	0.11	0.12	0.07	0.06	0.25	0.14	1						
Tegumentum	0.08	0.31	0.37	0.04	0.16	0.13	0.02	0.09	0.56	0.08	0.18	0.13	0.06	0.19	0.09	0.10	0.18	0.03	1					
Tetrapodorhabdus	0.30	0.00	0.15	0.47	0.13	0.12	0.12	0.24	0.08	0.15	0.08	0.18	0.00	0.30	0.32	0.18	0.12	0.20	0.11	1				
Tranolithus	0.41	0.26	0.09	0.24	0.02	0.03	0.29	0.12	0.13	0.02	0.01	0.26	0.04	0.21	0.25	0.07	0.05	0.13	0.23	0.11	1			
Unipolanarius	0.19	0.08	0.12	0.09	0.06	0.15	0.09	0.25	0.12	0.11	0.28	0.09	0.03	0.02	0.30	0.15	0.23	0.05	0.21	0.10	0.01	1		
Watznaueria	0.17	0.13	0.41	0.00	0.45	0.24	0.16	0.47	**-0.73**	0.02	0.23	0.05	0.04	0.01	0.42	0.28	0.46	0.25	0.39	0.02	0.17	0.35	1	
Zeugrhabdotus	0.12	0.04	0.44	0.15	0.23	0.30	0.07	0.34	0.34	0.15	0.15	0.12	0.07	0.20	0.24	0.28	0.27	0.08	0.24	0.45	0.32	0.21	0.41	1

Appendix 14B
Correlation matrix of species - TDP39

The quantitative data used to produce this matrix are available upon request

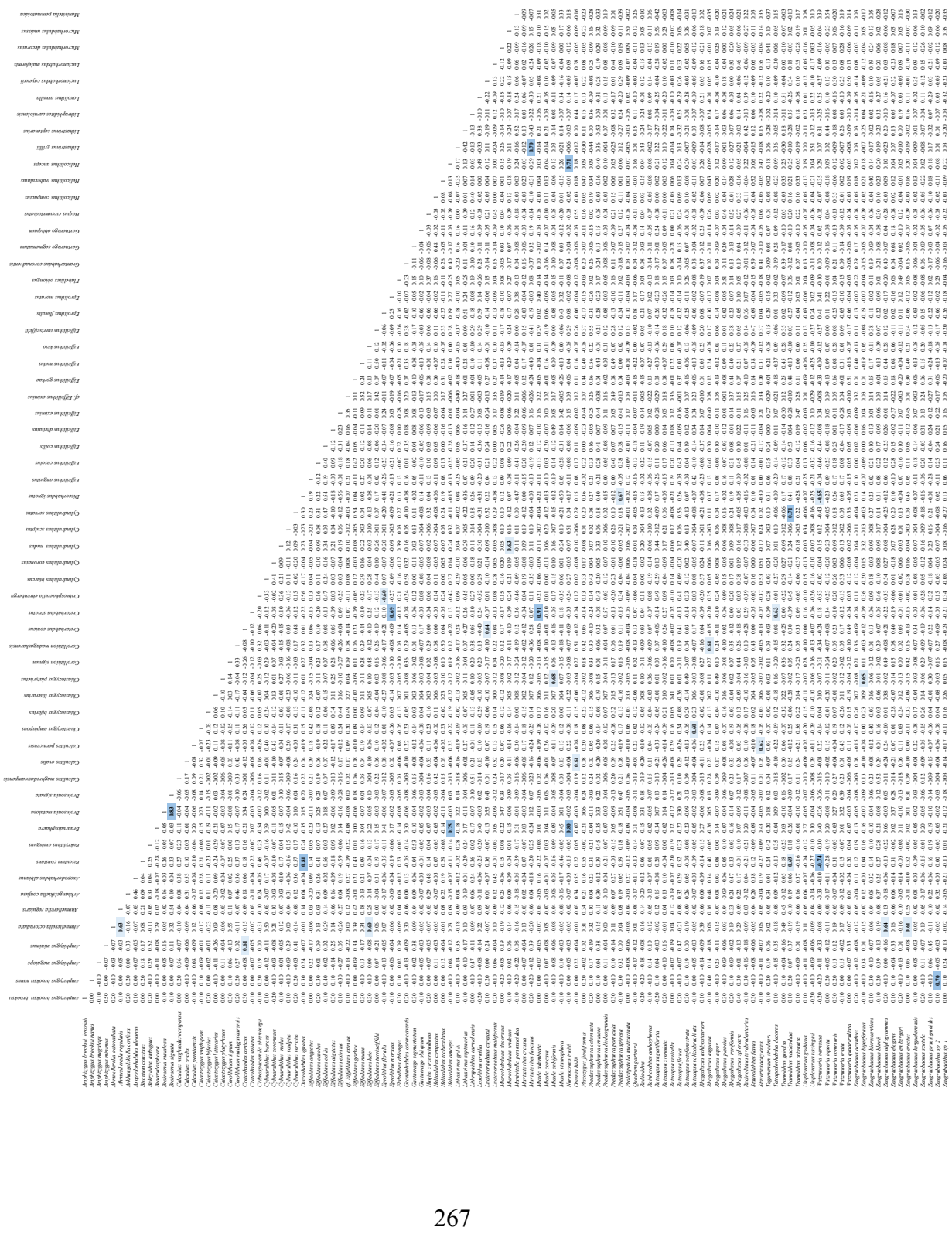

	Retecapsa surirella	*Retecapsa ficula*	*Retecapsa octofenestrata*	*Retecapsa schizobrachiata*	*Rhagodiscus achlyostaurion*	*Rhagodiscus angustus*	*Rhagodiscus asper*	*Rhagodiscus pleheius*	*Rhagodiscus reniformis*	*Rhagodiscus splendens*	*Rucinolithus terebrodentarius*	*Staurolithites flavus*	*Sloverius achylosus*	*Tegumentum stradneri*	*Tetrapodorhabdus decorus*	*Tranolithus gabalus*	*Tranolithus macleodiae*	*Tranolithus orionatus*	*Uniplanarius gothicus*	*Uniplanarius sissinghii*	*Watznaueria barnesae*	*Watznaueria biporta*	*Watznaueria communis*	*Watznaueria ovata*	*Watznaueria quadriradiata*	*Zeugrhabdotus acanthus*	*Zeugrhabdotus hiperforatus*	*Zeugrhabdotus bicrescentiicus*	*Zeugrhabdotus blowii*	*Zeugrhabdotus diplogrammus*	*Zeugrhabdotus elegans*	*Zeugrhabdotus embergeri*	*Zeugrhabdotus erectus*	*Zeugrhabdotus kerguelenensis*	*Zeugrhabdotus scutula*	*Zeugrhabdotus praesigmoides*	*Zeugrabdolithus sp. 2*	*Zeugrabdolithus sp. 1*
Retecapsa surirella	1																																					
Retecapsa ficula	-0.23	1																																					
Retecapsa octofenestrata	-0.11	0.08	1																																				
Retecapsa schizobrachiata	0.20	-0.13	0.08	1																																			
Rhagodiscus achlyostaurion	-0.05	-0.20	-0.06	-0.06	1																																		
Rhagodiscus angustus	0.12	0.14	0.23	-0.14	-0.06	1																																	
Rhagodiscus asper	0.16	-0.09	0.37	-0.07	-0.03	0.26	1																																
Rhagodiscus plebeius	0.11	-0.03	0.01	-0.04	0.03	-0.11	-0.13	1																															
Rhagodiscus reniformis	0.07	0.39	0.17	-0.14	0.00	0.49	-0.03	0.11	1																														
Rhagodiscus splendens	0.11	0.02	0.16	-0.09	0.19	0.32	-0.01	-0.02	0.28	1																													
Rucinolithus terebrodentarius	0.02	-0.30	-0.24	-0.11	-0.14	-0.06	0.01	-0.11	-0.13	0.07	1																												
Staurolithites flavus	-0.10	0.14	0.12	-0.04	0.14	0.24	-0.01	-0.07	0.44	-0.07	-0.03	1																											
Sloverius achylosus	0.20	-0.11	-0.16	-0.05	0.20	-0.09	0.10	-0.09	0.03	0.20	0.25	0.02	1																										
Tegumentum stradneri	0.01	0.06	-0.02	-0.12	-0.04	0.27	0.19	-0.06	-0.17	0.17	-0.10	-0.15	-0.03	1																									
Tetrapodorhabdus decorus	-0.19	0.12	-0.05	-0.08	-0.14	-0.31	-0.11	-0.07	-0.16	-0.20	0.18	-0.07	-0.20	0.11	1																									
Tranolithus gabalus	0.07	-0.21	-0.18	-0.10	0.08	0.40	-0.02	0.00	0.38	0.01	0.07	0.34	0.05	-0.09	-0.18	1																							
Tranolithus macleodiae	-0.14	**0.63**	0.03	0.01	-0.14	0.26	0.02	0.07	0.29	0.11	-0.17	0.02	-0.19	0.15	-0.04	-0.09	1																							
Tranolithus orionatus	0.16	0.22	-0.02	0.38	0.05	0.07	-0.11	-0.03	0.23	-0.05	-0.01	0.21	-0.07	-0.32	-0.09	-0.16	0.19	1																					
Uniplanarius gothicus	0.05	0.03	-0.11	-0.05	0.10	-0.17	-0.01	0.17	-0.15	0.07	-0.02	-0.09	0.14	-0.09	0.06	-0.11	0.09	0.01	1																				
Uniplanarius sissinghii	-0.18	-0.16	-0.18	-0.04	-0.12	-0.27	-0.13	-0.08	-0.27	-0.17	-0.27	-0.07	-0.09	-0.24	0.08	-0.04	-0.19	0.06	0.03	1																			
Watznaueria barnesae	0.15	-0.54	-0.09	0.17	-0.04	-0.44	-0.11	0.04	-0.36	-0.08	0.28	-0.19	0.23	0.00	-0.38	-0.17	-0.57	0.08	0.02	0.55	1																		
Watznaueria biporta	-0.01	-0.14	-0.06	-0.08	-0.10	-0.18	-0.18	0.00	0.01	0.07	0.41	-0.01	0.11	-0.27	0.14	-0.06	-0.09	0.11	0.00	0.21	0.36	1																	
Watznaueria communis	-0.05	0.14	0.19	0.19	-0.01	-0.01	0.00	-0.11	0.07	0.32	-0.23	-0.02	-0.07	0.01	-0.23	0.05	0.22	-0.10	0.02	-0.25	-0.38	-0.03	1																
Watznaueria ovata	0.08	0.05	-0.21	-0.09	0.05	0.03	-0.02	-0.06	-0.09	-0.02	-0.12	0.03	0.13	-0.02	-0.21	0.05	-0.16	-0.22	-0.06	-0.08	-0.10	0.15	0.31	1															
Watznaueria quadriradiata	-0.17	0.24	0.01	-0.03	0.28	-0.07	0.03	-0.06	-0.04	-0.12	-0.06	-0.05	-0.07	0.01	-0.07	-0.14	0.44	0.20	-0.07	-0.06	-0.16	-0.11	0.02	-0.12	1														
Zeugrhabdotus acanthus	-0.06	0.04	-0.10	-0.05	-0.16	0.02	-0.07	-0.11	0.17	-0.04	0.01	0.43	-0.01	-0.13	-0.08	0.20	-0.09	-0.16	-0.04	0.00	-0.11	-0.07	0.10	0.06	-0.08	1													
Zeugrhabdotus hiperforatus	-0.04	-0.04	0.43	-0.07	-0.04	0.11	0.52	-0.13	-0.01	-0.12	-0.30	-0.07	-0.11	0.20	-0.04	-0.15	0.07	-0.10	-0.16	-0.13	-0.21	-0.25	0.10	-0.10	0.05	-0.05	1												
Zeugrhabdotus bicrescentiicus	-0.08	0.21	0.08	-0.04	0.09	0.10	-0.14	-0.08	0.34	-0.03	-0.01	0.55	0.08	-0.10	-0.10	0.07	0.13	0.31	-0.10	-0.08	-0.19	0.06	0.11	0.06	-0.06	0.03	-0.01	1											
Zeugrhabdotus blowii	-0.01	0.06	-0.01	-0.08	-0.11	0.33	0.24	0.02	0.20	0.25	-0.11	-0.11	-0.05	0.45	-0.20	-0.16	0.26	0.08	0.03	-0.16	-0.28	-0.14	0.08	-0.03	-0.01	-0.11	0.29	0.16	1										
Zeugrhabdotus diplogrammus	0.28	-0.36	-0.08	0.03	0.41	0.08	-0.07	-0.08	-0.07	0.22	0.01	0.11	0.18	0.10	-0.32	0.36	-0.31	-0.23	-0.12	-0.14	-0.03	-0.29	0.15	0.29	-0.08	0.01	-0.03	0.01	-0.28	1									
Zeugrhabdotus elegans	0.12	0.26	-0.04	-0.02	0.00	0.13	-0.10	-0.04	-0.17	-0.08	-0.18	0.01	-0.23	0.07	-0.10	0.02	0.18	-0.11	0.05	-0.17	-0.25	-0.23	0.14	0.31	0.20	-0.04	-0.24	-0.12	-0.27	0.23	1								
Zeugrhabdotus embergeri	0.13	-0.02	-0.16	-0.10	-0.18	-0.15	0.10	0.41	-0.13	-0.01	0.06	-0.10	0.13	-0.07	-0.09	-0.06	0.12	0.08	0.36	-0.04	0.06	0.00	-0.02	-0.10	-0.14	-0.10	-0.10	0.05	0.09	-0.17	-0.11	1							
Zeugrhabdotus erectus	-0.15	-0.03	-0.20	-0.10	0.23	0.24	-0.10	0.23	0.28	-0.02	-0.15	0.11	-0.10	-0.05	-0.24	0.54	0.08	-0.29	0.18	-0.20	-0.40	-0.23	0.16	0.24	-0.09	**0.70**	-0.05	0.03	0.00	0.31	0.08	0.03	1						
Zeugrhabdotus kerguelenensis	-0.12	-0.13	0.10	-0.02	0.46	0.05	0.12	-0.04	-0.14	-0.09	0.03	-0.04	-0.05	-0.05	-0.08	-0.10	-0.04	0.23	-0.05	0.04	0.05	-0.08	-0.13	-0.09	-0.05	-0.07	-0.04	0.07	-0.01	0.06	-0.10	-0.08	1						
Zeugrhabdotus scutula	0.19	-0.27	-0.11	-0.05	0.08	-0.18	-0.10	-0.09	0.02	0.28	0.17	-0.08	0.08	-0.14	-0.10	0.03	-0.19	-0.14	0.02	0.08	0.18	-0.04	0.10	0.01	-0.06	0.18	-0.01	-0.09	0.04	0.31	-0.17	-0.14	-0.02	-0.05	1				
Zeugrhabdotus praesigmoides	0.02	0.32	0.09	-0.10	0.05	-0.01	0.04	-0.03	0.04	-0.21	-0.42	0.02	-0.21	0.18	0.07	-0.26	0.39	-0.02	0.00	-0.06	-0.26	-0.28	-0.07	-0.11	0.29	-0.10	0.48	-0.03	0.11	-0.10	0.22	-0.17	-0.10	-0.10	-0.12	1			
Zeugrabdolithus sp. 2	0.00	-0.08	0.25	-0.02	-0.06	0.39	-0.07	-0.04	0.02	0.39	0.24	-0.04	-0.05	0.22	-0.01	-0.10	0.09	-0.07	-0.05	-0.04	-0.06	0.13	0.07	-0.09	-0.03	-0.05	-0.07	-0.04	-0.02	0.01	0.06	0.03	-0.08	-0.02	-0.05	0.01	1		
Zeugrabdolithus sp. 1	0.14	-0.21	0.25	0.04	-0.02	-0.04	0.15	-0.02	-0.16	0.16	-0.21	-0.22	-0.12	0.23	-0.26	-0.23	-0.21	-0.23	-0.12	-0.24	-0.11	-0.14	0.26	-0.02	-0.19	-0.01	0.34	-0.02	0.23	0.21	-0.20	0.05	-0.03	-0.14	0.23	0.11	0.20	1	

Appendix 15
Range chart of ODP Site 763

Full range chart of nannofossil taxa recognized at **ODP Site 763** is available upon request. Semi-quantitative abundance of all taxa detected are reported, as well as total abundance and preservation of calcareous nannofossils in each studied sample.

Total abundance: Abundant (A) = 21-30 specimens in each field of view; Common (C) = 11-20 specimens in each field of view; Few (F)= 6-10 specimens in each field of view; Rare (R) = 1-5 specimens in each field of view.

Species abundance: Abundant (A) = $\geq$ 1 specimen in each field of view; Common (C) = 1 specimen in 2-10 fields of view; Few (F) = 1 specimen in 11-30 fields of view; Rare (R) = 1 specimen in > 31 fields of view.

Preservation was characterized as follows:

Good (G) if nannofossil specimens show little or no evidence of dissolution and/or overgrowth and the primary morphological characters are only slightly altered allowing species identification;

Moderate (M) if specimens exhibit some etching and/or overgrowth, primary morphological characters are somewhat altered allowing, however, identification at the species level;

Poor (P) if specimens show severe etching and/or overgrowth, primary morphological characters are obliterated, hampering identification at the species and/or even generic level

Appendix 16A
Correlation matrix of genera - ODP Site 763

The quantitative data used to produce this matrix are available upon request

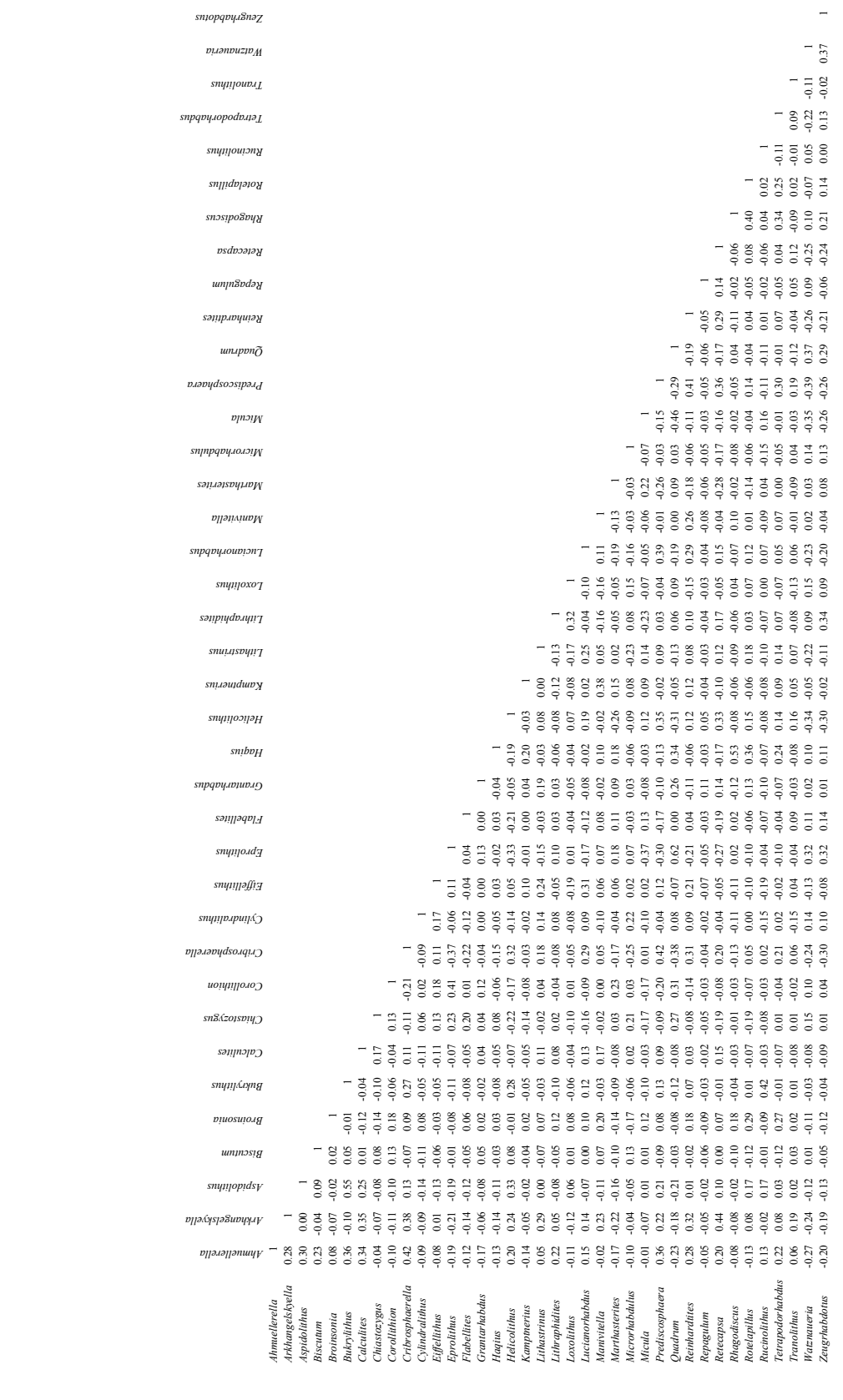

Appendix 16B
Correlation matrix of species - ODP 763

The quantitative data used to produce this matrix are available upon request

	Ahmuellerell a octoradiata	*Arkhangelskyella cymbiformis*	*Aspidolithus enormis*	*Aspidolithus furtivus*	*Aspidolithus parcus constrictus*	*Aspidolithus parcus expansus*	*Aspidolithus parcus parcus*	*Biscutum constans*	*Biscutum large*	*Broinsonia matalosa*	*Broinsonia signata*	*Bukrylithus ambiguus*	*Calculites sp.*	*Chiastozygus litterarius*	*Corollithion signum*	*Cribrosphaerella ehrenbergii*	*Cylindralithus nudus*	*Cylindralithus sculptus*	*Eiffellithus eximius*	*Eiffellithus gorkae*	*Eiffellithus turriseiffelii*	*Eprolithus floralis*	*Eprolithus eptapetalus*	*Flabellites oblongus*	*Gartnerago segmentatum*	*Grantarhabdus coronadventis*	*Haqius circumradiatus*	*Helicolithus anceps*	*Helicolithus trabeculatus*	*Kamptnerius magnificus*	*Lithastrinus grillii*	*Lithastrinus septenarius*	*Lithraphidites carniolensis*
Ahmuellerell a octoradiata	1																																
Arkhangelskyella cymbiformis	0.42	1																															
Aspidolithus enormis	0.16	0.21	1																														
Aspidolithus furtivus	0.13	0.20	0.27	1																													
Aspidolithus parcus constrictus	0.35	0.37	0.35	0.33	1																												
Aspidolithus parcus expansus	0.46	0.33	0.33	0.37	0.37	1																											
Aspidolithus parcus parcus	0.34	0.15	0.23	0.21	0.37	0.55	1																										
Biscutum constans	0.39	0.22	0.26	0.20	0.37	0.36	0.26	1																									
Biscutum large	0.08	0.17	0.20	0.31	0.48	0.25	0.19	0.14	1																								
Broinsonia matalosa	0.23	0.13	0.21	0.29	0.30	0.20	0.10	0.21	0.16	1																							
Broinsonia signata	0.21	0.28	0.35	0.34	0.42	0.37	0.29	0.28	0.27	0.15	1																						
Bukrylithus ambiguus	0.49	0.20	0.28	0.28	0.34	**0.70**	0.54	0.30	0.23	0.19	0.35	1																					
Calculites sp.	0.48	0.54	0.33	0.32	0.40	0.58	0.27	0.32	0.25	0.13	0.41	0.32	1																				
Chiastozygus litterarius	0.14	0.15	0.29	0.16	0.24	0.24	0.12	0.29	0.11	0.03	0.31	0.16	0.39	1																			
Corollithion signum	0.17	0.23	0.37	0.31	0.39	0.33	0.26	0.40	0.25	0.33	0.46	0.31	0.37	0.36	1																		
Cribrosphaerella ehrenbergii	0.49	0.47	0.06	0.20	0.18	0.30	0.21	0.09	0.18	0.24	0.12	0.38	0.27	0.04	0.04	1																	
Cylindralithus nudus	0.08	0.10	0.16	0.16	0.32	0.10	0.11	0.10	0.16	0.20	0.15	0.16	0.13	0.10	0.11	0.06	1																
Cylindralithus sculptus	0.22	0.31	0.36	0.36	0.43	0.40	0.30	0.27	0.27	0.30	0.44	0.35	0.41	0.48	**0.65**	0.17	0.21	1															
Eiffellithus eximius	-0.03	0.19	0.07	0.08	0.19	0.20	0.33	-0.06	0.24	-0.01	0.23	0.25	0.09	0.19	0.20	0.25	0.21	0.37	1														
Eiffellithus gorkae	0.16	0.25	0.31	0.39	0.35	0.30	0.26	0.20	0.37	0.28	0.36	0.26	0.33	0.32	0.43	0.13	0.16	0.37	0.19	1													
Eiffellithus turriseiffelii	0.27	0.13	0.19	0.05	0.17	0.06	0.08	0.38	0.04	0.22	0.14	0.04	0.23	0.18	0.32	0.08	0.06	0.29	-0.26	0.11	1												
Eprolithus floralis	0.09	0.14	0.35	0.24	0.33	0.25	0.19	0.29	0.22	0.13	0.35	0.25	0.32	0.39	**0.62**	-0.10	0.11	0.42	0.16	0.36	0.30	1											
Eprolithus eptapetalus	0.05	0.12	0.44	0.19	0.27	0.20	0.14	0.15	0.10	0.13	**0.62**	0.19	0.25	0.34	0.30	0.05	0.24	0.34	0.10	0.22	0.22	0.22	1										
Flabellites oblongus	0.10	0.13	0.40	0.22	0.30	0.23	0.17	0.21	0.20	0.19	0.40	0.22	0.28	0.37	0.32	-0.02	0.08	0.31	0.18	0.30	0.07	0.30	0.32	1									
Gartnerago segmentatum	0.00	0.12	0.13	0.36	0.16	0.17	0.07	0.22	0.16	0.16	0.20	0.19	0.26	0.20	0.30	0.11	0.15	0.16	0.21	0.22	0.01	0.31	0.20	0.18	1								
Grantarhabdus coronadventis	0.18	0.29	0.31	0.35	0.37	0.31	0.24	0.27	0.22	0.20	0.38	0.30	0.36	0.21	0.39	0.07	0.27	0.39	0.08	0.40	0.19	0.31	0.22	0.27	0.23	1							
Haqius circumradiatus	0.09	0.14	0.25	0.23	0.31	0.24	0.32	0.20	0.31	0.05	**0.68**	0.23	0.29	0.28	0.28	0.04	0.15	0.32	0.25	0.28	0.07	0.25	0.43	0.27	0.14	0.33	1						
Helicolithus anceps	0.30	0.39	0.10	0.14	0.19	0.50	0.36	0.29	0.15	0.10	0.16	0.36	0.18	-0.03	0.11	0.37	-0.07	0.16	0.06	0.15	0.21	-0.01	0.01	0.02	0.09	0.22	0.04	1					
Helicolithus trabeculatus	0.28	0.27	0.30	0.29	0.37	0.39	0.26	0.21	0.21	0.32	0.38	0.48	0.35	0.22	0.34	0.30	0.34	0.53	0.41	0.32	0.06	0.28	0.21	0.25	0.19	0.32	0.26	0.20	1				
Kamptnerius magnificus	0.05	0.16	0.19	0.19	0.54	0.21	0.27	0.13	0.35	0.18	0.25	0.19	0.23	0.07	0.21	0.11	0.14	0.25	0.29	0.22	0.05	0.24	0.16	0.21	0.20	0.20	0.37	0.15	0.20	1			
Lithastrinus grillii	0.28	0.50	0.18	0.29	0.35	0.33	0.23	0.20	0.22	0.27	0.25	0.26	0.38	0.12	0.20	0.41	0.20	0.28	0.24	0.33	0.21	0.09	0.09	0.15	0.25	0.30	0.22	0.30	0.37	0.24	1		
Lithastrinus septenarius	0.07	0.14	0.35	0.21	0.29	0.21	0.16	0.20	0.12	0.12	0.37	0.21	0.27	0.36	0.58	-0.06	0.35	0.45	0.11	0.37	0.30	0.39	**0.63**	0.36	0.33	0.30	0.24	0.00	0.23	0.11	0.10	1	
Lithraphidites carniolensis	0.34	0.23	0.32	0.15	0.22	0.21	0.10	0.13	0.29	0.26	0.23	0.15	0.31	0.19	0.22	0.06	0.24	0.23	-0.02	0.25	0.27	0.32	0.12	0.22	0.18	0.24	0.16	0.09	0.22	0.07	0.08	0.20	1
Loxolithus armilla	0.11	0.16	**0.62**	0.24	0.31	0.35	0.19	0.21	0.40	0.25	0.32	0.24	0.30	0.14	0.33	0.12	0.11	0.32	0.04	0.26	0.12	0.29	0.28	0.23	0.15	0.27	0.23	0.26	0.27	0.15	0.13	0.19	0.46
Lucianorhabdus cayeuxii	0.26	0.30	0.20	0.18	0.25	0.20	0.13	0.18	0.23	0.33	0.25	0.31	0.23	0.08	0.22	0.41	0.23	0.33	0.31	0.27	0.19	0.15	0.11	0.14	0.10	0.21	0.23	0.14	0.52	0.19	0.45	0.12	0.07
Lucianorhabdus maleformis	0.28	0.32	0.28	0.26	0.34	0.40	0.24	0.29	0.26	0.06	0.34	0.35	0.57	0.17	0.31	0.16	0.14	0.35	0.15	0.27	0.35	0.25	0.20	0.22	0.18	0.29	0.23	0.34	0.32	0.24	0.30	0.21	0.33
Manivitella pemmatoidea	0.15	0.39	0.13	0.15	0.50	0.17	0.09	0.23	0.30	0.29	0.33	0.20	0.37	0.16	0.25	0.18	0.10	0.20	0.22	0.17	0.12	0.28	0.16	0.26	0.15	0.17	0.28	0.14	0.24	0.48	0.28	0.09	0.03
Marthasterites furcatus	0.03	0.05	0.28	0.21	0.24	0.14	0.31	0.11	0.30	0.05	0.29	0.18	0.23	0.22	0.44	0.01	0.12	0.31	0.14	0.27	0.21	0.35	0.46	0.31	0.27	0.19	0.37	-0.03	0.21	0.31	0.11	0.47	0.14
Microrhabdulus decoratus	0.09	0.18	0.39	0.21	0.32	0.22	0.14	0.34	0.09	0.04	0.23	0.19	0.28	0.35	0.29	-0.07	0.26	0.45	0.14	0.17	0.20	0.29	0.27	0.19	0.19	0.23	0.17	0.08	0.27	0.24	-0.01	0.27	0.25
Micula cubiformis	0.31	0.22	0.20	0.22	0.32	0.38	0.40	0.16	0.13	0.09	0.41	0.23	0.33	0.07	0.23	0.32	0.20	0.30	0.40	0.19	0.11	0.14	0.19	0.15	0.00	0.24	0.28	0.24	0.31	0.11	0.24	0.11	0.19
Micula staurophora	0.10	0.11	0.14	0.29	0.21	0.15	0.29	0.20	0.13	0.25	0.20	0.12	0.18	0.04	0.10	0.10	0.06	0.16	-0.03	0.16	0.29	-0.08	0.35	0.29	0.13	0.10	0.14	0.25	0.13	0.24	0.22	0.32	-0.05
Predisosphaera cretacea	0.48	0.46	0.13	0.20	0.16	0.51	0.21	0.19	0.16	0.07	0.20	0.28	0.44	0.04	0.07	0.40	-0.02	0.18	0.02	0.13	0.26	0.01	0.03	-0.03	0.09	0.22	0.11	0.44	0.26	0.06	0.30	-0.01	0.23
Predisosphaera columnata	0.25	0.14	0.25	0.18	0.34	0.14	0.07	0.08	0.12	0.28	0.24	0.23	0.14	0.24	0.21	0.30	0.19	0.28	0.24	0.32	0.05	0.16	0.17	0.24	0.11	0.24	0.15	0.12	0.43	0.25	0.29	0.10	0.12
Predisosphaera grandis	0.25	0.29	0.17	0.15	0.23	0.49	0.27	0.18	0.34	0.28	0.23	0.35	0.21	0.04	0.19	0.39	0.24	0.34	0.39	0.42	-0.04	0.11	0.07	0.11	0.04	0.18	0.16	0.25	0.51	0.14	0.28	0.09	0.14
Quadrum gartneri	0.06	0.19	0.32	0.20	0.28	0.21	0.17	0.33	0.17	0.14	0.29	0.20	0.27	0.43	**0.63**	-0.08	0.19	0.31	0.11	0.34	0.14	**0.69**	0.21	0.27	0.30	0.33	0.41	0.02	0.23	0.19	0.12	0.41	0.21
Quadrum intermedium	0.03	0.09	0.36	0.17	0.25	0.17	0.12	0.08	0.10	0.09	0.36	0.19	0.23	0.22	0.36	-0.13	0.27	0.30	0.14	0.35	0.07	0.54	0.33	0.20	0.35	0.48	0.40	-0.04	0.21	0.09	0.03	0.41	0.20
Quadrum octobrachium	0.07	0.12	0.23	0.20	0.27	0.20	0.16	0.24	0.41	0.11	0.28	0.20	0.26	0.48	0.27	0.07	0.14	0.28	-0.02	0.20	0.25	0.42	0.22	0.22	0.12	0.38	0.47	0.05	0.23	0.30	0.12	0.17	0.30
Reinhardtites anthophorus	0.13	0.18	0.34	0.17	0.38	0.22	0.17	0.12	0.15	0.18	0.28	0.21	0.30	0.36	0.26	0.07	0.28	0.30	0.38	0.39	0.02	0.29	0.26	0.48	0.30	0.27	0.38	-0.08	0.30	0.35	0.11	0.38	0.26
Reinhardtites levis	0.47	0.52	0.07	0.10	0.37	0.26	0.13	0.22	0.16	0.35	0.13	0.27	0.21	-0.08	0.08	0.52	0.16	0.16	0.13	0.17	0.19	-0.04	-0.06	0.00	-0.11	0.14	-0.01	0.40	0.30	0.14	0.35	-0.05	0.18
Repagulum parvidentatum	0.24	0.31	0.38	0.46	0.45	0.40	0.32	0.30	0.29	0.18	0.45	0.37	0.43	0.27	0.42	0.19	0.22	0.47	0.14	0.46	0.21	0.37	0.30	0.33	0.23	**0.72**	0.34	0.28	0.40	0.27	0.31	0.32	0.25
Retecapsa angustiforata	0.22	0.28	0.36	0.35	0.43	0.38	0.30	0.29	0.28	0.15	0.44	0.35	0.41	0.25	0.41	0.15	0.42	0.45	0.20	0.36	0.21	0.37	0.28	0.31	0.21	0.39	0.32	0.22	0.38	0.25	0.25	0.30	0.23
Retecapsa crenulata	0.20	0.42	0.29	0.30	0.28	0.23	0.14	0.19	0.23	0.16	0.29	0.20	0.34	0.13	0.32	0.15	0.20	0.33	0.04	0.37	0.19	0.20	0.16	0.16	0.24	**0.69**	0.21	0.34	0.24	0.11	0.34	0.17	0.27
Retecapsa surirella	0.37	0.57	0.15	0.29	0.28	0.36	0.21	0.20	0.21	0.27	0.20	0.23	0.36	0.01	0.17	0.37	0.10	0.19	0.11	0.28	0.08	0.03	-0.02	0.04	0.19	0.39	0.05	0.49	0.19	0.10	0.36	0.03	0.31
Rhagodiscus asper	0.21	0.27	0.45	0.34	0.43	0.41	0.29	0.26	0.28	0.15	**0.90**	0.35	0.41	0.28	0.41	0.12	0.15	0.44	0.16	0.38	0.16	0.35	0.58	0.35	0.15	0.39	**0.68**	0.19	0.38	0.24	0.25	0.33	0.23
Rotelapillus coronatus	0.06	0.28	0.33	0.30	0.23	0.40	0.17	0.14	0.10	0.28	0.56	0.25	0.22	0.04	0.22	0.18	0.14	0.30	0.17	0.19	0.00	0.14	0.40	0.17	0.27	0.25	0.50	0.23	0.39	0.13	0.38	0.15	0.20
Rucinolithus terebrodentarius	0.32	0.26	0.28	0.27	0.35	0.44	0.43	0.27	0.24	0.13	0.35	**0.60**	0.33	0.19	0.33	0.19	0.07	0.36	0.07	0.27	0.13	0.30	0.20	0.23	0.13	0.30	0.24	0.15	0.30	0.18	0.21	0.22	0.18
Tetrapodorhabdus decorus	0.34	0.25	0.14	0.12	0.42	0.27	0.12	0.07	0.22	0.23	0.55	0.20	0.18	0.17	0.20	0.31	0.15	0.26	0.10	0.14	0.17	0.12	0.35	0.15	0.08	0.22	0.38	0.23	0.31	0.24	0.33	0.10	0.22
Tranolithus gabalus	0.28	0.22	0.25	0.24	0.31	0.37	0.39	0.40	0.17	0.09	0.32	0.55	0.30	0.29	0.28	0.18	0.04	0.32	0.13	0.24	0.17	0.39	0.25	0.32	0.09	0.30	0.31	0.08	0.27	0.26	0.13	0.19	0.13
Tranolithus orionatus	0.20	0.39	0.18	0.28	0.35	0.27	0.22	0.21	0.19	0.22	0.25	0.19	0.23	0.18	0.28	0.19	0.00	0.38	0.15	0.40	0.13	0.20	0.15	0.28	0.13	0.37	0.15	0.33	0.31	0.23	0.33	0.18	0.14
Watznaueria barnesiae	-0.18	-0.14	0.18	0.11	0.06	-0.02	-0.01	0.06	0.11	-0.05	0.13	0.03	0.01	0.19	0.17	-0.16	0.15	0.14	0.01	0.10	-0.03	0.33	0.08	0.17	0.09	0.13	0.15	-0.18	-0.03	0.01	-0.12	0.12	0.13
Watznaueria biporta	0.14	0.24	0.14	0.16	0.39	0.29	0.26	0.09	0.20	0.10	0.15	0.19	0.41	0.21	0.14	0.17	0.13	0.15	0.11	0.11	0.15	0.12	0.03	0.02	0.12	0.22	0.13	0.08	0.18	0.24	0.16	-0.01	0.12
Watznaueria fossacincta	0.20	0.11	0.11	0.19	0.23	0.22	0.16	0.40	0.23	0.20	0.37	0.17	0.20	0.23	0.20	0.07	0.07	0.17	0.01	0.15	0.08	0.10	0.31	0.45	0.05	0.21	0.21	-0.01	0.19	0.06	0.13	0.09	0.22
Watznaueria manivitiae	0.38	0.45	0.12	0.09	0.34	0.37	0.15	0.18	0.25	0.17	0.18	0.35	0.38	0.05	0.13	0.46	0.26	0.26	0.41	0.15	0.01	0.07	0.00	0.04	0.02	0.12	0.16	0.23	0.52	0.23	0.36	0.03	0.14
Zeugrhabdotus bicrescenticus	0.01	0.16	0.29	0.16	0.37	0.18	0.10	0.19	0.15	0.00	0.42	0.19	0.22	0.20	0.22	-0.05	0.20	0.24	0.09	0.33	0.01	0.39	0.23	0.29	0.18	0.25	0.33	0.04	0.19	0.24	0.13	0.18	0.20
Zeugrhabdotus embergeri	0.08	0.13	0.33	0.31	0.32	0.26	0.18	0.20	0.24	0.08	0.37	0.23	0.30	0.28	0.32	0.02	0.25	0.33	0.05	0.29	0.32	0.47	0.32	0.44	0.22	0.27	0.24	0.01	0.26	0.20	0.16	0.33	0.51
Zeugrhabdotus scutula	0.14	0.09	0.36	0.18	0.25	0.27	0.24	0.26	0.14	0.08	0.52	0.34	0.24	0.12	0.44	-0.04	0.30	0.26	-0.01	0.25	0.31	0.36	0.53	0.15	0.12	0.26	0.37	-0.03	0.22	0.10	0.05	0.50	0.45

	Loxolithus armilla	*Lucianorhabdus cayeuxii*	*Lucianorhabdus maleformis*	*Manivitella pemmatoidea*	*Marthasterites furcatus*	*Microrhabdulus decoratus*	*Micula cubiformis*	*Micula staurophora*	*Prediscosphaera cretacea*	*Prediscosphaera columnata*	*Prediscosphaera grandis*	*Quadrum gartneri*	*Quadrum intermedium*	*Quadrum octobrachium*	*Reinhardtites anthophorus*	*Reinhardtites levis*	*Repagulum parvidentatum*	*Retecapsa angustiforata*	*Retecapsa crenulata*	*Retecapsa surirella*	*Rhagodiscus asper*	*Rotelapillus coronatus*	*Rucinolithus terebrodentarius*	*Tetrapodorhabdus decorus*	*Tranolithus gabalus*	*Tranolithus orionatus*	*Watznaueria barnesiae*	*Watznaueria biporta*	*Watznaueria fossacincta*	*Watznaueria manivitiae*	*Zeugrhabdotus bicrescenticus*	*Zeugrhabdotus embergeri*	*Zeugrhabdotus scutula*
Loxolithus armilla	1																																
Lucianorhabdus cayeuxii	0.16	1																															
Lucianorhabdus maleformis	0.24	0.18	1																														
Manivitella pemmatoidea	0.08	0.31	0.14	1																													
Marthasterites furcatus	0.19	0.07	0.16	0.08	1																												
Microrhabdulus decoratus	0.33	0.02	0.27	0.15	0.18	1																											
Micula cubiformis	0.16	0.20	0.34	0.11	0.06	0.07	1																										
Micula staurophora	0.13	0.11	0.14	0.11	0.37	0.12	0.00	1																									
Prediscosphaera cretacea	0.18	0.31	0.46	0.07	-0.02	0.14	0.32	0.04	1																								
Prediscosphaera columnata	0.20	0.28	0.28	0.27	0.12	0.24	0.19	0.08	0.12	1																							
Prediscosphaera grandis	0.13	0.36	0.20	0.10	0.02	0.00	0.25	0.03	0.28	0.21	1																						
Quadrum gartneri	0.28	0.12	0.21	0.25	0.26	0.21	0.11	-0.05	-0.03	0.09	0.08	1																					
Quadrum intermedium	0.29	0.09	0.20	0.17	0.28	0.22	0.11	-0.16	0.02	0.22	0.05	0.39	1																				
Quadrum octobrachium	0.30	0.12	0.20	0.12	0.22	0.25	0.12	0.02	0.09	0.06	0.09	0.50	0.21	1																			
Reinhardtites anthophorus	0.17	0.21	0.22	0.30	0.28	0.37	0.18	0.09	0.05	0.39	0.17	0.21	0.46	0.11	1																		
Reinhardtites levis	0.06	0.41	0.30	0.33	-0.11	-0.06	0.40	0.00	0.39	0.33	0.44	-0.04	-0.09	-0.03	0.17	1																	
Repagulum parvidentatum	0.34	0.27	0.36	0.23	0.28	0.27	0.30	0.22	0.24	0.25	0.26	0.32	0.28	0.30	0.31	0.18	1																
Retecapsa angustiforata	0.35	0.26	0.35	0.20	0.34	0.50	0.27	0.24	0.14	0.31	0.24	0.31	0.31	0.28	0.38	0.13	0.47	1															
Retecapsa crenulata	0.23	0.14	0.44	0.12	0.13	0.20	0.22	0.05	0.26	0.28	0.20	0.22	0.34	0.25	0.20	0.28	0.42	0.40	1														
Retecapsa surirella	0.16	0.23	0.40	0.16	-0.07	-0.01	0.29	0.00	0.52	0.26	0.30	0.06	0.03	0.04	0.15	0.52	0.36	0.24	**0.65**	1													
Rhagodiscus asper	0.37	0.25	0.34	0.34	0.29	0.23	0.41	0.19	0.24	0.23	0.23	0.30	0.38	0.28	0.29	0.12	0.46	0.44	0.28	0.22	1												
Rotelapillus coronatus	0.28	0.30	0.22	0.19	0.09	0.14	0.28	0.10	0.29	0.15	0.34	0.14	0.25	0.11	0.23	0.16	0.26	0.24	0.30	0.22	0.56	1											
Rucinolithus terebrodentarius	0.29	0.32	0.27	0.15	0.28	0.12	0.22	0.32	0.12	0.19	0.18	0.22	0.19	0.21	0.26	0.17	0.37	0.36	0.20	0.19	0.41	0.26	1										
Tetrapodorhabdus decorus	0.14	0.25	0.13	0.21	0.17	0.12	0.21	0.12	0.39	0.27	0.19	0.08	0.21	0.26	0.17	0.20	0.23	0.36	0.17	0.19	0.48	0.37	0.13	1									
Tranolithus gabalus	0.22	0.16	0.24	0.31	0.21	0.33	0.19	0.12	0.21	0.23	0.15	0.22	0.17	0.36	0.33	0.06	0.34	0.32	0.20	0.16	0.32	0.22	0.56	0.10	1								
Tranolithus orionatus	0.14	0.29	0.20	0.15	0.13	0.20	0.24	0.14	0.33	0.26	0.19	0.14	0.14	0.16	0.12	0.18	0.35	0.25	0.26	0.32	0.25	0.22	0.17	0.27	0.33	1							
Watznaueria barnesiae	0.20	-0.09	-0.08	0.06	0.14	0.22	0.03	-0.14	-0.21	0.00	-0.14	0.28	0.30	0.24	0.05	-0.24	0.17	0.15	0.02	-0.14	0.16	0.00	0.11	-0.09	0.11	-0.01	1						
Watznaueria biporta	0.15	0.03	0.13	0.29	0.06	0.15	0.20	0.16	0.12	0.05	0.11	0.14	0.01	0.23	0.16	0.15	0.34	0.15	0.11	0.16	0.20	0.01	0.29	0.09	0.16	0.16	0.04	1					
Watznaueria fossacincta	0.15	0.08	0.15	0.08	0.19	0.11	0.21	0.13	0.07	0.13	0.16	0.06	0.00	0.27	0.22	0.10	0.30	0.16	0.12	0.12	0.24	0.12	0.21	0.15	0.28	0.11	0.11	0.08	1				
Watznaueria manivitiae	0.07	0.44	0.36	0.29	-0.04	0.00	0.32	-0.03	0.31	0.22	**0.67**	0.05	-0.02	0.09	0.13	0.55	0.21	0.18	0.17	0.31	0.17	0.30	0.13	0.09	0.13	0.07	-0.18	0.20	0.16	1			
Zeugrhabdotus bicrescenticus	0.23	0.08	0.19	0.24	0.16	0.24	0.12	-0.12	0.07	0.27	0.05	0.28	0.53	0.17	0.36	-0.05	0.26	0.33	0.19	0.09	0.45	0.31	0.17	0.34	0.21	0.25	0.30	0.11	0.09	0.03	1		
Zeugrhabdotus embergeri	0.32	0.14	0.24	0.13	0.33	0.33	0.14	0.10	-0.01	0.16	0.11	0.32	0.32	0.44	0.25	-0.03	0.35	0.41	0.16	-0.01	0.33	0.21	0.30	0.21	0.21	0.24	0.32	0.28	0.20	0.05	0.44	1	
Zeugrhabdotus scutula	0.33	0.10	0.19	0.15	0.30	0.24	0.22	0.14	0.05	-0.02	0.11	0.31	0.27	0.22	0.12	-0.03	0.28	0.26	0.17	0.03	0.52	0.37	0.35	0.21	0.31	0.10	0.19	0.17	0.15	0.04	0.30	0.46	1

Appendix 17

Miniati et al., 2020

CALCAREOUS PLANKTON BIOSTRATIGRAPHY OF THE SANTONIAN-CAMPANIAN BOUNDARY INTERVAL IN THE BOTTACCIONE SECTION (UMBRIA-MARCHE BASIN, CENTRAL ITALY)

Francesco Miniati, Maria Rose Petrizzo, Francesca Falzoni & Elisabetta Erba *

Rivista Italiana di Paleontologia e Stratigrafia vol. 126(3): 771-789.

Rivista Italiana di Paleontologia e Stratigrafia
(*Research in Paleontology and Stratigraphy*)
vol. 126(3): 771-789. **November 2020**

CALCAREOUS PLANKTON BIOSTRATIGRAPHY OF THE SANTONIAN-CAMPANIAN BOUNDARY INTERVAL IN THE BOTTACCIONE SECTION (UMBRIA-MARCHE BASIN, CENTRAL ITALY)

FRANCESCO MINIATI, MARIA ROSE PETRIZZO, FRANCESCA FALZONI & ELISABETTA ERBA*

Dipartimento di Scienze della Terra "Ardito Desio", Università degli Studi di Milano, Via Mangiagalli 34, 20133 Milano, Italy.
*Corresponding author. E-mail: elisabetta.erba@unimi.it

To cite this article: Miniati F., Petrizzo M.R., Falzoni F. & Erba E. (2020) - Calcareous plankton biostratigraphy of the Santonian-Campanian boundary interval in the Bottaccione Section (Umbria-Marche Basin, Central Italy). *Riv. It. Paleontol. Strat.*, 126(3): 771-789.

Keywords: Calcareous nannofossils; planktonic foraminifera; biostratigraphy; Santonian-Campanian boundary.

Abstract: The Bottaccione section (Umbria-Marche Basin, central Italy) was analyzed for calcareous nannofossil and planktonic foraminiferal biostratigraphy across the Santonian-Campanian boundary interval to achieve a high-resolution and updated zonation directly calibrated with magnetostratigraphy. Several calcareous plankton events were detected, including zonal markers and additional potential biohorizons. The base of magnetochron C33r, proposed for placement of the base of the Campanian, lies between the first occurrence of *Aspidolithus parcus parcus* and the last occurrence of *Dicarinella asymetrica* in the Bottaccione section. The literature survey indicates that these events were found in the Santonian-Campanian boundary interval at supraregional scale and, may be used to confidently approximate the base of the Campanian.

Introduction

The Bottaccione section, located near the city of Gubbio in central Italy (coordinates: 43°21'56.05" N, 12°34'57.56" E; Fig. 1), consists of a continuous Jurassic to Paleocene pelagic sequence deposited in the Umbria-Marche Basin (central-western Tethys). The portion of the Bottaccione section investigated in this study is entirely comprised in the Scaglia Rossa Formation and is exposed in the Bottaccione Gorge. The Scaglia Rossa Formation spans from the lower Turonian to the middle Eocene (e.g., Arthur & Fischer 1977; Cresta et al. 1989) and consists of pink to red pelagic limestone that is a lithified nannofossil-planktonic foraminiferal ooze, deposited at some 1500 m paleodepth (Arthur & Premoli Silva 1982). Bedding thickness ranges from 10 to 30 cm with common stylolites in the thicker beds. The Cretaceous Scaglia Rossa is divided in two members, the lower R1 member (Turonian-lower Campanian) is characterized by chert nodules and layers and the upper R2 member (lower Campanian-Maastrichtian) is predominantly made of pink to red-brown limestone without chert (Alvarez & Montanari 1988). The Bottaccione sequence represents a reference section used also in the Geologic Time Scale (GTS2012, Gradstein et al. 2012) for the Late Cretaceous.

We investigated calcareous nannofossils and planktonic foraminifera across the uppermost San-

Received: March 4, 2020; accepted: September 25, 2020

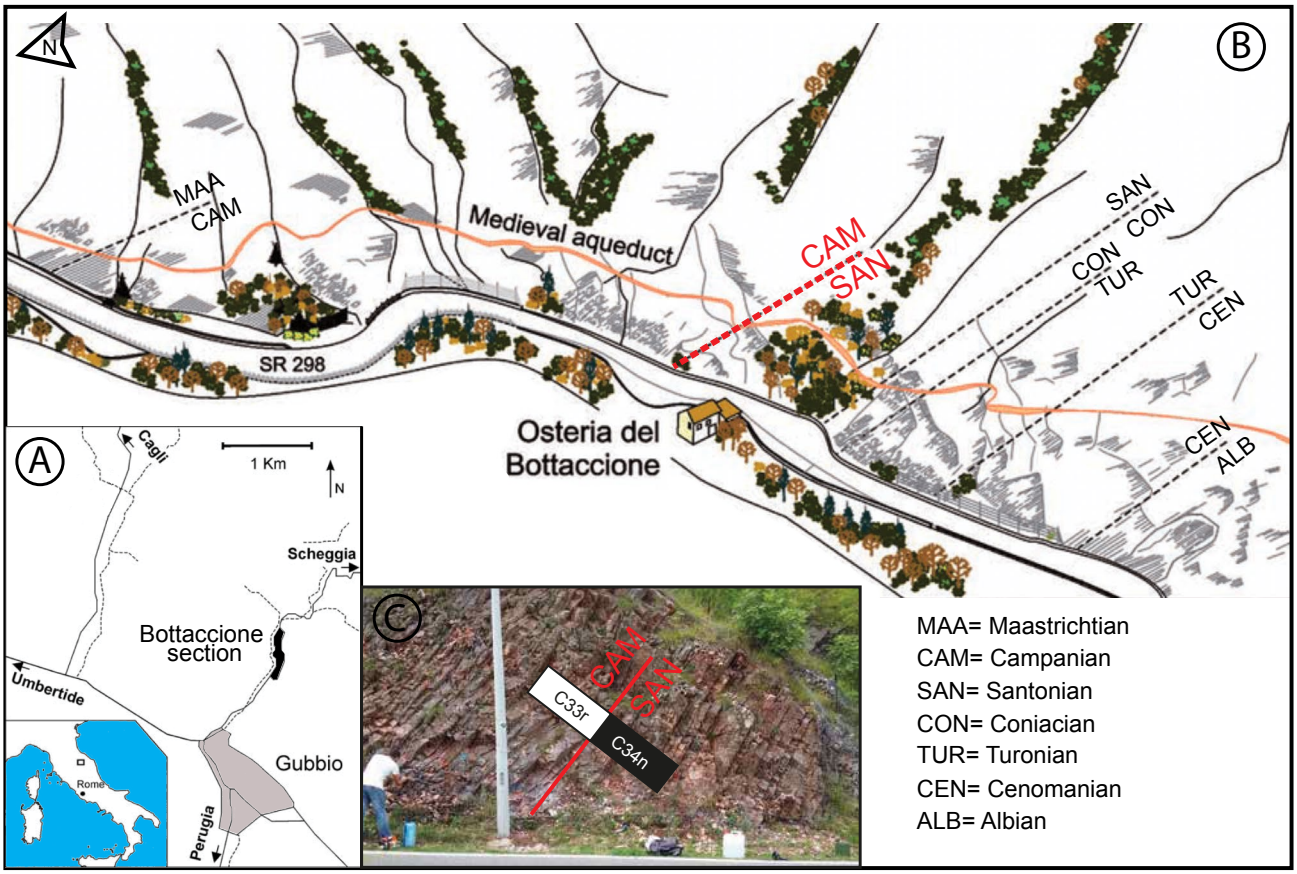

Fig. 1 - A) Location of the Bottaccione section. B) Schematic picture of the outcrop. The dashed lines indicate the position of the stage boundaries along the succession, the Santonian-Campanian boundary is in red (modified after Coccioni & Premoli Silva 2015). C) Photograph of the outcrop across the C34n/C33r magnetostratigraphic boundary at 221.525 ± 0.075 m (after Maron & Muttoni, accepted).

tonian to lowermost Campanian interval, within the lower R1 member. The Bottaccione section has been appointed as a candidate for the Campanian Global Stratotype Section and Point (GSSP) and revised/updated calcareous plankton biostratigraphy is meant to concur to the integrated characterization of the Santonian-Campanian boundary interval (minutes ISCS meeting at Strati 2019, http://cretaceous.stratigraphy.org/archives/). Following the suggestion by the Campanian Working Group of the International Subcommission on Cretaceous Stratigraphy (see minutes of the ISCS meeting at Strati 2019, http://cretaceous.stratigraphy.org/archives/), the base of the Campanian Stage is placed at the base of magnetic Chron 33r that in the Bottaccione section falls at 221.60 m according to the detailed paleomagnetic study by Maron & Muttoni (accepted). As described by Maron & Muttoni (accepted) a negligible fault, with a few decimeters-displacement, occurs at 221.20 m: the lithostratigraphy has been controlled in detail and proved to be continuous. The calcareous plankton biostratigraphy is directly calibrated with polarity magnetozones (Maron & Muttoni, accepted) to improve, revise and/or consolidate the integrated bio-magnetostratigraphy of the Santonian-Campanian boundary interval (Premoli Silva & Sliter 1995; Gardin et al. 2001; Tremolada 2002; Petrizzo et al. 2011; Coccioni & Premoli Silva 2015).

Material and Methods

Calcareous nannofossils

A total of 45 samples were analyzed for calcareous nannofossil biostratigraphy in the interval from meter 211 to meter 233 (Premoli Silva & Sliter 1995) across the Santonian-Campanian boundary (Fig. 3) using subsamples of magnetostratigraphy samples. An average sampling resolution of 0.50 cm was applied, but sampling resolution was increased to 0.10 cm between 220 m and 221 m (across the C34n/C33r magnetic polarity boundary).

	Family	Arkhangelskiellaceae	
	Genus	*Aspidolithus*	*Broinsonia*
	Schematic sketch (not in scale)	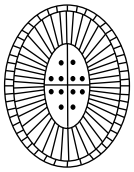	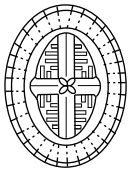
	Margin	Bicyclic (Radial)	Bicyclic (Radial)
Central area structures	Cross	No	Yes
	Plates	Yes	No
	Perforations	Yes	No

Fig. 2 - Illustration of diagnostic characters (distal view) for separating genera *Aspidolithus* and *Broinsonia*.

Samples were prepared as simple smear slide following the standard preparation techniques (Monechi & Thierstein 1985). Each sample was analyzed using a polarizing microscope at 1250X magnification, investigating 6 full traverses (= 1000 fields of view). Semiquantitative data were achieved for total nannofossil and individual taxa abundances and preservation characterized based on the degree of overgrowth and/or dissolution (Suppl. Tab. 1). The biostratigraphy was conducted following the zonations of Sissingh (1977) as modified by Perch-Nielsen (1985), Roth (1978), Bralower et al. (1995) and Burnett (1998) applying the CC, NC, NC* and UC codes, respectively.

Morphometric data were acquired for *Aspidolithus parcus* subspecies using pictures captured with a Q-imaging Micropublisher 5.0 RTV camera (Q-capture Prosuite software) mounted on a Leitz Laborlux light microscope. Measurements were obtained using the Image J64 software, with an error of ± 0.08 μm.

Planktonic foraminifera

Planktonic foraminifera were studied by integrating thin sections and washed residues obtained from the samples used for magnetostratigraphy (Maron & Muttoni, accepted). A total of 33 samples were studied in thin sections and 19 sample out of 33 were also studied in washed residues (Suppl. Tab. 2) which were obtained by processing about 80-100 g of rock samples with acetic acid (see procedure in Lirer 2000 and Falzoni et al. 2016). Santonian-Campanian limestones of the Scaglia Rossa Formation contain cherts that are particularly indurated and, as a consequence, rock samples were immersed in acetic acid for several hours to be disaggregated resulting in the common occurrence of broken or corroded specimens not identifiable at species level. Therefore, because of the poor preservation of planktonic foraminifera in the washed residues, only 19 samples were used for biostratigraphic analyses as they contained sufficiently well-preserved specimens to ensure reliable identification at species level.

Relative abundance data of planktonic foraminifera were collected for thin sections by screening the entire surface of the thin section (Suppl. Tab. 2). Planktonic foraminifera in the washed residues were studied on the >63 μm size fraction and because of the generally poor preservation of the assemblages only the occurrence of species is reported in Supplementary Table 2.

Taxonomic concepts for planktonic foraminiferal species identification follow their original descriptions and illustrations, Premoli Silva & Sliter (1995), Petrizzo et al. (2011), Haynes et al. (2015) and the online taxonomic database for Mesozoic Planktonic Foraminifera "PF@mikrotax" available at http://www.mikrotax.org/pforams/index.html (see Huber et al. 2016). Biozonation is according to Premoli Silva & Sliter (1995) and Robaszynski & Caron (1995).

Taxonomic remarks

Calcareous nannofossils

The investigated interval is characterized by the evolution of two important lineages, namely of genera *Arkhangelskiella* and *Aspidolithus*. Changes in coccolith morphometry are used to separate different species that are biostratigraphically relevant in the Upper Cretaceous. Following Burnett (1997), within the genus *Arkhangelskiella* we grouped the specimens <8 μm into *A. confusa* and specimens >8 μm into *A. cymbiformis* (Pl. 1).

The *Aspidolithus* genus is differentiated here from genus *Broinsonia* as the latter is characterized by the presence of a cross instead of plates in the central area (Lauer 1975; Prins in Perch Nielsen 1979; Perch-Nielsen 1985). Bukry (1969) intro-

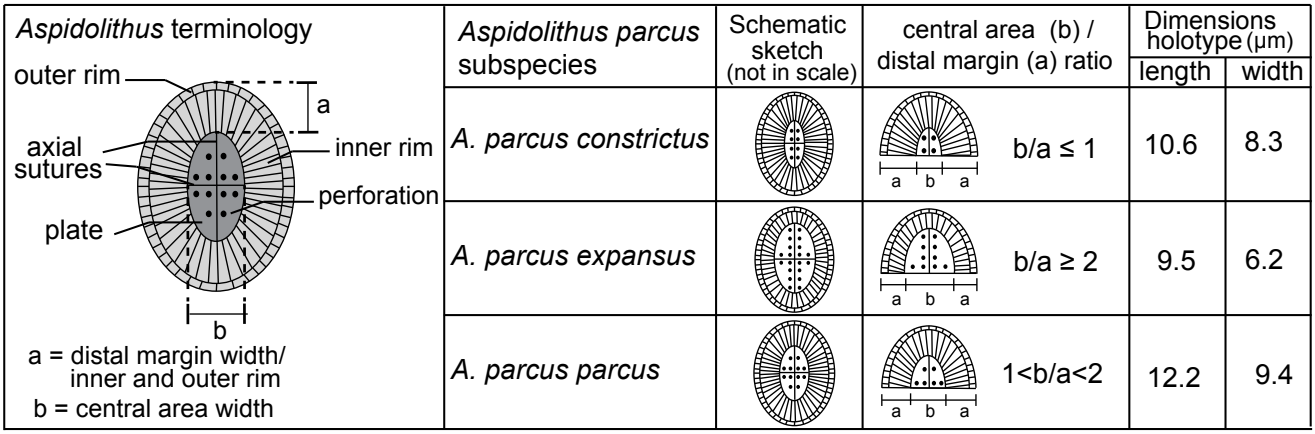

Fig. 3 - Schematic morphological characters (distal view) and their terminology of *Aspidolithus* specimens. *Aspidolithus parcus* subspecies are typified by the b (central area width)/a (distal margin width) ratio. The dimensions of length and width of the holotypes are reported.

duced the genus *Broinsonia* and selected *Broinsonia dentata* as type species. According to the original description, *B. dentata* is characterized by a central area divided by axial crossbars. The genus *Aspidolithus* was originally defined by Noël (1969) who indicated *Aspidolithus angustus* as type species. The holotype of *Aspidolithus angustus* (Noël 1969, Pl.1, figs 1a-c) is characterized by a central area filled by plates.

Lauer (1975) kept genera *Broinsonia* and *Aspidolithus* separated, but Veerbek (1977) and Hattner et al. (1980) considered them to be synonymous, *Broinsonia* having priority. Perch-Nielsen (1979), incorporating observations by Prins (personal communication in Perch-Nielsen 1979), returned to a differentiation of the two genera, due to presence of a distinct central cross in *Broinsonia* and perforated segments closing the central area in *Aspidolithus*.

Crux (1982) considered the genus *Aspidolithus* a junior synonym of *Broinsonia* and rejected the distinction between the two genera proposed by Perch Nielsen (1979) for various reasons: a) both Burky (1969) and Noël (1969) included in *Broinsonia* and *Aspidolithus*, respectively, forms with plates closing the central area as well as forms with a central cross; b) the margin structure (bicyclic) is the same in the two genera and considered highly diagnostic; c) poor preservation obliterates original characteristics of the central area, often producing apparent (but not real) crosses as a result of advanced etching of the plates. Analogously, *Aspidolithus* was disregarded by Bralower and Sissier (1992), Wise (1983), Burnett (1998) and Wolfgring et al. (2018).

Similarly to Almogi-Labin et al. (1991), Gardin et al. (2001), Tremolada (2002), we follow the diagnostic taxonomic characters synthetized by Perch-Nielsen (1985; Fig 14, p. 352) and, accordingly, maintain the distinction between *Broinsonia* and *Aspidolithus* as illustrated in Figure 2.

Within the *Aspidolithus* lineage, the subsequent appearances of *A. parcus expansus*, *A. parcus parcus* and *A. parcus constrictus* are marked by a gradual reduction of the central area/margin ratio as described by Wise (1983). We follow and apply the indications of Wise (1983) as illustrated in Figure 3.

Specimens of *Aspidolithus parcus* are characterized by changes in the central area/margin ratio, as well as by a variability in the coccolith length. An increase in coccolith length from smaller early specimens to larger later specimens of *Aspidolithus parcus* was observed by Bralower and Sissier (1982) and Almogi-Labin et al. (1991). Conversely, at the Falkland Plateau Wise (1983) did not observe any increase in the length of *Aspidolithus parcus* specimens.

In the Bottaccione section, Gardin et al. (2001) distinguished two morphogroups within the *Aspidolithus parcus* subspecies characterized by a total length <10 μm named as *A. parcus expansus* "small" and *A. parcus parcus* "small". According to Gardin et al. (2001) the small specimens of *A. parcus* have a distinct stratigraphic distribution compared to larger morphotypes. Similarly, at Postalm, Wolfgring et al. (2018) recognized five morphotypes within *Aspidolithus parcus* according to the b/a ratio and coccolith length. The *Aspidolithus* speci-

mens characterized by a length <9 μm (usually 6–8 μm) were placed within the species *Aspidolithus enormis*, as *A. enormis* sp.1 (b/a ratio ≥2) and *A. enormis* sp. 2 (b/a ratio <2). Based on coccolith size, Wolfgring et al. (2018) assigned specimens of *Aspidolithus* with a length >9 μm (usually >10 μm) to *A. parcus expansus* (b/a ratio ≥2), *A. parcus parcus* (b/a ratio between 1 and 2) and *A. parcus constrictus* (b/a ratio <1).

Here, we apply the criteria of Gardin et al. (2001) to divide the small from the large morphogroups within genus *Aspidolithus*. Further details on the subspecies subdivisions are discussed in the Appendix.

Planktonic foraminifera

Taxonomic remarks are provided for some taxa in order to clarify the taxonomic concept applied in this study (Suppl. Tab. 2). The supra-specific classification of biserial taxa follows Haynes et al. (2015). The biserial *Sigalia* specimens observed in thin section and not identifiable at species level because only observed in edge view, were assigned to *Sigalia* sp. Multiserial specimens with depressed intercameral sutures and identified in edge view in thin sections were not classified at species level and thus assigned to *Ventilabrella* sp. The multiserial *Ventilabrella alpina*, a species largely overlooked in the literature and often regarded as a junior synonym of either *V. eggeri* (Nederbragt, 1991) or *V. multicamerata* (http://www.mikrotax.org/pforams/index.html), has been confidently identified in the studied assemblages.

The genus "*Globigerinelloides*" is quoted in the text and in the distribution chart (Suppl. Tab. 2) because it is polyphyletic and currently under taxonomic revision (see taxonomic notes in Petrizzo et al. 2017).

Very small-sized and/or poorly preserved hedbergellids not identifiable at species level were assigned to *Muricohedbergella* sp. Specimens here assigned to *Muricohedbergella delrioensis* s.l. usually possess 5 chambers in the last whorl, a moderate to fast chamber size increasing rate in the last whorl and include morphotypes showing a full range of morphologic variability between the neotypes designated by Longoria (1974) and by Masters (1976) (see Petrizzo & Huber 2006). Globigeriniform morphotypes with a thick wall resembling that shown by *Whiteinella, Rugoglobigerina* and *Costellagerina* species were identified in thin section only, however the observed cuts did not allow discrimination among these genera.

Results

Calcareous nannofossils

The preservation of calcareous nannofossil assemblages in the studied interval ranges from moderate to poor with the presence of both overgrowth and etching. The total nannofossil abundances vary from common to rare with a higher abundance in the upper part of the studied interval (Suppl. Tab. 1). The assemblages are dominated by genera *Watznaueria*, *Eiffellithus* and *Retecapsa* as well as by the species *Cribrosphaerella ehrenbergii*. Marker and additional species are illustrated in Plates 1 and 2. Five bioevents were detected within the Santonian-Campanian boundary interval of the Bottaccione section (Fig. 3), allowing the identification of the CC17-CC18 zones of Sissingh (1977), NC17-NC18 zones of Roth (1978), NC17*-NC18a* zones of Bralower et al. (1995) and UC12 to UC14b zones of Burnett (1998).

The first occurrence (FO) of *Arkhangelskiella cymbiformis* was observed at 219.10 m where the base of the UC13 zone was placed. All the observed specimens have a rim width >1 μm, in contrast to what originally reported by Burnett (1997) for *A. cymbiformis*.

The FO of *Aspidolithus parcus parcus* at 220.5 m defines the base of the CC17, NC17, NC17* and UC14 zones. In the Bottaccione section, *A. parcus parcus* is extremely rare and discontinuous at the beginning of its range, becoming continuous and frequent from 224.6 m upwards: we labeled this change as first common occurrence (FCO) in this study. The FO of *Aspidolithus parcus constrictus* was detected at 229 m where the base of the UC14b subzone of Burnett (1998) was placed.

In the lower part of its range (between 220.5 and 225.75 m), the length dimensions of *A. parcus parcus* vary between 10 μm and 10.2 μm, with a single specimen of 9.6 μm in length at 221.3 m. According to Gardin et al. (2001), therefore, the older specimens are in the size range of *A. parcus parcus* (≥10 μm) although very close to the lower limit of size range. A relative increase in length size (>10.5 μm) of *A. parcus parcus* coccoliths is observed from 226.55 m upwards; these specimens co-occur with small and normal *A. parcus parcus* coccoliths with length varying from 8.4 to 11.7 μm**.** The presence of "small" *A. parcus parcus* was noted up to 232.85 m in the early Campanian. Our data indicate a gen-

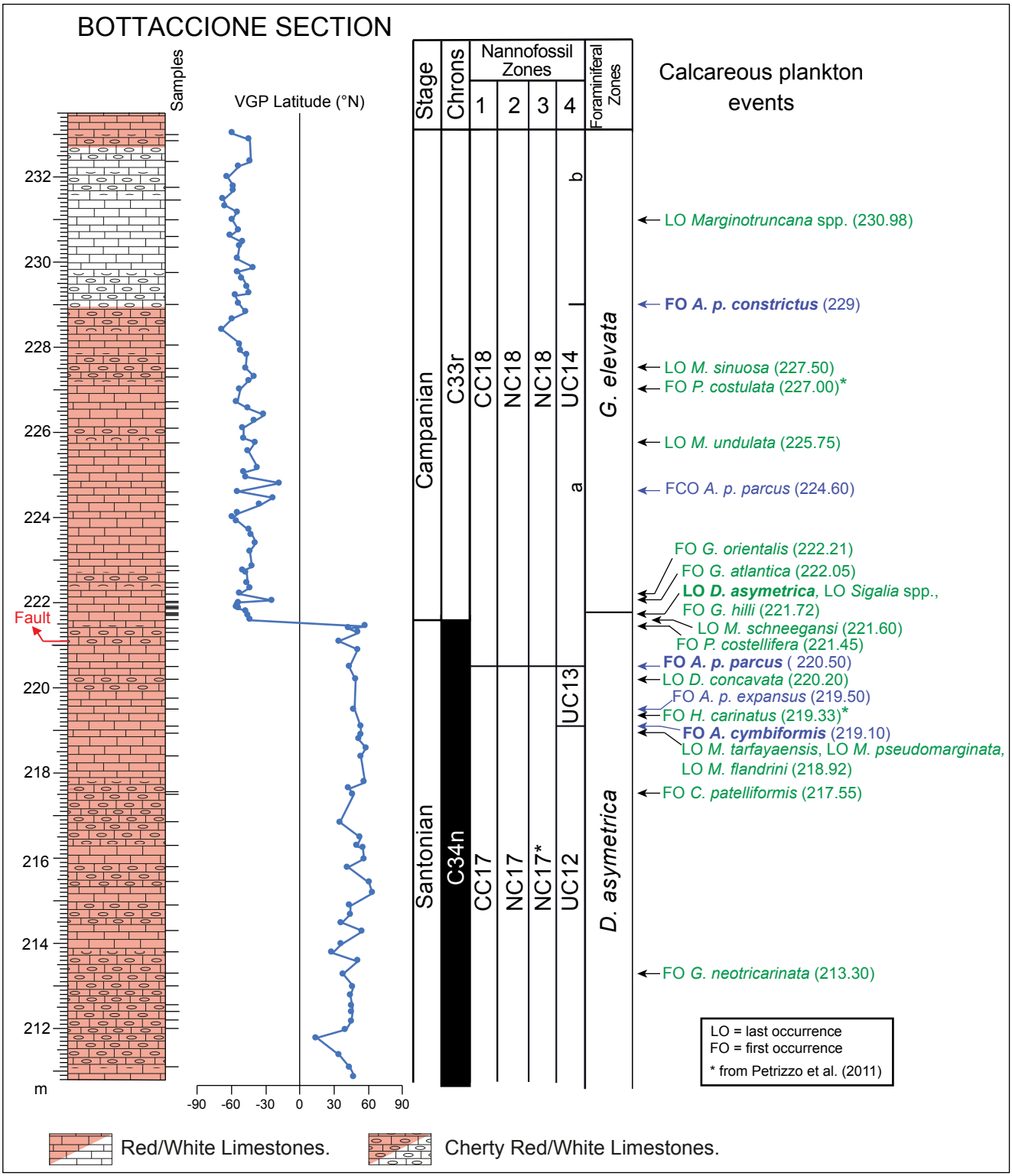

Fig. 4 - Calcareous plankton events recorded in the Bottaccione section (this study) correlated with magnetostratigraphy (Maron & Muttoni, accepted). The base of magnetochron C33r at 221.525 m is used to define the Santonian-Campanian boundary. Lithostratigraphy after Maron & Muttoni (accepted). The sample studied for calcareous plankton biostratigraphy are on the right side of the lithostratigraphic column. The calcareous nannofossil events are in blue, and the zonal marker evidenced in bold. Planktonic foraminiferal events are in green, and the zonal marker in bold. FO = first occurrence, LO = last occurrence. Events marked with an asterisk are according to Petrizzo et al. (2011).

eral increase in size (coccolith length) of *A. parcus parcus* specimens, consistently with previous records (Gardin et al. 2001; Wolfgring et al. 2018).

As far as *A. parcus expansus* is concerned, specimens in the lower part of the range (219.5–221.1 m) are rather small (coccolith length of 10–10.2 μm) and co-occur with "small" *A. parcus expansus* (coccolith length varying between 9.5 and 9.9 μm) from 220.2 m upwards. The coccolith length increases at 221.3 m as testified by presence of some relatively large specimens with length of 11–12.3 μm, together with small specimens (coccolith length varying between 9.5 and 9.9 μm) through the rest of the studied interval.

Planktonic foraminifera

The test of the specimens observed in thin section is generally well-preserved. The preservation of specimens in the washed residues varies from poor to moderate as a result of the procedure applied to process the rock samples. Planktonic foraminiferal assemblages are generally diverse and yield a typical tropical Tethyan assemblage (Suppl. Tab. 2) with unkeeled globigeriniform (genera *Whiteinella*, *Archaeoglobigerina*, *Costellagerina*, *Rugoglobigerina*), planispiral (genus "*Globigerinelloides*") and biserial (genera *Planoheterohelix*, *Pseudotextularia* and *Pseudoguembelina*) taxa as well as abundant single- (genus *Globotruncanita*) and double-keeled (genera *Dicarinella*, *Marginotruncana*, *Contusotruncana* and *Globotruncana*) taxa. Marker and the most common species are illustrated in Plate 3.

In addition to the taxonomically well-known species, we have also found specimens that resemble the species holotypes but possess some morphological differences. For instance, specimens assigned to *Globotruncanella* cf. *petaloidea* (Suppl. Tab. 2) resemble the holotype but show a more pinched lateral profile and a slightly smaller umbilical area. These specimens are found in the Bottaccione section well below the usually documented first occurrence of *Globotruncanella petaloidea* in middle-upper Campanian (Gradstein 1978; Premoli Silva & Sliter 1995; Zepeda 1998). Further studies are needed to evaluate their taxonomic and biostratigraphic significance.

Planktonic foraminiferal assemblages from the base of the studied interval (212.20 m) to 221.45 m show a moderate preservation and are generally diverse, whereas assemblages from 221.60 to 226.10 m are less well-preserved and diverse and contain abundant small-sized biserial and common globigeriniform taxa, while keeled specimens are rare.

The stratigraphic interval from 212.20 to 221.72 m is assigned to the *Dicarinella asymetrica* Taxon Range Zone based on the extinction of the marker species *D. asymetrica* at 221.72 m, while the overlying interval from 221.72 to 232.33 m is assigned to the *Globotruncanita elevata* Interval Zone (Fig. 3), following the subtropical biozonation by Premoli Silva & Sliter (1995) and Robaszynski & Caron (1995).

Secondary planktonic foraminiferal events identified in the *Dicarinella asymetrica* Zone are listed below in stratigraphic order from bottom to top (Fig. 3): a) the FO of *Globotruncana neotricarinata* at 213.30 m, b) the FO of *Contusotruncana patelliformis* at 217.55 m, c) the LO (last occurrence) of *Marginotruncana tarfayaensis*, *Marginotruncana pseudomarginata* and *Muricohedbergella flandrini* at 218.92 m, d) the FO of *Hendersonites carinatus* at 219.33 m, e) the LO of *Dicarinella concavata* at 220.20 m, f) the FO of *Pseudoguembelina costellifera* at 221.45 m, g) the LO of *Marginotruncana schneegansi* at 221.60 m, and h) the LO of *Sigalia* species and the FO of *Globotruncana hilli* at 221.72 m. Planktonic foraminiferal events in the *Globotruncanita elevata* Zone (Fig. 3) include: a) the FO of *Globotruncanita atlantica* at 222.05 m, b) the FO of *Globotruncanita orientalis* at 222.21 m, c) the LO of *Marginotruncana undulata* at 225.75 m, d) the FO of *Pseudoguembelina costulata* at 227.00 m, and e) the LO of *Marginotruncana sinuosa* at 227.50 m.

Discussion

Calcareous plankton biostratigraphy

Calcareous nannofossil assemblages of the Santonian-Campanian interval of the Bottaccione section were investigated in the 60s and 70s (Mohler 1966; Monechi & Pirini 1975; Monechi 1977). Monechi & Thierstein (1985) established a first nannofossil biostratigraphy of the upper Campanian-lower Eocene interval of the Bottaccione section calibrated with planktonic foraminifera (Premoli Silva et al. 1977; Napoleone et al. 1983) and magnetostratigraphy (Alvarez et al. 1977). Gardin et al. (2001) revised and implemented the biostratigraphy of the Santonian-Maastrichtian interval and Tremolada (2002) focused on the upper Albian - lowermost Campanian interval, in both cases

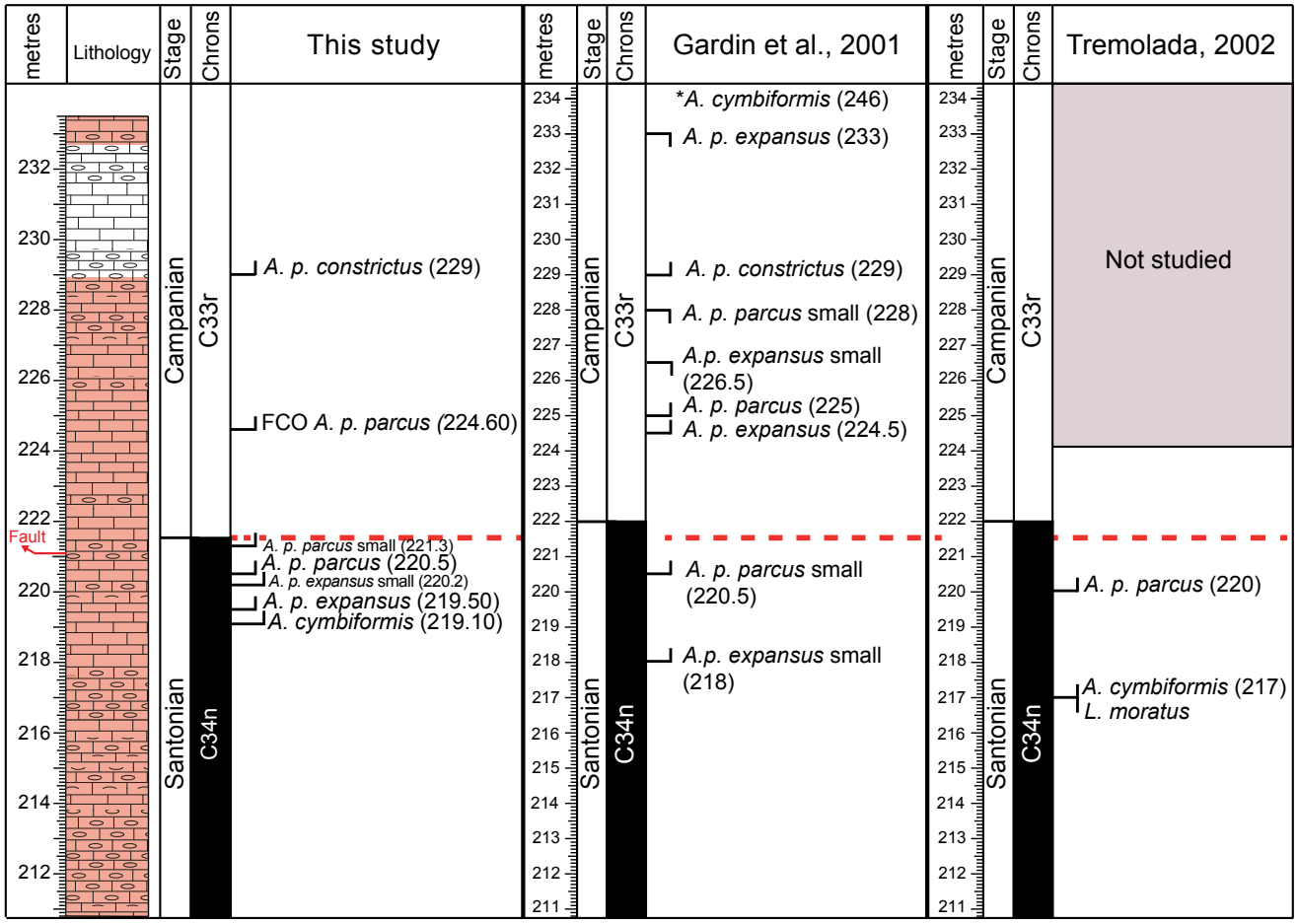

Fig. 5 - Comparison of calcareous nannofossil events found in this study and previously recorded (Gardin et al. 2001; Tremolada 2002) in the Bottaccione section. The Santonian-Campanian boundary is placed at 221.525 m according to updated magnetostratigraphy (Maron & Muttoni, accepted). The asterisk (*) added to *A. cymbiformis* was used to illustrate the FO documented at a meter level (246 m) above the studied interval.

investigating the samples previously used for planktonic foraminiferal studies by Premoli Silva & Sliter (1995).

In Fig. 5 our results are compared to the nannofossil biostratigraphies of Gardin et al. (2001) and Tremolada (2002). *Arkhangelskiella cymbiformis* (length >8 μm) was first observed at 219.10 m, while Tremolada (2002) reported the FO of this species at 217 m in the upper Santonian. Both these results differ from data by Gardin et al. (2001) who found *A. cymbiformis* in the Campanian at 246 m. The earliest species of *Aspidolithus* recorded in this study is *A. parcus expansus* (length ≥10 μm) which occurs for the first time at 219.50 m in the uppermost Santonian. The presence of *A. parcus expansus* in the Bottaccione section was not documented by Tremolada (2002). Otherwise, Gardin et al. (2001) observed the occurrence of "small" *A. parcus expansus* at 218 m in the uppermost Santonian, and *A. parcus expansus* (length ≥10 μm) at 224.5 m in the lowermost Campanian.

The FO of *A. parcus parcus* (length ≥10 μm) was detected at 220.5 m in the topmost Santonian, very close to the FO of *A. parcus parcus* at 220 m documented by Tremolada (2002), and at the same level of the FO of "small" *A. parcus parcus* reported by Gardin et al. (2001).

In this study, we distinguish the FO of *A. parcus parcus* (length ≥10 μm) characterized by rare and sporadic abundance from its first common occurrence (FCO), marked by a continuous and frequent presence in the assemblage in the lowermost Campanian (224.6 m). This FCO is very close to the level where Gardin et al. (2001) placed the FO of *A. parcus parcus*.

The FO of *A. parcus constrictus* is observed at 229 m in the lower Campanian and corresponds to same level reported by Gardin et al. (2001). The

presence of "small" *A. parcus expansus*, "small" *A. parcus parcus* and "small" *A. parcus constrictus* (length <10 μm) is recorded in this study in co-occurrence with normal specimens. As discussed above, we observed a gradual minor increase in size of *Aspidolithus* specimens as also reported by Gardin et al. (2001) and Wolfgring et al. (2018).

The different positions of nannofossil events in this study relative to previous investigations of the Bottaccione section (Gardin et al. 2001; Tremolada 2002) may be ascribed to various reasons: a) the overall nannofossil abundance is low and the preservation is moderate to poor; b) both *A. cymbiformis* and *A. parcus parcus* show rare and sporadic occurrences at the beginning of their range; c) the sampling resolution applied for this study is much higher than previous investigations.

The sequence of the nannofossil events calibrated with the magnetostratigraphy at the Bottaccione section (Maron & Muttoni, accepted), from the oldest to the youngest, is as follow (Fig. 4): 1) FO *A. cymbiformis* (base of biozone UC13) in the uppermost part of 34n magnetochron; 2) FO *A. parcus expansus* in the uppermost part of magnetochron C34n; 3) FO *A. parcus parcus* (base of biozones CC18, NC18, NC*18a and UC14a) in the topmost part of magnetochron C34n; 4) FCO *A. parcus parcus* in the lowermost part of magnetochron C33r; 5) FO *A. parcus constrictus* (base of biozone UC14b) in the lower part of magnetochron C33r.

The planktonic foraminiferal biostratigraphy of the Santonian-Campanian boundary interval in the Bottaccione section was investigated several times (Premoli Silva & Sliter 1995; Petrizzo et al. 2011; Premoli Silva & Coccioni 2015). The LO of *D. asymetrica* in sample 221.72 m is here identified 32 cm above the stratigraphic level reported in previous papers (Premoli Silva & Sliter 1995; Petrizzo et al. 2011; Coccioni & Premoli Silva 2015), thanks to the higher sampling resolution adopted in this study. Therefore, it falls 19.5 cm above the base of magnetochron C33r (Fig. 4). Additional bioevents that coincide with the LO of *D. asymetrica* are the LO of *Sigalia* sp. and the FO of *G. hilli*. These events are followed upward by the FO of *G. atlantica* at 222.05 m and the FO of *G. orientalis* at 222.21 m in the lower part of magnetochron C33r. The top of magnetochron C34n at 221.60 m coincides with the LO of *M. schneegansi* which is preceded at 221.45 m by the FO of *P. costellifera*. Therefore, we document a high-resolution sequence of planktonic foraminifera events across the boundary between magnetochrons C34n and C33r that allow the identification of the Santonian-Campanian boundary with a high degree of precision (Fig. 4).

The stratigraphic position of the secondary events (Fig. 4) is here revised compared to previous studies (Petrizzo et al. 2011; Coccioni & Premoli Silva 2015) with the exception of the FOs of the small-sized species *Hendersonites carinatus* and *Pseudoguembelina costulata*, as these events were detected in slightly younger stratigraphic intervals during this study (Suppl. Tab. 2), possibly as a result of the relatively poor preservation of small sized specimens in the studied samples and because of their rarity at the beginning of their stratigraphic distribution. These events are therefore placed in Fig. 4 according to Petrizzo et al. (2011).

Calcareous plankton events versus magnetostratigraphy

An integrated bio-magnetostratigraphy of the Santonian-Campanian transition (Fig. 6) has been described from the Tethys Ocean (Wolfgring et al. 2017; Wolfgring et al. 2018), Western Interior Sea (Kita et al. 2017), Poland (i.e. Dubicka et al. 2017), DSDP Site 530 (Stradner & Steinmetz 1984) and ODP Site 762 (Bralower & Siesser 1992; Petrizzo 2000).

In the Postalm section (Austrian Alps; north western Tethys), Wolfgring et al. (2018) recorded the LO of *D. asymetrica* at 1.24 m above the base of magnetochron C33r and the FO *A. parcus parcus* (length ≥10 μm) at 1. 66 m above the base of C33r, estimated to correspond to ~80 kyrs after the beginning of magnetochron C33r (Fig. 4). Other events lying close to the Santonian-Campanian boundary are the FO *C. obscurus* var. W at the top of C34n, and the FO *Ceratolithoides* cf. *C. verbeekii* in the lower C33r (Wolfgring et al. 2018). Specimens similar to *Ceratolithoides* cf. *C. verbeekii* were observed in only two samples from the Bottaccione section in the uppermost part of C34n. Regarding the planktonic foraminifera in the Postalm section Wolfgring et al. (2018) recorded the LO of *M. flandrini* at 0.64 m above the base of magnetochron C33r, whereas the species at the Bottaccione section disappears in the upper part of C34n (Fig. 6).

The FO of *A. parcus parcus* was found in the Mudurnu-Göynük area (Turkey; north-western Teth-

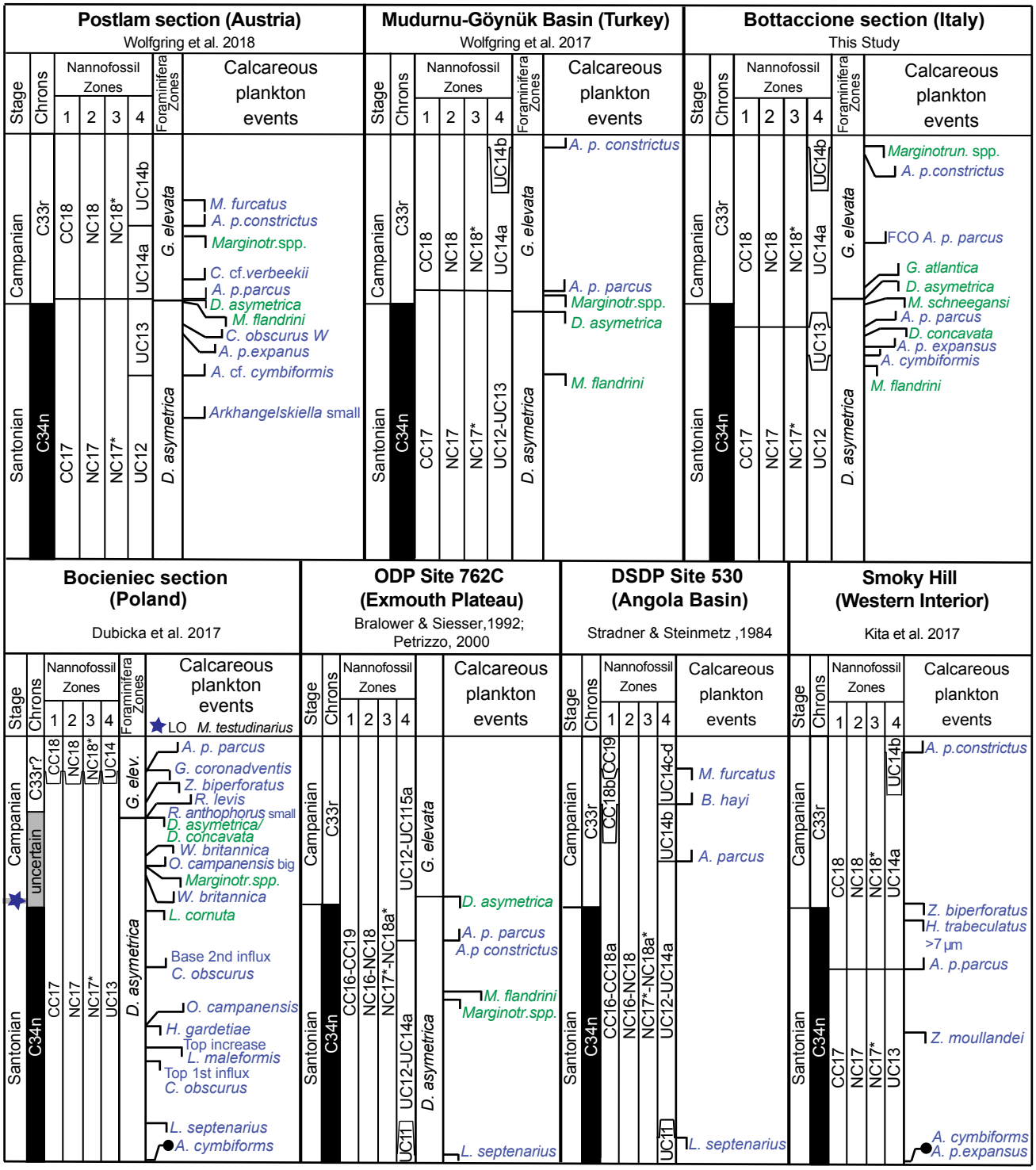

Fig. 6 - Comparison of calcareous plankton events relative to magnetostratigraphy in the Bottaccione section and in other sections across the Santonian-Campanian boundary interval. Calcareous nannofossils events are in blue, planktonic foraminiferal events are in green. The base of magnetic chron C33r is used to place the base of the Campanian Stage. In the Bocieniec section the Santonian-Campanian boundary is placed according to the LO of crinoid *Marsupites testudinarius*.

ys) approximately 500 ka after the beginning of magnetic reversal C33r (Wolfgring et al. 2017) (Fig. 6). However, this taxon is rare in this composite section characterized by poorly preserved assemblages. *Dicarinella asymetrica* is also rare and occurs discontinuously till its disappearance near the top of magnetochron C34n in a slightly older stratigraphic level than documented in the Bottaccione section. *Marginotruncana* spp. and *M. flandrini* disappear in the lower part of magnetochron C33r and in the upper part of C34n,

respectively (Fig. 6). Although the planktonic foraminifera events are recorded in the same sequence, the disappearance of *Marginotruncana* spp. is clearly older in the Turkish section compared to the Bottaccione section.

Kita et al. (2017) indicated two additional potential markers close to the Santonian-Campanian boundary: the LO *H. trabeculatus* (>7 μm) at the top of magnetochron C34n and the LO *Z. biperforatus* in the lowermost C33r. In the Bottaccione section, *H. trabeculatus* specimens larger than 7 μm were not observed, whereas the presence of *Z. biperforatus* was noticed only in one sample (in the lower part of C34n).

At the Exmouth plateau (ODP Hole 762C), Bralower & Siesser (1992) found the FOs *A. parcus parcus* and *A. parcus constrictus* around 2.67 meter, in the uppermost part of magnetochron C34n, while the LO *D. asymetrica* falls 0.98 m above the base of magnetochron C33r (Petrizzo 2000). Instead, *Marginotruncana* spp. and *M. flandrini* have their LOs in the upper part of magnetochron C34n. Compared to the Bottaccione section, the LOs *M. flandrini* and *D. asymetrica* do occur in equivalent stratigraphic levels, whereas the LO of *Marginotruncana* spp. is recorded in definitively older levels at Exmouth Plateau.

The results of Stradner & Steinmetz (1984) show the FO of *A. parcus* in the lower part of magnetochron C33r in the Angola Basin (DSDP Hole 530A) (Fig. 6). Stradner & Steinmetz (1984) included in *A. parcus* only specimens with a rim/central area ratio between 1 and 1.25, thus excluding potential *A. parcus parcus* specimens having a rim/central area ratio between 1.25 and 2.0 with a possible lower occurrence (Kita et al. 2017).

In the Bocieniec section (Poland), the Santonian-Campanian boundary was placed according to the LO of crinoid *Marsupites testudinarius* (Dubicka et al. 2017). The available magnetostratigraphy for this section is uncertain due to the anomalous values of the magnetic polarities. As a consequence, the boundary between magnetochrons C34n and C33r remains indefinite. According to Dubicka et al. (2017), the LO of *D. asymetrica* and the extinction of *Marginotruncana* spp. occur in the stratigraphic interval inferred to contain the boundary between magnetochrons C34n and C33r, whereas the FO *A. parcus parcus* was observed in the lower part of magnetochron C33r. In the Bocieniec section all these events (LO *D. asymetrica;* LO of *Marginotruncana* spp.; FO *A. parcus parcus*) fall above the LO of crinoid *M. testudinarius* (Fig. 4).

The comparison with available bio-magnetostratigraphic data show that the FO of *A. parcus parcus* has been found in a stratigraphic interval between the topmost part of magnetochron C34n and the lowermost part of magnetochron C33r, whereas the extinction of *D. asymetrica* is recorded slightly above the base of magnetochron C33r at all localities except for the Göynük area in Turkey where it falls at the top of magnetochron C34n. In conclusion, according to our findings, the base of magnetochron C33r lies between the FO of *A. parcus parcus* and the LO of *D. asymetrica* in the Bottaccione section and both microfossil events may be used to approximate the base of the Campanian Stage equated to the base of magnetochron C33r.

Conclusions

High-resolution calcareous nannofossil and planktonic foraminiferal biostratigraphy in the Santonian-Campanian boundary interval of the Bottaccione section results in the identification of several FO and LO directly calibrated against magnetostratigraphy. The comparison with previous data obtained for the Bottaccione section displays some discrepancies mainly due to different sampling rate, taxonomic ambiguities, general rarity and moderate to poor preservation of both nannofossil and foraminiferal assemblages. A critical review of all available calcareous plankton data directly correlated with magnetostratigraphy shows that the FO of *A. parcus parcus* is comprised within the topmost part of magnetochron C34n and the lowermost portion of magnetochron C33r, whereas the LO of *D. asymetrica* is documented in the lowermost part of magnetochron 33r, with the only exception of one section in Turkey where this datum correlates with the topmost magnetochron C34n. Adopting the base of magnetochron C33r to place the base of the Campanian stage, the FO of *A. parcus parcus* and the LO of *D. asymetrica* are proposed as the microfossil events to approximate the Santonian-Campanian boundary.

Acknowledgements: The Associate Editor Luca Giusberti, Simonetta Monechi and an anonymous Reviewer are warmly acknowledged for their constructive detailed criticism that greatly improved the quality of the manuscript. This research was funded through the "Piano di Sostegno alla Ricerca of the University of Milan". This study was partially supported by the International Subcommission on Cretaceous Stratigraphy of the International Commission on Stratigraphy (ICS).

PLATE 1

Selected calcareous nannofossil species from the Bottaccione section. For each taxon (a) cross-polarized light; (b) quartz lamina.

1) *Ahmuellerella regularis*, sample 213.8 m.
2) *Amphizygus minimus*, sample 219.75 m.
3) *Arkhangelskiella confusa*, sample 219.5 m.
4) *Arkhangelskiella cymbiformis*, sample 221.4 m.
5) *Aspidolithus parcus expansus* var. "small", sample 220.5 m.
6) *Aspidolithus parcus expansus*, sample 227.5 m.
7) *Aspidolithus parcus parcus* var. "small", sample 229 m.
8) *Aspidolithus parcus parcus*, sample 232.33 m.
9) *Aspidolithus parcus parcus*, sample 233 m.
10) *Aspidolithus parcus constrictus* var. "small", sample 230.6 m.
11) *Aspidolithus parcus constrictus* var. "small", sample 232.85 m.
12) *Aspidolithus parcus constrictus*, sample 230.6 m.
13) *Biscutum constans*, sample 220.9 m.
14) *Biscutum* sp., sample 212.40 m.
15) *Biscutum* sp., sample 220.2 m.
16) *Chiastozygus bifarius*, sample 218.4 m.
17) *Cyclagelosphaera reinhardtii*, sample 221.4 m.
18) *Cribrosphaerella ehrenbergii*, sample 221.9 m.

PLATE 2

Selected calcareous nannofossil species from the Bottaccione section. For each taxon (a) cross-polarized light; (b) quartz lamina.

1) *Cylindralithus biarcus*, sample 221.9 m.
2) *Cylindralithus sculptus*, sample 221.9 m.
3) *Discorhabdus ignotus*, sample 220.9 m.
4) *Eiffellithus eximius*, sample 221.3 m.
5) *Eiffellithus gorkae*, sample 216.3 m.
6) *Eiffellithus nudus*, sample 222 m.
7) *Helicolithus trabeculatus*, sample 221.4 m.
8) *Lithastrinus grillii,* sample 216.85 m.
9) *Lucianorhabdus cayeuxii*, sample 214.9 m.
10) *Microrhabdulus decoratus*, (a) cross-polarized;(b) quartz lamina, sample 220.5.
11) *Micula staurophora,* (a) cross-polarized; (b) quartz lamina, sample 230.6 m.
12) *Quadrum gartneri*, sample 219.1 m.
13) *Reinhardtites anthophorus,* sample 232.85 m.
14) *Reinhardtites* sp., sample 218.4 m.
15) *Retecapsa ficula*, sample 222 m.
16) *Rucinolithus hayi*, sample 229.75 m.
17) *Rucinolithus terebrodentarius*, sample 219.5 m.
18) *Zeugrhabdotus biperforatus*, sample 219.75 m.

PLATE 3

Selected planktonic foraminifera species from the Bottaccione section. Scale bars = 100 mm.

1) *Dicarinella asymetrica*, sample 221.72 m.
2) *Globotruncana linneiana*, sample 212.20 m.
3) *Globotruncanita elevata*, sample 224.60 m.
4) *Contusotruncana fornicata*, sample 221.71 m.
5) *Globotruncana arca*, sample 223.92 m.
6) *Marginotruncana coronata*, sample 212.20 m.
7) *Marginotruncana pseudolinneiana*, sample 224.60 m.
8) *Marginotruncana undulata*, sample 225.75 m.
9) *Marginotruncana sinuosa*, sample 218.92 m.
10) *Marginotruncana schneegansi*, sample 217.55 m.
11) *Marginotruncana pseudomarginata*, sample 218.40 m.
12) *Globotruncana neotricarinata*, sample 221.71 m.
13) *Globotruncana bulloides*, sample 222.05 m.
14) *Globotruncanita stuartiformis*, sample 220.25 m.
15) *Contusotruncana patelliformis*, sample 221.71 m.
16) *Globotruncana orientalis*, sample 221.21 m.
17) *Globotruncanita atlantica*, sample 222.05 m.
18) *Sigalia* sp., sample 221.71 m.
19) *Pseudotextularia nutttalli*, sample 229.75 m.
20) *Ventilabrella eggeri*, sample 214.30 m.
21) *Globotruncana hilli*, sample 224.60 m.
22) *"Globigerinelloides" prairiehillensis*, sample 231.76.
23) *"Globigerinelloides" bollii*, sample 213.30 m.
24) *Laeviheterohelix pulchra*, sample 232.33 m.

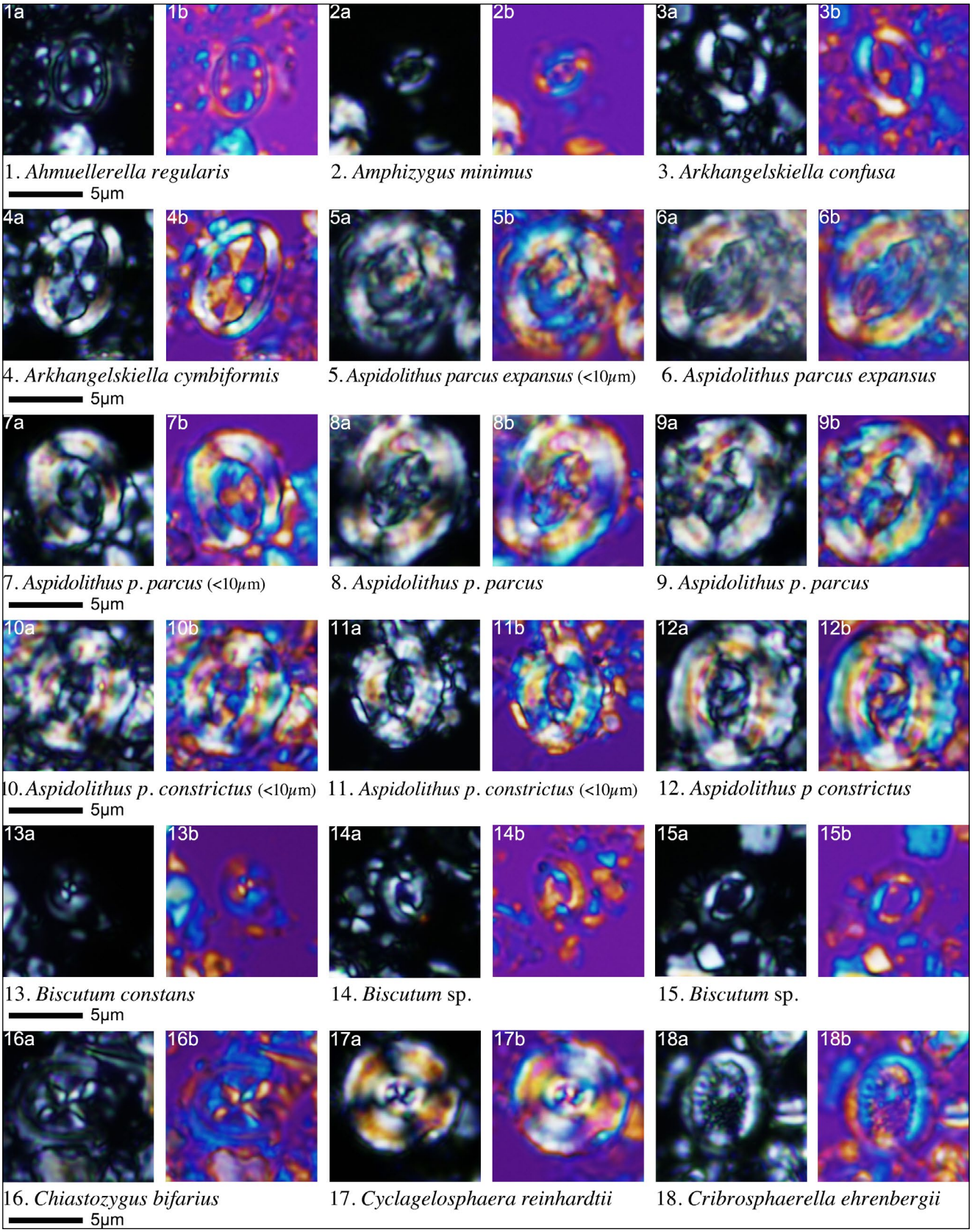
1a
1b
2a
2b
3a
3b
1. *Ahmuellerella regularis*
2. *Amphizygus minimus*
3. *Arkhangelskiella confusa*
5µm
4a
4b
5a
5b
6a
6b
4. *Arkhangelskiella cymbiformis*
5. *Aspidolithus parcus expansus* (<10µm)
6. *Aspidolithus parcus expansus*
5µm
7a
7b
8a
8b
9a
9b
7. *Aspidolithus p. parcus* (<10µm)
8. *Aspidolithus p. parcus*
9. *Aspidolithus p. parcus*
5µm
10a
10b
11a
11b
12a
12b
10. *Aspidolithus p. constrictus* (<10µm)
11. *Aspidolithus p. constrictus* (<10µm)
12. *Aspidolithus p constrictus*
5µm
13a
13b
14a
14b
15a
15b
13. *Biscutum constans*
14. *Biscutum* sp.
15. *Biscutum* sp.
5µm
16a
16b
17a
17b
18a
18b
16. *Chiastozygus bifarius*
17. *Cyclagelosphaera reinhardtii*
18. *Cribrosphaerella ehrenbergii*
5µm

PLATE 1

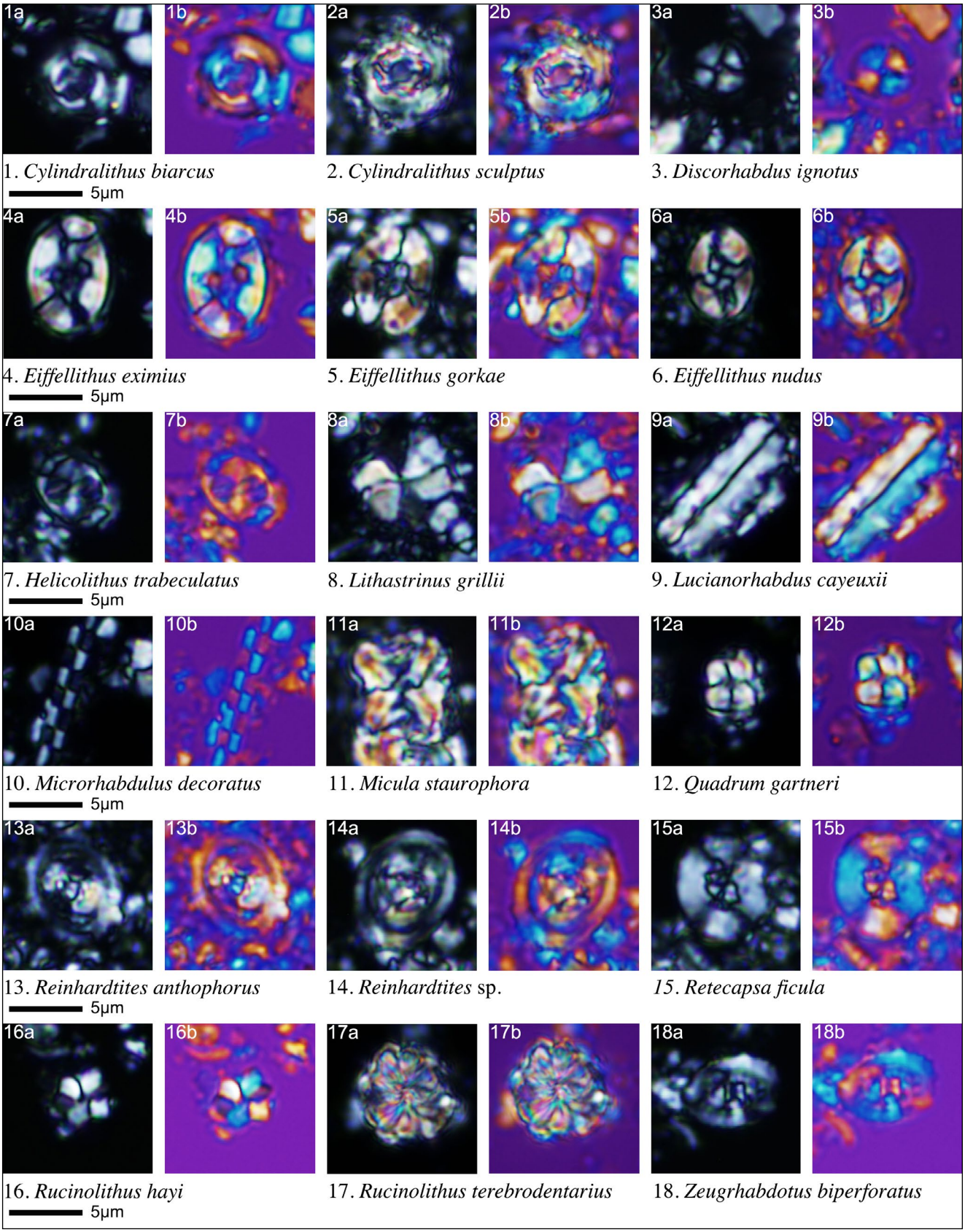
1a
1b
2a
2b
3a
3b
1. Cylindralithus biarcus
2. Cylindralithus sculptus
3. Discorhabdus ignotus
5µm
4a
4b
5a
5b
6a
6b
4. Eiffellithus eximius
5. Eiffellithus gorkae
6. Eiffellithus nudus
5µm
7a
7b
8a
8b
9a
9b
7. Helicolithus trabeculatus
8. Lithastrinus grillii
9. Lucianorhabdus cayeuxii
5µm
10a
10b
11a
11b
12a
12b
10. Microrhabdulus decoratus
11. Micula staurophora
12. Quadrum gartneri
5µm
13a
13b
14a
14b
15a
15b
13. Reinhardtites anthophorus
14. Reinhardtites sp.
15. Retecapsa ficula
5µm
16a
16b
17a
17b
18a
18b
16. Rucinolithus hayi
17. Rucinolithus terebrodentarius
18. Zeugrhabdotus biperforatus
5µm

PLATE 2

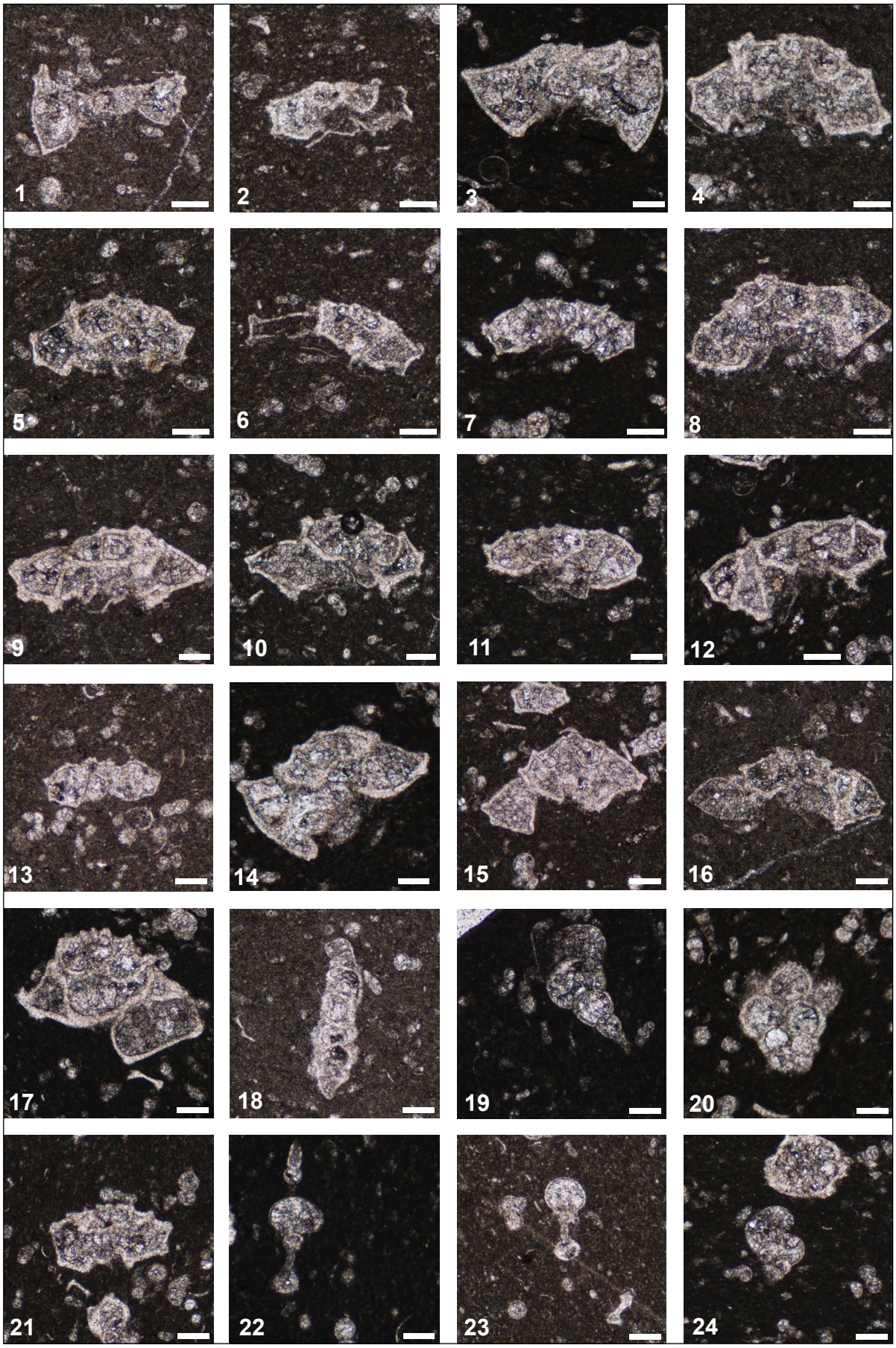

PLATE 3

APPENDIX

In this appendix we describe the diagnostic characters of the genus *Aspidolithus* and of the *Aspidolithus parcus* subspecies. The morphometric data observed in the studied interval of the Bottaccione section are also reported and compared to previous results from the Santonian-Campanian boundary interval.

Order **Arkhangelskiales** Bown & Hampton in Young and Bown, (1997)
Family Arkhangelskiellaceae Bown & Hampton, 1997 *in* Bown & Young, 1997
Genus *Aspidolithus* Noël, 1969

Type-species: *Aspidolithus angustus* Noël, 1969.

Description. Elliptical coccolith with a tired bicyclic rim and a central area filled by perforated plates with axial sutures. At polarizing light microscope, the inner and outer cycles of the rim are visible in distal view, whereas in proximal view only the outer cycle in visible. At crossed nicols, the inner cycle appears brighter than the outer cycle.

Remarks. In this work, we follow Lauer (1974), Prins in Perch Nielsen (1979) and Perch-Nielsen (1985) and, accordingly, genus *Aspidolithus* is differentiated from genus *Broinsonia* due to the presence of plates instead of a cross in the central area. Within the *Aspidolithus* lineage, the subsequent appearances of *A. parcus expansus*, *A. parcus parcus* and *A. parcus constrictus* are marked by a gradual reduction of the central area/margin ratio as described by Wise (1983).

Aspidolithus parcus constrictus (Hattner et al., 1980) Perch-Nielsen, 1984

1980 *Broinsonia parca constricta* – Hattner, Wind and Wise, p. 23; Plate 2, Figs 1-3, 5-8.
1984 *Aspidolithus parcus constrictus* – Perch-Nielsen, p. 43.

Remarks. A subspecies of *Aspidolithus parcus* with a small central area spanned by a perforated plate divided by axial sutures. One to three perforations per quadrants lie parallel to the major axis. The width of the central area is small compared to the shield margin and have a width equivalent or less than the shield margin (b/a ratio ≤1). *A. parcus constrictus* evolved during the early Campanian from *A. parcus parcus* and represents the youngest subspecies in the *Aspidolithus* lineage.

Specimens with the same b/a ratio but a total length <10 μm were considered as "small" *A. parcus constrictus* by Gardin et al. (2001). Wolfgring et al. (2018), instead, considered small the specimens with a total length <9 μm. Both papers outline an increase in size in younger levels.

In the studied Bottaccione section (this work) *A. parcus constrictus* specimens display a total length varying between 8 and 10.3 μm with no correlation with the stratigraphic position.

Aspidolithus parcus expansus (Wise and Watkins in Wise, 1983) Perch-Nielsen, 1984

1983 *Broinsonia parca expansa* – Wise and Watkins in Wise, p. 506; plate 9, Figs. 1-5; plate 10, Figs. 5-9; Plate 11, Figs. 1-9.
1984 *Aspidolithus parcus expansus* – Perch-Nielsen, p. 43.

Remarks. A subspecies of *Aspidolithus parcus* with a wide central area spanned by a perforated plate divided by axial sutures. Central area perforations lie parallel to the ellipse axes. The width of the central area is approximately twice or more than twice the width of the shield margin (the b/a ratio is ≥2). *A. parcus expansus* represents the oldest subspecies belongings to the *Aspidolithus parcus* lineage starting in the late Santonian (Wise 1983; Perch-Nielsen 1985).

Specimens with this b/a ratio but a total length <10 μm or <9 μm were considered as "small" *A. parcus expansus* by Gardin et al (2001) and Wolfgring et al. (2018), respectively.

The specimens observed in the studied Bottaccione section have a length variable between 9 and 12.3 μm. In the lowermost part of the subspecies range (latest Santonian) specimens are rather small (coccolith length of 10–10.2 μm) and co-occur with "small" *A. parcus expansus* (coccolith length varying between 9 and 9.9 μm) from just prior to the Santonian-Campanian boundary. The coccolith length increases in the earliest Campanian as testified by presence of some relatively large specimens (total length of 11–12.3 μm) together with small specimens (length varying between 9.5 and 9.9 μm) through the rest of the studied interval.

Aspidolithus parcus parcus (Stradner, 1963) Noël, 1969

1963 *Arkhangelskiella parca* – Stradner, p. 10; Plate 1, Figs. 3, 3a.
1969 *Aspidolithus parcus* – Noël, p. 196; Plate 1, Figs. 3, 4.

Remarks. A subspecies of *Aspidolithus parcus* with a central area spanned by a perforated plate divided by axial sutures. Central area perforations lie parallel to the ellipse axes. The width of the central area is approximately between one to two times the width of the shield margin (b/a ratio between 1 and 2). In the latest Santonian, *A. parcus parcus* evolved from *A. parcus expansus* with a reduction of the central area width.

Specimens with this b/a ratio but a total length <10 μm were considered as "small" *A. parcus parcus* by Gardin et al. (2001); Wolfgring et al. (2018), instead, considered small the specimens with total length <9 μm. Both studies outline an increase in size upwards.

In the studied Bottaccione section *A. parcus parcus* specimens have a length varying between 9.5 and 11.8 μm, with a general increase in coccolith length upwards in analogy to previous records (Gardin et al. 2001; Wolfgring et al. 2018). However, in the lowermost part of its range (latest Santonian), the coccolith length varies between 10 μm and 10.2 μm, thus, within the size range of *A. parcus parcus* (≥10 μm, following Gardin et al. 2001) although very close to the lower limit of size range. A single specimen with total length of 9.6 μm (small *A. parcus parcus*) was observed in this interval. A minor increase in length size (10.5–11.7 μm) of *A. parcus parcus* coccoliths is observed in the lower Campanian; these specimens co-occur with small *A. parcus parcus* coccoliths with length varying from 8.4 to 9.9 μm.

References

Almogi-Labin A., Eshet Y., Flexer A., Honigstein A., Moshkovitz S. & Rosenfeld A. (1991) - Detailed biostratigraphy of the Santonian/Campanian boundary interval in Northern Israel. *Journal of Micropalaeontology*, 10: 39-50.

Alvarez W. & Montanari A. (1988) - The Scaglia limestone (Late Cretaceous–Oligocene) in the northeastern Apennines carbonate sequence: stratigraphic context and geological significance. In: Premoli Silva I., Coccioni R. & Montanari A. (Eds.) - The Eocene–Oligocene boundary in the Marche–Umbria basin (Italy), 1: 13-29. Industrie Grafiche F.lli Aniballi, Ancona.

Alvarez W., Arthur M.A., Fischer A.G., Lowrie W., Napoleone G., Premoli Silva I. & Roggenthen W.M. (1977) - Upper Cretaceous–Paleocene magnetic stratigraphy at Gubbio, Italy. Type section for the Late Cretaceous-Paleocene geomagnetic reversal time scale. *Geological Society of America Bulletin*, 88: 383-389.

Arthur M.A. & Fischer A.G. (1977) - Upper Cretaceous–Paleocene magnetic stratigraphy at Gubbio, Italy I. Lithostratigraphy and sedimentology. *Geological Society of America Bulletin,* 88: 367-371.

Boersma A. (1981) - Cretaceous and early Tertiary foraminifers from Deep Sea Drilling Project Leg 62 sites in the central Pacific. In: Thiede J., Valuer T.L. et al. (Eds.) - Initial Reports of the Deep Sea Drilling Project, 62: 377-396. U.S. Government Printing Office, Washington.

Bralower T.J. & Siesser W.G. (1992) - Cretaceous calcareous nannofossil biostratigraphy of ODP Leg 122 Sites 761,762 and 763, Exmouth and Wombat Plateaus, N.W. Australia. In: von Rad U., Haq B.U. et al. (Eds.) - Proceedings Ocean Drilling Program Scientific Results, 122: 529-556. Ocean Drilling Program, College Station, Texas.

Bralower T.J., Leckie R.M., Sliter W.V. & Thierstein H.R. (1995) - An integrated Cretaceous microfossil biostratigraphy. In: Berggren W.A., Kent D.V., Aubry M.-P. & Hardenbol J. (Eds.) - Geochronology, Time Scales and Global Stratigraphic Correlation, 54: 65-79. Society of Economic Paleontologists and Mineralogists, Special Publication.

Bukry D. (1969) - Upper Cretaceous coccoliths from Texas and Europe. *The University of Kansas Paleontological Contributions*: *Article 51 (Protista 2)*: 1-79.

Burnett J. A. (1997) - New species and new combinations of Cretaceous nannofossils and a note on the origin of *Petrarhabdus* (Deflandre) Wise & Wind. *Journal of Nannoplankton Research*, 19: 133-146.

Burnett J.A. (1998) - Upper Cretaceous. In: Bown P.R. (Eds.) - Calcareous Nannofossil Biostratigraphy: 132-199. Kluwer Academic Publishers, London.

Coccioni R. & Premoli Silva I. (2015) - Revised Upper Albian–Maastrichtian planktonic foraminiferal biostratigraphy and magneto-stratigraphy of the classical Tethyan Gubbio section (Italy). *Newsletters on Stratigraphy*, 48: 47-90.

Cresta S., Monechi S. & Parisi G. (1989) - Stratigrafia del Mesozoico e Cenozoico nell'area Umbro–Marchigiana. Memorie descrittive della Carta Geologica d'Italia 39, 185 pp.

Crux J.A. (1982) - Upper Cretaceous (Cenomanian to Campanian) calcareous nannofossils. In: Lord A.R. (Eds.) - A Stratigraphical Index of Calcareous Nannofossils 5: 81-135. British Micropalaeontological Society Series, Chichester.

Dubicka Z., Jurkowska A., Thibault N., Rasmjooei M.J.,Wojcik K., Gorzelak P. & Felisiak I. (2017) - An integrated stratigraphic study across the Santonian/Campanian boundary at Bocieniec, southern Poland: a new boundary stratotype candidate. *Cretaceous Research,* 80: 61-85.

Falzoni F., Petrizzo M.R., Jenkyns H.C., Gale A.S. & Tsikos H. (2016) - Planktonic foraminiferal biostratigraphy and assemblage composition across the Cenomanian–Turonian boundary interval at Clot Chevalier (Vocontian Basin, SE France). *Cretaceous Research,* 59: 69-97.

Gardin S., Del Panta F., Monechi S. & Pozzi M. (2001) - A Tethyan reference record for the Campanian and Maastrichtian stages: The Bottaccione section (Central Italy); review of data and new calcareous nannofossil results. In: G.S. Odin (Eds.) - The Campanian–Maastrichtian Stage Boundary, 19: 745-757. Developments in Palaeontology and Stratigraphy, Elsevier.

Gradstein F.M. (1978) - Biostratigraphy of Lower Cretaceous Blake Nose and Blake-Bahama basin foraminifers DSDP Leg 44, western north Atlantic Ocean. In: Benson W.E., Sheridan R.E. et al. (Eds.) - Initial Reports of the Deep Sea Drilling Project, 44: 663-701. U.S. Government Printing Office, Washington.

Gradstein F.M., Ogg J.G., Schmitz M.D. & Ogg G.M. (2012) - The Geologic Time Scale 2012. Elsevier, 1144 pp.

Hancock J.M. & Gale A.S. (1996) - The Campanian Stage. *Bulletin de l'Institut royal des Sciences naturelles de Belgique: Sciences de la Terre*, 66: 103-109.

Hattner J.G., Wind F.H. & Wise S.W. (1980) - The Santonian-Campanian boundary: comparison of nearshore-offshore calcareous nannofossil assemblages. *Cahiers de Micropaléontologie*, 3: 9-26.

Haynes S.J., Huber B.T. & Macleod K.G. (2015) - Evolution and phylogeny of mid-Cretaceous (Albian–Coniacian) biserial planktic foraminifera. *Journal of Foraminiferal Research*, 45: 42-81.

Huber B.T., Petrizzo M.R., Young J.R., Falzoni F., Gilardoni S. E., Bown P.R. & Wade B.S. (2016) - Pforams@microtax: A new online taxonomic database for planktonic foraminifera. *Micropaleontology*, 62: 429-438.

Kita Z.A., Watkins D.K. & Sageman B.B. (2017) - High resolution calcareous nannofossil biostratigraphy of the Santonian/Campanian Stage boundary, Western Interior Basin, USA. *Cretaceous Research*, 69: 49-55.

Lauer G. (1975) - Evolutionary trends in the Arkhangelskiellaceae (calcareous nannoplankton) of the Upper Cretaceous of Central Oman, SE Arabia. *Archives de Sciences Genève*, 28: 259-262.

Lirer F. (2000) - A new technique for retrieving calcareous microfossils from lithified lime deposits. *Micropaleontology*, 46: 365-369.

Longoria J.F. (1974) - Stratigraphic, morphologic and taxonomic studies of Aptian planktonic foraminifera. *Revista Espanola de Micropaleontologia*, Numero Extraordinario:

5-107.

Maron M. & Muttoni G. (accepted) - A detailed record of the C34n/C33r magnetozone boundary for the definition of the base of the Campanian Stage at the Bottaccione section (Gubbio, Italy). *Newsletters on Stratigraphy*. DOI:10.1127/nos/2020/0607.

Masters B.A. (1977) - The neotype of *Globigerina cretacea* var. *delrioensis* Carsey. *Journal of Paleontology*, 51: 643.

Mohler H.P. (1966) - Stratigraphische Untersuchungen in den Giswiler Klippen (Prealpes Medianes) und ihrer helvetisch-ultrahelvetischen Unterlage. *Beiträge zur Geologischen Karte der Schweiz*, 129:15-84.

Monechi S. (1977) - Upper Cretaceous and Early Tertiary nannoplankton from Scaglia Umbra Formation (Gubbio, Italy). *Rivista Italiana di Paleontologia e Stratigrafia*, 83: 759-802.

Monechi S. & Pirini Radrizzani C. (1975) - Nannoplankton from Scaglia Umbra Formation (Gubbio) at the Cretaceous-Tertiary boundary. *Rivista Italiana di Paleontologia e Stratigrafia*, 81: 85-96.

Monechi S. & Thierstein H.R. (1985) - Late Cretaceous-Eocene nannofossil and magnetostratigraphic correlations near Gubbio, Italy. *Marine Micropaleontology*, 9: 419-440.

Napoleone G., Premoli Silva I., Heller F., Cheli P., Corezzi S., & Fischer A.G. (1983) - Eocene magnetic stratigraphy at Gubbio, Italy, and its implications for Paleogene geochronology. *Geological Society of America Bulletin*, 94: 181-191.

Nederbragt A.J. (1991) - Late Cretaceous biostratigraphy and development of Heterohelicidae (planktic foraminifera). *Micropaleontology*, 37: 329-372.

Noël D. (1969) - *Arkhangelskiella* (coccolithes Crétacés) et formes affines du Bassin de Paris. *Revue de Micropaléontologie*, 11: 191-204.

Perch-Nielsen K. (1979) - Calcareous nannofossils from the Cretaceous between the North Sea and the Mediterranean. Aspecte der Kriede Europas: Stuttgart. *IUGS Series A*, 6: 223-272.

Perch-Nielsen K. (1984) - Validation of new combinations. *INA Newsletter*, 6: 42-46.

Perch-Nielsen K. (1985) - Mesozoic calcareous nannofossils. In: Bolli H.M., Saunders J.B. & Perch-Nielsen K. (Eds.) - Plankton Stratigraphy: 329-426. Cambridge University Press.

Petrizzo M.R. (2000) - Upper Turonian-lower Campanian planktonic foraminifera from southern mid high latitudes (Exmouth Plateau, NW Australia): biostratigraphy and taxonomic notes. *Cretaceous Research,* 21: 479-505.

Petrizzo M.R. & Huber B.T. (2006) - Biostratigraphy and taxonomy of Late Albian planktonic foraminifera from ODP Leg 171b (western north Atlantic Ocean). *Journal of Foraminiferal Research*, 36: 165-189.

Petrizzo M.R., Falzoni F. & Premoli Silva I. (2011) - Identification of the base of the lower-to-middle Campanian *Globotruncana ventricosa* Zone: Comments on reliability and global correlations. *Cretaceous Research*, 32: 387-405.

Petrizzo M.R., Berrocoso A.J., Falzoni F., Huber B.T. & Macleod K.G. (2017) - The Coniacian–Santonian sedimentary record in southern Tanzania (Ruvuma Basin, East Africa): Planktonic foraminiferal evolutionary, geochemical and palaeoceanographic patterns. *Sedimentology*, 64: 252-285.

Premoli Silva I. (1977) - Upper Cretaceous-Paleocene magnetic stratigraphy at Gubbio, Italy II. Biostratigraphy. *Geological Society of America Bulletin*, 88: 371-374.

Premoli Silva I. & Sliter W.V. (1995) - Cretaceous planktonic foraminiferal biostratigraphy and evolutionary trends from the Bottaccione section, Gubbio, Italy. *Palaeontographia Italica*, 82: 1-85.

Robaszynski F. & Caron M. (1995) - Foraminiféres planctoniques du Crétacé: commentaire de la zonation Europe-Méditerranée. *Bulletin de la Société Géologique de France*, 166: 681-692.

Roth P.H. (1978) - Cretaceous nannoplankton biostratigraphy and oceanography of the northwestern Atlantic Ocean. In: Benson W.E., Sheridan R.E. et al. (Eds.) - Initial Reports ofthe Deep Sea Drilling Project 44: 663-701. U.S. Government Printing Office, Washington.

Sissingh W. (2007) - Biostratigraphy of Cretaceous calcareous nannoplankton. *Netherlands Journal of Geosciences/Geologie en Mijnbouw*, 56: 37-65.

Stradner H. & Steinmetz J. (1984) - Cretaceous calcareous nannofossils from the Angola Basin, Deep Sea Drilling Project Site 530. In: Hay W.W., Sibuet J.-C et al. (Eds) - Initial Reports of the Deep Sea Drilling Project 75: 565-649. U.S. Government Printing Office, Washington.

Tremolada F. (2002) - Aptian to Campanian calcareous nannofossils biostratigraphy from the Bottaccione section, Gubbio, central Italy. *Rivista Italiana di Paleontologia e Stratigrafia*, 108: 441-456.

Wise S.W. (1983) - Mesozoic and Cenozoic calcareous nannofossils recovered by deep sea drilling project Leg 71 in the Falkland Plateau region, south-west Atlantic Ocean. In: Ludwig W.J., Krasheninikov V.A. et al. (Eds.) - Initial Reports of the Deep Sea Drilling Project 71: 481-550. U.S. Government Printing Office, Washington.

Wolfgring E., Wagreich M., Dinarès-Turell J., Gier S., Böhm K., Sames B., Spötl C. & Popp F. (2018) - The Santonian–Campanian boundary and the end of the Long Cretaceous Normal Polarity–Chron: isotope and plankton stratigraphy of a pelagic reference section in the NW Tethys (Austria). *Newsletter on Stratigraphy*, 51: 445-476.

Verbeek J.W. (1977) - Calcareous nannoplankton biostratigraphy of Middle and Upper Cretaceous deposits in Tunisia, southern Spain and France. *Utrecht Micropaleontological Bulletin*, 16: 1-157.

Wolfgring E., Wagreich M., Dinares-Turell J., Yilmaz I.O., Bohm K. (2017) - Plankton biostratigraphy and magnetostratigraphy of the Santonian–Campanian boundary interval in the Mudurnu-G.ynük Basin, northwestern Turkey. *Cretaceous Research*, 87: 296-311.

Zepeda M.A. (1998) - Planktonic foraminiferal diversity, equitability and biostratigraphy of the uppermost Campanian–Maastrichtian, ODP leg 122, hole 762C, Exmouth Plateau, NW Australia, eastern Indian Ocean. *Cretaceous Research*, 19: 117-152.

Acknowledgements

I am very grateful to Prof. Elisabetta Erba for the opportunity she gave me to work in such a great Ph.D. project. She kindly supported my work with inspiring discussions and her experience, providing help whenever needed. I'm also very grateful to Prof. Cinzia Bottini for her help and scientific discussion.

Thanks to Prof. Isabella Premoli Silva and Prof. Maria Rose Petrizzo for their every good advice.

I would like to thank Matteo Pegoraro for the valuable help in the lab and samples preparation.

I am grateful to Prof. Nicolas Rudolph Thibault for the opportunity he gave me for a four-months research stay at the University of Copenhagen. I would also like to thank Sarah, Johannes, Samer, Juan, Toms, Janina for the friendship and company at the institute that made the stay an incredible experience.

I would like to thank my colleague and friends at the University, Francesca, Silvia, Victor, Stefano, Liyenne, Giulia, Anna and Gaia for their support, discussion and the good time spent together.

I am grateful to Martina and Diego that they never made me miss their support in this adventure. They patiently endured my long periods away and my nights working. Thanks to my parents and all my family and friends for their continuous encouragement.